TYPE SYNTHESIS AND PERFORMANCE OPTIMIZATION OF PARALLEL MANIPULATORS

QI ZOU

A DISSERTATION SUBMITTED TO
THE FACULTY OF GRADUATE STUDIES
IN PARTIAL FULFILLMENT OF THE REQUIREMENTS
FOR THE DEGREE OF

DOCTOR OF PHILOSOPHY

GRADUATE PROGRAM IN
MECHANICAL ENGINEERING
YORK UNIVERSITY
TORONTO, ONTARIO

DECEMBER 2022

Abstract

Parallel robots have been widely employed in industrial applications. There are still some challenging topics in the fundamental research, e.g., the primary problem mobility analysis has not been solved for about 150 years. A universal mobility equation for all kinds of parallel architectures has not been found. Another issue lies on the performance measurements for parallel manipulators. There are plenty of kinematic and dynamic performance indices. However, the various ranges and scales of these indicators make the optimal design considering multiple indices complicated. It is essential to search for a unified approach to normalize performance indicators. More dynamic performance measurement indicators should be raised to explore the dynamic features and complete the theory for parallel mechanisms.

In this research, an improved mobility equation is designed to reveal the degrees of freedom for a special class of parallel robots. A novel methodology called the kinematic joint matrix is proposed. It possesses the mapping relations with parallel manipulators. A series of 2-6 degrees of freedom parallel architectures is denoted by the kinematic joint matrix. The theory of screw is employed to check the feasibility from several kinds of parallel structures. A special block diagram is introduced to distinguish various kinematic joint matrices.

Since this family of parallel robots contains various motion characteristics, four parallel robots with distinct features are selected. Based on the kinematic models, three categories of singularities are explored. The operational and reachable workspaces of the pure-translational parallel robots are searched and the parametric analyses are reported. The linkage's impacts for the reachable workspace of the mixed-motion parallel architectures are investigated. The novel performance level index is designed to unify the positive performance index and demonstrated the performance rank for any pose (position and orientation). The dexterity index is utilized as an example to verify the characteristics of the level index. The distributions and parametric analyses of two novel mass-related performances are studied. The dimension synthesis of a selected planar parallel robot is presented based on the non-dominated genetic algorithm II. The experiment results testify the correctness of the mobility and kinematic mathematical models of this mechanism.

Acknowledgements

I want to express my sincere gratitude to my supervisor Prof. Dan Zhang. During my whole study in the Advanced robotics and mechatronics lab of York University, he has provided me lots of detailed guidance, which helps me to dive into this research field. Being a modest, patient, diligent and talented researcher, he would like to encourage students to explore the intrinsic problems and concentrate on one research issue deeply during the whole process. He has endeavored to support and encourage students, share his knowledge to young people. His genuine help and inspiration have significant meanings for me, both in research career and life. He is my lifetime role model.

I would like to thank my supervisory committee members, Dr. Aleksander (Alex) Czekanski and Dr. Zheng Hong (George) Zhu. They have leaded me to review my research topics and improve my research skills. Their suggestive comments assist me to enhance my research.

I want to thank the other members in our lab, Shuo Zhang, XueLing Luo, ZhongXing Yang, GuanYu Huang, HongYan Tang, XiaoDong Jin, HaiQiang Zhang, NaiJiang Jiang, Chong Zhao, ZhiBo Sun, Lei Zhang, Moritz Arns, ShiTao Ge. I really appreciate your help and encouragements during my research.

I am deeply grateful to my family whose sincere support and love have encouraged me to study happily in York University. Especially, I want to express my deep appreciation to my wife Shuo Zhang. I will never complete my study without your selfless support, accompany and understanding. Thank you.

At last, I want to thank everyone who has helped me in my PhD program. I wish you all the best.

Contents

Abstract ii
Acknowledgements iii
Contents iv
List of Tables vi
List of Figures vii
List of Nomenclatures xiii
Chapter 1 Introduction 1
1.1 Backgrounds of the research 1
1.2 Motivations and research objectives 4
1.3 Organization of this dissertation 6
Chapter 2 Literature review 8
2.1 Type synthesis of parallel robots 8
2.2 Kinematic performance measurements of parallel robots 10
2.3 Dynamic analysis of parallel mechanisms 17
2.4 Linkage optimization research 20
2.5 Summary 23
Chapter 3 Structural synthesis of a group of parallel manipulators 24
3.1 Revised mobility equation for a group of parallel robots 24
3.2 Kinematic joint matrix 29
3.3 Enumeration of a family of parallel mechanisms 34
3.3.1 Two-DOF parallel mechanism 34
3.3.2 Three-DOF parallel mechanism 39
3.3.3 Four-DOF parallel mechanism 54
3.3.4 Five-DOF parallel mechanism 80
3.3.5 Six-DOF parallel mechanism 116
3.4 Summary 177
Chapter 4 Performance analysis of parallel mechanisms 178
4.1 Performance index: Level index 178
4.2 Case one: 2T parallel mechanism 180
4.3 Case two: 2T1R parallel mechanism 189
4.4 Case three: 3T parallel mechanism 204
4.5 Case four: 3T1R parallel mechanism 216
4.6 Summary 229
Chapter 5 Dynamic modelling of parallel structures 230
5.1 Inertia-related indices 230
5.2 Case one: 2T parallel mechanism 231
5.3 Case two: 2T1R parallel mechanism 239
5.4 Case three: 3T parallel mechanism 249
5.5 Case four: 3T1R parallel mechanism 258
5.6 Summary 273
Chapter 6 Design optimization and experiments 274
6.1 Dimension optimization 274
6.2 Experiments 278

6.3 Summary 283
Chapter 7 Conclusion and future work 284
7.1 Conclusions 284
7.2 Contributions of the dissertation 284
7.3 Future work 286
Bibliography 288

List of Tables

Table 3-1 Possible parallel mechanisms in this group.....28
Table 4-1 The comparisons among four selected parallel structures.....180
Table 6-1 Performances of the last generations.....277

List of Figures

Figure 3-1 Schematic diagram of this planar parallel mechanism 25
Figure 3-2 Block patterns for kinematic joint matrix 32
Figure 3-3 The block pattern for two similar matrices 34
Figure 3-4 Prototype of a 6-DOF parallel structure 34
Figure 3-5 Schematic diagram of 2-DOF parallel structure (1) 35
Figure 3-6 Schematic diagram of 2-DOF parallel structure (2) 36
Figure 3-7 The first branch of 2R mechanism 36
Figure 3-8 1T1R mechanism 38
Figure 3-9 Schematic diagram of 3-DOF parallel structure (1) 40
Figure 3-10 Schematic diagram of 3-DOF parallel structure (2) 41
Figure 3-11 Schematic diagram of 3-DOF parallel structure (3) 41
Figure 3-12 Schematic diagram of 3-DOF parallel structure (4) 42
Figure 3-13 Schematic diagram of 3-DOF parallel structure (5) 42
Figure 3-14 Schematic diagram of 3-DOF parallel structure (6) 43
Figure 3-15 Schematic diagram of 3-DOF parallel structure (7) 43
Figure 3-16 Schematic diagram of 3-DOF parallel structure (8) 44
Figure 3-17 Schematic diagram of 3-DOF parallel structure (9) 44
Figure 3-18 Schematic diagram of 3-DOF parallel structure (10) 45
Figure 3-19 The first branch of 3R mechanism 45
Figure 3-20 The first kind of 1T2R mechanism 47
Figure 3-21 The second kind of 1T2R mechanism 49
Figure 3-22 Schematic diagram of 2T1R parallel structure (1) 51
Figure 3-23 Schematic diagram of 2T1R parallel structure (2) 52
Figure 3-24 Diagram of 3-DOF parallel structure 52
Figure 3-25 Schematic diagram of 4-DOF parallel structure (1) 57
Figure 3-26 Schematic diagram of 4-DOF parallel structure (2) 58
Figure 3-27 Schematic diagram of 4-DOF parallel structure (3) 58
Figure 3-28 Schematic diagram of 4-DOF parallel structure (4) 59
Figure 3-29 Schematic diagram of 4-DOF parallel structure (5) 60
Figure 3-30 Schematic diagram of 4-DOF parallel structure (6) 60
Figure 3-31 Schematic diagram of 4-DOF parallel structure (7) 61
Figure 3-32 Schematic diagram of 4-DOF parallel structure (8) 62
Figure 3-33 Schematic diagram of 4-DOF parallel structure (9) 62
Figure 3-34 Schematic diagram of 4-DOF parallel structure (10) 63
Figure 3-35 Schematic diagram of 4-DOF parallel structure (11) 64
Figure 3-36 Schematic diagram of 4-DOF parallel structure (12) 64

Figure 3-37 Schematic diagram of 4-DOF parallel structure (13)....65
Figure 3-38 Schematic diagram of 4-DOF parallel structure (14)....66
Figure 3-39 Schematic diagram of 4-DOF parallel structure (15)....66
Figure 3-40 Schematic diagram of 4-DOF parallel structure (16)....67
Figure 3-41 Schematic diagram of 4-DOF parallel structure (17)....68
Figure 3-42 Schematic diagram of 4-DOF parallel structure (18)....69
Figure 3-43 Schematic diagram of 4-DOF parallel structure (19)....69
Figure 3-44 Schematic diagram of 4-DOF parallel structure (20)....70
Figure 3-45 Schematic diagram of 4-DOF parallel structure (21)....71
Figure 3-46Schematic diagram of 4-DOF parallel structure (22)....71
Figure 3-47 Schematic diagram of 4-DOF parallel structure (23)....72
Figure 3-48 Schematic diagram of 4-DOF parallel structure (24)....73
Figure 3-49 2T2R mechanism....74
Figure 3-50 1T3R mechanism....77
Figure 3-51 Schematic diagram of 5-DOF parallel structure (1)....82
Figure 3-52 Schematic diagram of 5-DOF parallel structure (2)....83
Figure 3-53 Schematic diagram of 5-DOF parallel structure (3)....84
Figure 3-54 Schematic diagram of 5-DOF parallel structure (4)....84
Figure 3-55 Schematic diagram of 5-DOF parallel structure (5)....85
Figure 3-56 Schematic diagram of 5-DOF parallel structure (6)....86
Figure 3-57 Schematic diagram of 5-DOF parallel structure (7)....86
Figure 3-58 Schematic diagram of 5-DOF parallel structure (8)....87
Figure 3-59 Schematic diagram of 5-DOF parallel structure (9)....88
Figure 3-60 Schematic diagram of 5-DOF parallel structure (10)....88
Figure 3-61 Schematic diagram of 5-DOF parallel structure (11)....89
Figure 3-62Schematic diagram of 5-DOF parallel structure (12)....90
Figure 3-63 Schematic diagram of 5-DOF parallel structure (13)....91
Figure 3-64 Schematic diagram of 5-DOF parallel structure (14)....91
Figure 3-65 Schematic diagram of 5-DOF parallel structure (15)....92
Figure 3-66 Schematic diagram of 5-DOF parallel structure (16)....93
Figure 3-67 Schematic diagram of 5-DOF parallel structure (17)....93
Figure 3-68 Schematic diagram of 5-DOF parallel structure (18)....94
Figure 3-69 Schematic diagram of 5-DOF parallel structure (19)....95
Figure 3-70 Schematic diagram of 5-DOF parallel structure (20)....95
Figure 3-71 Schematic diagram of 5-DOF parallel structure (21)....96
Figure 3-72 Schematic diagram of 5-DOF parallel structure (22)....97
Figure 3-73 Schematic diagram of 5-DOF parallel structure (23)....98

Figure 3-74 Schematic diagram of 5-DOF parallel structure (24) 98
Figure 3-75 Schematic diagram of 5-DOF parallel structure (25) 99
Figure 3-76 Schematic diagram of 5-DOF parallel structure (26) 100
Figure 3-77 Schematic diagram of 5-DOF parallel structure (27) 101
Figure 3-78 Schematic diagram of 5-DOF parallel structure (28) 102
Figure 3-79 Schematic diagram of 5-DOF parallel structure (29) 103
Figure 3-80 Schematic diagram of 5-DOF parallel structure (30) 104
Figure 3-81 Schematic diagram of 5-DOF parallel structure (31) 105
Figure 3-82 Schematic diagram of 5-DOF parallel structure (32) 106
Figure 3-83 Schematic diagram of 5-DOF parallel structure (33) 106
Figure 3-84 Schematic diagram of 5-DOF parallel structure (34) 107
Figure 3-85 Schematic diagram of 5-DOF parallel structure (35) 108
Figure 3-86 Schematic diagram of 5-DOF parallel structure (36) 109
Figure 3-87 Schematic diagram of 5-DOF parallel structure (37) 110
Figure 3-88 Schematic diagram of 5-DOF parallel structure (38) 111
Figure 3-89 Schematic diagram of 5-DOF parallel structure (39) 111
Figure 3-90 Schematic diagram of 5-DOF parallel structure (40) 112
Figure 3-91 2T3R mechanism 113
Figure 3-92 Schematic diagram of 6-DOF parallel structure (1) 118
Figure 3-93 Schematic diagram of 6-DOF parallel structure (2) 118
Figure 3-94 Schematic diagram of 6-DOF parallel structure (3) 119
Figure 3-95 Schematic diagram of 6-DOF parallel structure (4) 120
Figure 3-96 Schematic diagram of 6-DOF parallel structure (5) 120
Figure 3-97 Schematic diagram of 6-DOF parallel structure (6) 121
Figure 3-98 Schematic diagram of 6-DOF parallel structure (7) 122
Figure 3-99 Schematic diagram of 6-DOF parallel structure (8) 122
Figure 3-100 Schematic diagram of 6-DOF parallel structure (9) 123
Figure 3-101 Schematic diagram of 6-DOF parallel structure (10) 124
Figure 3-102 Schematic diagram of 6-DOF parallel structure (11) 125
Figure 3-103 Schematic diagram of 6-DOF parallel structure (12) 125
Figure 3-104 Schematic diagram of 6-DOF parallel structure (13) 126
Figure 3-105 Schematic diagram of 6-DOF parallel structure (14) 127
Figure 3-106 Schematic diagram of 6-DOF parallel structure (15) 128
Figure 3-107 Schematic diagram of 6-DOF parallel structure (16) 129
Figure 3-108 Schematic diagram of 6-DOF parallel structure (17) 129
Figure 3-109 Schematic diagram of 6-DOF parallel structure (18) 130
Figure 3-110 Schematic diagram of 6-DOF parallel structure (19) 131

Figure 3-111 Schematic diagram of 6-DOF parallel structure (20).....132
Figure 3-112 Schematic diagram of 6-DOF parallel structure (21).....132
Figure 3-113 Schematic diagram of 6-DOF parallel structure (22).....133
Figure 3-114 Schematic diagram of 6-DOF parallel structure (23).....134
Figure 3-115 Schematic diagram of 6-DOF parallel structure (24).....134
Figure 3-116 Schematic diagram of 6-DOF parallel structure (25).....135
Figure 3-117 Schematic diagram of 6-DOF parallel structure (26).....136
Figure 3-118 Schematic diagram of 6-DOF parallel structure (27).....137
Figure 3-119 Schematic diagram of 6-DOF parallel structure (28).....137
Figure 3-120 Schematic diagram of 6-DOF parallel structure (29).....138
Figure 3-121 Schematic diagram of 6-DOF parallel structure (30).....139
Figure 3-122 Schematic diagram of 6-DOF parallel structure (31).....140
Figure 3-123 Schematic diagram of 6-DOF parallel structure (32).....140
Figure 3-124 Schematic diagram of 6-DOF parallel structure (33).....141
Figure 3-125 Schematic diagram of 6-DOF parallel structure (34).....142
Figure 3-126 Schematic diagram of 6-DOF parallel structure (35).....143
Figure 3-127 Schematic diagram of 6-DOF parallel structure (36).....144
Figure 3-128 Schematic diagram of 6-DOF parallel structure (37).....145
Figure 3-129 Schematic diagram of 6-DOF parallel structure (38).....145
Figure 3-130 Schematic diagram of 6-DOF parallel structure (39).....146
Figure 3-131 Schematic diagram of 6-DOF parallel structure (40).....147
Figure 3-132 Schematic diagram of 6-DOF parallel structure (41).....148
Figure 3-133 Schematic diagram of 6-DOF parallel structure (42).....149
Figure 3-134 Schematic diagram of 6-DOF parallel structure (43).....150
Figure 3-135 Schematic diagram of 6-DOF parallel structure (44).....151
Figure 3-136 Schematic diagram of 6-DOF parallel structure (45).....152
Figure 3-137 Schematic diagram of 6-DOF parallel structure (46).....153
Figure 3-138 Schematic diagram of 6-DOF parallel structure (47).....154
Figure 3-139 Schematic diagram of 6-DOF parallel structure (48).....154
Figure 3-140 Schematic diagram of 6-DOF parallel structure (49).....155
Figure 3-141 Schematic diagram of 6-DOF parallel structure (50).....156
Figure 3-142 Schematic diagram of 6-DOF parallel structure (51).....157
Figure 3-143 Schematic diagram of 6-DOF parallel structure (52).....158
Figure 3-144 Schematic diagram of 6-DOF parallel structure (53).....159
Figure 3-145 Schematic diagram of 6-DOF parallel structure (54).....159
Figure 3-146 Schematic diagram of 6-DOF parallel structure (55).....160
Figure 3-147 Schematic diagram of 6-DOF parallel structure (56).....161

Figure 3-148 Schematic diagram of 6-DOF parallel structure (57) 162
Figure 3-149 Schematic diagram of 6-DOF parallel structure (58) 163
Figure 3-150 Schematic diagram of 6-DOF parallel structure (59) 163
Figure 3-151 Schematic diagram of 6-DOF parallel structure (60) 164
Figure 3-152 Schematic diagram of 6-DOF parallel structure (61) 165
Figure 3-153 Schematic diagram of 6-DOF parallel structure (62) 166
Figure 3-154 Schematic diagram of 6-DOF parallel structure (63) 167
Figure 3-155 Schematic diagram of 6-DOF parallel structure (64) 168
Figure 3-156 Schematic diagram of 6-DOF parallel structure (65) 169
Figure 3-157 Schematic diagram of 6-DOF parallel structure (66) 170
Figure 3-158 Schematic diagram of 6-DOF parallel structure (67) 171
Figure 3-159 Schematic diagram of 6-DOF parallel structure (68) 172
Figure 3-160 Schematic diagram of 6-DOF parallel structure (69) 173
Figure 3-161 Schematic diagram of 6-DOF parallel structure (70) 174
Figure 3-162 Schematic diagram of 6-DOF parallel structure (71) 175
Figure 3-163 Schematic diagram of 6-DOF parallel structure (72) 176
Figure 3-164 Schematic diagram of 6-DOF parallel structure (73) 177
Figure 4-1 Schematic diagram of the 2T parallel mechanism 181
Figure 4-2 Singularity configurations of 2T parallel mechanism 184
Figure 4-3 Reachable and task workspaces of 2T parallel mechanism 185
Figure 4-4 Parametric analysis of the reachable and task workspaces 186
Figure 4-5 Distributions of the LCI 188
Figure 4-6 Layout of the local level condition index 189
Figure 4-7 Schematic diagram of this planar 2T1R robot 190
Figure 4-8 Flow diagram for reachable workspace 199
Figure 4-9 Reachable workspace and specific layers 200
Figure 4-10 Parametric analysis on the reachable workspace 201
Figure 4-11 Distributions of LTCI and LRCI 203
Figure 4-12 Layouts of LTLCI and LRLCI 204
Figure 4-13 Schematic diagram of the 3T parallel robot 205
Figure 4-14 Singularity configurations of the 3T parallel robot 210
Figure 4-15 Reachable workspaces (rw) and task workspaces (tw) 212
Figure 4-16 Parametric effects on reachable and task workspace 213
Figure 4-17 The distribution of the LCI of 3T mechanism 215
Figure 4-18 The distribution of the LLCI of 3T mechanism 215
Figure 4-19 Schematic diagram of the 3T1R mechanism 217
Figure 4-20 Reachable workspace of the 4-DOF parallel robot 224

Figure 4-21 Linkages' impacts on the reachable workspace of the 4-DOF robot 225
Figure 4-22 LTCI and LRCI Distributions of the 4-DOF robot 228
Figure 4-23 LTLCI and LRLCI Distributions of the 4-DOF robot 229
Figure 5-1 Diagram of a rigid linkage in 3-dimensional space 232
Figure 5-2 JRI index of the parallel mechanism 236
Figure 5-3 CVI index of this parallel mechanism 237
Figure 5-4 BCAI index of this 2T parallel mechanism 238
Figure 5-5 VBCI index of this 2T parallel structure 239
Figure 5-6 JRI index of this 2T1R parallel mechanism 246
Figure 5-7 CVI index of this 2T1R parallel mechanism 247
Figure 5-8 BCAI index of this 2T1R parallel mechanism 248
Figure 5-9 VBCI index of this 2T1R parallel mechanism 249
Figure 5-10 JRI index of the 3T parallel robot 255
Figure 5-11 CVI index of the 3T parallel robot 256
Figure 5-12 BCAI index of the 3T parallel robot 257
Figure 5-13 VBCI index of the 3T parallel robot 258
Figure 5-14 JRI index of the 3T1R parallel robot 269
Figure 5-15 CVI index of the 3T1R parallel robot 270
Figure 5-16 BCAI index of the 3T1R parallel robot 271
Figure 5-17 VBCI index of the 3T1R parallel robot 273
Figure 6-1 Flow diagram of the non-dominated genetic algorithm-II 276
Figure 6-2 Optimization process 276
Figure 6-3 The Pareto optimal solutions 278
Figure 6-4 The 2T parallel robot prototype 279
Figure 6-5 The experiment results without controller 280
Figure 6-6 Control strategy of the parallel robot 281
Figure 6-7 The experiment results with controller 282

List of Nomenclatures

3D	3-dimensional
BCAI	branch-coupling absolute inertia
C	Cylindrical
CVI	Coefficient of variation of joint-space inertia
DOF	Degree of freedom
G_F set	Generalized function set
JRI	Joint-reflected Inertia
LI	Level index
LCI	Local condition index
LLCI	Local level condition index
LTCI	Local translational condition index
LRCI	Local rotational condition index
LTLCI	Local translational level condition index
LRLCI	Local rotational level condition index
P	Prismatic
P_a	Parallelogram
PID	Proportional-integral-derivative
R	Rotation or Revolute
S	Spherical
T	Translation
U	Universal
VBCI	Variation of branch-coupling inertia

Chapter 1 Introduction

1.1 Backgrounds of the research

The conventional parallel mechanism is composed of at least two kinematic limbs between the fixed platform and the moving plate. Compared with the serial counterpart, parallel robot can achieve higher acceleration, stiffness and larger payload capacity, since there are multiple supporting chains and actuations are attached to the fixed platform [1]. There are also many shortcomings. The forward kinematic solutions are complicated to be solved. The parallel robot generally has smaller workspace compared with serial robot in the similar scale. The movement of the mobile platform is constrained by these kinematic chains containing of active/passive joints and rods. The parallel structure exists many singularity configurations. In 1954, the Stewart platform was invented by Eric Gough and this robot was used as a tire testing machine [2]. Since that, parallel mechanisms have been widely employed in various applications, i.e., parallel kinematic machine [3], picking-and-placing robot arm [4,5], flight simulator [6], rehabilitation robot [7], etc.

The drawbacks of parallel mechanism that restrict its wider applications have received increasing interests. The first fundamental problem is mobility analysis. The theory of screw can be used to obtain the specific motions of the mobile platform. The general mobility formula is the Grübler–Kutzbach equation. It is stated that the order in this equation is 3 for planar mechanisms and 6 for spatial manipulators. It is noteworthy that this statement is not for all parallel mechanisms. Some exceptional mechanisms include Sarrus linkage, Bennett linkage, Goldberg 5-bar linkage, Myard linkage, Bricard linkage, Trihedral linkage and Schatz linkage [8]. Take the Sarrus linkage 2-RRR (R denotes revolute joint) as an example and the order is three, its degree of freedom (DOF) is calculated as three using this formula. In fact, its DOF should be one and the order is five due to extra constraints. The order within this equation can be calculated by the screw theory. A more complete formulator for mobility analysis is the modified Grübler–Kutzbach equation. However, this is not a universal equation that can directly calculate the DOFs of all parallel mechanisms. This issue becomes complicated when there are various class of parallel structures. For example, the over-constrained mechanisms are constructed with special configurations that can provide redundant constraint(s). The generalized parallel mechanism can have additional limb(s) to connect different kinematic chains, or a

configurable mobile platform instead of a fixed traveling plate. These kinds of mechanisms build barriers for the DOF calculations employing this equation.

It is still a challenging task to design compact and simple parallel mechanisms that can easily fulfill the industrial application requirements. One of the concerns is the limited translational and orientational workspace volumes. The spatial kinematic pairs generally have smaller ranges of motion when compared with planar joints [9]. The spherical (S) joint has -23 degrees to +23 degrees for each rotational axis. The universal (U) joint in each rotary direction may have small ranges, special when there is already rotation in its orthogonal axis. Furthermore, the reachable workspace can be unregular shapes, especial for parallel structures with more legs and kinematic pairs, which builds barriers to design a proper operational workspace in future applications. Generally speaking, the usage of S and U joints will cause smaller stiffness and payload capacity when compared with prismatic (P) and R joints. Another significant concern is the parasite motions within workspace. This kind of movement is an intrinsic feature for some parallel manipulators. The mobile platform of the 2T1R 3-PRS robot has diminutive movements in the restricted directions [10]. This phenomenon can be tolerable in some cases but not in applications with high precision demands. The same issue happens in the 3-PRS parallel mechanism. In the research of [11], the inner parasite motion of 1T2R parallel structure is caused by the geometric relations from the arrangements of three kinematic legs. Following this research, a more detailed analysis of the parasite motions for 3-PRS mechanism with various limb assembly conditions was mentioned in [12]. In the work of [13], the detailed parasite movements of 2 1T2R parallel structures 3-RCU (C indicates cylindrical joint) and 3-UCR were computed. The latter mechanism had smaller unexpected motions according to the kinematic analysis and the layouts of the global average parasitic motion index.

The direct kinematic models of parallel robots are generally complicated. It is hard to find the simple analytical solutions for some parallel mechanisms. The forward kinematic solution of the famous Gough-Stewart parallel robot could be generated as a 40th degree univariate polynomial expression through the algebraic elimination approach [14,15]. Raghavan [16] employed the numerical polynomial continuation approach to resolve the direct kinematics of the Stewart platform. Merlet [17] calculated this issue with the interval analysis method. This approach could compute an accuracy result since the round-off factor

was already considered. The forward kinematic mathematical model was constructed with the assistance of the Sylvester dialytic elimination approach [18]. There are also some other approaches, e.g., Newton-Raphson method, utilizing extra encoder information, Newton-Gauss methodology [19]. The recent methods are based on artificial intelligent algorithms, i.e., back propagation neural network, support vector machines, fuzzy inference system [20-22].

The forward kinematic solution is very a complex problem when all these system outputs are associated with all motion inputs. The complexity of this issue can be alleviated when some system outputs are only pertinent to a part of the active joints. When it comes to the complete decoupling that each position or orientation of the mobile platform is only related to one driving joint, the forward kinematic model should be significantly simplified and the control strategy of the robot is simple [23]. One of the most famous parallel structures is the cartesian Tripteron robot [24]. This assumption is too difficult to be realized in most applications. The partial decoupled features of the parallel robots are already excellent in most scenarios and the corresponding forward kinematic solutions are simple to be found. This phenomenon will be desired when the translational and rotational movements are decoupled. Under this situation, the actuators of parallel robots will be actively chosen to be adapt for various operations. This case belongs to the group decoupling mentioned in [25]. Within group decoupling, the mobile platform movements can be divided into various groups (each group is composed of at least one component) and every set of motions will be monitored by its unique actuator(s).

The various singularity configurations of parallel robots hugely restrict the researchable workspace. Generally speaking, the workspace might display a hollow shape or separate regions due to three sets of singularities. The first kind is the inverse kinematic singularity. It takes place mostly in the boundary of the reachable workspace. In this case, the mobile platform may fail to move in one or more degree(s) of freedom, which also leads to the whole parallel manipulator can stand the force or torque in the specific direction(s) exerted on the moving platform even without system inputs. The second type is the direct kinematic singularity. Under this situation, the travelling plate might earn one or more degrees of freedom. Thus, the whole structure fails to bear the external force or torque although all driving joints are monitored and can not move. This type of singularity is complex and

maybe it is difficult to obtain all the possible results. The last one is the combined singularity where this pose is qualified for both the inverse and direct singularities [26]. The singularity configurations of the parallel robot can be calculated by the Jacobian matrix. Therefore, some singularities are related to the pose of the parallel architecture. The rest singularities are not pertinent to its position or orientation [27]. More kinematic joints and limbs and complicated limb arrangements may cause more complex singularity situations. It is common to employ the symmetrical kinematic chains to list all possible singularities conveniently. Furthermore, the constraint singularity, which does not belong to the above three types, can not be directly obtained based on Jacobian matrix [28].

The performance measurement is the key point for parallel robots. According to the pose range, the various performance indices can be grouped as local indices and global indices. Corresponding to the kinematic and dynamic models, the performance indicators can be divided as kinematic indicators, dynamic indicators and others. Another classification method is the intrinsic and extrinsic indicators. The former one is a built-in feature. It is related to the overall configurations of the parallel structures. The other one is only associated with the specific operations. These indices had been concluded in [29]. It is noteworthy that some indicators are computed using Jacobian matrix. When it comes to the non-square matrix, it is not possible to directly obtain its inverse matrix. Then the pseudo-inverse Jacobian matrix will be employed [30]. The Jacobian matrix contains linear and angular velocity connections for the mixed-motion parallel robots. The non-homogeneous units arise concerns in utilizing these indices. The most popular solutions include normalization and respectively formulating the translational and rotational indices [31]. It is noting that these performance measurements distributions can be employed for the selections of parallel structures and operational workspace. These indices can be regarded as the objectives in dimensional synthesis by intelligent algorithms or physical model of the solution space [32]. However, some indicators should be questioned and reviewed. For example, the concept of the manipulability index did not adopt a scientific and practical manner [33].

1.2 Motivations and research objectives

(A) Motivations of the research

The parallel mechanism theory has been developed for about 150 years. The fundamental mobility analysis has not been solved due to plentiful of parallel manipulator configurations. Although a general mobility equation could not be proposed, it is an improvement to design a novel formula that might only be applicable to a part of parallel robots. The mobility disclosure of more parts of the parallel robots might raise more ignored constraints those have never mentioned before.

Although there are many advantages and tremendous industrial applications, the parallel manipulator is not as popular as the serial robot in various scenarios due to its intrinsic issues, i.e., restricted reachable workspace, limited orientational workspace, lots of singularity configurations, complicated dynamic models, coupled movements. These issues have to be reduced gradually to unlock the potential of parallel mechanisms. A good parallel robot design can decide its performance and potential applications. This is one of the key points to mitigate these burdens. For example, the preference should be given to planar kinematic joints instead of spatial joints to enhance the range of motion for this joint and increase the overall workspace of this kinematic chain and the mobile platform. In another word, it is suggested to replace some joints with equivalent joint sets, e.g., using two orthogonal R joint to replace U joint, three orthogonal R joints to substitute S joint. Some special techniques can be provided to expand the range of motion for kinematic joints. Such as, one kind of rotation in a U joint can be manufactured with larger range of motion to satisfy the large range of motion requirement. If the desired parallel mechanism has translational and rotational motions, it is better to allow the decoupled features for mobile platform. The last but not the least, the parallel architecture with identical chains is preferable. Beyond the design of one single parallel architecture with good performance, it is desirable to propose a family of parallel structures with a systematic approach.

Compared with the wide applications of serial robot, the usages of parallel robots are too limited. Taking the well-known picking-and-placing operations of parallel robots as an example, the target objects can be light-weighted, fixed shapes. In the whole picking-and-placing operations, the objects may have various shapes and size. Their weights have large scales. The objective surface stiffness varies. The objects are randomly placed with any kind of position and orientation. There might be interference and other uncertainties in some complex stacking manners. Another common application is the machining for the

large-scale components. In these manufacturing process, the workpiece may have a super large size that the overall parallel mechanism has to move along this workpiece to finish all the operations and remain the predefined precision demands. The machining parts have complicated shapes and surface. In some cases, this machining parts may be consisting of different composite materials. The latest technology provides more challenges for the parts and the parts thereby challenge the parallel kinematic machine tools with higher levels. These conditions require techniques from many subjects. However, the most primary performance is initially identified by the parallel mechanism design.

(B) Research objectives

Considering the mentioned problems and limitations of parallel mechanisms, this research concentrates on the structural synthesis and modelling for a special family of parallel structures. The objectives of this dissertation are listed below,

(i) To propose a systematic structural synthesis approach for a family of feasible 2-6 degrees-of-freedom parallel manipulators with parallelogram joint in every kinematic chain. All these parallel mechanisms should be further determined whether they are equipped with/without qualified movements.

(ii) To design a convenient method for discrimination of different parallel structures. This straightforward approach should also be able to disclose more configuration information, to be easily identified from other structures.

(iii) To design novel indices for performance evaluation. These indices can be utilized to reveal more characteristics of the parallel mechanisms. This will assist to better performance measurements for future selection of parallel architectures. These indicators can also be regarded as target objectives in linkage optimizations with a predefined operation in the future.

1.3 Organization of this dissertation

This dissertation is arranged as follows,

Chapter one provides the introductions of this research. The questions and limitations of parallel robots include the unsolved general mobility formula, limited translational and orientational workspaces, parasitic movements, complicated forward kinematic mathematical models, singularity configurations and feasible performance analysis. The

motivations are introduced, followed by the research objectives of this research. The layout of this dissertation is presented at the end.

In Chapter two, the latest research on parallel robots is listed in detail. It shows the improvements in various topics, e.g., type synthesis approaches, dynamic modelling and performance evaluations.

Chapter three proposes a supplementary term to form a novel mobility equation that is applicable for a family of parallel mechanisms with parallelogram joints. The novel kinematic joint matrix is designed to represent parallel architectures and a unique block pattern is provided for matrices discrimination. Then a group of 2 to 6 DOFs parallel mechanisms is completely enumerated according to this matrix. The theory of screw is utilized to examine the unrealistic structures.

In Chapter four, a novel level index for all performance indices that are composed of positive values is presented. To testify the characteristics of this level index, four general parallel mechanisms are chosen. The detailed kinematic models are constructed, based on which, all the singularity configurations are explored for further avoidance. The linkage's impacts on the reachable workspace are investigated. The layouts of the local condition index and the corresponding level index are provided.

Chapter five displays the novel mass related indices, the branch-coupling absolute inertia indicator and the variation of branch-coupling inertia indicator. The inverse dynamic models for these four different parallel robots are established by the Lagrange equation, followed by the construction of inertia matrices. The distributions of four mass-related indices (joint-reflected inertia index, the coefficient of variation of joint-space inertia index and these two new indices) are outlined, as well as the linkage's influences.

Chapter six searches the optimal linkages dimensions of the selected planar mechanism via the non-dominated genetic algorithm II. A physical prototype is completed. The experiments are designed to verify the primary kinematic models of this parallel structure.

Chapter seven concludes the overall research and points out the innovative parts of this dissertation. The following research objectives are provided based on the current progress.

Chapter 2 Literature review

2.1 Type synthesis of parallel robots

There are several primary theories for type synthesis of parallel structures, i.e., screw theory, differential geometry (specifically Lie group and Lie algebra), generalized function (G_F) set theory, Single open chain method [34].

The constraint systems of the 2R1T (T indicates translation) parallel mechanisms with three and four kinematic chains were calculated by means of the theory of screw in [35]. The possible kinematic branches with the simplest joint configurations in the 3-legged and 4-legged mechanisms were enumerated and the overall structures were confirmed. A detailed synthesis steps of the mobile parallel robots was presented in [36]. The kinematic limbs with 3 to 5 force/torque constraints were analyzed by the theory of screw, based on which, the total parallel structures were obtained. The dual quaternion method was employed in [37] to represent a finite motion of the 1T2R parallel mechanism with parasite movements. All the available kinematic chains were generated after some basic rules were defined. A group of 1T2R parallel manipulators was constructed with various assembly conditions. In the work of [38], a general type synthesis approach was proposed to explore a family of 4-DOF mixed motion parallel structures with a similar idea. Different from the linkage mechanism with one single loop [39], the two-loop linkage mechanism with two layers were more complex. The twist equation of this kind of mechanisms were outlined, based on which, the mobility situations were figured out. Then a general approach to design a family of this class of mechanisms was proposed.

Wei and Jian [40] studied the transitions of various parallel robot configurations (1R2T and 2R1T) through the theory of Lie subgroups and submanifolds, and then designed a unique kinematic joint that contained of six operational modes. A family of parallel structures with metamorphic functions was constructed based on this special joints. Li *et al.* [41] brought an approach to design a group of five-DOF parallel architectures via the theory of Lie group. There were fourteen new parallel robots within the results. This method could also be referred to design structures with other kinds of DOFs. The subgroup features and intersection operations of the kinematic chains within spherical parallel architectures were revealed by the effective approach the Lie group, and the qualified

kinematic limbs with 3-DOF, 4-DOF, 5-DOF, 6-DOF were completely searched. The feasible parallel structures were then constructed considering the basic assembly rules [42]. The G_F set theory was utilized to calculate the motion of a point fixed on a rigid linkage. On the basis of this advantage, the movement features of the leg and the actuation mechanism for the mobile robot were explained. Therefore, fifteen different types of mixed-motion legs and eight groups of actuating mechanisms were explored [43]. The G_F set theory was adopted to design legs for quadruped mobile robots. These legs were contained of serial, parallel and hybrid connections [44]. With the brief introductions of the G_F set theory, the design principles were predefined for the press machine with 4 degrees-of-freedom parallel legs. Then the structural synthesis for the target parallel mechanisms were listed [45]. Gao *et al.* [46] utilized the G_F set theory to establish the rotational axes intersections of two rotational joints. The feasible kinematic chains were designed based on the intersection equations. Then a set of parallel mechanisms with 2-4 DOFs with two rotary functions were illustrated.

Jin and Yang [47] defined two primary limb structures, single-open-chain and hybrid-single-open-chain, for topology synthesis of parallel mechanisms. A general procedure was proposed to design a family of reliable parallel structures and this approach was employed for 3-DOF parallel architectures with pure translations. Shen *et al.* [48] introduced a systematic approach to design all feasible parallel mechanisms with six DOFs under given requirements. The authors found 28 novel structures among the obtained 29 results. Yang *et al.* [49] developed the composition rules for general parallel mechanisms. These rules were contained of not only the loop of over-constrained linkage mechanism but also the relationships among them. Based on this improvement, the authors built a general structural synthesis by using single-open-chain module.

In addition to type synthesis of a family of parallel mechanisms with a mature procedure, it is essential to design an approach to represent the parallel structures. The naming convention for the parallel mechanisms does not fully qualify this requirement. For example, 3-RPS denotes the types and numbers of kinematic joints in the overall structure. The limb configuration is also symmetric and all the corresponding linkages in each limb own the identical lengths, respectively. However, the overall topology is not disclosed. Employing matrix to present and identify the linkage mechanism has various advantages

and has attracted a lot of research. The first widely used matrix is topology matrix, which was proposed by Yan [50] to represent the topological structure of linkage mechanism. This matrix was constituted of linkages, joint types and connection points. It was also a practical approach to represent the mechanisms with variable topologies [51]. Yan and Kuo [52] designed a directionality topology matrices to describe linkage mechanisms. The joint types, connection points and joint sequence incident for any two rods were included in this method. To represent the joint types and sequences with a unified method, they further developed the hexadecimal topology matrix to be conveniently utilized in coding. In a similar manner, the authors in [53] introduced the 3-dimensional adjacency matrix in which a 16-bit coding string could include the displacement subsets data and relative joints relationships. The adjacency matrix is another popular research. Slaboch and Voglewede [54] designed the adjacency matrix to denote the topology structures of planar linkage mechanisms. Only two elements 1 and 0 were employed in this matrix to indicate the connection status. This adjacent matrix was also utilized in [55] to identify two distinct configurations of a polygonal linkage mechanism. Moreover, Li and Dai [56] developed the augmented adjacency matrix that contained the joint axis relations. Pucheta and Cardona [57] introduced the type adjacency matrix, where the rigid rod and flexible rod were indicated separately. Different elements 0-4 were used for various joint types. There are also some other kinds of matrices, e.g., the authors in [58] utilized two classes of matrices for linkage mechanisms with multiple loops. The first class was the circuit matrix that containing the joints information based on the loop directions. The other was the sequence matrix where the joint sequences were provided in each closed loop.

2.2 Kinematic performance measurements of parallel robots

A proper parallel structure is very important since there are some complicated mathematical models for some parallel mechanisms. One of the well-known issues is the difficult analytic solutions for forward kinematic models of some parallel robots.

To study the direct problem of parallel mechanisms with six DOFs, Seibel *et al.* [59] classified the parallel manipulators and concluded that, for a special kind of parallel robots, the only forward kinematic solution set could be obtained when measuring the rotational angles of each driving prismatic joint. Considering the simple structures of the planar 3-RRR parallel mechanism, Oetomo *et al.* [60] derived the forward kinematic solution and

found the result was an eighth univariate polynomial. The whole problem could be further simplified when the additional assumptions were implemented and yielded the decoupled translations and rotations. The 3-RS parallel structures could be achieved when locking the active kinematic joints within some mechanisms [61]. Under this situation, a general procedure was suggested to deal with the corresponding forward position problem with the assistance of the conformal geometric algebra methodology. Five parallel architectures were utilized to verify this systematic method. Shen *et al.* [62] brought forward a spatial parallel robot with pure translational movements. The analytic solutions for both the inverse and forward position problems could be solved easily on the basis of the special joint configurations in the overall workspace. This was helpful in path planning and controller designing. The geometrical relationships of the 3-PRS parallel mechanism were written in [63]. The Bezout's elimination approach was utilized to realize 64 groups of configurations. The essential steps to assess these solutions were not efficient on time and could not be used for real prototypes. The alternative optimization methodology was then presented to meet the minimal constraints errors. This method could not provide the analytic solutions but take less time to generate the numerical solutions. Bonev [64] classified 3-PPS, 3-RPS, 3-PRS symmetrical structures as the parallel mechanisms without torsion. He found that the Tilt-and-Torsion angles method was the only way to calculate the forward kinematic issues for these parallel architectures and these results corresponded to only one or two groups of solutions. This approach was far more applicable than the Bezout's elimination method on these mechanisms. A compendious and effective algorithm was proposed in the work of [65] intended for the forward position problem of the 6-6 Steward parallel robot. A final fourteenth polynomial was described in the special condition.

Kim and Park [66] resolved the direct kinematic problem of the 3-RS parallel robot and a sixteenth univariate polynomial equation was finally realized by using the Sylvester's elimination approach. The direct position analysis of the 3-PRS parallel manipulator was expressed in detail and a sixteenth univariate polynomial was formulated employing the Sylvester elimination approach [67]. Due to the complexity of the direct position problem of 3-RPS mechanism, Zarkandi and Esmaili [68] made a different driving style that the R joints as the active joints and the P joints as passive. In this case, the nonlinear constraint

equations could be resolved as an eighth univariate polynomial employing the Sylvester elimination methodology. Ye *et al.* [69] claimed that the serial-parallel hybrid parallel structures could not formula the analytical forward kinematic solutions in most cases. The authors built a 5-DOF hybrid machine containing of 2-UPU/SP parallel structure. Due to the special configuration of the parallel unit, its direct kinematic solutions could be simplified by the Sylvester's elimination approach and the final values could be generated through the Ferrari's approach. The special 1-CCC/5-SPS parallel mechanism was brought forward in [70]. Due to its unique configuration, the constraint equations were composed of five fixed-length expressions and one constant angle relationship. Then the direct kinematic solution was formulated by the Sylvester's elimination methodology and the result was reduced as four fortieth polynomials. The final values could be obtained by the theory of Gröbner.

To avoid the time-consuming analytic forward displacement analysis of the parallel mechanism, the improved global Newton-Raphson method was proposed in [71]. This approach was constructed with extra Tailor expansion equation on the basis of Newton-Raphson iteration method. A 6-UPU mechanism was taken as an example to testify the high accuracy and convergent characteristics of this approach. The authors in [72] found that most research solving the direct kinematics of parallel mechanisms via Newton-Raphson method were mechanism-related and there was not a general methodology that could be applicable to other mechanisms in a convenient manner. Therefore, such an algorithm was presented and several commonly used parallel mechanisms were taken as examples for testing. The authors in [73] selected the Newton-Raphson approach to search for the corresponding platform pose of a spatial structure with the given the displacements of the six active sliding joints. The solution was obtained in the dynamic model within the proportional-derivative control strategy.

A cable-driven parallel manipulator with six DOFs was proposed in [74]. The forward kinematic issue was solved by the iterative Newton-Gauss methodology. Schreiber and Gosselin [75] realized that the direct kinematic problem of the Gough-Stewart Platform was contained of 40 set of solutions. The forward kinematics of the redundant version of the classic parallel structure would be more complicated to be solved by the analytic methodologies. They applied the Newton-Gauss approach to explore the numerical

solutions of this parallel architecture efficiently. The authors in [76] proposed a kinematically redundant parallel manipulator. The structure was too complicated to ensure a computational efficient analytic direct kinematic solution. The Newton-Gauss method was then applied to promise a fast and stable result with proper original guess. This approach was integrated in its control policy to realize desired movements.

Besides measuring the extended lengths of the driving linkages, Schulz installed inertia measurement units to detect the linkages orientations and used this data in the computation of forward kinematic problem of 3-RPR planar parallel mechanism [77]. In the work of [78], the usage of this methodology did not require a nice initial guess value and could keep convergence and save time, compared with other widely used numerical solutions. The authors employed the homotopy continuation approach to calculate the direct kinematic problem of the 3-UPU parallel architecture. This case study verified its advantages.

To solve the tricky direct kinematics of parallel mechanisms, Parikh and Lam [79] trained the neural network to obtain an approximate result, then the well-known Newton-Raphson method was employed to generate the final solutions. This hybrid strategy could run in real time and achieve the target accuracy, which was confirmed by the calculations on a six-degrees-of-freedom spatial mechanism. Zhang *et al.* [80] brought forward a 2-RPU/2-SPR asymmetrical parallel mechanism and it was driven by four pairs of extendable linkages. The hybrid approach consisting of Newton-Raphson and back propagation neural network was utilized to solve its displacement problem. The simulation results demonstrated this hybrid algorithm was fast and accurate, which enabled it for future real-time applications. Elsheikh *et al.* [81] established neural networks to mimic the direct kinematic model for three classic planar parallel structures, 3-RPR, 3-PRR and 3-RRR. Several neural networks were applied to the direct kinematics of the spherical 3-RRR parallel robot used for haptic device in [82]. A neural network module was employed for rough guess and the remaining networks were responsible for the target high accuracy solutions. This proposed algorithm only used a quarter of time using the conventional Newton-Raphson approach. Since some numerical direct kinematic approaches had poor and unstable convergency, the authors in [83] adopted the multi-layer perceptron neural network to predict the corresponding solutions of the HEXA robot with given displacements of driving joints. The results contained tolerable errors in experience. Zhang and Lei [84] compared the several

intelligent algorithms' performance on the forward kinematic problem of the 3-DOF parallel structure with one passive kinematic chain. The support vector machine method won with better convergence feature than those of multilayer perceptron and radial basis function neural networks. Morell *et al.* [85] brought forward a support vector machine approach to replace the complicated analytic direct kinematic model for the Gough-Stewart robot. This methodology after proper training and validation displayed superior performance on time and accuracy.

In addition to the complex direct kinematic models, the other problems in kinematic analysis have been widely investigated by researchers around the world. In the work of [86], the authors proposed a reconfigurable parallel mechanism 3-SvPS (Sv denotes the spherical joint with changing axis direction). The unique structure could have three to six DOFs for different operation modes. Its workspace was explored by the spatial searching algorithm. The Jacobian matrix that could cover all operations modes was constructed by the theory of screw. The dimension-independant local transmission index and the global transmission behavior were established and their distributions were discussed. A 3-RRR parallel manipulator with only rotations and reconfigurable characteristics was proposed in [87]. The loci for two groups of singularity configurations were explored and its symmetrical rotational workspace was obtained, based on which, the authors defined an operational workspace without singularities. The layouts of its local condition index and global condition index were illustrated to find out the best performance.

The authors in [88] proposed a planar 5-R parallel structure with nine kinds of driving strategies. The new performance orthogonal-degree-based local transmission index, which was inspired from the branch transmission index and end-effector transmission index, was defined and evaluated to assess this mechanism under various operation modes. Plitea *et al.* [89] designed a hybrid parallel robot for surgery operation. The spatial search method was employed for the workspace and the dexterous workspace was implemented for the surgical operation requirements. Three family of singularities were computed based on Jacobian matrix. Several surgical operation paths were tested on this hybrid structure.

Schreiber and Gosselin [90] introduced two kinematically redundant planar parallel mechanisms, 2-RPR/2-(RPR)R and 2-RPR/R-2-(RPR). The singularity configurations were obtained by the Jacobian matrices. The reachable workspace of each of them

indicated that one platform could rotate without constraints while another could not rotate one round. These researchers [91] then presented a kinematically redundant spatial parallel robot with nine driving joints. The singularity analysis based on Jacobian matrix revealed that the additional kinematic chains could be employed to avoid singularity configurations. In additional to its translational workspace, the rotational workspace was huge. The maximal torsion angle is 200° and the tilt angles range from 80° to 160°. The trajectories along several single direction demonstrated that the platform could achieve large orientation angles and keep far from singularities at some conditions. Nurahmi *et al.* [92] further studied the singularity configurations of the 3-PRS cubic parallel structure mentioned by Huang and Fang [93]. These unexpected singularities were illustrated into the joint space. There was only one operation mode for the mobile platform, as denoted by the eight kinematic constraint functions. Except for the three vertices of the moving platform, the other points fixed on the moving platform could move within a Steiner surface. The vertical Darboux motion was also found on this structure.

A special rR (reconfigurable R) joint was designed in [94] and could be driven by the worm gear system or bevel gear system. The adoption of this unique joint in the 3-RPS parallel mechanism gained two working modes for the mobile platform, 3-rotations and 1-translation-and-2-rotations. The singularity loci in various modes were found through the Jacobian matrix constructed by the screw theory. The workspace without singularity was obtained and the parametric impacts on this workspace were discussed. Gosselin *et al.* [95] designed a group of planar parallel manipulators. They all included redundant kinematic limb to gain full cycle movements. They could avoid all kinds of direct singularities by make full use of the additional kinematic chain. This special design could cause singularity-free workspace for all of them. An over-constrained 2-RPU/SPR parallel structure was displayed in [96]. Both the analytical solutions for the inverse and forward kinematic models were generated based on the geometry relation in each kinematic chain. Instead of using the inverse kinematics in workspace analysis as seen in most research, the direct kinematic model was adopted to obtain the reachable workspace with the spatial search algorithm. The parasitic motion was also revealed and its workspace was also found. The pressure angles within this parallel mechanism were applied to establish two performance indicators to measure the transmission performance. The 2-DOF RPaR-RRPRR (Pa

denotes parallelogram linkage, 2(R-R)) was developed in [97]. On the basis of the analytic inverse/forward kinematic solutions, this structure owned the fully decoupled feature. All the possible singularity conditions were explored completely based on the theory of screw. The whole reachable workspace was its isotropic workspace, which indicated this structure had excellent motion/force transmission in any position and orientation.

The Hexarot robot was proposed in [98] and the detailed kinematic models were constructed due to its special configuration. Its reachable workspace was provided by considering the constraints originated from kinematic joints and chains. Taking the six movements of the mobile platform into account, its workspace in various planes were plotted in 3D images, for better understanding of its borders. The authors also found the symmetrical plane for this reachable workspace. The authors in [99] brought forward the 3-PRS parallel architecture. The active prismatic joints owned two types of configurations. According to the inverse kinematic model, the Jacobian matrix was established and the singularities were discussed. The Jacobian matrix based indices, the minimum singular value, condition number, kinematic configuration index and local/global conditioning indices were evaluated within reachable workspace. The 3-P$(US)_2$ parallel robot without orientation workspace was proposed in [100]. In accordance with the constant linkage length relationship in each chain, the constraint equations set were obtained and then the kinematic models were solved. The numerical approach was employed to determine the reachable translational workspace. The global dexterity index and manipulability were measured with respect to the angles of driving linkages. Xie *et al.* [101] investigated the 5-DOF parallel robot with asymmetrical limbs, URPR-2[R-$(RP)_2$-RUR]. The corresponding mobility analysis was carried out through the combination of line graph approach and Grassmann line geometry. The tilt-and-torsion angles were applied and the results showed that the travelling plate had flexible rotational performances within workspace. The unwanted parasite motion was explained and its distribution was revealed. At last, four operation modes were identified for future applications to avoid the singularities. In the work of [102], the authors presented a novel parallel structure where the mobile platform had two modes and could achieve Schönflies movement. Four steps of the line graph approach were employed to capture the mobility of overall mechanism. The symmetrical rotational range index and maximum rotational range indicator were proposed and

evaluated. The maximum symmetrical circle workspace was investigated with the reachable workspace.

2.3 Dynamic analysis of parallel mechanisms

There are many approaches employed for dynamic solution of parallel robot. The factors of the dynamic performance, e.g., the joint friction, clearance and deformation, were formulated in detail to generate comprehensive models for kinematic pairs. Their impacts for specific joints were further discussed. They were contained in the integrated dynamic model of the parallel mechanism 2[$(PUS)_3$-S] through Newton–Euler method [103]. The contact models of the spherical joints in dry and lubricated situations were constructed, based on which, the spherical joints' influences on the active torques were derived and testified by comparing with simulation results. To obtain an efficient model of the 2PUR-PSR parallel mechanism [104], the natural orthogonal complement matrix was computed by the theory of screw. The complete dynamic solution considering compatible deformation was then derived based on the Newton-Euler approach. Both the translational and rotary dynamic manipulability ellipsoid of this manipulator were generated to measure its thorough isotropy characteristics. A serial-parallel hybrid space robot (2UPS-UP)+RRRR for grasping operation was presented in [105]. The analytical dynamic solution was completed after the corresponding dynamic models in recursive forms for the serial and parallel parts were generated by the Newton-Euler method. This dynamic model was verified in a case study under given conditions and employed in the control strategy. The isotropic and fully decoupled 3-DOF parallel mechanism Tripteron robot proposed by Kong and Gosselin [106] was studied in [107]. Some simplification assumptions were provided firstly and the dynamic model was derived considering joints frictions.

To achieve a dynamic model with high precision, the authors in [108] constructed a linkage flexibility model and spherical joint clearance model for the dynamic solution for a 4-SPS/PS mechanism based on the Lagrangian equation. This model was then examined by a case study. The Lagrange equation was employed [109] to derive the inverse dynamic model of a compact spherical parallel mechanism in operational workspace. Modelling errors and external disturbances were included to obtain a complete and high-precision model. The HEXA parallel mechanism was proposed in [110]. The local mobility of each branch was eliminated and this architecture was reduced as a 6-RUS parallel mechanism,

based on which, the corresponding dynamic solution was established through D'Alembert's principle. This approach assisted to estimate the absorbed power on every driving joint and loading characteristics of all kinematic chains. They provided a strong proof for proper arrangements of system inputs for safety issue and long-term reliability. A novel methodology integrated with the Hessian matrix was introduced to construct Lagrange–D'Alembert equation for the dynamic model of parallel robot. The 3-RRR parallel mechanism was taken as an example for method validation[111].

Moreover, the principle of virtual work was utilized for inverse dynamic model of a planar parallel structure in [112], it was further tested and verified by comparison with simulation result of ADAMS prototype. The Kane's method without unnecessary forces/moments and joint reaction forces/torques was employed for the dynamic modeling of the parallel mechanism 3RSS/S [113]. Two cases were implemented to validate the proposed algorithm. The complicated dynamic modeling process required a large amount of computations and it was time-consuming. It needed to be further combined or simplified to realize increased computation efficiency and equivalent accuracy. The Lagrangian formulation was utilized for the dynamic modeling of the 2UPS/UP parallel mechanism while the principle of virtual work was integrated to promise a feasible and efficient process. The combined algorithm proposed in this research was verified to reduce computation time [114]. In the work of [115], The main dynamic modeling approaches were reviewed. Their completed and simplified models were discussed, and computation times and precisions were derived and compared when the classic Delta robot was taken as an example. Nabavi *et al.* [116] compared the results of accurate and simplified dynamic models for the 6-PUS parallel robot. The latter model could save computation time compared with the first solution. Du and Lou [117] proposed a methodology to simplify the dynamic model of the parallel mechanism. The comparisons based on the Delta manipulator were conducted and the simplified algorithm won on efficiency, which was beneficial for real-time control.

Apart from the various modelling issues for the dynamic solutions, the dynamic performance has attracted a lot of interests. The dynamic isotropy indices[118] were suggested for pure translation/rotation and mixed movements. The coupling acceleration capacity was derived for selection of feasible acceleration sets. An intrinsic approach related to inertia and an extrinsic approach concerning the active force/torque vector [119]

were discussed comprehensively, based on which, the linkage optimization was provided within the pre-set workspace. A dynamic performance factor containing gravity [120] was outlined and demonstrated and compared on 2UPU/SP and Tricept parallel robots. The configuration's impacts on this index were also explored to future selections. Fontes and Silva [121] defined a dynamic index to indicate the maximal driving forces/torques demanded by a pre-set operation. This assisted to measure and compare the features of a group of planar parallel mechanisms with and without kinematic redundancy.

The Generalized inertia ellipsoid designed by Asada [122,123] and dynamic manipulability ellipsoid developed by Yoshikawa [124] were widely applied to measure various parallel manipulators. In [125], both the translational and rotary dynamic manipulability ellipsoids for the 3-PRRU parallel structure, to quantitatively describe the level of transformation of the pose (position and orientation). A solution was also mentioned to achieve the dynamic isotropy. The same index was employed to conduct the dynamic performance of the over-constrained 2-PUR/PSR parallel robot [126]. In the work of [127], a 2-RPU/PRS/UPS parallel system was proposed. The dynamic manipulability ellipsoid was classified into a pure translational dynamic manipulability ellipsoid and a pure rotary dynamic manipulability ellipsoid. A special index was further developed to describe the relationship between the dynamic performances and its pure-translational DOFs. The dynamic model of 2PRU-UPR parallel robot [128] was derived through the principle of virtual work. The dynamic manipulability ellipsoid was selected to evaluate its local performance. A 2UPS/RRR mechanism for ankle rehabilitation was introduced in [129]. Based on the kinetostatic model, the motion isotropy, force transfer ratio and isotropic force radius were calculated. Its dynamic uniformity within the desirable workspace was computed and discussed.

The other inertia-matrix related indices also play important roles to assess and optimize parallel manipulators. The joint-reflected inertia index was investigated for the Stewart parallel manipulator in [130]. The corresponding index denoted the inertia capacity of all limbs and its distribution was obtained and discussed. Then Mo *et al.* [131] further developed the coefficient of variation of joint-space inertia index, based on which the dynamic performance of a four-legged picking-and-placing parallel mechanism was evaluated comprehensively. However, Muralidharan *et al.* [132] adopted the Euclidean

norm of the inertia matrix, which was applied to estimate the 3-RRR and 3-RRS parallel manipulators. To understand the performance of the redundant-actuation parallel manipulators with various operation modes, the authors in [133] defined the inertia torque index by combining the inertia matrix and the acceleration of the mobile platform.

2.4 Linkage optimization research

Optimization relating to motion performance and geometry [134] is one essential problem that has been discussed in many research. There are various methods for this topic. The Genetic algorithm is widely employed to search for the optimal set of linkages lengths. Kelaiaia *et al.* [135] studied linear Delta parallel mechanism's multi-performance. The multi-objecitve optimization was conducted via the genetic algorithm Strength Pareto Evolutionary Algorithm-II and the targets were larger dexterous workspace, better kinematic and dynamic indices. A three-DOF spherical parallel robot was proposed in [136]. The requirements of smaller mass of all the moving bodies and modified global conditioning index were met by searching through the well known non-dominated genetic algorithm II. Garcia and Campos [137] computed all types of singularity configurations of the 6-UPS parallel structure based on the theory of screw. These special conditions provided supportive unwanted configurations and were avoided in the optimization process. To acquire the initial orientation of moving platform corresponding to the biggest sphere in workspace, there were two steps in optimization. The golden search method was employed in the first step to obtain the optimal radius of the sphere and the genetic algorithm was then applied to locate the origin of this sphere. Song *et al.* [138] calculated a five-DOF parallel structure with passive limb and two-layer mobile platforms. The mean value of generalized virtual power transmissibility and its discrete value within a given workspace were desired and the nondominated sorting genetic algorithm II provided the optimal process. The lower-limb rehabilitation robot with 3 DOFs was presented in [139]. A special objective demonstrating the global transmission index was designed to pursue the optimal set of linkages by the assistant of genetic algorithm.

Liu *et al.* [140] designed a five-bar mechanism with only revolute joints. The physical model of the solution space was employed to classify the linkage lengths relationships into several cases. The various singularity loci in each working mode were presented. Proper linkages lengths in the design space were searched in the pursuit of larger workspace

volume and global condition index. In the work of [141], three dimensionless linkages lengths were defined for the 3-PRS robot. Then the parameter design space was established. The good-transmission orientation capability and the global transmission index were plotted in this design space. On the basis of the demands retaining the predefined smallest values of these indices, the optimal set of rod dimensions could be chosen from the distributions of the target performances. The detailed kinematic problems of the planar parallel robot containing of three P_a joints were presented in [142]. The dimensionless design space of all parameters was plotted and the whole cases could be classified as 12 groups. The area and the range along *X* axis of the good transmission workspace were chosen as the target in the optimization process. The optimal results could be selected based on the layouts of these two indicators. The parallel robot with high accuracy positioning level was presented in [143]. The layouts of the conditioning index and global mobility conditioning indicator under specific conditions were illustrated on its solution space, to search for the best set of rods dimensions.

The multi-objective differential evolution algorithm was employed in [144] on the 3-UPU parallel mechanism. The optimal target was the global condition index and the sampling points were generated by the Monte Carlo method. An ankle rehabilitation robot with redundant actuations was proposed in [145]. The workspace, two global transmission indices and the global torque index were adopted as the targets in the optimization based on various differential evolution algorithms. The 2-UPS/RRR parallel architecture for medical robot was introduced in [146]. Nine different indices were integrated into one expression, which served as the objective. The differential evolution algorithm was applied to search for the optimal linkage dimensions. The planar 3-RRR parallel structure was developed in [147]. The objective of the case study included the geometric wrench and extra penalties. Both the differential evolution methodology and the modified algorithm were used for the optimization under various working modes and driving situations.

Shirazi *et al.* [148] conducted the optimal dimensions for the 6-UPS parallel mechanism. Three lengths variables were constrained between zero and one. Three kinds of indices including the workspace volume, global condition number and stiffness index were optimized through the particle swarm optimization. Gao and Zhang [149] designed a compliant parallel structure with three DOFs. The particle swarm optimization approach

was utilized to search for the largest volume of the reachable workspace. In the work of [150], the 4-PUS/PS parallel architecture was presented. The particle swarm optimization and the quantum particle swarm optimization were adopted to conduct the single-objective optimization while the objective as the workspace volume or the dexterity index. Both scenarios demonstrated the latter algorithm converged faster. The parallel kinematic machine Tricept was analyzed in [151]. The basic optimal designs of the workspace volume or the global condition index were implemented by the particle swarm optimization. The multi-objective particle swarm optimization methodology employing weight coefficients and the epsilon constraint were both carried out.

Enfereadi and Nikrooz [152] conducted detailed optimizations for the 3-UPS/S parallel robot. The global workspace conditioning index, global conditioning index, gradient global index and dynamic dexterity index were calculated for this mechanism. Four single-objective optimizations using them were implemented. The optimal results and the processing times by genetic algorithm and pattern search approach in each case were both recorded and compared. Four dual-objective optimizations employing non-dominated sorting genetic algorithm-II were reported. At last, one triple-objective optimization was represented. The 4-RUPaR parallel robot with mixed movements was presented in [153]. The searching for the maximal effective transmission positional workspace was provided by the differential evolution algorithm, genetic algorithm and particle swarm optimization. The comparison results showed the differential evolution obtained the best performance.

Russo *et al.* [154] conducted the linkage optimization of a 3-UPR robot where the objectives contained of workspace and several Jacobian-matrix-based kinematic behaviors, dexterity, stiffness and force transmission. Two variables were selected as the references and the remaining dimensions could be represented. All these targets were mapped into the parameter space for optimal design. Sun *et al.* [155] proposed an effective workspace decomposition approach. After normalizing linkage parameters, dimensional synthesis of the novel five-DOF Tricept-IV robot was conducted considering two subsystems classified by the proposed method. Two global indices, inertia torque index and centrifugal/Coriolis torque index were established in [156], based on which, optimal design of a redundantly actuated parallel mechanism was obtained with several kinematic constraints satisfied. The 2-translations and 2-rotations parallel manipulator 2-RPS/2-UPS was proposed in [157].

The singularity loci were fully found within reachable workspace, based on which, the zero-singularity workspace was obtained and the maximum was search by predefined sets of linkage dimensions. Karimi *et al.* [158] derived the singularity configurations of the 3-RPR parallel mechanism in detail. Two coefficients related to the reachable workspace and zero-singularity workspace were combined as single objective. The branch-and-prune intelligent algorithm was proposed for this optimal problem. The detailed kinematic analysis of the Exechon parallel machine was introduced in [159]. The discrete workspace volume and the global condition index were combined into one single objective with flexible weight coefficients. The dimensional synthesis was conducted five times with this target and the results were compared.

2.5 Summary

Four existing problems of parallel mechanisms are discussed in this chapter. The latest researches on these four issues are cited to represent different approaches and results.

Chapter 3 Structural synthesis of a group of parallel manipulators

3.1 Revised mobility equation for a group of parallel robots

The Grübler–Kutzbach equation [8] for the mobility of a linkage mechanism with multiple chains is listed below.

$$M = d(n-g-1)+\sum_{i=1}^{g} f_i \tag{3-1}$$

where M denotes the degrees of freedom (DOFs) of the mobile platform (or end-effector), d represents the order of the mechanism($d=6-\lambda$, where λ is the number of common constraints, it is generally 6 for spatial mechanisms and 3 for planar mechanisms), n and g are the number of moving linages and joints, respectively. f_i represents the DOFs for the i-th linkage.

However, this expression can not reveal the mobility features for some parallel mechanisms, i.e., the Sarrus Linkage, Delta robot. The modified Grübler–Kutzbach formula [8] is then proposed, as shown below

$$M = d(n-g-1)+\sum_{i=1}^{g} f_i + \nu - \zeta \tag{3-2}$$

where ν denotes the redundant constraints (can be determined by the screw theory), expect the common constraints of the mechanism. ζ indicates the passive degrees of freedom within the linkage mechanism.

Beside λ, if any limb's reciprocal screw is more than (all limbs' reciprocal screw system), this part belongs to ν. If there is no S-S joint linkage or cam-roller, there is no ζ for this mechanism and ζ =0. Equation (3-2) is suitable for most parallel mechanisms. There can be some excepts when the mechanism contains of special relations for joint arrangements or linkage lengths. An example is shown in figure 3-1. In this two-legged parallel structure, each chain has one prismatic joint connected to the fixed platform, and one parallelogram joint connected to the moving platform.

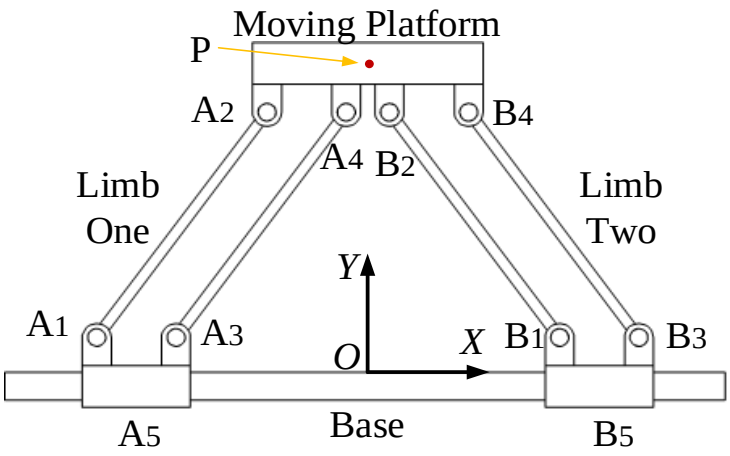

Figure 3-1 Schematic diagram of this planar parallel mechanism

The coordinate system of the parallel mechanism is attached in figure 3-1. The linkages A_1A_3, A_2A_4, B_1B_3 and B_2B_4 are in the same dimension of $2L_3$. Point A_5 (x_1,0,0) is the center of linkage A_1A_3. Point B_5 (x_2,0,0) is located at the center of linkage B_1B_3. Point P (x,y,0) is the center of linkage A_4B_2. The positions for dots A_1, A_2, A_3 and A_4 are respectively denoted as (x_1-L_3,0,0), (x-3L_3,0,0), (x_1+L_3,0,0) and (x-L_3,0,0). The positions for dots B_1, B_2, B_3 and B_4 are respectively denoted as (x_2-L_3,0,0), (x+L_3,0,0), (x_2+L_3,0,0) and (x+3L_3,0,0). In the limb one of this parallel structure, the kinematic screws for the linkages A_1A_2 and A_3A_4 are listed as

$$\begin{cases} \$_{A1} = \begin{bmatrix} 0 & 0 & 1; & 0 & L_3 - x_1 & 0 \end{bmatrix}^{\mathrm{T}} \\ \$_{A2} = \begin{bmatrix} 0 & 0 & 1; & y & 3L_3 - x & 0 \end{bmatrix}^{\mathrm{T}} \end{cases} \tag{3-3}$$

$$\begin{cases} \$_{A3} = \begin{bmatrix} 0 & 0 & 1; & 0 & -L_3 - x_1 & 0 \end{bmatrix}^{\mathrm{T}} \\ \$_{A4} = \begin{bmatrix} 0 & 0 & 1; & y & L_3 - x & 0 \end{bmatrix}^{\mathrm{T}} \end{cases} \tag{3-4}$$

The reciprocal screws of these limbs are calculated as below

$$\begin{cases} \$^r_{e1,11} = \begin{bmatrix} (x - 2L_3 - x_1)/y & 1 & 0; & 0 & 0 & x_1 - L_3 \end{bmatrix}^{\mathrm{T}} \\ \$^r_{e1,12} = \begin{bmatrix} 0 & 0 & 1; & 0 & 0 & 0 \end{bmatrix}^{\mathrm{T}} \\ \$^r_{e1,13} = \begin{bmatrix} 0 & 0 & 0; & 0 & 1 & 0 \end{bmatrix}^{\mathrm{T}} \\ \$^r_{e1,14} = \begin{bmatrix} 0 & 0 & 0; & 1 & 0 & 0 \end{bmatrix}^{\mathrm{T}} \end{cases} \tag{3-5}$$

$$\begin{cases} \$_{e1,21}^{r} = \left[(x - 2L_3 - x_1)/y \quad 1 \quad 0; \quad 0 \quad 0 \quad x_1 + L_3 \right]^{\mathrm{T}} \\ \$_{e1,22}^{r} = \left[0 \quad 0 \quad 1; \quad 0 \quad 0 \quad 0 \right]^{\mathrm{T}} \\ \$_{e1,23}^{r} = \left[0 \quad 0 \quad 0; \quad 0 \quad 1 \quad 0 \right]^{\mathrm{T}} \\ \$_{e1,24}^{r} = \left[0 \quad 0 \quad 0; \quad 1 \quad 0 \quad 0 \right]^{\mathrm{T}} \end{cases} \tag{3-6}$$

where the superscript r denotes reciprocal. It is the same for the following equations. The subscripts e1 and e2 mean the equivalent joints of the parallelogram joint $A_1A_2\,A_3A_4$ and $B_1B_2\,B_3B_4$, respectively.

Based on the definition of reciprocal screw, the equivalent kinematic pair of this parallelogram $A_1A_2\,A_3A_4$ is calculated as

$$\$_{e1} = \left[0 \quad 0 \quad 0; \quad y/(2L_3 + x_1 - x) \quad 1 \quad 0 \right]^{\mathrm{T}} \tag{3-7}$$

Considering the kinematic screw of the first sliding joint

$$\$_{A5} = \left[0 \quad 0 \quad 0; \quad 1 \quad 0 \quad 0 \right]^{\mathrm{T}} \tag{3-8}$$

The twist screw system is solved as the reciprocal screw of Eqs. (3-7) and (3-8), as

$$\begin{cases} \$_{11}^{r} = \left[0 \quad 0 \quad 0; \quad 1 \quad 0 \quad 0 \right]^{\mathrm{T}} \\ \$_{12}^{r} = \left[0 \quad 0 \quad 0; \quad 0 \quad 1 \quad 0 \right]^{\mathrm{T}} \\ \$_{13}^{r} = \left[0 \quad 0 \quad 0; \quad 0 \quad 0 \quad 1 \right]^{\mathrm{T}} \\ \$_{14}^{r} = \left[0 \quad 0 \quad 1; \quad 0 \quad 0 \quad 0 \right]^{\mathrm{T}} \end{cases} \tag{3-9}$$

In the second limb, the kinematic screws for the linkages B_1B_2 and B_3B_4 are listed as

$$\begin{cases} \$_{B1} = \left[0 \quad 0 \quad 1; \quad 0 \quad L_3 - x_2 \quad 0 \right]^{\mathrm{T}} \\ \$_{B2} = \left[0 \quad 0 \quad 1; \quad y \quad -L_3 - x \quad 0 \right]^{\mathrm{T}} \end{cases} \tag{3-10}$$

$$\begin{cases} \$_{B3} = \left[0 \quad 0 \quad 1; \quad 0 \quad -L_3 - x_2 \quad 0 \right]^{\mathrm{T}} \\ \$_{B4} = \left[0 \quad 0 \quad 1; \quad y \quad -3L_3 - x \quad 0 \right]^{\mathrm{T}} \end{cases} \tag{3-11}$$

The reciprocal screws of these two limbs are derived as

$$\begin{cases} \$_{e2,11}^{r} = \left[(x + 2L_3 - x_2)/y \quad 1 \quad 0; \quad 0 \quad 0 \quad x_2 - L_3 \right]^{\mathrm{T}} \\ \$_{e2,12}^{r} = \left[0 \quad 0 \quad 1; \quad 0 \quad 0 \quad 0 \right]^{\mathrm{T}} \\ \$_{e2,13}^{r} = \left[0 \quad 0 \quad 0; \quad 0 \quad 1 \quad 0 \right]^{\mathrm{T}} \\ \$_{e2,14}^{r} = \left[0 \quad 0 \quad 0; \quad 1 \quad 0 \quad 0 \right]^{\mathrm{T}} \end{cases} \tag{3-12}$$

$$\begin{cases} \$_{e2,21}^{r} = \left[(x + 2L_3 - x_2)/y \quad 1 \quad 0; \quad 0 \quad 0 \quad x_1 + L_3 \right]^{\mathrm{T}} \\ \$_{e2,22}^{r} = \left[0 \quad 0 \quad 1; \quad 0 \quad 0 \quad 0 \right]^{\mathrm{T}} \\ \$_{e2,23}^{r} = \left[0 \quad 0 \quad 0; \quad 0 \quad 1 \quad 0 \right]^{\mathrm{T}} \\ \$_{e2,24}^{r} = \left[0 \quad 0 \quad 0; \quad 1 \quad 0 \quad 0 \right]^{\mathrm{T}} \end{cases} \tag{3-13}$$

the equivalent kinematic pair of this parallelogram $B_1B_2\,B_3B_4$ is calculated as

$$\$_{e2} = \left[0 \quad 0 \quad 0; \quad -y/(2L_3 + x - x_2) \quad 1 \quad 0 \right]^{\mathrm{T}} \tag{3-14}$$

Combined with the kinematic screw of the first sliding joint

$$\$_{B5} = \left[0 \quad 0 \quad 0; \quad 1 \quad 0 \quad 0 \right]^{\mathrm{T}} \tag{3-15}$$

The twist screw system is solved as the reciprocal screw of Equations (3-14) and (3-15), as

$$\begin{cases} \$_{21}^{r} = \$_{11}^{r} \\ \$_{22}^{r} = \$_{12}^{r} \\ \$_{23}^{r} = \$_{12}^{r} \\ \$_{24}^{r} = \$_{12}^{r} \end{cases} \tag{3-16}$$

According to the Equation (3-16), the common constraints λ for two kinematic chains are 4. Therefore d=6-4=2. ν and ζ both are zeroes. Employing the Equation (3-2) yields

$$M = 2(8-10-1)+10+0-0 = 4 \tag{3-17}$$

Based on the structure of the mechanism in figure 3-1, its mobility should be 2. Equation (3-17) shows Equation (3-2) is not feasible in this kind of parallel structures.

This kind of parallel structures has one P_a joint in each kinematic chain. There are three kinds of planes for P_a joint, parallel to XOY, XOZ, or YOZ planes. In each parallel architecture, the joints numbers and types should be the same. The prismatic joint can be added if the mobile platform requires more translations. There are three directions for prismatic joint, parallel to X, Y or Z directions. The revolute joints can be provided in each kinematic limb if the moving platform needs rotational workspace. There are three kinds of axis directions for revolute joint, parallel to X, Y or Z directions. Assuming the parallelogram module as one generalized kinematic joint, this kind of mechanisms belongs to fully parallel robot, where the number of chains is same as the degrees-of-freedom of

the whole manipulator. In addition, the number of joints of each chain is equal to the degrees-of-freedom of the parallel mechanism and only the joint connected to the fixed platform is equipped with an actuator.

Since the order of the planar parallel mechanism with 2 branches is special, a term containing of the order is added to achieve a revised mobility equation, to be suitable for this class of parallel manipulators, as seen below

$$M = d(n-g-1)+\sum_{i=1}^{g} f_i + \nu - \zeta + d(d-3) \tag{3-18}$$

Based on Equation (3-18), the mobility analysis of the 2-PPa structure is

$$M_2 = 2(8-10-1)+10+0-0+2(2-3)=2 \tag{3-19}$$

where the subscript 2 means 2 kinematic chains.

There are some other parallel mechanisms within this group, 3-PPaP, 4-PPaPR, 5-PPaPRR, 6-PPaPRRR. Considering the cases of the 2-PPa, the common constraints λ for them are 3, 2, 1 and 0, respectively. Their degrees of freedom can be solved by utilizing Equation (3-18), as shown below

$$\begin{cases} M_3 = 3(14-18-1)+18+0-0+3(3-3)=3 \\ M_4 = 4(22-28-1)+28+0-0+4(4-3)=4 \\ M_5 = 5(32-40-1)+40+0-0+5(5-3)=5 \\ M_6 = 6(44-54-1)+54+0-0+6(6-3)=6 \end{cases} \tag{3-20}$$

The possible parallel structures are listed below, according to the modified equation. Each case will be explained and infeasible structures will be verified by screw theory.

Table 3-1 Possible parallel mechanisms in this group

Number of Chains	DOFs	d	n	g	$\sum_{i=1}^{g} f_i$	Mechanism type (T-Translation, R-Rotation)	Mechanism
2	2	2	8	10	10	2T	2-PPa
						1T1R	2-RPa
						2R	2-RPa
3	3	3	14	18	18	3T	3-PPaP
						2T1R	3-PPaR
						1T2R	3-PaRR

						3R	3-PaRR
						3T1R	4-PPaPR
4	4	4	22	28	28	2T2R	4-PPaRR
						1T3R	4-PaRRR
5	5	5	32	40	40	3T2R	5-PPaPRR
						2T3R	5-PPaRRR
6	6	6	44	54	54	3T3R	6-PPaPRRR

3.2 Kinematic joint matrix

In this section, the novel concept kinematic joint matrix that can represent linkage mechanism is introduced in detail. The basic module of the kinematic joint matrix can be represented as

$$\begin{bmatrix} m_{11} & m_{12} & m_{13} \\ m_{21} & m_{22} & m_{23} \\ m_{31} & m_{32} & m_{33} \end{bmatrix} \tag{3-21}$$

where m_{ij} (i,j=1,2,3) in the i-th row and j-th column element of this square matrix denotes the kinematic joint type within the parallel mechanism.

This matrix can be divided into three categories. The diagonal elements m_{ii} of Equation (3-21) can display one kind of kinematic joint. Three elements above or below the main diagonal can indicate additional two kinds of kinematic pairs, respectively. In such a way, this matrix has the ability to imply linkage mechanisms under some conditions. The parallel mechanism with three kinds of joints can be expressed by the kinematic joint matrix, as demonstrated below

$$\left[\begin{array}{ccc:ccc:ccc} j_1 & j_2 & j_2 & j_1 & j_2 & j_2 & j_1 & j_2 & j_2 \\ j_3 & j_1 & j_2 & j_3 & j_1 & j_2 & \cdots j_3 & j_1 & j_2 \\ j_3 & j_3 & j_1 & j_3 & j_3 & j_1 & j_3 & j_3 & j_1 \end{array}\right] \tag{3-22}$$

where j_1, j_2 and j_3 indicate three sorts of kinematic joints respectively. The vertical dash line is employed to distinguish adjacent square matrices.

In the kinematic joint matrix, the written sequence is from left to right. In each group of kinematic pair, the corresponding joint position will be filled once this position in the left square matrix is already filled, to achieve a compact format.

The widely used prismatic (P) joint, revolute (R) joint and parallelogram (Pa) joint are taken as examples. The elementary kinematic pairs P and R joints with larger ranges of

motion, higher stiffness compared with U and S joints. As a result, the intrinsic shortcomings of parallel mechanisms can be decreased and the target performance including large translational and rotational workspaces, high stiffness and load capacity can be realized. These joints are further constrained in this case. Each prismatic joint axis can be parallel to *X*, *Y* or *Z* direction, denoted as P_X, P_Y and P_Z, respectively. The rotational joint axis can parallel to *X*, *Y* or *Z* direction separately, represented respectively as R_X, R_Y and R_Z. Every P_a joint can be placed in planes that are parallel to *XOY*, *XOZ* or *YOZ* plane, and respectively shown as P_{XY}, P_{XZ} and P_{YZ}. Thereafter, each category of kinematic joint is further divided into three cases, which reveals that each component position is unique. According to definition of Equation (3-21), the kinematic joint matrix under this circumstance can be formulated as

$$\begin{bmatrix} P_X & P_{XY} & P_{XZ} \\ R_Z & P_Y & P_{YZ} \\ R_Y & R_X & P_Z \end{bmatrix} \tag{3-23}$$

There are two reasons indicating the kinematic joint matrix is insufficient to directly distinguish any two parallel structures. The first factor is the mapping relations with parallel mechanisms. The matrix can have one-to-one mapping relationship with the parallel mechanism if this matrix is simple and there are few elements. If there are more kinematic joints, the matrix becomes complicated and may exist one-to-many relationship with parallel mechanisms. For example, three joints P_X, R_X and P_{XY} in Equation (3-23) can be treated in the same branch or different branches to construct various parallel structures. The second factor is that various kinematic joint matrices can be obtained if the parallel manipulator is placed in different coordinate systems (e.g., the P_X joint in one coordinate system might be P_Y or P_Z joint in another reference system).

However, it is meaningful to propose an approach for discriminating different kinds of matrices, since any two parallel manipulators expressed by different categories of kinematic joint matrices are distinct. It also means the second factor can be resolved. It is evident that two kinematic joint matrices are different if the total numbers for prismatic joints or revolute joints or P_a joints are not the same. This question is further constrained to distinguish the matrices with identical numbers for prismatic joints, rotary joints and P_a joints, respectively. For a given kinematic joint matrix representing parallel mechanisms,

The total numbers of P_X, P_Y, P_Z, R_X, R_Y, R_Z, P_{XY}, P_{XZ} and P_{YZ} joints are expressed separately as N_{11}, N_{22}, N_{33}, N_{32}, N_{31}, N_{21}, N_{12}, N_{13} and N_{23}. The i, j, k are integers ranging from 1 to 3. The following numbers are pre-defined

$$\begin{cases} a1 = \min(i, j) & a2 = \max(i, j) \\ a3 = \min(i, k) & a4 = \max(i, k) \\ a5 = \min(j, k) & a6 = \max(j, k) \end{cases} \tag{3-24}$$

A unique block pattern is introduced, as shown in Figure 3-2(a). In this block pattern, the first column is for N_{ii}. The second column is filled by N_{32}, N_{31} and N_{21}. The last column is for N_{12}, N_{13} and N_{23}. An example is illustrated in Figure 3-2 (b). Take the N_{11}, N_{32}, N_{12} and N_{13} as examples, the physical relevance (inner feature) among them is the common subscript X in P_X, R_X, P_{XY} and P_{XZ}. The external feature is based on the subscripts of these filled elements N_{ij} in this pattern. If the first column is selected, each element of the second column can be decided by the elements of the first column and the other rows. For example, the subscripts a5 and a6 of N_{a6a5} are respectively the minimal and maximum values between j and k (subscripts of N_{jj}, N_{kk}). Each element of the third column can be concluded by the directly connected two columns (the two elements of the first column), i.e. N_{a1a2} is directly connected by N_{a6a5} and N_{a4a3}. Then the subscripts a1 and a2 are solved respectively as the minimal and maximum elements of the subscripts of N_{ii}, N_{jj}.

Before filling elements into the block pattern, comparing N_{ii}, N_{jj}, N_{kk} (i, j, k=1,2,3.) and the following expression can be obtained

$$N_{ii} \geq N_{jj} \geq N_{kk} \tag{3-25}$$

The following scenarios can be found

$$\begin{aligned} &\text{(I)} && N_{ii} > N_{jj} > N_{kk} \\ &\text{(II)} && N_{ii} > N_{jj} = N_{kk} \;\&\; N_{a1a2} > N_{a3a4} \\ &\text{(III)} && N_{ii} > N_{jj} = N_{kk} \;\&\; N_{a1a2} = N_{a3a4} \\ &\text{(IV)} && N_{ii} > N_{jj} = N_{kk} \;\&\; N_{a1a2} < N_{a3a4} \\ &\text{(V)} && N_{ii} = N_{jj} > N_{kk} \;\&\; N_{a3a4} > N_{a5a6} \\ &\text{(VI)} && N_{ii} = N_{jj} > N_{kk} \;\&\; N_{a3a4} = N_{a5a6} \\ &\text{(VII)} && N_{ii} = N_{jj} > N_{kk} \;\&\; N_{a3a4} < N_{a5a6} \end{aligned} \tag{3-26}$$

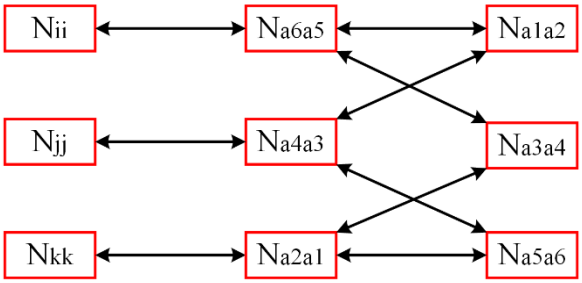

(a) Block pattern

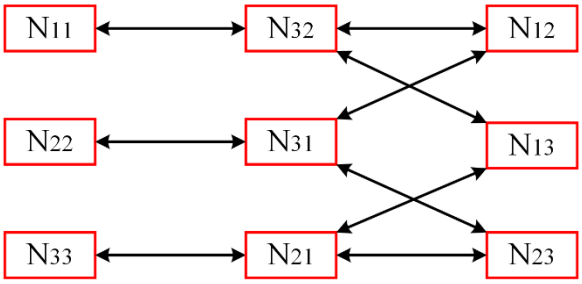

(b) Block pattern of a sample

Figure 3-2 Block patterns for kinematic joint matrix

(The red block is filled with the sum for one kind of joint.

The double arrow line implies two blocks are pertinent.)

In cases (I), (II), (V), the first column of the block pattern is N_{ii}, N_{jj} and N_{kk}. The final pattern is the same as in Figure 3-2 (a). For case (III), the first column of the pattern can be N_{ii}, N_{jj} and N_{kk}, or N_{ii}, N_{kk} and N_{jj}. The whole patterns are the same. In case (IV), the first column of the pattern is listed as N_{ii}, N_{kk} and N_{jj}. In case (VI), the first column of the block pattern can be N_{ii}, N_{jj} and N_{kk}, or N_{jj}, N_{ii} and N_{kk}. The contents are identical in any selection. In case (VII), the first column of the block pattern is listed as N_{jj}, N_{ii} and N_{kk}.

The other situations happen when N_{11}= N_{22}= N_{33}. Before classifying the remaining cases, comparing N_{a1a2}, N_{a3a4} and N_{a5a6} yields

$$N_{b1b2} \geq N_{b3b4} \geq N_{b5b6} \tag{3-27}$$

where N_{b1b2} and N_{b5b6} are respectively the largest and smallest among N_{a1a2}, N_{a3a4} and N_{a5a6}. N_{b3b4} is the rest of them.

The remaining scenarios are concluded as

$$
\begin{aligned}
&\text{(VIII)}\ N_{ii} = N_{jj} = N_{kk}\ \&\ N_{b1b2} > N_{b3b4} > N_{b5b6} \\
&\text{(IX)}\ \ N_{ii} = N_{jj} = N_{kk}\ \&\ N_{b1b2} > N_{b3b4} = N_{b5b6} \\
&\text{(X)}\ \ \ N_{ii} = N_{jj} = N_{kk}\ \&\ N_{b1b2} = N_{b3b4} > N_{b5b6} \\
&\text{(XI)}\ \ N_{ii} = N_{jj} = N_{kk}\ \&\ N_{b1b2} = N_{b3b4} = N_{b5b6}
\end{aligned}
\qquad (3\text{-}28)
$$

In case (VIII), the first column of the block pattern is N_{ii}, N_{jj} and N_{kk}. In case (IX), the first column of the pattern can be either N_{ii}, N_{jj} and N_{kk}, or N_{jj}, N_{ii} and N_{kk}. In case (X), the first column of the pattern can be either N_{ii}, N_{jj} and N_{kk}, or N_{ii}, N_{kk} and N_{jj}. In case (XI), the first column of the pattern can be listed in any sequence to finally derive a unique pattern. All the feasible situations for the block pattern are summarized in Equations (3-26) and (3-28). As long as two kinematic joint matrices can create identical block patterns, these two matrices belong to the same kind of matrix and can express the same parallel mechanism(s). One sample is provided below. Two kinematic joint matrices are listed as

$$
\left[\begin{array}{ccc|ccc|ccc|ccc|ccc|ccc}
P_X & \_ & P_{XZ} & P_X & \_ & P_{XZ} & P_X & \_ & \_ & P_X & \_ & \_ & P_X & \_ & \_ & P_X & \_ & \_ \\
R_Z & P_Y & P_{YZ} & R_Z & P_Y & P_{YZ} & R_Z & P_Y & P_{YZ} & R_Z & P_Y & P_{YZ} & R_Z & \_ & \_ & R_Z & \_ & \_ \\
R_Y & R_X & P_Z & R_Y & R_X & P_Z & R_Y & R_X & \_ & R_Y & R_X & \_ & R_Y & R_X & \_ & R_Y & R_X & \_
\end{array}\right]
\qquad (3\text{-}29)
$$

$$
\left[\begin{array}{ccc|ccc|ccc|ccc|ccc|ccc}
P_X & \_ & P_{XZ} & P_X & \_ & P_{XZ} & P_X & \_ & P_{XZ} & P_X & \_ & P_{XZ} & \_ & \_ & \_ & \_ & \_ & \_ \\
R_Z & P_Y & P_{YZ} & R_Z & P_Y & P_{YZ} & R_Z & P_Y & \_ & R_Z & P_Y & \_ & R_Z & P_Y & \_ & R_Z & P_Y & \_ \\
R_Y & R_X & P_Z & R_Y & R_X & P_Z & R_Y & R_X & \_ & R_Y & R_X & \_ & R_Y & R_X & \_ & R_Y & R_X & \_
\end{array}\right]
\qquad (3\text{-}30)
$$

The parameters for these two aforementioned matrices are computed separately. They correspond to $N_{11}=6, N_{12}=0, N_{13}=2, N_{21}=6, N_{22}=4, N_{23}=4, N_{31}=6, N_{32}=6, N_{33}=2$ and $N_{11}=4, N_{12}=0, N_{13}=4, N_{21}=6, N_{22}=6, N_{23}=2, N_{31}=6, N_{32}=6, N_{33}=2$. Following the above method, these two scenarios can be classified into the case (I). Their final block patterns can both be written as seen in figure 3-3, which indicates they belong to the same kind of kinematic joint matrix. One feasible 6-DOF parallel structure is illustrated in figure 3-4. According to figure 3-4, one is based on the X1-Y1-Z1 coordinate system while the other is generated in accordance with the X2-Y2-Z2 coordinate system. These two coordinate systems can be transformed by rotation operations (The directions of the corresponding axes are separately parallel. The same origins are not required).

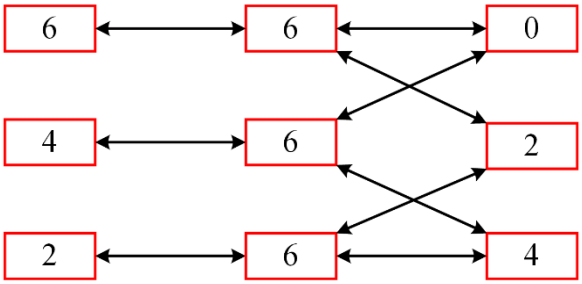

Figure 3-3 The block pattern for two similar matrices

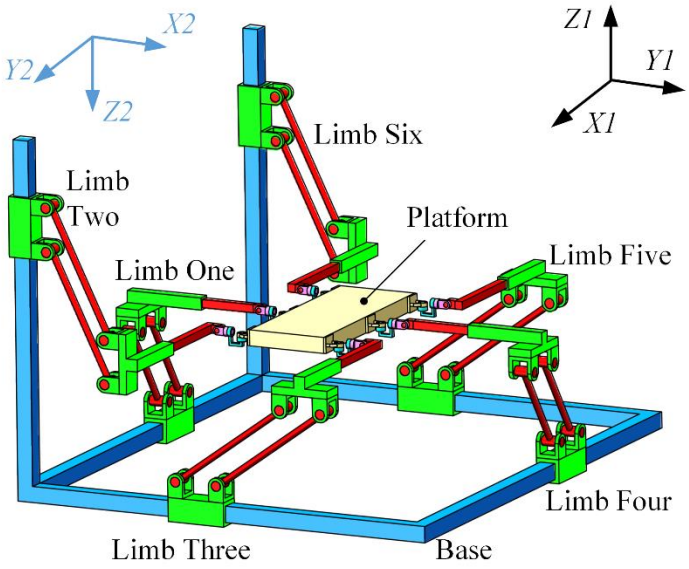

Figure 3-4 Prototype of a 6-DOF parallel structure

Therefore, this block pattern is helpful for the enumerations of every possible kinematic joint matrix with predefined conditions.

3.3 Enumeration of a family of parallel mechanisms

3.3.1 Two-DOF parallel mechanism

(i) Case one: 2T mechanism

There are two limbs

$$\begin{cases} P_X - P_{XY} \\ P_Y - P_{XY} \end{cases} \tag{3-31}$$

Limbs are shown in matrix form

$$\begin{bmatrix} P_X & P_{XY} \\ - & - \end{bmatrix} \begin{bmatrix} - & P_{XY} \\ - & P_Y \end{bmatrix} \tag{3-32}$$

The limb can be represented as Q_i. In enumeration, there will be $Q_i^2 + Q_i Q_j = 2 + C_2^2 = 3$ (The superscript n means n such limbs in mechanism) kinds of matrices. The same matrices are ones with similar cell configuration, while their orientations in the global coordinate system are different. At last, there are 2 kinds of feasible matrices. The first matrix can be represented as

$$\left[\begin{array}{cc:cc} P_X & P_{XY} & P_X & P_{XY} \\ - & - & - & - \end{array}\right] \tag{3-33}$$

P_i means there are i prismatic joint(s) in this parallel manipulator and R_i denotes there are i revolute joint(s) in this parallel manipulator. Its corresponding planar translational parallel mechanism is illustrated in figure 3-5. There is one P_2 joint(P_X). There are two same P_a joints(P_{XY}) related to the P_2 joint(P_X).

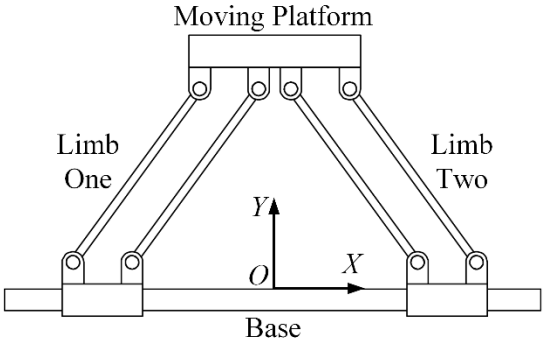

Figure 3-5 Schematic diagram of 2-DOF parallel structure (1)

The second kinematic joint matrix is

$$\left[\begin{array}{cc:cc} P_X & P_{XY} & - & P_{XY} \\ - & P_Y & - & - \end{array}\right] \tag{3-34}$$

Its corresponding parallel mechanism is illustrated in figure 3-6. There are two P_1 joints(P_X and P_Y). Two same P_a joints are both related to P_1 joint(P_X) and P_1 joint(P_Y).

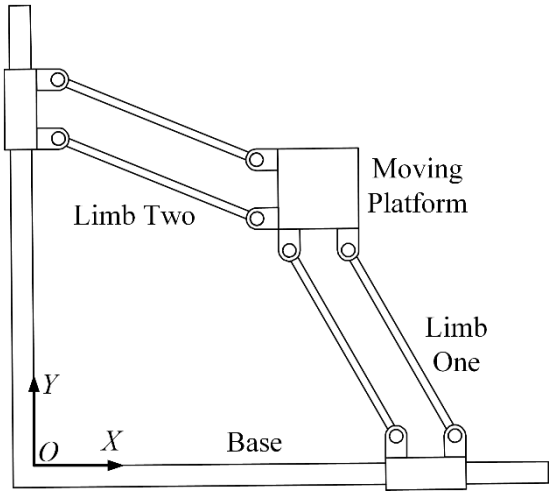

Figure 3-6 Schematic diagram of 2-DOF parallel structure (2)

(ii) Case two: 2R mechanism

The only possible solution is 2-RP$_a$, since each limb supports one rotation and one decoupled translation, it may not be feasible for a 2-rotational mechanism. One such limb is presented in figure 3-7.

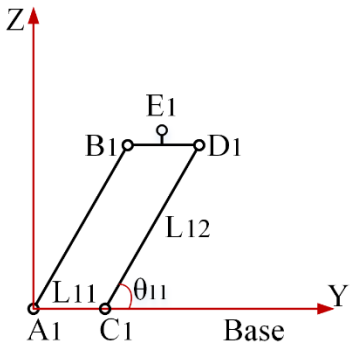

Figure 3-7 The first branch of 2R mechanism

The coordinates of these points are provided as, $A_1(0,0,0)$, $B_1(0, L_{12}\cos\theta_{11}, L_{12}\sin\theta_{11})$, $C_1(0, L_{11}, 0)$, $D_1(0, L_{11}+L_{12}\cos\theta_{11}, L_{12}\sin\theta_{11})$, $E_1(0, 0.5L_{11}+L_{12}\cos\theta_{11}, L_{12}\sin\theta_{11})$.

In this case, only one possible branch is provided and analyzed. The kinematic screws of four joints of P$_a$ joint

$$\begin{cases} \$_{A1} = \begin{bmatrix} 1 & 0 & 0; & 0 & 0 & 0 \end{bmatrix}^{\mathrm{T}} \\ \$_{B1} = \begin{bmatrix} 1 & 0 & 0; & 0 & L_{12}\sin\theta_{11} & -L_{12}\cos\theta_{11} \end{bmatrix}^{\mathrm{T}} \\ \$_{C1} = \begin{bmatrix} 1 & 0 & 0; & 0 & 0 & -L_{11} \end{bmatrix}^{\mathrm{T}} \\ \$_{D1} = \begin{bmatrix} 1 & 0 & 0; & 0 & L_{12}\sin\theta_{11} & -L_{11}-L_{12}\cos\theta_{11} \end{bmatrix}^{\mathrm{T}} \end{cases} \tag{3-35}$$

The equivalent screw

$$\$_{Pa1} = \begin{bmatrix} 0 & 0 & 0; & 0 & \sin\theta_{11} & -\cos\theta_{11} \end{bmatrix}^{\mathrm{T}} \tag{3-36}$$

It denotes the equivalent movement is an arc and the translational direction is the tangential direction of this arc.

The kinematic screw of joint E_1

$$\$_{E1} = \begin{bmatrix} 1 & 0 & 0; & 0 & L_{12}\sin\theta_{11} & -0.5L_{11}-L_{12}\cos\theta_{11} \end{bmatrix}^{\mathrm{T}} \tag{3-37}$$

The reciprocal screw of this branch

$$\begin{cases} \$_{11}^{r} = \begin{bmatrix} 1 & 0 & 0; & 0 & 0 & 0 \end{bmatrix}^{\mathrm{T}} \\ \$_{12}^{r} = \begin{bmatrix} 0 & 0 & 0; & 0 & 0 & 1 \end{bmatrix}^{\mathrm{T}} \\ \$_{13}^{r} = \begin{bmatrix} 0 & 0 & 0; & 0 & 1 & 0 \end{bmatrix}^{\mathrm{T}} \\ \$_{14}^{r} = \begin{bmatrix} 0 & \cos\theta_{11} & \sin\theta_{11}; & 0.5L_{11} & 0 & 0 \end{bmatrix}^{\mathrm{T}} \end{cases} \tag{3-38}$$

The first screw is a constraint force along X direction. The second screw is the constraint moment about Z axis. The third screw is the constraint couple about Y direction. The last screw is a constraint force (the direction is parallel to radial direction of the arc). This branch constrains two rotations. Therefore, the moving platform has one rotation at most. The 2R mechanism can not be constructed.

(iii) Case three: 1T1R mechanism

The only possible solution is 2-RPa, since each limb supports one rotation and one decoupled translation, it may not be feasible for a 1T1R mechanism. One such parallel structure is presented in figure 3-8.

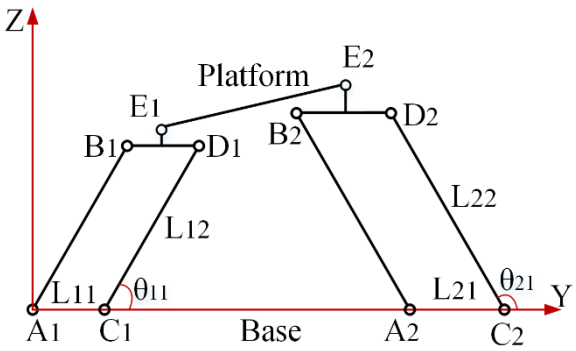

Figure 3-8 1T1R mechanism

The coordinates of these points are provided as, $A_1(0,0,0)$, $B_1(0, L_{12}\cos\theta_{11}, L_{12}\sin\theta_{11})$, $C_1(0, L_{11}, 0)$, $D_1(0, L_{11}+L_{12}\cos\theta_{11}, L_{12}\sin\theta_{11})$, $E_1(0, 0.5L_{11}+L_{12}\cos\theta_{11}, L_{12}\sin\theta_{11})$, $A_2(0, L_{20}, 0)$, $B_2(0, L_{20}+L_{22}\cos\theta_{21}, L_{22}\sin\theta_{21})$, $C_2(0, L_{20}+L_{21}, 0)$, $D_2(0, L_{20}+L_{21}+L_{22}\cos\theta_{21}, L_{22}\sin\theta_{21})$, $E_2(0, L_{20}+0.5L_{21}+L_{22}\cos\theta_{21}, L_{22}\sin\theta_{21})$.

The screw systems for the P_a joints in two chains

$$\begin{cases} \$_{A1} = [1 \quad 0 \quad 0; \quad 0 \quad 0 \quad 0]^{\mathrm{T}} \\ \$_{B1} = [1 \quad 0 \quad 0; \quad 0 \quad L_{12}\sin\theta_{11} \quad -L_{12}\cos\theta_{11}]^{\mathrm{T}} \\ \$_{C1} = [1 \quad 0 \quad 0; \quad 0 \quad 0 \quad -L_{11}]^{\mathrm{T}} \\ \$_{D1} = [1 \quad 0 \quad 0; \quad 0 \quad L_{12}\sin\theta_{11} \quad -L_{11}-L_{12}\cos\theta_{11}]^{\mathrm{T}} \end{cases} \tag{3-39}$$

$$\begin{cases} \$_{A2} = [1 \quad 0 \quad 0; \quad 0 \quad 0 \quad -L_{20}]^{\mathrm{T}} \\ \$_{B2} = [1 \quad 0 \quad 0; \quad 0 \quad L_{22}\sin\theta_{21} \quad -L_{20}-L_{22}\cos\theta_{21}]^{\mathrm{T}} \\ \$_{C2} = [1 \quad 0 \quad 0; \quad 0 \quad 0 \quad -L_{20}-L_{21}]^{\mathrm{T}} \\ \$_{D2} = [1 \quad 0 \quad 0; \quad 0 \quad L_{22}\sin\theta_{21} \quad -L_{20}-L_{21}-L_{22}\cos\theta_{21}]^{\mathrm{T}} \end{cases} \tag{3-40}$$

Their equivalent screws are respectively

$$\$_{Pa1} = [0 \quad 0 \quad 0; \quad 0 \quad \sin\theta_{11} \quad -\cos\theta_{11}]^{\mathrm{T}} \tag{3-41}$$

$$\$_{Pa2} = [0 \quad 0 \quad 0; \quad 0 \quad \sin\theta_{21} \quad -\cos\theta_{21}]^{\mathrm{T}} \tag{3-42}$$

The kinematic screws for the remaining joints

$$\$_{E1} = [1 \quad 0 \quad 0; \quad 0 \quad L_{12}\sin\theta_{11} \quad -0.5L_{11}-L_{12}\cos\theta_{11}]^{\mathrm{T}} \tag{3-43}$$

$$\$_{E2} = [1 \quad 0 \quad 0; \quad 0 \quad L_{22}\sin\theta_{21} \quad -L_{20}-0.5L_{11}-L_{22}\cos\theta_{21}]^{\mathrm{T}} \tag{3-44}$$

The corresponding reciprocal screws for the first and second chains are separately

$$\begin{cases} \$_{11}^{r} = \begin{bmatrix} 1 & 0 & 0; & 0 & 0 & 0 \end{bmatrix}^{\mathrm{T}} \\ \$_{12}^{r} = \begin{bmatrix} 0 & 0 & 0; & 0 & 0 & 1 \end{bmatrix}^{\mathrm{T}} \\ \$_{13}^{r} = \begin{bmatrix} 0 & 0 & 0; & 0 & 1 & 0 \end{bmatrix}^{\mathrm{T}} \\ \$_{14}^{r} = \begin{bmatrix} 0 & \cos\theta_{11} & \sin\theta_{11}; & 0.5L_{11} & 0 & 0 \end{bmatrix}^{\mathrm{T}} \end{cases} \tag{3-45}$$

$$\begin{cases} \$_{21}^{r} = \begin{bmatrix} 1 & 0 & 0; & 0 & 0 & 0 \end{bmatrix}^{\mathrm{T}} \\ \$_{22}^{r} = \begin{bmatrix} 0 & 0 & 0; & 0 & 0 & 1 \end{bmatrix}^{\mathrm{T}} \\ \$_{23}^{r} = \begin{bmatrix} 0 & 0 & 0; & 0 & 1 & 0 \end{bmatrix}^{\mathrm{T}} \\ \$_{24}^{r} = \begin{bmatrix} 0 & \cos\theta_{21} & \sin\theta_{21}; & 0.5L_{21}+L_{20} & 0 & 0 \end{bmatrix}^{\mathrm{T}} \end{cases} \tag{3-46}$$

The kinematic screw for the moving platform

$$\$_{m} = \begin{bmatrix} 0 & -\dfrac{L_{11}-L_{21}-2L_{20}}{-L_{21}\cot\theta_{11}-2L_{20}\cot\theta_{11}+L_{11}\cot\theta_{21}} & 1; & 0 & 0 & -L_{20} \end{bmatrix}^{\mathrm{T}} \tag{3-47}$$

This illustrates the moving platform has only one rotation. The 1T1R movement can not be achieved.

3.3.2 Three-DOF parallel mechanism

(i) Case one: 3T mechanism

The possible limbs are provided as

$$\begin{cases} P_Y - P_{YZ} - P_X & P_Y - P_{XY} - P_Z & P_X - P_{XY} - P_Z \\ P_X - P_{XZ} - P_Y & P_Z - P_{XZ} - P_Y & P_Z - P_{YZ} - P_X \end{cases} \tag{3-48}$$

Limbs shown in matrix form:

$$\begin{cases} \begin{bmatrix} P_X & P_{XY} & - \\ - & P_Y & - \\ - & - & - \end{bmatrix} & \begin{bmatrix} - & P_{XY} & - \\ - & P_Y & - \\ - & - & P_Z \end{bmatrix} & \begin{bmatrix} P_X & P_{XY} & - \\ - & - & - \\ - & - & P_Z \end{bmatrix} \\ \begin{bmatrix} P_X & - & P_{XZ} \\ - & P_Y & - \\ - & - & - \end{bmatrix} & \begin{bmatrix} - & - & P_{XZ} \\ - & P_Y & - \\ - & - & P_Z \end{bmatrix} & \begin{bmatrix} P_X & - & - \\ - & - & P_{YZ} \\ - & - & P_Z \end{bmatrix} \end{cases} \tag{3-49}$$

The limb can be represented as Q_i. In enumeration, there will be $Q_i^3 + Q_i^2 Q_j + Q_i Q_j Q_k = 6 + A_6^2 + C_6^3 = 56$ kinds of matrices. The same matrices are ones with similar cell configuration. There are two different scenarios for 3/4/5/6 DOFs parallel

mechanisms. The first one is that their orientations in the global coordinate system are different or represent. The next one means they represent different mechanisms.

At last, there are 10 kinds of feasible matrices. These mechanisms are shown in matrix form. The first matrix is listed as

$$\left[\begin{array}{ccc:ccc} P_X & P_{XY} & P_{XZ} & P_X & \_ & \_ \\ \_ & P_Y & P_{YZ} & \_ & P_Y & \_ \\ \_ & \_ & P_Z & \_ & \_ & P_Z \end{array}\right] \tag{3-50}$$

One possible parallel architecture is seen in figure 3-9. There are three P_2 joints (P_X, P_Y and P_Z) and three different P_a joints (P_{XY}, P_{XZ} and P_{YZ}). Each P_a joint is related to two different P_2 joints. Two different Pa joints (P_{XY}, P_{XZ}) are related to P_2 joints (P_X). Two different P_a joints (P_{XY}, P_{YZ}) are related to P_2 joints (P_Y). Two different P_a joints (P_{XZ}, P_{YZ}) are related to P_2 joints (P_Z).

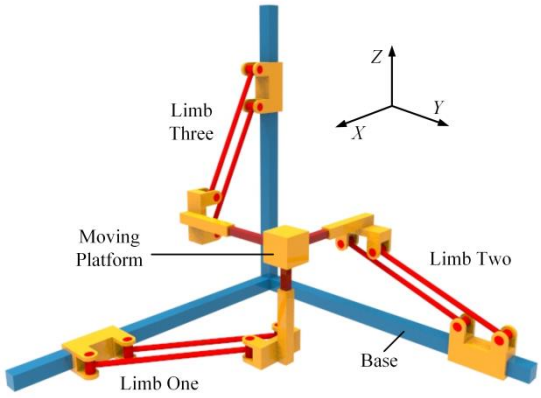

Figure 3-9 Schematic diagram of 3-DOF parallel structure (1)

The second matrix is provided as

$$\left[\begin{array}{ccc:ccc:ccc} P_X & P_{XY} & \_ & P_X & \_ & \_ & P_X & \_ & \_ \\ \_ & P_Y & P_{YZ} & \_ & \_ & P_{YZ} & \_ & \_ & \_ \\ \_ & \_ & P_Z & \_ & \_ & P_Z & \_ & \_ & \_ \end{array}\right] \tag{3-51}$$

One possible parallel architecture is seen in figure 3-10. There are one P_1 joint (P_Y), one P_2 joint (P_Z), one P_3 joint (P_X), one P_a joint (P_{XY}) and two same P_a joints (P_{YZ}). Three P_a joints

(P_{XY}, P_{YZ}) are related to P_1 joint (P_Y). Two identical P_a joints (P_{YZ}) are related to P_2 joint (P_Z). One P_a joint (P_{XY}) is related to P_3 joint (P_X).

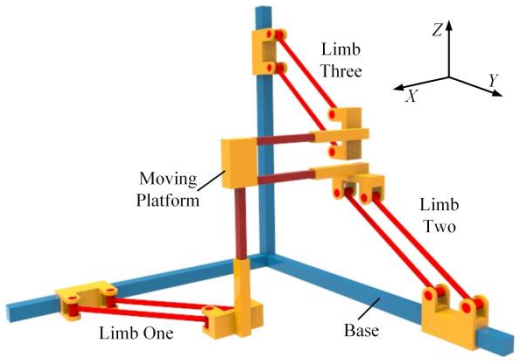

Figure 3-10 Schematic diagram of 3-DOF parallel structure (2)

The third matrix is provided as

$$\left[\begin{array}{ccc:ccc} P_X & P_{XY} & - & P_X & P_{XY} & - \\ - & P_Y & P_{YZ} & - & P_Y & - \\ - & - & P_Z & - & - & P_Z \end{array}\right] \tag{3-52}$$

One possible parallel architecture is seen in figure 3-11. There are three P_2 joints (P_X, P_Y and P_Z), one P_a joint (P_{YZ}) and two identical P_a joints (P_{XY}). Two same P_a joints (P_{XY}) are related to P_2 joints (P_X). Three P_a joints (P_{XY}, P_{YZ}) are related to P_2 joints (P_Y). One P_a joint (P_{YZ}) is related to P_2 joints (P_Z).

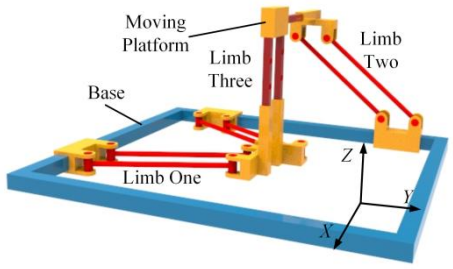

Figure 3-11 Schematic diagram of 3-DOF parallel structure (3)

The fourth matrix is denoted as

$$\left[\begin{array}{ccc:ccc:ccc} P_X & P_{XY} & P_{XZ} & P_X & - & - & P_X & - & - \\ - & P_Y & P_{YZ} & - & P_Y & - & - & - & - \\ - & - & P_Z & - & - & - & - & - & - \end{array}\right] \tag{3-53}$$

One feasible parallel architecture is shown in figure 3-12. There are one P_1 joint (P_Z), one P_2 joint (P_Y), one P_3 joint (P_X), and three different P_a joints (P_{XY}, P_{XZ} and P_{YZ}). Two P_a joints

(P_{XZ}, P_{YZ}) are related to P_1 joint (P_Z). Two P_a joints (P_{XZ}, P_{YZ}) are related to P_2 joint (P_Y). Two P_a joints (P_{XY}, P_{XZ}) are related to P_3 joint (P_X).

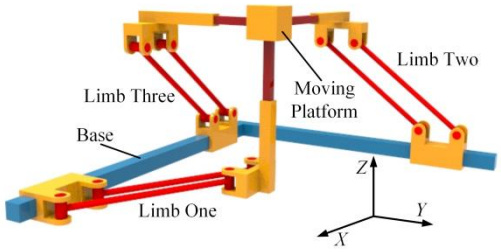

Figure 3-12 Schematic diagram of 3-DOF parallel structure (4)

The fifth matrix is denoted as

$$\left[\begin{array}{ccc|ccc|ccc} P_X & P_{XY} & - & P_X & - & - & - & - & - \\ - & P_Y & P_{YZ} & - & P_Y & P_{YZ} & - & P_Y & - \\ - & - & P_Z & - & - & - & - & - & - \end{array}\right] \tag{3-54}$$

One feasible parallel architecture is shown in figure 3-13. There are one P_1 joint (P_Z), one P_2 joint (P_X), one P_3 joint (P_Y), one P_a joint (P_{XY}) and two identical P_a joints (P_{YZ}). Two same P_a joints (P_{YZ}) are related to P_1 joint (P_Z). One P_a joint (P_{XY}) is related to P_2 joint (P_X). Three P_a joints (P_{XY}, P_{YZ}) are related to P_3 joint (P_Y).

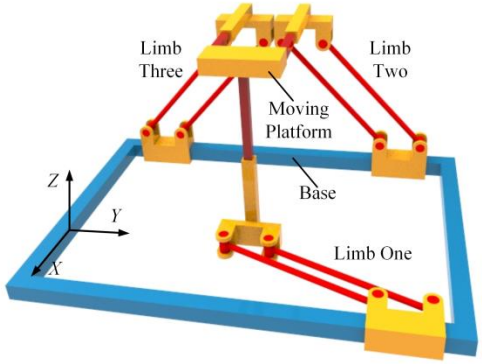

Figure 3-13 Schematic diagram of 3-DOF parallel structure (5)

The sixth matrix is denoted as

$$\left[\begin{array}{ccc|ccc|ccc} P_X & - & - & P_X & - & - & P_X & - & - \\ - & P_Y & P_{YZ} & - & P_Y & P_{YZ} & - & - & P_{YZ} \\ - & - & P_Z & - & - & - & - & - & - \end{array}\right] \tag{3-55}$$

One feasible parallel architecture is shown in figure 3-14. There are one P_1 joint (P_Z), one P_2 joint (P_Y), one P_3 joint (P_X) and three identical P_a joints (P_{YZ}). Three same P_a joints (P_{YZ}) are both related to P_1 joint (P_Z) and P_2 joint (P_Y). No P_a joint is related to P_3 joint (P_X).

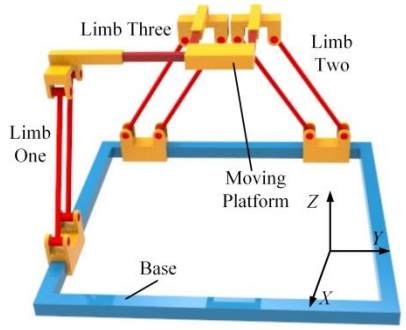

Figure 3-14 Schematic diagram of 3-DOF parallel structure (6)

The seventh matrix is represented as

$$\left[\begin{array}{ccc|ccc|ccc} P_X & - & - & P_X & - & - & P_X & - & - \\ - & P_Y & P_{YZ} & - & P_Y & P_{YZ} & - & P_Y & P_{YZ} \\ - & - & - & - & - & - & - & - & - \end{array}\right] \tag{3-56}$$

One feasible parallel structure is shown in figure 3-15. There are two P_3 joint (P_X, P_Y) and three identical P_a joints (P_{YZ}). Three P_a joints (P_{YZ}) are related to P_3 joint (P_Y). No P_a joint is related to P_3 joint (P_X).

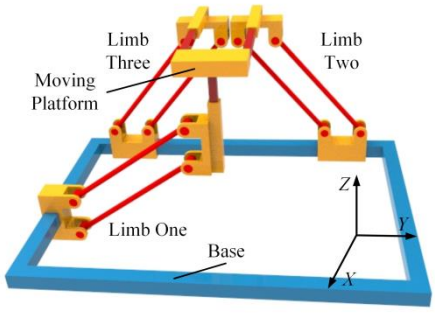

Figure 3-15 Schematic diagram of 3-DOF parallel structure (7)

The eighth matrix is represented as

$$\left[\begin{array}{ccc|ccc|ccc} P_X & - & P_{XZ} & P_X & - & - & P_X & - & - \\ - & P_Y & P_{YZ} & - & P_Y & P_{YZ} & - & P_Y & - \\ - & - & - & - & - & - & - & - & - \end{array}\right] \tag{3-57}$$

One feasible parallel structure is shown in figure 3-16. There are two P_3 joint (P_X, P_Y), one Pa joint (P_{XZ}) and two identical P_a joints (P_{YZ}). One P_a joint (P_{XZ}) is related to P_3 joint (P_X) and two same P_a joints (P_{YZ}) are related to P_3 joint (P_Y).

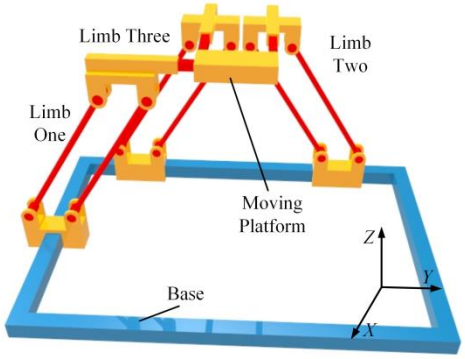

Figure 3-16 Schematic diagram of 3-DOF parallel structure (8)

The nineth matrix is represented as

$$\left[\begin{array}{ccc:ccc:ccc} P_X & - & P_{XZ} & P_X & - & - & & - & - \\ - & P_Y & P_{YZ} & - & P_Y & P_{YZ} & - & P_Y & - \\ - & - & \underline{P_Z} & - & - & - & - & - & - \end{array}\right] \tag{3-58}$$

One feasible parallel structure is shown in figure 3-17. There are one P_1 joint(P_Z), one P_2 joint (P_X), one P_3 joint (P_Y), one P_a joint (P_{XZ}) and two identical P_a joints (P_{YZ}). Three P_a joints (P_{XZ}, P_{YZ}) are related to P_1 joint(P_Z). One P_a joint (P_{XZ}) is related to P_2 joint (P_X). Two same identical P_a joints (P_{YZ}) are related to P_3 joint (P_Y).

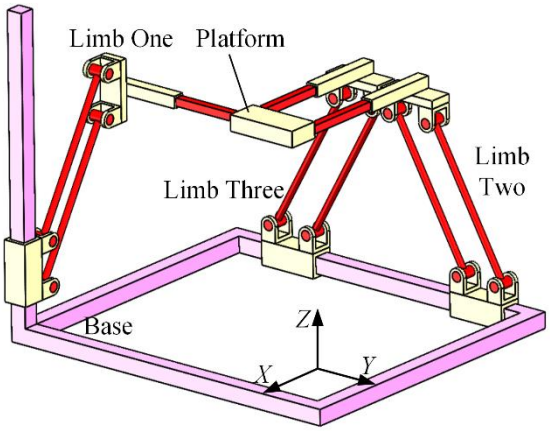

Figure 3-17 Schematic diagram of 3-DOF parallel structure (9)

The last matrix is represented as

$$\left[\begin{array}{ccc|ccc|ccc} P_X & P_{XY} & - & P_X & - & - & P_X & - & - \\ - & P_Y & P_{YZ} & - & P_Y & P_{YZ} & - & & - \\ - & - & P_Z & - & - & - & - & - & - \end{array}\right] \tag{3-59}$$

One feasible parallel structure is shown in figure 3-18. There are one P_1 joint(P_Z), one P_2 joint (P_Y), one P_3 joint (P_X), one P_a joint (P_{XZ}) and two identical P_a joints (P_{YZ}). Two same P_a joints (P_{YZ}) are related to P_1 joint(P_Z). Three P_a joints (P_{XZ}, P_{YZ}) are related to P_2 joint (P_Y). One P_a joint (P_{XY}) is related to P_3 joint (P_X).

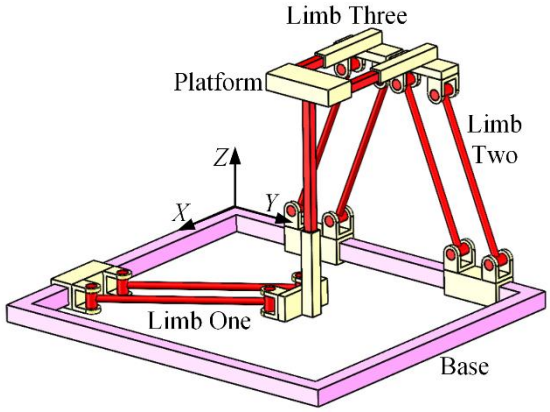

Figure 3-18 Schematic diagram of 3-DOF parallel structure (10)

(ii) Case two: 3R mechanism

The possible structure is 3- P_aRR. The following demonstration is provided.

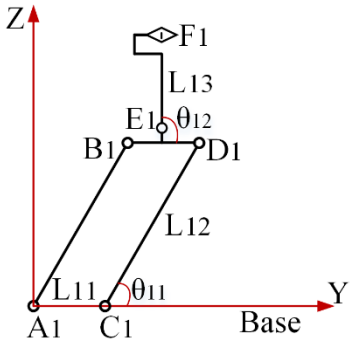

Figure 3-19 The first branch of 3R mechanism

The main points are represented as, $A_1(0,0,0)$, $B_1(0, L_{12}\cos\theta_{11}, L_{12}\sin\theta_{11})$, $C_1(0, L_{11}, 0)$, $D_1(0, L_{11}+L_{12}\cos\theta_{11}, L_{12}\sin\theta_{11})$, $E_1(0, 0.5L_{11}+L_{12}\cos\theta_{11}, L_{12}\sin\theta_{11})$, $F_1(0, 0.5L_{11}+L_{12}\cos\theta_{11}+L_{13}\cos\theta_{12}, L_{12}\sin\theta_{11}+L_{13}\sin\theta_{12})$.

In this case, one possible chain is provided and calculated via screw theory. The kinematic screws of the Pa joint

$$\begin{cases} \$_{A1} = \begin{bmatrix} 1 & 0 & 0; & 0 & 0 & 0 \end{bmatrix}^{\mathrm{T}} \\ \$_{B1} = \begin{bmatrix} 1 & 0 & 0; & 0 & L_{12}\sin\theta_{11} & -L_{12}\cos\theta_{11} \end{bmatrix}^{\mathrm{T}} \\ \$_{C1} = \begin{bmatrix} 1 & 0 & 0; & 0 & 0 & -L_{11} \end{bmatrix}^{\mathrm{T}} \\ \$_{D1} = \begin{bmatrix} 1 & 0 & 0; & 0 & L_{12}\sin\theta_{11} & -L_{11}-L_{12}\cos\theta_{11} \end{bmatrix}^{\mathrm{T}} \end{cases} \tag{3-60}$$

The equivalent screw is computed as

$$\$_{Pa1} = \begin{bmatrix} 0 & 0 & 0; & 0 & \sin\theta_{11} & -\cos\theta_{11} \end{bmatrix}^{\mathrm{T}} \tag{3-61}$$

Equation (3-61) shows the trajectory of this Pa joint is an arc.

The kinematic screws for the remaining joints in this limb

$$\begin{cases} \$_{E1} = \begin{bmatrix} 1 & 0 & 0; & 0 & L_{12}\sin\theta_{11} & -0.5L_{11}-L_{12}\cos\theta_{11} \end{bmatrix}^{\mathrm{T}} \\ \$_{F1} = \begin{bmatrix} 0 & 1 & 0; & -L_{12}\sin\theta_{11}-L_{13}\sin\theta_{12} & 0 & 0 \end{bmatrix}^{\mathrm{T}} \end{cases} \tag{3-62}$$

The reciprocal screws for this limb

$$\begin{cases} \$_{11}^{r} = \begin{bmatrix} 0 & 0 & 0; & 0 & 0 & 1 \end{bmatrix}^{\mathrm{T}} \\ \$_{12}^{r} = \begin{bmatrix} 1 & 0 & 0; & L_{12}\sin\theta_{11}+L_{13}\sin\theta_{12} & 0 & 0 \end{bmatrix}^{\mathrm{T}} \\ \$_{13}^{r} = \begin{bmatrix} 0 & \cos\theta_{11} & \sin\theta_{11}; & 0.5L_{11} & 0 & 0 \end{bmatrix}^{\mathrm{T}} \end{cases} \tag{3-63}$$

The first screw denotes a constraint couple about Z axis. The second screw means a constraint force (parallel to X axis). The last screw stands for a constraint force(parallel to radial direction of the arc path).

This branch constrains two rotations. Therefore, the moving platform could not achieve 3R movement.

(iii) Case three: 1T2R mechanism

The possible structure is 3-P_aRR. The following calculations will verify its mobility. If the first two chains are both $P_{YZ}R_XR_Y$ joint configuration, the permitted translation of these two chains are along Y and Z axes, the permitted rotations of them are about X and Y axes. There are three possible scenarios for the last chain, $P_{YZ}R_XR_Y$ and $P_{XZ}R_YR_X$. If any of them fails to achieve 1T2R movement, the 1T2R mechanism will not be possible.

1) 3-$P_{YZ}R_XR_Y$

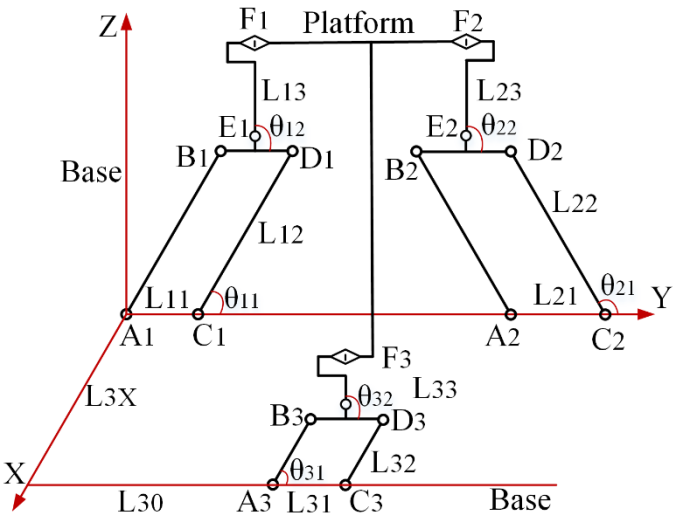

Figure 3-20 The first kind of 1T2R mechanism

The positions of the main points are calculated as, $A_1(0,0,0)$, $B_1(0, L_{12}\cos\theta_{11}, L_{12}\sin\theta_{11})$, $C_1(0, L_{11}, 0)$, $D_1(0, L_{11}+L_{12}\cos\theta_{11}, L_{12}\sin\theta_{11})$, $E_1(0, 0.5L_{11}+L_{12}\cos\theta_{11}, L_{12}\sin\theta_{11})$, $F_1(0, 0.5L_{11}+L_{12}\cos\theta_{11}+L_{13}\cos\theta_{12}, L_{12}\sin\theta_{11}+L_{13}\sin\theta_{12})$, $A_2(0, L_{20}, 0)$, $B_2(0, L_{20}+L_{22}\cos\theta_{21}, L_{22}\sin\theta_{21})$, $C_2(0, L_{20}+L_{21}, 0)$, $D_2(0, L_{20}+L_{21}+L_{22}\cos\theta_{21}, L_{22}\sin\theta_{21})$, $E_2(0, L_{20}+0.5L_{21}+L_{22}\cos\theta_{21}, L_{22}\sin\theta_{21})$, $F_2(0, L_{20}+0.5L_{21}+L_{22}\cos\theta_{21}+L_{23}\cos\theta_{22}, L_{22}\sin\theta_{21}+L_{23}\sin\theta_{22})$, $A_3(L_{3X}, L_{30}, 0)$, $B_3(L_{3X}, L_{30}+L_{32}\cos\theta_{31}, L_{32}\sin\theta_{31})$, $C_3(L_{3X}, L_{30}+L_{31}, 0)$, $D_3(L_{3X}, L_{30}+L_{31}+L_{32}\cos\theta_{31}, L_{32}\sin\theta_{31})$, $E_3(L_{3X}, L_{30}+0.5L_{31}+L_{32}\cos\theta_{31}, L_{32}\sin\theta_{31})$, $F_3(L_{3X}, L_{30}+0.5L_{31}+L_{32}\cos\theta_{31}+L_{33}\cos\theta_{32}, L_{32}\sin\theta_{31}+L_{33}\sin\theta_{32})$.

Kinematic screw systems for three branches

$$\begin{cases} \$_{A1} = \begin{bmatrix} 1 & 0 & 0; & 0 & 0 & 0 \end{bmatrix}^{\mathrm{T}} \\ \$_{B1} = \begin{bmatrix} 1 & 0 & 0; & 0 & L_{12}\sin\theta_{11} & -L_{12}\cos\theta_{11} \end{bmatrix}^{\mathrm{T}} \\ \$_{C1} = \begin{bmatrix} 1 & 0 & 0; & 0 & 0 & -L_{11} \end{bmatrix}^{\mathrm{T}} \\ \$_{D1} = \begin{bmatrix} 1 & 0 & 0; & 0 & L_{12}\sin\theta_{11} & -L_{11}-L_{12}\cos\theta_{11} \end{bmatrix}^{\mathrm{T}} \end{cases} \tag{3-64}$$

$$\begin{cases} \$_{A2}=\begin{bmatrix}1 & 0 & 0; & 0 & 0 & -L_{20}\end{bmatrix}^{\mathrm{T}} \\ \$_{B2}=\begin{bmatrix}1 & 0 & 0; & 0 & L_{22}\sin\theta_{21} & -L_{20}-L_{22}\cos\theta_{21}\end{bmatrix}^{\mathrm{T}} \\ \$_{C2}=\begin{bmatrix}1 & 0 & 0; & 0 & 0 & -L_{20}-L_{21}\end{bmatrix}^{\mathrm{T}} \\ \$_{D2}=\begin{bmatrix}1 & 0 & 0; & 0 & L_{22}\sin\theta_{21} & -L_{20}-L_{21}-L_{22}\cos\theta_{21}\end{bmatrix}^{\mathrm{T}} \end{cases} \tag{3-65}$$

$$\begin{cases} \$_{A3}=\begin{bmatrix}1 & 0 & 0; & 0 & 0 & -L_{30}\end{bmatrix}^{\mathrm{T}} \\ \$_{B3}=\begin{bmatrix}1 & 0 & 0; & 0 & L_{32}\sin\theta_{31} & -L_{30}-L_{32}\cos\theta_{31}\end{bmatrix}^{\mathrm{T}} \\ \$_{C3}=\begin{bmatrix}1 & 0 & 0; & 0 & 0 & -L_{30}-L_{31}\end{bmatrix}^{\mathrm{T}} \\ \$_{D3}=\begin{bmatrix}1 & 0 & 0; & 0 & L_{32}\sin\theta_{31} & -L_{30}-L_{31}-L_{32}\cos\theta_{31}\end{bmatrix}^{\mathrm{T}} \end{cases} \tag{3-66}$$

The equivalent kinematic screws for each Pa joint

$$\$_{Pa1}=\begin{bmatrix}0 & 0 & 0; & 0 & \sin\theta_{11} & -\cos\theta_{11}\end{bmatrix}^{\mathrm{T}} \tag{3-67}$$

$$\$_{Pa2}=\begin{bmatrix}0 & 0 & 0; & 0 & \sin\theta_{21} & -\cos\theta_{21}\end{bmatrix}^{\mathrm{T}} \tag{3-68}$$

$$\$_{Pa3}=\begin{bmatrix}0 & 0 & 0; & 0 & \sin\theta_{31} & -\cos\theta_{31}\end{bmatrix}^{\mathrm{T}} \tag{3-69}$$

The remaining kinematic screws for each limb

$$\begin{cases} \$_{E1}=\begin{bmatrix}1 & 0 & 0; & 0 & L_{12}\sin\theta_{11} & -0.5L_{11}-L_{12}\cos\theta_{11}\end{bmatrix}^{\mathrm{T}} \\ \$_{F1}=\begin{bmatrix}0 & 1 & 0; & -L_{12}\sin\theta_{11}-L_{13}\sin\theta_{12} & 0 & 0\end{bmatrix}^{\mathrm{T}} \end{cases} \tag{3-70}$$

$$\begin{cases} \$_{E2}=\begin{bmatrix}1 & 0 & 0; & 0 & L_{22}\sin\theta_{21} & -L_{20}-0.5L_{11}-L_{22}\cos\theta_{21}\end{bmatrix}^{\mathrm{T}} \\ \$_{F2}=\begin{bmatrix}0 & 1 & 0; & -L_{22}\sin\theta_{21}-L_{23}\sin\theta_{22} & 0 & 0\end{bmatrix}^{\mathrm{T}} \end{cases} \tag{3-71}$$

$$\begin{cases} \$_{E3}=\begin{bmatrix}1 & 0 & 0; & 0 & L_{32}\sin\theta_{31} & -L_{30}-0.5L_{31}-L_{32}\cos\theta_{31}\end{bmatrix}^{\mathrm{T}} \\ \$_{F3}=\begin{bmatrix}0 & 1 & 0; & -L_{32}\sin\theta_{31}-L_{33}\sin\theta_{32} & 0 & L_{3X}\end{bmatrix}^{\mathrm{T}} \end{cases} \tag{3-72}$$

Through the definition of reciprocal screw, the constrain screws for each branch

$$\begin{cases} \$_{11}^{r}=\begin{bmatrix}0 & 0 & 0; & 0 & 0 & 1\end{bmatrix}^{\mathrm{T}} \\ \$_{12}^{r}=\begin{bmatrix}1 & 0 & 0; & L_{12}\sin\theta_{11}+L_{13}\sin\theta_{12} & 0 & 0\end{bmatrix}^{\mathrm{T}} \\ \$_{13}^{r}=\begin{bmatrix}0 & \cos\theta_{11} & \sin\theta_{11}; & 0.5L_{11} & 0 & 0\end{bmatrix}^{\mathrm{T}} \end{cases} \tag{3-73}$$

$$\begin{cases} \$_{21}^{r} = \begin{bmatrix} 0 & 0 & 0; & 0 & 0 & 1 \end{bmatrix}^{\mathrm{T}} \\ \$_{22}^{r} = \begin{bmatrix} 1 & 0 & 0; & L_{22}\sin\theta_{21} + L_{23}\sin\theta_{22} & 0 & 0 \end{bmatrix}^{\mathrm{T}} \\ \$_{23}^{r} = \begin{bmatrix} 0 & \cos\theta_{21} & \sin\theta_{21}; & L_{20} + 0.5L_{21} & 0 & 0 \end{bmatrix}^{\mathrm{T}} \end{cases} \tag{3-74}$$

$$\begin{cases} \$_{31}^{r} = \begin{bmatrix} 0 & 0 & 0; & 0 & 0 & 1 \end{bmatrix}^{\mathrm{T}} \\ \$_{32}^{r} = \begin{bmatrix} 1 & 0 & 0; & L_{32}\sin\theta_{31} + L_{33}\sin\theta_{32} & 0 & 0 \end{bmatrix}^{\mathrm{T}} \\ \$_{33}^{r} = \begin{bmatrix} 0 & \cos\theta_{31} & \sin\theta_{31}; & L_{30} + 0.5L_{31} & 0 & 0 \end{bmatrix}^{\mathrm{T}} \end{cases} \tag{3-75}$$

Therefore, the kinematic screw of the moving platform can be obtained by the reciprocal screw of all constraint screws of each limb. The kinematic screw of the moving platform is null. The moving platform can not translate or rotate.

2) 2-$P_{YZ}R_XR_Y$+$P_{XZ}R_YR_X$

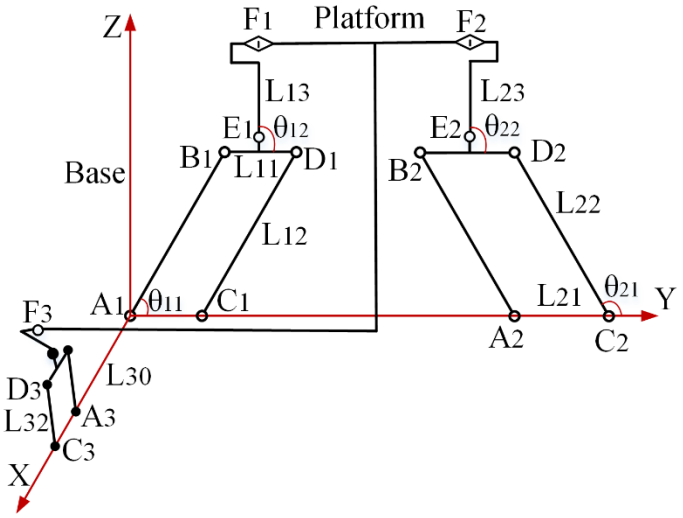

Figure 3-21 The second kind of 1T2R mechanism

(Solid dot denotes the R joint with the axis being parallel to Y axis)

The first chain and second chain are the same with that of 3-$P_{YZ}R_XR_Y$. Therefore, only the third chain is provided below. The positions for main points are listed as $A_3(L_{30},0,0)$, $B_3(L_{30}+L_{32}\cos\theta_{31},0,L_{32}\sin\theta_{31})$, $C_3(L_{30}+L_{31},0,0)$, $D_3(L_{30}+L_{31}+L_{32}\cos\theta_{31},0,L_{32}\sin\theta_{31})$, $E_3(L_{30}+0.5L_{31}+L_{32}\cos\theta_{31},0,L_{32}\sin\theta_{31})$, $F_3(L_{30}+0.5L_{31}+L_{32}\cos\theta_{31}+L_{33}\cos\theta_{32},0,L_{32}\sin\theta_{31}+L_{33}\sin\theta_{32})$.

The kinematic screws for the P_a joint in the third limb

$$\begin{cases} \$_{A3} = \left[0 \quad 1 \quad 0; \quad 0 \quad 0 \quad -L_{30}\right]^{\mathrm{T}} \\ \$_{B3} = \left[0 \quad 1 \quad 0; \quad -L_{32}\sin\theta_{31} \quad 0 \quad -L_{30} - L_{32}\cos\theta_{31}\right]^{\mathrm{T}} \\ \$_{C3} = \left[0 \quad 1 \quad 0; \quad 0 \quad 0 \quad L_{30} + L_{31}\right]^{\mathrm{T}} \\ \$_{D3} = \left[0 \quad 1 \quad 0; \quad -L_{32}\sin\theta_{31} \quad 0 \quad L_{30} + L_{31} + L_{32}\cos\theta_{31}\right]^{\mathrm{T}} \end{cases} \tag{3-76}$$

The equivalent kinematic screw for the P_a joint

$$\$_{Pa3} = \left[0 \quad 0 \quad 0; \quad \sin\theta_{31} \quad 0 \quad -\cos\theta_{31}\right]^{\mathrm{T}} \tag{3-77}$$

The kinematic screws of the following two revolute joints

$$\begin{cases} \$_{E3} = \left[0 \quad 1 \quad 0; \quad -L_{32}\sin\theta_{31} \quad 0 \quad L_{30} + 0.5L_{31} + L_{32}\cos\theta_{31}\right]^{\mathrm{T}} \\ \$_{F3} = \left[1 \quad 0 \quad 0; \quad 0 \quad L_{32}\sin\theta_{31} + L_{33}\sin\theta_{32} \quad 0\right]^{\mathrm{T}} \end{cases} \tag{3-78}$$

The above equations form the kinematic screw system of the third limb. The reciprocal screws

$$\begin{cases} \$_{31}^{r} = \left[0 \quad 0 \quad 0; \quad 0 \quad 0 \quad 1\right]^{\mathrm{T}} \\ \$_{32}^{r} = \left[0 \quad 1 \quad 0; \quad -L_{32}\sin\theta_{31} - L_{33}\sin\theta_{32} \quad 0 \quad 0\right]^{\mathrm{T}} \\ \$_{33}^{r} = \left[c\cos\theta_{31} \quad 0 \quad \sin\theta_{31}; \quad 0 \quad -L_{30} - 0.5L_{31} \quad 0\right]^{\mathrm{T}} \end{cases} \tag{3-79}$$

Combined with the constraint screws in Equation (3-79), the kinematic screw of the moving platform can be calculated and it is null. It shows the moving platform can not move.

The results of the 3-$P_{YZ}R_XR_Y$ and 2-$P_{YZ}R_XR_Y$+$P_{XZ}R_YR_X$ are both null. The 1T2R mechanism can not be constructed.

(iv) Case four: 2T1R mechanism

limbs:

$$\begin{cases} \mathrm{P}_X - \mathrm{P}_{XY} - R_Z \\ \mathrm{P}_Y - \mathrm{P}_{XY} - R_Z \end{cases} \tag{3-80}$$

Limbs shown in matrix form

$$\left\{\begin{bmatrix} \mathrm{P}_X & \mathrm{P}_{XY} & - \\ R_Z & - & - \\ - & - & - \end{bmatrix} \begin{bmatrix} \mathrm{P}_X & \mathrm{P}_{XY} & - \\ R_Z & \mathrm{P}_Y & - \\ - & - & - \end{bmatrix}\right. \tag{3-81}$$

The limb can be represented as Q_i. In enumeration, there will be $Q_i^3 + Q_i^2 Q_j = 2 + C_2^1 = 4$ kinds of mechanism. They are all planar parallel mechanisms. The same matrices are ones with similar cell configuration. At last, there are 2 kinds of feasible Mechanisms. These matrices and corresponding parallel structures are listed below.

$$\left[\begin{array}{ccc:ccc:ccc} \mathrm{P}_X & \mathrm{P}_{XY} & - & \mathrm{P}_X & \mathrm{P}_{XY} & - & \mathrm{P}_X & \mathrm{P}_{XY} & - \\ R_Z & - & - & R_Z & - & - & R_Z & - & - \\ - & - & - & - & - & - & - & - & - \end{array}\right] \tag{3-82}$$

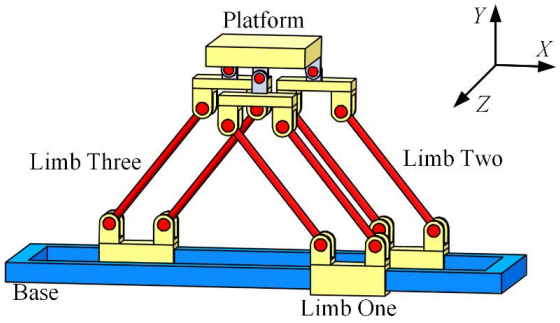

Figure 3-22 Schematic diagram of 2T1R parallel structure (1)

Feature: There are one P_3 joint (P_X), one R_3 joint (R_Z) and three identical P_a joints (P_{XY}). Three P_a joints (P_{XY}) are related to P_3 joint (P_X) but irrelevant to R_3 joint (R_X). The translational direction (X axis) of P_3 joint (P_X) and the rotational axis (Z direction) of R_3 joint (R_X) are not parallel.

$$\left[\begin{array}{ccc:ccc:ccc} \mathrm{P}_X & \mathrm{P}_{XY} & - & \mathrm{P}_X & \mathrm{P}_{XY} & - & - & \mathrm{P}_{XY} & - \\ R_Z & \mathrm{P}_Y & - & R_Z & - & - & R_Z & - & - \\ - & - & - & - & - & - & - & - & - \end{array}\right] \tag{3-83}$$

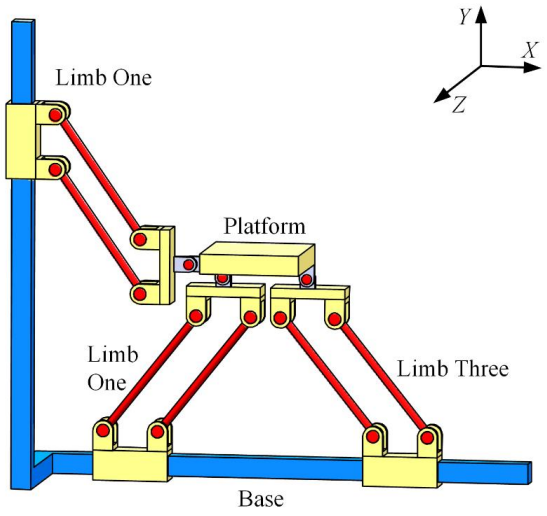

Figure 3-23 Schematic diagram of 2T1R parallel structure (2)

Feature: There are one P_1 joint (P_Y), one P_2 joint (P_X), one R_3 joint (R_Z) and three identical P_a joints (P_{XY}). Three P_a joints (P_{XY}) are both related to P_1 joint (P_Y) and P_2 joint (P_X) but irrelevant to R_3 joint (R_Z).

A sample is provided below to demonstrate the above 2T1R mechanisms can not have anther rotation (parallel to *Y* axis). In the following figure, the mechanism can move in the YOZ plane, but the rotation for each chain is parallel to Y axis.

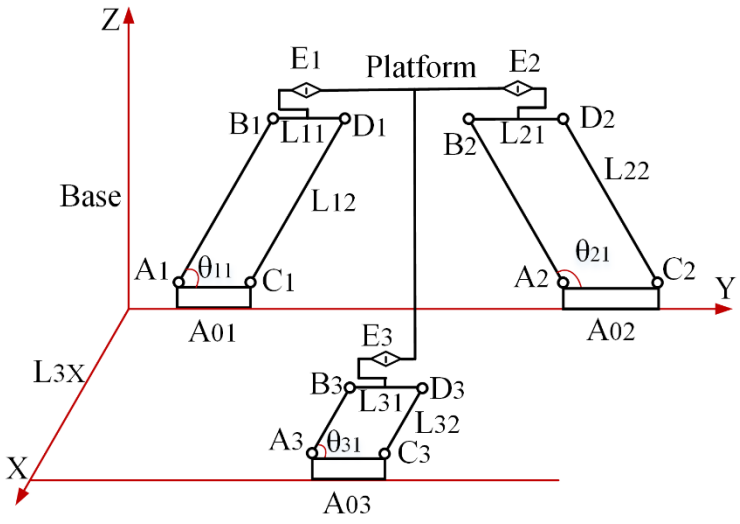

Figure 3-24 Diagram of 3-DOF parallel structure

The coordinates of these points are listed as: $A_{01}(0, x_1, 0)$, $A_1(0, x_1 - 0.5L_{11}, 0)$, $B_1(0, x_1 - 0.5L_{11} + L_{12}\cos\theta_{11}, L_{12}\sin\theta_{11})$, $C_1(0, x_1 + 0.5L_{11}, 0)$,

$D_1(0, x_1 + 0.5L_{11} + L_{12}\cos\theta_{11}, L_{12}\sin\theta_{11})$, $E_1(0, x_1 + L_{12}\cos\theta_{11}, L_{12}\sin\theta_{11})$, $A_{02}(0, x_2, 0)$, $A_2(0, x_2 - 0.5L_{21}, 0)$, $B_2(0, x_2 - 0.5L_{21} + L_{22}\cos\theta_{21}, L_{22}\sin\theta_{21})$, $C_2(0, x_2 + 0.5L_{21}, 0)$, $D_2(0, x_2 + 0.5L_{21} + L_{22}\cos\theta_{21}, L_{22}\sin\theta_{21})$, $E_2(0, x_2 + L_{22}\cos\theta_{21}, L_{22}\sin\theta_{21})$, $A_{03}(L_{3X}, x_3, 0)$, $A_3(L_{3X}, x_3 - 0.5L_{31}, 0)$, $B_3(L_{3X}, x_3 - 0.5L_{31} + L_{32}\cos\theta_{31}, L_{32}\sin\theta_{31})$, $C_3(L_{3X}, x_3 + 0.5L_{31}, 0)$, $D_3(L_{3X}, x_3 + 0.5L_{31} + L_{32}\cos\theta_{31}, L_{32}\sin\theta_{31})$, $E_3(L_{3X}, x_3 + L_{32}\cos\theta_{31}, L_{32}\sin\theta_{31})$,

The kinematic screws of Pa joint in each limb

$$\begin{cases} \$_{A1} = [1 \quad 0 \quad 0; \quad 0 \quad 0 \quad 0.5L_{11} - x_1]^{\mathrm{T}} \\ \$_{B1} = [1 \quad 0 \quad 0; \quad 0 \quad L_{12}\sin\theta_{11} \quad 0.5L_{11} - x_1 - L_{12}\cos\theta_{11}]^{\mathrm{T}} \\ \$_{C1} = [1 \quad 0 \quad 0; \quad 0 \quad 0 \quad -0.5L_{11} - x_1]^{\mathrm{T}} \\ \$_{D1} = [1 \quad 0 \quad 0; \quad 0 \quad L_{12}\sin\theta_{11} \quad -0.5L_{11} - x_1 - L_{12}\cos\theta_{11}]^{\mathrm{T}} \end{cases} \tag{3-84}$$

$$\begin{cases} \$_{A2} = [1 \quad 0 \quad 0; \quad 0 \quad 0 \quad 0.5L_{21} - x_2]^{\mathrm{T}} \\ \$_{B2} = [1 \quad 0 \quad 0; \quad 0 \quad L_{22}\sin\theta_{21} \quad 0.5L_{21} - x_2 - L_{22}\cos\theta_{21}]^{\mathrm{T}} \\ \$_{C2} = [1 \quad 0 \quad 0; \quad 0 \quad 0 \quad -0.5L_{21} - x_2]^{\mathrm{T}} \\ \$_{D2} = [1 \quad 0 \quad 0; \quad 0 \quad L_{22}\sin\theta_{21} \quad -0.5L_{21} - x_2 - L_{22}\cos\theta_{21}]^{\mathrm{T}} \end{cases} \tag{3-85}$$

$$\begin{cases} \$_{A3} = [1 \quad 0 \quad 0; \quad 0 \quad 0 \quad 0.5L_{31} - x_3]^{\mathrm{T}} \\ \$_{B3} = [1 \quad 0 \quad 0; \quad 0 \quad L_{32}\sin\theta_{31} \quad 0.5L_{31} - x_3 - L_{32}\cos\theta_{31}]^{\mathrm{T}} \\ \$_{C3} = [1 \quad 0 \quad 0; \quad 0 \quad 0 \quad -0.5L_{31} - x_3]^{\mathrm{T}} \\ \$_{D3} = [1 \quad 0 \quad 0; \quad 0 \quad L_{32}\sin\theta_{31} \quad -0.5L_{31} - x_3 - L_{32}\cos\theta_{31}]^{\mathrm{T}} \end{cases} \tag{3-86}$$

The equivalent kinematic screw of the Pa joint in each chain

$$\$_{Pa1} = [0 \quad 0 \quad 0; \quad 0 \quad \sin\theta_{11} \quad -\cos\theta_{11}]^{\mathrm{T}} \tag{3-87}$$

$$\$_{Pa2} = [0 \quad 0 \quad 0; \quad 0 \quad \sin\theta_{21} \quad -\cos\theta_{21}]^{\mathrm{T}} \tag{3-88}$$

$$\$_{Pa3} = [0 \quad 0 \quad 0; \quad 0 \quad \sin\theta_{31} \quad -\cos\theta_{31}]^{\mathrm{T}} \tag{3-89}$$

The kinematic screws for the remaining joints of each limb

$$\begin{cases} \$_{A01} = [0 \quad 0 \quad 0; \quad 0 \quad 1 \quad 0]^{\mathrm{T}} \\ \$_{E1} = [0 \quad 1 \quad 0; \quad -L_{12}\sin\theta_{11} \quad 0 \quad 0]^{\mathrm{T}} \end{cases} \tag{3-90}$$

$$\begin{cases} \$_{A02} = \begin{bmatrix} 0 & 0 & 0; & 0 & 1 & 0 \end{bmatrix}^{\mathrm{T}} \\ \$_{E2} = \begin{bmatrix} 0 & 1 & 0; & -L_{22}\sin\theta_{21} & 0 & 0 \end{bmatrix}^{\mathrm{T}} \end{cases} \tag{3-91}$$

$$\begin{cases} \$_{A03} = \begin{bmatrix} 0 & 0 & 0; & 0 & 1 & 0 \end{bmatrix}^{\mathrm{T}} \\ \$_{E3} = \begin{bmatrix} 0 & 1 & 0; & -L_{32}\sin\theta_{31} & 0 & 0 \end{bmatrix}^{\mathrm{T}} \end{cases} \tag{3-92}$$

The corresponding reciprocal screws for each limb

$$\begin{cases} \$_{11}^{r} = \begin{bmatrix} 0 & 0 & 0; & 0 & 0 & 1 \end{bmatrix}^{\mathrm{T}} \\ \$_{12}^{r} = \begin{bmatrix} 0 & 0 & 0; & 1 & 0 & 0 \end{bmatrix}^{\mathrm{T}} \\ \$_{13}^{r} = \begin{bmatrix} 1 & 0 & 0; & 0 & L_{12}\sin\theta_{11} & 0 \end{bmatrix}^{\mathrm{T}} \end{cases} \tag{3-93}$$

$$\begin{cases} \$_{21}^{r} = \begin{bmatrix} 0 & 0 & 0; & 0 & 0 & 1 \end{bmatrix}^{\mathrm{T}} \\ \$_{22}^{r} = \begin{bmatrix} 0 & 0 & 0; & 1 & 0 & 0 \end{bmatrix}^{\mathrm{T}} \\ \$_{23}^{r} = \begin{bmatrix} 1 & 0 & 0; & 0 & L_{22}\sin\theta_{21} & 0 \end{bmatrix}^{\mathrm{T}} \end{cases} \tag{3-94}$$

$$\begin{cases} \$_{31}^{r} = \begin{bmatrix} 0 & 0 & 0; & 0 & 0 & 1 \end{bmatrix}^{\mathrm{T}} \\ \$_{32}^{r} = \begin{bmatrix} 0 & 0 & 0; & 1 & 0 & 0 \end{bmatrix}^{\mathrm{T}} \\ \$_{33}^{r} = \begin{bmatrix} 1 & 0 & 0; & 0 & L_{32}\sin\theta_{31} & 0 \end{bmatrix}^{\mathrm{T}} \end{cases} \tag{3-95}$$

The kinematic screw system for the moving platform

$$\begin{cases} \$_{m1} = \begin{bmatrix} 0 & 0 & 0; & 0 & 1 & 0 \end{bmatrix}^{\mathrm{T}} \\ \$_{m2} = \begin{bmatrix} 0 & 0 & 0; & 0 & 0 & 1 \end{bmatrix}^{\mathrm{T}} \end{cases} \tag{3-96}$$

The Equation (3-69) denotes the moving platform can move along Y and Z axes. It can not conduct 2T1R motion.

Even the rotational axis of joint E in each chain is parallel to Z axis, the same result will be obtained if applying for the above procedure. Since these calculations are similar, the calculation process is not provided. The result is still two translations along Y and Z axes. The moving platform can not achieve 2T1R motion. These calculations also prove 2T1R mechanism is a planar mechanism and only two feasible branches are provided in this case.

3.3.3 Four-DOF parallel mechanism

(i) Case one: 3T1R mechanism

The possible limbs are:

$$\begin{cases} \mathrm{P}_X - \mathrm{P}_{XZ} - \mathrm{P}_Y - R_X \\ \mathrm{P}_X - \mathrm{P}_{YZ} - \mathrm{P}_Y - R_X \\ \mathrm{P}_X - \mathrm{P}_{XY} - \mathrm{P}_Z - R_X \\ \mathrm{P}_X - \mathrm{P}_{YZ} - \mathrm{P}_Z - R_X \\ \mathrm{P}_Y - \mathrm{P}_{XY} - \mathrm{P}_Z - R_X \\ \mathrm{P}_Y - \mathrm{P}_{XZ} - \mathrm{P}_Z - R_X \end{cases} \tag{3-97}$$

$$\begin{cases} \mathrm{P}_X - \mathrm{P}_{XZ} - \mathrm{P}_Y - R_Y \\ \mathrm{P}_X - \mathrm{P}_{YZ} - \mathrm{P}_Y - R_Y \\ \mathrm{P}_X - \mathrm{P}_{XY} - \mathrm{P}_Z - R_Y \\ \mathrm{P}_X - \mathrm{P}_{YZ} - \mathrm{P}_Z - R_Y \\ \mathrm{P}_Y - \mathrm{P}_{XY} - \mathrm{P}_Z - R_Y \\ \mathrm{P}_Y - \mathrm{P}_{XZ} - \mathrm{P}_Z - R_Y \end{cases} \tag{3-98}$$

$$\begin{cases} \mathrm{P}_X - \mathrm{P}_{XZ} - \mathrm{P}_Y - R_Z \\ \mathrm{P}_X - \mathrm{P}_{YZ} - \mathrm{P}_Y - R_Z \\ \mathrm{P}_X - \mathrm{P}_{XY} - \mathrm{P}_Z - R_Z \\ \mathrm{P}_X - \mathrm{P}_{YZ} - \mathrm{P}_Z - R_Z \\ \mathrm{P}_Y - \mathrm{P}_{XY} - \mathrm{P}_Z - R_Z \\ \mathrm{P}_Y - \mathrm{P}_{XZ} - \mathrm{P}_Z - R_Z \end{cases} \tag{3-99}$$

Limbs are shown in matrix form, corresponding to Equations (3-97) to (3-99),

$$\begin{bmatrix} \mathrm{P}_X & - & \mathrm{P}_{XZ} \\ - & \mathrm{P}_Y & - \\ - & R_X & - \\ - & - & - \\ - & - & - \\ - & - & - \end{bmatrix}, \begin{bmatrix} \mathrm{P}_X & - & - \\ - & \mathrm{P}_Y & \mathrm{P}_{YZ} \\ - & R_X & - \\ - & - & - \\ - & - & - \\ - & - & - \end{bmatrix}, \begin{bmatrix} \mathrm{P}_X & \mathrm{P}_{XY} & - \\ - & - & - \\ - & R_X & \mathrm{P}_Z \\ - & - & - \\ - & - & - \\ - & - & - \end{bmatrix}$$

$$\begin{bmatrix} \mathrm{P}_X & - & - \\ - & - & \mathrm{P}_{YZ} \\ - & R_X & \mathrm{P}_Z \\ - & - & - \\ - & - & - \\ - & - & - \end{bmatrix}, \begin{bmatrix} - & \mathrm{P}_{XY} & - \\ - & \mathrm{P}_Y & - \\ - & R_X & \mathrm{P}_Z \\ - & - & - \\ - & - & - \\ - & - & - \end{bmatrix}, \begin{bmatrix} - & - & \mathrm{P}_{XZ} \\ - & \mathrm{P}_Y & - \\ - & R_X & \mathrm{P}_Z \\ - & - & - \\ - & - & - \\ - & - & - \end{bmatrix} \tag{3-100}$$

$$\begin{bmatrix} \mathrm{P}_X & - & \mathrm{P}_{XZ} \\ - & \mathrm{P}_Y & - \\ R_Y & - & - \\ - & - & - \\ - & - & - \\ - & - & - \end{bmatrix}, \begin{bmatrix} \mathrm{P}_X & - & - \\ - & \mathrm{P}_Y & \mathrm{P}_{YZ} \\ R_Y & - & - \\ - & - & - \\ - & - & - \\ - & - & - \end{bmatrix}, \begin{bmatrix} \mathrm{P}_X & \mathrm{P}_{XY} & - \\ - & - & - \\ R_Y & - & \mathrm{P}_Z \\ - & - & - \\ - & - & - \\ - & - & - \end{bmatrix}$$

$$\begin{bmatrix} \mathrm{P}_X & - & - \\ - & - & \mathrm{P}_{YZ} \\ R_Y & - & \mathrm{P}_Z \\ - & - & - \\ - & - & - \\ - & - & - \end{bmatrix}, \begin{bmatrix} - & \mathrm{P}_{XY} & - \\ - & \mathrm{P}_Y & - \\ R_Y & - & \mathrm{P}_Z \\ - & - & - \\ - & - & - \\ - & - & - \end{bmatrix}, \begin{bmatrix} - & - & \mathrm{P}_{XZ} \\ - & \mathrm{P}_Y & - \\ R_Y & - & \mathrm{P}_Z \\ - & - & - \\ - & - & - \\ - & - & - \end{bmatrix} \quad (3\text{-}101)$$

$$\begin{bmatrix} \mathrm{P}_X & - & \mathrm{P}_{XZ} \\ R_Z & \mathrm{P}_Y & - \\ - & - & - \\ - & - & - \\ - & - & - \\ - & - & - \end{bmatrix}, \begin{bmatrix} \mathrm{P}_X & - & - \\ R_Z & \mathrm{P}_Y & \mathrm{P}_{YZ} \\ - & - & - \\ - & - & - \\ - & - & - \\ - & - & - \end{bmatrix}, \begin{bmatrix} \mathrm{P}_X & \mathrm{P}_{XY} & - \\ R_Z & - & - \\ - & - & \mathrm{P}_Z \\ - & - & - \\ - & - & - \\ - & - & - \end{bmatrix}$$

$$\begin{bmatrix} \mathrm{P}_X & - & - \\ R_Z & - & \mathrm{P}_{YZ} \\ - & - & \mathrm{P}_Z \\ - & - & - \\ - & - & - \\ - & - & - \end{bmatrix}, \begin{bmatrix} - & \mathrm{P}_{XY} & - \\ R_Z & \mathrm{P}_Y & - \\ - & - & \mathrm{P}_Z \\ - & - & - \\ - & - & - \\ - & - & - \end{bmatrix}, \begin{bmatrix} - & - & \mathrm{P}_{XZ} \\ R_Z & \mathrm{P}_Y & - \\ - & - & \mathrm{P}_Z \\ - & - & - \\ - & - & - \\ - & - & - \end{bmatrix} \quad (3\text{-}102)$$

The limb can be represented as Q_i. In enumeration, there will be $3\times(Q_i^4+Q_i^3Q_j+Q_i^2Q_j^2+Q_i^2Q_jQ_k+Q_iQ_jQ_kQ_l)=3\times(6+A_6^2+C_6^2+6\times C_5^2+C_6^4)=378$ kinds of matrices. The same matrices are ones with similar cell configuration. At last, there are 24 kinds of reliable matrices. These matrices and corresponding parallel structures are listed below.

$$\left[\begin{array}{ccc:ccc} P_X & - & P_{XZ} & P_X & - & P_{XZ} \\ - & P_Y & - & - & P_Y & - \\ - & R_X & - & - & R_X & - \\ P_X & - & P_{XZ} & P_X & - & P_{XZ} \\ - & P_Y & - & - & P_Y & - \\ - & R_X & - & - & R_X & - \end{array}\right] \tag{3-103}$$

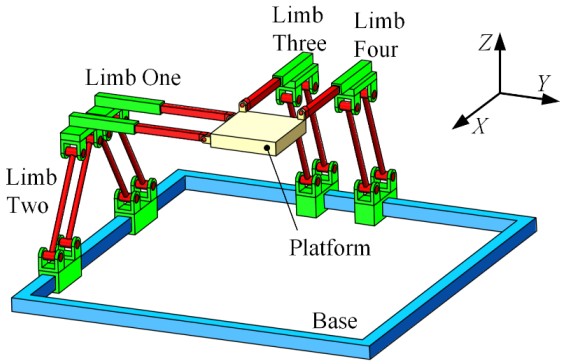

Figure 3-25 Schematic diagram of 4-DOF parallel structure (1)

Feature: There are two P_4 joints (P_X, P_Y), one R_4 joint (R_X) and four identical P_a joints (P_{XZ}). Four P_a joints (P_{XZ}) are related to P_4 joint (P_X). No P_a joint is related to P_4 joint (P_Y). The translational direction of P_4 joint (P_X) and the rotational axis of R_4 joint (R_X) are parallel (*X* axis).

$$\left[\begin{array}{ccc:ccc} P_X & - & P_{XZ} & P_X & - & P_{XZ} \\ - & P_Y & P_{YZ} & - & P_Y & - \\ - & R_X & - & - & R_X & - \\ P_X & - & P_{XZ} & P_X & - & - \\ - & P_Y & - & - & P_Y & - \\ - & R_X & - & - & R_X & - \end{array}\right] \tag{3-104}$$

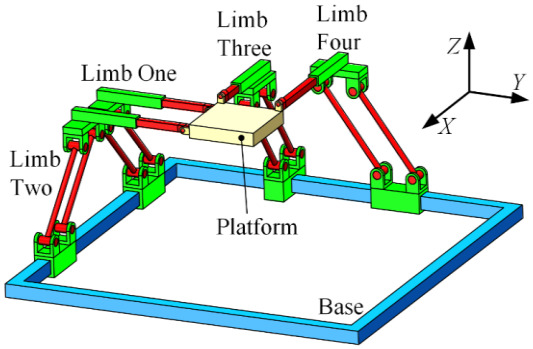

Figure 3-26 Schematic diagram of 4-DOF parallel structure (2)

Feature: There are two P_4 joints (P_X, P_Y), one R_4 joint (R_X), one P_a joint (P_{YZ}) and three identical P_a joints (P_{XZ}). Three P_a joints (P_{XZ}) are related to P_4 joint (P_X). One P_a joint (P_{YZ}) is related to P_4 joint (P_Y). The translational direction of P_4 joint (P_X) and the rotational axis of R_4 joint (R_X) are parallel (X axis).

$$\left[\begin{array}{ccc:ccc} P_X & P_{XY} & P_{XZ} & P_X & - & P_{XZ} \\ - & P_Y & - & - & P_Y & - \\ - & R_X & - & - & R_X & - \\ P_X & - & P_{XZ} & P_X & - & - \\ - & P_Y & - & - & P_Y & - \\ - & R_X & - & - & R_X & - \end{array}\right] \tag{3-105}$$

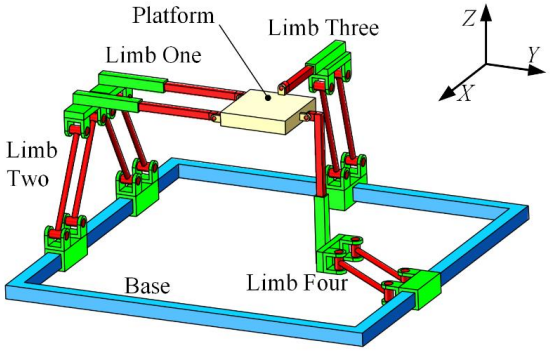

Figure 3-27 Schematic diagram of 4-DOF parallel structure (3)

Feature: There are two P_4 joints (P_X, P_Y), one R_4 joint (R_X), one P_a joint (P_{XY}) and three identical P_a joints (P_{XZ}). Four P_a joints (P_{XY}, P_{XZ}) are related to P_4 joint (P_X). One P_a joint (P_{XY}) is related to P_4 joint (P_Y). The translational direction of P_4 joint (P_X) and the rotational axis of R_4 joint (R_X) are parallel (X axis).

$$\left[\begin{array}{ccc:ccc} P_X & - & P_{XZ} & P_X & - & P_{XZ} \\ - & P_Y & P_{YZ} & - & P_Y & - \\ - & R_X & P_Z & - & R_X & - \\ P_X & - & P_{XZ} & P_X & - & - \\ - & P_Y & - & - & - & - \\ - & R_X & - & - & R_X & - \end{array}\right] \tag{3-106}$$

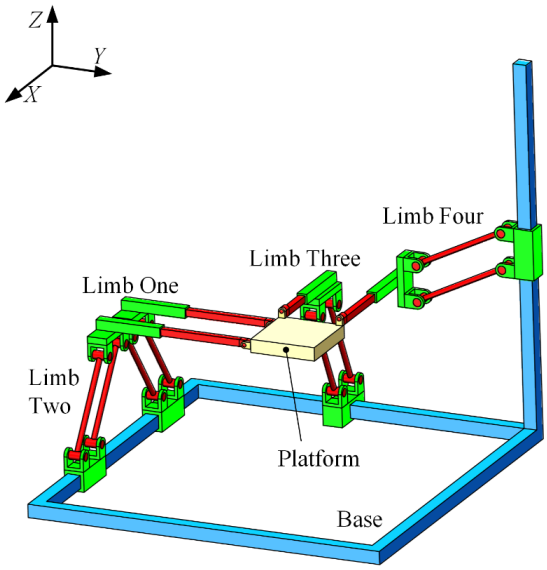

Figure 3-28 Schematic diagram of 4-DOF parallel structure (4)

Feature: There are one P_1 joint (P_Z), one P_3 joint (P_Y), one P_4 joint (P_X), one R_4 joint (R_X), one P_a joint (P_{YZ}) and three identical P_a joints (P_{XZ}). Four P_a joints (P_{XZ}, P_{YZ}) are related to P_1 joint (P_Z). One P_a joint (P_{YZ}) is related to P_3 joint (P_Y). Three P_a joints (P_{XY}) are related to P_4 joint (P_X). The translational direction of P_4 joint (P_X) and the rotational axis of R_4 joint (R_X) are parallel (X axis).

$$\left[\begin{array}{ccc:ccc} P_X & P_{XY} & P_{XZ} & P_X & - & P_{XZ} \\ - & P_Y & - & - & P_Y & - \\ - & R_X & P_Z & - & R_X & - \\ P_X & - & P_{XZ} & P_X & - & - \\ - & P_Y & - & - & - & - \\ - & R_X & - & - & R_X & - \end{array}\right] \tag{3-107}$$

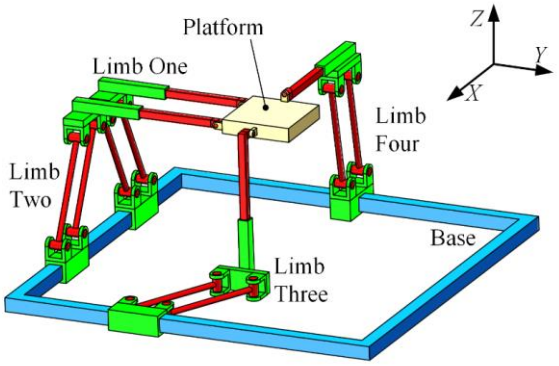

Figure 3-29 Schematic diagram of 4-DOF parallel structure (5)

Feature: There are one P_1 joint (P_Z), one P_3 joint (P_Y), one P_4 joint (P_X), one R_4 joint (R_X), one P_a joint (P_{XY}) and three identical P_a joints (P_{XZ}). Three P_a joints (P_{XZ}) are related to P_1 joint (P_Z). One P_a joint (P_{XY}) is related to P_3 joint (P_Y). Four P_a joints (P_{XY}, P_{XZ}) are related to P_4 joint (P_X). The translational direction of P_4 joint (P_X) and the rotational axis of R_4 joint (R_X) are parallel (X axis).

$$\left[\begin{array}{ccc|ccc} P_X & - & P_{XZ} & P_X & - & P_{XZ} \\ - & P_Y & - & - & P_Y & - \\ - & R_X & P_Z & - & R_X & - \\ P_X & - & P_{XZ} & - & - & P_{XZ} \\ - & P_Y & - & - & P_Y & - \\ - & R_X & - & - & R_X & - \end{array}\right] \tag{3-108}$$

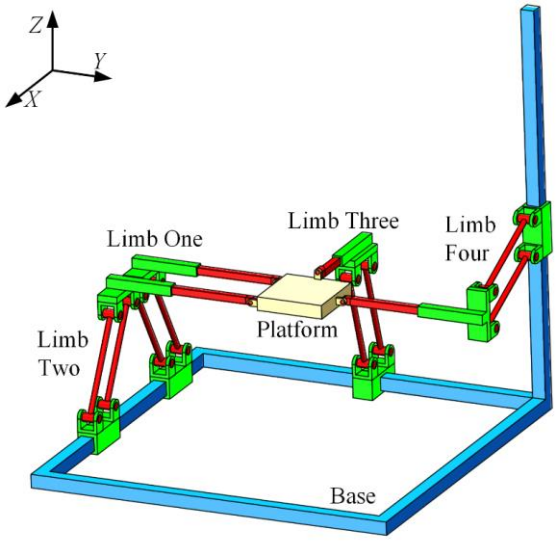

Figure 3-30 Schematic diagram of 4-DOF parallel structure (6)

Feature: There are one P_1 joint (P_Z), one P_3 joint (P_X), one P_4 joint (P_Y), one R_4 joint (R_X) and four identical P_a joints (P_{XZ}). Four P_a joints (P_{XZ}) are related to P_1 joint (P_Z). Four P_a joints (P_{XZ}) are related to P_3 joint (P_X). Zero P_a joint is related to P_4 joint (P_Y). The translational direction of P_3 joint (P_X) and the rotational axis of R_4 joint (R_X) are parallel (X axis).

$$\left[\begin{array}{cccccc} P_X & - & P_{XZ} & P_X & - & - \\ - & P_Y & P_{YZ} & - & P_Y & - \\ - & R_X & - & - & R_X & - \\ P_X & - & P_{XZ} & P_X & - & - \\ - & P_Y & P_{YZ} & - & P_Y & - \\ - & R_X & - & - & R_X & - \end{array}\right] \tag{3-109}$$

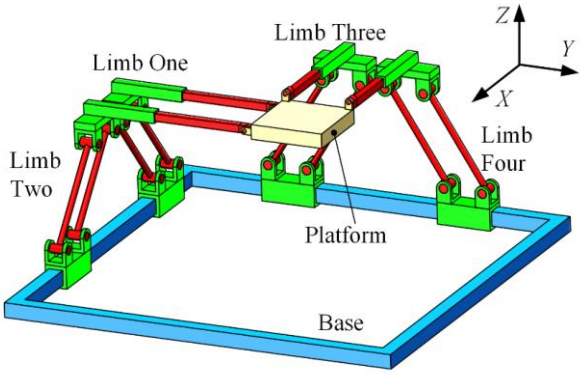

Figure 3-31 Schematic diagram of 4-DOF parallel structure (7)

Feature: There are two P_4 joints (P_X, P_Y), one R_4 joint (R_X), two same P_a joints (P_{XZ}) and two same P_a joints (P_{YZ}). Two P_a joints (P_{XZ}) are related to P_4 joint (P_X). Two P_a joints (P_{YZ}) are related to P_4 joint (P_Y). The translational direction of P_4 joint (P_X) and the rotational axis of R_4 joint (R_X) are parallel (X axis).

$$\left[\begin{array}{cccccc} P_X & P_{XY} & P_{XZ} & P_X & - & - \\ - & P_Y & - & - & - & - \\ - & R_X & P_Z & - & R_X & - \\ P_X & P_{XY} & P_{XZ} & P_X & - & - \\ - & P_Y & - & - & - & - \\ - & R_X & P_Z & - & R_X & - \end{array}\right] \tag{3-110}$$

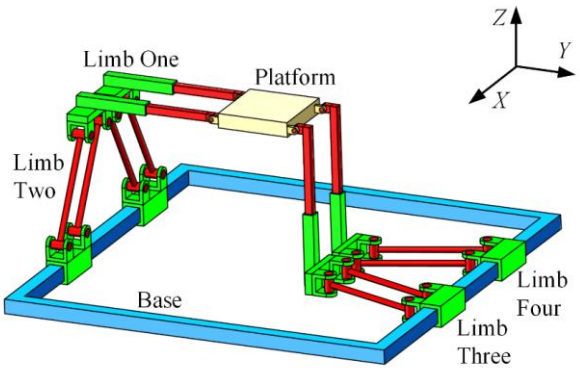

Figure 3-32 Schematic diagram of 4-DOF parallel structure (8)

Feature: There are two P_2 joints (P_Y, P_Z), one P_4 joints (P_X), one R_4 joint (R_X), two same P_a joints (P_{XY}) and two same P_a joints (P_{XZ}). Two Pa joints (P_{XY}) are related to P_2 joint (P_Y). Two P_a joints (P_{XZ}) are related to P_2 joint (P_Z). Four P_a joints (P_{XY}, P_{XZ}) are related to P_4 joint (P_X). The translational direction of P_4 joint (P_X) and the rotational axis of R_4 joint (R_X) are parallel (X axis).

$$\left[\begin{array}{ccc:ccc} P_X & - & P_{XZ} & P_X & - & - \\ - & P_Y & P_{YZ} & - & - & - \\ - & R_X & P_Z & - & R_X & - \\ P_X & - & P_{XZ} & P_X & - & - \\ - & P_Y & P_{YZ} & - & - & - \\ - & R_X & P_Z & - & R_X & - \end{array}\right] \tag{3-111}$$

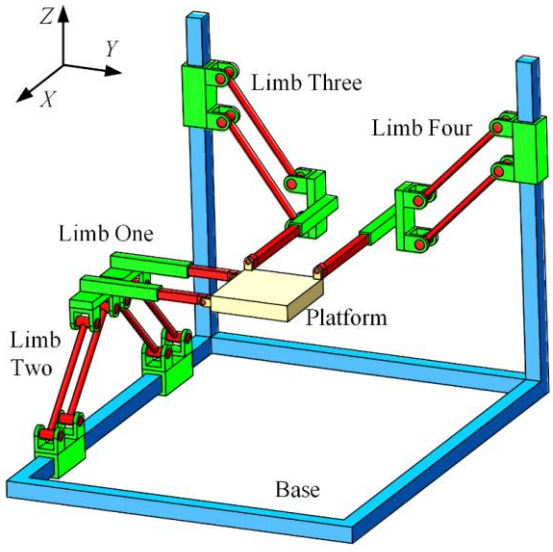

Figure 3-33 Schematic diagram of 4-DOF parallel structure (9)

Feature: There are two P_2 joints (P_Y, P_Z), one P_4 joints (P_X), one R_4 joint (R_X), two same P_a joints (P_{XZ}) and two same P_a joints (P_{YZ}). Two P_a joints (P_{YZ}) are related to P_2 joint (P_Y). Four P_a joints (P_{XZ}, P_{YZ}) are related to P_2 joint (P_Z). Two P_a joints (P_{XZ}) are related to P_4 joint (P_X). The translational direction of P_4 joint (P_X) and the rotational axis of R_4 joint (R_X) are parallel (X axis).

$$\left[\begin{array}{ccc:ccc} P_X & - & P_{XZ} & - & - & P_{XZ} \\ - & P_Y & - & - & P_Y & - \\ - & R_X & P_Z & - & R_X & - \\ P_X & - & P_{XZ} & - & - & P_{XZ} \\ - & P_Y & - & - & P_Y & - \\ - & R_X & P_Z & - & R_X & - \end{array}\right] \tag{3-112}$$

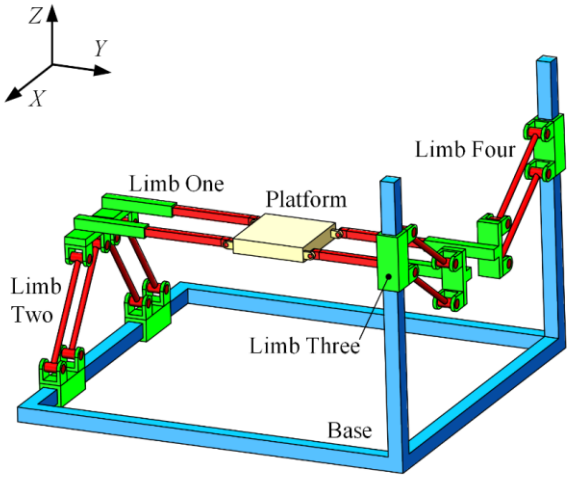

Figure 3-34 Schematic diagram of 4-DOF parallel structure (10)

Feature: There are two P_2 joints (P_X, P_Z), one P_4 joints (P_Y), one R_4 joint (R_X) and four identical P_a joints (P_{XZ}). Four P_a joints (P_{XZ}) are related to both P_2 joint (P_X) and P_2 joint (P_Z). There is no P_a joint relating to P_4 joint (P_Y). The translational direction of P_2 joint (P_X) and the rotational axis of R_4 joint (R_X) are parallel (X axis).

$$\left[\begin{array}{ccc:ccc} P_X & P_{XY} & P_{XZ} & P_X & - & - \\ - & P_Y & P_{YZ} & - & P_Y & - \\ - & R_X & P_Z & - & R_X & - \\ P_X & - & P_{XZ} & P_X & - & - \\ - & P_Y & - & - & - & - \\ - & R_X & - & - & R_X & - \end{array}\right] \tag{3-113}$$

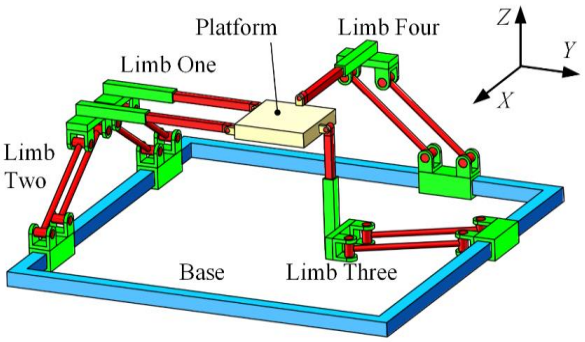

Figure 3-35 Schematic diagram of 4-DOF parallel structure (11)

Feature: There are one P_1 joints (P_Z), one P_3 joints (P_Y), one P_4 joints (P_X), one R_4 joint (R_X), one P_a joint (P_{XY}), one P_a joint (P_{YZ}) and two identical P_a joints (P_{XZ}). Three P_a joints (P_{XZ}, P_{YZ}) are related to P_1 joint (P_Z). Two different P_a joints (P_{XY}, P_{YZ}) are related to P_3 joint (P_Y). Three P_a joints (P_{XY}, P_{XZ}) are related to P_4 joint (P_X). The translational direction of P_4 joint (P_X) and the rotational axis of R_4 joint (R_X) are parallel (X axis).

$$\left[\begin{array}{ccc:ccc} P_X & - & P_{XZ} & P_X & - & - \\ - & P_Y & P_{YZ} & - & P_Y & - \\ - & R_X & P_Z & - & R_X & - \\ P_X & - & P_{XZ} & P_X & - & - \\ - & P_Y & P_{YZ} & - & - & - \\ - & R_X & - & - & R_X & - \end{array}\right] \tag{3-114}$$

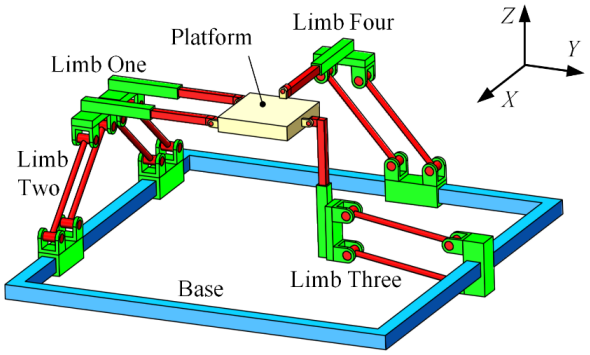

Figure 3-36 Schematic diagram of 4-DOF parallel structure (12)

Feature: There are one P_1 joints (P_Z), one P_3 joints (P_Y), one P_4 joints (P_X), one R_4 joint (R_X), two identical P_a joints (P_{XZ}) and two identical P_a joints (P_{YZ}). Four P_a joints (P_{XZ}, P_{YZ}) are related to P_1 joint (P_Z). Two same P_a joints (P_{YZ}) are related to P_3 joint (P_Y). Two same P_a

joints (P_{XZ}) are related to P_4 joint (P_X). The translational direction of P_4 joint (P_X) and the rotational axis of R_4 joint (R_X) are parallel (X axis).

$$\left[\begin{array}{ccc:ccc} P_X & - & P_{XZ} & P_X & - & P_{XZ} \\ - & P_Y & P_{YZ} & - & P_Y & - \\ - & R_X & P_Z & - & R_X & - \\ P_X & - & P_{XZ} & - & - & - \\ - & P_Y & - & - & P_Y & - \\ - & R_X & - & - & R_X & - \end{array}\right] \tag{3-115}$$

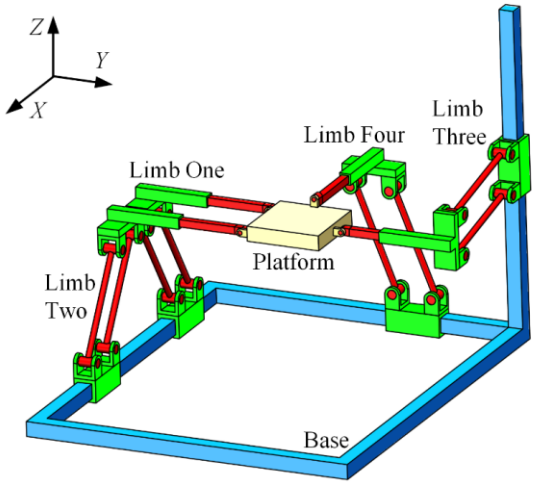

Figure 3-37 Schematic diagram of 4-DOF parallel structure (13)

Feature: There are one P_1 joints (P_Z), one P_3 joints (P_X), one P_4 joints (P_Y), one R_4 joint (R_X), one P_a joint (P_{YZ}) and three identical P_a joints (P_{XZ}). Four P_a joints (P_{XZ}, P_{YZ}) are related to P_1 joint (P_Z). Three same P_a joints (P_{XZ}) are related to P_3 joint (P_X). One P_a joint (P_{YZ}) is related to P_4 joint (P_Y). The translational direction of P_3 joint (P_X) and the rotational axis of R_4 joint (R_X) are parallel (X axis).

$$\left[\begin{array}{ccc:ccc} P_X & P_{XY} & P_{XZ} & P_X & - & - \\ - & P_Y & P_{YZ} & - & - & - \\ - & R_X & P_Z & - & R_X & - \\ P_X & - & P_{XZ} & P_X & - & - \\ - & P_Y & - & - & - & - \\ - & R_X & P_Z & - & R_X & - \end{array}\right] \tag{3-116}$$

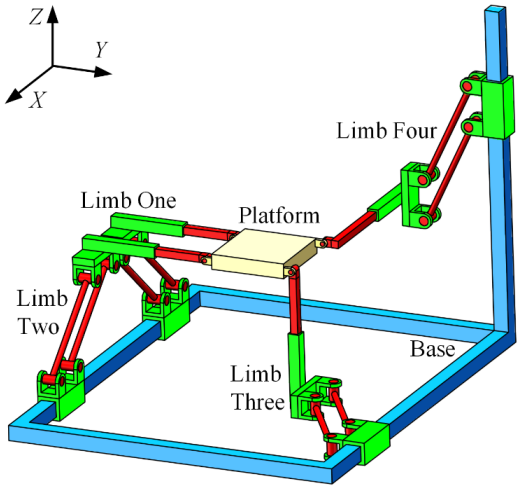

Figure 3-38 Schematic diagram of 4-DOF parallel structure (14)

Feature: There are one P_2 joints (P_Y), one P_2 joints (P_Z), one P_4 joints (P_X), one R_4 joint (R_X), one P_a joint (P_{XY}), one P_a joint (P_{YZ}) and two identical P_a joints (P_{XZ}). Two P_a joints (P_{XY}, P_{YZ}) are related to P_2 joint (P_Y). Three P_a joints (P_{XZ}, P_{YZ}) are related to P_2 joint (P_Z). Three P_a joints (P_{XY}, P_{XZ}) are related to P_4 joint (P_X). The translational direction of P_4 joint (P_X) and the rotational axis of R_4 joint (R_X) are parallel (X axis).

$$\left[\begin{array}{ccc:ccc} P_X & P_{XY} & P_{XZ} & P_X & - & - \\ - & P_Y & - & - & P_Y & - \\ - & R_X & P_Z & - & R_X & - \\ P_X & P_{XY} & P_{XZ} & - & - & - \\ - & P_Y & - & - & - & - \\ - & R_X & P_Z & - & R_X & - \end{array}\right] \tag{3-117}$$

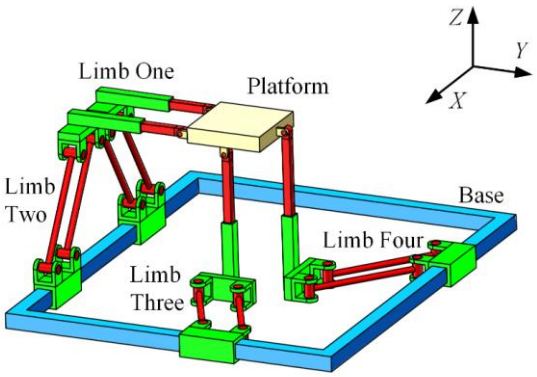

Figure 3-39 Schematic diagram of 4-DOF parallel structure (15)

Feature: There are one P_2 joint (P_Z), one P_3 joint (P_X), one P_3 joint (P_Y), one R_4 joint (R_X), two same P_a joints (P_{XY}), two P_a joints (P_{XZ}). Two same P_a joints (P_{XZ}) are related to P_2 joint (P_Z). Four P_a joints (P_{XY}, P_{XZ}) are related to P_3 joint (P_X). Two identical P_a joints (P_{XY}) are related to P_3 joint (P_Y). The translational direction of P_3 joint (P_X) and the rotational axis of R_4 joint (R_X) are parallel (X axis).

$$\left[\begin{array}{cccc:ccc} P_X & P_{XY} & P_{XZ} & P_X & - & P_{XZ} \\ - & P_Y & - & - & P_Y & - \\ - & R_X & P_Z & - & R_X & - \\ P_X & - & P_{XZ} & - & - & - \\ - & P_Y & - & - & - & - \\ - & R_X & P_Z & - & R_X & - \end{array}\right] \tag{3-118}$$

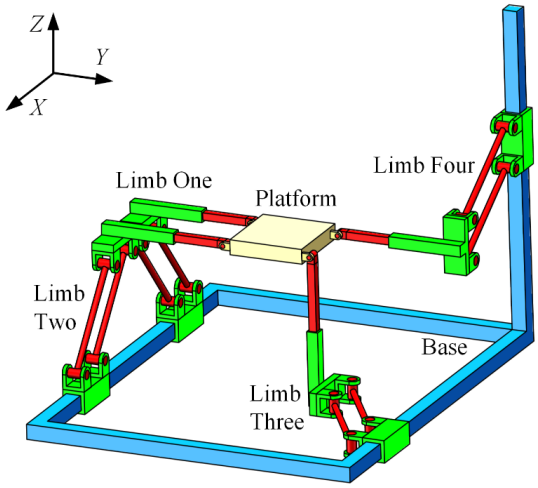

Figure 3-40 Schematic diagram of 4-DOF parallel structure (16)

Feature: There are one P_2 joint (P_Z), one P_3 joint (P_X), one P_3 joint (P_Y), one R_4 joint (R_X), one Pa joint (P_{XY}), three identical P_a joints (P_{XZ}). Three same P_a joints (P_{XZ}) are related to P_2 joint (P_Z). Four P_a joints (P_{XY}, P_{XZ}) are related to P_3 joint (P_X). One P_a joint (P_{XY}) is related to P_3 joint (P_Y). The translational direction of P_3 joint (P_X) and the rotational axis of R_4 joint (R_X) are parallel (X axis).

$$\left[\begin{array}{ccc:ccc} P_X & P_{XY} & P_{XZ} & P_X & - & - \\ - & P_Y & P_{YZ} & - & P_Y & - \\ - & R_X & P_Z & - & R_X & - \\ P_X & - & P_{XZ} & - & - & - \\ - & P_Y & - & - & - & - \\ - & R_X & P_Z & - & R_X & - \end{array}\right] \tag{3-119}$$

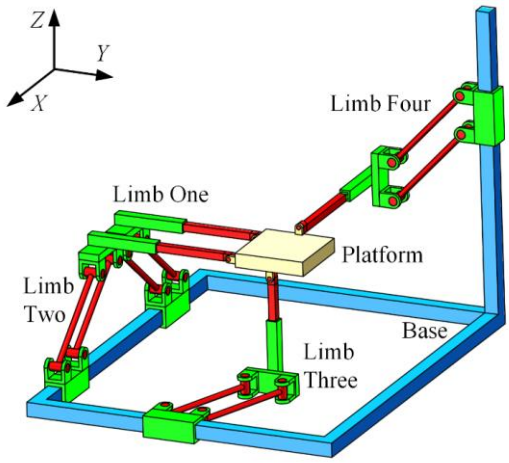

Figure 3-41 Schematic diagram of 4-DOF parallel structure (17)

Feature: There are one P_2 joint (P_Z), one P_3 joint (P_X), one P_3 joint (P_Y), one R_4 joint (R_X), one P_a joint (P_{XY}), one P_a joint (P_{YZ}) and two same P_a joints (P_{XZ}). Three P_a joints (P_{XZ}, P_{YZ}) are related to P_2 joint (P_Z). Three P_a joints (P_{XY}, P_{XZ}) are related to P_3 joint (P_X). Two different P_a joints (P_{XY}, P_{YZ}) are related to P_3 joint (P_Y). The translational direction of P_3 joint (P_X) and the rotational axis of R_4 joint (R_X) are parallel (X axis).

$$\left[\begin{array}{ccc:ccc} P_X & - & P_{XZ} & P_X & - & P_{XZ} \\ - & P_Y & P_{YZ} & - & P_Y & - \\ - & R_X & P_Z & - & R_X & - \\ P_X & - & P_{XZ} & - & - & - \\ - & P_Y & - & - & - & - \\ - & R_X & P_Z & - & R_X & - \end{array}\right] \tag{3-120}$$

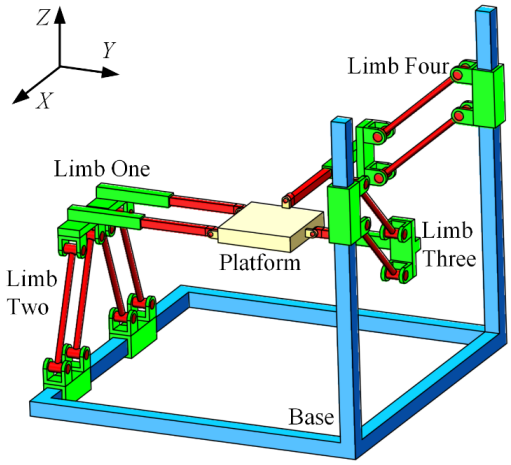

Figure 3-42 Schematic diagram of 4-DOF parallel structure (18)

Feature: There are one P_2 joint (P_Z), one P_3 joint (P_X), one P_3 joint (P_Y), one R_4 joint (R_X), one P_a joint (P_{YZ}) and three same P_a joints (P_{XZ}). Four P_a joints (P_{XZ}, P_{YZ}) are related to P_2 joint (P_Z). Three same P_a joints (P_{XZ}) are related to P_3 joint (P_X). One P_a joint (P_{YZ}) is related to P_3 joint (P_Y). The translational direction of P_3 joint (P_X) and the rotational axis of R_4 joint (R_X) are parallel (X axis).

$$\left[\begin{array}{ccc:ccc} P_X & P_{XY} & P_{XZ} & - & - & P_{XZ} \\ - & P_Y & - & - & P_Y & - \\ - & R_X & P_Z & - & R_X & - \\ P_X & - & P_{XZ} & - & - & - \\ - & P_Y & - & - & P_Y & - \\ - & R_X & P_Z & - & R_X & - \end{array}\right] \tag{3-121}$$

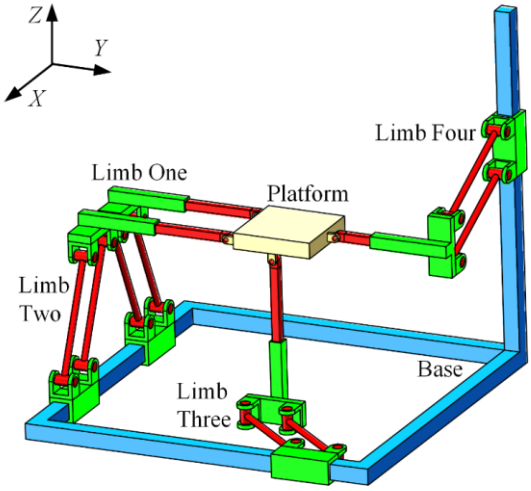

Figure 3-43 Schematic diagram of 4-DOF parallel structure (19)

Feature: There are two P_2 joint (P_X, P_Z), one P_4 joint (P_Y), one R_4 joint (R_X), one P_a joint (P_{XY}) and three same P_a joints (P_{XZ}). Four P_a joints (P_{XY}, P_{XZ}) are related to P_2 joint (P_X). Three same P_a joints (P_{XZ}) are related to P_2 joint (P_Z). One P_a joint (P_{XY}) is related to P_4 joint (P_Y). The translational direction of P_2 joint (P_X) and the rotational axis of R_4 joint (R_X) are parallel (X axis).

$$\left[\begin{array}{ccc:ccc} P_X & P_{XY} & P_{XZ} & P_X & \_ & \_ \\ \_ & P_Y & P_{YZ} & \_ & P_Y & \_ \\ \_ & R_X & P_Z & \_ & R_X & \_ \\ P_X & \_ & P_{XZ} & \_ & \_ & \_ \\ \_ & P_Y & \_ & \_ & P_Y & \_ \\ \_ & R_X & \_ & \_ & R_X & \_ \end{array}\right] \tag{3-122}$$

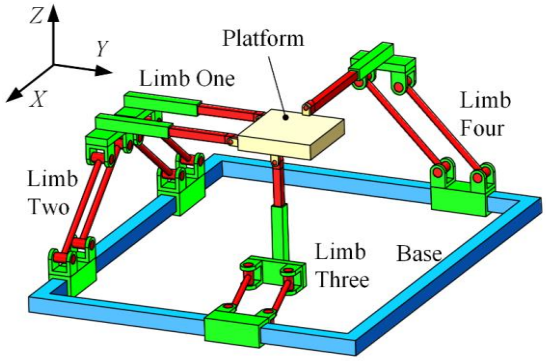

Figure 3-44 Schematic diagram of 4-DOF parallel structure (20)

Feature: There are one P_1 joint (P_Z), one P_3 joint (P_X), one P_4 joint (P_Y), one R_4 joint (R_X), one P_a joint (P_{XY}), one P_a joint (P_{YZ}) and two same P_a joints (P_{XZ}). Three P_a joints (P_{XZ}, P_{YZ}) are related to P_1 joint (P_Z). Three P_a joints (P_{XY}, P_{XZ}) are related to P_3 joint (P_X). Two different P_a joints (P_{XY}, P_{YZ}) are related to P_4 joint (P_Y). The translational direction of P_3 joint (P_X) and the rotational axis of R_4 joint (R_X) are parallel (X axis).

$$\left[\begin{array}{ccc:ccc} P_X & P_{XY} & P_{XZ} & P_X & \_ & \_ \\ \_ & P_Y & P_{YZ} & \_ & \_ & \_ \\ \_ & R_X & P_Z & \_ & R_X & \_ \\ P_X & \_ & \_ & P_X & \_ & \_ \\ \_ & P_Y & P_{YZ} & \_ & \_ & \_ \\ \_ & R_X & P_Z & \_ & R_X & \_ \end{array}\right] \tag{3-123}$$

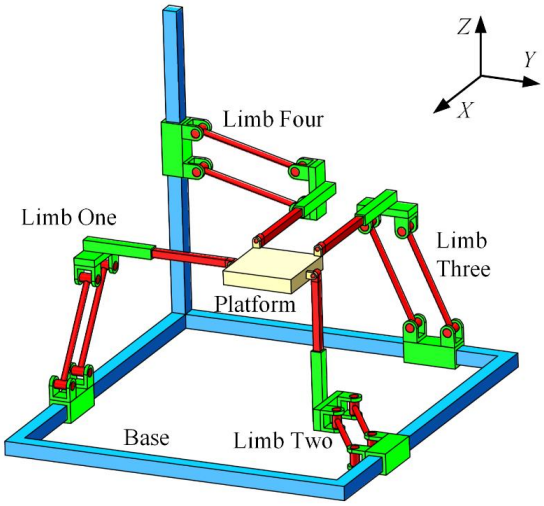

Figure 3-45 Schematic diagram of 4-DOF parallel structure (21)

Feature: There are two P_2 joint (P_Y, P_Z), one P_4 joint (P_X), one R_4 joint (R_X), one P_a joint (P_{XY}), one P_a joint (P_{XZ}) and two same P_a joints (P_{YZ}). Three P_a joints (P_{XY}, P_{YZ}) are related to P_2 joint (P_Y). Three P_a joints (P_{XZ}, P_{XZ}) are related to P_2 joint (P_X). Two different P_a joints (P_{XY}, P_{XZ}) are related to P_4 joint (P_X). The translational direction of P_4 joint (P_X) and the rotational axis of R_4 joint (R_X) are parallel (X axis).

$$\left[\begin{array}{ccc:ccc} P_X & P_{XY} & P_{XZ} & P_X & - & - \\ - & P_Y & P_{YZ} & - & P_Y & - \\ - & R_X & P_Z & - & R_X & - \\ P_X & P_{XY} & - & - & - & - \\ - & P_Y & - & - & - & - \\ - & R_X & P_Z & - & R_X & - \end{array}\right] \tag{3-124}$$

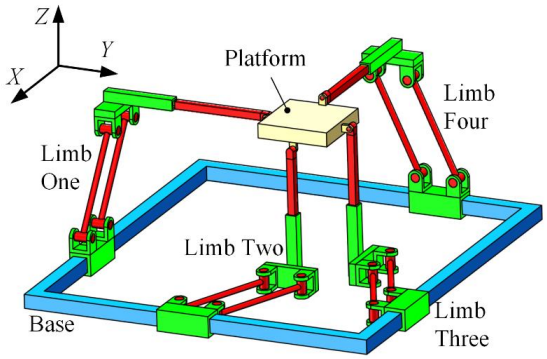

Figure 3-46Schematic diagram of 4-DOF parallel structure (22)

Feature: There are one P_2 joint (P_Z), two P_3 joint (P_X, P_Y), one R_4 joint (R_X), one P_a joint (P_{XZ}), one P_a joint (P_{YZ}) and two same P_a joints (P_{XY}). Two different P_a joints (P_{XZ}, P_{YZ}) are related to P_2 joint (P_Z). Three different P_a joints (P_{XY}, P_{XZ}) are related to P_3 joint (P_X). Three P_a joints (P_{XY}, P_{YZ}) are related to P_3 joint (P_Y). The translational direction of P_3 joint (P_X) and the rotational axis of R_4 joint (R_X) are parallel (X axis).

$$\left[\begin{array}{ccc:ccc} P_X & P_{XY} & P_{XZ} & P_X & - & - \\ - & P_Y & P_{YZ} & - & P_Y & - \\ - & R_X & P_Z & - & R_X & - \\ P_X & - & - & - & - & - \\ - & P_Y & P_{YZ} & - & - & - \\ - & R_X & P_Z & - & R_X & - \end{array}\right] \tag{3-125}$$

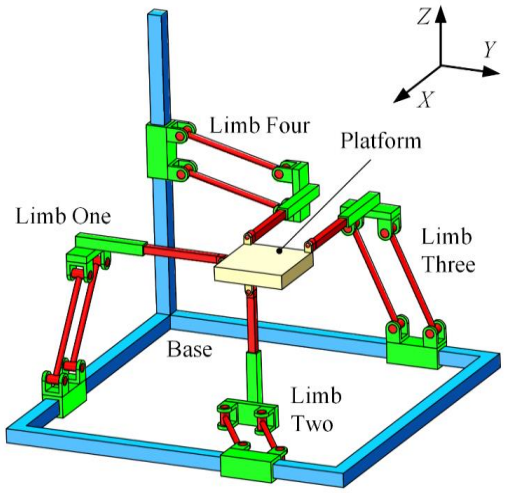

Figure 3-47 Schematic diagram of 4-DOF parallel structure (23)

Feature: There are one P_2 joint (P_Z), two P_3 joint (P_X, P_Y), one R_4 joint (R_X), one P_a joint (P_{XY}), one P_a joint (P_{XZ}) and one P_a joint (P_{YZ}). Three P_a joints (P_{XZ}, P_{YZ}) are related to P_2 joint (P_Z). Two different P_a joints (P_{XY}, P_{XZ}) are related to P_3 joint (P_X). Two different P_a joints (P_{XY}, P_{YZ}) are related to P_3 joint (P_Y). The translational direction of P_3 joint (P_X) and the rotational axis of R_4 joint (R_X) are parallel (X axis).

$$\left[\begin{array}{ccc:ccc} P_X & - & P_{XZ} & P_X & - & - \\ - & P_Y & P_{YZ} & - & P_Y & - \\ - & R_X & P_Z & - & R_X & - \\ P_X & - & P_{XZ} & - & - & - \\ - & P_Y & P_{YZ} & - & - & - \\ - & R_X & P_Z & - & R_X & - \end{array}\right] \tag{3-126}$$

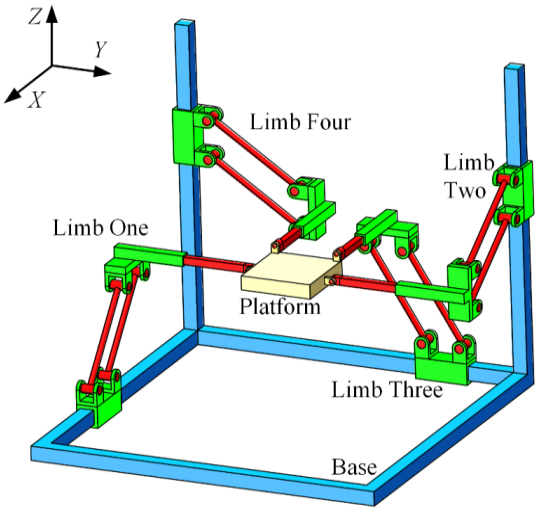

Figure 3-48 Schematic diagram of 4-DOF parallel structure (24)

Feature: There are one P_2 joint (P_Z), two P_3 joints (P_X, P_Y), one R_4 joint (R_X), two same P_a joints (P_{XZ}) and two same P_a joints (P_{YZ}). Four P_a joints (P_{XZ}, P_{YZ}) are related to P_2 joint (P_Z). Two identical P_a joints (P_{XZ}) are related to P_3 joint (P_X). Two identical P_a joints (P_{YZ}) are related to P_3 joint (P_Y). The translational direction of P_3 joint (P_X) and the rotational axis of R_4 joint (R_X) are parallel (X axis).

(ii) Case two: 2T2R mechanism

The possible mechanism is 4-PPaRR, as demonstrated in figure 3-49.

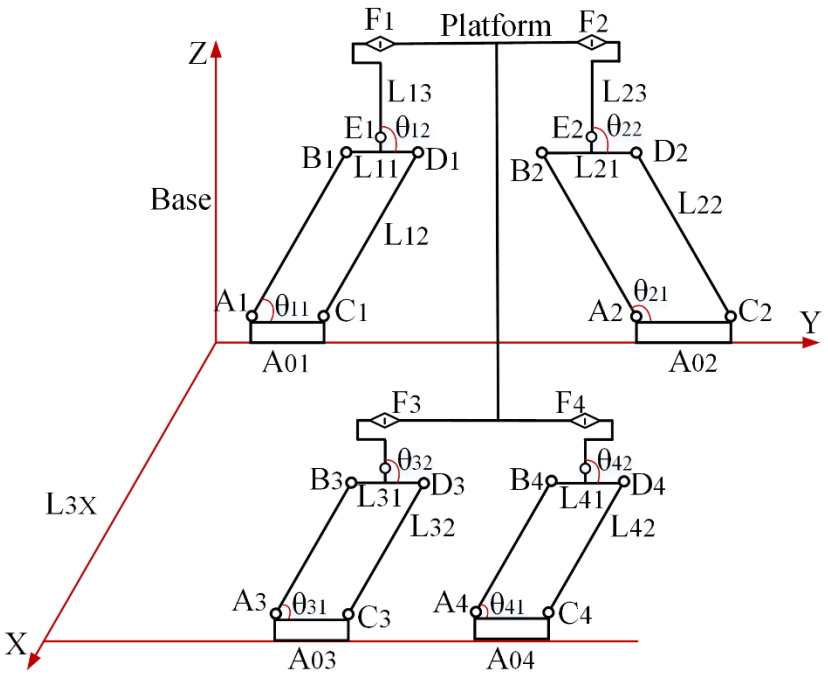

Figure 3-49 2T2R mechanism

These coordinates are given as: $A_{01}(0, x_1, 0)$, $A_1(0, x_1 - 0.5L_{11}, 0)$, $B_1(0, x_1 - 0.5L_{11} + L_{12}\cos\theta_{11}, L_{12}\sin\theta_{11})$, $C_1(0, x_1 + 0.5L_{11}, 0)$, $D_1(0, x_1 + 0.5L_{11} + L_{12}\cos\theta_{11}, L_{12}\sin\theta_{11})$, $E_1(0, x_1 + L_{12}\cos\theta_{11}, L_{12}\sin\theta_{11})$, $F_1(0, x_1 + L_{12}\cos\theta_{11} + L_{13}\cos\theta_{12}, L_{12}\sin\theta_{11} + L_{13}\sin\theta_{12})$, $A_{02}(0, x_2, 0)$, $A_2(0, x_2 - 0.5L_{21}, 0)$, $B_2(0, x_2 - 0.5L_{21} + L_{22}\cos\theta_{21}, L_{22}\sin\theta_{21})$, $C_2(0, x_2 + 0.5L_{21}, 0)$, $D_2(0, x_2 + 0.5L_{21} + L_{22}\cos\theta_{21}, L_{22}\sin\theta_{21})$, $E_2(0, x_2 + L_{22}\cos\theta_{21}, L_{22}\sin\theta_{21})$, $F_2(0, x_2 + L_{22}\cos\theta_{21} + L_{23}\cos\theta_{22}, L_{22}\sin\theta_{21} + L_{23}\sin\theta_{22})$, $A_{03}(L_{3X}, x_3, 0)$, $A_3(L_{3X}, x_3 - 0.5L_{31}, 0)$, $B_3(L_{3X}, x_3 - 0.5L_{31} + L_{32}\cos\theta_{31}, L_{32}\sin\theta_{31})$, $C_3(L_{3X}, x_3 + 0.5L_{31}, 0)$, $D_3(L_{3X}, x_3 + 0.5L_{31} + L_{32}\cos\theta_{31}, L_{32}\sin\theta_{31})$, $E_3(L_{3X}, x_3 + L_{32}\cos\theta_{31}, L_{32}\sin\theta_{31})$, $F_3(L_{3X}, x_3 + L_{32}\cos\theta_{21} + L_{33}\cos\theta_{32}, L_{32}\sin\theta_{31} + L_{33}\sin\theta_{32})$, $A_{04}(L_{4X}, x_4, 0)$, $A_4(L_{4X}, x_4 - 0.5L_{41}, 0)$, $B_4(L_{4X}, x_4 - 0.5L_{41} + L_{42}\cos\theta_{41}, L_{42}\sin\theta_{41})$, $C_4(L_{4X}, x_4 + 0.5L_{41}, 0)$, $D_4(L_{4X}, x_4 + 0.5L_{41} + L_{42}\cos\theta_{41}, L_{42}\sin\theta_{41})$, $E_4(L_{4X}, x_4 + L_{42}\cos\theta_{41}, L_{42}\sin\theta_{41})$, $F_4(L_{4X}, x_4 + L_{42}\cos\theta_{41} + L_{43}\cos\theta_{42}, L_{42}\sin\theta_{41} + L_{43}\sin\theta_{42})$.

The kinematic screws of Pa joint in each limb

$$\begin{cases} \$_{A1}=\begin{bmatrix}1 & 0 & 0; & 0 & 0 & 0.5L_{11}-x_1\end{bmatrix}^{\mathrm{T}} \\ \$_{B1}=\begin{bmatrix}1 & 0 & 0; & 0 & L_{12}\sin\theta_{11} & 0.5L_{11}-x_1-L_{12}\cos\theta_{11}\end{bmatrix}^{\mathrm{T}} \\ \$_{C1}=\begin{bmatrix}1 & 0 & 0; & 0 & 0 & -0.5L_{11}-x_1\end{bmatrix}^{\mathrm{T}} \\ \$_{D1}=\begin{bmatrix}1 & 0 & 0; & 0 & L_{12}\sin\theta_{11} & -0.5L_{11}-x_1-L_{12}\cos\theta_{11}\end{bmatrix}^{\mathrm{T}} \end{cases} \tag{3-127}$$

$$\begin{cases} \$_{A2}=\begin{bmatrix}1 & 0 & 0; & 0 & 0 & 0.5L_{21}-x_2\end{bmatrix}^{\mathrm{T}} \\ \$_{B2}=\begin{bmatrix}1 & 0 & 0; & 0 & L_{22}\sin\theta_{21} & 0.5L_{21}-x_2-L_{22}\cos\theta_{21}\end{bmatrix}^{\mathrm{T}} \\ \$_{C2}=\begin{bmatrix}1 & 0 & 0; & 0 & 0 & -0.5L_{21}-x_2\end{bmatrix}^{\mathrm{T}} \\ \$_{D2}=\begin{bmatrix}1 & 0 & 0; & 0 & L_{22}\sin\theta_{21} & -0.5L_{21}-x_2-L_{22}\cos\theta_{21}\end{bmatrix}^{\mathrm{T}} \end{cases} \tag{3-128}$$

$$\begin{cases} \$_{A3}=\begin{bmatrix}1 & 0 & 0; & 0 & 0 & 0.5L_{31}-x_3\end{bmatrix}^{\mathrm{T}} \\ \$_{B3}=\begin{bmatrix}1 & 0 & 0; & 0 & L_{32}\sin\theta_{31} & 0.5L_{31}-x_3-L_{32}\cos\theta_{31}\end{bmatrix}^{\mathrm{T}} \\ \$_{C3}=\begin{bmatrix}1 & 0 & 0; & 0 & 0 & -0.5L_{31}-x_3\end{bmatrix}^{\mathrm{T}} \\ \$_{D3}=\begin{bmatrix}1 & 0 & 0; & 0 & L_{32}\sin\theta_{31} & -0.5L_{31}-x_3-L_{32}\cos\theta_{31}\end{bmatrix}^{\mathrm{T}} \end{cases} \tag{3-129}$$

$$\begin{cases} \$_{A4}=\begin{bmatrix}1 & 0 & 0; & 0 & 0 & 0.5L_{41}-x_4\end{bmatrix}^{\mathrm{T}} \\ \$_{B4}=\begin{bmatrix}1 & 0 & 0; & 0 & L_{42}\sin\theta_{41} & 0.5L_{41}-x_4-L_{42}\cos\theta_{41}\end{bmatrix}^{\mathrm{T}} \\ \$_{C4}=\begin{bmatrix}1 & 0 & 0; & 0 & 0 & -0.5L_{41}-x_4\end{bmatrix}^{\mathrm{T}} \\ \$_{D4}=\begin{bmatrix}1 & 0 & 0; & 0 & L_{42}\sin\theta_{41} & -0.5L_{41}-x_4-L_{42}\cos\theta_{41}\end{bmatrix}^{\mathrm{T}} \end{cases} \tag{3-130}$$

The equivalent kinematic screw of the Pa joint in each chain

$$\$_{Pa1}=\begin{bmatrix}0 & 0 & 0; & 0 & \sin\theta_{11} & -\cos\theta_{11}\end{bmatrix}^{\mathrm{T}} \tag{3-131}$$

$$\$_{Pa2}=\begin{bmatrix}0 & 0 & 0; & 0 & \sin\theta_{21} & -\cos\theta_{21}\end{bmatrix}^{\mathrm{T}} \tag{3-132}$$

$$\$_{Pa3}=\begin{bmatrix}0 & 0 & 0; & 0 & \sin\theta_{31} & -\cos\theta_{31}\end{bmatrix}^{\mathrm{T}} \tag{3-133}$$

$$\$_{Pa4}=\begin{bmatrix}0 & 0 & 0; & 0 & \sin\theta_{41} & -\cos\theta_{41}\end{bmatrix}^{\mathrm{T}} \tag{3-134}$$

The kinematic screws for the remaining joints of each limb

$$\begin{cases} \$_{A01}=\begin{bmatrix}0 & 0 & 0; & 0 & 1 & 0\end{bmatrix}^{\mathrm{T}} \\ \$_{E1}=\begin{bmatrix}1 & 0 & 0; & 0 & L_{12}\sin\theta_{11} & -x_1-L_{12}\cos\theta_{11}\end{bmatrix}^{\mathrm{T}} \\ \$_{F1}=\begin{bmatrix}0 & 1 & 0; & -L_{12}\sin\theta_{11}-L_{13}\sin\theta_{12} & 0 & 0\end{bmatrix}^{\mathrm{T}} \end{cases} \tag{3-135}$$

$$\begin{cases} \$_{A02} = \begin{bmatrix} 0 & 0 & 0; & 0 & 1 & 0 \end{bmatrix}^{\mathrm{T}} \\ \$_{E2} = \begin{bmatrix} 1 & 0 & 0; & 0 & L_{22}\sin\theta_{21} & -x_2 - L_{22}\cos\theta_{21} \end{bmatrix}^{\mathrm{T}} \\ \$_{F2} = \begin{bmatrix} 0 & 1 & 0; & -L_{22}\sin\theta_{21} - L_{23}\sin\theta_{22} & 0 & 0 \end{bmatrix}^{\mathrm{T}} \end{cases} \tag{3-136}$$

$$\begin{cases} \$_{A03} = \begin{bmatrix} 0 & 0 & 0; & 0 & 1 & 0 \end{bmatrix}^{\mathrm{T}} \\ \$_{E3} = \begin{bmatrix} 1 & 0 & 0; & 0 & L_{32}\sin\theta_{31} & -x_3 - L_{32}\cos\theta_{31} \end{bmatrix}^{\mathrm{T}} \\ \$_{F3} = \begin{bmatrix} 0 & 1 & 0; & -L_{32}\sin\theta_{31} - L_{33}\sin\theta_{32} & 0 & L_{3X} \end{bmatrix}^{\mathrm{T}} \end{cases} \tag{3-137}$$

$$\begin{cases} \$_{A04} = \begin{bmatrix} 0 & 0 & 0; & 0 & 1 & 0 \end{bmatrix}^{\mathrm{T}} \\ \$_{E4} = \begin{bmatrix} 1 & 0 & 0; & 0 & L_{42}\sin\theta_{41} & -x_4 - L_{42}\cos\theta_{41} \end{bmatrix}^{\mathrm{T}} \\ \$_{F4} = \begin{bmatrix} 0 & 1 & 0; & -L_{42}\sin\theta_{41} - L_{43}\sin\theta_{42} & 0 & L_{4X} \end{bmatrix}^{\mathrm{T}} \end{cases} \tag{3-138}$$

The corresponding reciprocal screws for each limb

$$\begin{cases} \$_{11}^{r} = \begin{bmatrix} 0 & 0 & 0; & 0 & 0 & 1 \end{bmatrix}^{\mathrm{T}} \\ \$_{12}^{r} = \begin{bmatrix} 1 & 0 & 0; & 0 & L_{12}\sin\theta_{11} + L_{13}\sin\theta_{12} & 0 \end{bmatrix}^{\mathrm{T}} \end{cases} \tag{3-139}$$

$$\begin{cases} \$_{21}^{r} = \begin{bmatrix} 0 & 0 & 0; & 0 & 0 & 1 \end{bmatrix}^{\mathrm{T}} \\ \$_{22}^{r} = \begin{bmatrix} 1 & 0 & 0; & 0 & L_{22}\sin\theta_{21} + L_{23}\sin\theta_{22} & 0 \end{bmatrix}^{\mathrm{T}} \end{cases} \tag{3-140}$$

$$\begin{cases} \$_{31}^{r} = \begin{bmatrix} 0 & 0 & 0; & 0 & 0 & 1 \end{bmatrix}^{\mathrm{T}} \\ \$_{32}^{r} = \begin{bmatrix} 1 & 0 & 0; & 0 & L_{32}\sin\theta_{31} + L_{33}\sin\theta_{32} & 0 \end{bmatrix}^{\mathrm{T}} \end{cases} \tag{3-141}$$

$$\begin{cases} \$_{41}^{r} = \begin{bmatrix} 0 & 0 & 0; & 0 & 0 & 1 \end{bmatrix}^{\mathrm{T}} \\ \$_{42}^{r} = \begin{bmatrix} 1 & 0 & 0; & 0 & L_{42}\sin\theta_{41} + L_{43}\sin\theta_{42} & 0 \end{bmatrix}^{\mathrm{T}} \end{cases} \tag{3-142}$$

The kinematic screw system for the moving platform

$$\begin{cases} \$_{m1} = \begin{bmatrix} 0 & 0 & 0; & 0 & 1 & 0 \end{bmatrix}^{\mathrm{T}} \\ \$_{m2} = \begin{bmatrix} 0 & 0 & 0; & 0 & 0 & 1 \end{bmatrix}^{\mathrm{T}} \\ \$_{m3} = \begin{bmatrix} 1 & 0 & 0; & 0 & 0 & 0 \end{bmatrix}^{\mathrm{T}} \end{cases} \tag{3-143}$$

Equation (4-116) denotes the moving platform can move along Y and Z axes, rotate about X axis. It can not conduct 2T2R motion.

(iii) Case three: 1T3R mechanism

The possible mechanism is 4-P_aRRR, as shown in figure 3-50.

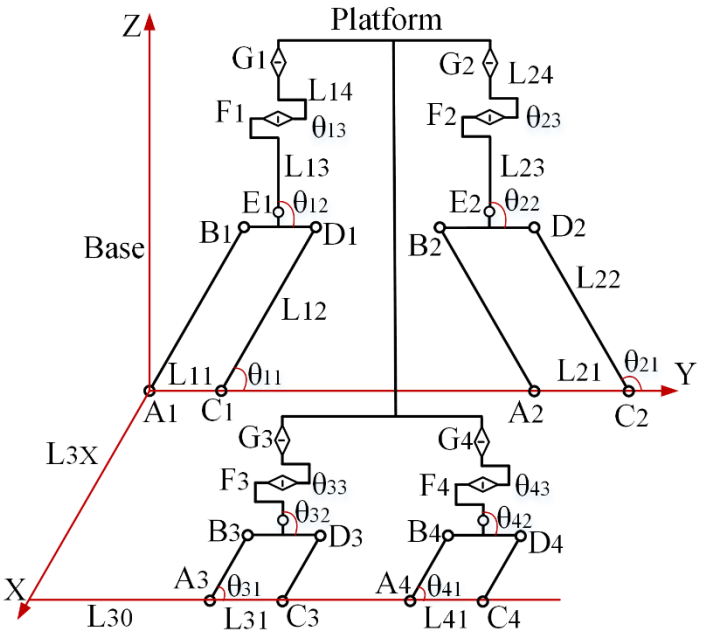

Figure 3-50 1T3R mechanism

The coordinates for these points are provided as follows,

$A_1(0,0,0)$, $B_1(0, L_{12}\cos\theta_{11}, L_{12}\sin\theta_{11})$, $C_1(0, L_{11}, 0)$, $D_1(0, L_{11}+L_{12}\cos\theta_{11}, L_{12}\sin\theta_{11})$,

$E_1(0, 0.5L_{11}+L_{12}\cos\theta_{11}, L_{12}\sin\theta_{11})$,

$F_1(0, 0.5L_{11}+L_{12}\cos\theta_{11}+L_{13}\cos\theta_{12}, L_{12}\sin\theta_{11}+L_{13}\sin\theta_{12})$,

$G_1(L_{14}\cos\theta_{13}, 0.5L_{11}+L_{12}\cos\theta_{11}+L_{13}\cos\theta_{12}, L_{12}\sin\theta_{11}+L_{13}\sin\theta_{12}+L_{14}\sin\theta_{13})$,

$A_2(0, L_{20}, 0)$, $B_2(0, L_{20}+L_{22}\cos\theta_{21}, L_{22}\sin\theta_{21})$, $C_2(0, L_{20}+L_{21}, 0)$,

$D_2(0, L_{20}+L_{21}+L_{22}\cos\theta_{21}, L_{22}\sin\theta_{21})$, $E_2(0, L_{20}+0.5L_{21}+L_{22}\cos\theta_{21}, L_{22}\sin\theta_{21})$,

$F_2(0, L_{20}+0.5L_{21}+L_{22}\cos\theta_{21}+L_{23}\cos\theta_{22}, L_{22}\sin\theta_{21}+L_{23}\sin\theta_{22})$,

$G_2(L_{24}\cos\theta_{23}, L_{20}+0.5L_{21}+L_{22}\cos\theta_{21}+L_{23}\cos\theta_{22}, L_{22}\sin\theta_{21}+L_{23}\sin\theta_{22}+L_{24}\sin\theta_{23})$,

$A_3(L_{3X}, L_{30}, 0)$, $B_3(L_{3X}, L_{30}+L_{32}\cos\theta_{31}, L_{32}\sin\theta_{31})$, $C_3(L_{3X}, L_{30}+L_{31}, 0)$,

$D_3(L_{3X}, L_{30}+L_{31}+L_{32}\cos\theta_{31}, L_{32}\sin\theta_{31})$, $E_3(L_{3X}, L_{30}+0.5L_{31}+L_{32}\cos\theta_{31}, L_{32}\sin\theta_{31})$,

$F_3(L_{3X}, L_{30}+0.5L_{31}+L_{32}\cos\theta_{31}+L_{33}\cos\theta_{32}, L_{32}\sin\theta_{31}+L_{33}\sin\theta_{32})$,

$G_3(L_{3X}+L_{34}\cos\theta_{33}, L_{30}+0.5L_{31}+L_{32}\cos\theta_{31}+L_{33}\cos\theta_{32}, L_{32}\sin\theta_{31}+L_{33}\sin\theta_{32}+L_{34}\sin\theta_{33})$

, $A_4(L_{4X}, L_{40}, 0)$, $B_4(L_{4X}, L_{40}+L_{42}\cos\theta_{41}, L_{42}\sin\theta_{41})$, $C_4(L_{4X}, L_{40}+L_{41}, 0)$,

$D_4(L_{4X}, L_{40}+L_{41}+L_{42}\cos\theta_{41}, L_{42}\sin\theta_{41})$, $E_4(L_{4X}, L_{40}+0.5L_{41}+L_{42}\cos\theta_{41}, L_{42}\sin\theta_{41})$,

$F_4(L_{4X}, L_{40}+0.5L_{41}+L_{42}\cos\theta_{41}+L_{43}\cos\theta_{42}, L_{42}\sin\theta_{41}+L_{43}\sin\theta_{42})$,

$G_4(L_{4X}+L_{44}\cos\theta_{43}, L_{40}+0.5L_{41}+L_{42}\cos\theta_{41}+L_{43}\cos\theta_{42}, L_{42}\sin\theta_{41}+L_{43}\sin\theta_{42}+L_{44}\sin\theta_{43})$

.The kinematic screws for the P_a joint of each limb

$$\begin{cases} \$_{A1}=\begin{bmatrix}1 & 0 & 0; & 0 & 0 & 0\end{bmatrix}^{\mathrm{T}} \\ \$_{B1}=\begin{bmatrix}1 & 0 & 0; & 0 & L_{12}\sin\theta_{11} & -L_{12}\cos\theta_{11}\end{bmatrix}^{\mathrm{T}} \\ \$_{C1}=\begin{bmatrix}1 & 0 & 0; & 0 & 0 & -L_{11}\end{bmatrix}^{\mathrm{T}} \\ \$_{D1}=\begin{bmatrix}1 & 0 & 0; & 0 & L_{12}\sin\theta_{11} & -L_{11}-L_{12}\cos\theta_{11}\end{bmatrix}^{\mathrm{T}} \end{cases} \tag{3-144}$$

$$\begin{cases} \$_{A2}=\begin{bmatrix}1 & 0 & 0; & 0 & 0 & -L_{20}\end{bmatrix}^{\mathrm{T}} \\ \$_{B2}=\begin{bmatrix}1 & 0 & 0; & 0 & L_{22}\sin\theta_{21} & -L_{20}-L_{22}\cos\theta_{21}\end{bmatrix}^{\mathrm{T}} \\ \$_{C2}=\begin{bmatrix}1 & 0 & 0; & 0 & 0 & -L_{20}-L_{21}\end{bmatrix}^{\mathrm{T}} \\ \$_{D2}=\begin{bmatrix}1 & 0 & 0; & 0 & L_{22}\sin\theta_{21} & -L_{20}-L_{21}-L_{22}\cos\theta_{21}\end{bmatrix}^{\mathrm{T}} \end{cases} \tag{3-145}$$

$$\begin{cases} \$_{A3}=\begin{bmatrix}1 & 0 & 0; & 0 & 0 & -L_{40}\end{bmatrix}^{\mathrm{T}} \\ \$_{B3}=\begin{bmatrix}1 & 0 & 0; & 0 & L_{42}\sin\theta_{41} & -L_{40}-L_{42}\cos\theta_{41}\end{bmatrix}^{\mathrm{T}} \\ \$_{C3}=\begin{bmatrix}1 & 0 & 0; & 0 & 0 & -L_{40}-L_{41}\end{bmatrix}^{\mathrm{T}} \\ \$_{D3}=\begin{bmatrix}1 & 0 & 0; & 0 & L_{42}\sin\theta_{41} & -L_{40}-L_{41}-L_{42}\cos\theta_{41}\end{bmatrix}^{\mathrm{T}} \end{cases} \tag{3-146}$$

$$\begin{cases} \$_{A4}=\begin{bmatrix}1 & 0 & 0; & 0 & 0 & -L_{30}\end{bmatrix}^{\mathrm{T}} \\ \$_{B4}=\begin{bmatrix}1 & 0 & 0; & 0 & L_{32}\sin\theta_{31} & -L_{30}-L_{32}\cos\theta_{31}\end{bmatrix}^{\mathrm{T}} \\ \$_{C4}=\begin{bmatrix}1 & 0 & 0; & 0 & 0 & -L_{30}-L_{31}\end{bmatrix}^{\mathrm{T}} \\ \$_{D4}=\begin{bmatrix}1 & 0 & 0; & 0 & L_{32}\sin\theta_{31} & -L_{30}-L_{31}-L_{32}\cos\theta_{31}\end{bmatrix}^{\mathrm{T}} \end{cases} \tag{3-147}$$

Their corresponding kinematic screws are obtained respectively

$$\$_{Pa1}=\begin{bmatrix}0 & 0 & 0; & 0 & \sin\theta_{11} & -\cos\theta_{11}\end{bmatrix}^{\mathrm{T}} \tag{3-148}$$

$$\$_{Pa2}=\begin{bmatrix}0 & 0 & 0; & 0 & \sin\theta_{21} & -\cos\theta_{21}\end{bmatrix}^{\mathrm{T}} \tag{3-149}$$

$$\$_{Pa3}=\begin{bmatrix}0 & 0 & 0; & 0 & \sin\theta_{31} & -\cos\theta_{31}\end{bmatrix}^{\mathrm{T}} \tag{3-150}$$

$$\$_{Pa4}=\begin{bmatrix}0 & 0 & 0; & 0 & \sin\theta_{41} & -\cos\theta_{41}\end{bmatrix}^{\mathrm{T}} \tag{3-151}$$

Considering the remaining kinematic joints in each branch,

$$\begin{cases} \$_{E1} = \begin{bmatrix} 1 & 0 & 0; & 0 & L_{12}\sin\theta_{11} & -0.5L_{11} - L_{12}\cos\theta_{11} \end{bmatrix}^{\mathrm{T}} \\ \$_{F1} = \begin{bmatrix} 0 & 1 & 0; & -L_{12}\sin\theta_{11} - L_{13}\sin\theta_{12} & 0 & 0 \end{bmatrix}^{\mathrm{T}} \\ \$_{G1} = \begin{bmatrix} 0 & 0 & 1; & 0.5L_{11} + L_{12}\cos\theta_{11} + L_{13}\cos\theta_{12} & -L_{14}\cos\theta_{13} & 0 \end{bmatrix}^{\mathrm{T}} \end{cases} \tag{3-152}$$

$$\begin{cases} \$_{E2} = \begin{bmatrix} 1 & 0 & 0; & 0 & L_{22}\sin\theta_{21} & -L_{20} - 0.5L_{11} - L_{22}\cos\theta_{21} \end{bmatrix}^{\mathrm{T}} \\ \$_{F2} = \begin{bmatrix} 0 & 1 & 0; & -L_{22}\sin\theta_{21} - L_{23}\sin\theta_{22} & 0 & 0 \end{bmatrix}^{\mathrm{T}} \\ \$_{G2} = \begin{bmatrix} 0 & 0 & 1; & L_{20} + 0.5L_{21} + L_{22}\cos\theta_{21} + L_{23}\cos\theta_{22} & -L_{24}\cos\theta_{23} & 0 \end{bmatrix}^{\mathrm{T}} \end{cases} \tag{3-153}$$

$$\begin{cases} \$_{E3} = \begin{bmatrix} 1 & 0 & 0; & 0 & L_{32}\sin\theta_{31} & -L_{30} - 0.5L_{31} - L_{32}\cos\theta_{31} \end{bmatrix}^{\mathrm{T}} \\ \$_{F3} = \begin{bmatrix} 0 & 1 & 0; & -L_{32}\sin\theta_{31} - L_{33}\sin\theta_{32} & 0 & L_{3X} \end{bmatrix}^{\mathrm{T}} \\ \$_{G3} = \begin{bmatrix} 0 & 0 & 1; & L_{30} + 0.5L_{31} + L_{32}\cos\theta_{31} + L_{33}\cos\theta_{32} & -L_{3X} - L_{34}\cos\theta_{33} & 0 \end{bmatrix}^{\mathrm{T}} \end{cases} \tag{3-154}$$

$$\begin{cases} \$_{E4} = \begin{bmatrix} 1 & 0 & 0; & 0 & L_{42}\sin\theta_{41} & -L_{40} - 0.5L_{41} - L_{42}\cos\theta_{41} \end{bmatrix}^{\mathrm{T}} \\ \$_{F4} = \begin{bmatrix} 0 & 1 & 0; & -L_{42}\sin\theta_{41} - L_{43}\sin\theta_{42} & 0 & L_{4X} \end{bmatrix}^{\mathrm{T}} \\ \$_{G4} = \begin{bmatrix} 0 & 0 & 1; & L_{40} + 0.5L_{41} + L_{42}\cos\theta_{41} + L_{43}\cos\theta_{42} & -L_{4X} - L_{44}\cos\theta_{43} & 0 \end{bmatrix}^{\mathrm{T}} \end{cases} \tag{3-155}$$

The constraint screws from each branch are listed below

$$\begin{cases} \$_{11}^{r} = \begin{bmatrix} 1 & 0 & 0; & 0 & L_{12}\sin\theta_{11} + L_{13}\sin\theta_{12} & -0.5L_{11} - L_{12}\cos\theta_{11} - L_{13}\cos\theta_{12} \end{bmatrix}^{\mathrm{T}} \\ \$_{12}^{r} = \begin{bmatrix} 0 & \cos\theta_{11} & \sin\theta_{11}; & 0.5L_{11} & 0 & L_{14}\cos\theta_{13}\cot\theta_{11} \end{bmatrix}^{\mathrm{T}} \end{cases} \tag{3-156}$$

$$\begin{cases} \$_{21}^{r} = \begin{bmatrix} 1 & 0 & 0; & 0 & L_{22}\sin\theta_{21} + L_{23}\sin\theta_{22} & -L_{20} - 0.5L_{21} - L_{22}\cos\theta_{21} - L_{23}\cos\theta_{22} \end{bmatrix}^{\mathrm{T}} \\ \$_{22}^{r} = \begin{bmatrix} 0 & \cos\theta_{21} & \sin\theta_{21}; & L_{20} + 0.5L_{21} & 0 & L_{24}\cos\theta_{23}\cot\theta_{21} \end{bmatrix}^{\mathrm{T}} \end{cases}$$

(3-157)

$$\begin{cases} \$_{31}^{r} = \begin{bmatrix} 1 & 0 & 0; & 0 & L_{32}\sin\theta_{31} + L_{33}\sin\theta_{32} & -L_{30} - 0.5L_{31} - L_{32}\cos\theta_{31} - L_{33}\cos\theta_{32} \end{bmatrix}^{\mathrm{T}} \\ \$_{32}^{r} = \begin{bmatrix} 0 & \cos\theta_{31} & \sin\theta_{31}; & L_{30} + 0.5L_{31} & -L_{3X} & (L_{3X} + L_{34}\cos\theta_{33})\cot\theta_{21} \end{bmatrix}^{\mathrm{T}} \end{cases}$$

(3-158)

$$\begin{cases} \$_{41}^{r} = \begin{bmatrix} 1 & 0 & 0; & 0 & L_{42}\sin\theta_{41} + L_{43}\sin\theta_{42} & -L_{40} - 0.5L_{41} - L_{42}\cos\theta_{41} - L_{43}\cos\theta_{42} \end{bmatrix}^{\mathrm{T}} \\ \$_{42}^{r} = \begin{bmatrix} 0 & \cos\theta_{41} & \sin\theta_{41}; & L_{40} + 0.5L_{41} & -L_{4X} & (L_{4X} + L_{44}\cos\theta_{43})\cot\theta_{41} \end{bmatrix}^{\mathrm{T}} \end{cases}$$

(3-159)

Based on Equations (3-156) to (3-159), the kinematic screws of the moving platform can be derived and the result is null. It means the moving platform can not move.

However, in some special cases, the moving platform can gain some movements. A scenario is provided below. Assuming all L_{i1}, L_{i2}, L_{i3}, L_{i4} and θ_{i1} (i=1,2,3,4) are in the same value respectively. L_{3X}=L_{4X}. L_{20}= L_{40}. L_{30}=0. Then the kinematic screw of the moving platform is $\$_m = \begin{bmatrix} 0 & 0 & 0; & 0 & \sin\theta_{11} & -\cos\theta_{11} \end{bmatrix}^{\mathrm{T}}$. The moving platform has a decoupled translational movement along Y and Z axes under the previous condition.

3.3.4 Five-DOF parallel mechanism

(i) Case one: 3T2R mechanism

The qualified limbs are:

$$\begin{cases} \mathrm{P}_X - \mathrm{P}_{XZ} - \mathrm{P}_Y - R_X - R_Y \\ \mathrm{P}_X - \mathrm{P}_{YZ} - \mathrm{P}_Y - R_X - R_Y \\ \mathrm{P}_X - \mathrm{P}_{XY} - \mathrm{P}_Z - R_X - R_Y \\ \mathrm{P}_X - \mathrm{P}_{YZ} - \mathrm{P}_Z - R_X - R_Y \\ \mathrm{P}_Y - \mathrm{P}_{XY} - \mathrm{P}_Z - R_X - R_Y \\ \mathrm{P}_Y - \mathrm{P}_{XZ} - \mathrm{P}_Z - R_X - R_Y \end{cases} \tag{3-160}$$

$$\begin{cases} \mathrm{P}_X - \mathrm{P}_{XZ} - \mathrm{P}_Y - R_X - R_Z \\ \mathrm{P}_X - \mathrm{P}_{YZ} - \mathrm{P}_Y - R_X - R_Z \\ \mathrm{P}_X - \mathrm{P}_{XY} - \mathrm{P}_Z - R_X - R_Z \\ \mathrm{P}_X - \mathrm{P}_{YZ} - \mathrm{P}_Z - R_X - R_Z \\ \mathrm{P}_Y - \mathrm{P}_{XY} - \mathrm{P}_Z - R_X - R_Z \\ \mathrm{P}_Y - \mathrm{P}_{XZ} - \mathrm{P}_Z - R_X - R_Z \end{cases} \tag{3-161}$$

$$\begin{cases} \mathrm{P}_X - \mathrm{P}_{XZ} - \mathrm{P}_Y - R_Y - R_Z \\ \mathrm{P}_X - \mathrm{P}_{YZ} - \mathrm{P}_Y - R_Y - R_Z \\ \mathrm{P}_X - \mathrm{P}_{XY} - \mathrm{P}_Z - R_Y - R_Z \\ \mathrm{P}_X - \mathrm{P}_{YZ} - \mathrm{P}_Z - R_Y - R_Z \\ \mathrm{P}_Y - \mathrm{P}_{XY} - \mathrm{P}_Z - R_Y - R_Z \\ \mathrm{P}_Y - \mathrm{P}_{XZ} - \mathrm{P}_Z - R_Y - R_Z \end{cases} \tag{3-162}$$

Limbs are shown in matrix form, corresponding to Equations (3-160) to (3-162),

$$\begin{bmatrix} P_X & - & P_{XZ} \\ - & P_Y & - \\ R_Y & R_X & - \\ - & - & - \\ - & - & - \\ - & - & - \end{bmatrix}, \begin{bmatrix} P_X & - & - \\ - & P_Y & P_{YZ} \\ R_Y & R_X & - \\ - & - & - \\ - & - & - \\ - & - & - \end{bmatrix}, \begin{bmatrix} P_X & P_{XY} & - \\ - & - & - \\ R_Y & R_X & P_Z \\ - & - & - \\ - & - & - \\ - & - & - \end{bmatrix}$$

$$\begin{bmatrix} P_X & - & - \\ - & - & P_{YZ} \\ R_Y & R_X & P_Z \\ - & - & - \\ - & - & - \\ - & - & - \end{bmatrix}, \begin{bmatrix} - & P_{XY} & - \\ - & P_Y & - \\ R_Y & R_X & P_Z \\ - & - & - \\ - & - & - \\ - & - & - \end{bmatrix}, \begin{bmatrix} - & - & P_{XZ} \\ - & P_Y & - \\ R_Y & R_X & P_Z \\ - & - & - \\ - & - & - \\ - & - & - \end{bmatrix} \quad (3\text{-}163)$$

$$\begin{bmatrix} P_X & - & P_{XZ} \\ R_Z & P_Y & - \\ - & R_X & - \\ - & - & - \\ - & - & - \\ - & - & - \end{bmatrix}, \begin{bmatrix} P_X & - & - \\ R_Z & P_Y & P_{YZ} \\ - & R_X & - \\ - & - & - \\ - & - & - \\ - & - & - \end{bmatrix}, \begin{bmatrix} P_X & P_{XY} & - \\ R_Z & - & - \\ - & R_X & P_Z \\ - & - & - \\ - & - & - \\ - & - & - \end{bmatrix}$$

$$\begin{bmatrix} P_X & - & - \\ R_Z & - & P_{YZ} \\ - & R_X & P_Z \\ - & - & - \\ - & - & - \\ - & - & - \end{bmatrix}, \begin{bmatrix} - & P_{XY} & - \\ R_Z & P_Y & - \\ - & R_X & P_Z \\ - & - & - \\ - & - & - \\ - & - & - \end{bmatrix}, \begin{bmatrix} - & - & P_{XZ} \\ R_Z & P_Y & - \\ - & R_X & P_Z \\ - & - & - \\ - & - & - \\ - & - & - \end{bmatrix} \quad (3\text{-}164)$$

$$\begin{bmatrix} P_X & - & P_{XZ} \\ R_Z & P_Y & - \\ R_Y & - & - \\ - & - & - \\ - & - & - \\ - & - & - \end{bmatrix}, \begin{bmatrix} P_X & - & - \\ R_Z & P_Y & P_{YZ} \\ R_Y & - & - \\ - & - & - \\ - & - & - \\ - & - & - \end{bmatrix}, \begin{bmatrix} P_X & P_{XY} & - \\ R_Z & - & - \\ R_Y & - & P_Z \\ - & - & - \\ - & - & - \\ - & - & - \end{bmatrix}$$

$$\begin{bmatrix} \mathrm{P}_X & - & - \\ R_Z & - & \mathrm{P}_{YZ} \\ R_Y & - & \mathrm{P}_Z \\ - & - & - \\ - & - & - \\ - & - & - \end{bmatrix}, \begin{bmatrix} - & \mathrm{P}_{XY} & - \\ R_Z & \mathrm{P}_Y & - \\ R_Y & - & \mathrm{P}_Z \\ - & - & - \\ - & - & - \\ - & - & - \end{bmatrix}, \begin{bmatrix} - & - & \mathrm{P}_{XZ} \\ R_Z & \mathrm{P}_Y & - \\ R_Y & - & \mathrm{P}_Z \\ - & - & - \\ - & - & - \\ - & - & - \end{bmatrix} \tag{3-165}$$

The limb can be represented as Q_i. In enumeration, there will be

$$\begin{aligned} &3\times(Q_i^5+Q_i^4Q_j+Q_i^3Q_j^2+Q_i^3Q_jQ_k+Q_i^2Q_j^2Q_k+Q_i^2Q_jQ_kQ_l+Q_iQ_jQ_kQ_lQ_m) \\ &=3\times(6+A_6^2+A_6^2+6\times C_5^2+C_6^2\times 4+6\times C_5^3+C_6^5) \\ &=756 \end{aligned} \tag{3-166}$$

kinds of matrices. The same matrices are ones with similar cell configuration. At last, there are 40 kinds of qualified matrices. These matrices and corresponding parallel structures are listed below.

$$\left[\begin{array}{ccc:ccc:ccc} \mathrm{P}_X & - & \mathrm{P}_{XZ} & \mathrm{P}_X & - & \mathrm{P}_{XZ} & \mathrm{P}_X & - & \mathrm{P}_{XZ} \\ - & \mathrm{P}_Y & - & - & \mathrm{P}_Y & - & - & \mathrm{P}_Y & - \\ R_Y & R_X & - & R_Y & R_X & - & R_Y & R_X & - \\ \mathrm{P}_X & - & \mathrm{P}_{XZ} & \mathrm{P}_X & - & \mathrm{P}_{XZ} & - & - & - \\ - & \mathrm{P}_Y & - & - & \mathrm{P}_Y & - & - & - & - \\ R_Y & R_X & - & R_Y & R_X & - & - & - & - \end{array}\right] \tag{3-167}$$

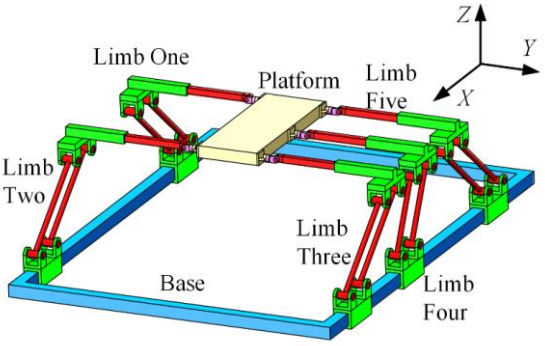

Figure 3-51 Schematic diagram of 5-DOF parallel structure (1)

Feature: There are two P_5 joints (P_X, P_Y), two R_5 joints (R_X, R_Y) and five same P_a joints (P_{XZ}). Five same P_a joints (P_{XZ}) are related to P_5 joint (P_X) but nor related to P_5 joint (P_Y). The translational direction of P_5 joint (P_X) and the rotational axis of R_5 joint (R_X) are parallel (X axis). The translational direction of P_5 joint (P_Y) and the rotational axis of R_5 joint (R_Y) are parallel (Y axis).

$$\left[\begin{array}{ccc:ccc:ccc} \mathrm{P}_X & - & \mathrm{P}_{XZ} & \mathrm{P}_X & - & \mathrm{P}_{XZ} & \mathrm{P}_X & - & - \\ - & \mathrm{P}_Y & \mathrm{P}_{YZ} & - & \mathrm{P}_Y & - & - & \mathrm{P}_Y & - \\ R_Y & R_X & - & R_Y & R_X & - & R_Y & R_X & - \\ \mathrm{P}_X & - & \mathrm{P}_{XZ} & \mathrm{P}_X & - & \mathrm{P}_{XZ} & - & - & - \\ - & \mathrm{P}_Y & - & - & \mathrm{P}_Y & - & - & - & - \\ R_Y & R_X & - & R_Y & R_X & - & - & - & - \end{array}\right] \tag{3-168}$$

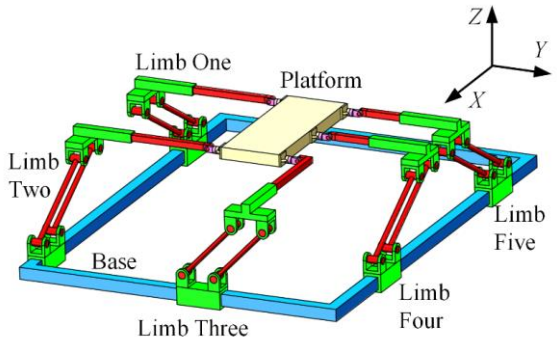

Figure 3-52 Schematic diagram of 5-DOF parallel structure (2)

Feature: There are two P_5 joints (P_X, P_Y), two R_5 joints (R_X, R_Y), one P_a joint (P_{YZ}) and four same P_a joints (P_{XZ}). Four same P_a joints (P_{XZ}) are related to P_5 joint (P_X). One P_a joint (P_{YZ}) is related to P_5 joint (P_Y). The translational direction of P_5 joint (P_X) and the rotational axis of R_5 joint (R_X) are parallel (*X* axis). The translational direction of P_5 joint (P_Y) and the rotational axis of R_5 joint (R_Y) are parallel (*Y* axis).

$$\left[\begin{array}{ccc:ccc:ccc} \mathrm{P}_X & \mathrm{P}_{XY} & \mathrm{P}_{XZ} & \mathrm{P}_X & - & \mathrm{P}_{XZ} & \mathrm{P}_X & - & - \\ - & \mathrm{P}_Y & - & - & \mathrm{P}_Y & - & - & - & - \\ R_Y & R_X & \mathrm{P}_Z & R_Y & R_X & - & R_Y & R_X & - \\ \mathrm{P}_X & - & \mathrm{P}_{XZ} & \mathrm{P}_X & - & \mathrm{P}_{XZ} & - & - & - \\ - & \mathrm{P}_Y & - & - & \mathrm{P}_Y & - & - & - & - \\ R_Y & R_X & - & R_Y & R_X & - & - & - & - \end{array}\right] \tag{3-169}$$

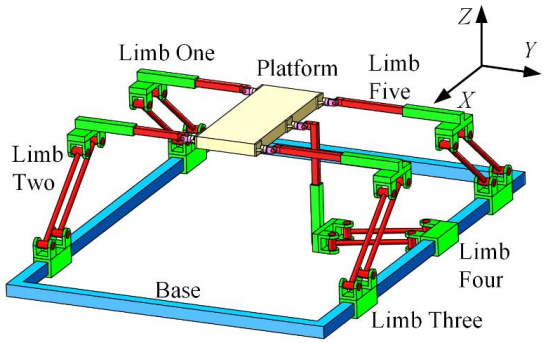

Figure 3-53 Schematic diagram of 5-DOF parallel structure (3)

Feature: There are one P_1 joint (P_Z), one P_4 joint (P_Y), one P_5 joint (P_X), two R_5 joints (R_X, R_Y), one P_a joint (P_{XY}) and four same P_a joints (P_{XZ}). Four same P_a joints (P_{XZ}) are related to P_1 joint (P_Z). One P_a joint (P_{XY}) is related to P_4 joint (P_Y). Five P_a joints (P_{XY}, P_{XZ}) are related to P_5 joint (P_X). The translational direction of P_5 joint (P_X) and the rotational axis of R_5 joint (R_X) are parallel (X axis). The translational direction of P_4 joint (P_Y) and the rotational axis of R_5 joint (R_Y) are parallel (Y axis).

$$\left[\begin{array}{ccc:ccc:ccc} P_X & - & P_{XZ} & P_X & - & P_{XZ} & P_X & - & - \\ - & P_Y & P_{YZ} & - & P_Y & - & - & - & - \\ R_Y & R_X & P_Z & R_Y & R_X & - & R_Y & R_X & - \\ P_X & - & P_{XZ} & P_X & - & P_{XZ} & - & - & - \\ - & P_Y & - & - & P_Y & - & - & - & - \\ R_Y & R_X & - & R_Y & R_X & - & - & - & - \end{array}\right] \tag{3-170}$$

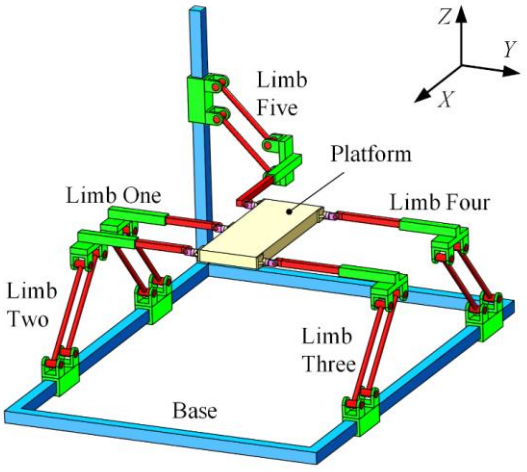

Figure 3-54 Schematic diagram of 5-DOF parallel structure (4)

Feature: There are one P_1 joint (P_Z), one P_4 joint (P_Y), one P_5 joint (P_X), two R_5 joints (R_X, R_Y), one P_a joint (P_{YZ}) and four same P_a joints (P_{XZ}). Five P_a joints (P_{XZ}, P_{YZ}) are related to P_1 joint (P_Z). One P_a joint (P_{YZ}) is related to P_4 joint (P_Y). Four identical P_a joints (P_{XZ}) are related to P_5 joint (P_X). The translational direction of P_5 joint (P_X) and the rotational axis of R_5 joint (R_X) are parallel (X axis). The translational direction of P_4 joint (P_Y) and the rotational axis of R_5 joint (R_Y) are parallel (Y axis).

$$\left[\begin{array}{ccc:ccc:ccc} P_X & P_{XY} & P_{XZ} & P_X & - & P_{XZ} & - & - & - \\ - & P_Y & - & - & P_Y & - & - & P_Y & - \\ R_Y & R_X & P_Z & R_Y & R_X & - & R_Y & R_X & - \\ P_X & - & P_{XZ} & P_X & - & P_{XZ} & - & - & - \\ - & P_Y & - & - & P_Y & - & - & - & - \\ R_Y & R_X & - & R_Y & R_X & - & - & - & - \end{array}\right] \tag{3-171}$$

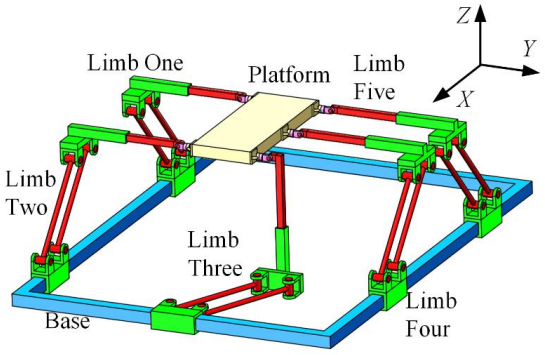

Figure 3-55 Schematic diagram of 5-DOF parallel structure (5)

Feature: There are one P_1 joint (P_Z), one P_4 joint (P_X), one P_5 joint (P_Y), two R_5 joints (R_X, R_Y), one P_a joint (P_{XY}) and four same P_a joints (P_{XZ}). Four identical P_a joints (P_{XZ}) are related to P_1 joint (P_Z). Five P_a joints (P_{XY}, P_{XZ}) are related to P_4 joint (P_X). One P_a joint (P_{XY}) is related to P_5 joint (P_Y). The translational direction of P_4 joint (P_X) and the rotational axis of R_5 joint (R_X) are parallel (X axis). The translational direction of P_5 joint (P_Y) and the rotational axis of R_5 joint (R_Y) are parallel (Y axis).

$$\left[\begin{array}{ccc:ccc:ccc} P_X & - & P_{XZ} & P_X & - & P_{XZ} & - & - & P_{XZ} \\ - & P_Y & - & - & P_Y & - & - & P_Y & - \\ R_Y & R_X & P_Z & R_Y & R_X & - & R_Y & R_X & - \\ P_X & - & P_{XZ} & P_X & - & P_{XZ} & - & - & - \\ - & P_Y & - & - & P_Y & - & - & - & - \\ R_Y & R_X & - & R_Y & R_X & - & - & - & - \end{array}\right] \tag{3-172}$$

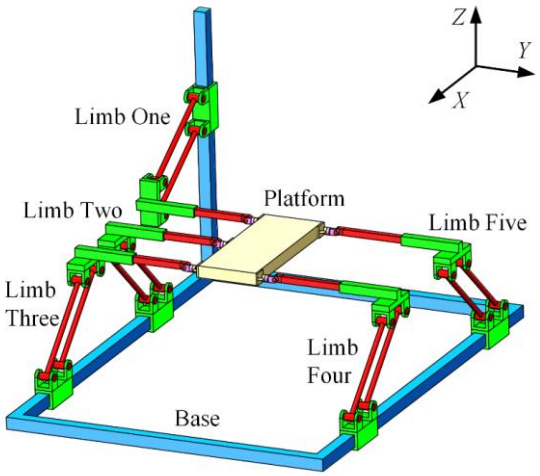

Figure 3-56 Schematic diagram of 5-DOF parallel structure (6)

Feature: There are one P_1 joint (P_Z), one P_4 joint (P_X), one P_5 joint (P_Y), two R_5 joints (R_X, R_Y) and five same P_a joints (P_{XZ}). Five identical P_a joints (P_{XZ}) are related to P_1 joint (P_Z). Five identical P_a joints (P_{XZ}) are related to P_4 joint (P_X). Zero P_a joint (P_{XY}) is related to P_5 joint (P_Y). The translational direction of P_4 joint (P_X) and the rotational axis of R_5 joint (R_X) are parallel (X axis). The translational direction of P_5 joint (P_Y) and the rotational axis of R_5 joint (R_Y) are parallel (Y axis).

$$\left[\begin{array}{ccc:ccc:ccc} P_X & \_ & P_{XZ} & P_X & \_ & P_{XZ} & P_X & \_ & \_ \\ \_ & P_Y & P_{YZ} & \_ & P_Y & \_ & \_ & P_Y & \_ \\ R_Y & R_X & \_ & R_Y & R_X & \_ & R_Y & R_X & \_ \\ P_X & \_ & P_{XZ} & P_X & \_ & \_ & \_ & \_ & \_ \\ \_ & P_Y & P_{YZ} & \_ & P_Y & \_ & \_ & \_ & \_ \\ R_Y & R_X & \_ & R_Y & R_X & \_ & \_ & \_ & \_ \end{array}\right] \tag{3-173}$$

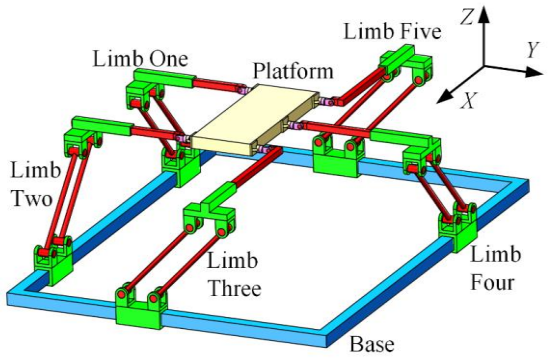

Figure 3-57 Schematic diagram of 5-DOF parallel structure (7)

Feature: There are two P_5 joints (P_X, P_Y), two R_5 joints (R_X, R_Y), two same P_a joints (P_{YZ}) and three same P_a joints (P_{XZ}). Three identical P_a joints (P_{XZ}) are related to P_5 joint (P_X). Two same P_a joints (P_{YZ}) are related to P_5 joint (P_Y). The translational direction of P_5 joint (P_X) and the rotational axis of R_5 joint (R_X) are parallel (X axis). The translational direction of P_5 joint (P_Y) and the rotational axis of R_5 joint (R_Y) are parallel (Y axis).

$$\left[\begin{array}{ccc:ccc:ccc} P_X & P_{XY} & P_{XZ} & P_X & - & P_{XZ} & P_X & - & - \\ - & P_Y & - & - & P_Y & - & - & - & - \\ R_Y & R_X & P_Z & R_Y & R_X & - & R_Y & R_X & - \\ P_X & P_{XY} & P_{XZ} & P_X & - & - & - & - & - \\ - & P_Y & - & - & - & - & - & - & - \\ R_Y & R_X & P_Z & R_Y & R_X & - & - & - & - \end{array}\right] \tag{3-174}$$

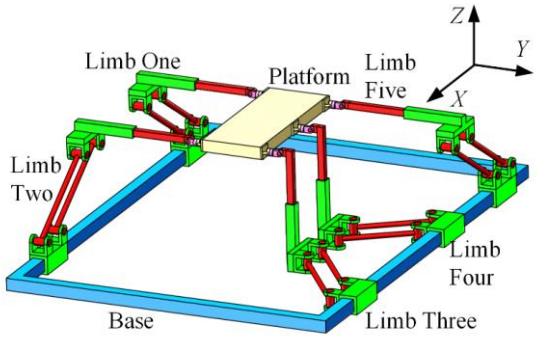

Figure 3-58 Schematic diagram of 5-DOF parallel structure (8)

Feature: There are one P_2 joint (P_Z), one P_3 joint (P_Y), one P_5 joint (P_X), two R_5 joints (R_X, R_Y), two same P_a joints (P_{XY}) and three same P_a joints (P_{XZ}). Three identical Pa joints (P_{XZ}) are related to P_2 joint (P_Z). Two identical P_a joints (P_{XY}) are related to P_3 joint (P_Y). Five P_a joints (P_{XY}, P_{XZ}) are related to P_5 joint (P_X). The translational direction of P_5 joint (P_X) and the rotational axis of R_5 joint (R_X) are parallel (X axis). The translational direction of P_3 joint (P_Y) and the rotational axis of R_5 joint (R_Y) are parallel (Y axis).

$$\left[\begin{array}{ccc:ccc:ccc} P_X & - & P_{XZ} & P_X & - & P_{XZ} & P_X & - & - \\ - & P_Y & P_{YZ} & - & P_Y & - & - & - & - \\ R_Y & R_X & P_Z & R_Y & R_X & - & R_Y & R_X & - \\ P_X & - & P_{XZ} & P_X & - & - & - & - & - \\ - & P_Y & P_{YZ} & - & - & - & - & - & - \\ R_Y & R_X & P_Z & R_Y & R_X & - & - & - & - \end{array}\right] \tag{3-175}$$

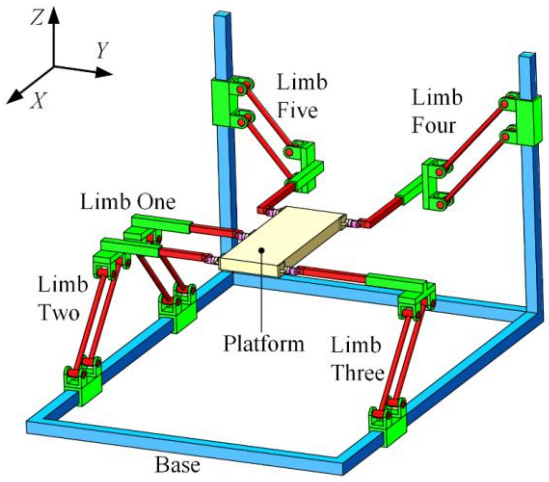

Figure 3-59 Schematic diagram of 5-DOF parallel structure (9)

Feature: There are one P_2 joint (P_Z), one P_3 joint (P_Y), one P_5 joint (P_X), two R_5 joints (R_X, R_Y), two same P_a joints (P_{YZ}) and three same P_a joints (P_{XZ}). Five P_a joints (P_{XZ}, P_{YZ}) are related to P_2 joint (P_Z). Two identical P_a joints (P_{YZ}) are related to P_3 joint (P_Y). Three identical P_a joints (P_{XZ}) are related to P_5 joint (P_X). The translational direction of P_5 joint (P_X) and the rotational axis of R_5 joint (R_X) are parallel (X axis). The translational direction of P_3 joint (P_Y) and the rotational axis of R_5 joint (R_Y) are parallel (Y axis).

$$\left[\begin{array}{ccc:ccc:ccc} P_X & P_{XY} & P_{XZ} & P_X & - & P_{XZ} & - & - & - \\ - & P_Y & - & - & P_Y & - & - & P_Y & - \\ R_Y & R_X & P_Z & R_Y & R_X & - & R_Y & R_X & - \\ P_X & P_{XY} & P_{XZ} & - & - & - & - & - & - \\ - & P_Y & - & - & P_Y & - & - & - & - \\ R_Y & R_X & P_Z & R_Y & R_X & - & - & - & - \end{array}\right] \tag{3-176}$$

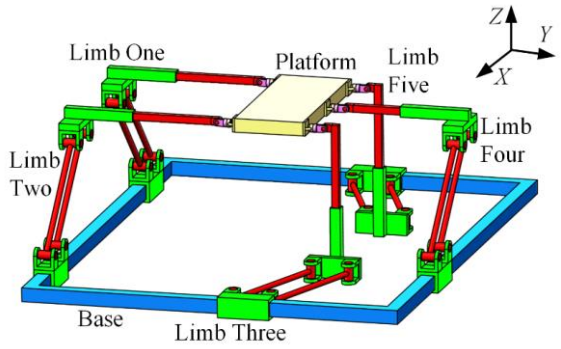

Figure 3-60 Schematic diagram of 5-DOF parallel structure (10)

Feature: There are one P_2 joint (P_Z), one P_3 joint (P_X), one P_5 joint (P_Y), two R_5 joints (R_X, R_Y), two same P_a joints (P_{XY}) and three same P_a joints (P_{XZ}). Three same P_a joints (P_{XZ}) are related to P_2 joint (P_Z). Two identical P_a joints (P_{XY}) are related to P_5 joint (P_Y). Five P_a joints (P_{XY}, P_{XZ}) are related to P_3 joint (P_X). The translational direction of P_3 joint (P_X) and the rotational axis of R_5 joint (R_X) are parallel (X axis). The translational direction of P_5 joint (P_Y) and the rotational axis of R_5 joint (R_Y) are parallel (Y axis).

$$\left[\begin{array}{ccc:ccc:ccc} P_X & - & P_{XZ} & P_X & - & P_{XZ} & - & - & P_{XZ} \\ - & P_Y & - & - & P_Y & - & - & P_Y & - \\ R_Y & R_X & P_Z & R_Y & R_X & - & R_Y & R_X & - \\ P_X & - & P_{XZ} & - & - & P_{XZ} & - & - & - \\ - & P_Y & - & - & P_Y & - & - & - & - \\ R_Y & R_X & P_Z & R_Y & R_X & - & - & - & - \end{array}\right] \tag{3-177}$$

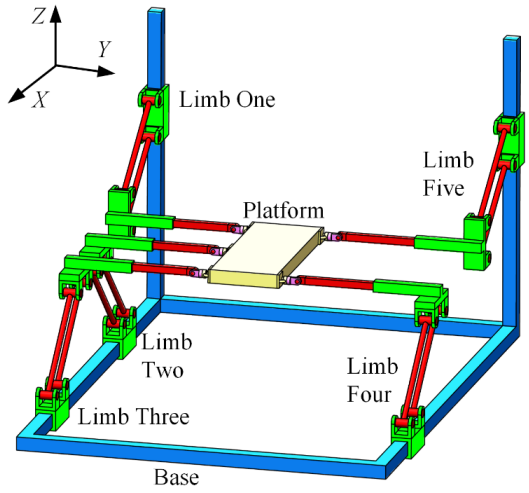

Figure 3-61 Schematic diagram of 5-DOF parallel structure (11)

Feature: There are one P_2 joint (P_Z), one P_3 joint (P_X), one P_5 joint (P_Y), two R_5 joints (R_X, R_Y) and five same P_a joints (P_{XZ}). Five same P_a joints (P_{XZ}) are related to P_2 joint (P_Z). Zero P_a joint is related to P_5 joint (P_Y). Five same P_a joints (P_{XZ}) are related to P_3 joint (P_X). The translational direction of P_3 joint (P_X) and the rotational axis of R_5 joint (R_X) are parallel (X axis). The translational direction of P_5 joint (P_Y) and the rotational axis of R_5 joint (R_Y) are parallel (Y axis).

$$\left[\begin{array}{ccc|ccc|ccc} P_X & P_{XY} & P_{XZ} & P_X & - & P_{XZ} & P_X & - & - \\ - & P_Y & P_{YZ} & - & P_Y & - & - & - & - \\ R_Y & R_X & P_Z & R_Y & R_X & - & R_Y & R_X & - \\ P_X & - & P_{XZ} & P_X & - & - & - & - & - \\ - & P_Y & - & - & P_Y & - & - & - & - \\ R_Y & R_X & - & R_Y & R_X & - & - & - & - \end{array}\right] \tag{3-178}$$

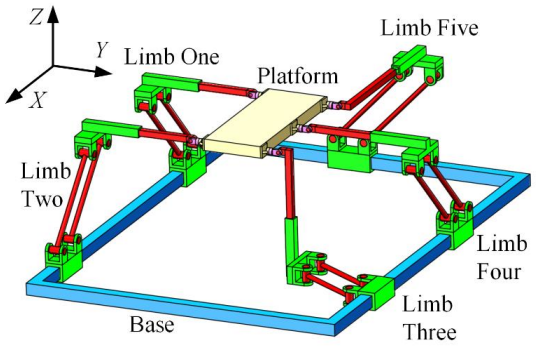

Figure 3-62Schematic diagram of 5-DOF parallel structure (12)

Figure 3-62 Schematic diagram of 5-DOF parallel structure (12)

Feature: There are one P_1 joint (P_Z), one P_4 joint (P_Y), one P_5 joint (P_X), two R_5 joints (R_X, R_Y), one P_a joint (P_{XY}), one P_a joint (P_{YZ}) and three same Pa joints (P_{XZ}). Four P_a joints (P_{XZ}, P_{YZ}) are related to P_1 joint (P_Z). Two different P_a joints (P_{XY}, P_{YZ}) are related to P_4 joint (P_Y). Four P_a joints (P_{XY}, P_{XZ}) are related to P_5 joint (P_X). The translational direction of P_5 joint (P_X) and the rotational axis of R_5 joint (R_X) are parallel (*X* axis). The translational direction of P_4 joint (P_Y) and the rotational axis of R_5 joint (R_Y) are parallel (*Y* axis).

$$\left[\begin{array}{ccc|ccc|ccc} P_X & - & P_{XZ} & P_X & - & P_{XZ} & P_X & - & - \\ - & P_Y & P_{YZ} & - & P_Y & - & - & - & - \\ R_Y & R_X & P_Z & R_Y & R_X & - & R_Y & R_X & - \\ P_X & - & P_{XZ} & P_X & - & - & - & - & - \\ - & P_Y & P_{YZ} & - & P_Y & - & - & - & - \\ R_Y & R_X & - & R_Y & R_X & - & - & - & - \end{array}\right] \tag{3-179}$$

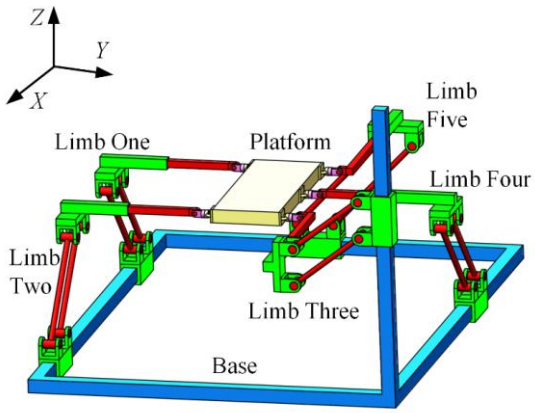

Figure 3-63 Schematic diagram of 5-DOF parallel structure (13)

Feature: There are one P_1 joint (P_Z), one P_4 joint (P_Y), one P_5 joint (P_X), two R_5 joints (R_X, R_Y), two same P_a joints (P_{YZ}) and three same P_a joints (P_{XZ}). Five P_a joints (P_{XZ}, P_{YZ}) are related to P_1 joint (P_Z). Two same P_a joints (P_{YZ}) are related to P_4 joint (P_Y). Three identical P_a joints (P_{XZ}) are related to P_5 joint (P_X). The translational direction of P_5 joint (P_X) and the rotational axis of R_5 joint (R_X) are parallel (X axis). The translational direction of P_4 joint (P_Y) and the rotational axis of R_5 joint (R_Y) are parallel (Y axis).

$$\left[\begin{array}{ccc:ccc:ccc} P_X & P_{XY} & P_{XZ} & P_X & \_ & P_{XZ} & \_ & \_ & \_ \\ \_ & P_Y & P_{YZ} & \_ & P_Y & \_ & \_ & P_Y & \_ \\ R_Y & R_X & P_Z & R_Y & R_X & \_ & R_Y & R_X & \_ \\ P_X & \_ & P_{XZ} & P_X & \_ & \_ & \_ & \_ & \_ \\ \_ & P_Y & \_ & \_ & P_Y & \_ & \_ & \_ & \_ \\ R_Y & R_X & \_ & R_Y & R_X & \_ & \_ & \_ & \_ \end{array}\right] \tag{3-180}$$

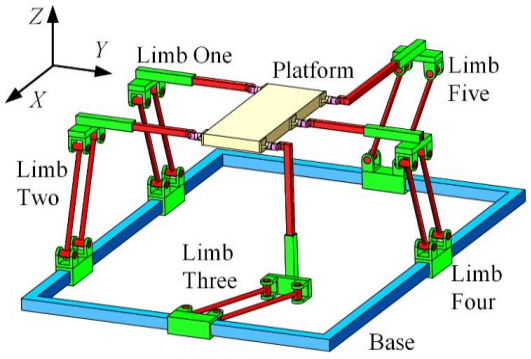

Figure 3-64 Schematic diagram of 5-DOF parallel structure (14)

Feature: There are one P_1 joint (P_Z), one P_4 joint (P_X), one P_5 joint (P_Y), two R_5 joints (R_X, R_Y), one P_a joint (P_{XY}), one P_a joint (P_{YZ}) and three same P_a joints (P_{XZ}). Four P_a joints (P_{XZ},

P_{YZ}) are related to P_1 joint (P_Z). Four P_a joints (P_{XY}, P_{XZ}) are related to P_4 joint (P_X). Two different P_a joints (P_{XY}, P_{YZ}) are related to P_5 joint (P_Y). The translational direction of P_4 joint (P_X) and the rotational axis of R_5 joint (R_X) are parallel (X axis). The translational direction of P_5 joint (P_Y) and the rotational axis of R_5 joint (R_Y) are parallel (Y axis).

$$\left[\begin{array}{ccc|ccc|ccc} P_X & - & P_{XZ} & P_X & - & P_{XZ} & - & - & - \\ - & P_Y & P_{YZ} & - & P_Y & - & - & P_Y & - \\ R_Y & R_X & P_Z & R_Y & R_X & - & R_Y & R_X & - \\ P_X & - & P_{XZ} & P_X & - & P_{XZ} & - & - & - \\ - & P_Y & - & - & P_Y & - & - & - & - \\ R_Y & R_X & - & R_Y & R_X & - & - & - & - \end{array}\right] \tag{3-181}$$

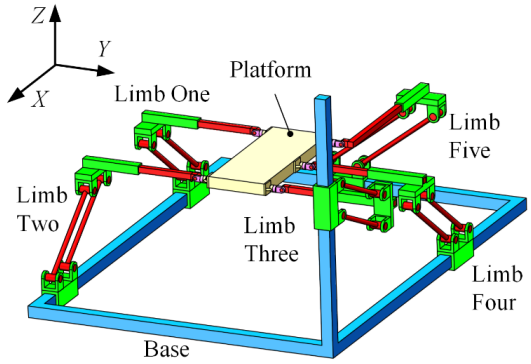

Figure 3-65 Schematic diagram of 5-DOF parallel structure (15)

Feature: There are one P_1 joint (P_Z), one P_4 joint (P_X), one P_5 joint (P_Y), two R_5 joints (R_X, R_Y), one P_a joint (P_{YZ}) and four same P_a joints (P_{XZ}). Four Pa joints (P_{XZ}, P_{YZ}) are related to P_1 joint (P_Z). Four same P_a joints (P_{XZ}) are related to P_4 joint (P_X). One P_a joint (P_{YZ}) is related to P_5 joint (P_Y). The translational direction of P_4 joint (P_X) and the rotational axis of R_5 joint (R_X) are parallel (X axis). The translational direction of P_5 joint (P_Y) and the rotational axis of R_5 joint (R_Y) are parallel (Y axis).

$$\left[\begin{array}{ccc|ccc|ccc} P_X & P_{XY} & P_{XZ} & P_X & - & P_{XZ} & P_X & - & - \\ - & P_Y & P_{YZ} & - & P_Y & - & - & - & - \\ R_Y & R_X & P_Z & R_Y & R_X & - & R_Y & R_X & - \\ P_X & - & P_{XZ} & P_X & - & - & - & - & - \\ - & P_Y & - & - & - & - & - & - & - \\ R_Y & R_X & P_Z & R_Y & R_X & - & - & - & - \end{array}\right] \tag{3-182}$$

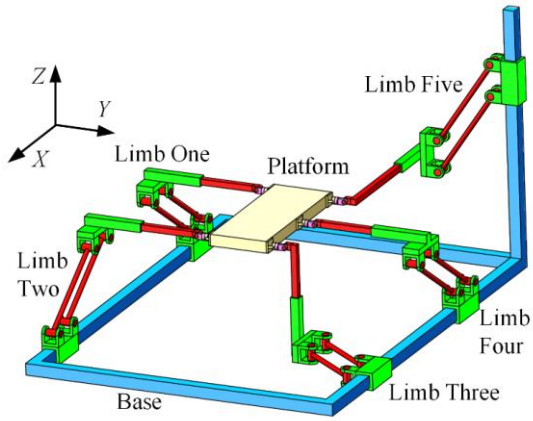

Figure 3-66 Schematic diagram of 5-DOF parallel structure (16)

Feature: There are one P_2 joint (P_Z), one P_3 joint (P_Y), one P_5 joint (P_X), two R_5 joints (R_X, R_Y), one P_a joint (P_{XY}), one P_a joint (P_{YZ}) and three same P_a joints (P_{XZ}). Four P_a joints (P_{XZ}, P_{YZ}) are related to P_2 joint (P_Z). Two different P_a joints (P_{XZ}, P_{YZ}) are related to P_3 joint (P_Y). Four P_a joints (P_{XY}, P_{XZ}) are related to P_5 joint (P_X). The translational direction of P_5 joint (P_X) and the rotational axis of R_5 joint (R_X) are parallel (X axis). The translational direction of P_3 joint (P_Y) and the rotational axis of R_5 joint (R_Y) are parallel (Y axis).

$$\left[\begin{array}{ccc:ccc:ccc} P_X & P_{XY} & P_{XZ} & P_X & - & P_{XZ} & - & - & - \\ - & P_Y & - & - & P_Y & - & - & - & - \\ R_Y & R_X & P_Z & R_Y & R_X & - & R_Y & R_X & - \\ P_X & P_{XY} & P_{XZ} & P_X & - & - & - & - & - \\ - & P_Y & - & - & P_Y & - & - & - & - \\ R_Y & R_X & P_Z & R_Y & R_X & - & - & - & - \end{array}\right] \tag{3-183}$$

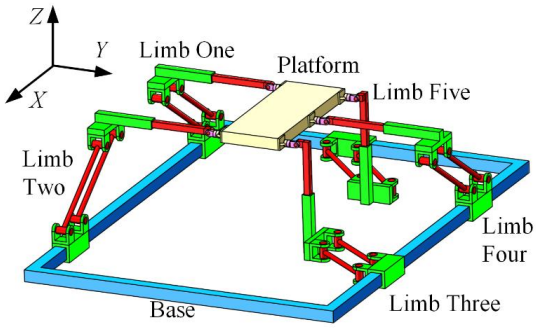

Figure 3-67 Schematic diagram of 5-DOF parallel structure (17)

Feature: There are one P_2 joint (P_Z), two P_4 joints (P_X, P_Y), two R_5 joints (R_X, R_Y), two same P_a joints (P_{XY}) and three same P_a joints (P_{XZ}). Three same P_a joints (P_{XZ}) are related to P_2 joint (P_Z). Five P_a joints (P_{XY}, P_{XZ}) are related to P_4 joint (P_X). Two same P_a joints (P_{XY}) are

related to P_4 joint (P_Y). The translational direction of P_4 joint (P_X) and the rotational axis of R_5 joint (R_X) are parallel (X axis). The translational direction of P_4 joint (P_Y) and the rotational axis of R_5 joint (R_Y) are parallel (Y axis).

$$\left[\begin{array}{ccc|ccc|ccc} P_X & P_{XY} & P_{XZ} & P_X & - & P_{XZ} & - & - & - \\ - & P_Y & - & - & P_Y & - & - & - & - \\ R_Y & R_X & P_Z & R_Y & R_X & - & R_Y & R_X & - \\ P_X & - & P_{XZ} & P_X & - & P_{XZ} & - & - & - \\ - & P_Y & - & - & P_Y & - & - & - & - \\ R_Y & R_X & P_Z & R_Y & R_X & - & - & - & - \end{array}\right] \tag{3-184}$$

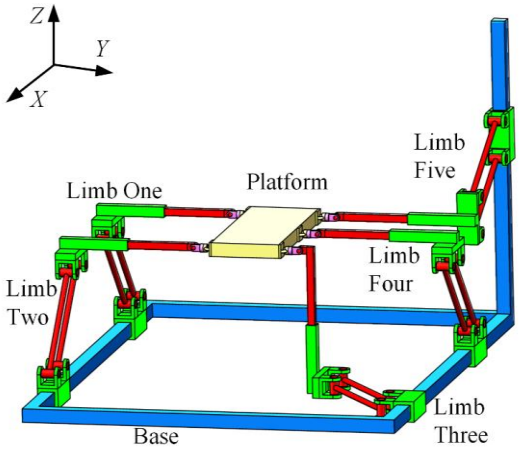

Figure 3-68 Schematic diagram of 5-DOF parallel structure (18)

Feature: There are one P_2 joint (P_Z), two P_4 joints (P_X, P_Y), two R_5 joints (R_X, R_Y), one P_a joint (P_{XY}) and four same P_a joints (P_{XZ}). Four same P_a joints (P_{XZ}) are related to P_2 joint (P_Z). Five P_a joints (P_{XY}, P_{XZ}) are related to P_4 joint (P_X). One P_a joint (P_{XY}) is related to P_4 joint (P_Y). The translational direction of P_4 joint (P_X) and the rotational axis of R_5 joint (R_X) are parallel (X axis). The translational direction of P_4 joint (P_Y) and the rotational axis of R_5 joint (R_Y) are parallel (Y axis).

$$\left[\begin{array}{ccc|ccc|ccc} P_X & P_{XY} & P_{XZ} & P_X & - & P_{XZ} & - & - & - \\ - & P_Y & P_{YZ} & - & P_Y & - & - & - & - \\ R_Y & R_X & P_Z & R_Y & R_X & - & R_Y & R_X & - \\ P_X & - & P_{XZ} & P_X & - & - & - & - & - \\ - & P_Y & - & - & P_Y & - & - & - & - \\ R_Y & R_X & P_Z & R_Y & R_X & - & - & - & - \end{array}\right] \tag{3-185}$$

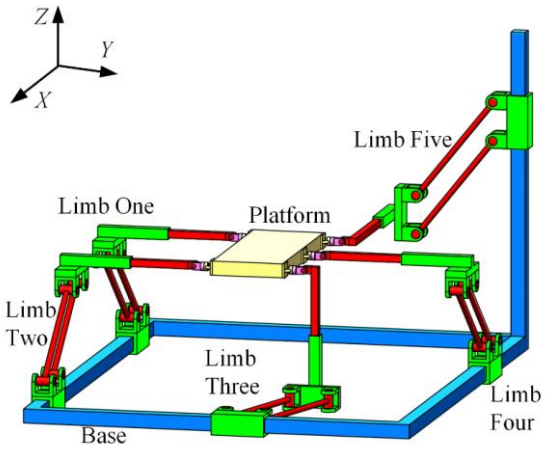

Figure 3-69 Schematic diagram of 5-DOF parallel structure (19)

Feature: There are one P_2 joint (P_Z), two P_4 joints (P_X, P_Y), two R_5 joints (R_X, R_Y), one P_a joint (P_{XY}), one P_a joint (P_{YZ}) and three same P_a joints (P_{XZ}). Four P_a joints (P_{XZ}, P_{YZ}) are related to P_2 joint (P_Z). Four P_a joints (P_{XY}, P_{XZ}) are related to P_4 joint (P_X). Two different P_a joints (P_{XY}, P_{YZ}) are related to P_4 joint (P_Y). The translational direction of P_4 joint (P_X) and the rotational axis of R_5 joint (R_X) are parallel (X axis). The translational direction of P_4 joint (P_Y) and the rotational axis of R_5 joint (R_Y) are parallel (Y axis).

$$\left[\begin{array}{ccc:ccc:ccc} P_X & \_ & P_{XZ} & P_X & \_ & P_{XZ} & \_ & \_ & \_ \\ \_ & P_Y & P_{YZ} & \_ & P_Y & \_ & \_ & \_ & \_ \\ R_Y & R_X & P_Z & R_Y & R_X & \_ & R_Y & R_X & \_ \\ P_X & \_ & P_{XZ} & P_X & \_ & P_{XZ} & \_ & \_ & \_ \\ \_ & P_Y & \_ & \_ & P_Y & \_ & \_ & \_ & \_ \\ R_Y & R_X & P_Z & R_Y & R_X & \_ & \_ & \_ & \_ \end{array}\right] \tag{3-186}$$

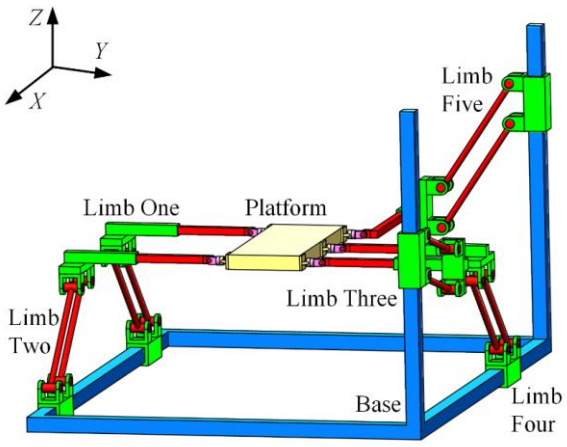

Figure 3-70 Schematic diagram of 5-DOF parallel structure (20)

Feature: There are one P_2 joint (P_Z), two P_4 joints (P_X, P_Y), two R_5 joints (R_X, R_Y), one P_a joint (P_{YZ}) and four same P_a joints (P_{XZ}). Five P_a joints (P_{XZ}, P_{YZ}) are related to P_2 joint (P_Z). Four same P_a joints (P_{XZ}) are related to P_4 joint (P_X). One P_a joint (P_{YZ}) is related to P_4 joint (P_Y). The translational direction of P_4 joint (P_X) and the rotational axis of R_5 joint (R_X) are parallel (X axis). The translational direction of P_4 joint (P_Y) and the rotational axis of R_5 joint (R_Y) are parallel (Y axis).

$$\left[\begin{array}{ccc:ccc:ccc} P_X & P_{XY} & P_{XZ} & P_X & - & P_{XZ} & - & - & - \\ - & P_Y & - & - & P_Y & - & - & P_Y & - \\ R_Y & R_X & P_Z & R_Y & R_X & - & R_Y & R_X & - \\ P_X & - & P_{XZ} & - & - & P_{XZ} & - & - & - \\ - & P_Y & - & - & P_Y & - & - & - & - \\ R_Y & R_X & P_Z & R_Y & R_X & - & - & - & - \end{array}\right] \tag{3-187}$$

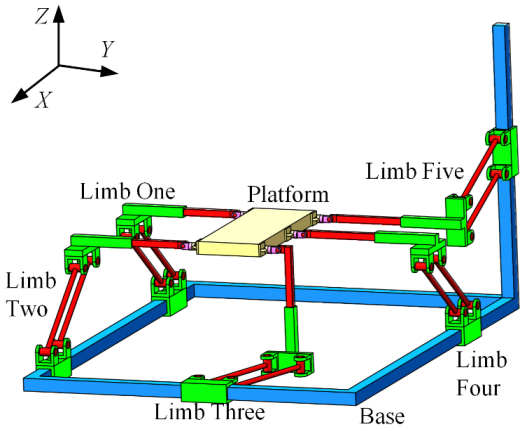

Figure 3-71 Schematic diagram of 5-DOF parallel structure (21)

Feature: There are one P_2 joint (P_Z), one P_3 joint (P_X), one P_5 joints (P_Y), two R_5 joints (R_X, R_Y), one P_a joint (P_{XY}) and four same P_a joints (P_{XZ}). Four same P_a joints (P_{XZ}) are related to P_2 joint (P_Z). Five P_a joints (P_{XY}, P_{XZ}) are related to P_3 joint (P_X). One P_a joint (P_{XY}) is related to P_5 joint (P_Y). The translational direction of P_3 joint (P_X) and the rotational axis of R_5 joint (R_X) are parallel (X axis). The translational direction of P_5 joint (P_Y) and the rotational axis of R_5 joint (R_Y) are parallel (Y axis).

$$\left[\begin{array}{ccc:ccc:ccc} P_X & P_{XY} & P_{XZ} & P_X & - & - & P_X & - & - \\ - & P_Y & P_{YZ} & - & P_Y & - & - & - & - \\ R_Y & R_X & P_Z & R_Y & R_X & - & R_Y & R_X & - \\ P_X & - & P_{XZ} & P_X & - & - & - & - & - \\ - & P_Y & P_{YZ} & - & P_Y & - & - & - & - \\ R_Y & R_X & - & R_Y & R_X & - & - & - & - \end{array}\right] \tag{3-188}$$

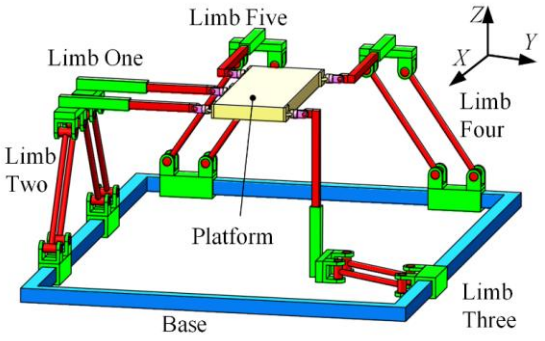

Figure 3-72 Schematic diagram of 5-DOF parallel structure (22)

Feature: There are one P_1 joint (P_Z), one P_4 joint (P_Y), one P_5 joints (P_X), two R_5 joints (R_X, R_Y), one P_a joint (P_{XY}), two same P_a joints (P_{XZ}) and two same P_a joints (P_{YZ}). Four P_a joints (P_{XZ}, P_{YZ}) are related to P_1 joint (P_Z). Three P_a joints (P_{XZ}, P_{YZ}) are related to P_4 joint (P_Y). Three P_a joints (P_{XY}, P_{XZ}) are related to P_5 joint (P_X). The translational direction of P_5 joint (P_X) and the rotational axis of R_5 joint (R_X) are parallel (X axis). The translational direction of P_4 joint (P_Y) and the rotational axis of R_5 joint (R_Y) are parallel (Y axis).

$$\left[\begin{array}{ccc:ccc:ccc} P_X & - & P_{XZ} & P_X & - & - & P_X & - & - \\ - & P_Y & P_{YZ} & - & P_Y & P_{YZ} & - & - & - \\ R_Y & R_X & P_Z & R_Y & R_X & - & R_Y & R_X & - \\ P_X & - & P_{XZ} & P_X & - & - & - & - & - \\ - & P_Y & P_{YZ} & - & P_Y & - & - & - & - \\ R_Y & R_X & - & R_Y & R_X & - & - & - & - \end{array}\right] \tag{3-189}$$

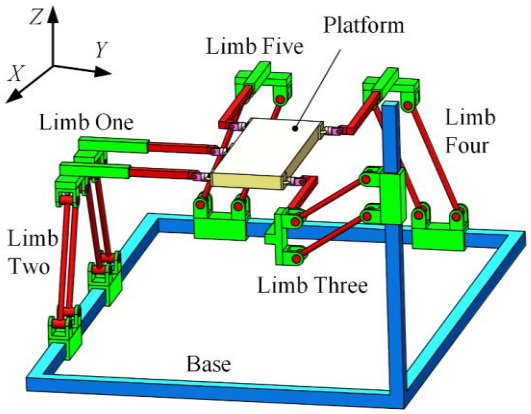

Figure 3-73 Schematic diagram of 5-DOF parallel structure (23)

Feature: There are one P_1 joint (P_Z), one P_4 joint (P_Y), one P_5 joints (P_X), two R_5 joints (R_X, R_Y), two same P_a joints (P_{XZ}) and three same P_a joints (P_{YZ}). Five P_a joints (P_{XZ}, P_{YZ}) are related to P_1 joint (P_Z). Three same P_a joints (P_{YZ}) are related to P_4 joint (P_Y). Two same P_a joints (P_{XZ}) are related to P_5 joint (P_X). The translational direction of P_5 joint (P_X) and the rotational axis of R_5 joint (R_X) are parallel (*X* axis). The translational direction of P_4 joint (P_Y) and the rotational axis of R_5 joint (R_Y) are parallel (*Y* axis).

$$\left[\begin{array}{ccc:ccc:ccc} P_X & P_{XY} & P_{XZ} & P_X & \_ & \_ & P_X & \_ & \_ \\ \_ & P_Y & P_{YZ} & \_ & P_Y & \_ & \_ & \_ & \_ \\ R_Y & R_X & P_Z & R_Y & R_X & \_ & R_Y & R_X & \_ \\ P_X & P_{XY} & P_{XZ} & P_X & \_ & \_ & \_ & \_ & \_ \\ \_ & P_Y & \_ & \_ & \_ & \_ & \_ & \_ & \_ \\ R_Y & R_X & P_Z & R_Y & R_X & \_ & \_ & \_ & \_ \end{array}\right] \tag{3-190}$$

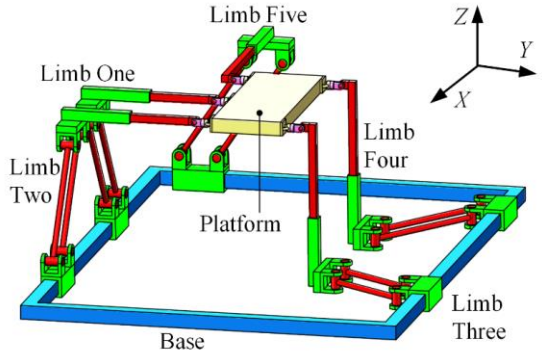

Figure 3-74 Schematic diagram of 5-DOF parallel structure (24)

Feature: There are one P_2 joint (P_Z), one P_3 joint (P_Y), one P_5 joints (P_X), two R_5 joints (R_X, R_Y), one P_a joint (P_{YZ}), two same P_a joints (P_{XY}) and two same P_a joints (P_{XZ}). Three P_a joints

(P_{XZ}, P_{YZ}) are related to P_2 joint (P_Z). Three P_a joints (P_{XY}, P_{YZ}) are related to P_3 joint (P_Y). Four P_a joints (P_{XY}, P_{XZ}) are related to P_5 joint (P_X). The translational direction of P_5 joint (P_X) and the rotational axis of R_5 joint (R_X) are parallel (*X* axis). The translational direction of P_3 joint (P_Y) and the rotational axis of R_5 joint (R_Y) are parallel (*Y* axis).

$$\left[\begin{array}{ccc:ccc:ccc} P_X & P_{XY} & P_{XZ} & P_X & P_{XY} & - & - & - & - \\ - & P_Y & - & - & P_Y & - & - & - & - \\ R_Y & R_X & P_Z & R_Y & R_X & P_Z & R_Y & R_X & - \\ P_X & P_{XY} & P_{XZ} & P_X & - & - & - & - & - \\ - & P_Y & - & - & - & - & - & - & - \\ R_Y & R_X & P_Z & R_Y & R_X & - & - & - & - \end{array}\right] \tag{3-191}$$

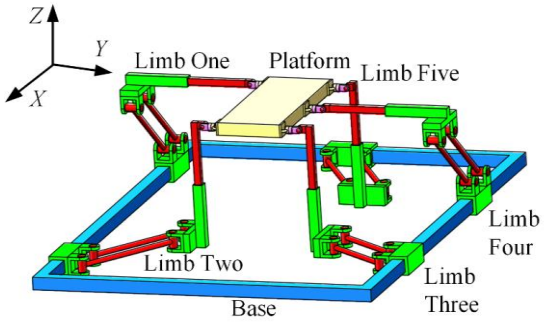

Figure 3-75 Schematic diagram of 5-DOF parallel structure (25)

Feature: There are two P_3 joints (P_Y, P_Z), one P_4 joint (P_X), two R_5 joints (R_X, R_Y), two same P_a joints (P_{XZ}) and three same P_a joints (P_{XY}). Three same P_a joints (P_{XY}) are related to P_3 joint (P_Y). Two same P_a joints (P_{XZ}) are related to P_3 joint (P_Z). Five P_a joints (P_{XY}, P_{XZ}) are related to P_4 joint (P_X). The translational direction of P_4 joint (P_X) and the rotational axis of R_5 joint (R_X) are parallel (*X* axis). The translational direction of P_3 joint (P_Y) and the rotational axis of R_5 joint (R_Y) are parallel (*Y* axis).

$$\left[\begin{array}{ccc:ccc:ccc} P_X & - & P_{XZ} & P_X & - & - & P_X & - & - \\ - & P_Y & P_{YZ} & - & P_Y & P_{YZ} & - & - & - \\ R_Y & R_X & P_Z & R_Y & R_X & - & R_Y & R_X & - \\ P_X & - & P_{XZ} & P_X & - & - & - & - & - \\ - & P_Y & P_{YZ} & - & - & - & - & - & - \\ R_Y & R_X & P_Z & R_Y & R_X & - & - & - & - \end{array}\right] \tag{3-192}$$

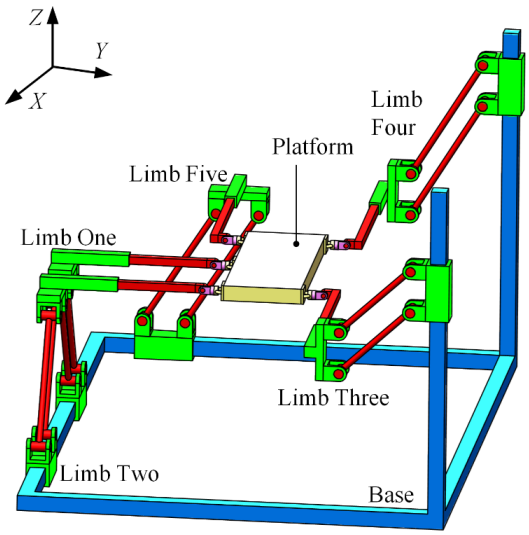

Figure 3-76 Schematic diagram of 5-DOF parallel structure (26)

Feature: There are one P_2 joint (P_Z), one P_3 joint (P_Y), one P_5 joint (P_X), two R_5 joints (R_X, R_Y), two same P_a joints (P_{XZ}) and three same P_a joints (P_{YZ}). Five P_a joints (P_{XZ}, P_{YZ}) are related to P_2 joint (P_Z). Three same P_a joints (P_{YZ}) are related to P_3 joint (P_Y). Three same P_a joints (P_{XZ}) are related to P_5 joint (P_X). The translational direction of P_5 joint (P_X) and the rotational axis of R_5 joint (R_X) are parallel (X axis). The translational direction of P_3 joint (P_Y) and the rotational axis of R_5 joint (R_Y) are parallel (Y axis).

$$\left[\begin{array}{ccc:ccc:ccc} P_X & P_{XY} & P_{XZ} & P_X & - & - & P_X & - & - \\ - & P_Y & P_{YZ} & - & - & - & - & - & - \\ R_Y & R_X & P_Z & R_Y & R_X & P_Z & R_Y & R_X & - \\ P_X & - & P_{XZ} & P_X & - & - & - & - & - \\ - & P_Y & P_{YZ} & - & - & - & - & - & - \\ R_Y & R_X & P_Z & R_Y & R_X & - & - & - & - \end{array}\right] \tag{3-193}$$

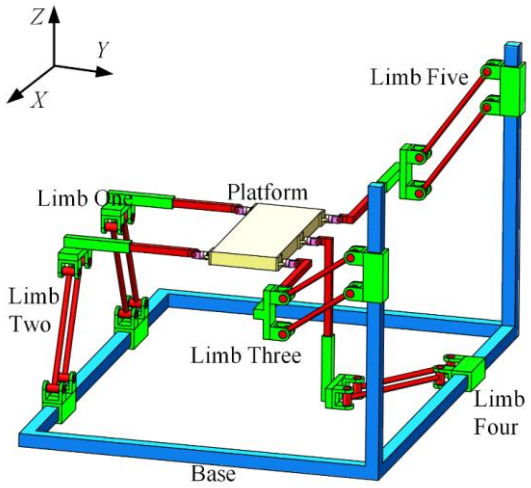

Figure 3-77 Schematic diagram of 5-DOF parallel structure (27)

Feature: There are one P_2 joint (P_Y), one P_3 joint (P_Z), one P_5 joint (P_X), two R_5 joints (R_X, R_Y), one P_a joint (P_{XY}), two same P_a joints (P_{XZ}) and two same P_a joints (P_{YZ}). Three P_a joints (P_{XY}, P_{YZ}) are related to P_2 joint (P_Y). Four P_a joints (P_{XZ}, P_{YZ}) are related to P_3 joint (P_Z). Three P_a joints (P_{XY}, P_{XZ}) are related to P_5 joint (P_X). The translational direction of P_5 joint (P_X) and the rotational axis of R_5 joint (R_X) are parallel (X axis). The translational direction of P_2 joint (P_Y) and the rotational axis of R_5 joint (R_Y) are parallel (Y axis).

$$\left[\begin{array}{ccc:ccc:ccc} P_X & P_{XY} & P_{XZ} & P_X & - & - & - & - & - \\ - & P_Y & P_{YZ} & - & P_Y & - & - & - & - \\ R_Y & R_X & P_Z & R_Y & R_X & P_Z & R_Y & R_X & - \\ P_X & - & P_{XZ} & P_X & - & - & - & - & - \\ - & P_Y & P_{YZ} & - & - & - & - & - & - \\ R_Y & R_X & P_Z & R_Y & R_X & - & - & - & - \end{array}\right] \tag{3-194}$$

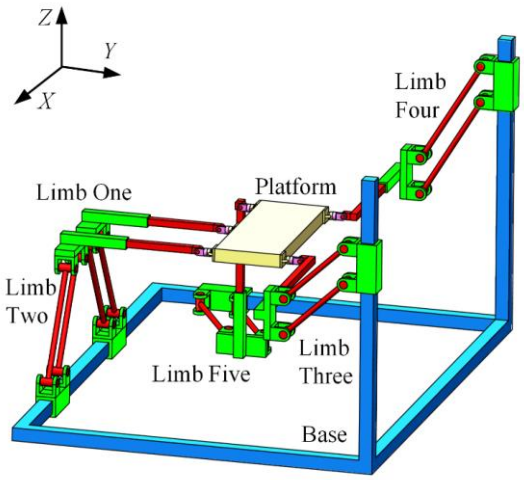

Figure 3-78 Schematic diagram of 5-DOF parallel structure (28)

Feature: There are two P_3 joints (P_Y, P_Z), one P_4 joint (P_X), two R_5 joints (R_X, R_Y), one P_a joint (P_{XY}), two same P_a joints (P_{XZ}) and two same Pa joints (P_{YZ}). Three P_a joints (P_{XY}, P_{YZ}) are related to P_3 joint (P_Y). Four P_a joints (P_{XZ}, P_{YZ}) are related to P_3 joint (P_Z). Three P_a joints (P_{XY}, P_{XZ}) are related to P_4 joint (P_X). The translational direction of P_4 joint (P_X) and the rotational axis of R_5 joint (R_X) are parallel (X axis). The translational direction of P_3 joint (P_Y) and the rotational axis of R_5 joint (R_Y) are parallel (Y axis).

$$\left[\begin{array}{ccc:ccc:ccc} P_X & - & P_{XZ} & P_X & - & P_{XZ} & - & - & - \\ - & P_Y & P_{YZ} & - & P_Y & - & - & - & - \\ R_Y & R_X & P_Z & R_Y & R_X & P_Z & R_Y & R_X & - \\ P_X & - & P_{XZ} & P_X & - & - & - & - & - \\ - & P_Y & P_{YZ} & - & - & - & - & - & - \\ R_Y & R_X & P_Z & R_Y & R_X & - & - & - & - \end{array}\right] \tag{3-195}$$

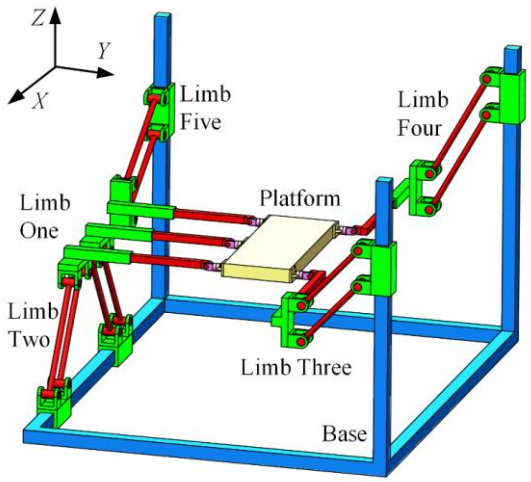

Figure 3-79 Schematic diagram of 5-DOF parallel structure (29)

Feature: There are two P_3 joints (P_Y, P_Z), one P_4 joint (P_X), two R_5 joints (R_X, R_Y), two same P_a joints (P_{YZ}) and three same P_a joints (P_{YZ}). Two same P_a joints (P_{YZ}) are related to P_3 joint (P_Y). Five P_a joints (P_{XZ}, P_{YZ}) are related to P_3 joint (P_Z). Three same P_a joints (P_{XZ}) are related to P_4 joint (P_X). The translational direction of P_4 joint (P_X) and the rotational axis of R_5 joint (R_X) are parallel (X axis). The translational direction of P_3 joint (P_Y) and the rotational axis of R_5 joint (R_Y) are parallel (Y axis).

$$\left[\begin{array}{ccc:ccc:ccc} P_X & - & P_{XZ} & P_X & - & P_{XZ} & - & - & - \\ - & P_Y & P_{YZ} & - & P_Y & - & - & P_Y & - \\ R_Y & R_X & P_Z & R_Y & R_X & - & R_Y & R_X & - \\ P_X & - & P_{XZ} & - & - & P_{XZ} & - & - & - \\ - & P_Y & - & - & P_Y & - & - & - & - \\ R_Y & R_X & P_Z & R_Y & R_X & - & - & - & - \end{array}\right] \tag{3-196}$$

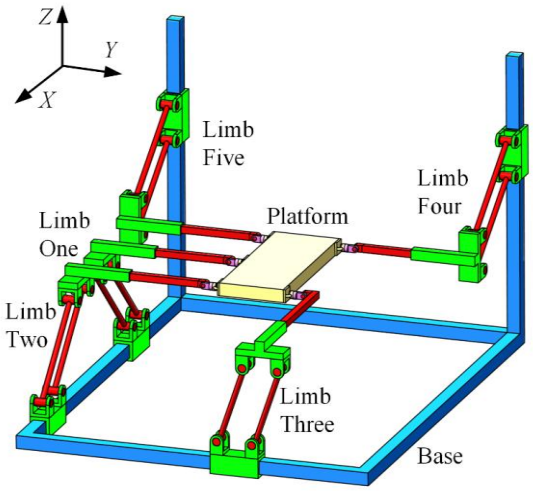

Figure 3-80 Schematic diagram of 5-DOF parallel structure (30)

Feature: There are one P_2 joint (P_Z), one P_3 joint (P_X), one P_5 joint (P_Y), two R_5 joints (R_X, R_Y), one P_a joint (P_{YZ}) and four same P_a joints (P_{XZ}). Five P_a joints (P_{XZ}, P_{YZ}) are related to P_2 joint (P_Z). Three same P_a joints (P_{XZ}) are related to P_3 joint (P_X). One P_a joint (P_{YZ}) is related to P_5 joint (P_Y). The translational direction of P_3 joint (P_X) and the rotational axis of R_5 joint (R_X) are parallel (X axis). The translational direction of P_5 joint (P_Y) and the rotational axis of R_5 joint (R_Y) are parallel (Y axis).

$$\left[\begin{array}{ccc:ccc:ccc} P_X & P_{XY} & P_{XZ} & P_X & - & P_{XZ} & - & - & - \\ - & P_Y & - & - & P_Y & - & - & - & - \\ R_Y & R_X & P_Z & R_Y & R_X & P_Z & R_Y & R_X & - \\ P_X & - & P_{XZ} & - & - & P_{XZ} & - & - & - \\ - & P_Y & - & - & P_Y & - & - & - & - \\ R_Y & R_X & P_Z & R_Y & R_X & - & - & - & - \end{array}\right] \tag{3-197}$$

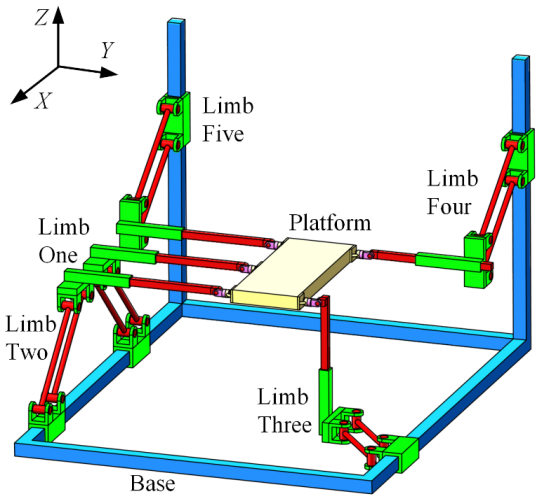

Figure 3-81 Schematic diagram of 5-DOF parallel structure (31)

Feature: There are two P_3 joints (P_X, P_Z), one P_4 joint (P_Y), two R_5 joints (R_X, R_Y), one P_a joint (P_{XY}) and four same P_a joints (P_{XZ}). Five P_a joints (P_{XY}, P_{XZ}) are related to P_3 joint (P_X). Four same P_a joints (P_{XZ}) are related to P_3 joint (P_Z). One P_a joint (P_{XY}) is related to P_4 joint (P_Y). The translational direction of P_3 joint (P_X) and the rotational axis of R_5 joint (R_X) are parallel (X axis). The translational direction of P_4 joint (P_Y) and the rotational axis of R_5 joint (R_Y) are parallel (Y axis).

$$\left[\begin{array}{ccc:ccc:ccc} P_X & P_{XY} & P_{XZ} & P_X & - & - & P_X & - & - \\ - & P_Y & P_{YZ} & - & P_Y & - & - & - & - \\ R_Y & R_X & P_Z & R_Y & R_X & - & R_Y & R_X & - \\ P_X & - & P_{XZ} & P_X & - & - & - & - & - \\ - & P_Y & P_{YZ} & - & - & - & - & - & - \\ R_Y & R_X & P_Z & R_Y & R_X & - & - & - & - \end{array}\right] \tag{3-198}$$

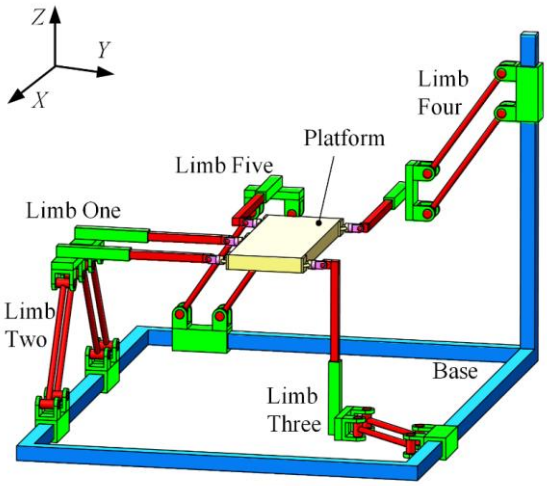

Figure 3-82 Schematic diagram of 5-DOF parallel structure (32)

Feature: There are one P_2 joint (P_Z), one P_3 joint (P_Y), one P_5 joint (P_X), two R_5 joints (R_X, R_Y), one P_a joint (P_{XY}), two same P_a joints (P_{XZ}) and two same P_a joints (P_{YZ}). Four P_a joints (P_{XZ}, P_{YZ}) are related to P_2 joint (P_Z). Three P_a joints (P_{XY}, P_{YZ}) are related to P_3 joint (P_Y). Three P_a joints (P_{XY}, P_{XZ}) are related to P_5 joint (P_X). The translational direction of P_5 joint (P_X) and the rotational axis of R_5 joint (R_X) are parallel (X axis). The translational direction of P_3 joint (P_Y) and the rotational axis of R_5 joint (R_Y) are parallel (Y axis).

$$\left[\begin{array}{ccc:ccc:ccc} P_X & P_{XY} & P_{XZ} & P_X & - & - & - & - & - \\ - & P_Y & P_{YZ} & - & P_Y & - & - & - & - \\ R_Y & R_X & P_Z & R_Y & R_X & - & R_Y & R_X & - \\ P_X & P_{XY} & P_{XZ} & P_X & - & - & - & - & - \\ - & P_Y & - & - & P_Y & - & - & - & - \\ R_Y & R_X & P_Z & R_Y & R_X & - & - & - & - \end{array}\right] \tag{3-199}$$

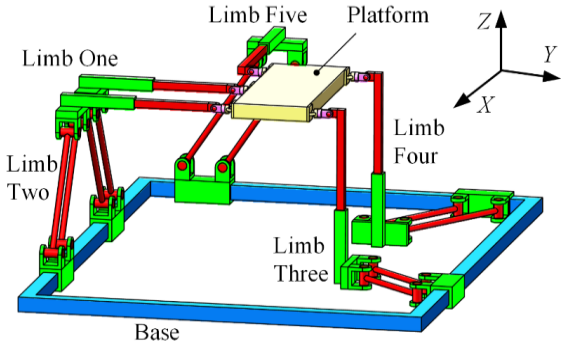

Figure 3-83 Schematic diagram of 5-DOF parallel structure (33)

Feature: There are one P_2 joint (P_Z), two P_4 joints (P_X, P_Y), two R_5 joints (R_X, R_Y), one P_a joint (P_{YZ}), two same P_a joints (P_{XY}) and two same Pa joints (P_{XZ}). Three P_a joints (P_{XZ}, P_{YZ}) are related to P_2 joint (P_Z). Four P_a joints (P_{XY}, P_{XZ}) are related to P_4 joint (P_X). Three P_a joints (P_{XY}, P_{YZ}) are related to P_4 joint (P_Y). The translational direction of P_4 joint (P_X) and the rotational axis of R_5 joint (R_X) are parallel (X axis). The translational direction of P_4 joint (P_Y) and the rotational axis of R_5 joint (R_Y) are parallel (Y axis).

$$\left[\begin{array}{ccc:ccc:ccc} P_X & P_{XY} & P_{XZ} & P_X & - & - & - & - & - \\ - & P_Y & P_{YZ} & - & P_Y & - & - & - & - \\ R_Y & R_X & P_Z & R_Y & R_X & - & R_Y & R_X & - \\ P_X & - & P_{XZ} & P_X & - & - & - & - & - \\ - & P_Y & P_{YZ} & - & P_Y & - & - & - & - \\ R_Y & R_X & P_Z & R_Y & R_X & - & - & - & - \end{array}\right] \tag{3-200}$$

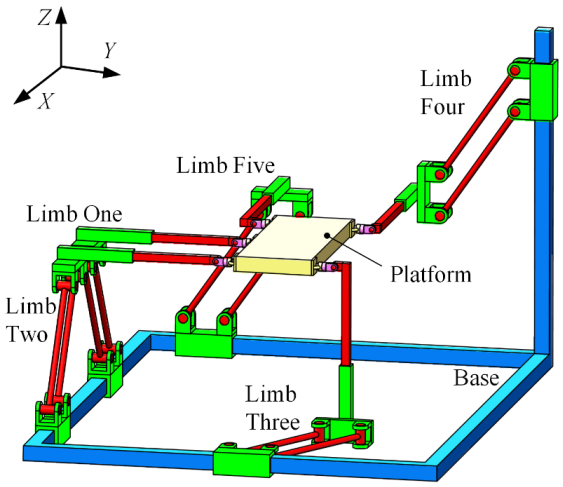

Figure 3-84 Schematic diagram of 5-DOF parallel structure (34)

Feature: There are one P_2 joint (P_Z), two P_4 joints (P_X, P_Y), two R_5 joints (R_X, R_Y), one P_a joint (P_{XY}), two same P_a joints (P_{XZ}) and two same P_a joints (P_{YZ}). Four P_a joints (P_{XZ}, P_{YZ}) are related to P_2 joint (P_Z). Three P_a joints (P_{XY}, P_{XZ}) are related to P_4 joint (P_X). Three P_a joints (P_{XY}, P_{YZ}) are related to P_4 joint (P_Y). The translational direction of P_4 joint (P_X) and the rotational axis of R_5 joint (R_X) are parallel (X axis). The translational direction of P_4 joint (P_Y) and the rotational axis of R_5 joint (R_Y) are parallel (Y axis).

$$\left[\begin{array}{ccc:ccc:ccc} P_X & - & P_{XZ} & P_X & - & P_{XZ} & - & - & - \\ - & P_Y & P_{YZ} & - & P_Y & - & - & - & - \\ R_Y & R_X & P_Z & R_Y & R_X & - & R_Y & R_X & - \\ P_X & - & P_{XZ} & P_X & - & - & - & - & - \\ - & P_Y & P_{YZ} & - & P_Y & - & - & - & - \\ R_Y & R_X & P_Z & R_Y & R_X & - & - & - & - \end{array}\right] \tag{3-201}$$

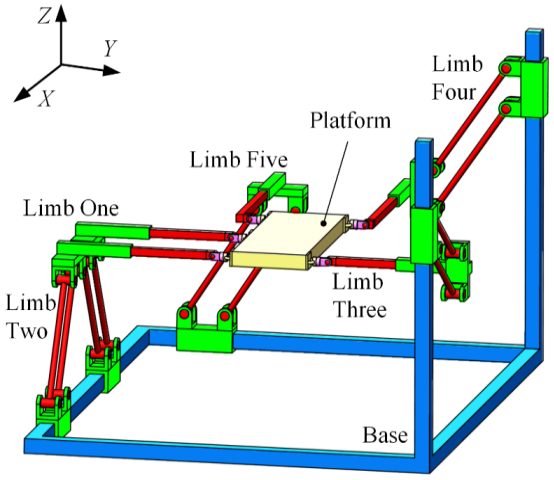

Figure 3-85 Schematic diagram of 5-DOF parallel structure (35)

Feature: There are one P_2 joint (P_Z), two P_4 joints (P_X, P_Y), two R_5 joints (R_X, R_Y), two same P_a joints (P_{YZ}) and three same P_a joints (P_{XZ}). Five P_a joints (P_{XZ}, P_{YZ}) are related to P_2 joint (P_Z). Three identical P_a joints (P_{XZ}) are related to P_4 joint (P_X). Two same P_a joints (P_{YZ}) are related to P_4 joint (P_Y). The translational direction of P_4 joint (P_X) and the rotational axis of R_5 joint (R_X) are parallel (X axis). The translational direction of P_4 joint (P_Y) and the rotational axis of R_5 joint (R_Y) are parallel (Y axis).

$$\left[\begin{array}{ccc:ccc:ccc} P_X & P_{XY} & P_{XZ} & P_X & - & P_{XZ} & - & - & - \\ - & P_Y & P_{YZ} & - & P_Y & - & - & P_Y & - \\ R_Y & R_X & P_Z & R_Y & R_X & - & R_Y & R_X & - \\ P_X & - & P_{XZ} & - & - & - & - & - & - \\ - & P_Y & - & - & P_Y & - & - & - & - \\ R_Y & R_X & P_Z & R_Y & R_X & - & - & - & - \end{array}\right] \tag{3-202}$$

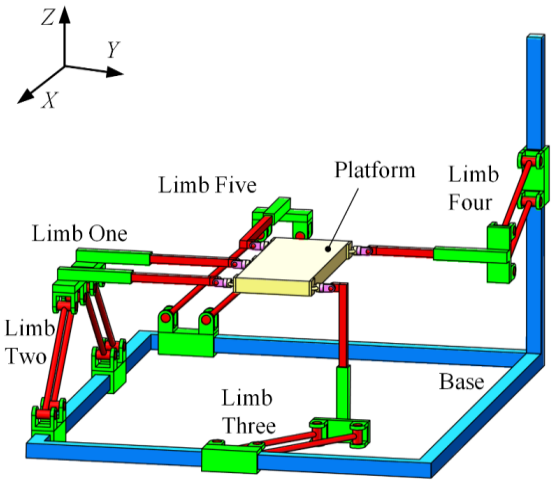

Figure 3-86 Schematic diagram of 5-DOF parallel structure (36)

Feature: There are one P_2 joint (P_Z), one P_3 joint (P_X), one P_5 joint (P_Y), two R_5 joints (R_X, R_Y) , one P_a joint (P_{XY}), one P_a joint (P_{YZ}) and three same P_a joints (P_{XZ}). Four P_a joints (P_{XZ}, P_{YZ}) are related to P_2 joint (P_Z). Four P_a joints (P_{XY}, P_{XZ}) are related to P_3 joint (P_X). Two different P_a joints (P_{XY}, P_{YZ}) are related to P_5 joint (P_Y). The translational direction of P_3 joint (P_X) and the rotational axis of R_5 joint (R_X) are parallel (X axis). The translational direction of P_5 joint (P_Y) and the rotational axis of R_5 joint (R_Y) are parallel (Y axis).

$$\left[\begin{array}{ccc:ccc:ccc} P_X & P_{XY} & P_{XZ} & P_X & - & - & - & - & - \\ - & P_Y & P_{YZ} & - & P_Y & - & - & - & - \\ R_Y & R_X & P_Z & R_Y & R_X & P_Z & R_Y & R_X & - \\ P_X & P_{XY} & P_{XZ} & P_X & - & - & - & - & - \\ - & P_Y & - & - & - & - & - & - & - \\ R_Y & R_X & P_Z & R_Y & R_X & - & - & - & - \end{array}\right] \tag{3-203}$$

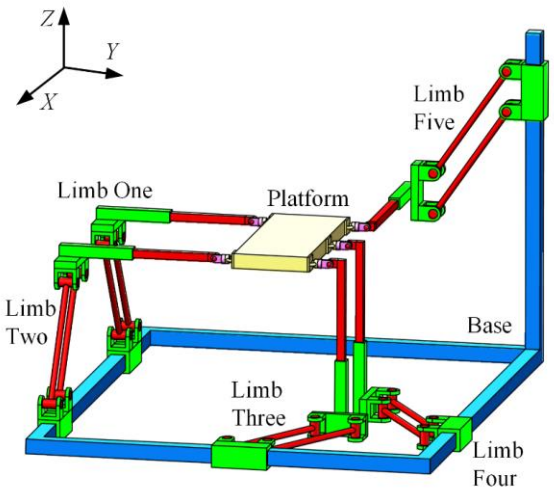

Figure 3-87 Schematic diagram of 5-DOF parallel structure (37)

Feature: There are two P_3 joints (P_Y, P_Z), one P_4 joint (P_X), two R_5 joints (R_X, R_Y) , one P_a joint (P_{YZ}), two same P_a joints (P_{XY}) and two same Pa joints (P_{XZ}). Three P_a joints (P_{XY}, P_{YZ}) are related to P_3 joint (P_Y). Three P_a joints (P_{XZ}, P_{YZ}) are related to P_3 joint (P_Z). Four P_a joints (P_{XY}, P_{XZ}) are related to P_4 joint (P_X). The translational direction of P_4 joint (P_X) and the rotational axis of R_5 joint (R_X) are parallel (X axis). The translational direction of P_3 joint (P_Y) and the rotational axis of R_5 joint (R_Y) are parallel (Y axis).

$$\left[\begin{array}{ccc:ccc:ccc} P_X & P_{XY} & P_{XZ} & P_X & - & P_{XZ} & - & - & - \\ - & P_Y & P_{YZ} & - & P_Y & - & - & - & - \\ R_Y & R_X & P_Z & R_Y & R_X & P_Z & R_Y & R_X & - \\ P_X & - & P_{XZ} & P_X & - & - & - & - & - \\ - & P_Y & - & - & - & - & - & - & - \\ R_Y & R_X & P_Z & R_Y & R_X & - & - & - & - \end{array}\right] \tag{3-204}$$

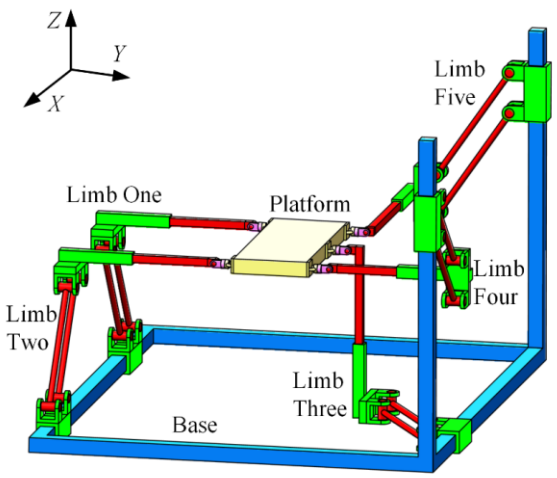

Figure 3-88 Schematic diagram of 5-DOF parallel structure (38)

Feature: There are two P_3 joints (P_Y, P_Z), one P_4 joint (P_X), two R_5 joints (R_X, R_Y) , one P_a joint (P_{XY}), one P_a joint (P_{YZ}) and three same P_a joints (P_{XZ}). Two different P_a joints (P_{XY}, P_{YZ}) are related to P_3 joint (P_Y). Four P_a joints (P_{XZ}, P_{YZ}) are relevant to P_3 joint (P_Z). Four P_a joints (P_{XY}, P_{XZ}) are relevant to P_4 joint (P_X). The translational direction of P_4 joint (P_X) and the rotational axis of R_5 joint (R_X) are parallel (X axis). The translational direction of P_3 joint (P_Y) and the rotational axis of R_5 joint (R_Y) are parallel (Y axis).

$$\left[\begin{array}{ccc:ccc:ccc} P_X & P_{XY} & P_{XZ} & P_X & - & P_{XZ} & - & - & - \\ - & P_Y & - & - & P_Y & - & - & - & - \\ R_Y & R_X & P_Z & R_Y & R_X & P_Z & R_Y & R_X & - \\ P_X & P_{XY} & P_{XZ} & - & - & - & - & - & - \\ - & P_Y & - & - & P_Y & - & - & - & - \\ R_Y & R_X & P_Z & R_Y & R_X & - & - & - & - \end{array}\right] \tag{3-205}$$

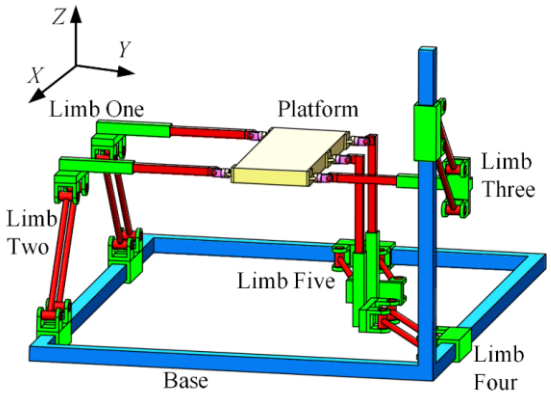

Figure 3-89 Schematic diagram of 5-DOF parallel structure (39)

Feature: There are two P_3 joints (P_X, P_Z), one P_4 joint (P_Y), two R_5 joints (R_X, R_Y) , two same P_a joints (P_{XY}) and three same P_a joints (P_{XZ}). Five P_a joints (P_{XY}, P_{XZ}) are related to P_3 joint (P_X). Three identical P_a joints (P_{XZ}) are relevant to P_3 joint (P_Z). Two same P_a joints (P_{XY}) are relevant to P_4 joint (P_Y). The translational direction of P_3 joint (P_X) and the rotational axis of R_5 joint (R_X) are parallel (X axis). The translational direction of P_4 joint (P_Y) and the rotational axis of R_5 joint (R_Y) are parallel (Y axis).

$$\left[\begin{array}{ccc:ccc:ccc} P_X & P_{XY} & P_{XZ} & P_X & - & P_{XZ} & - & - & - \\ - & P_Y & P_{YZ} & - & P_Y & - & - & - & - \\ R_Y & R_X & P_Z & R_Y & R_X & P_Z & R_Y & R_X & - \\ P_X & - & P_{XZ} & - & - & - & - & - & - \\ - & P_Y & - & - & P_Y & - & - & - & - \\ R_Y & R_X & P_Z & R_Y & R_X & - & - & - & - \end{array}\right] \tag{3-206}$$

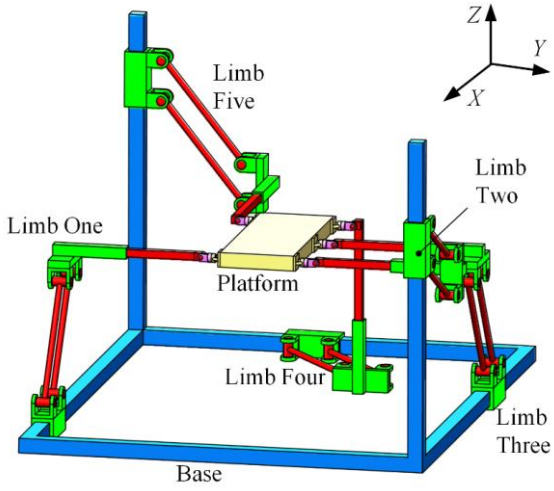

Figure 3-90 Schematic diagram of 5-DOF parallel structure (40)

Feature: There are two P_3 joints (P_X, P_Z), one P_4 joint (P_Y), two R_5 joints (R_X, R_Y) , one P_a joint (P_{XY}), one P_a joint (P_{YZ}) and three same P_a joints (P_{XZ}). Four P_a joints (P_{XY}, P_{XZ}) are related to P_3 joint (P_X). Four P_a joints (P_{XZ}, P_{YZ}) are relevant to P_3 joint (P_Z). Two different P_a joints (P_{XY}, P_{YZ}) are relevant to P_4 joint (P_Y). The translational direction of P_3 joint (P_X) and the rotational axis of R_5 joint (R_X) are parallel (X axis). The translational direction of P_4 joint (P_Y) and the rotational axis of R_5 joint (R_Y) are parallel (Y axis).

(ii) Case two: 2T3R mechanism

The possible mechanism is 5-PP_aRRR, as illustrated in figure 3-91.

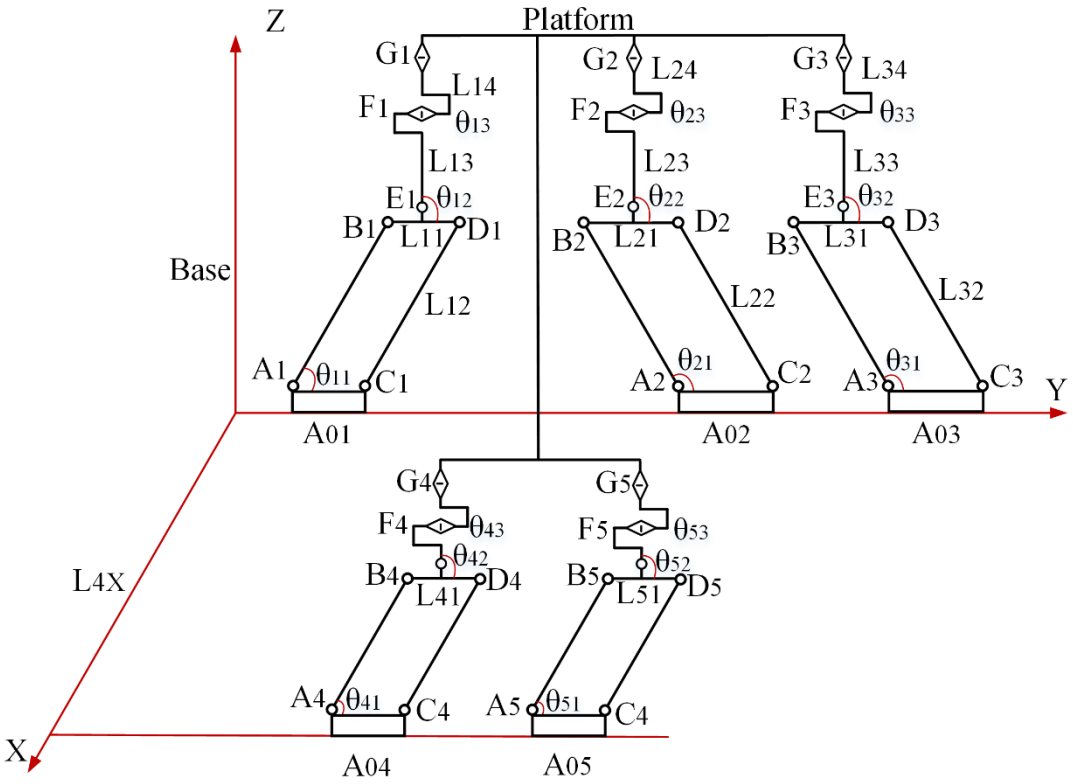

Figure 3-91 2T3R mechanism

The coordinates of the main points in this mechanisms are listed as, $A_{01}(0, x_1, 0)$, $A_1(0, x_1 - 0.5L_{11}, 0)$, $B_1(0, x_1 - 0.5L_{11} + L_{12}\cos\theta_{11}, L_{12}\sin\theta_{11})$, $C_1(0, x_1 + 0.5L_{11}, 0)$, $D_1(0, x_1 + 0.5L_{11} + L_{12}\cos\theta_{11}, L_{12}\sin\theta_{11})$, $E_1(0, x_1 + L_{12}\cos\theta_{11}, L_{12}\sin\theta_{11})$, $F_1(0, x_1 + L_{12}\cos\theta_{11} + L_{13}\cos\theta_{12}, L_{12}\sin\theta_{11} + L_{13}\sin\theta_{12})$, $G_1(L_{14}\cos\theta_{13}, x_1 + L_{12}\cos\theta_{11} + L_{13}\cos\theta_{12}, L_{12}\sin\theta_{11} + L_{13}\sin\theta_{12} + L_{14}\sin\theta_{13})$, $A_{02}(0, x_2, 0)$, $A_2(0, x_2 - 0.5L_{21}, 0)$, $B_2(0, x_2 - 0.5L_{21} + L_{22}\cos\theta_{21}, L_{22}\sin\theta_{21})$, $C_2(0, x_2 + 0.5L_{21}, 0)$, $D_2(0, x_2 + 0.5L_{21} + L_{22}\cos\theta_{21}, L_{22}\sin\theta_{21})$, $E_2(0, x_2 + L_{22}\cos\theta_{21}, L_{22}\sin\theta_{21})$, $F_2(0, x_2 + L_{22}\cos\theta_{21} + L_{23}\cos\theta_{22}, L_{22}\sin\theta_{21} + L_{23}\sin\theta_{22})$, $G_2(L_{24}\cos\theta_{23}, x_2 + L_{22}\cos\theta_{21} + L_{23}\cos\theta_{22}, L_{22}\sin\theta_{21} + L_{23}\sin\theta_{22} + L_{24}\sin\theta_{23})$, $A_{03}(0, x_3, 0)$, $A_3(0, x_3 - 0.5L_{31}, 0)$, $B_3(0, x_3 - 0.5L_{31} + L_{32}\cos\theta_{31}, L_{32}\sin\theta_{31})$, $C_3(0, x_3 + 0.5L_{31}, 0)$, $D_3(0, x_3 + 0.5L_{31} + L_{32}\cos\theta_{31}, L_{32}\sin\theta_{31})$, $E_3(0, x_3 + L_{32}\cos\theta_{31}, L_{32}\sin\theta_{31})$, $F_3(0, x_3 + L_{32}\cos\theta_{21} + L_{33}\cos\theta_{32}, L_{32}\sin\theta_{31} + L_{33}\sin\theta_{32})$,

$G_3(L_{34}\cos\theta_{33}, x_3+L_{32}\cos\theta_{31}+L_{33}\cos\theta_{32}, L_{32}\sin\theta_{31}+L_{33}\sin\theta_{32}+L_{34}\sin\theta_{33})$,

$A_{04}(L_{4X}, x_4, 0)$, $A_4(L_{4X}, x_4-0.5L_{41}, 0)$, $B_4(L_{4X}, x_4-0.5L_{41}+L_{42}\cos\theta_{41}, L_{42}\sin\theta_{41})$,

$C_4(L_{4X}, x_4+0.5L_{41}, 0)$, $D_4(L_{4X}, x_4+0.5L_{41}+L_{42}\cos\theta_{41}, L_{42}\sin\theta_{41})$,

$E_4(L_{4X}, x_4+L_{42}\cos\theta_{41}, L_{42}\sin\theta_{41})$,

$F_4(L_{4X}, x_4+L_{42}\cos\theta_{41}+L_{43}\cos\theta_{42}, L_{42}\sin\theta_{41}+L_{43}\sin\theta_{42})$,

$G_4(L_{4X}+L_{44}\cos\theta_{43}, x_4+L_{42}\cos\theta_{41}+L_{43}\cos\theta_{42}, L_{42}\sin\theta_{41}+L_{43}\sin\theta_{42}+L_{44}\sin\theta_{43})$,

$A_{05}(L_{5X}, x_5, 0)$, $A_5(L_{5X}, x_5-0.5L_{51}, 0)$, $B_5(L_{5X}, x_5-0.5L_{51}+L_{52}\cos\theta_{51}, L_{52}\sin\theta_{51})$,

$C_5(L_{5X}, x_5+0.5L_{51}, 0)$, $D_5(L_{5X}, x_5+0.5L_{51}+L_{52}\cos\theta_{51}, L_{52}\sin\theta_{51})$,

$E_5(L_{5X}, x_5+L_{52}\cos\theta_{51}, L_{52}\sin\theta_{51})$,

$F_5(L_{5X}, x_5+L_{52}\cos\theta_{51}+L_{53}\cos\theta_{52}, L_{52}\sin\theta_{51}+L_{53}\sin\theta_{52})$,

$G_5(L_{5X}+L_{54}\cos\theta_{53}, x_5+L_{52}\cos\theta_{51}+L_{53}\cos\theta_{52}, L_{52}\sin\theta_{51}+L_{53}\sin\theta_{52}+L_{54}\sin\theta_{53})$.

The kinematic screws of the P_a joint in each branch

$$\begin{cases} \$_{A1}=\begin{bmatrix}1 & 0 & 0; & 0 & 0 & 0.5L_{11}-x_1\end{bmatrix}^{\mathrm{T}} \\ \$_{B1}=\begin{bmatrix}1 & 0 & 0; & 0 & L_{12}\sin\theta_{11} & 0.5L_{11}-x_1-L_{12}\cos\theta_{11}\end{bmatrix}^{\mathrm{T}} \\ \$_{C1}=\begin{bmatrix}1 & 0 & 0; & 0 & 0 & -0.5L_{11}-x_1\end{bmatrix}^{\mathrm{T}} \\ \$_{D1}=\begin{bmatrix}1 & 0 & 0; & 0 & L_{12}\sin\theta_{11} & -0.5L_{11}-x_1-L_{12}\cos\theta_{11}\end{bmatrix}^{\mathrm{T}} \end{cases} \tag{3-207}$$

$$\begin{cases} \$_{A2}=\begin{bmatrix}1 & 0 & 0; & 0 & 0 & 0.5L_{21}-x_2\end{bmatrix}^{\mathrm{T}} \\ \$_{B2}=\begin{bmatrix}1 & 0 & 0; & 0 & L_{22}\sin\theta_{21} & 0.5L_{21}-x_2-L_{22}\cos\theta_{21}\end{bmatrix}^{\mathrm{T}} \\ \$_{C2}=\begin{bmatrix}1 & 0 & 0; & 0 & 0 & -0.5L_{21}-x_2\end{bmatrix}^{\mathrm{T}} \\ \$_{D2}=\begin{bmatrix}1 & 0 & 0; & 0 & L_{22}\sin\theta_{21} & -0.5L_{21}-x_2-L_{22}\cos\theta_{21}\end{bmatrix}^{\mathrm{T}} \end{cases} \tag{3-208}$$

$$\begin{cases} \$_{A3}=\begin{bmatrix}1 & 0 & 0; & 0 & 0 & 0.5L_{31}-x_3\end{bmatrix}^{\mathrm{T}} \\ \$_{B3}=\begin{bmatrix}1 & 0 & 0; & 0 & L_{32}\sin\theta_{31} & 0.5L_{31}-x_3-L_{32}\cos\theta_{31}\end{bmatrix}^{\mathrm{T}} \\ \$_{C3}=\begin{bmatrix}1 & 0 & 0; & 0 & 0 & -0.5L_{31}-x_3\end{bmatrix}^{\mathrm{T}} \\ \$_{D3}=\begin{bmatrix}1 & 0 & 0; & 0 & L_{32}\sin\theta_{31} & -0.5L_{31}-x_3-L_{32}\cos\theta_{31}\end{bmatrix}^{\mathrm{T}} \end{cases} \tag{3-209}$$

$$\begin{cases} \$_{A4} = \begin{bmatrix} 1 & 0 & 0; & 0 & 0 & 0.5L_{41} - x_4 \end{bmatrix}^{\mathrm{T}} \\ \$_{B4} = \begin{bmatrix} 1 & 0 & 0; & 0 & L_{42}\sin\theta_{41} & 0.5L_{41} - x_4 - L_{42}\cos\theta_{41} \end{bmatrix}^{\mathrm{T}} \\ \$_{C4} = \begin{bmatrix} 1 & 0 & 0; & 0 & 0 & -0.5L_{41} - x_4 \end{bmatrix}^{\mathrm{T}} \\ \$_{D4} = \begin{bmatrix} 1 & 0 & 0; & 0 & L_{42}\sin\theta_{41} & -0.5L_{41} - x_4 - L_{42}\cos\theta_{41} \end{bmatrix}^{\mathrm{T}} \end{cases} \tag{3-210}$$

$$\begin{cases} \$_{A5} = \begin{bmatrix} 1 & 0 & 0; & 0 & 0 & 0.5L_{51} - x_5 \end{bmatrix}^{\mathrm{T}} \\ \$_{B5} = \begin{bmatrix} 1 & 0 & 0; & 0 & L_{52}\sin\theta_{51} & 0.5L_{51} - x_5 - L_{52}\cos\theta_{51} \end{bmatrix}^{\mathrm{T}} \\ \$_{C5} = \begin{bmatrix} 1 & 0 & 0; & 0 & 0 & -0.5L_{51} - x_5 \end{bmatrix}^{\mathrm{T}} \\ \$_{D5} = \begin{bmatrix} 1 & 0 & 0; & 0 & L_{52}\sin\theta_{51} & -0.5L_{51} - x_5 - L_{52}\cos\theta_{51} \end{bmatrix}^{\mathrm{T}} \end{cases} \tag{3-211}$$

The equivalent kinematic screw of the P_a joint in each branch

$$\$_{Pa1} = \begin{bmatrix} 0 & 0 & 0; & 0 & \sin\theta_{11} & -\cos\theta_{11} \end{bmatrix}^{\mathrm{T}} \tag{3-212}$$

$$\$_{Pa2} = \begin{bmatrix} 0 & 0 & 0; & 0 & \sin\theta_{21} & -\cos\theta_{21} \end{bmatrix}^{\mathrm{T}} \tag{3-213}$$

$$\$_{Pa3} = \begin{bmatrix} 0 & 0 & 0; & 0 & \sin\theta_{31} & -\cos\theta_{31} \end{bmatrix}^{\mathrm{T}} \tag{3-214}$$

$$\$_{Pa4} = \begin{bmatrix} 0 & 0 & 0; & 0 & \sin\theta_{41} & -\cos\theta_{41} \end{bmatrix}^{\mathrm{T}} \tag{3-215}$$

$$\$_{Pa5} = \begin{bmatrix} 0 & 0 & 0; & 0 & \sin\theta_{51} & -\cos\theta_{51} \end{bmatrix}^{\mathrm{T}} \tag{3-216}$$

The kinematic screws of the remaining kinematic joints for each branch

$$\begin{cases} \$_{A01} = \begin{bmatrix} 0 & 0 & 0; & 0 & 1 & 0 \end{bmatrix}^{\mathrm{T}} \\ \$_{E1} = \begin{bmatrix} 1 & 0 & 0; & 0 & L_{12}\sin\theta_{11} & -x_1 - L_{12}\cos\theta_{11} \end{bmatrix}^{\mathrm{T}} \\ \$_{F1} = \begin{bmatrix} 0 & 1 & 0; & -L_{12}\sin\theta_{11} - L_{13}\sin\theta_{12} & 0 & 0 \end{bmatrix}^{\mathrm{T}} \\ \$_{G1} = \begin{bmatrix} 0 & 0 & 1; & x_1 + L_{12}\cos\theta_{11} + L_{13}\cos\theta_{12} & -L_{14}\cos\theta_{13} & 0 \end{bmatrix}^{\mathrm{T}} \end{cases} \tag{3-217}$$

$$\begin{cases} \$_{A02} = \begin{bmatrix} 0 & 0 & 0; & 0 & 1 & 0 \end{bmatrix}^{\mathrm{T}} \\ \$_{E2} = \begin{bmatrix} 1 & 0 & 0; & 0 & L_{22}\sin\theta_{21} & -x_2 - L_{22}\cos\theta_{21} \end{bmatrix}^{\mathrm{T}} \\ \$_{F2} = \begin{bmatrix} 0 & 1 & 0; & -L_{22}\sin\theta_{21} - L_{23}\sin\theta_{22} & 0 & 0 \end{bmatrix}^{\mathrm{T}} \\ \$_{G2} = \begin{bmatrix} 0 & 0 & 1; & x_2 + L_{22}\cos\theta_{21} + L_{23}\cos\theta_{22} & -L_{24}\cos\theta_{23} & 0 \end{bmatrix}^{\mathrm{T}} \end{cases} \tag{3-218}$$

$$\begin{cases} \$_{A03} = \begin{bmatrix} 0 & 0 & 0; & 0 & 1 & 0 \end{bmatrix}^{\mathrm{T}} \\ \$_{E3} = \begin{bmatrix} 1 & 0 & 0; & 0 & L_{32}\sin\theta_{31} & -x_3 - L_{32}\cos\theta_{31} \end{bmatrix}^{\mathrm{T}} \\ \$_{F3} = \begin{bmatrix} 0 & 1 & 0; & -L_{32}\sin\theta_{31} - L_{33}\sin\theta_{32} & 0 & 0 \end{bmatrix}^{\mathrm{T}} \\ \$_{G3} = \begin{bmatrix} 0 & 0 & 1; & x_3 + L_{32}\cos\theta_{31} + L_{33}\cos\theta_{32} & -L_{34}\cos\theta_{33} & 0 \end{bmatrix}^{\mathrm{T}} \end{cases} \tag{3-219}$$

$$\begin{cases} \$_{A04} = \begin{bmatrix} 0 & 0 & 0; & 0 & 1 & 0 \end{bmatrix}^{\mathrm{T}} \\ \$_{E4} = \begin{bmatrix} 1 & 0 & 0; & 0 & L_{42}\sin\theta_{41} & -x_4 - L_{42}\cos\theta_{41} \end{bmatrix}^{\mathrm{T}} \\ \$_{F4} = \begin{bmatrix} 0 & 1 & 0; & -L_{42}\sin\theta_{41} - L_{43}\sin\theta_{42} & 0 & L_{4X} \end{bmatrix}^{\mathrm{T}} \\ \$_{G4} = \begin{bmatrix} 0 & 0 & 1; & x_4 + L_{42}\cos\theta_{41} + L_{43}\cos\theta_{42} & -L_{4X} - L_{44}\cos\theta_{43} & 0 \end{bmatrix}^{\mathrm{T}} \end{cases} \tag{3-220}$$

$$\begin{cases} \$_{A05} = \begin{bmatrix} 0 & 0 & 0; & 0 & 1 & 0 \end{bmatrix}^{\mathrm{T}} \\ \$_{E5} = \begin{bmatrix} 1 & 0 & 0; & 0 & L_{52}\sin\theta_{51} & -x_5 - L_{52}\cos\theta_{51} \end{bmatrix}^{\mathrm{T}} \\ \$_{F5} = \begin{bmatrix} 0 & 1 & 0; & -L_{52}\sin\theta_{51} - L_{53}\sin\theta_{52} & 0 & L_{5X} \end{bmatrix}^{\mathrm{T}} \\ \$_{G5} = \begin{bmatrix} 0 & 0 & 1; & x_5 + L_{52}\cos\theta_{51} + L_{53}\cos\theta_{52} & -L_{5X} - L_{54}\cos\theta_{53} & 0 \end{bmatrix}^{\mathrm{T}} \end{cases} \tag{3-221}$$

The corresponding constraint screw for each branch

$$\$_{11}^{r} = \begin{bmatrix} 1 & 0 & 0; & 0 & L_{12}\sin\theta_{11} + L_{13}\sin\theta_{12} & -x_1 - L_{12}\cos\theta_{11} - L_{13}\cos\theta_{12} \end{bmatrix}^{\mathrm{T}} \tag{3-222}$$

$$\$_{21}^{r} = \begin{bmatrix} 1 & 0 & 0; & 0 & L_{22}\sin\theta_{21} + L_{23}\sin\theta_{22} & -x_2 - L_{22}\cos\theta_{21} - L_{23}\cos\theta_{22} \end{bmatrix}^{\mathrm{T}} \tag{3-223}$$

$$\$_{31}^{r} = \begin{bmatrix} 1 & 0 & 0; & 0 & L_{32}\sin\theta_{31} + L_{33}\sin\theta_{32} & -x_3 - L_{32}\cos\theta_{31} - L_{33}\cos\theta_{32} \end{bmatrix}^{\mathrm{T}} \tag{3-224}$$

$$\$_{41}^{r} = \begin{bmatrix} 1 & 0 & 0; & 0 & L_{42}\sin\theta_{41} + L_{43}\sin\theta_{42} & -x_4 - L_{42}\cos\theta_{41} - L_{43}\cos\theta_{42} \end{bmatrix}^{\mathrm{T}} \tag{3-225}$$

$$\$_{51}^{r} = \begin{bmatrix} 1 & 0 & 0; & 0 & L_{52}\sin\theta_{51} + L_{53}\sin\theta_{52} & -x_5 - L_{52}\cos\theta_{51} - L_{53}\cos\theta_{52} \end{bmatrix}^{\mathrm{T}} \tag{3-226}$$

Therefore, the kinematic screw system of the moving platform can be calculated as

$$\begin{cases} \$_{m1} = \begin{bmatrix} 0 & 0 & 0; & 0 & 1 & 0 \end{bmatrix}^{\mathrm{T}} \\ \$_{m2} = \begin{bmatrix} 0 & 0 & 0; & 0 & 0 & 1 \end{bmatrix}^{\mathrm{T}} \\ \$_{m3} = \begin{bmatrix} 1 & 0 & 0; & 0 & 0 & 0 \end{bmatrix}^{\mathrm{T}} \end{cases} \tag{3-227}$$

Equation (3-227) illustrates the moving platform has translational movements along Y and Z directions, rotational movement about X direction.

3.3.5 Six-DOF parallel mechanism

The possible limbs are:

$$\begin{cases} \mathrm{P}_X - \mathrm{P}_{XZ} - \mathrm{P}_Y - R_X - R_Y - R_Z \\ \mathrm{P}_X - \mathrm{P}_{YZ} - \mathrm{P}_Y - R_X - R_Y - R_Z \\ \mathrm{P}_X - \mathrm{P}_{XY} - \mathrm{P}_Z - R_X - R_Y - R_Z \\ \mathrm{P}_X - \mathrm{P}_{YZ} - \mathrm{P}_Z - R_X - R_Y - R_Z \\ \mathrm{P}_Y - \mathrm{P}_{XY} - \mathrm{P}_Z - R_X - R_Y - R_Z \\ \mathrm{P}_Y - \mathrm{P}_{XZ} - \mathrm{P}_Z - R_X - R_Y - R_Z \end{cases} \tag{3-228}$$

Limbs shown in matrix form:

$$\begin{bmatrix} \mathrm{P}_X & - & \mathrm{P}_{XZ} \\ R_Z & \mathrm{P}_Y & - \\ R_Y & R_X & - \\ - & - & - \\ - & - & - \\ - & - & - \end{bmatrix}, \begin{bmatrix} \mathrm{P}_X & - & - \\ R_Z & \mathrm{P}_Y & \mathrm{P}_{YZ} \\ R_Y & R_X & - \\ - & - & - \\ - & - & - \\ - & - & - \end{bmatrix}, \begin{bmatrix} \mathrm{P}_X & \mathrm{P}_{XY} & - \\ R_Z & - & - \\ R_Y & R_X & \mathrm{P}_Z \\ - & - & - \\ - & - & - \\ - & - & - \end{bmatrix}$$

$$\begin{bmatrix} \mathrm{P}_X & - & - \\ R_Z & - & \mathrm{P}_{YZ} \\ R_Y & R_X & \mathrm{P}_Z \\ - & - & - \\ - & - & - \\ - & - & - \end{bmatrix}, \begin{bmatrix} - & \mathrm{P}_{XY} & - \\ R_Z & \mathrm{P}_Y & - \\ R_Y & R_X & \mathrm{P}_Z \\ - & - & - \\ - & - & - \\ - & - & - \end{bmatrix}, \begin{bmatrix} - & - & \mathrm{P}_{XZ} \\ R_Z & \mathrm{P}_Y & - \\ R_Y & R_X & \mathrm{P}_Z \\ - & - & - \\ - & - & - \\ - & - & - \end{bmatrix} \tag{3-229}$$

The limb can be represented as Q_i. In enumeration, there will be

$$\begin{aligned} & Q_i^6 + + Q_i^5 Q_j + + Q_i^4 (Q_j^2 + Q_j Q_k) + Q_i^3 (Q_j^3 + Q_j^2 Q_k + Q_j Q_k Q_l) \\ & \quad + Q_i^2 (Q_j^2 Q_k^2 + Q_j^2 Q_k Q_l + Q_j Q_k Q_l Q_m) + Q_i Q_j Q_k Q_l Q_m Q_n \\ & = 6 + A_6^2 + A_6^2 + 6 \times C_5^2 + C_6^2 + A_6^3 + 6 \times C_5^3 + C_6^3 + C_6^2 C_4^2 + 6 \times C_5^4 + 1 \\ & = 362 \end{aligned} \tag{3-230}$$

kinds of matrices. The same matrices are ones with similar cell configuration. At last, there are 73 kinds of practical matrices. These matrices and corresponding parallel structures are listed below.

$$\left[\begin{array}{ccc:ccc:ccc} \mathrm{P}_X & - & \mathrm{P}_{XZ} & \mathrm{P}_X & - & \mathrm{P}_{XZ} & \mathrm{P}_X & - & \mathrm{P}_{XZ} \\ R_Z & \mathrm{P}_Y & - & R_Z & \mathrm{P}_Y & - & R_Z & \mathrm{P}_Y & - \\ R_Y & R_X & - & R_Y & R_X & - & R_Y & R_X & - \\ \mathrm{P}_X & - & \mathrm{P}_{XZ} & \mathrm{P}_X & - & \mathrm{P}_{XZ} & \mathrm{P}_X & - & \mathrm{P}_{XZ} \\ R_Z & \mathrm{P}_Y & - & R_Z & \mathrm{P}_Y & - & R_Z & \mathrm{P}_Y & - \\ R_Y & R_X & - & R_Y & R_X & - & R_Y & R_X & - \end{array}\right] \tag{3-231}$$

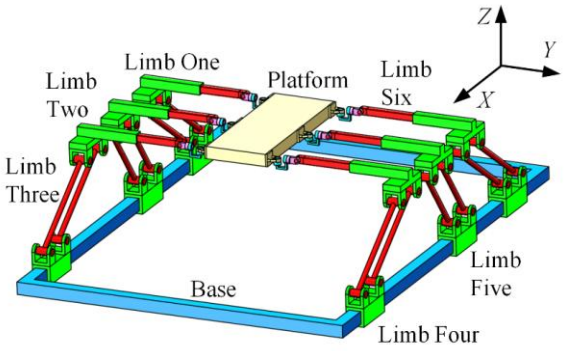

Figure 3-92 Schematic diagram of 6-DOF parallel structure (1)

Feature: There are two P_6 joints (P_X, P_Y), three R_6 joints (R_X, R_Y, R_Z) and six same P_a joints (P_{XZ}). Six identical P_a joints (P_{XZ}) are related to P_6 joint (P_X). Zero P_a joint is relevant to P_6 joint (P_Y). The translational direction of P_6 joint (P_X) and the rotational axis of R_6 joint (R_X) are parallel (X axis). The translational direction of P_6 joint (P_Y) and the rotational axis of R_6 joint (R_Y) are parallel (Y axis).

$$\left[\begin{array}{ccc:ccc:ccc} P_X & - & P_{XZ} & P_X & - & P_{XZ} & P_X & - & P_{XZ} \\ R_Z & P_Y & P_{YZ} & R_Z & P_Y & - & R_Z & P_Y & - \\ R_Y & R_X & - & R_Y & R_X & - & R_Y & R_X & - \\ P_X & - & P_{XZ} & P_X & - & P_{XZ} & P_X & - & - \\ R_Z & P_Y & - & R_Z & P_Y & - & R_Z & P_Y & - \\ R_Y & R_X & - & R_Y & R_X & - & R_Y & R_X & - \end{array}\right] \tag{3-232}$$

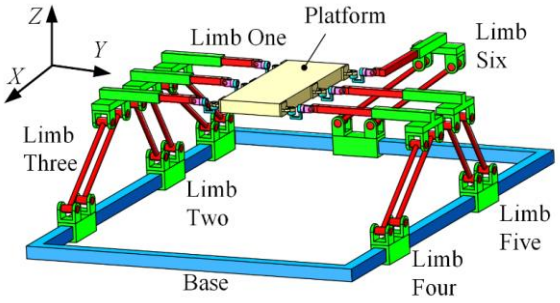

Figure 3-93 Schematic diagram of 6-DOF parallel structure (2)

Feature: There are two P_6 joints (P_X, P_Y), three R_6 joints (R_X, R_Y, R_Z), one P_a joint (P_{YZ}) and five same P_a joints (P_{XZ}). Five identical P_a joints (P_{XZ}) are related to P_6 joint (P_X). One P_a joint (P_{YZ}) is relevant to P_6 joint (P_Y). The translational direction of P_6 joint (P_X) and the rotational axis of R_6 joint (R_X) are parallel (X axis). The translational direction of P_6 joint (P_Y) and the rotational axis of R_6 joint (R_Y) are parallel (Y axis).

$$\left[\begin{array}{ccc|ccc|ccc} P_X & P_{XY} & P_{XZ} & P_X & - & P_{XZ} & P_X & - & P_{XZ} \\ R_Z & P_Y & - & R_Z & P_Y & - & R_Z & P_Y & - \\ R_Y & R_X & P_Z & R_Y & R_X & - & R_Y & R_X & - \\ P_X & - & P_{XZ} & P_X & - & P_{XZ} & P_X & - & - \\ R_Z & P_Y & - & R_Z & P_Y & - & R_Z & - & - \\ R_Y & R_X & - & R_Y & R_X & - & R_Y & R_X & - \end{array}\right] \tag{3-233}$$

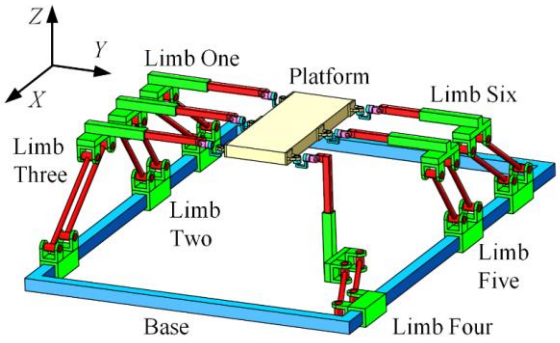

Figure 3-94 Schematic diagram of 6-DOF parallel structure (3)

Feature: There are one P_1 joint (P_Z), one P_5 joint (P_Y), one P_6 joint (P_X), three R_6 joints (R_X, R_Y, R_Z), one P_a joint (P_{XY}) and five same P_a joints (P_{XZ}). Five identical P_a joints (P_{XZ}) are relevant to P_1 joint (P_Z). One P_a joint (P_{XY}) is relevant to P_5 joint (P_Y). Six P_a joints (P_{XY}, P_{XZ}) are related to P_6 joint (P_X). The translational direction of P_6 joint (P_X) and the rotational axis of R_6 joint (R_X) are parallel (*X* axis). The translational direction of P_5 joint (P_Y) and the rotational axis of R_6 joint (R_Y) are parallel (*Y* axis). The translational direction of P_1 joint (P_Z) and the rotational axis of R_6 joint (R_Z) are parallel (*Z* axis).

$$\left[\begin{array}{ccc|ccc|ccc} P_X & - & P_{XZ} & P_X & - & P_{XZ} & P_X & - & P_{XZ} \\ R_Z & P_Y & P_{YZ} & R_Z & P_Y & - & R_Z & P_Y & - \\ R_Y & R_X & P_Z & R_Y & R_X & - & R_Y & R_X & - \\ P_X & - & P_{XZ} & P_X & - & P_{XZ} & P_X & - & - \\ R_Z & P_Y & - & R_Z & P_Y & - & R_Z & - & - \\ R_Y & R_X & - & R_Y & R_X & - & R_Y & R_X & - \end{array}\right] \tag{3-234}$$

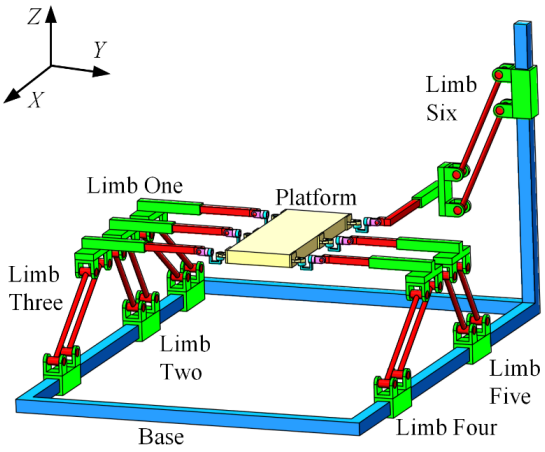

Figure 3-95 Schematic diagram of 6-DOF parallel structure (4)

Feature: There are one P_1 joint (P_Z), one P_5 joint (P_Y), one P_6 joint (P_X), three R_6 joints (R_X, R_Y, R_Z), one P_a joint (P_{YZ}) and five same P_a joints (P_{XZ}). Six P_a joints (P_{XZ}, P_{YZ}) are relevant to P_1 joint (P_Z). One P_a joint (P_{YZ}) is relevant to P_5 joint (P_Y). Five identical P_a joints (P_{XZ}) are related to P_6 joint (P_X). The translational direction of P_6 joint (P_X) and the rotational axis of R_6 joint (R_X) are parallel (*X* axis). The translational direction of P_5 joint (P_Y) and the rotational axis of R_6 joint (R_Y) are parallel (*Y* axis). The translational direction of P_1 joint (P_Z) and the rotational axis of R_6 joint (R_Z) are parallel (*Z* axis).

$$\left[\begin{array}{ccc:ccc:ccc} P_X & P_{XY} & P_{XZ} & P_X & \_ & P_{XZ} & P_X & \_ & P_{XZ} \\ R_Z & P_Y & \_ & R_Z & P_Y & \_ & R_Z & P_Y & \_ \\ R_Y & R_X & P_Z & R_Y & R_X & \_ & R_Y & R_X & \_ \\ P_X & \_ & P_{XZ} & P_X & \_ & P_{XZ} & \_ & \_ & \_ \\ R_Z & P_Y & \_ & R_Z & P_Y & \_ & R_Z & P_Y & \_ \\ R_Y & R_X & \_ & R_Y & R_X & \_ & R_Y & R_X & \_ \end{array}\right] \tag{3-235}$$

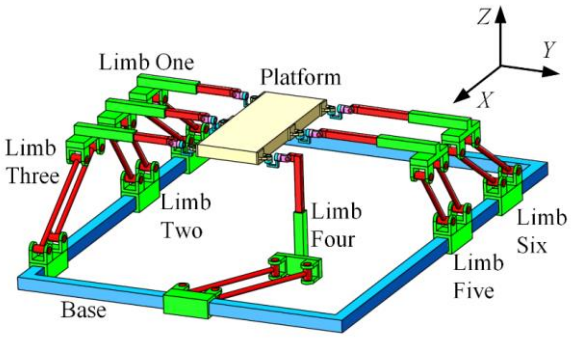

Figure 3-96 Schematic diagram of 6-DOF parallel structure (5)

Feature: There are one P_1 joint (P_Z), one P_5 joint (P_X), one P_6 joint (P_Y), three R_6 joints (R_X, R_Y, R_Z), one P_a joint (P_{XY}) and five same P_a joints (P_{XZ}). Five P_a joints (P_{XZ}) are relevant to P_1 joint (P_Z). Five P_a joints (P_{XY}, P_{XZ}) are relevant to P_5 joint (P_X). One P_a joint (P_{XY}) is related to P_6 joint (P_Y). The translational direction of P_5 joint (P_X) and the rotational axis of R_6 joint (R_X) are parallel (X axis). The translational direction of P_6 joint (P_Y) and the rotational axis of R_6 joint (R_Y) are parallel (Y axis). The translational direction of P_1 joint (P_Z) and the rotational axis of R_6 joint (R_Z) are parallel (Z axis).

$$\left[\begin{array}{ccc:ccc:ccc} P_X & - & P_{XZ} & P_X & - & P_{XZ} & P_X & - & P_{XZ} \\ R_Z & P_Y & - & R_Z & P_Y & - & R_Z & P_Y & - \\ R_Y & R_X & P_Z & R_Y & R_X & - & R_Y & R_X & - \\ P_X & - & P_{XZ} & P_X & - & P_{XZ} & - & - & P_{XZ} \\ R_Z & P_Y & - & R_Z & P_Y & - & R_Z & P_Y & - \\ R_Y & R_X & - & R_Y & R_X & - & R_Y & R_X & - \end{array}\right] \tag{3-236}$$

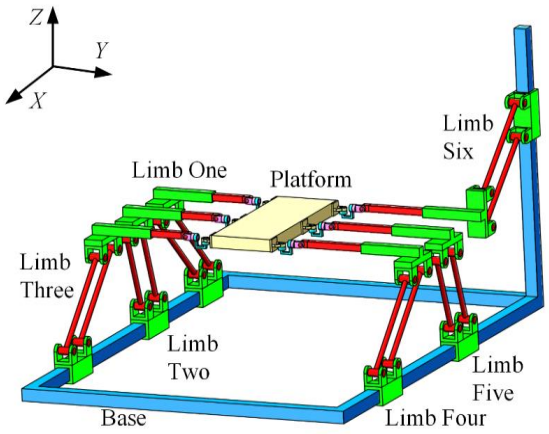

Figure 3-97 Schematic diagram of 6-DOF parallel structure (6)

Feature: There are one P_1 joint (P_Z), one P_5 joint (P_X), one P_6 joint (P_Y), three R_6 joints (R_X, R_Y, R_Z) and six same P_a joints (P_{XZ}). Six identical P_a joints (P_{XZ}) are relevant to P_1 joint (P_Z). Six same P_a joints (P_{XZ}) are relevant to P_5 joint (P_X). No P_a joint is related to P_6 joint (P_Y). The translational direction of P_5 joint (P_X) and the rotational axis of R_6 joint (R_X) are parallel (X axis). The translational direction of P_6 joint (P_Y) and the rotational axis of R_6 joint (R_Y) are parallel (Y axis). The translational direction of P_1 joint (P_Z) and the rotational axis of R_6 joint (R_Z) are parallel (Z axis).

$$\begin{bmatrix} P_X & - & P_{XZ} & P_X & - & P_{XZ} & P_X & - & - \\ R_Z & P_Y & P_{YZ} & R_Z & P_Y & - & R_Z & P_Y & - \\ R_Y & R_X & - & R_Y & R_X & - & R_Y & R_X & - \\ P_X & - & P_{XZ} & P_X & - & P_{XZ} & P_X & - & - \\ R_Z & P_Y & P_{YZ} & R_Z & P_Y & - & R_Z & P_Y & - \\ R_Y & R_X & - & R_Y & R_X & - & R_Y & R_X & - \end{bmatrix} \tag{3-237}$$

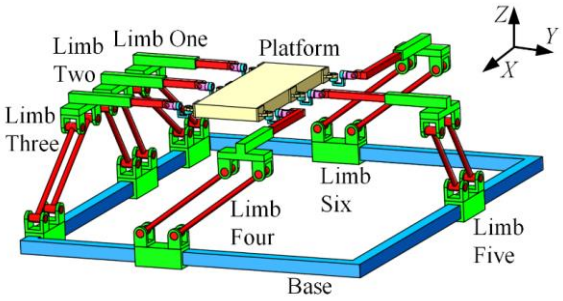

Figure 3-98 Schematic diagram of 6-DOF parallel structure (7)

Feature: There are two P_6 joints (P_X, P_Y), three R_6 joints (R_X, R_Y, R_Z), two identical P_a joints (P_{YZ}) and four same P_a joints (P_{XZ}). Four same P_a joints (P_{XZ}) are relevant to P_6 joint (P_X). Two identical P_a joints (P_{YZ}) are related to P_6 joint (P_Y). The translational direction of P_6 joint (P_X) and the rotational axis of R_6 joint (R_X) are parallel (*X* axis). The translational direction of P_6 joint (P_Y) and the rotational axis of R_6 joint (R_Y) are parallel (*Y* axis).

$$\begin{bmatrix} P_X & P_{XY} & P_{XZ} & P_X & - & P_{XZ} & P_X & - & - \\ R_Z & P_Y & - & R_Z & P_Y & - & R_Z & - & - \\ R_Y & R_X & P_Z & R_Y & R_X & - & R_Y & R_X & - \\ P_X & P_{XY} & P_{XZ} & P_X & - & P_{XZ} & P_X & - & - \\ R_Z & P_Y & - & R_Z & P_Y & - & R_Z & - & - \\ R_Y & R_X & P_Z & R_Y & R_X & - & R_Y & R_X & - \end{bmatrix} \tag{3-238}$$

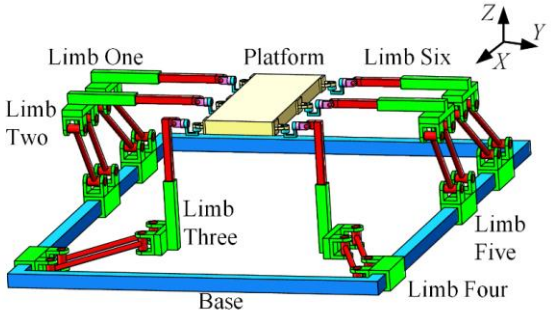

Figure 3-99 Schematic diagram of 6-DOF parallel structure (8)

Feature: There are one P_2 joint (P_Z), one P_4 joint (P_Y), one P_6 joint (P_X), three R_6 joints (R_X, R_Y, R_Z), two same P_a joints (P_{XY}) and four same P_a joints (P_{XZ}). Four identical P_a joints (P_{XZ}) are relevant to P_2 joint (P_Z). Two same P_a joints (P_{XY}) are relevant to P_4 joint (P_Y). Six P_a joints (P_{XY}, P_{XZ}) are related to P_6 joint (P_X). The translational direction of P_6 joint (P_X) and the rotational axis of R_6 joint (R_X) are parallel (X axis). The translational direction of P_5 joint (P_Y) and the rotational axis of R_6 joint (R_Y) are parallel (Y axis). The translational direction of P_2 joint (P_Z) and the rotational axis of R_6 joint (R_Z) are parallel (Z axis).

$$\left[\begin{array}{ccc:ccc:ccc} P_X & - & P_{XZ} & P_X & - & P_{XZ} & P_X & - & - \\ R_Z & P_Y & P_{YZ} & R_Z & P_Y & - & R_Z & - & - \\ R_Y & R_X & P_Z & R_Y & R_X & - & R_Y & R_X & - \\ P_X & - & P_{XZ} & P_X & - & P_{XZ} & P_X & - & - \\ R_Z & P_Y & P_{YZ} & R_Z & P_Y & - & R_Z & - & - \\ R_Y & R_X & P_Z & R_Y & R_X & - & R_Y & R_X & - \end{array}\right] \tag{3-239}$$

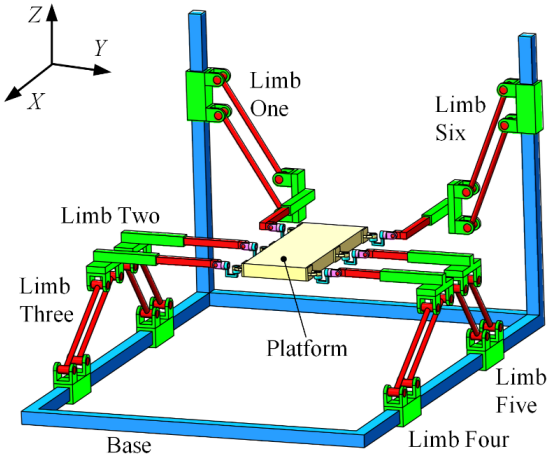

Figure 3-100 Schematic diagram of 6-DOF parallel structure (9)

Feature: There are one P_2 joint (P_Z), one P_4 joint (P_Y), one P_6 joint (P_X), three R_6 joints (R_X, R_Y, R_Z), two same P_a joints (P_{YZ}) and four same P_a joints (P_{XZ}). Six P_a joints (P_{XZ}, P_{YZ}) are relevant to P_2 joint (P_Z). Two same P_a joints (P_{YZ}) are relevant to P_4 joint (P_Y). Four identical P_a joints (P_{XZ}) are related to P_6 joint (P_X). The translational direction of P_6 joint (P_X) and the rotational axis of R_6 joint (R_X) are parallel (X axis). The translational direction of P_5 joint (P_Y) and the rotational axis of R_6 joint (R_Y) are parallel (Y axis). The translational direction of P_2 joint (P_Z) and the rotational axis of R_6 joint (R_Z) are parallel (Z axis).

$$\left[\begin{array}{ccc|ccc|ccc}
\mathrm{P}_X & \mathrm{P}_{XY} & \mathrm{P}_{XZ} & \mathrm{P}_X & _ & \mathrm{P}_{XZ} & _ & _ & _ \\
R_Z & \mathrm{P}_Y & _ & R_Z & \mathrm{P}_Y & _ & R_Z & \mathrm{P}_Y & _ \\
R_Y & R_X & \mathrm{P}_Z & R_Y & R_X & _ & R_Y & R_X & _ \\
\mathrm{P}_X & \mathrm{P}_{XY} & \mathrm{P}_{XZ} & \mathrm{P}_X & _ & \mathrm{P}_{XZ} & _ & _ & _ \\
R_Z & \mathrm{P}_Y & _ & R_Z & \mathrm{P}_Y & _ & R_Z & \mathrm{P}_Y & _ \\
R_Y & R_X & \mathrm{P}_Z & R_Y & R_X & _ & R_Y & R_X & _
\end{array}\right] \tag{3-240}$$

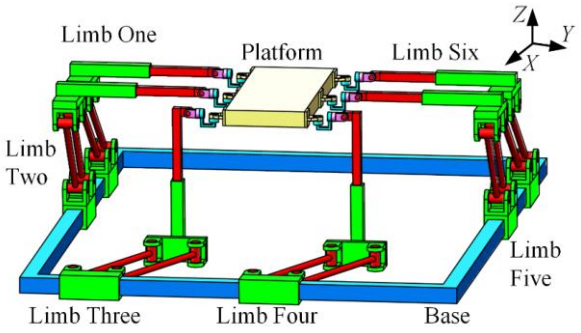

Figure 3-101 Schematic diagram of 6-DOF parallel structure (10)

Feature: There are one P_2 joint (P_Z), one P_4 joint (P_X), one P_6 joint (P_Y), three R_6 joints (R_X, R_Y, R_Z), two same P_a joints (P_{XY}) and four same P_a joints (P_{XZ}). Four identical P_a joints (P_{XZ}) are relevant to P_2 joint (P_Z). Six P_a joints (P_{XY}, P_{XZ}) are relevant to P_4 joint (P_X). Two identical P_a joints (P_{XY}) are related to P_6 joint (P_Y). The translational direction of P_4 joint (P_X) and the rotational axis of R_6 joint (R_X) are parallel (X axis). The translational direction of P_6 joint (P_Y) and the rotational axis of R_6 joint (R_Y) are parallel (Y axis). The translational direction of P_2 joint (P_Z) and the rotational axis of R_6 joint (R_Z) are parallel (Z axis).

$$\left[\begin{array}{ccc|ccc|ccc}
\mathrm{P}_X & _ & \mathrm{P}_{XZ} & \mathrm{P}_X & _ & \mathrm{P}_{XZ} & _ & _ & \mathrm{P}_{XZ} \\
R_Z & \mathrm{P}_Y & _ & R_Z & \mathrm{P}_Y & _ & R_Z & \mathrm{P}_Y & _ \\
R_Y & R_X & \mathrm{P}_Z & R_Y & R_X & _ & R_Y & R_X & _ \\
\mathrm{P}_X & _ & \mathrm{P}_{XZ} & \mathrm{P}_X & _ & \mathrm{P}_{XZ} & _ & _ & \mathrm{P}_{XZ} \\
R_Z & \mathrm{P}_Y & _ & R_Z & \mathrm{P}_Y & _ & R_Z & \mathrm{P}_Y & _ \\
R_Y & R_X & \mathrm{P}_Z & R_Y & R_X & _ & R_Y & R_X & _
\end{array}\right] \tag{3-241}$$

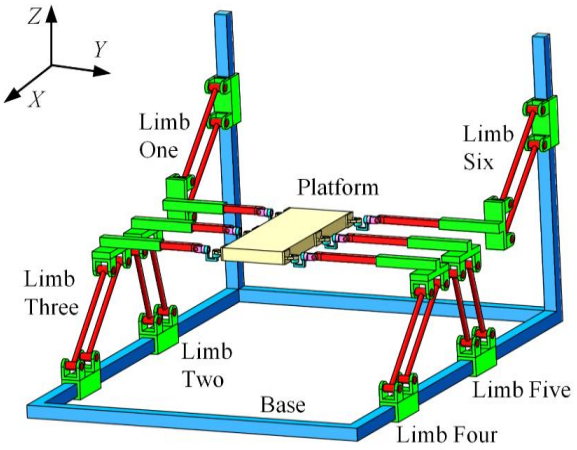

Figure 3-102 Schematic diagram of 6-DOF parallel structure (11)

Feature: There are one P_2 joint (P_Z), one P_4 joint (P_X), one P_6 joint (P_Y), three R_6 joints (R_X, R_Y, R_Z) and six same P_a joints (P_{XZ}). Six identical P_a joints (P_{XZ}) are relevant to P_2 joint (P_Z). Six same P_a joints (P_{XZ}) are relevant to P_4 joint (P_X). No P_a joint is related to P_6 joint (P_Y). The translational direction of P_4 joint (P_X) and the rotational axis of R_6 joint (R_X) are parallel (X axis). The translational direction of P_6 joint (P_Y) and the rotational axis of R_6 joint (R_Y) are parallel (Y axis). The translational direction of P_2 joint (P_Z) and the rotational axis of R_6 joint (R_Z) are parallel (Z axis).

$$\left[\begin{array}{ccc:ccc:ccc} P_X & P_{XY} & P_{XZ} & P_X & - & P_{XZ} & P_X & - & - \\ R_Z & P_Y & P_{YZ} & R_Z & P_Y & - & R_Z & P_Y & - \\ R_Y & R_X & P_Z & R_Y & R_X & - & R_Y & R_X & - \\ P_X & - & P_{XZ} & P_X & - & P_{XZ} & P_X & - & - \\ R_Z & P_Y & - & R_Z & P_Y & - & R_Z & - & - \\ R_Y & R_X & - & R_Y & R_X & - & R_Y & R_X & - \end{array}\right] \tag{3-242}$$

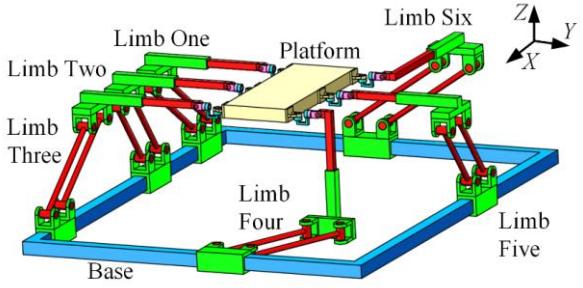

Figure 3-103 Schematic diagram of 6-DOF parallel structure (12)

Feature: There are one P_1 joint (P_Z), one P_5 joint (P_Y), one P_6 joint (P_X), three R_6 joints (R_X, R_Y, R_Z), one P_a joint (P_{XY}), one P_a joint (P_{YZ}) and four same P_a joints (P_{XZ}). Five P_a joints

(P_{XZ}, P_{YZ}) are relevant to P_1 joint (P_Z). Two P_a joints (P_{XY}, P_{YZ}) are relevant to P_5 joint (P_Y). Five P_a joints (P_{XY}, P_{XZ}) are related to P_6 joint (P_X). The translational direction of P_6 joint (P_X) and the rotational axis of R_6 joint (R_X) are parallel (X axis). The translational direction of P_5 joint (P_Y) and the rotational axis of R_6 joint (R_Y) are parallel (Y axis). The translational direction of P_1 joint (P_Z) and the rotational axis of R_6 joint (R_Z) are parallel (Z axis).

$$\left[\begin{array}{ccc:ccc:ccc} P_X & - & P_{XZ} & P_X & - & P_{XZ} & P_X & - & - \\ R_Z & P_Y & P_{YZ} & R_Z & P_Y & - & R_Z & P_Y & - \\ R_Y & R_X & P_Z & R_Y & R_X & - & R_Y & R_X & - \\ P_X & - & P_{XZ} & P_X & - & P_{XZ} & P_X & - & - \\ R_Z & P_Y & P_{YZ} & R_Z & P_Y & - & R_Z & - & - \\ R_Y & R_X & - & R_Y & R_X & - & R_Y & R_X & - \end{array}\right] \tag{3-243}$$

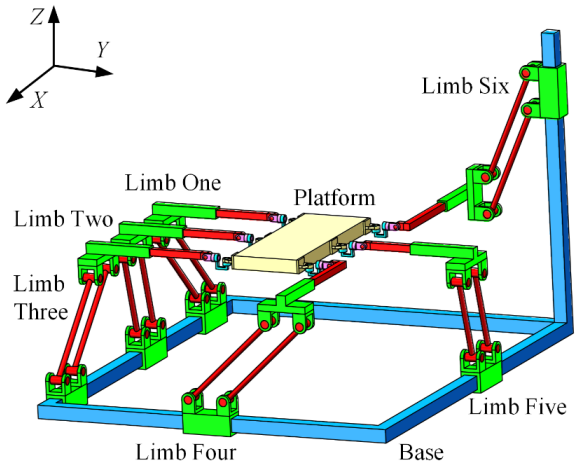

Figure 3-104 Schematic diagram of 6-DOF parallel structure (13)

Feature: There are one P_1 joint (P_Z), one P_5 joint (P_Y), one P_6 joint (P_X), three R_6 joints (R_X, R_Y, R_Z), two identical P_a joints (P_{YZ}) and four same P_a joints (P_{XZ}). Six P_a joints (P_{XZ}, P_{YZ}) are relevant to P_1 joint (P_Z). Two identical P_a joints (P_{YZ}) are relevant to P_5 joint (P_Y). Four same P_a joints (P_{XZ}) are related to P_6 joint (P_X). The translational direction of P_6 joint (P_X) and the rotational axis of R_6 joint (R_X) are parallel (X axis). The translational direction of P_5 joint (P_Y) and the rotational axis of R_6 joint (R_Y) are parallel (Y axis). The translational direction of P_1 joint (P_Z) and the rotational axis of R_6 joint (R_Z) are parallel (Z axis).

$$\left[\begin{array}{ccc:ccc:ccc} P_X & P_{XY} & P_{XZ} & P_X & - & P_{XZ} & P_X & - & - \\ R_Z & P_Y & P_{YZ} & R_Z & P_Y & - & R_Z & P_Y & - \\ R_Y & R_X & P_Z & R_Y & R_X & - & R_Y & R_X & - \\ P_X & - & P_{XZ} & P_X & - & P_{XZ} & - & - & - \\ R_Z & P_Y & - & R_Z & P_Y & - & R_Z & P_Y & - \\ R_Y & R_X & - & R_Y & R_X & - & R_Y & R_X & - \end{array}\right] \tag{3-244}$$

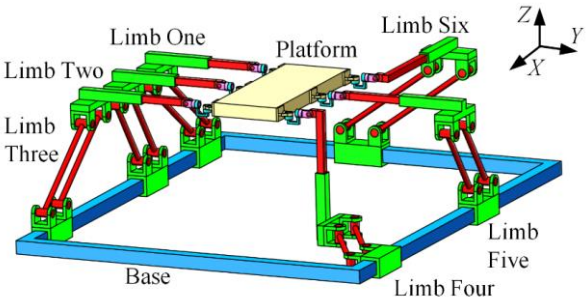

Figure 3-105 Schematic diagram of 6-DOF parallel structure (14)

Feature: There are one P_1 joint (P_Z), one P_5 joint (P_X), one P_6 joint (P_Y), three R_6 joints (R_X, R_Y, R_Z), one P_a joint (P_{XY}), one P_a joint (P_{YZ}) and four same P_a joints (P_{XZ}). Five P_a joints (P_{XZ}, P_{YZ}) are relevant to P_1 joint (P_Z). Five P_a joints (P_{XY}, P_{XZ}) are relevant to P_5 joint (P_X). Two P_a joints (P_{XY}, P_{YZ}) are related to P_6 joint (P_Y). The translational direction of P_5 joint (P_X) and the rotational axis of R_6 joint (R_X) are parallel (*X* axis). The translational direction of P_6 joint (P_Y) and the rotational axis of R_6 joint (R_Y) are parallel (*Y* axis). The translational direction of P_1 joint (P_Z) and the rotational axis of R_6 joint (R_Z) are parallel (*Z* axis).

$$\left[\begin{array}{ccc:ccc:ccc} P_X & - & P_{XZ} & P_X & - & P_{XZ} & P_X & - & P_{XZ} \\ R_Z & P_Y & P_{YZ} & R_Z & P_Y & - & R_Z & P_Y & - \\ R_Y & R_X & P_Z & R_Y & R_X & - & R_Y & R_X & - \\ P_X & - & P_{XZ} & P_X & - & P_{XZ} & - & - & - \\ R_Z & P_Y & - & R_Z & P_Y & - & R_Z & P_Y & - \\ R_Y & R_X & - & R_Y & R_X & - & R_Y & R_X & - \end{array}\right] \tag{3-245}$$

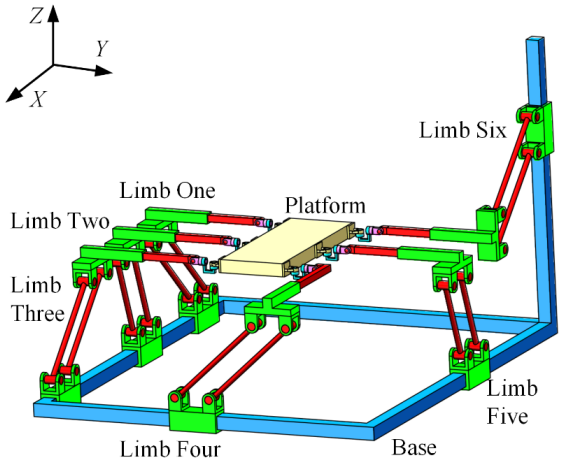

Figure 3-106 Schematic diagram of 6-DOF parallel structure (15)

Feature: There are one P_1 joint (P_Z), one P_5 joint (P_X), one P_6 joint (P_Y), three R_6 joints (R_X, R_Y, R_Z), one P_a joint (P_{YZ}) and five same P_a joints (P_{XZ}). Six P_a joints (P_{XZ}, P_{YZ}) are relevant to P_1 joint (P_Z). Five identical P_a joints (P_{XZ}) are relevant to P_5 joint (P_X). One P_a joint (P_{XZ}) is related to P_6 joint (P_Y). The translational direction of P_5 joint (P_X) and the rotational axis of R_6 joint (R_X) are parallel (X axis). The translational direction of P_6 joint (P_Y) and the rotational axis of R_6 joint (R_Y) are parallel (Y axis). The translational direction of P_1 joint (P_Z) and the rotational axis of R_6 joint (R_Z) are parallel (Z axis).

$$\left[\begin{array}{ccc:ccc:ccc} P_X & P_{XY} & P_{XZ} & P_X & \_ & P_{XZ} & P_X & \_ & \_ \\ R_Z & P_Y & P_{YZ} & R_Z & P_Y & \_ & R_Z & \_ & \_ \\ R_Y & R_X & P_Z & R_Y & R_X & \_ & R_Y & R_X & \_ \\ P_X & \_ & P_{XZ} & P_X & \_ & P_{XZ} & P_X & \_ & \_ \\ R_Z & P_Y & \_ & R_Z & P_Y & \_ & R_Z & \_ & \_ \\ R_Y & R_X & P_Z & R_Y & R_X & \_ & R_Y & R_X & \_ \end{array}\right] \tag{3-246}$$

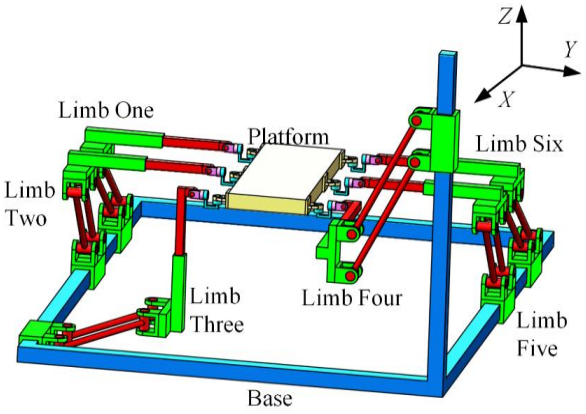

Figure 3-107 Schematic diagram of 6-DOF parallel structure (16)

Feature: There are one P_2 joint (P_Z), one P_4 joint (P_Y), one P_6 joint (P_X), three R_6 joints (R_X, R_Y, R_Z), one P_a joint (P_{XY}), one P_a joint (P_{YZ}) and four same P_a joints (P_{XZ}). Five P_a joints (P_{XZ}, P_{YZ}) are relevant to P_2 joint (P_Z). Two P_a joints (P_{XY}, P_{YZ}) are relevant to P_4 joint (P_Y). Five P_a joints (P_{XY}, P_{XZ}) are related to P_6 joint (P_X). The translational direction of P_6 joint (P_X) and the rotational axis of R_6 joint (R_X) are parallel (X axis). The translational direction of P_4 joint (P_Y) and the rotational axis of R_6 joint (R_Y) are parallel (Y axis). The translational direction of P_2 joint (P_Z) and the rotational axis of R_6 joint (R_Z) are parallel (Z axis).

$$\left[\begin{array}{ccc:ccc:ccc} P_X & P_{XY} & P_{XZ} & P_X & - & P_{XZ} & P_X & - & - \\ R_Z & P_Y & - & R_Z & P_Y & - & R_Z & P_Y & - \\ R_Y & R_X & P_Z & R_Y & R_X & - & R_Y & R_X & - \\ P_X & P_{XY} & P_{XZ} & P_X & - & P_{XZ} & - & - & - \\ R_Z & P_Y & - & R_Z & P_Y & - & R_Z & - & - \\ R_Y & R_X & P_Z & R_Y & R_X & - & R_Y & R_X & - \end{array}\right] \tag{3-247}$$

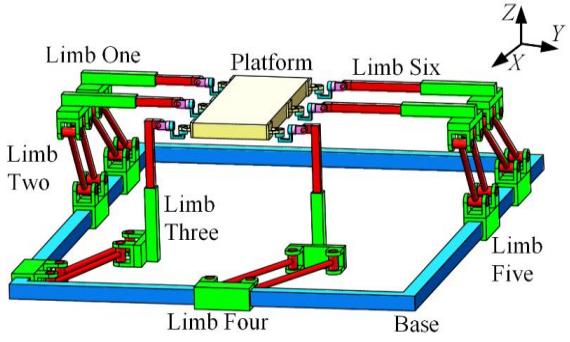

Figure 3-108 Schematic diagram of 6-DOF parallel structure (17)

Feature: There are one P_2 joint (P_Z), one P_5 joint (P_X), one P_5 joint (P_Y), three R_6 joints (R_X, R_Y, R_Z), two identical P_a joint (P_{XY}) and four same P_a joints (P_{XZ}). Four identical P_a joints

(P_{XZ}) are relevant to P_2 joint (P_Z). Six P_a joints (P_{XY}, P_{YZ}) are relevant to P_5 joint (P_X). Two identical P_a joints (P_{XY}) are related to P_5 joint (P_Y). The translational direction of P_5 joint (P_X) and the rotational axis of R_6 joint (R_X) are parallel (X axis). The translational direction of P_5 joint (P_Y) and the rotational axis of R_6 joint (R_Y) are parallel (Y axis). The translational direction of P_2 joint (P_Z) and the rotational axis of R_6 joint (R_Z) are parallel (Z axis).

$$\left[\begin{array}{ccc:ccc:ccc} P_X & P_{XY} & P_{XZ} & P_X & - & P_{XZ} & P_X & - & P_{XZ} \\ R_Z & P_Y & - & R_Z & P_Y & - & R_Z & P_Y & - \\ R_Y & R_X & P_Z & R_Y & R_X & - & R_Y & R_X & - \\ P_X & - & P_{XZ} & P_X & - & P_{XZ} & - & - & - \\ R_Z & P_Y & - & R_Z & P_Y & - & R_Z & - & - \\ R_Y & R_X & P_Z & R_Y & R_X & - & R_Y & R_X & - \end{array}\right] \tag{3-248}$$

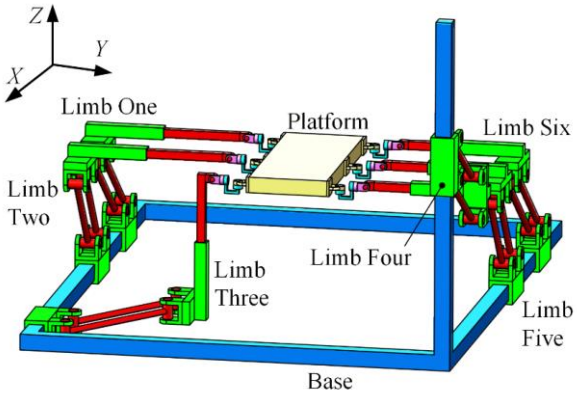

Figure 3-109 Schematic diagram of 6-DOF parallel structure (18)

Feature: There are one P_2 joint (P_Z), one P_5 joint (P_X), one P_5 joint (P_Y), three R_6 joints (R_X, R_Y, R_Z), one P_a joint (P_{XY}) and five same P_a joints (P_{XZ}). Five identical P_a joints (P_{XZ}) are relevant to P_2 joint (P_Z). Six P_a joints (P_{XY}, P_{YZ}) are relevant to P_5 joint (P_X). One P_a joint (P_{XY}) is related to P_5 joint (P_Y). The translational direction of P_5 joint (P_X) and the rotational axis of R_6 joint (R_X) are parallel (X axis). The translational direction of P_5 joint (P_Y) and the rotational axis of R_6 joint (R_Y) are parallel (Y axis). The translational direction of P_2 joint (P_Z) and the rotational axis of R_6 joint (R_Z) are parallel (Z axis).

$$\left[\begin{array}{ccc:ccc:ccc} P_X & P_{XY} & P_{XZ} & P_X & - & P_{XZ} & P_X & - & - \\ R_Z & P_Y & P_{YZ} & R_Z & P_Y & - & R_Z & P_Y & - \\ R_Y & R_X & P_Z & R_Y & R_X & - & R_Y & R_X & - \\ P_X & - & P_{XZ} & P_X & - & P_{XZ} & - & - & - \\ R_Z & P_Y & - & R_Z & P_Y & - & R_Z & - & - \\ R_Y & R_X & P_Z & R_Y & R_X & - & R_Y & R_X & - \end{array}\right] \tag{3-249}$$

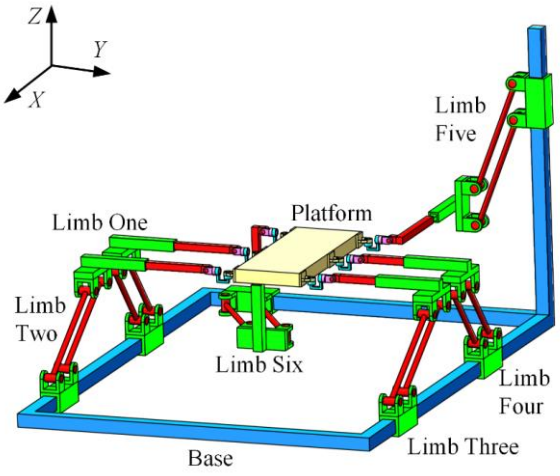

Figure 3-110 Schematic diagram of 6-DOF parallel structure (19)

Feature: There are one P_2 joint (P_Z), one P_5 joint (P_X), one P_5 joint (P_Y), three R_6 joints (R_X, R_Y, R_Z), one P_a joint (P_{XY}), one P_a joint (P_{YZ}) and four same P_a joints (P_{XZ}). Five P_a joints (P_{XY}, P_{XZ}) are relevant to P_2 joint (P_Z). Five P_a joints (P_{XY}, P_{XZ}) are relevant to P_5 joint (P_X). Two different P_a joints (P_{XY}, P_{YZ}) are related to P_5 joint (P_Y). The translational direction of P_5 joint (P_X) and the rotational axis of R_6 joint (R_X) are parallel (X axis). The translational direction of P_5 joint (P_Y) and the rotational axis of R_6 joint (R_Y) are parallel (Y axis). The translational direction of P_2 joint (P_Z) and the rotational axis of R_6 joint (R_Z) are parallel (Z axis).

$$\left[\begin{array}{ccc:ccc:ccc} P_X & - & P_{XZ} & P_X & - & P_{XZ} & P_X & - & P_{XZ} \\ R_Z & P_Y & P_{YZ} & R_Z & P_Y & - & R_Z & P_Y & - \\ R_Y & R_X & P_Z & R_Y & R_X & - & R_Y & R_X & - \\ P_X & - & P_{XZ} & P_X & - & P_{XZ} & - & - & - \\ R_Z & P_Y & - & R_Z & P_Y & - & R_Z & - & - \\ R_Y & R_X & P_Z & R_Y & R_X & - & R_Y & R_X & - \end{array}\right] \tag{3-250}$$

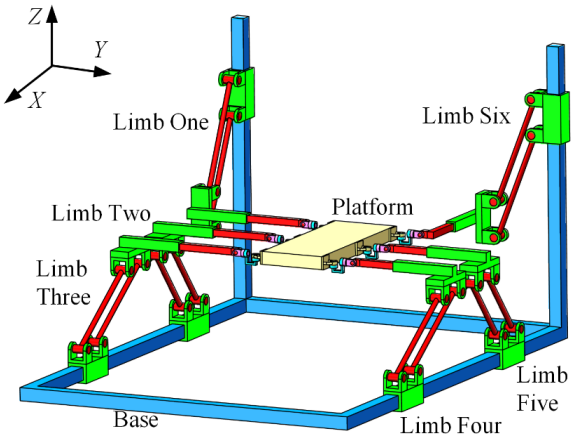

Figure 3-111 Schematic diagram of 6-DOF parallel structure (20)

Feature: There are one P_2 joint (P_Z), one P_5 joint (P_X), one P_5 joint (P_Y), three R_6 joints (R_X, R_Y, R_Z), one Pa joint (P_{YZ}) and five same P_a joints (P_{XZ}). Six P_a joints (P_{XY}, P_{XZ}) are relevant to P_2 joint (P_Z). Five identical P_a joints (P_{XZ}) are relevant to P_5 joint (P_X). One P_a joint (P_{YZ}) is related to P_5 joint (P_Y). The translational direction of P_5 joint (P_X) and the rotational axis of R_6 joint (R_X) are parallel (X axis). The translational direction of P_5 joint (P_Y) and the rotational axis of R_6 joint (R_Y) are parallel (Y axis). The translational direction of P_2 joint (P_Z) and the rotational axis of R_6 joint (R_Z) are parallel (Z axis).

$$\left[\begin{array}{ccc:ccc:ccc} P_X & P_{XY} & P_{XZ} & P_X & \_ & P_{XZ} & \_ & \_ & P_{XZ} \\ R_Z & P_Y & \_ & R_Z & P_Y & \_ & R_Z & P_Y & \_ \\ R_Y & R_X & P_Z & R_Y & R_X & \_ & R_Y & R_X & \_ \\ P_X & \_ & P_{XZ} & P_X & \_ & P_{XZ} & \_ & \_ & \_ \\ R_Z & P_Y & \_ & R_Z & P_Y & \_ & R_Z & P_Y & \_ \\ R_Y & R_X & P_Z & R_Y & R_X & \_ & R_Y & R_X & \_ \end{array}\right] \tag{3-251}$$

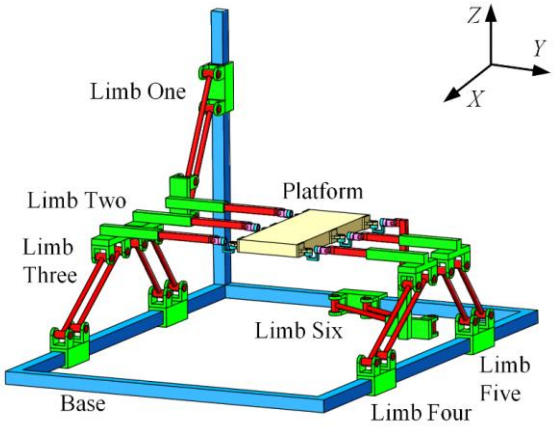

Figure 3-112 Schematic diagram of 6-DOF parallel structure (21)

Feature: There are one P_2 joint (P_Z), one P_4 joint (P_X), one P_6 joint (P_Y), three R_6 joints (R_X, R_Y, R_Z), one P_a joint (P_{XY}) and five same P_a joints (P_{XZ}). Five same P_a joints (P_{XZ}) are relevant to P_2 joint (P_Z). Six P_a joints (P_{XY}, P_{XZ}) are relevant to P_4 joint (P_X). One P_a joint (P_{XY}) is related to P_6 joint (P_Y). The translational direction of P_4 joint (P_X) and the rotational axis of R_6 joint (R_X) are parallel (*X* axis). The translational direction of P_6 joint (P_Y) and the rotational axis of R_6 joint (R_Y) are parallel (*Y* axis). The translational direction of P_2 joint (P_Z) and the rotational axis of R_6 joint (R_Z) are parallel (*Z* axis).

$$\left[\begin{array}{ccc:ccc:ccc} P_X & - & P_{XZ} & P_X & - & P_{XZ} & P_X & - & - \\ R_Z & P_Y & P_{YZ} & R_Z & P_Y & P_{YZ} & R_Z & P_Y & - \\ R_Y & R_X & - & R_Y & R_X & - & R_Y & R_X & - \\ P_X & - & P_{XZ} & P_X & - & - & P_X & - & - \\ R_Z & P_Y & P_{YZ} & R_Z & P_Y & - & R_Z & P_Y & - \\ R_Y & R_X & - & R_Y & R_X & - & R_Y & R_X & - \end{array}\right] \tag{3-252}$$

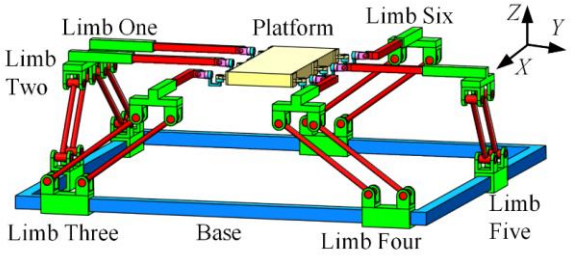

Figure 3-113 Schematic diagram of 6-DOF parallel structure (22)

Feature: There are one P_6 joint (P_X), one P_6 joint (P_Y), three R_6 joints (R_X, R_Y, R_Z), three identical P_a joints (P_{XZ}) and three same P_a joints (P_{YZ}). Three identical P_a joints (P_{XZ}) are relevant to P_6 joint (P_X). Three identical P_a joints (P_{YZ}) are related to P_6 joint (P_Y). The translational direction of P_4 joint (P_X) and the rotational axis of R_6 joint (R_X) are parallel (*X* axis). The translational direction of P_6 joint (P_Y) and the rotational axis of R_6 joint (R_Y) are parallel (*Y* axis).

$$\left[\begin{array}{ccc:ccc:ccc} P_X & P_{XY} & P_{XZ} & P_X & P_{XY} & P_{XZ} & P_X & - & - \\ R_Z & P_Y & - & R_Z & P_Y & - & R_Z & - & - \\ R_Y & R_X & P_Z & R_Y & R_X & P_Z & R_Y & R_X & - \\ P_X & P_{XY} & P_{XZ} & P_X & - & - & P_X & - & - \\ R_Z & P_Y & - & R_Z & - & - & R_Z & - & - \\ R_Y & R_X & P_Z & R_Y & R_X & - & R_Y & R_X & - \end{array}\right] \tag{3-253}$$

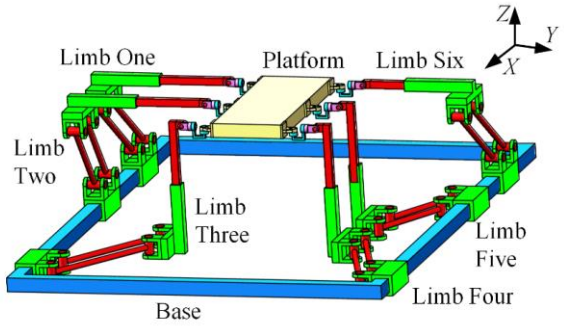

Figure 3-114 Schematic diagram of 6-DOF parallel structure (23)

Feature: There are two P_3 joints (P_Y, P_Z), one P_6 joint (P_X), three R_6 joints (R_X, R_Y, R_Z), three identical P_a joints (P_{XY}) and three same P_a joints (P_{XZ}). Three identical P_a joints (P_{XY}) are relevant to P_3 joint (P_Y). Three identical P_a joints (P_{XZ}) are relevant to P_3 joint (P_Z). Six P_a joints (P_{XY}, P_{XZ}) are related to P_6 joint (P_X). The translational direction of P_6 joint (P_X) and the rotational axis of R_6 joint (R_X) are parallel (X axis). The translational direction of P_3 joint (P_Y) and the rotational axis of R_6 joint (R_Y) are parallel (Y axis). The translational direction of P_3 joint (P_Z) and the rotational axis of R_6 joint (R_Z) are parallel (Z axis).

$$\left[\begin{array}{ccc:ccc:ccc} P_X & - & P_{XZ} & P_X & - & P_{XZ} & P_X & - & - \\ R_Z & P_Y & P_{YZ} & R_Z & P_Y & P_{YZ} & R_Z & - & - \\ R_Y & R_X & P_Z & R_Y & R_X & P_Z & R_Y & R_X & - \\ P_X & - & P_{XZ} & P_X & - & - & P_X & - & - \\ R_Z & P_Y & P_{YZ} & R_Z & - & - & R_Z & - & - \\ R_Y & R_X & P_Z & R_Y & R_X & - & R_Y & R_X & - \end{array}\right] \tag{3-254}$$

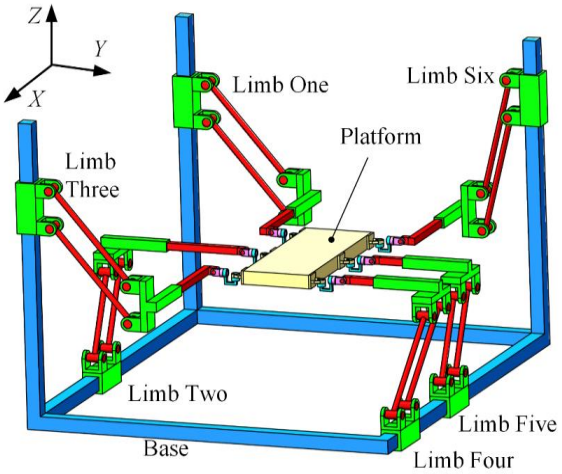

Figure 3-115 Schematic diagram of 6-DOF parallel structure (24)

Feature: There are two P_3 joints (P_Y, P_Z), one P_6 joint (P_X), three R_6 joints (R_X, R_Y, R_Z), three identical P_a joints (P_{XZ}) and three same P_a joints (P_{YZ}). Three identical P_a joints (P_{YZ}) are relevant to P_3 joint (P_Y). Six P_a joints (P_{XZ}, P_{YZ}) are relevant to P_3 joint (P_Z). Three identical P_a joints (P_{XZ}) are related to P_6 joint (P_X). The translational direction of P_6 joint (P_X) and the rotational axis of R_6 joint (R_X) are parallel (X axis). The translational direction of P_3 joint (P_Y) and the rotational axis of R_6 joint (R_Y) are parallel (Y axis). The translational direction of P_3 joint (P_Z) and the rotational axis of R_6 joint (R_Z) are parallel (Z axis).

$$\left[\begin{array}{ccc:ccc:ccc} P_X & - & P_{XZ} & P_X & - & P_{XZ} & - & - & P_{XZ} \\ R_Z & P_Y & - & R_Z & P_Y & - & R_Z & P_Y & - \\ R_Y & R_X & P_Z & R_Y & R_X & P_Z & R_Y & R_X & - \\ P_X & - & P_{XZ} & - & - & P_{XZ} & - & - & P_{XZ} \\ R_Z & P_Y & - & R_Z & P_Y & - & R_Z & P_Y & - \\ R_Y & R_X & P_Z & R_Y & R_X & - & R_Y & R_X & - \end{array}\right] \tag{3-255}$$

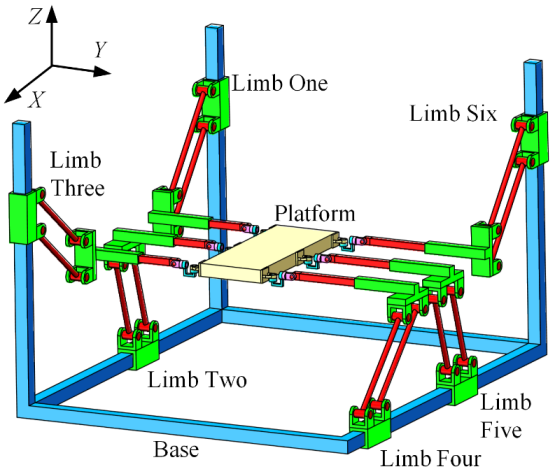

Figure 3-116 Schematic diagram of 6-DOF parallel structure (25)

Feature: There are two P_3 joints (P_X, P_Z), one P_6 joint (P_Y), three R_6 joints (R_X, R_Y, R_Z) and six identical P_a joints (P_{XZ}). Six identical P_a joints (P_{XZ}) are relevant to both P_3 joint (P_X) and P_3 joint (P_Z). Zero P_a joint is related to P_6 joint (P_Y). The translational direction of P_3 joint (P_X) and the rotational axis of R_6 joint (R_X) are parallel (X axis). The translational direction of P_6 joint (P_Y) and the rotational axis of R_6 joint (R_Y) are parallel (Y axis). The translational direction of P_3 joint (P_Z) and the rotational axis of R_6 joint (R_Z) are parallel (Z axis).

$$\begin{bmatrix} P_X & P_{XY} & P_{XZ} & P_X & - & P_{XZ} & P_X & - & - \\ R_Z & P_Y & P_{YZ} & R_Z & P_Y & - & R_Z & P_Y & - \\ R_Y & R_X & P_Z & R_Y & R_X & - & R_Y & R_X & - \\ P_X & - & P_{XZ} & P_X & - & - & P_X & - & - \\ R_Z & P_Y & P_{YZ} & R_Z & P_Y & - & R_Z & - & - \\ R_Y & R_X & - & R_Y & R_X & - & R_Y & R_X & - \end{bmatrix} \tag{3-256}$$

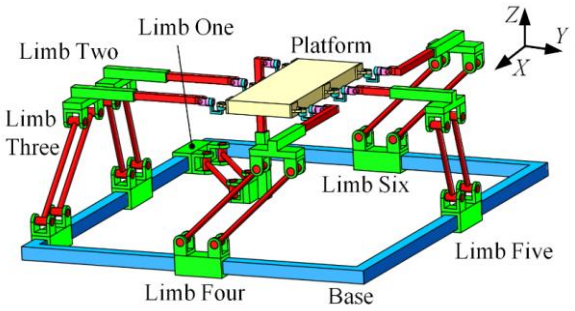

Figure 3-117 Schematic diagram of 6-DOF parallel structure (26)

Feature: There are one P_1 joint (P_Z), one P_5 joint (P_Y), one P_6 joint (P_X), three R_6 joints (R_X, R_Y, R_Z), one P_a joint (P_{XY}), two identical P_a joints (P_{YZ}) and three identical P_a joints (P_{XZ}). Five P_a joints (P_{XZ}) are relevant to P_1 joint (P_Z). Three P_a joints (P_{XY}, P_{YZ}) are relevant to P_5 joint (P_Y). Four P_a joints (P_{XY}, P_{XZ}) are related to P_6 joint (P_X). The translational direction of P_6 joint (P_X) and the rotational axis of R_6 joint (R_X) are parallel (*X* axis). The translational direction of P_5 joint (P_Y) and the rotational axis of R_6 joint (R_Y) are parallel (*Y* axis). The translational direction of P_1 joint (P_Z) and the rotational axis of R_6 joint (R_Z) are parallel (*Z* axis).

$$\begin{bmatrix} P_X & - & P_{XZ} & P_X & - & P_{XZ} & P_X & - & - \\ R_Z & P_Y & P_{YZ} & R_Z & P_Y & P_{YZ} & R_Z & P_Y & - \\ R_Y & R_X & P_Z & R_Y & R_X & - & R_Y & R_X & - \\ P_X & - & P_{XZ} & P_X & - & - & P_X & - & - \\ R_Z & P_Y & P_{YZ} & R_Z & P_Y & - & R_Z & - & - \\ R_Y & R_X & - & R_Y & R_X & - & R_Y & R_X & - \end{bmatrix} \tag{3-257}$$

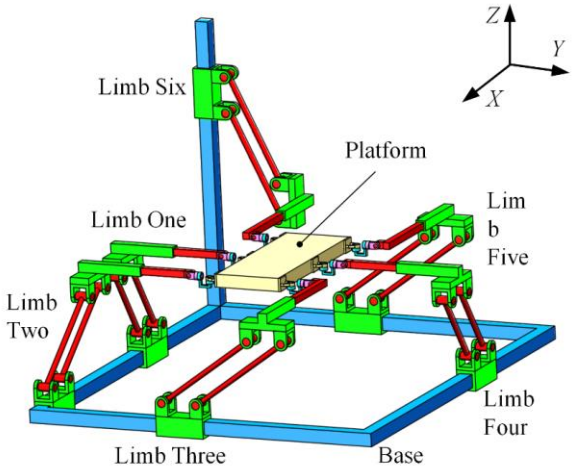

Figure 3-118 Schematic diagram of 6-DOF parallel structure (27)

Feature: There are one P_1 joint (P_Z), one P_5 joint (P_Y), one P_6 joint (P_X), three R_6 joints (R_X, R_Y, R_Z), three identical P_a joints (P_{XZ}) and three identical P_a joints (P_{YZ}). Six P_a joints (P_{XZ}, P_{YZ}) are relevant to P_1 joint (P_Z). Three same P_a joints (P_{YZ}) are relevant to P_5 joint (P_Y). Three identical P_a joints (P_{XZ}) are related to P_6 joint (P_X). The translational direction of P_6 joint (P_X) and the rotational axis of R_6 joint (R_X) are parallel (X axis). The translational direction of P_5 joint (P_Y) and the rotational axis of R_6 joint (R_Y) are parallel (Y axis). The translational direction of P_1 joint (P_Z) and the rotational axis of R_6 joint (R_Z) are parallel (Z axis).

$$\left[\begin{array}{ccc:ccc:ccc} P_X & P_{XY} & P_{XZ} & P_X & - & P_{XZ} & P_X & - & - \\ R_Z & P_Y & P_{YZ} & R_Z & P_Y & - & R_Z & P_Y & - \\ R_Y & R_X & P_Z & R_Y & R_X & - & R_Y & R_X & - \\ P_X & - & P_{XZ} & P_X & - & - & - & - & - \\ R_Z & P_Y & P_{YZ} & R_Z & P_Y & - & R_Z & P_Y & - \\ R_Y & R_X & - & R_Y & R_X & - & R_Y & R_X & - \end{array}\right] \tag{3-258}$$

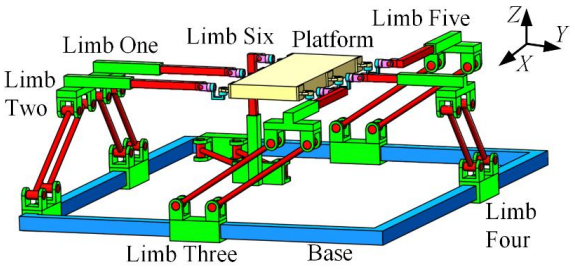

Figure 3-119 Schematic diagram of 6-DOF parallel structure (28)

Feature: There are one P_1 joint (P_Z), one P_5 joint (P_X), one P_6 joint (P_Y), three R_6 joints (R_X, R_Y, R_Z), one P_a joint (P_{XY}), two same P_a joints (P_{YZ}) and three identical P_a joints (P_{XZ}). Five P_a joints (P_{XZ}, P_{YZ}) are relevant to P_1 joint (P_Z). Four P_a joints (P_{XY}, P_{XZ}) are relevant to P_5 joint (P_X). Three P_a joints (P_{XY}, P_{YZ}) are related to P_6 joint (P_Y). The translational direction of P_5 joint (P_X) and the rotational axis of R_6 joint (R_X) are parallel (X axis). The translational direction of P_6 joint (P_Y) and the rotational axis of R_6 joint (R_Y) are parallel (Y axis). The translational direction of P_1 joint (P_Z) and the rotational axis of R_6 joint (R_Z) are parallel (Z axis).

$$\left[\begin{array}{ccc:ccc:ccc} P_X & - & P_{XZ} & P_X & - & P_{XZ} & P_X & - & - \\ R_Z & P_Y & P_{YZ} & R_Z & P_Y & - & R_Z & P_Y & - \\ R_Y & R_X & P_Z & R_Y & R_X & - & R_Y & R_X & - \\ P_X & - & P_{XZ} & P_X & - & P_{XZ} & - & - & - \\ R_Z & P_Y & P_{YZ} & R_Z & P_Y & - & R_Z & P_Y & - \\ R_Y & R_X & - & R_Y & R_X & - & R_Y & R_X & - \end{array}\right] \tag{3-259}$$

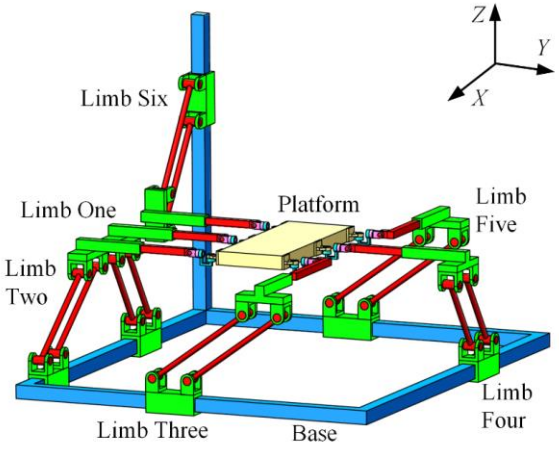

Figure 3-120 Schematic diagram of 6-DOF parallel structure (29)

Feature: There are one P_1 joint (P_Z), one P_5 joint (P_X), one P_6 joint (P_Y), three R_6 joints (R_X, R_Y, R_Z), two same P_a joints (P_{YZ}) and four identical P_a joints (P_{XZ}). All P_a joints (P_{XZ}, P_{YZ}) are relevant to P_1 joint (P_Z). Three identical P_a joints (P_{XZ}) are relevant to P_5 joint (P_X). Two same P_a joints (P_{YZ}) are related to P_6 joint (P_Y). The translational direction of P_5 joint (P_X) and the rotational axis of R_6 joint (R_X) are parallel (X axis). The translational direction of P_6 joint (P_Y) and the rotational axis of R_6 joint (R_Y) are parallel (Y axis). The translational direction of P_1 joint (P_Z) and the rotational axis of R_6 joint (R_Z) are parallel (Z axis).

$$\left[\begin{array}{ccc:ccc:ccc} P_X & P_{XY} & P_{XZ} & P_X & - & P_{XZ} & P_X & - & - \\ R_Z & P_Y & P_{YZ} & R_Z & P_Y & - & R_Z & - & - \\ R_Y & R_X & P_Z & R_Y & R_X & - & R_Y & R_X & - \\ P_X & - & P_{XZ} & P_X & - & - & P_X & - & - \\ R_Z & P_Y & P_{YZ} & R_Z & P_Y & - & R_Z & - & - \\ R_Y & R_X & P_Z & R_Y & R_X & - & R_Y & R_X & - \end{array}\right] \tag{3-260}$$

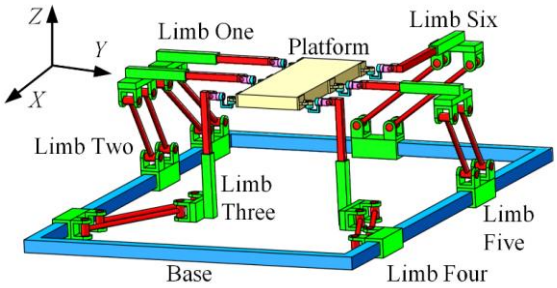

Figure 3-121 Schematic diagram of 6-DOF parallel structure (30)

Feature: There are one P_2 joint (P_Z), one P_4 joint (P_Y), one P_6 joint (P_X), three R_6 joints (R_X, R_Y, R_Z), one P_a joint (P_{XY}), two same P_a joints (P_{YZ}) and three identical P_a joints (P_{XZ}). Five P_a joints (P_{XZ}, P_{YZ}) are relevant to P_2 joint (P_Z). Three P_a joints (P_{XY}, P_{YZ}) are relevant to P_4 joint (P_Y). Four P_a joints (P_{XY}, P_{XZ}) are related to P_6 joint (P_X). The translational direction of P_6 joint (P_X) and the rotational axis of R_6 joint (R_X) are parallel (X axis). The translational direction of P_4 joint (P_Y) and the rotational axis of R_6 joint (R_Y) are parallel (Y axis). The translational direction of P_2 joint (P_Z) and the rotational axis of R_6 joint (R_Z) are parallel (Z axis).

$$\left[\begin{array}{ccc:ccc:ccc} P_X & P_{XY} & P_{XZ} & P_X & - & P_{XZ} & P_X & - & - \\ R_Z & P_Y & P_{YZ} & R_Z & P_Y & - & R_Z & - & - \\ R_Y & R_X & P_Z & R_Y & R_X & P_Z & R_Y & R_X & - \\ P_X & - & P_{XZ} & P_X & - & - & P_X & - & - \\ R_Z & P_Y & P_{YZ} & R_Z & - & - & R_Z & - & - \\ R_Y & R_X & P_Z & R_Y & R_X & - & R_Y & R_X & - \end{array}\right] \tag{3-261}$$

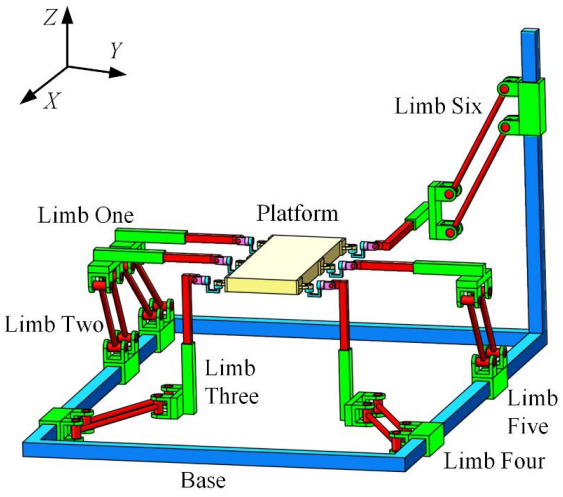

Figure 3-122 Schematic diagram of 6-DOF parallel structure (31)

Feature: There are two P_3 joints (P_Y, P_Z), one P_6 joint (P_X), three R_6 joints (R_X, R_Y, R_Z), one P_a joint (P_{XY}), two same P_a joints (P_{YZ}) and three identical P_a joints (P_{XZ}). Three P_a joints (P_{XY}, P_{YZ}) are relevant to P_3 joint (P_Y). Five P_a joints (P_{XZ}, P_{YZ}) are relevant to P_3 joint (P_Z). Four P_a joints (P_{XY}, P_{XZ}) are related to P_6 joint (P_X). The translational direction of P_6 joint (P_X) and the rotational axis of R_6 joint (R_X) are parallel (X axis). The translational direction of P_3 joint (P_Y) and the rotational axis of R_6 joint (R_Y) are parallel (Y axis). The translational direction of P_3 joint (P_Z) and the rotational axis of R_6 joint (R_Z) are parallel (Z axis).

$$\left[\begin{array}{ccc:ccc:ccc} P_X & P_{XY} & P_{XZ} & P_X & P_{XY} & P_{XZ} & P_X & \_ & \_ \\ R_Z & P_Y & \_ & R_Z & P_Y & \_ & R_Z & \_ & \_ \\ R_Y & R_X & P_Z & R_Y & R_X & P_Z & R_Y & R_X & \_ \\ P_X & P_{XY} & P_{XZ} & P_X & \_ & \_ & \_ & \_ & \_ \\ R_Z & P_Y & \_ & R_Z & P_Y & \_ & R_Z & \_ & \_ \\ R_Y & R_X & P_Z & R_Y & R_X & \_ & R_Y & R_X & \_ \end{array}\right] \tag{3-262}$$

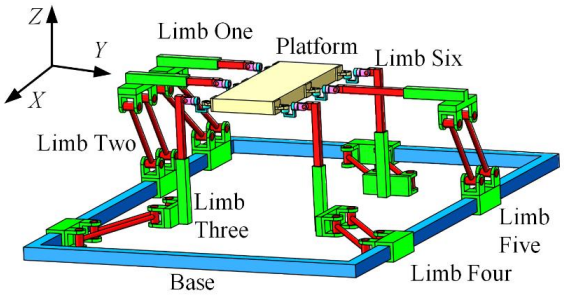

Figure 3-123 Schematic diagram of 6-DOF parallel structure (32)

Feature: There are one P_3 joint (P_Z), one P_4 joint (P_Y), one P_5 joint (P_X), three R_6 joints (R_X, R_Y, R_Z), three same P_a joints (P_{XY}) and three identical P_a joints (P_{XZ}). Three same P_a joints (P_{XZ}) are relevant to P_3 joint (P_Z). Three identical P_a joints (P_{XY}) are relevant to P_4 joint (P_Y). Six P_a joints (P_{XY}, P_{XZ}) are related to P_5 joint (P_X). The translational direction of P_5 joint (P_X) and the rotational axis of R_6 joint (R_X) are parallel (X axis). The translational direction of P_4 joint (P_Y) and the rotational axis of R_6 joint (R_Y) are parallel (Y axis). The translational direction of P_3 joint (P_Z) and the rotational axis of R_6 joint (R_Z) are parallel (Z axis).

$$\left[\begin{array}{ccc:ccc:ccc} P_X & P_{XY} & P_{XZ} & P_X & - & P_{XZ} & P_X & - & - \\ R_Z & P_Y & - & R_Z & P_Y & - & R_Z & - & - \\ R_Y & R_X & P_Z & R_Y & R_X & P_Z & R_Y & R_X & - \\ P_X & P_{XY} & P_{XZ} & P_X & - & P_{XZ} & - & - & - \\ R_Z & P_Y & - & R_Z & P_Y & - & R_Z & - & - \\ R_Y & R_X & P_Z & R_Y & R_X & - & R_Y & R_X & - \end{array}\right] \tag{3-263}$$

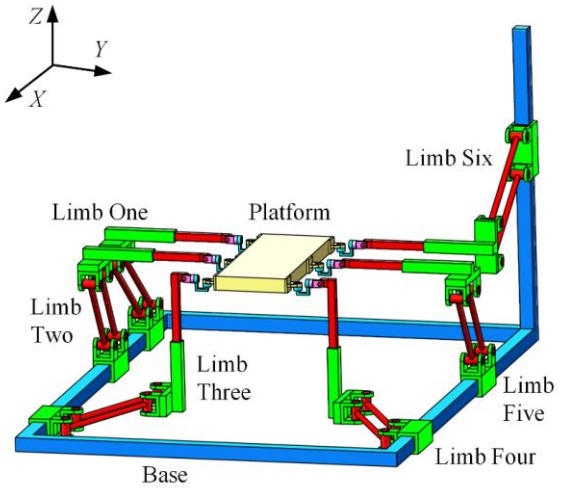

Figure 3-124 Schematic diagram of 6-DOF parallel structure (33)

Feature: There are one P_3 joint (P_Z), one P_4 joint (P_Y), one P_5 joint (P_X), three R_6 joints (R_X, R_Y, R_Z), two same P_a joints (P_{XY}) and four identical P_a joints (P_{XZ}). Four identical P_a joints (P_{XZ}) are relevant to P_3 joint (P_Z). Two identical P_a joints (P_{XY}) are relevant to P_4 joint (P_Y). Six P_a joints (P_{XY}, P_{XZ}) are related to P_5 joint (P_X). The translational direction of P_5 joint (P_X) and the rotational axis of R_6 joint (R_X) are parallel (X axis). The translational direction of P_4 joint (P_Y) and the rotational axis of R_6 joint (R_Y) are parallel (Y axis). The translational direction of P_3 joint (P_Z) and the rotational axis of R_6 joint (R_Z) are parallel (Z axis).

$$\left[\begin{array}{ccc:ccc:ccc} P_X & - & P_{XZ} & P_X & - & P_{XZ} & P_X & - & - \\ R_Z & P_Y & P_{YZ} & R_Z & P_Y & P_{YZ} & R_Z & - & - \\ R_Y & R_X & P_Z & R_Y & R_X & - & R_Y & R_X & - \\ P_X & - & P_{XZ} & P_X & - & - & P_X & - & - \\ R_Z & P_Y & P_{YZ} & R_Z & P_Y & - & R_Z & - & - \\ R_Y & R_X & P_Z & R_Y & R_X & - & R_Y & R_X & - \end{array}\right] \tag{3-264}$$

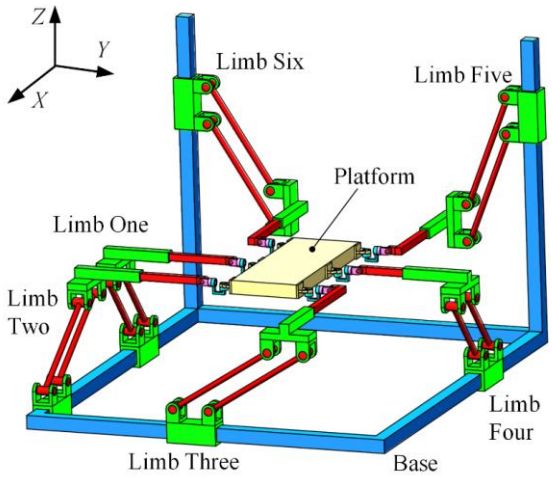

Figure 3-125 Schematic diagram of 6-DOF parallel structure (34)

Feature: There are one P_2 joint (P_Z), one P_4 joint (P_Y), one P_6 joint (P_X), three R_6 joints (R_X, R_Y, R_Z), three same P_a joints (P_{XZ}) and three identical P_a joints (P_{YZ}). Six P_a joints (P_{XZ}, P_{YZ}) are relevant to P_2 joint (P_Z). Three identical P_a joints (P_{YZ}) are relevant to P_4 joint (P_Y). Three same P_a joints (P_{XZ}) are related to P_6 joint (P_X). The translational direction of P_6 joint (P_X) and the rotational axis of R_6 joint (R_X) are parallel (X axis). The translational direction of P_4 joint (P_Y) and the rotational axis of R_6 joint (R_Y) are parallel (Y axis). The translational direction of P_2 joint (P_Z) and the rotational axis of R_6 joint (R_Z) are parallel (Z axis).

$$\left[\begin{array}{ccc:ccc:ccc} P_X & P_{XY} & P_{XZ} & P_X & - & P_{XZ} & P_X & - & - \\ R_Z & P_Y & P_{YZ} & R_Z & P_Y & - & R_Z & - & - \\ R_Y & R_X & P_Z & R_Y & R_X & P_Z & R_Y & R_X & - \\ P_X & - & P_{XZ} & P_X & - & - & P_X & - & - \\ R_Z & P_Y & P_{YZ} & R_Z & - & - & R_Z & - & - \\ R_Y & R_X & P_Z & R_Y & R_X & - & R_Y & R_X & - \end{array}\right] \tag{3-265}$$

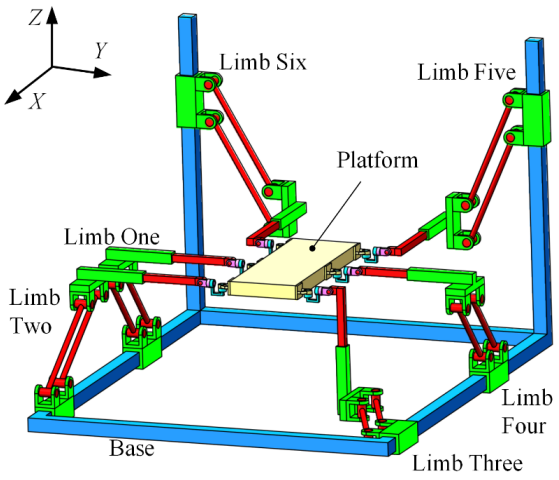

Figure 3-126 Schematic diagram of 6-DOF parallel structure (35)

Feature: There are two P_3 joints (P_Y, P_Z), one P_6 joint (P_X), three R_6 joints (R_X, R_Y, R_Z), one P_a joint (P_{XY}), two same P_a joints (P_{YZ}) and three identical P_a joints (P_{XZ}). Three P_a joints (P_{XY}, P_{YZ}) are relevant to P_3 joint (P_Y). Five P_a joints (P_{XZ}, P_{YZ}) are relevant to P_3 joint (P_Z). Four P_a joints (P_{XY}, P_{XZ}) are related to P_6 joint (P_X). The translational direction of P_6 joint (P_X) and the rotational axis of R_6 joint (R_X) are parallel (X axis). The translational direction of P_3 joint (P_Y) and the rotational axis of R_6 joint (R_Y) are parallel (Y axis). The translational direction of P_3 joint (P_Z) and the rotational axis of R_6 joint (R_Z) are parallel (Z axis).

$$\left[\begin{array}{ccc:ccc:ccc} P_X & P_{XY} & P_{XZ} & P_X & - & P_{XZ} & P_X & - & - \\ R_Z & P_Y & P_{YZ} & R_Z & P_Y & - & R_Z & - & - \\ R_Y & R_X & P_Z & R_Y & R_X & P_Z & R_Y & R_X & - \\ P_X & - & P_{XZ} & P_X & - & - & - & - & - \\ R_Z & P_Y & P_{YZ} & R_Z & P_Y & - & R_Z & - & - \\ R_Y & R_X & P_Z & R_Y & R_X & - & R_Y & R_X & - \end{array}\right] \tag{3-266}$$

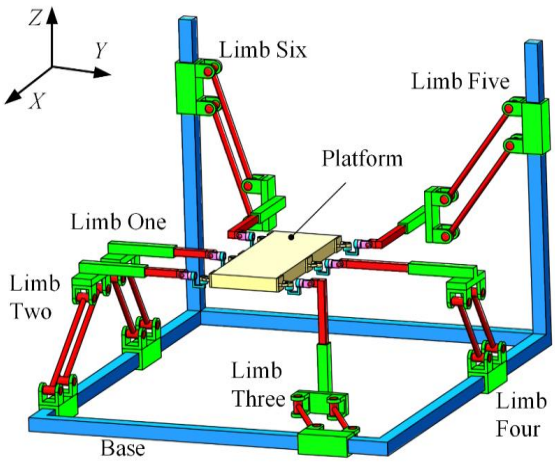

Figure 3-127 Schematic diagram of 6-DOF parallel structure (36)

Feature: There are one P_3 joint (P_Z), one P_4 joint (P_Y), one P_5 joint (P_X), three R_6 joints (R_X, R_Y, R_Z), one P_a joint (P_{XY}), two same P_a joints (P_{YZ}) and three identical P_a joints (P_{XZ}). Five P_a joints (P_{XZ}, P_{YZ}) are relevant to P_3 joint (P_Z). Three P_a joints (P_{XY}, P_{YZ}) are relevant to P_4 joint (P_Y). Four P_a joints (P_{XY}, P_{XZ}) are related to P_5 joint (P_X). The translational direction of P_5 joint (P_X) and the rotational axis of R_6 joint (R_X) are parallel (*X* axis). The translational direction of P_4 joint (P_Y) and the rotational axis of R_6 joint (R_Y) are parallel (*Y* axis). The translational direction of P_3 joint (P_Z) and the rotational axis of R_6 joint (R_Z) are parallel (*Z* axis).

$$\left[\begin{array}{ccc:ccc:ccc} P_X & - & P_{XZ} & P_X & - & P_{XZ} & P_X & - & - \\ R_Z & P_Y & P_{YZ} & R_Z & P_Y & - & R_Z & - & - \\ R_Y & R_X & P_Z & R_Y & R_X & P_Z & R_Y & R_X & - \\ P_X & - & P_{XZ} & P_X & - & P_{XZ} & - & - & - \\ R_Z & P_Y & P_{YZ} & R_Z & P_Y & - & R_Z & - & - \\ R_Y & R_X & P_Z & R_Y & R_X & - & R_Y & R_X & - \end{array}\right] \tag{3-267}$$

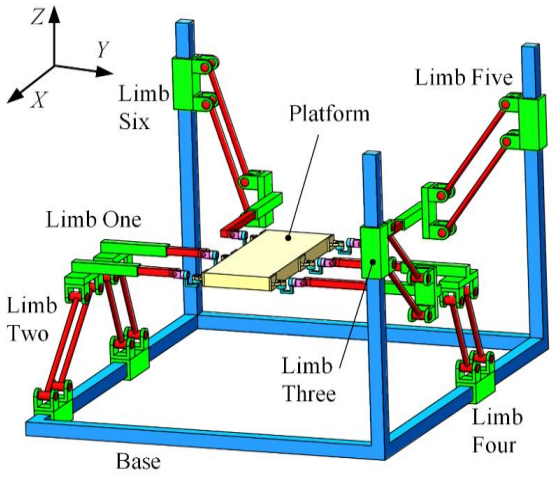

Figure 3-128 Schematic diagram of 6-DOF parallel structure (37)

Feature: There are one P_3 joint (P_Z), one P_4 joint (P_Y), one P_5 joint (P_X), three R_6 joints (R_X, R_Y, R_Z), two same P_a joints (P_{YZ}) and four identical P_a joints (P_{XZ}). Six P_a joints (P_{XZ}, P_{YZ}) are relevant to P_3 joint (P_Z). Two same P_a joints (P_{YZ}) are relevant to P_4 joint (P_Y). Four identical P_a joints (P_{XZ}) are related to P_5 joint (P_X). The translational direction of P_5 joint (P_X) and the rotational axis of R_6 joint (R_X) are parallel (X axis). The translational direction of P_4 joint (P_Y) and the rotational axis of R_6 joint (R_Y) are parallel (Y axis). The translational direction of P_3 joint (P_Z) and the rotational axis of R_6 joint (R_Z) are parallel (Z axis).

$$\left[\begin{array}{ccc|ccc|ccc} P_X & P_{XY} & P_{XZ} & P_X & \_ & P_{XZ} & \_ & \_ & \_ \\ R_Z & P_Y & P_{YZ} & R_Z & P_Y & \_ & R_Z & P_Y & \_ \\ R_Y & R_X & P_Z & R_Y & R_X & \_ & R_Y & R_X & \_ \\ P_X & P_{XY} & P_{XZ} & P_X & \_ & \_ & \_ & \_ & \_ \\ R_Z & P_Y & \_ & R_Z & P_Y & \_ & R_Z & P_Y & \_ \\ R_Y & R_X & P_Z & R_Y & R_X & \_ & R_Y & R_X & \_ \end{array}\right] \tag{3-268}$$

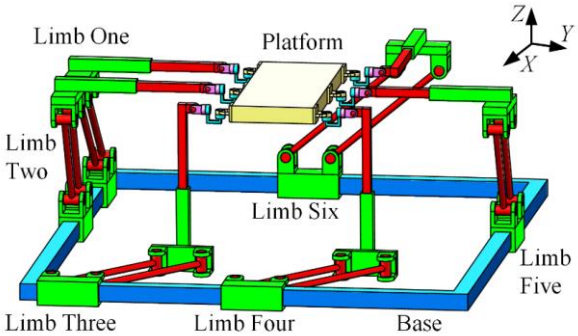

Figure 3-129 Schematic diagram of 6-DOF parallel structure (38)

Feature: There are one P_2 joint (P_Z), one P_4 joint (P_X), one P_6 joint (P_Y), three R_6 joints (R_X, R_Y, R_Z), one P_a joint (P_{YZ}), two same P_a joints (P_{XY}) and three identical P_a joints (P_{XZ}). Four P_a joints (P_{XZ}, P_{YZ}) are relevant to P_2 joint (P_Z). Five P_a joints (P_{XY}, P_{XZ}) are related to P_4 joint (P_X). Three P_a joints (P_{XY}, P_{YZ}) are relevant to P_6 joint (P_Y). The translational direction of P_4 joint (P_X) and the rotational axis of R_6 joint (R_X) are parallel (X axis). The translational direction of P_6 joint (P_Y) and the rotational axis of R_6 joint (R_Y) are parallel (Y axis). The translational direction of P_2 joint (P_Z) and the rotational axis of R_6 joint (R_Z) are parallel (Z axis).

$$\left[\begin{array}{ccc:ccc:ccc} P_X & P_{XY} & P_{XZ} & P_X & P_{XY} & P_{XZ} & - & - & - \\ R_Z & P_Y & - & R_Z & P_Y & - & R_Z & P_Y & - \\ R_Y & R_X & P_Z & R_Y & R_X & P_Z & R_Y & R_X & - \\ P_X & P_{XY} & P_{XZ} & P_X & - & - & - & - & - \\ R_Z & P_Y & - & R_Z & P_Y & - & R_Z & - & - \\ R_Y & R_X & P_Z & R_Y & R_X & - & R_Y & R_X & - \end{array}\right] \tag{3-269}$$

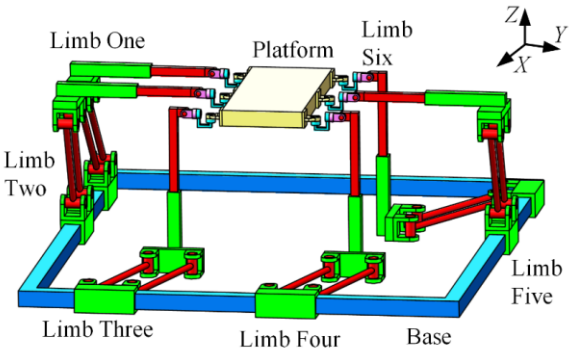

Figure 3-130 Schematic diagram of 6-DOF parallel structure (39)

Feature: There are one P_3 joint (P_Z), one P_4 joint (P_X), one P_5 joint (P_Y), three R_6 joints (R_X, R_Y, R_Z), three same P_a joints (P_{XY}) and three identical P_a joints (P_{XZ}). Three identical P_a joints (P_{XZ}) are relevant to P_3 joint (P_Z). Six P_a joints (P_{XY}, P_{XZ}) are related to P_4 joint (P_X). Three identical P_a joints (P_{XY}) are relevant to P_5 joint (P_Y). The translational direction of P_4 joint (P_X) and the rotational axis of R_6 joint (R_X) are parallel (X axis). The translational direction of P_5 joint (P_Y) and the rotational axis of R_6 joint (R_Y) are parallel (Y axis). The translational direction of P_3 joint (P_Z) and the rotational axis of R_6 joint (R_Z) are parallel (Z axis).

$$\left[\begin{array}{ccc:ccc:ccc} P_X & P_{XY} & P_{XZ} & P_X & - & P_{XZ} & - & - & - \\ R_Z & P_Y & P_{YZ} & R_Z & P_Y & - & R_Z & P_Y & - \\ R_Y & R_X & P_Z & R_Y & R_X & P_Z & R_Y & R_X & - \\ P_X & P_{XY} & P_{XZ} & P_X & - & - & - & - & - \\ R_Z & P_Y & - & R_Z & P_Y & - & R_Z & - & - \\ R_Y & R_X & P_Z & R_Y & R_X & - & R_Y & R_X & - \end{array}\right] \tag{3-270}$$

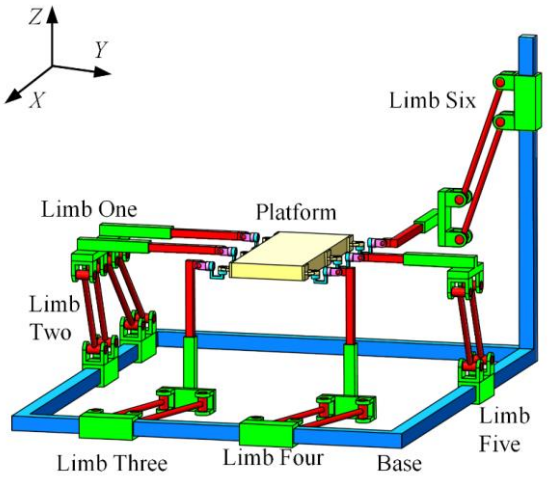

Figure 3-131 Schematic diagram of 6-DOF parallel structure (40)

Feature: There are one P_3 joint (P_Z), one P_4 joint (P_X), one P_5 joint (P_Y), three R_6 joints (R_X, R_Y, R_Z), one P_a joint (P_{YZ}), two same P_a joints (P_{XY}) and three identical P_a joints (P_{XZ}). Four P_a joints (P_{XZ}, P_{YZ}) are relevant to P_3 joint (P_Z). Five P_a joints (P_{XY}, P_{XZ}) are related to P_4 joint (P_X). Three P_a joints (P_{XY}, P_{YZ}) are relevant to P_5 joint (P_Y). The translational direction of P_4 joint (P_X) and the rotational axis of R_6 joint (R_X) are parallel (X axis). The translational direction of P_5 joint (P_Y) and the rotational axis of R_6 joint (R_Y) are parallel (Y axis). The translational direction of P_3 joint (P_Z) and the rotational axis of R_6 joint (R_Z) are parallel (Z axis).

$$\left[\begin{array}{ccc:ccc:ccc} P_X & P_{XY} & P_{XZ} & P_X & - & P_{XZ} & - & - & - \\ R_Z & P_Y & - & R_Z & P_Y & - & R_Z & P_Y & - \\ R_Y & R_X & P_Z & R_Y & R_X & P_Z & R_Y & R_X & - \\ P_X & P_{XY} & P_{XZ} & - & - & P_{XZ} & - & - & - \\ R_Z & P_Y & - & R_Z & P_Y & - & R_Z & P_Y & - \\ R_Y & R_X & P_Z & R_Y & R_X & - & R_Y & R_X & - \end{array}\right] \tag{3-271}$$

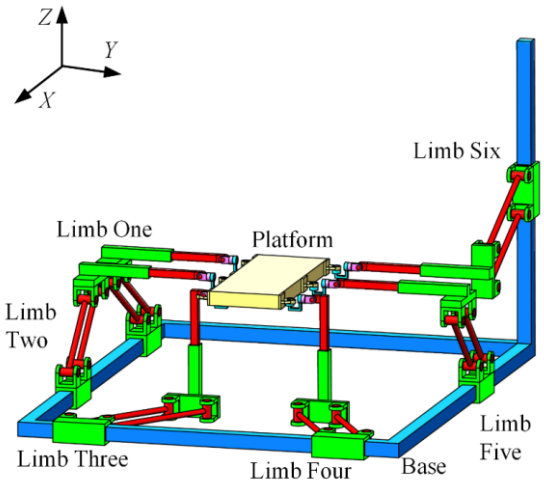

Figure 3-132 Schematic diagram of 6-DOF parallel structure (41)

Feature: There are two P_3 joints (P_X, P_Z), one P_6 joint (P_Y), three R_6 joints (R_X, R_Y, R_Z), two same P_a joints (P_{XY}) and four identical P_a joints (P_{XZ}). Six P_a joints (P_{XY}, P_{XZ}) are related to P_3 joint (P_X). Four same P_a joints (P_{XZ}) are relevant to P_3 joint (P_Z). Two identical P_a joints (P_{XY}) are relevant to P_6 joint (P_Y). The translational direction of P_3 joint (P_X) and the rotational axis of R_6 joint (R_X) are parallel (X axis). The translational direction of P_6 joint (P_Y) and the rotational axis of R_6 joint (R_Y) are parallel (Y axis). The translational direction of P_3 joint (P_Z) and the rotational axis of R_6 joint (R_Z) are parallel (Z axis).

$$\left[\begin{array}{ccc:ccc:ccc} P_X & - & P_{XZ} & P_X & - & P_{XZ} & - & - & P_{XZ} \\ R_Z & P_Y & P_{YZ} & R_Z & P_Y & - & R_Z & P_Y & - \\ R_Y & R_X & P_Z & R_Y & R_X & - & R_Y & R_X & - \\ P_X & - & P_{XZ} & P_X & - & P_{XZ} & - & - & - \\ R_Z & P_Y & - & R_Z & P_Y & - & R_Z & P_Y & - \\ R_Y & R_X & P_Z & R_Y & R_X & - & R_Y & R_X & - \end{array}\right] \tag{3-272}$$

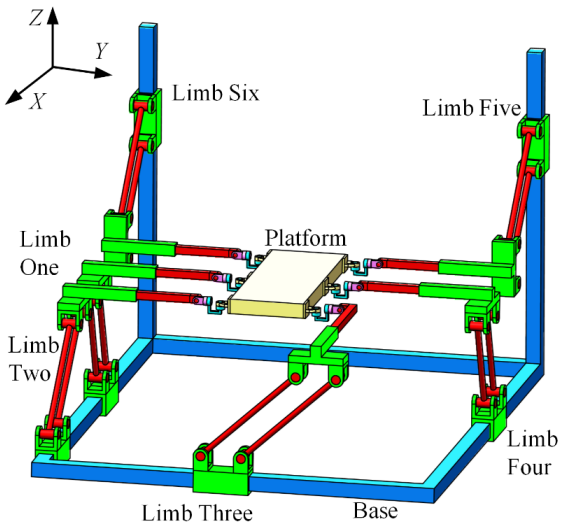

Figure 3-133 Schematic diagram of 6-DOF parallel structure (42)

Feature: There are one P_2 joint (P_Z), one P_4 joint (P_X), one P_6 joint (P_Y), three R_6 joints (R_X, R_Y, R_Z), one P_a joint (P_{YZ}) and five identical P_a joints (P_{XZ}). Six P_a joints (P_{XZ}, P_{YZ}) are relevant to P_2 joint (P_Z). Five identical P_a joints (P_{XZ}) are related to P_4 joint (P_X). One P_a joint (P_{YZ}) is relevant to P_6 joint (P_Y). The translational direction of P_4 joint (P_X) and the rotational axis of R_6 joint (R_X) are parallel (X axis). The translational direction of P_6 joint (P_Y) and the rotational axis of R_6 joint (R_Y) are parallel (Y axis). The translational direction of P_2 joint (P_Z) and the rotational axis of R_6 joint (R_Z) are parallel (Z axis).

$$\left[\begin{array}{ccc:ccc:ccc} P_X & P_{XY} & P_{XZ} & P_X & - & P_{XZ} & - & - & P_{XZ} \\ R_Z & P_Y & - & R_Z & P_Y & - & R_Z & P_Y & - \\ R_Y & R_X & P_Z & R_Y & R_X & P_Z & R_Y & R_X & - \\ P_X & - & P_{XZ} & P_X & - & P_{XZ} & - & - & - \\ R_Z & P_Y & - & R_Z & P_Y & - & R_Z & - & - \\ R_Y & R_X & P_Z & R_Y & R_X & - & R_Y & R_X & - \end{array}\right] \tag{3-273}$$

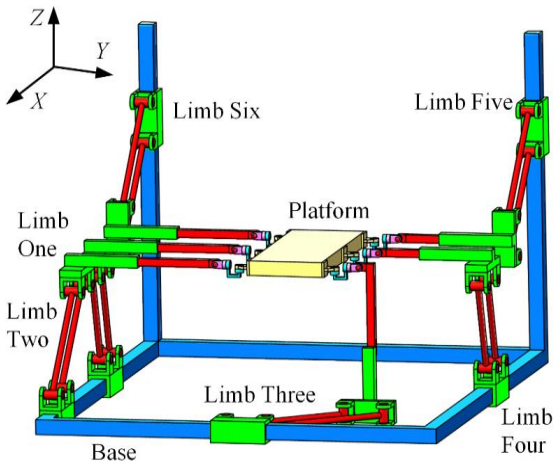

Figure 3-134 Schematic diagram of 6-DOF parallel structure (43)

Feature: There are one P_3 joint (P_Z), one P_4 joint (P_X), one P_5 joint (P_Y), three R_6 joints (R_X, R_Y, R_Z), one P_a joint (P_{XY}) and five identical P_a joints (P_{XZ}). Five identical P_a joints (P_{XZ}) are relevant to P_3 joint (P_Z). Six P_a joints (P_{XY}, P_{XZ}) are related to P_4 joint (P_X). One P_a joint (P_{XY}) is relevant to P_5 joint (P_Y). The translational direction of P_4 joint (P_X) and the rotational axis of R_6 joint (R_X) are parallel (*X* axis). The translational direction of P_5 joint (P_Y) and the rotational axis of R_6 joint (R_Y) are parallel (*Y* axis). The translational direction of P_3 joint (P_Z) and the rotational axis of R_6 joint (R_Z) are parallel (*Z* axis).

$$\left[\begin{array}{ccc:ccc:ccc} P_X & \_ & P_{XZ} & P_X & \_ & P_{XZ} & \_ & \_ & P_{XZ} \\ R_Z & P_Y & P_{YZ} & R_Z & P_Y & \_ & R_Z & P_Y & \_ \\ R_Y & R_X & P_Z & R_Y & R_X & P_Z & R_Y & R_X & \_ \\ P_X & \_ & P_{XZ} & P_X & \_ & P_{XZ} & \_ & \_ & \_ \\ R_Z & P_Y & \_ & R_Z & P_Y & \_ & R_Z & \_ & \_ \\ R_Y & R_X & P_Z & R_Y & R_X & \_ & R_Y & R_X & \_ \end{array}\right] \tag{3-274}$$

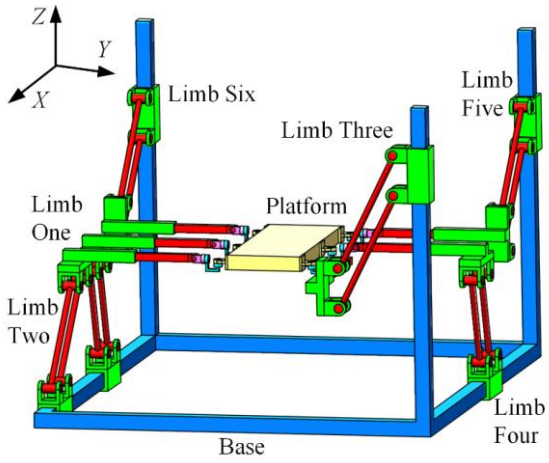

Figure 3-135 Schematic diagram of 6-DOF parallel structure (44)

Feature: There are one P_3 joint (P_Z), one P_4 joint (P_X), one P_5 joint (P_Y), three R_6 joints (R_X, R_Y, R_Z), one P_a joint (P_{YZ}) and five identical P_a joints (P_{XZ}). All P_a joints (P_{XZ}, P_{YZ}) are relevant to P_3 joint (P_Z). Five identical P_a joints (P_{XZ}) are related to P_4 joint (P_X). One P_a joint (P_{YZ}) is relevant to P_5 joint (P_Y). The translational direction of P_4 joint (P_X) and the rotational axis of R_6 joint (R_X) are parallel (X axis). The translational direction of P_5 joint (P_Y) and the rotational axis of R_6 joint (R_Y) are parallel (Y axis). The translational direction of P_3 joint (P_Z) and the rotational axis of R_6 joint (R_Z) are parallel (Z axis).

$$\left[\begin{array}{ccc:ccc:ccc} P_X & P_{XY} & P_{XZ} & P_X & - & P_{XZ} & - & - & P_{XZ} \\ R_Z & P_Y & - & R_Z & P_Y & - & R_Z & P_Y & - \\ R_Y & R_X & P_Z & R_Y & R_X & P_Z & R_Y & R_X & - \\ P_X & - & P_{XZ} & - & - & P_{XZ} & - & - & - \\ R_Z & P_Y & - & R_Z & P_Y & - & R_Z & P_Y & - \\ R_Y & R_X & P_Z & R_Y & R_X & - & R_Y & R_X & - \end{array}\right] \tag{3-275}$$

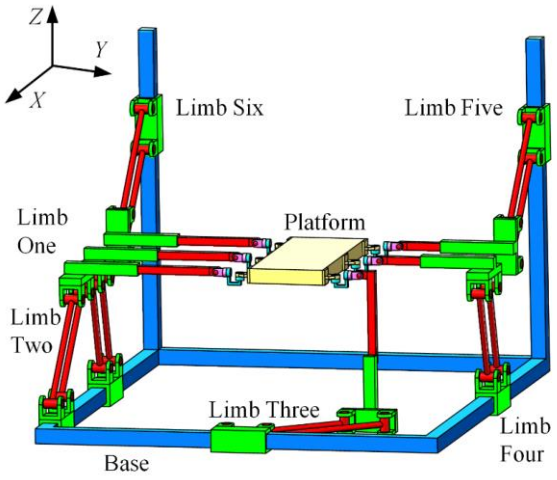

Figure 3-136 Schematic diagram of 6-DOF parallel structure (45)

Feature: There are one P_3 joint (P_X), one P_3 joint (P_Z), one P_6 joint (P_Y), three R_6 joints (R_X, R_Y, R_Z), one P_a joint (P_{XY}) and five identical P_a joints (P_{XZ}). All P_a joints (P_{XY}, P_{XZ}) are relevant to P_3 joint (P_X). Five identical P_a joints (P_{XZ}) are related to P_3 joint (P_Z). One P_a joint (P_{XY}) is relevant to P_6 joint (P_Y). The translational direction of P_3 joint (P_X) and the rotational axis of R_6 joint (R_X) are parallel (X axis). The translational direction of P_6 joint (P_Y) and the rotational axis of R_6 joint (R_Y) are parallel (Y axis). The translational direction of P_3 joint (P_Z) and the rotational axis of R_6 joint (R_Z) are parallel (Z axis).

$$\left[\begin{array}{ccc:ccc:ccc} P_X & P_{XY} & P_{XZ} & P_X & - & P_{XZ} & P_X & - & - \\ R_Z & P_Y & P_{YZ} & R_Z & P_Y & - & R_Z & - & - \\ R_Y & R_X & P_Z & R_Y & R_X & - & R_Y & R_X & - \\ P_X & - & P_{XZ} & P_X & - & - & P_X & - & - \\ R_Z & P_Y & P_{YZ} & R_Z & P_Y & - & R_Z & - & - \\ R_Y & R_X & P_Z & R_Y & R_X & - & R_Y & R_X & - \end{array}\right] \tag{3-276}$$

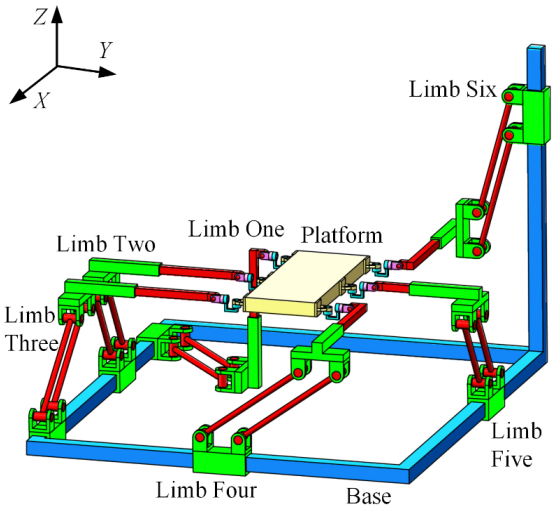

Figure 3-137 Schematic diagram of 6-DOF parallel structure (46)

Feature: There are one P_2 joint (P_Z), one P_4 joint (P_Y), one P_6 joint (P_X), three R_6 joints (R_X, R_Y, R_Z), one P_a joint (P_{XY}), two same P_a joints (P_{YZ}) and three identical P_a joints (P_{XZ}). Five P_a joints (P_{XZ}, P_{YZ}) are relevant to P_2 joint (P_Z). Three P_a joints (P_{XY}, P_{YZ}) are related to P_4 joint (P_Y). Four P_a joints (P_{XY}, P_{XZ}) are relevant to P_6 joint (P_X). The translational direction of P_6 joint (P_X) and the rotational axis of R_6 joint (R_X) are parallel (X axis). The translational direction of P_4 joint (P_Y) and the rotational axis of R_6 joint (R_Y) are parallel (Y axis). The translational direction of P_2 joint (P_Z) and the rotational axis of R_6 joint (R_Z) are parallel (Z axis).

$$\left[\begin{array}{ccc:ccc:ccc} P_X & P_{XY} & P_{XZ} & P_X & \_ & P_{XZ} & P_X & \_ & \_ \\ R_Z & P_Y & P_{YZ} & R_Z & P_Y & \_ & R_Z & P_Y & \_ \\ R_Y & R_X & P_Z & R_Y & R_X & \_ & R_Y & R_X & \_ \\ P_X & P_{XY} & P_{XZ} & P_X & \_ & \_ & \_ & \_ & \_ \\ R_Z & P_Y & \_ & R_Z & P_Y & \_ & R_Z & \_ & \_ \\ R_Y & R_X & P_Z & R_Y & R_X & \_ & R_Y & R_X & \_ \end{array}\right] \tag{3-277}$$

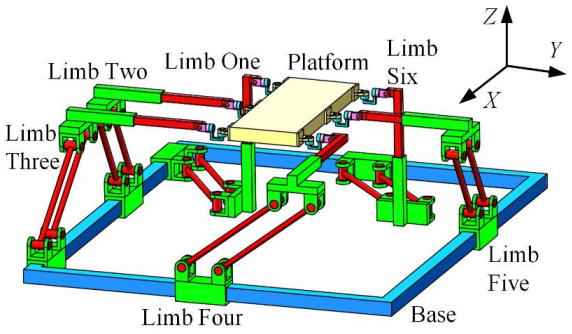

Figure 3-138 Schematic diagram of 6-DOF parallel structure (47)

Feature: There are one P_2 joint (P_Z), one P_5 joint (P_X), one P_5 joint (P_Y), three R_6 joints (R_X, R_Y, R_Z), one P_a joint (P_{YZ}), two same P_a joints (P_{XY}) and three identical P_a joints (P_{XZ}). Four P_a joints (P_{XZ}, P_{YZ}) are relevant to P_2 joint (P_Z). Five P_a joints (P_{XY}, P_{XZ}) are related to P_5 joint (P_X). Three P_a joints (P_{XY}, P_{YZ}) are relevant to P_5 joint (P_Y). The translational direction of P_5 joint (P_X) and the rotational axis of R_6 joint (R_X) are parallel (X axis). The translational direction of P_5 joint (P_Y) and the rotational axis of R_6 joint (R_Y) are parallel (Y axis). The translational direction of P_2 joint (P_Z) and the rotational axis of R_6 joint (R_Z) are parallel (Z axis).

$$\left[\begin{array}{ccc:ccc:ccc} P_X & P_{XY} & P_{XZ} & P_X & - & P_{XZ} & P_X & - & - \\ R_Z & P_Y & P_{YZ} & R_Z & P_Y & - & R_Z & P_Y & - \\ R_Y & R_X & P_Z & R_Y & R_X & - & R_Y & R_X & - \\ P_X & - & P_{XZ} & P_X & - & - & - & - & - \\ R_Z & P_Y & P_{YZ} & R_Z & P_Y & - & R_Z & - & - \\ R_Y & R_X & P_Z & R_Y & R_X & - & R_Y & R_X & - \end{array}\right] \tag{3-278}$$

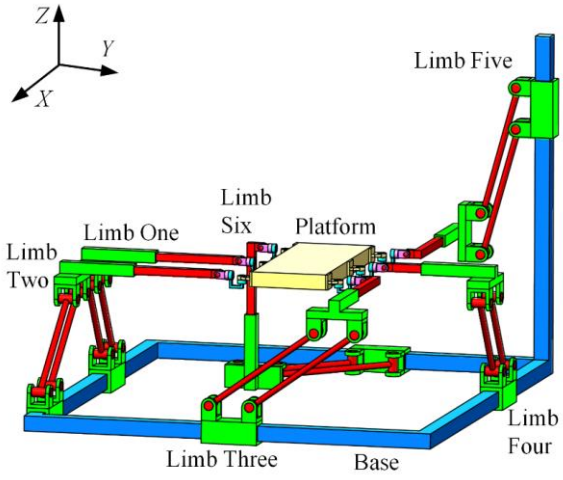

Figure 3-139 Schematic diagram of 6-DOF parallel structure (48)

Feature: There are one P_2 joint (P_Z), one P_5 joint (P_X), one P_5 joint (P_Y), three R_6 joints (R_X, R_Y, R_Z), one P_a joint (P_{XY}), two same P_a joints (P_{YZ}) and three identical P_a joints (P_{XZ}). Five P_a joints (P_{XZ}, P_{YZ}) are relevant to P_2 joint (P_Z). Four P_a joints (P_{XY}, P_{XZ}) are related to P_5 joint (P_X). Three P_a joints (P_{XY}, P_{YZ}) are relevant to P_5 joint (P_Y). The translational direction of P_5 joint (P_X) and the rotational axis of R_6 joint (R_X) are parallel (X axis). The translational direction of P_5 joint (P_Y) and the rotational axis of R_6 joint (R_Y) are parallel (Y axis). The translational direction of P_2 joint (P_Z) and the rotational axis of R_6 joint (R_Z) are parallel (Z axis).

$$\left[\begin{array}{ccc:ccc:ccc} P_X & - & P_{XZ} & P_X & - & P_{XZ} & P_X & - & - \\ R_Z & P_Y & P_{YZ} & R_Z & P_Y & - & R_Z & P_Y & - \\ R_Y & R_X & P_Z & R_Y & R_X & - & R_Y & R_X & - \\ P_X & - & P_{XZ} & P_X & - & P_{XZ} & - & - & - \\ R_Z & P_Y & P_{YZ} & R_Z & P_Y & - & R_Z & - & - \\ R_Y & R_X & P_Z & R_Y & R_X & - & R_Y & R_X & - \end{array}\right] \tag{3-279}$$

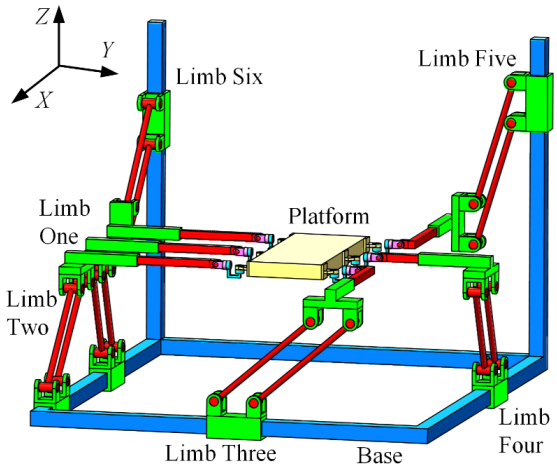

Figure 3-140 Schematic diagram of 6-DOF parallel structure (49)

Feature: There are one P_2 joint (P_Z), one P_5 joint (P_X), one P_5 joint (P_Y), three R_6 joints (R_X, R_Y, R_Z), two same P_a joints (P_{YZ}) and four identical P_a joints (P_{XZ}). Six P_a joints (P_{XZ}, P_{YZ}) are relevant to P_2 joint (P_Z). Four identical P_a joints (P_{XZ}) are related to P_5 joint (P_X). Two identical P_a joints (P_{YZ}) are relevant to P_5 joint (P_Y). The translational direction of P_5 joint (P_X) and the rotational axis of R_6 joint (R_X) are parallel (X axis). The translational direction of P_5 joint (P_Y) and the rotational axis of R_6 joint (R_Y) are parallel (Y axis). The translational direction of P_2 joint (P_Z) and the rotational axis of R_6 joint (R_Z) are parallel (Z axis).

$$\left[\begin{array}{ccc:ccc:ccc}
P_X & P_{XY} & P_{XZ} & P_X & - & P_{XZ} & - & - & - \\
R_Z & P_Y & P_{YZ} & R_Z & P_Y & - & R_Z & P_Y & - \\
R_Y & R_X & P_Z & R_Y & R_X & - & R_Y & R_X & - \\
P_X & - & P_{XZ} & P_X & - & P_{XZ} & - & - & - \\
R_Z & P_Y & - & R_Z & P_Y & - & R_Z & P_Y & - \\
R_Y & R_X & P_Z & R_Y & R_X & - & R_Y & R_X & -
\end{array}\right] \tag{3-280}$$

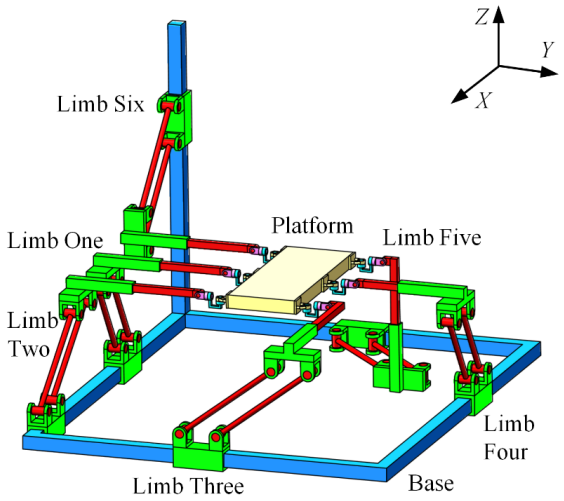

Figure 3-141 Schematic diagram of 6-DOF parallel structure (50)

Feature: There are one P_2 joint (P_Z), one P_4 joint (P_X), one P_6 joint (P_Y), three R_6 joints (R_X, R_Y, R_Z), one P_a joint (P_{XY}), one P_a joint (P_{YZ}) and four identical P_a joints (P_{XZ}). Five P_a joints (P_{XZ}, P_{YZ}) are relevant to P_2 joint (P_Z). Five P_a joints (P_{XY}, P_{XZ}) are related to P_4 joint (P_X). Two different P_a joints (P_{XY}, P_{YZ}) are relevant to P_6 joint (P_Y). The translational direction of P_4 joint (P_X) and the rotational axis of R_6 joint (R_X) are parallel (X axis). The translational direction of P_6 joint (P_Y) and the rotational axis of R_6 joint (R_Y) are parallel (Y axis). The translational direction of P_2 joint (P_Z) and the rotational axis of R_6 joint (R_Z) are parallel (Z axis).

$$\left[\begin{array}{ccc:ccc:ccc}
P_X & P_{XY} & P_{XZ} & P_X & - & P_{XZ} & P_X & - & - \\
R_Z & P_Y & P_{YZ} & R_Z & P_Y & - & R_Z & - & - \\
R_Y & R_X & P_Z & R_Y & R_X & P_Z & R_Y & R_X & - \\
P_X & P_{XY} & P_{XZ} & P_X & - & - & - & - & - \\
R_Z & P_Y & - & R_Z & P_Y & - & R_Z & - & - \\
R_Y & R_X & P_Z & R_Y & R_X & - & R_Y & R_X & -
\end{array}\right] \tag{3-281}$$

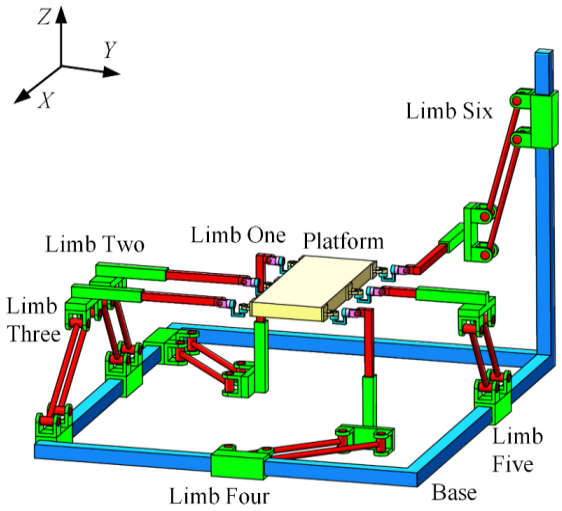

Figure 3-142 Schematic diagram of 6-DOF parallel structure (51)

Feature: There are one P_3 joint (P_Z), one P_4 joint (P_Y), one P_5 joint (P_X), three R_6 joints (R_X, R_Y, R_Z), one P_a joint (P_{YZ}), two identical P_a joints (P_{XY}) and three identical P_a joints (P_{XZ}). Four P_a joints (P_{XZ}, P_{YZ}) are relevant to P_3 joint (P_Z). Three P_a joints (P_{XY}, P_{YZ}) are related to P_4 joint (P_Y). Five P_a joints (P_{XY}, P_{XZ}) are relevant to P_5 joint (P_X). The translational direction of P_5 joint (P_X) and the rotational axis of R_6 joint (R_X) are parallel (X axis). The translational direction of P_4 joint (P_Y) and the rotational axis of R_6 joint (R_Y) are parallel (Y axis). The translational direction of P_3 joint (P_Z) and the rotational axis of R_6 joint (R_Z) are parallel (Z axis).

$$\left[\begin{array}{ccc:ccc:ccc} P_X & P_{XY} & P_{XZ} & P_X & \_ & P_{XZ} & P_X & \_ & \_ \\ R_Z & P_Y & P_{YZ} & R_Z & P_Y & \_ & R_Z & \_ & \_ \\ R_Y & R_X & P_Z & R_Y & R_X & P_Z & R_Y & R_X & \_ \\ P_X & \_ & P_{XZ} & P_X & \_ & P_{XZ} & \_ & \_ & \_ \\ R_Z & P_Y & \_ & R_Z & P_Y & \_ & R_Z & \_ & \_ \\ R_Y & R_X & P_Z & R_Y & R_X & \_ & R_Y & R_X & \_ \end{array}\right] \tag{3-282}$$

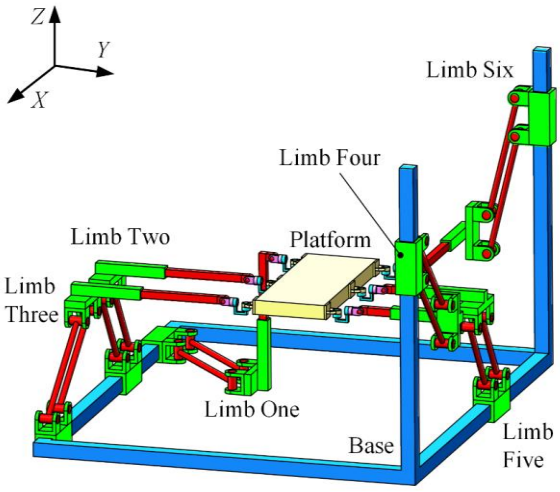

Figure 3-143 Schematic diagram of 6-DOF parallel structure (52)

Feature: There are one P_3 joint (P_Z), one P_4 joint (P_Y), one P_5 joint (P_X), three R_6 joints (R_X, R_Y, R_Z), one P_a joint (P_{XY}), one P_a joint (P_{YZ}) and four identical P_a joints (P_{XZ}). Five P_a joints (P_{XZ}, P_{YZ}) are relevant to P_3 joint (P_Z). Two different P_a joints (P_{XY}, P_{YZ}) are related to P_4 joint (P_Y). Five P_a joints (P_{XY}, P_{XZ}) are relevant to P_5 joint (P_X). The translational direction of P_5 joint (P_X) and the rotational axis of R_6 joint (R_X) are parallel (X axis). The translational direction of P_4 joint (P_Y) and the rotational axis of R_6 joint (R_Y) are parallel (Y axis). The translational direction of P_3 joint (P_Z) and the rotational axis of R_6 joint (R_Z) are parallel (Z axis).

$$\left[\begin{array}{ccc:ccc:ccc} P_X & P_{XY} & P_{XZ} & P_X & - & P_{XZ} & - & - & - \\ R_Z & P_Y & P_{YZ} & R_Z & P_Y & - & R_Z & P_Y & - \\ R_Y & R_X & P_Z & R_Y & R_X & P_Z & R_Y & R_X & - \\ P_X & - & P_{XZ} & P_X & - & P_{XZ} & - & - & - \\ R_Z & P_Y & - & R_Z & P_Y & - & R_Z & - & - \\ R_Y & R_X & P_Z & R_Y & R_X & - & R_Y & R_X & - \end{array}\right] \tag{3-283}$$

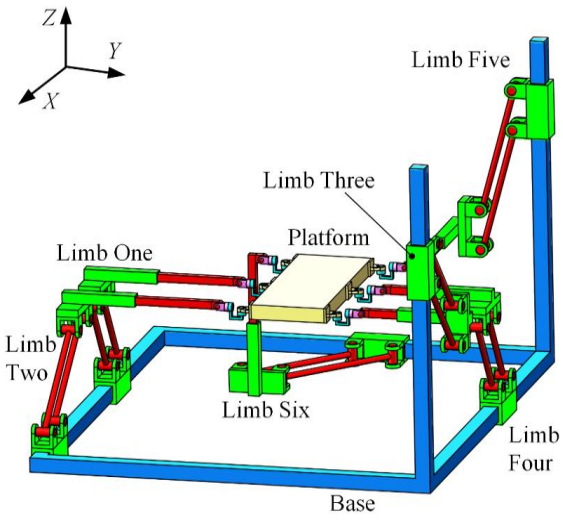

Figure 3-144 Schematic diagram of 6-DOF parallel structure (53)

Feature: There are one P_3 joint (P_Z), one P_4 joint (P_X), one P_5 joint (P_Y), three R_6 joints (R_X, R_Y, R_Z), one P_a joint (P_{XY}), one P_a joint (P_{YZ}) and four identical P_a joints (P_{XZ}). Five P_a joints (P_{XZ}, P_{YZ}) are relevant to P_3 joint (P_Z). Five P_a joints (P_{XY}, P_{XZ}) are related to P_4 joint (P_X). Two different P_a joints (P_{XY}, P_{YZ}) are relevant to P_5 joint (P_Y). The translational direction of P_4 joint (P_X) and the rotational axis of R_6 joint (R_X) are parallel (X axis). The translational direction of P_5 joint (P_Y) and the rotational axis of R_6 joint (R_Y) are parallel (Y axis). The translational direction of P_3 joint (P_Z) and the rotational axis of R_6 joint (R_Z) are parallel (Z axis).

$$\left[\begin{array}{ccc:ccc:ccc} P_X & P_{XY} & P_{XZ} & P_X & \_ & \_ & P_X & \_ & \_ \\ R_Z & P_Y & P_{YZ} & R_Z & P_Y & \_ & R_Z & \_ & \_ \\ R_Y & R_X & P_Z & R_Y & R_X & \_ & R_Y & R_X & \_ \\ P_X & P_{XY} & P_{XZ} & P_X & \_ & \_ & P_X & \_ & \_ \\ R_Z & P_Y & P_{YZ} & R_Z & P_Y & \_ & R_Z & \_ & \_ \\ R_Y & R_X & P_Z & R_Y & R_X & \_ & R_Y & R_X & \_ \end{array}\right] \tag{3-284}$$

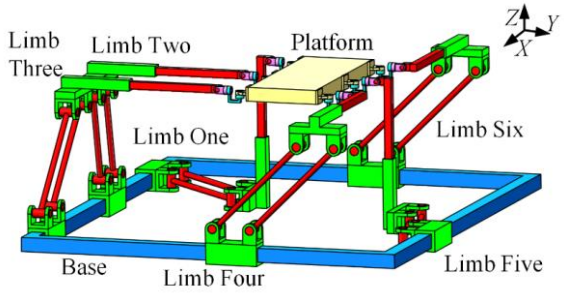

Figure 3-145 Schematic diagram of 6-DOF parallel structure (54)

Feature: There are one P_2 joint (P_Z), one P_4 joint (P_Y), one P_6 joint (P_X), three R_6 joints (R_X, R_Y, R_Z), two identical P_a joints (P_{XY}), two identical P_a joints (P_{XZ}) and two identical P_a joints (P_{YZ}). Four P_a joints (P_{XZ}, P_{YZ}) are relevant to P_2 joint (P_Z). Four P_a joints (P_{XY}, P_{YZ}) are related to P_4 joint (P_Y). Four different P_a joints (P_{XY}, P_{XZ}) are relevant to P_6 joint (P_X). The translational direction of P_6 joint (P_X) and the rotational axis of R_6 joint (R_X) are parallel (X axis). The translational direction of P_4 joint (P_Y) and the rotational axis of R_6 joint (R_Y) are parallel (Y axis). The translational direction of P_2 joint (P_Z) and the rotational axis of R_6 joint (R_Z) are parallel (Z axis).

$$\left[\begin{array}{ccc:ccc:ccc} P_X & - & P_{XZ} & P_X & - & - & P_X & - & - \\ R_Z & P_Y & P_{YZ} & R_Z & P_Y & P_{YZ} & R_Z & - & - \\ R_Y & R_X & P_Z & R_Y & R_X & - & R_Y & R_X & - \\ P_X & - & P_{XZ} & P_X & - & - & P_X & - & - \\ R_Z & P_Y & P_{YZ} & R_Z & P_Y & P_{YZ} & R_Z & - & - \\ R_Y & R_X & P_Z & R_Y & R_X & - & R_Y & R_X & - \end{array}\right] \tag{3-285}$$

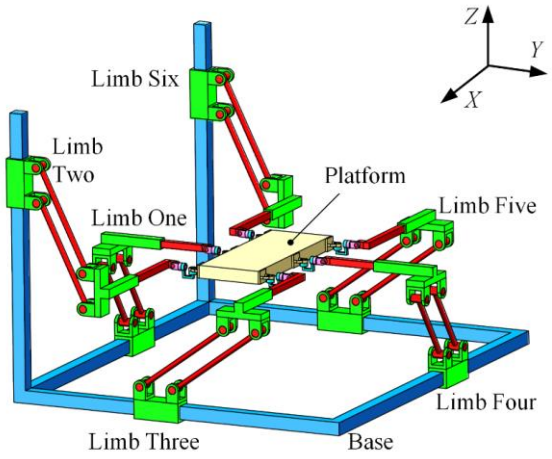

Figure 3-146 Schematic diagram of 6-DOF parallel structure (55)

Feature: There are one P_2 joint (P_Z), one P_4 joint (P_Y), one P_6 joint (P_X), three R_6 joints (R_X, R_Y, R_Z), two identical P_a joints (P_{XZ}) and four identical P_a joints (P_{YZ}). Six P_a joints (P_{XZ}, P_{YZ}) are relevant to P_2 joint (P_Z). Four same P_a joints (P_{YZ}) are related to P_4 joint (P_Y). Two same P_a joints (P_{XZ}) are relevant to P_6 joint (P_X). The translational direction of P_6 joint (P_X) and the rotational axis of R_6 joint (R_X) are parallel (X axis). The translational direction of P_4 joint (P_Y) and the rotational axis of R_6 joint (R_Y) are parallel (Y axis). The translational direction of P_2 joint (P_Z) and the rotational axis of R_6 joint (R_Z) are parallel (Z axis).

$$\left[\begin{array}{ccc:ccc:ccc}
\mathrm{P}_X & \mathrm{P}_{XY} & \mathrm{P}_{XZ} & \mathrm{P}_X & \mathrm{P}_{XY} & _ & _ & _ & _ \\
R_Z & \mathrm{P}_Y & _ & R_Z & \mathrm{P}_Y & _ & R_Z & _ & _ \\
R_Y & R_X & \mathrm{P}_Z & R_Y & R_X & \mathrm{P}_Z & R_Y & R_X & _ \\
\mathrm{P}_X & \mathrm{P}_{XY} & \mathrm{P}_{XZ} & \mathrm{P}_X & \mathrm{P}_{XY} & _ & _ & _ & _ \\
R_Z & \mathrm{P}_Y & _ & R_Z & \mathrm{P}_Y & _ & R_Z & _ & _ \\
R_Y & R_X & \mathrm{P}_Z & R_Y & R_X & \mathrm{P}_Z & R_Y & R_X & _
\end{array}\right] \tag{3-286}$$

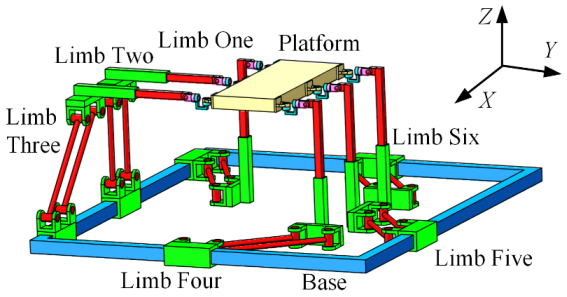

Figure 3-147 Schematic diagram of 6-DOF parallel structure (56)

Feature: There are three P_4 joints (P_X, P_Y, P_Z), three R_6 joints (R_X, R_Y, R_Z), two identical P_a joints (P_{XZ}) and four identical P_a joints (P_{XY}). Six P_a joints (P_{XY}, P_{XZ}) are relevant to P_4 joint (P_X). Four same P_a joints (P_{XY}) are related to P_4 joint (P_Y). Two same P_a joints (P_{XZ}) are relevant to P_4 joint (P_Z). The translational direction of P_4 joint (P_X) and the rotational axis of R_6 joint (R_X) are parallel (X axis). The translational direction of P_4 joint (P_Y) and the rotational axis of R_6 joint (R_Y) are parallel (Y axis). The translational direction of P_4 joint (P_Z) and the rotational axis of R_6 joint (R_Z) are parallel (Z axis).

$$\left[\begin{array}{ccc:ccc:ccc}
\mathrm{P}_X & \mathrm{P}_{XY} & \mathrm{P}_{XZ} & \mathrm{P}_X & _ & _ & _ & _ & _ \\
R_Z & \mathrm{P}_Y & \mathrm{P}_{YZ} & R_Z & \mathrm{P}_Y & _ & R_Z & _ & _ \\
R_Y & R_X & \mathrm{P}_Z & R_Y & R_X & \mathrm{P}_Z & R_Y & R_X & _ \\
\mathrm{P}_X & \mathrm{P}_{XY} & \mathrm{P}_{XZ} & \mathrm{P}_X & _ & _ & _ & _ & _ \\
R_Z & \mathrm{P}_Y & \mathrm{P}_{YZ} & R_Z & \mathrm{P}_Y & _ & R_Z & _ & _ \\
R_Y & R_X & \mathrm{P}_Z & R_Y & R_X & \mathrm{P}_Z & R_Y & R_X & _
\end{array}\right] \tag{3-287}$$

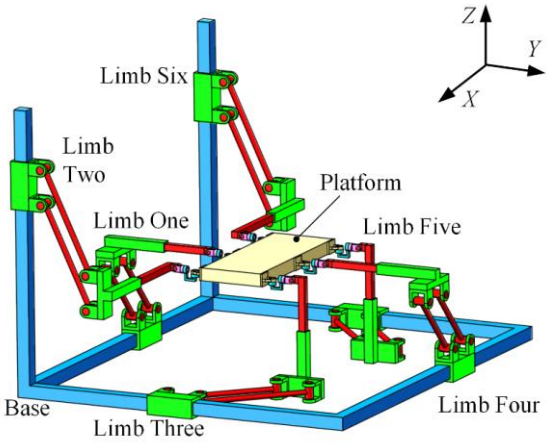

Figure 3-148 Schematic diagram of 6-DOF parallel structure (57)

Feature: There are three P_4 joints (P_X, P_Y, P_Z), three R_6 joints (R_X, R_Y, R_Z), two identical P_a joints (P_{XY}), two identical P_a joints (P_{XZ}) and two same P_a joints (P_{YZ}). Four P_a joints (P_{XY}, P_{XZ}) are relevant to P_4 joint (P_X). Four P_a joints (P_{XY}, P_{YZ}) are related to P_4 joint (P_Y). Four P_a joints (P_{XZ}, P_{YZ}) are relevant to P_4 joint (P_Z). The translational direction of P_4 joint (P_X) and the rotational axis of R_6 joint (R_X) are parallel (X axis). The translational direction of P_4 joint (P_Y) and the rotational axis of R_6 joint (R_Y) are parallel (Y axis). The translational direction of P_4 joint (P_Z) and the rotational axis of R_6 joint (R_Z) are parallel (Z axis).

$$\left[\begin{array}{ccc:ccc:ccc} P_X & P_{XY} & P_{XZ} & P_X & \_ & \_ & P_X & \_ & \_ \\ R_Z & P_Y & P_{YZ} & R_Z & P_Y & P_{YZ} & R_Z & \_ & \_ \\ R_Y & R_X & P_Z & R_Y & R_X & \_ & R_Y & R_X & \_ \\ P_X & \_ & P_{XZ} & P_X & \_ & \_ & P_X & \_ & \_ \\ R_Z & P_Y & P_{YZ} & R_Z & P_Y & \_ & R_Z & \_ & \_ \\ R_Y & R_X & P_Z & R_Y & R_X & \_ & R_Y & R_X & \_ \end{array}\right] \tag{3-288}$$

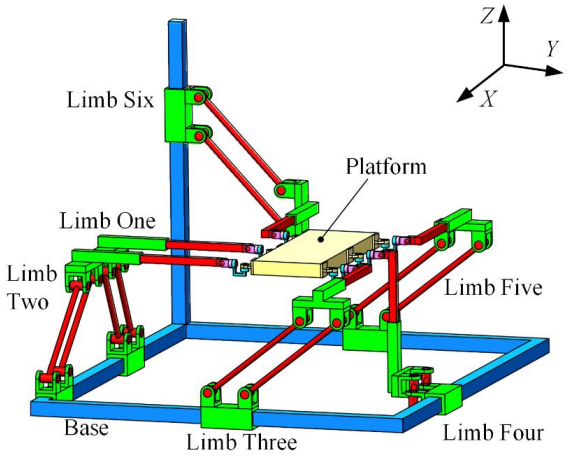

Figure 3-149 Schematic diagram of 6-DOF parallel structure (58)

Feature: There are one P_2 joint (P_Z), one P_4 joint (P_Y), one P_6 joint (P_X), three R_6 joints (R_X, R_Y, R_Z), one P_a joint (P_{XY}), two identical P_a joints (P_{XZ}) and three same P_a joints (P_{YZ}). Five P_a joints (P_{XZ}, P_{YZ}) are relevant to P_2 joint (P_Z). Four P_a joints (P_{XY}, P_{YZ}) are related to P_4 joint (P_Y). Three P_a joints (P_{XY}, P_{XZ}) are relevant to P_6 joint (P_X). The translational direction of P_6 joint (P_X) and the rotational axis of R_6 joint (R_X) are parallel (X axis). The translational direction of P_4 joint (P_Y) and the rotational axis of R_6 joint (R_Y) are parallel (Y axis). The translational direction of P_2 joint (P_Z) and the rotational axis of R_6 joint (R_Z) are parallel (Z axis).

$$\left[\begin{array}{ccc:ccc:ccc} P_X & P_{XY} & P_{XZ} & P_X & - & - & P_X & - & - \\ R_Z & P_Y & P_{YZ} & R_Z & P_Y & - & R_Z & P_Y & - \\ R_Y & R_X & P_Z & R_Y & R_X & - & R_Y & R_X & - \\ P_X & P_{XY} & P_{XZ} & P_X & - & - & - & - & - \\ R_Z & P_Y & P_{YZ} & R_Z & P_Y & - & R_Z & - & - \\ R_Y & R_X & P_Z & R_Y & R_X & - & R_Y & R_X & - \end{array}\right] \tag{3-289}$$

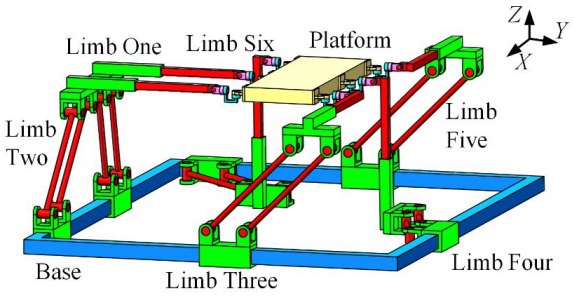

Figure 3-150 Schematic diagram of 6-DOF parallel structure (59)

Feature: There are one P_2 joint (P_Z), one P_5 joint (P_X), one P_5 joint (P_Y), three R_6 joints (R_X, R_Y, R_Z), two identical P_a joints (P_{XY}), two identical P_a joints (P_{XZ}) and three same P_a joints (P_{YZ}). Four P_a joints (P_{XZ}, P_{YZ}) are relevant to P_2 joint (P_Z). Four P_a joints (P_{XY}, P_{XZ}) are related to P_5 joint (P_X). Four P_a joints (P_{XY}, P_{YZ}) are relevant to P_5 joint (P_Y). The translational direction of P_5 joint (P_X) and the rotational axis of R_6 joint (R_X) are parallel (X axis). The translational direction of P_5 joint (P_Y) and the rotational axis of R_6 joint (R_Y) are parallel (Y axis). The translational direction of P_2 joint (P_Z) and the rotational axis of R_6 joint (R_Z) are parallel (Z axis).

$$\left[\begin{array}{ccc:ccc:ccc} P_X & \_ & P_{XZ} & P_X & \_ & P_{XZ} & P_X & \_ & \_ \\ R_Z & P_Y & P_{YZ} & R_Z & P_Y & P_{YZ} & R_Z & P_Y & \_ \\ R_Y & R_X & P_Z & R_Y & R_X & \_ & R_Y & R_X & \_ \\ P_X & \_ & P_{XZ} & P_X & \_ & \_ & \_ & \_ & \_ \\ R_Z & P_Y & P_{YZ} & R_Z & P_Y & \_ & R_Z & \_ & \_ \\ R_Y & R_X & P_Z & R_Y & R_X & \_ & R_Y & R_X & \_ \end{array}\right] \tag{3-290}$$

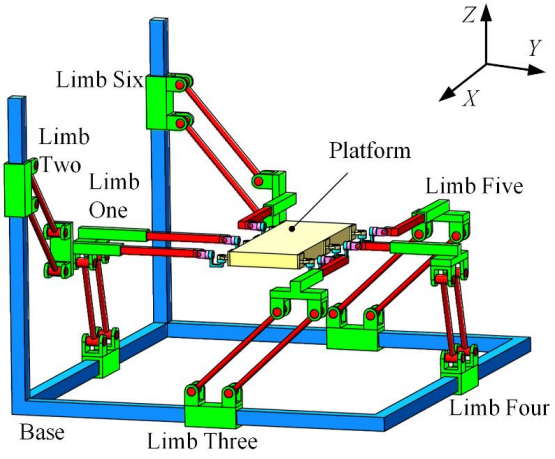

Figure 3-151 Schematic diagram of 6-DOF parallel structure (60)

Feature: There are one P_2 joint (P_Z), one P_5 joint (P_X), one P_5 joint (P_Y), three R_6 joints (R_X, R_Y, R_Z), three identical P_a joints (P_{XZ}) and three same P_a joints (P_{YZ}). Six P_a joints (P_{XZ}, P_{YZ}) are relevant to P_2 joint (P_Z). Three same P_a joints (P_{XZ}) are related to P_5 joint (P_X). Three identical P_a joints (P_{YZ}) are relevant to P_5 joint (P_Y). The translational direction of P_5 joint (P_X) and the rotational axis of R_6 joint (R_X) are parallel (X axis). The translational direction of P_5 joint (P_Y) and the rotational axis of R_6 joint (R_Y) are parallel (Y axis). The translational direction of P_2 joint (P_Z) and the rotational axis of R_6 joint (R_Z) are parallel (Z axis).

$$\left[\begin{array}{ccc:ccc:ccc} P_X & P_{XY} & P_{XZ} & P_X & - & - & P_X & - & - \\ R_Z & P_Y & P_{YZ} & R_Z & P_Y & - & R_Z & - & - \\ R_Y & R_X & P_Z & R_Y & R_X & P_Z & R_Y & R_X & - \\ P_X & P_{XY} & P_{XZ} & P_X & - & - & P_X & - & - \\ R_Z & P_Y & P_{YZ} & R_Z & - & - & R_Z & - & - \\ R_Y & R_X & P_Z & R_Y & R_X & - & R_Y & R_X & - \end{array}\right] \tag{3-291}$$

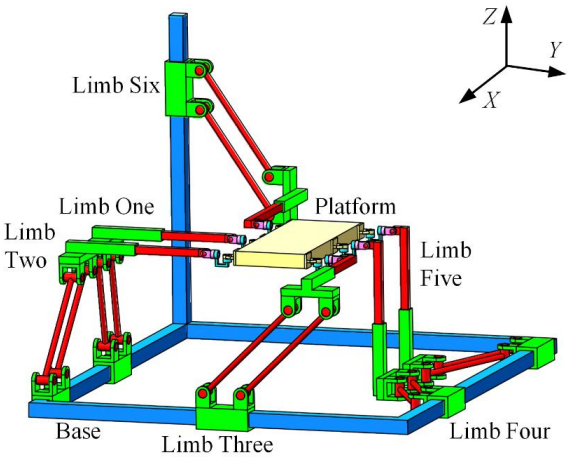

Figure 3-152 Schematic diagram of 6-DOF parallel structure (61)

Feature: There are one P_3 joint (P_Y), one P_3 joint (P_Z), one P_6 joint (P_X), three R_6 joints (R_X, R_Y, R_Z), two identical P_a joints (P_{XY}), two identical P_a joints (P_{XZ}) and two same P_a joints (P_{YZ}). Four P_a joints (P_{XY}, P_{YZ}) are relevant to P_3 joint (P_Y). Four P_a joints (P_{XZ}, P_{YZ}) are relevant to P_3 joint (P_Z). Four P_a joints (P_{XY}, P_{XZ}) are related to P_6 joint (P_X). The translational direction of P_6 joint (P_X) and the rotational axis of R_6 joint (R_X) are parallel (X axis). The translational direction of P_3 joint (P_Y) and the rotational axis of R_6 joint (R_Y) are parallel (Y axis). The translational direction of P_3 joint (P_Z) and the rotational axis of R_6 joint (R_Z) are parallel (Z axis).

$$\left[\begin{array}{ccc:ccc:ccc} P_X & P_{XY} & P_{XZ} & P_X & P_{XY} & - & P_X & - & - \\ R_Z & P_Y & P_{YZ} & R_Z & P_Y & - & R_Z & - & - \\ R_Y & R_X & P_Z & R_Y & R_X & P_Z & R_Y & R_X & - \\ P_X & P_{XY} & P_{XZ} & P_X & - & - & - & - & - \\ R_Z & P_Y & - & R_Z & P_Y & - & R_Z & - & - \\ R_Y & R_X & P_Z & R_Y & R_X & - & R_Y & R_X & - \end{array}\right] \tag{3-292}$$

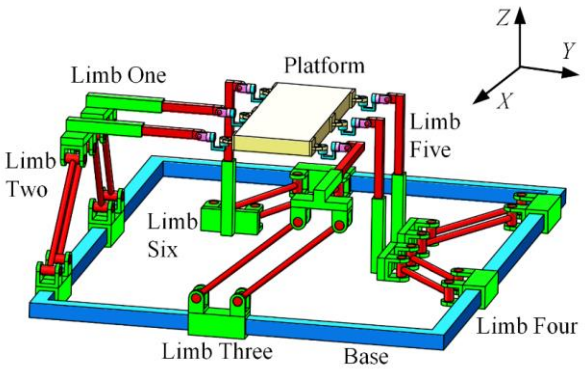

Figure 3-153 Schematic diagram of 6-DOF parallel structure (62)

Feature: There are one P_3 joint (P_Z), one P_4 joint (P_Y), one P_5 joint (P_X), three R_6 joints (R_X, R_Y, R_Z), one P_a joints (P_{YZ}), two identical P_a joints (P_{XZ}) and three same P_a joints (P_{XY}). Three P_a joints (P_{XZ}, P_{YZ}) are relevant to P_3 joint (P_Z). Four P_a joints (P_{XY}, P_{YZ}) are relevant to P_4 joint (P_Y). Five P_a joints (P_{XY}, P_{XZ}) are related to P_5 joint (P_X). The translational direction of P_5 joint (P_X) and the rotational axis of R_6 joint (R_X) are parallel (X axis). The translational direction of P_4 joint (P_Y) and the rotational axis of R_6 joint (R_Y) are parallel (Y axis). The translational direction of P_3 joint (P_Z) and the rotational axis of R_6 joint (R_Z) are parallel (Z axis).

$$\left[\begin{array}{ccc:ccc:ccc} P_X & P_{XY} & P_{XZ} & P_X & - & - & P_X & - & - \\ R_Z & P_Y & P_{YZ} & R_Z & P_Y & P_{YZ} & R_Z & - & - \\ R_Y & R_X & P_Z & R_Y & R_X & P_Z & R_Y & R_X & - \\ P_X & - & P_{XZ} & P_X & - & - & P_X & - & - \\ R_Z & P_Y & P_{YZ} & R_Z & - & - & R_Z & - & - \\ R_Y & R_X & P_Z & R_Y & R_X & - & R_Y & R_X & - \end{array}\right] \tag{3-293}$$

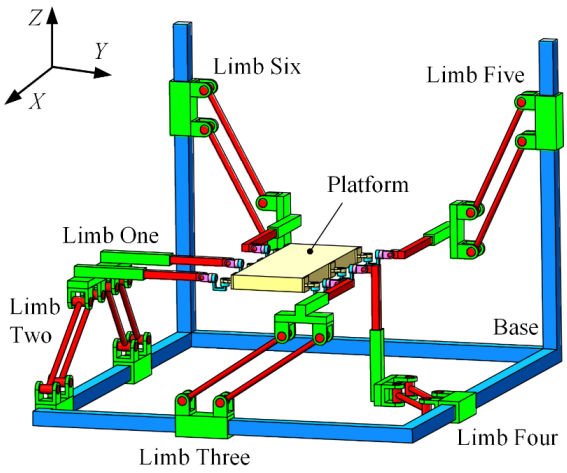

Figure 3-154 Schematic diagram of 6-DOF parallel structure (63)

Feature: There are one P_3 joint (P_Y), one P_3 joint (P_Z), one P_6 joint (P_X), three R_6 joints (R_X, R_Y, R_Z), one P_a joints (P_{XY}), two identical P_a joints (P_{XZ}) and three same P_a joints (P_{YZ}). Four P_a joints (P_{XY}, P_{YZ}) are relevant to P_3 joint (P_Y). Five P_a joints (P_{XZ}, P_{YZ}) are relevant to P_3 joint (P_Z). Three P_a joints (P_{XY}, P_{XZ}) are related to P_6 joint (P_X). The translational direction of P_6 joint (P_X) and the rotational axis of R_6 joint (R_X) are parallel (X axis). The translational direction of P_3 joint (P_Y) and the rotational axis of R_6 joint (R_Y) are parallel (Y axis). The translational direction of P_3 joint (P_Z) and the rotational axis of R_6 joint (R_Z) are parallel (Z axis).

$$\left[\begin{array}{ccc:ccc:ccc} P_X & P_{XY} & P_{XZ} & P_X & P_{XY} & P_{XZ} & \_ & \_ & \_ \\ R_Z & P_Y & \_ & R_Z & P_Y & \_ & R_Z & \_ & \_ \\ R_Y & R_X & P_Z & R_Y & R_X & P_Z & R_Y & R_X & \_ \\ P_X & P_{XY} & P_{XZ} & P_X & \_ & \_ & \_ & \_ & \_ \\ R_Z & P_Y & \_ & R_Z & P_Y & \_ & R_Z & \_ & \_ \\ R_Y & R_X & P_Z & R_Y & R_X & P_Z & R_Y & R_X & \_ \end{array}\right] \tag{3-294}$$

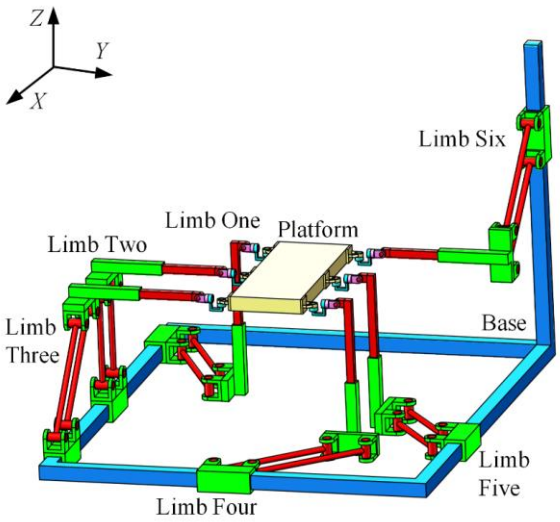

Figure 3-155 Schematic diagram of 6-DOF parallel structure (64)

Feature: There are three P_4 joints (P_X, P_Y, P_Z), three R_6 joints (R_X, R_Y, R_Z), three identical P_a joints (P_{XY}) and three same P_a joints (P_{XZ}). Six P_a joints (P_{XY}, P_{XZ}) are related to P_4 joint (P_X). Three same P_a joints (P_{XY}) are relevant to P_4 joint (P_Y). Three identical P_a joints (P_{XZ}) are relevant to P_4 joint (P_Z). The translational direction of P_4 joint (P_X) and the rotational axis of R_6 joint (R_X) are parallel (X axis). The translational direction of P_4 joint (P_Y) and the rotational axis of R_6 joint (R_Y) are parallel (Y axis). The translational direction of P_4 joint (P_Z) and the rotational axis of R_6 joint (R_Z) are parallel (Z axis).

$$\left[\begin{array}{ccc:ccc:ccc} P_X & P_{XY} & P_{XZ} & P_X & - & P_{XZ} & - & - & - \\ R_Z & P_Y & P_{YZ} & R_Z & P_Y & - & R_Z & - & - \\ R_Y & R_X & P_Z & R_Y & R_X & P_Z & R_Y & R_X & - \\ P_X & - & P_{XZ} & P_X & - & - & - & - & - \\ R_Z & P_Y & P_{YZ} & R_Z & P_Y & - & R_Z & - & - \\ R_Y & R_X & P_Z & R_Y & R_X & P_Z & R_Y & R_X & - \end{array}\right] \tag{3-295}$$

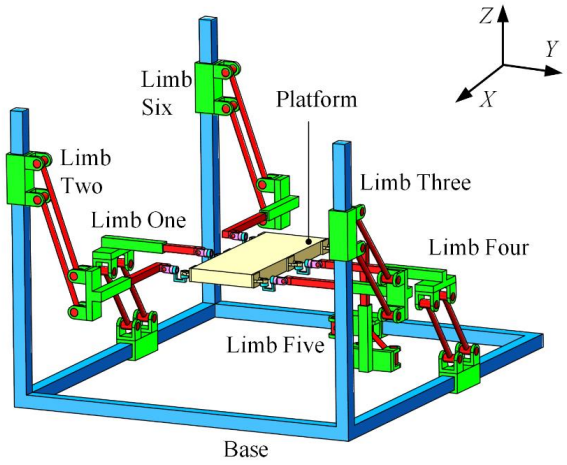

Figure 3-156 Schematic diagram of 6-DOF parallel structure (65)

Feature: There are three P_4 joints (P_X, P_Y, P_Z), three R_6 joints (R_X, R_Y, R_Z), one P_a joint (P_{XY}), two identical P_a joints (P_{YZ}) and three same P_a joints (P_{XZ}). Four P_a joints (P_{XY}, P_{XZ}) are related to P_4 joint (P_X). Three P_a joints (P_{XY}, P_{YZ}) are relevant to P_4 joint (P_Y). Five P_a joints (P_{XZ}, P_{YZ}) are relevant to P_4 joint (P_Z). The translational direction of P_4 joint (P_X) and the rotational axis of R_6 joint (R_X) are parallel (X axis). The translational direction of P_4 joint (P_Y) and the rotational axis of R_6 joint (R_Y) are parallel (Y axis). The translational direction of P_4 joint (P_Z) and the rotational axis of R_6 joint (R_Z) are parallel (Z axis).

$$\left[\begin{array}{ccc:ccc:ccc} P_X & P_{XY} & P_{XZ} & P_X & \_ & P_{XZ} & \_ & \_ & \_ \\ R_Z & P_Y & P_{YZ} & R_Z & P_Y & \_ & R_Z & \_ & \_ \\ R_Y & R_X & P_Z & R_Y & R_X & P_Z & R_Y & R_X & \_ \\ P_X & \_ & P_{XZ} & P_X & \_ & P_{XZ} & \_ & \_ & \_ \\ R_Z & P_Y & \_ & R_Z & P_Y & \_ & R_Z & \_ & \_ \\ R_Y & R_X & P_Z & R_Y & R_X & P_Z & R_Y & R_X & \_ \end{array}\right] \tag{3-296}$$

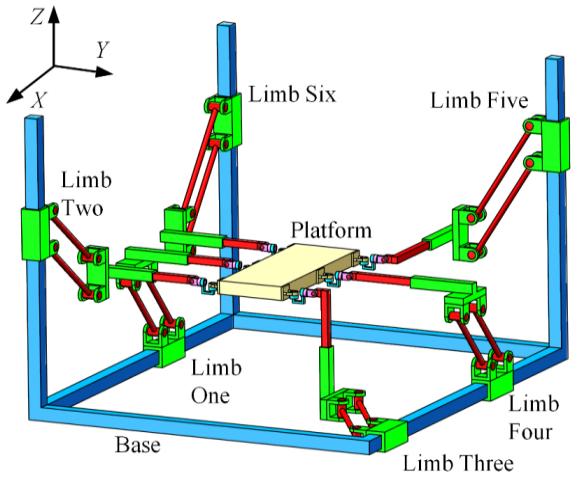

Figure 3-157 Schematic diagram of 6-DOF parallel structure (66)

Feature: There are three P_4 joints (P_X, P_Y, P_Z), three R_6 joints (R_X, R_Y, R_Z), one P_a joint (P_{XY}), one Pa joint (P_{YZ}) and four same P_a joints (P_{XZ}). Five P_a joints (P_{XY}, P_{XZ}) are related to P_4 joint (P_X). Two different P_a joints (P_{XY}, P_{YZ}) are relevant to P_4 joint (P_Y). Five P_a joints (P_{XZ}, P_{YZ}) are relevant to P_4 joint (P_Z). The translational direction of P_4 joint (P_X) and the rotational axis of R_6 joint (R_X) are parallel (*X* axis). The translational direction of P_4 joint (P_Y) and the rotational axis of R_6 joint (R_Y) are parallel (*Y* axis). The translational direction of P_4 joint (P_Z) and the rotational axis of R_6 joint (R_Z) are parallel (*Z* axis).

$$\left[\begin{array}{ccc:ccc:ccc} P_X & P_{XY} & P_{XZ} & P_X & - & - & P_X & - & - \\ R_Z & P_Y & P_{YZ} & R_Z & P_Y & P_{YZ} & R_Z & - & - \\ R_Y & R_X & P_Z & R_Y & R_X & P_Z & R_Y & R_X & - \\ P_X & - & P_{XZ} & P_X & - & - & - & - & - \\ R_Z & P_Y & P_{YZ} & R_Z & P_Y & - & R_Z & - & - \\ R_Y & R_X & P_Z & R_Y & R_X & - & R_Y & R_X & - \end{array}\right] \tag{3-297}$$

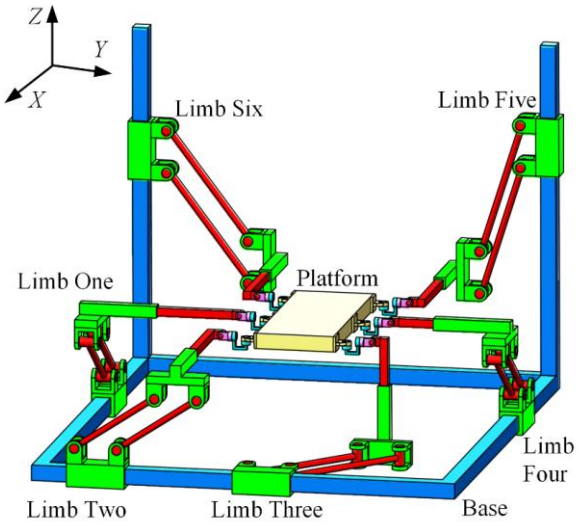

Figure 3-158 Schematic diagram of 6-DOF parallel structure (67)

Feature: There are one P_3 joint (P_Z), one P_4 joint (P_Y), one P_5 joint (P_X), three R_6 joints (R_X, R_Y, R_Z), one P_a joint (P_{XY}), two identical P_a joints (P_{XZ}) and three same P_a joints (P_{YZ}). Five P_a joints (P_{XZ}, P_{YZ}) are relevant to P_3 joint (P_Z). Four P_a joints (P_{XY}, P_{YZ}) are relevant to P_4 joint (P_Y). Three P_a joints (P_{XY}, P_{XZ}) are related to P_5 joint (P_X). The translational direction of P_5 joint (P_X) and the rotational axis of R_6 joint (R_X) are parallel (X axis). The translational direction of P_4 joint (P_Y) and the rotational axis of R_6 joint (R_Y) are parallel (Y axis). The translational direction of P_3 joint (P_Z) and the rotational axis of R_6 joint (R_Z) are parallel (Z axis).

$$\left[\begin{array}{ccc:ccc:ccc} P_X & - & P_{XZ} & P_X & - & P_{XZ} & P_X & - & - \\ R_Z & P_Y & P_{YZ} & R_Z & P_Y & P_{YZ} & R_Z & - & - \\ R_Y & R_X & P_Z & R_Y & R_X & P_Z & R_Y & R_X & - \\ P_X & - & P_{XZ} & P_X & - & - & - & - & - \\ R_Z & P_Y & P_{YZ} & R_Z & P_Y & - & R_Z & - & - \\ R_Y & R_X & P_Z & R_Y & R_X & - & R_Y & R_X & - \end{array}\right] \tag{3-298}$$

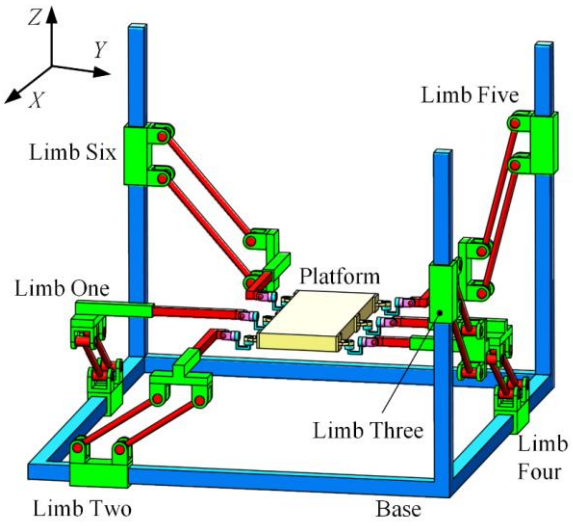

Figure 3-159 Schematic diagram of 6-DOF parallel structure (68)

Feature: There are one P_3 joint (P_Z), one P_4 joint (P_Y), one P_5 joint (P_X), three R_6 joints (R_X, R_Y, R_Z), three identical P_a joints (P_{XZ}) and three same P_a joints (P_{YZ}). Six P_a joints (P_{XZ}, P_{YZ}) are relevant to P_3 joint (P_Z). Three identical P_a joints (P_{YZ}) are relevant to P_4 joint (P_Y). Three identical P_a joints (P_{XZ}) are related to P_5 joint (P_X). The translational direction of P_5 joint (P_X) and the rotational axis of R_6 joint (R_X) are parallel (X axis). The translational direction of P_4 joint (P_Y) and the rotational axis of R_6 joint (R_Y) are parallel (Y axis). The translational direction of P_3 joint (P_Z) and the rotational axis of R_6 joint (R_Z) are parallel (Z axis).

$$\left[\begin{array}{ccc:ccc:ccc} P_X & P_{XY} & P_{XZ} & P_X & - & - & P_X & - & - \\ R_Z & P_Y & P_{YZ} & R_Z & P_Y & - & R_Z & - & - \\ R_Y & R_X & P_Z & R_Y & R_X & P_Z & R_Y & R_X & - \\ P_X & P_{XY} & P_{XZ} & P_X & - & - & - & - & - \\ R_Z & P_Y & P_{YZ} & R_Z & - & - & R_Z & - & - \\ R_Y & R_X & P_Z & R_Y & R_X & P_Z & R_Y & R_X & - \end{array}\right] \tag{3-299}$$

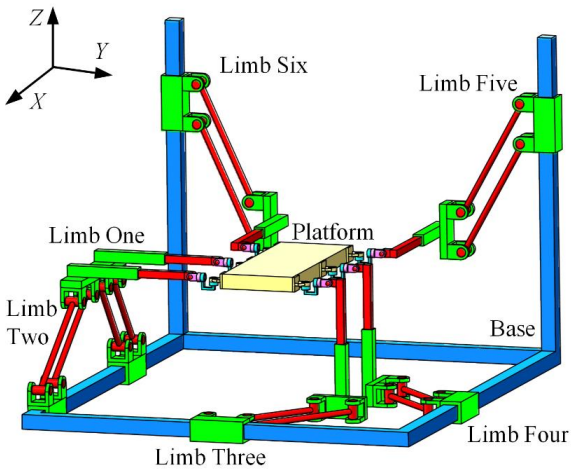

Figure 3-160 Schematic diagram of 6-DOF parallel structure (69)

Feature: There are one P_3 joint (P_Y), one P_4 joint (P_Z), one P_5 joint (P_X), three R_6 joints (R_X, R_Y, R_Z), two identical P_a joints (P_{XY}), two identical P_a joints (P_{XZ}) and two same P_a joints (P_{YZ}). Four P_a joints (P_{XY}, P_{YZ}) are relevant to P_3 joint (P_Y). Four P_a joints (P_{XZ}, P_{YZ}) are relevant to P_4 joint (P_Z). Four P_a joints (P_{XY}, P_{XZ}) are related to P_5 joint (P_X). The translational direction of P_5 joint (P_X) and the rotational axis of R_6 joint (R_X) are parallel (X axis). The translational direction of P_3 joint (P_Y) and the rotational axis of R_6 joint (R_Y) are parallel (Y axis). The translational direction of P_4 joint (P_Z) and the rotational axis of R_6 joint (R_Z) are parallel (Z axis).

$$\left[\begin{array}{ccc:ccc:ccc} P_X & P_{XY} & P_{XZ} & P_X & - & P_{XZ} & P_X & - & - \\ R_Z & P_Y & P_{YZ} & R_Z & P_Y & - & R_Z & - & - \\ R_Y & R_X & P_Z & R_Y & R_X & P_Z & R_Y & R_X & - \\ P_X & - & P_{XZ} & P_X & - & - & - & - & - \\ R_Z & P_Y & P_{YZ} & R_Z & - & - & R_Z & - & - \\ R_Y & R_X & P_Z & R_Y & R_X & P_Z & R_Y & R_X & - \end{array}\right] \tag{3-300}$$

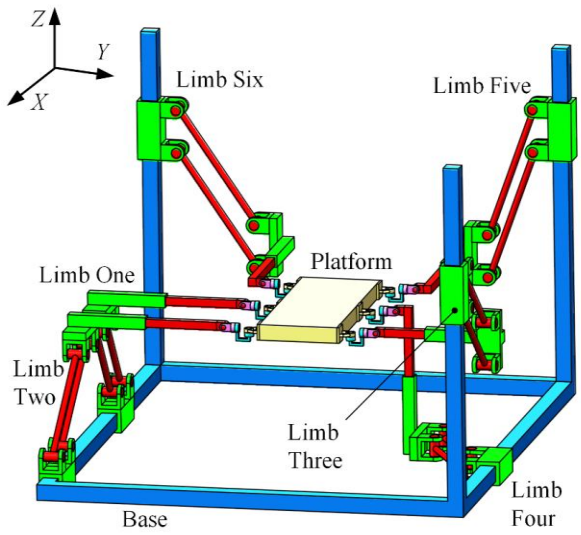

Figure 3-161 Schematic diagram of 6-DOF parallel structure (70)

Feature: There are one P_3 joint (P_Y), one P_4 joint (P_Z), one P_5 joint (P_X), three R_6 joints (R_X, R_Y, R_Z), one P_a joint (P_{XY}), two identical P_a joints (P_{YZ}) and three same P_a joints (P_{XZ}). Three P_a joints (P_{XY}, P_{YZ}) are relevant to P_3 joint (P_Y). Five P_a joints (P_{XZ}, P_{YZ}) are relevant to P_4 joint (P_Z). Four P_a joints (P_{XY}, P_{XZ}) are related to P_5 joint (P_X). The translational direction of P_5 joint (P_X) and the rotational axis of R_6 joint (R_X) are parallel (*X* axis). The translational direction of P_3 joint (P_Y) and the rotational axis of R_6 joint (R_Y) are parallel (*Y* axis). The translational direction of P_4 joint (P_Z) and the rotational axis of R_6 joint (R_Z) are parallel (*Z* axis).

$$\left[\begin{array}{ccc:ccc:ccc} P_X & - & P_{XZ} & P_X & - & P_{XZ} & - & - & - \\ R_Z & P_Y & P_{YZ} & R_Z & P_Y & - & R_Z & P_Y & - \\ R_Y & R_X & P_Z & R_Y & R_X & P_Z & R_Y & R_X & - \\ P_X & - & P_{XZ} & P_X & - & P_{XZ} & - & - & - \\ R_Z & P_Y & P_{YZ} & R_Z & P_Y & - & R_Z & - & - \\ R_Y & R_X & P_Z & R_Y & R_X & - & R_Y & R_X & - \end{array}\right] \tag{3-301}$$

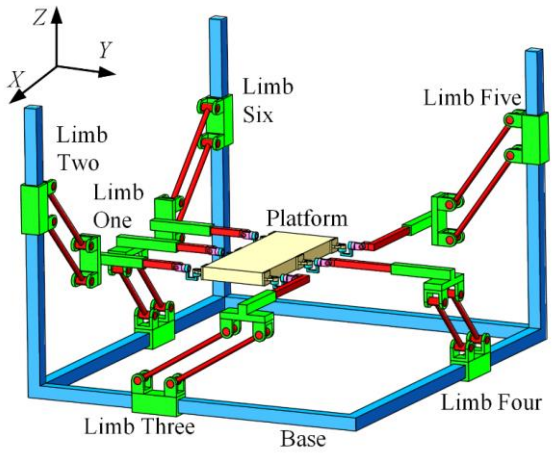

Figure 3-162 Schematic diagram of 6-DOF parallel structure (71)

Feature: There are one P_3 joint (P_Z), one P_4 joint (P_X), one P_5 joint (P_5), three R_6 joints (R_X, R_Y, R_Z), two identical P_a joints (P_{YZ}) and four same P_a joints (P_{XZ}). Six P_a joints (P_{XZ}, P_{YZ}) are relevant to P_3 joint (P_Z). Four identical P_a joints (P_{XZ}) are related to P_4 joint (P_X). Two same P_a joints (P_{YZ}) are relevant to P_5 joint (P_Y). The translational direction of P_4 joint (P_X) and the rotational axis of R_6 joint (R_X) are parallel (*X* axis). The translational direction of P_5 joint (P_Y) and the rotational axis of R_6 joint (R_Y) are parallel (*Y* axis). The translational direction of P_3 joint (P_Z) and the rotational axis of R_6 joint (R_Z) are parallel (*Z* axis).

$$\left[\begin{array}{ccc:ccc:ccc} P_X & P_{XY} & P_{XZ} & P_X & - & P_{XZ} & - & - & - \\ R_Z & P_Y & P_{YZ} & R_Z & P_Y & - & R_Z & P_Y & - \\ R_Y & R_X & P_Z & R_Y & R_X & P_Z & R_Y & R_X & - \\ P_X & - & P_{XZ} & - & - & P_{XZ} & - & - & - \\ R_Z & P_Y & - & R_Z & P_Y & - & R_Z & P_Y & - \\ R_Y & R_X & P_Z & R_Y & R_X & - & R_Y & R_X & - \end{array}\right] \tag{3-302}$$

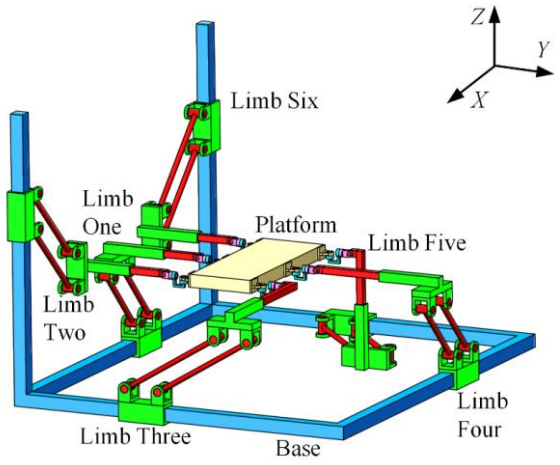

Figure 3-163 Schematic diagram of 6-DOF parallel structure (72)

Feature: There are one P_3 joint (P_X), one P_3 joint (P_Z), one P_6 joint (P_Y), three R_6 joints (R_X, R_Y, R_Z), one P_a joint (P_{XY}), one P_a joint (P_{YZ}) and four same P_a joints (P_{XZ}). Five P_a joints (P_{XY}, P_{XZ}) are related to P_3 joint (P_X). Five P_a joints (P_{XZ}, P_{YZ}) are relevant to P_3 joint (P_Z). Two different P_a joints (P_{XY}, P_{YZ}) are relevant to P_6 joint (P_Y). The translational direction of P_3 joint (P_X) and the rotational axis of R_6 joint (R_X) are parallel (X axis). The translational direction of P_6 joint (P_Y) and the rotational axis of R_6 joint (R_Y) are parallel (Y axis). The translational direction of P_3 joint (P_Z) and the rotational axis of R_6 joint (R_Z) are parallel (Z axis).

$$\left[\begin{array}{ccc:ccc:ccc} P_X & P_{XY} & P_{XZ} & P_X & - & P_{XZ} & - & - & - \\ R_Z & P_Y & - & R_Z & P_Y & - & R_Z & P_Y & - \\ R_Y & R_X & P_Z & R_Y & R_X & P_Z & R_Y & R_X & - \\ P_X & P_{XY} & P_{XZ} & P_X & - & P_{XZ} & - & - & - \\ R_Z & P_Y & - & R_Z & P_Y & - & R_Z & - & - \\ R_Y & R_X & P_Z & R_Y & R_X & - & R_Y & R_X & - \end{array}\right] \tag{3-303}$$

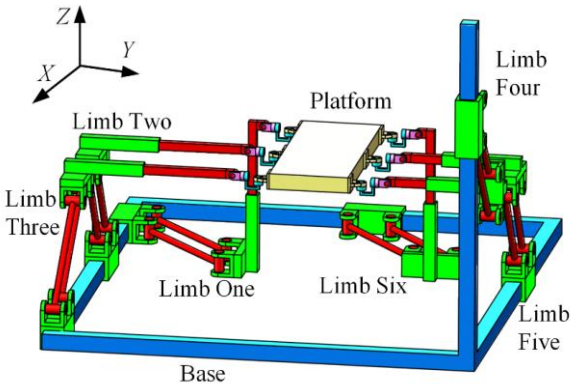

Figure 3-164 Schematic diagram of 6-DOF parallel structure (73)

Feature: There are one P_3 joint (P_Z), one P_4 joint (P_X), one P_5 joint (P_Y), three R_6 joints (R_X, R_Y, R_Z), two same P_a joints (P_{XY}) and four same P_a joints (P_{XZ}). Four identical P_a joints (P_{XZ}) are related to P_3 joint (P_Z). Six P_a joints (P_{XY}, P_{XZ}) are relevant to P_4 joint (P_X). Two identical P_a joints (P_{XY}) are relevant to P_5 joint (P_Y). The translational direction of P_4 joint (P_X) and the rotational axis of R_6 joint (R_X) are parallel (X axis). The translational direction of P_5 joint (P_Y) and the rotational axis of R_6 joint (R_Y) are parallel (Y axis). The translational direction of P_3 joint (P_Z) and the rotational axis of R_6 joint (R_Z) are parallel (Z axis).

3.4 Summary

A special term is added to the modified G-K equation, to be suitable for a group of parallel mechanisms with P, R and parallelogram joints. A novel methodology called the kinematic joint matrix is proposed. It possesses the mapping relations with parallel manipulators with three kinds of kinematic joints. A unique pattern is design to distinguish various kinematic joint matrices. A series of 2-6 DOFs parallel architectures is denoted by the kinematic joint matrix and the unreliable parallel structures are clarified by the screw theory.

Chapter 4 Performance analysis of parallel mechanisms

4.1 Performance index: Level index

There are various kinds of kinematic and dynamic indices to measure the performance of parallel manipulators. They are generally no less than 0 in the whole workspace of the parallel structure. In this section, the novel level index is proposed to evaluate the performance rank of any position/orientation in the overall performances in workspace, and to normalize various performance indices with positive values. The level index can be computed as

$$\text{Level Index} = \frac{\mu(\text{pose})}{\bar{\mu} + \mu(\text{pose})} \tag{4-1}$$

where $\mu(\text{pose})$ is the performance of any pose of the moving platform and $\bar{\mu}$ represents the mean value of this kind of performance in workspace.

There are three main advantages of this novel index.

(i) Based on the definition, the level index ranges from 0 to 1 and it is a monotonically increasing function with respect to $\mu(\text{pose})$. In another word, if one performance index is chosen, the mean level index is a constant, the pose with higher performance will own larger level index. The level index can maintain the feature of the original index.

A proof is provided. There are two positions for point *a* and point *b*. Their corresponding level indices of one specific indicator are $\text{LI(a)} = \mu(a)/[\bar{\mu} + \mu(a)]$ (LI is short for level index) and $\text{LI(b)} = \mu(b)/[\bar{\mu} + \mu(b)]$, respectively. The parameters $\mu(a)$, $\mu(b)$, $\bar{\mu}$, LI(a) and LI(b) are all positive values. Hence, the following expression can be generated

$$\begin{aligned} \text{LI(b)} - \text{LI(a)} &= \frac{\mu(b)}{\bar{\mu} + \mu(b)} - \frac{\mu(a)}{\bar{\mu} + \mu(a)} \\ &= \frac{\mu(b)[\bar{\mu} + \mu(a)] - \mu(a)[\bar{\mu} + \mu(b)]}{[\bar{\mu} + \mu(a)][\bar{\mu} + \mu(b)]} \\ &= \frac{\bar{\mu}[\mu(b) - \mu(a)]}{[\bar{\mu} + \mu(a)][\bar{\mu} + \mu(b)]} \end{aligned} \tag{4-2}$$

Equation (4-2) have the identical positive or negative symbol with $\mu(b) - \mu(a)$. Therefore, the level index can remain the original index distributions.

(ii) The usage of the level index can also assist to shrink/normalize the range of the performance index. For example, the local condition index (LCI) of a parallel mechanism

generally ranges from 1 to $+\infty$. The corresponding level index will be limited between 0 to 1. This process will make it easier to be depicted in figures, as the long axis for the performance index will be replaced.

(iii) The level index provides the performance rating in one parallel mechanism. When comparing two poses from two parallel mechanisms, the same kind of performances of these two poses are not sufficient. Their ratings in the corresponding manipulators are unknown. It is assumed that there are two parallel manipulators with provided LCI information. In the first parallel manipulator, the mean LCI is 4 and the LCI of point D_1 is 5. In the second parallel mechanism, the mean LCI is 10 while the LCI of point D_2 is 6. In one hand, the point D_1 has better LCI than that of point D_2. In another hand, the LCI of the point D_1 is larger than the mean value of the first mechanism. The LCI of the point D_2 is smaller than the mean value of the second mechanism. Considering this aspect, the point D_1 is worse than the point D_2. This conclusion can be verified by the local condition level index, which can be deduced through Equation (4-1). The local level condition indices of these two points are 5/9 and 3/8 respectively, which indicate their ranks in the corresponding mechanisms.

The local condition index of the mechanism is employed to examine this concept. Based on the definition in Equation (4-1), the local level condition index (LLCI) is formulated as follows

$$LLCI = \frac{LCI}{\overline{LCI} + LCI} \tag{4-3}$$

where $\overline{LCI}$ represents the mean value of local condition index (global condition index).

Since some parallel manipulators have mixed (translation and rotation) movements, it is better to compute this index separately to avoid the non-homogeneous unit[160]. In accordance with the definition in Equation (4-3), the local translational condition index (LTCI) and the local rotational condition index (LRCI) are generated respectively as

$$\begin{cases} \text{LTCI} = LCI(\boldsymbol{J}_V) = \left\|\boldsymbol{J}_V\right\|_f \left\|\boldsymbol{J}_V^{-1}\right\|_f \\ \text{LRCI} = LCI(\boldsymbol{J}_W) = \left\|\boldsymbol{J}_W\right\|_f \left\|\boldsymbol{J}_W^{-1}\right\|_f \end{cases} \tag{4-4}$$

where $\boldsymbol{J}_V$ and $\boldsymbol{J}_W$ own respectively the first i column(s) (i indicates the translational DOF(s) of the mobile platform) and the remaining column(s) of the whole Jacobian matrix $\boldsymbol{J}$.

Therefore, the LTCI and LRCI can be applied in Equation (4-1) to compute the corresponding local translational level condition index (LTLCI) and local rotational level condition index (LRLCI), respectively.

Several parallel structures should be chosen from Section 3.3 to verify the novel level index concept. Since there are planar and spatial DOFs, translational and mixed-motion (both translation(s) and rotation(s)), fully coupled or partial decoupled movements in this class of parallel architectures, four different structures are selected to represent the general cases, 2T (figure 3-5), 2T1R (figure 3-22), 3T (figure 3-14) and 3T1R (figure 3-33) mechanisms. Their characteristics are listed in Table. 4-1.

Table 4-1 The comparisons among four selected parallel structures

	Planar or spatial motion	Translational or mixed motion	(De)coupled
2T	Planar	Translational	Coupled
2T1R	Planar	Mixed	Coupled
3T	Spatial	Translational	Partial decoupled
3T1R	Spatial	Mixed	Partial decoupled

4.2 Case one: 2T parallel mechanism

The parallel manipulator illustrated in figure 4-1 is consisted of two identical branches. Each branch contains an active prismatic joint connected to the fixed platform and a parallelogram module (4R links) attached to the moving platform. The global coordinate system attached to the base is also established. The driving joints of two branches are along X axis. The revolute joints axes of two parallelogram modules are parallel to Z axis.

The midpoints of linkages $A_{11}A_{13}$, $A_{12}A_{14}$, $B_{11}B_{13}$ and $B_{12}B_{14}$ are denoted as A_{15}, A_{16}, B_{15} and B_{16}, respectively. The maximal range of the two sliding joints are defined as L_{11}. The lengths of linkage $A_{11}A_{12}$ or ($A_{13}A_{14}$) and $A_{11}A_{13}$ or ($A_{12}A_{14}$) are respectively L_{12} and $2L_{13}$.The linkage lengths of $B_{11}B_{12}$ or ($B_{13}B_{14}$) and $B_{11}B_{13}$ or ($B_{12}B_{14}$) are respectively L_{14} and $2L_{15}$. The distance between point A_{14} (or B_{12}) and point P_1 is represented as L_{16}. θ_{11} and θ_{12} present the inclined angles for linkages $A_{13}A_{14}$ and $B_{13}B_{14}$.

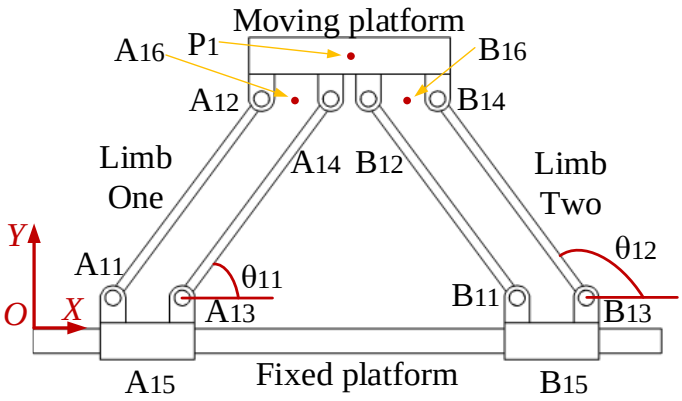

Figure 4-1 Schematic diagram of the 2T parallel mechanism

(i) Kinematic models

Two actuation displacements are defined as $\boldsymbol{Q}_1=[x_{A15},y_{B15}]^{\mathrm{T}}$. The mobile platform position is denoted as $\boldsymbol{X}_1=[x_{P1},y_{P1}]^{\mathrm{T}}$. The positions of some points are obtained in the given coordinate system. $P_{A15}(x_{A15},0)$, $P_{A16}(x_{P1}-L_{13}-L_{16},y_{P1})$, $P_{B15}(x_{B15},0)$, $P_{B16}(x_{P1}+L_{13}+L_{16},y_{P1})$.

To resolve the inverse kinematic model, the vector-loop equation of the first branch can be described as

$$\boldsymbol{OA}_{15}+\boldsymbol{A}_{15}\boldsymbol{A}_{16}+\boldsymbol{A}_{16}\boldsymbol{P}_1=\boldsymbol{OP}_1 \tag{4-5}$$

Equation (4-5) can be further explained in two orthogonal axes, as listed below

$$\begin{cases} x_{A15}+L_{12}\cos\theta_{11}+L_{13}+L_{16}=x_{P1} \\ L_{12}\sin\theta_{11}=y_{P1} \end{cases} \tag{4-6}$$

Then the inclined angle θ_{11} and the position of the first actuator can be solved as

$$\begin{cases} \theta_{11}=\arcsin(y_{P1}/L_{12}) \\ x_{A15}=x_{P1}-L_{13}-L_{16}-L_{12}\cos\theta_{11} \end{cases} \tag{4-7}$$

In a similar way, the vector-loop equation of the second limb can be expressed as

$$\boldsymbol{OB}_{15}+\boldsymbol{B}_{15}\boldsymbol{B}_{16}+\boldsymbol{B}_{16}\boldsymbol{P}_1=\boldsymbol{OP}_1 \tag{4-8}$$

Equation (4-8) can be split into *X* and *Y* axes, as

$$\begin{cases} x_{B15}+L_{14}\cos\theta_{12}-L_{15}-L_{16}=x_{P1} \\ L_{14}\sin\theta_{12}=y_{P1} \end{cases} \tag{4-9}$$

The inclined angle θ_{12} and the second prismatic joint position can be obtained

$$\begin{cases} \theta_{12} = \arcsin(y_{P1} / L_{14}) \\ x_{B15} = x_{P1} + L_{15} + L_{16} - L_{14}\cos\theta_{12} \end{cases} \tag{4-10}$$

The forward kinematic model can be computed based on Equations (4-6) and (4-9). The unknown inclined angles of these two equations are moved at one side of equations, then they can be rearranged as

$$\Gamma_{11} : \left(x_{P1} - x_{A15} - L_{13} - L_{16}\right)^2 + y_{P1}^2 - L_{12}^2 = 0 \tag{4-11}$$

$$\Gamma_{12} : \left(x_{P1} - x_{B15} + L_{15} + L_{16}\right)^2 + y_{P1}^2 - L_{14}^2 = 0 \tag{4-12}$$

Equation (4-11) minuses Equation (4-12) leading to

$$L_{12}^2 - L_{14}^2 = \left(x_{P1} - x_{A15} - L_{13} - L_{16}\right)^2 - \left(x_{P1} - x_{B15} + L_{15} + L_{16}\right)^2 \tag{4-13}$$

In accordance with Equation (4-13), the X component of the point P_1 in the mobile platform can be found

$$x_{P1} = \frac{\left(x_{A15} + L_{13} + L_{16}\right)^2 - \left(L_{15} + L_{16} - x_{B15}\right)^2 + L_{14}^2 - L_{12}^2}{2\left(x_{A15} - x_{B15} + L_{13} + L_{15} + 2L_{16}\right)} \tag{4-14}$$

Combining Equations (4-11) and (4-14) yields

$$y_{P1} = \pm\sqrt{L_{12}^2 - \left(x_{P1} - x_{A15} - L_{13} - L_{16}\right)^2} \tag{4-15}$$

Equations (4-14) and (4-15) are the corresponding forward kinematic solutions with a given positions of two driving prismatic joints.

(ii) Singularity configurations

Differentiating both sides of the constraint equations (4-11) and (4-12) with respect to time, the velocity relation between two actuators and the mobile platform is obtained

$$\boldsymbol{J}_{Q1}[\dot{x}_{A15}, \dot{y}_{B15}]^{\mathrm{T}} = \boldsymbol{J}_{X1}[\dot{x}_{P1}, \dot{y}_{P1}]^{\mathrm{T}} \tag{4-16}$$

where

$$\boldsymbol{J}_{Q1} = \begin{bmatrix} -\left(x_{P1} - x_{A15} - L_{13} - L_{16}\right) & 0 \\ 0 & -\left(x_{P1} - x_{B15} + L_{15} + L_{16}\right) \end{bmatrix}$$

$$\boldsymbol{J}_{X1} = \begin{bmatrix} x_{P1} - x_{A15} - L_{13} - L_{16} & y_{P1} \\ x_{P1} - x_{B15} + L_{15} + L_{16} & y_{P1} \end{bmatrix}$$

The Jacobian matrix of this parallel structure is then expressed as

$$\boldsymbol{J}_1 = \boldsymbol{J}_{Q1}^{-1}\boldsymbol{J}_{X1} \tag{4-17}$$

There are generally three kinds of singularity configurations [26] based on Equation (4-16). Type-I singularity happens when $Det(\boldsymbol{J}_{Q1})=0$. The first case is $x_{P1}=x_{A15}+L_{13}+L_{16}$ in the condition of $L_{12}\le L_{14}$. In this situation shown in figure 4-2(a), θ_{11} is $\pi/2$ rad and. The second case is similar with the first case. In this case illustrated in figure 4-2(b), $x_{P1}=x_{B15}-L_{15}-L_{16}$ in the condition of $L_{12}\ge L_{14}$. θ_{12} is $\pi/2$ rad. In both cases, the mobile platform can resist external force that is parallel to *Y* axis without actuation force.

Type-II singularity occurs when $Det(\boldsymbol{J}_{X1})=0$. The result is $y_{P1}=0$. The first case is $\sin\theta_{11}=\sin\theta_{12}=0\&L_{12}\neq 0\&L_{14}\neq 0$. The whole mechanism is trapped in the *X* axis and the mobile platform loses the translation along *Y* axis, as shown in figure 4-2(c-e). Another possible situation is $L_{12}=0$ or $L_{14}=0$. The moving platform loses the translational mobility along *Y* axis and only has one DOF, as presented in figure 4-2(f-h).

The combined singularity happens when both type-I and type-II scenarios happen. This case does not exist in according to its definition $Det(\boldsymbol{J}_{Q1})=0$ and $Det(\boldsymbol{J}_{X1})=0$. However, this case happens when $L_{12}=0$ or $L_{14}=0$, in according to the analysis of type-II singularities.

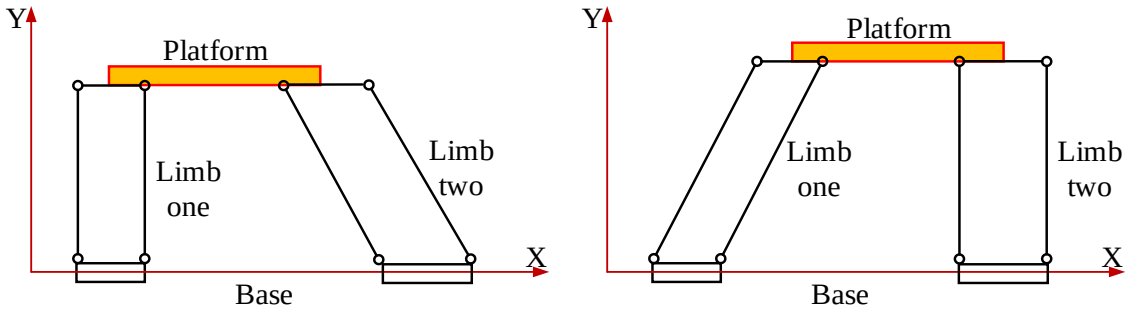

(a) $\theta_{11}=\pi/2$ (b) $\theta_{12}=\pi/2$

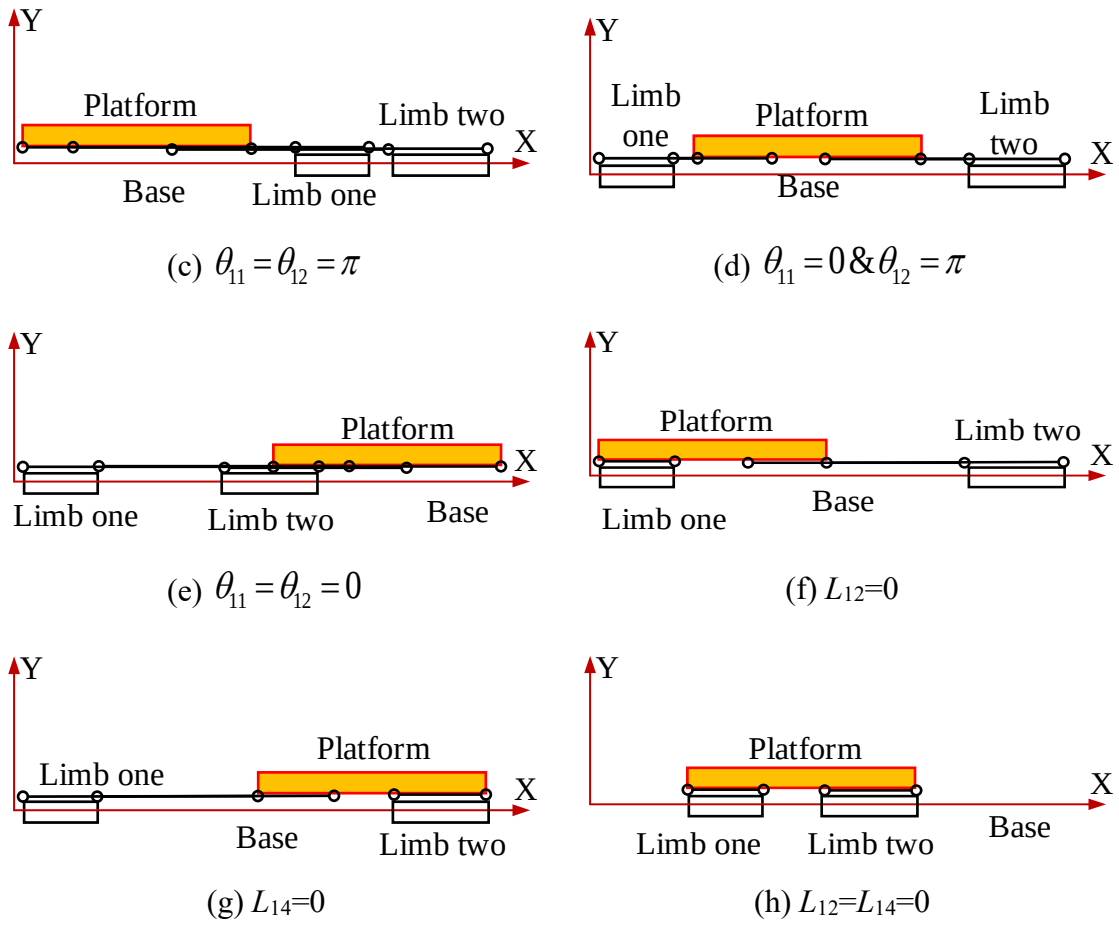

Figure 4-2 Singularity configurations of 2T parallel mechanism

(iii) Workspace analysis

The physically constraints of all kinematic joints should be considered in order to calculate workspace of the mobile platform. The strokes for two active prismatic joints are constrained as $L_{13} \le x_{A15} \le L_{11} - 4L_{13}$ and $4L_{13} \le x_{B15} \le L_{11} - L_{13}$. Revolute joint generally has a large rotational range. However, they are shrunk when considering singularity avoidance and real assembly condition. $\pi/36 \le \theta_{11} \le 17\pi/36$ and $19\pi/36 \le \theta_{11} \le 35\pi/36$. To avoid singularity configurations discussed above, the position of the mobile platform is given as $x_{A15} < x_{P1} < x_{B15}$. The spatial searching algorithm is applied to determine its

workspace. Given any possible point, the inverse kinematic solution is employed and it can be regarded feasible if all these above requirements can be satisfied.

These parameters are given as: L_{11}=100mm, L_{12}=30mm, L_{13}= 5mm, L_{16}=5mm. The symmetric features are selected for the workspace analysis and the following calculations. L_{13}=L_{15}, L_{12}=L_{14}.The reachable workspace is illustrated as red dot in figure 4-3. The reachable workspace is symmetric image about X=50mm. The workspace region keeps increasing as the height (along Y axis) of the mobile platform rises. However, the reachable workspace with irregular shape does not fit for real applications. The task workspace is defined as a rectangle within the reachable workspace as denoted in figure 4-3.

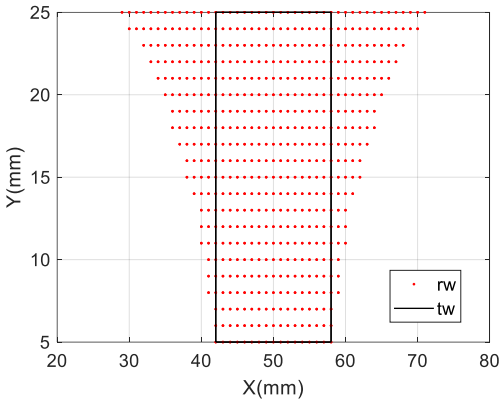

Figure 4-3 Reachable and task workspaces of 2T parallel mechanism
(rw-reachable workspace, tw-task workspace)

To understand the parametric effects on both the reachable workspace and operational workspace, a set of values for each parameter are selected to evaluate and compare their corresponding regions. The sum of qualified discrete poses is used for the reachable workspace since it is not a regular shape. The rectangle area is employed for the operation workspace. These effects are illustrated in figure 4-4. From figure 4-4(a), the reachable workspace gets larger as L_{11} increases. The task workspace decreases at first and then increases when L_{11} changes from 75mm to 125mm. From figure 4-4(b), the reachable workspace shrinks when L_{12} increases. The task workspace gets smaller when L_{12} increases from 30mm to 38mm and keeps zero when L_{12} increases until 50mm. Figure 4-4(c) illustrates that both workspaces decrease when L_{13} changes from 3mm to 10mm. The task

workspace does not exist when L_{13} equals to 10mm. Figure 4-4(d) demonstrates that both workspaces shrink as L_{13} gets larger.

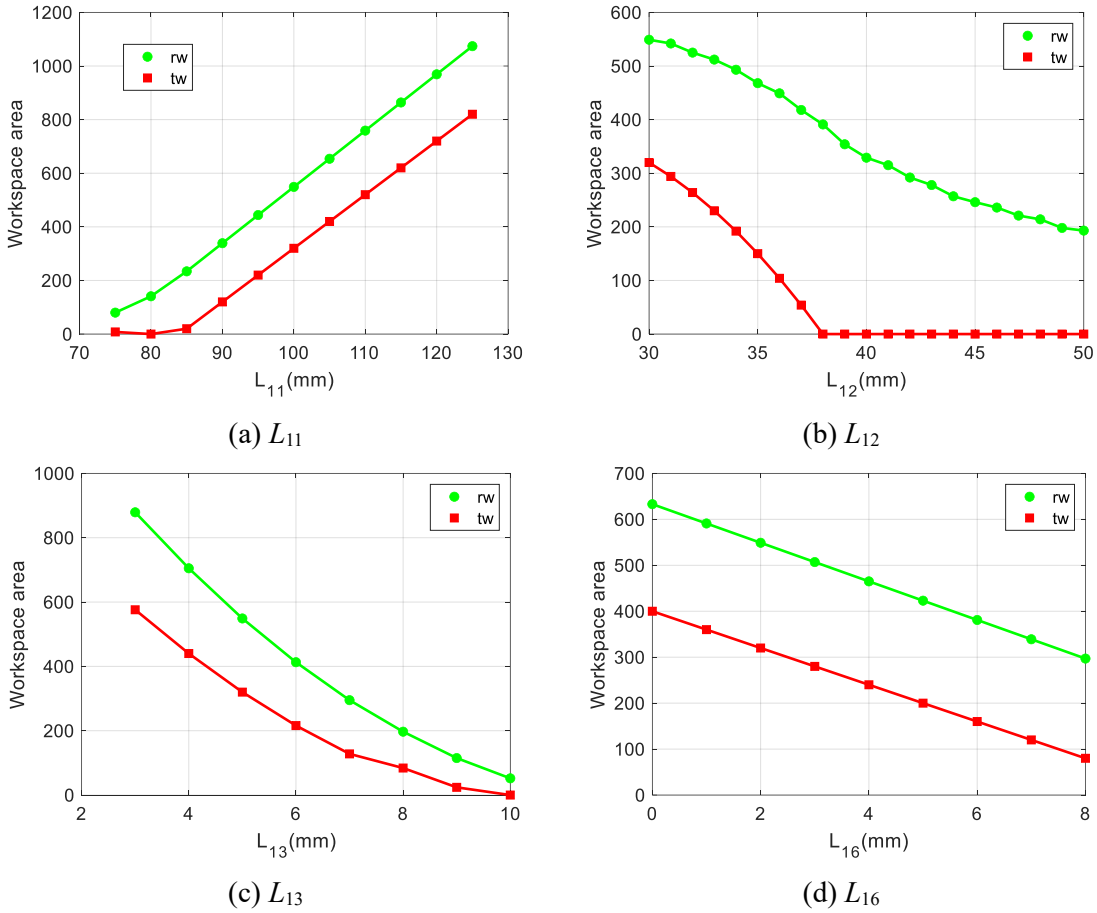

(a) L_{11} (b) L_{12}

(c) L_{13} (d) L_{16}

Figure 4-4 Parametric analysis of the reachable and task workspaces

(iv) Dexterity analysis and level index

For this parallel mechanism, its dexterity is studied to understand the transmission relationship's capability between two linear inputs and two translational outputs. The most commonly used indices are manipulability and condition number, and the latter one is applied here. Its local condition index (*LCI*) is calculated as the Frobenius norm of its Jacobian matrix, as provided below

$$
\begin{aligned}
LCI &= \sqrt{\frac{y_{P1}^2}{\left(x_{P1}-x_{A15}-L_{13}-L_{16}\right)^2}+\frac{y_{P1}^2}{\left(x_{P1}-x_{B15}+L_{15}+L_{16}\right)^2}+2} \\
&= \sqrt{\frac{y_{P1}^2}{L_{12}^2-y_{P1}^2}+\frac{y_{P1}^2}{L_{12}^2-y_{P1}^2}+2} \\
&= \sqrt{\frac{2L_{12}^2}{L_{12}^2-y_{P1}^2}}
\end{aligned}
\tag{4-18}
$$

Equation (4-18) indicates *LCI* is constantly greater than $\sqrt{2}$ for this mechanism. Its transmission performance is better when *LCI* is closer to $\sqrt{2}$. It can be concluded from Equation (4-18) that *LCI* is only related to L_{12} and y_{P1}. The impacts originated from these two parameters are depicted in figure 4-5.

In figure 4-5(a), L_{12} is a constant value of 30mm. It can be seen from figure 4-5(a) that *LCI* gets larger as y_{P1} increases with the smallest and largest *LCI* are 1.4343 and 2.5584, respectively. In figure 4-5(b), y_{P1} remain 15mm. Figure 4-5(b) indicates *LCI* gets smaller when L_{12} becomes longer. The velocity transmission capacity is getting better in this process. Figure 4-5(c) is required to show the overall impacts from both variables. Figure 4-5(c) presents the best LCI is located with the largest y_{P1} and the shortest L_{12}, while the worst performance can be obtained when y_{P1} is in the lowest position and L_{12} is selected as the longest length.

It is noteworthy that the linkage length's impacts on the global condition index is not provided. The most important reason is that various dimensions of one linkage may cause different areas/volumes of the whole reachable workspace. Therefore, the impacts on a global index are consisted of the effects on the workspace and this index. It is difficult to explore the linkage's direct impact on this global index. Hence, the linkages' impacts on global indices are not discussed in this research.

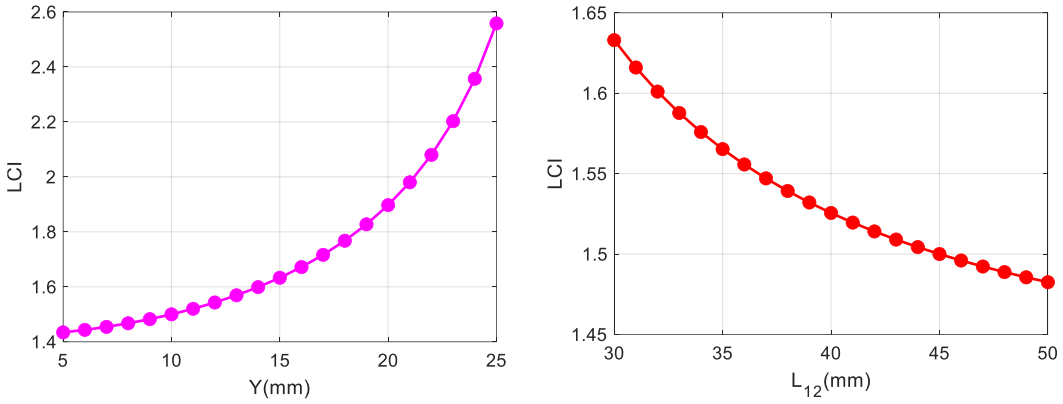

(a) y_{P1} (b) L_{12}

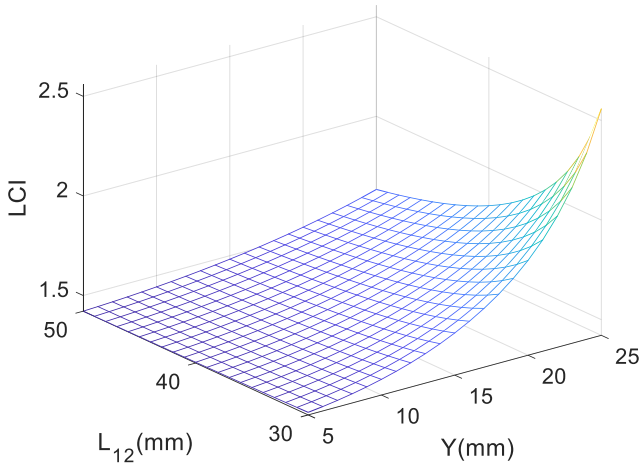

(c) y_{P1} and L_{12}

Figure 4-5 Distributions of the LCI

The corresponding distribution for LLCI is calculated from Equation (4-3) and is depicted in figure 4-6. Its trend is exactly the same as that in figure 4-5(a). The scale of LLCI is narrowed. In the whole workspace, the LLCI ranges from 0.4379 to 0.5816 and the mean value is 0.4834. The impact from L_{12} is ignored since the variance of L_{12} will lead to the changes of $\overline{LCI}$.

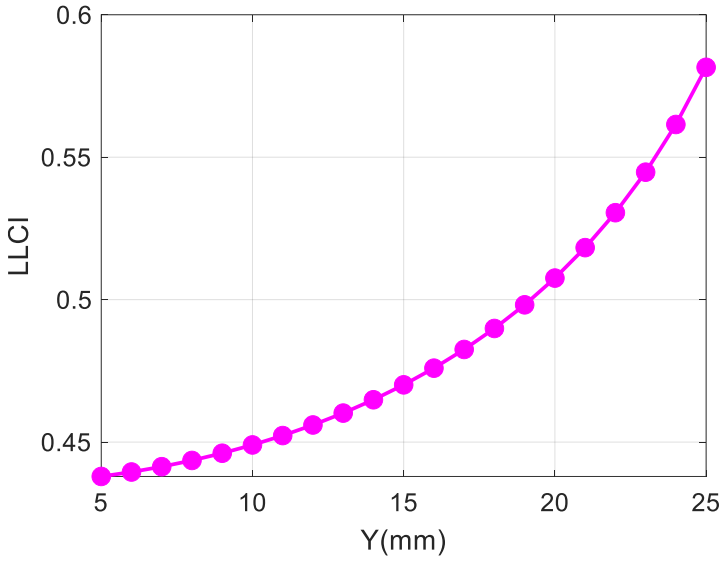

Figure 4-6 Layout of the local level condition index

4.3 Case two: 2T1R parallel mechanism

This planar parallel mechanism is depicted seen in figure 4-7. The coordinate system is located at the bottom left corner. Based on the right-hand rule, *Z*-axis is perpendicular to the *XOY* plane and points outward. This parallel robot includes one fixed platform and a mobile platform connected by three independent kinematic chains. Each chain is constituted of one active prismatic joint, one parallelogram joint ((R-R)$_2$ linkage) and a revolute joint. All the sliding joints moves along *X*-direction. The parallelogram joints are placed in the *XOY* plane. In each kinematic branch, one side of the parallelogram joint is installed on the driving sliding joint and another side is attached to the moving platform with a rotary joint. The axes of three rotational joints connected to the mobile platform are all parallel to *Z*-axis. This planar parallel architecture can achieve two translations along *X*-axis and *Y*-axis, one rotational movement about Z-axis.

The points A_{25}, B_{25}, C_{25} are the midpoints of $A_{21}A_{23}$, $B_{21}B_{23}$ and $C_{21}C_{23}$, respectively. The points A_{26}, B_{26}, C_{26} are the midpoints of $A_{22}A_{24}$, $B_{22}B_{24}$ and $C_{22}C_{24}$, respectively. The distance along *Y* direction between the active sliders $A_{21}A_{23}$ and $C_{21}C_{23}$ is defined as L_{21}.

$|A_{21}A_{22}|=|A_{23}A_{24}|=L_{22}$. $|A_{21}A_{23}|=|A_{22}A_{24}|=2L_{23}$. $|B_{21}B_{22}|=|B_{23}B_{24}|=L_{24}$.

$|B_{21}B_{23}|=|B_{22}B_{24}|=2L_{25}$. $|C_{21}C_{22}|=|C_{23}C_{24}|=L_{26}$. $|C_{21}C_{23}|=|C_{22}C_{24}|=2L_{27}$. $|A_{26}A_{27}|=L_{28}$.

$|B_{26}B_{27}|=L_{29}$. $|C_{26}C_{27}|=L_{210}$. The mobile platform $A_{27}B_{27}C_{27}$ forms a virtual equilateral triangle with the edge is L_{211} and the center is point P_2. According to the feature of this

triangle, $|A_{27}P_2|=|B_{27}P_2|=|C_{27}P_2|=\sqrt{3}L_{211}/3$. The sliding stroke along X direction for all actuators is set as L_{212}. The sloping angles between positive X-axis and the linkages $A_{23}A_{24}$, $B_{23}B_{24}$ and $C_{23}C_{24}$ are respectively represented as θ_{21}, θ_{22} and θ_{23}. The angle between the virtual edge $A_{27}B_{27}$ and the positive X-axis is φ_{21}.

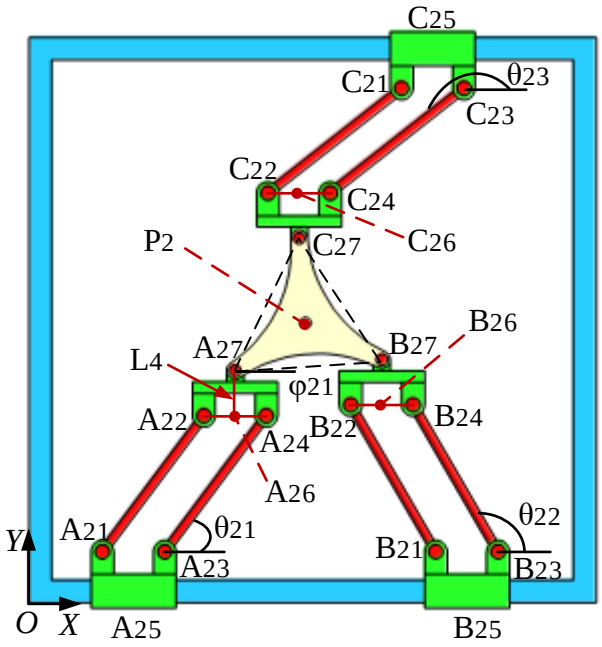

Figure 4-7 Schematic diagram of this planar 2T1R robot

(i) Kinematic models

The positions along X direction of the active sliding joint A_{25}, B_{25} and C_{25} are x_{A25}, x_{B25} and x_{C25}, separately. The system input of this parallel manipulator is defined as $\boldsymbol{Q}_2=[x_{A25},x_{B25},x_{C25}]^{\mathrm{T}}$. The position of point P_2 in the provided coordinate system is (x_{P2}, y_{P2}). Thereafter, the pose of the mobile platform is given as $\boldsymbol{X}_2=[x_{P2},y_{P2},\varphi_{21}]^{\mathrm{T}}$. The inverse kinematic problem can be computed with the given $\boldsymbol{X}_2$. For the first kinematic chain, the vector-loop equation is obtained as

$$\boldsymbol{OA}_{25}+\boldsymbol{A}_{25}\boldsymbol{A}_{26}+\boldsymbol{A}_{26}\boldsymbol{A}_{27}+\boldsymbol{A}_{27}\boldsymbol{P}_2=\boldsymbol{OP}_2 \tag{4-19}$$

Equation (4-19) can be expressed along two orthogonal directions

$$\begin{cases} x_{A25}+L_{22}\cos\theta_{21}+\sqrt{3}L_{211}/3\cos(\varphi_{21}+\pi/6)=x_{P2} \\ L_{22}\sin\theta_{21}+L_{28}+\sqrt{3}L_{211}/3\sin(\varphi_{21}+\pi/6)=y_{P2} \end{cases} \tag{4-20}$$

From Equation (4-20), the unknown parameter θ_{21} should be placed at one side while the others are in other side, to eliminate θ_{21}. Hence, Equation (4-20) is rephrased as

$$\begin{cases} L_{22}\cos\theta_{21} = x_{P2} - \sqrt{3}L_{211}/3\cos(\varphi_{21}+\pi/6) - x_{A25} \\ L_{22}\sin\theta_{21} = y_{P2} - \sqrt{3}L_{211}/3\sin(\varphi_{21}+\pi/6) - L_{28} \end{cases} \tag{4-21}$$

Adding the squares of both equations in Equation (4-21) leads to

$$\Gamma_{21}:\left[x_{P2} - \sqrt{3}L_{211}/3\cos(\varphi_{21}+\pi/6) - x_1\right]^2 + \left[y_{P2} - \sqrt{3}L_{211}/3\sin(\varphi_{21}+\pi/6) - L_{28}\right]^2 - L_{22}^2 = 0 \tag{4-22}$$

The position of the active prismatic joint A_{25} is then solved as

$$x_{A25} = \left[x_{P2} - \sqrt{3}L_{211}/3\cos(\varphi_{21}+\pi/6)\right] \pm \sqrt{L_{22}^2 - \left[y_{P2} - \sqrt{3}L_{211}/3\sin(\varphi_{21}+\pi/6) - L_{28}\right]^2} \tag{4-23}$$

The similar calculation steps for the first branch will be employed for the remaining supporting branches. The closed-loop equations for the other supporting branches are calculated as

$$\boldsymbol{OB}_{25} + \boldsymbol{B}_{25}\boldsymbol{B}_{26} + \boldsymbol{B}_{26}\boldsymbol{B}_{27} + \boldsymbol{B}_{27}\boldsymbol{P}_2 = \boldsymbol{OP}_2 \tag{4-24}$$

$$\boldsymbol{OC}_{25} + \boldsymbol{C}_{25}\boldsymbol{C}_{26} + \boldsymbol{C}_{26}\boldsymbol{C}_{27} + \boldsymbol{C}_{27}\boldsymbol{P}_2 = \boldsymbol{OP}_2 \tag{4-25}$$

Both Equations (4-24) and (4-25) will be described in two orthogonal directions and the passive parameters θ_{22} and θ_{23} will be placed in one side, as arranged below

$$\begin{cases} L_{24}\cos\theta_{22} = x_{P2} - \sqrt{3}L_{211}/3\cos(\varphi_{21}+5\pi/6) - x_{B25} \\ L_{24}\sin\theta_{22} = y_{P2} - \sqrt{3}L_{211}/3\sin(\varphi_{21}+5\pi/6) - L_{28} \end{cases} \tag{4-26}$$

$$\begin{cases} L_{26}\cos\theta_{23} = x_{P2} - \sqrt{3}L_{211}/3\cos(\varphi_{21}+3\pi/2) - x_{C25} \\ L_{26}\sin\theta_{23} = y_{P2} - \sqrt{3}L_{211}/3\sin(\varphi_{21}+3\pi/2) - L_{21} + L_{28} \end{cases} \tag{4-27}$$

Summing the squares of both equations in Equations (4-26) and (4-27) respectively. The following expressions can be deduced

$$\Gamma_{22}:\left[x_{P2} - \sqrt{3}L_{211}/3\cos(\varphi_{21}+5\pi/6) - x_2\right]^2 + \left[y_{P2} - \sqrt{3}L_{211}/3\sin(\varphi_{21}+5\pi/6) - L_{28}\right]^2 - L_{24}^2 = 0 \tag{4-28}$$

$$\Gamma_{23}:\left[x_{P2}-\sqrt{3}L_{211}/3\cos(\varphi_{21}+3\pi/2)-x_3\right]^2+\left[y_{P2}-\sqrt{3}L_{211}/3\sin(\varphi_{21}+3\pi/2)-L_{21}+L_{28}\right]^2-L_{26}^2=0 \tag{4-29}$$

The positions of the remaining actuation joints B_{25} and C_{25} can be formulated separately, as listed below

$$x_{B25}=\left[x_{P2}-\sqrt{3}L_{211}/3\cos(\varphi_{21}+5\pi/6)\right]\pm\sqrt{L_{24}^2-\left[y_{P2}-\sqrt{3}L_{211}/3\sin(\varphi_{21}+5\pi/6)-L_{28}\right]^2} \tag{4-30}$$

$$x_{C25}=\left[x_{P2}-\sqrt{3}L_{211}/3\cos(\varphi_{21}+3\pi/2)\right]\pm\sqrt{L_{26}^2-\left[y_{P2}-\sqrt{3}L_{211}/3\sin(\varphi_{21}+3\pi/2)-L_{21}+L_{28}\right]^2} \tag{4-31}$$

The analytical solution of the inverse kinematic model is concluded in Equations (4-23), (4-30) and (4-31).

The forward kinematic problem can be calculated with the predefined $\boldsymbol{Q}_2$. Equations (4-22), (4-28) and (4-29) can be deduced in the following form

$$x_{P2}^2+y_{P2}^2+e_{11}x_{P2}+e_{12}y_{P2}+e_{13}=0 \tag{4-32}$$

$$x_{P2}^2+y_{P2}^2+e_{21}x_{P2}+e_{22}y_{P2}+e_{23}=0 \tag{4-33}$$

$$x_{P2}^2+y_{P2}^2+e_{31}x_{P2}+e_{32}y_{P2}+e_{33}=0 \tag{4-34}$$

where

$$\begin{cases} e_{11}=-2\left[\sqrt{3}L_{211}/3\cos(\varphi_{21}+\pi/6)+x_{A25}\right] \\ e_{12}=-2\left[\sqrt{3}L_{211}/3\sin(\varphi_{21}+\pi/6)+L_{28}\right] \\ e_{13}=\left[\sqrt{3}L_{211}/3\cos(\varphi_{21}+\pi/6)+x_{A25}\right]^2+\left[\sqrt{3}L_{211}/3\sin(\varphi_{21}+\pi/6)+L_{28}\right]^2-L_{22}^2 \end{cases}$$

$$\begin{cases} e_{21}=-2\left[\sqrt{3}L_{211}/3\cos(\varphi_{21}+5\pi/6)+x_{B25}\right] \\ e_{22}=-2\left[\sqrt{3}L_{211}/3\sin(\varphi_{21}+5\pi/6)+L_{28}\right] \\ e_{23}=\left[\sqrt{3}L_{211}/3\cos(\varphi_{21}+5\pi/6)+x_{B25}\right]^2+\left[\sqrt{3}L_{211}/3\sin(\varphi_{21}+5\pi/6)+L_{28}\right]^2-L_{24}^2 \end{cases}$$

$$\begin{cases} e_{31} = -2\left[\sqrt{3}L_{211}/3\cos(\varphi_{21}+3\pi/2)+x_{C25}\right] \\ e_{32} = -2\left[\sqrt{3}L_{211}/3\sin(\varphi_{21}+3\pi/2)+L_{21}-L_{28}\right] \\ e_{33} = \left[\sqrt{3}L_{211}/3\cos(\varphi_{21}+3\pi/2)+x_{C25}\right]^2+\left[\sqrt{3}L_5/3\sin(\varphi_{21}+3\pi/2)+L_{21}-L_{28}\right]^2-L_{26}^2 \end{cases}$$

Subtracting Equation (4-33) from Equation (4-32) leads to

$$e_{41}x_{P2}+e_{42}y_{P2}+e_{43}=0 \tag{4-35}$$

where $e_{4i}=e_{1i}-e_{2i} \quad i=1,2,3.$

Subtracting Equation (4-34) from Equation (4-32) generates

$$e_{51}x_{P2}+e_{52}y_{P2}+e_{53}=0 \tag{4-36}$$

where $e_{5i}=e_{1i}-e_{3i} \quad i=1,2,3.$

The parameters *x* and *y* can be computed by solving Equations (4-35) and (4-36)

$$x_{P2}=\frac{e_{62}}{e_{61}},\ y_{P2}=\frac{-e_{63}}{e_{61}} \tag{4-37}$$

where

$$\begin{cases} e_{61}=e_{41}e_{52}-e_{42}e_{51} \\ e_{62}=e_{42}e_{53}-e_{43}e_{52} \\ e_{63}=e_{41}e_{53}-e_{43}e_{51} \end{cases}$$

Combining Equations (4-32) and (4-37) yields

$$e_{62}^2+e_{63}^2+e_{11}e_{61}e_{62}-e_{12}e_{61}e_{63}+e_{13}e_{61}^2=0 \tag{4-38}$$

Hence, the variable φ_{21} can be computed since it is the only unknown parameter in Equation (4-38).

(ii) Singularity configurations

Taking the derivatives of Equations (4-22), (4-28) and (4-29) with respect to time and rearranging the expression, yield

$$\boldsymbol{J}_{Q2}\cdot[\dot{x}_{A25},\dot{x}_{B25},\dot{x}_{C25}]^{\mathrm{T}}=\boldsymbol{J}_{X2}\cdot[\dot{x}_{P2},\dot{y}_{P2},\dot{\varphi}_{21}]^{\mathrm{T}} \tag{4-39}$$

where

$$\boldsymbol{J}_{Q2}=diag(M_{11},M_{13},M_{15})$$

$$\boldsymbol{J}_{X2}=\begin{bmatrix} M_{11} & M_{12} & M_{11}\sqrt{3}L_{211}/3\sin(\varphi_{21}+\pi/6)-M_{12}\sqrt{3}L_{211}/3\cos(\varphi_{21}+\pi/6) \\ M_{13} & M_{14} & M_{13}\sqrt{3}L_{211}/3\sin(\varphi_{21}+5\pi/6)-M_{14}\sqrt{3}L_{211}/3\cos(\varphi_{21}+5\pi/6) \\ M_{15} & M_{16} & M_{15}\sqrt{3}L_{211}/3\sin(\varphi_{21}+3\pi/2)-M_{16}\sqrt{3}L_{211}/3\cos(\varphi_{21}+3\pi/2) \end{bmatrix}$$

$$M_{11}=x_{P2}-\sqrt{3}L_{211}/3\cos(\varphi_{21}+\pi/6)-x_{A25}$$

$$M_{12}=y_{P2}-\sqrt{3}L_{211}/3\sin(\varphi_{21}+\pi/6)-L_{28}$$

$$M_{13}=x_{P2}-\sqrt{3}L_{211}/3\cos(\varphi_{21}+5\pi/6)-x_{B25}$$

$$M_{14}=y_{P2}-\sqrt{3}L_{211}/3\sin(\varphi_{21}+5\pi/6)-L_{28}$$

$$M_{15}=x_{P2}-\sqrt{3}L_{211}/3\cos(\varphi_{21}+3\pi/2)-x_{C25}$$

$$M_{16}=y_{P2}-\sqrt{3}L_{211}/3\sin(\varphi_{21}+3\pi/2)-L_{21}+L_{28}$$

Equation (4-39) can be further expressed as

$$\dot{\boldsymbol{Q}}_2=\boldsymbol{J}_2\dot{\boldsymbol{X}}_2=(\boldsymbol{J}_{Q2}^{-1}\boldsymbol{J}_{X2})\dot{\boldsymbol{X}}_2 \tag{4-40}$$

where $\boldsymbol{J}_2$ is the Jacobian matrix of this planar parallel mechanism.

The linkages $A_{26}A_{27}$, $B_{26}B_{27}$ and $C_{26}C_{27}$ are parallel to each other in figure 4-7. This already shows a singularity that the moving platform may cause an infinitesimal sliding movement along X direction even all the active sliding joints are fixed. Therefore, L_{28}= L_{29}= L_{210}=0 to avoid this singularity configuration. Under this situation, the singularity configurations of this planar parallel manipulator are listed below on the basis of Equation (4-39).

Type-I singularity happens when $Det(\boldsymbol{J}_{Q2})=0$. The first case is $x_{p2}=[3x_{A25}+\sqrt{3}L_{211}\cos(\varphi_{21}+\pi/6)]/3$. It implies that $L_{22}\cos\theta_{21}=0$, which can be realized when L_{22}=0 or $\theta_{21}=\pi/2rad$ (Considering the real application and assembly condition, the range of angle is from 0 to $\pi\ rad$. This consideration is also applied to other sloping angles). The latter scenario shows the sloping linkages $A_{21}A_{23}$ and $A_{22}A_{24}$ are perpendicular to X direction. The second case is $x_{p2}=[3x_{B25}-\sqrt{3}L_{211}\cos(\varphi-\pi/6)]/3$. It indicates that $L_{24}\cos\theta_{22}=0$. This result can be obtained when $L_{24}=0$ or $\theta_{22}=\pi/2rad$ (This means the inclined linkages $B_{21}B_{23}$ and $B_{22}B_{24}$ are perpendicular to X direction). The last case is $x_{p2}=(3x_{C25}-\sqrt{3}L_{211}\sin\varphi)/3$. It means $L_{26}\cos\theta_{23}=0$ which can be achieved

when $L_{26} = 0$ and $\theta_{23} = 3\pi / 2rad$ (The inclined linkages $C_{21}C_{23}$ and $C_{22}C_{24}$ are perpendicular to *X* direction). In summary, the first scenario of each case means the inclined linkages do not exist, while the second scenario depicts that the moving platform can bear the external force along *Y* axis without driving outputs.

Type-II singularity occurs when $Det(\boldsymbol{J}_{X2}) = 0$. There are two cases. The first case is expressed as

$$
\begin{aligned}
x_{p2} = -\{\ & [\sqrt{3}(24y_{P2}^2 + 2L_{211}^2)(x_{A25}^2 + x_{B25}^2 + x_{C25}^2) + 18L_{21}^2L_{211}^2 + 24L_{21}^2(x_{A25}^2 + x_{B25}^2) + \\
& 24L_{21}^2(y_{P2}^2 - x_{A25}^2\cos 2\varphi_{21} - x_{B25}^2\cos 2\varphi_{21} + y_{P2}^2\cos 2\varphi_{21}) + \\
& L_{211}^2(x_{A25}^2\cos 4\varphi_{21} + x_{B25}^2\cos 4\varphi_{21} - 2x_{C25}^2\cos 4\varphi_{21}) - 24y_{P2}^2(x_{A25}x_{B25} + x_{A25}x_{C25} + x_{B25}x_{C25}) \\
& + 12y_{P2}^2\cos 2\varphi_{21}(x_{A25}^2 + x_{B25}^2 - 2x_{C25}^2) + L_{21}^2(-16L_{211}^2\cos 2\varphi_{21} + 2L_{211}^2\cos 4\varphi_{21} - 48x_{A25}x_{B25}) \\
& - 2L_{211}^2(x_{A25}x_{B25} + x_{A25}x_{C25} + x_{B25}x_{C25}) - 24L_{21}y_{P2}(x_{A25}^2 + x_{B25}^2) + \\
& 24L_{21}^2L_{211}\cos 3\varphi_{21}(-x_{A25} + x_{B25}) - 8L_{21}L_{211}^2\sin 2\varphi_{21}(x_{A25} + x_{B25}) + \\
& 12L_{21}L_{211}\sin 3\varphi_{21}(-x_{A25}^2 + x_{B25}^2) + L_{21}L_{211}^2(2x_{A25}\sin 4\varphi_{21} + 16x_{C25}\sin 2\varphi_{21} + 2x_{B25}\sin 4\varphi_{21} - \\
& 4x_{C25}\sin 2\varphi_{21}) + 48L_{21}x_{A25}x_{B25}(y_{P2} + L_{21}\cos 2\varphi_{21}) + \\
& L_{211}^2\cos 4\varphi_{21}(-4x_{A25}x_{B25} + 2x_{A25}x_{C25} + 2x_{B25}x_{C25}) + 6\sqrt{3}L_{21}L_{211}^2(-x_{A25} + x_{B25}) + \\
& 24L_{21}y_{P2}(x_{A25}^2\cos 2\varphi_{21} + x_{B25}^2\cos 2\varphi_{21} + x_{A25}y_{P2}\sin 2\varphi_{21} + x_{B25}y_{P2}\sin 2\varphi_{21} - 2x_{C25}y_{P2}\sin 2\varphi_{21}) + \\
& 24y_{P2}^2\cos 2\varphi_{21}(-2x_{A25}x_{B25} + x_{A25}x_{C25} + x_{B25}x_{C25}) + \\
& 24\sqrt{3}L_{21}y_{P2}(3x_{A25}y_{P2} - 2L_{21}x_{A25} - 3x_{B25}y_{P2} + 2L_{21}x_{B25}) + \sqrt{3}L_{211}^2\sin 4\varphi_{21}(x_{A25}^2 - x_{B25}^2) + \\
& 24L_{21}^2L_{211}\cos\varphi_{21}(x_{A25} - x_{B25}) + 12\sqrt{3}y_{P2}^2\sin 2\varphi_{21}(-x_{A25}^2 + x_{B25}^2) + \\
& 12L_{211}\sin\varphi_{21}(L_{21}x_{A25}^2 - L_{21}x_{B25}^2 - x_{A25}^2y_{P2} + x_{B25}^2y_{P2}) - \\
& 4\sqrt{3}L_{21}L_{211}(x_{A25}^2\cos\varphi_{21} + x_{B25}^2\cos\varphi_{21} + 6L_{21}y_{P2}\cos\varphi_{21}) + 24L_{21}L_{211}x_{C25}\sin 3\varphi_{21}(x_{A25} - x_{B25}) + \\
& 4\sqrt{3}L_{211}y_{P2}\cos\varphi_{21}(-x_{A25}^2 - x_{B25}^2 + 2x_{C25}^2) - 48L_{21}x_{A25}x_{B25}y_{P2}\cos 2\varphi_{21} \\
& + 2\sqrt{3}L_{21}L_{211}(4L_{211}x_{A25}\cos 2\varphi_{21} + 2x_{A25}^2\cos 3\varphi_{21} - 4L_{211}x_{B25}\cos 2\varphi_{21} + 2x_{B25}^2\cos 3\varphi_{21} + \\
& L_{211}x_{A25}\cos 4\varphi_{21} - L_{211}x_{B25}\cos 4\varphi_{21} + 4L_{21}y_{P2}\cos 3\varphi_{21}) + \\
& 24\sqrt{3}L_{21}y_{P2}\cos 2\varphi_{21}(-x_{A25}y_{P2} + 2L_{21}x_{A25} + x_{B25}y_{P2} - 2L_{21}x_{B25}) - \\
& 8\sqrt{3}L_{211}y_{P2}\cos 3\varphi_{21}(x_{A25}^2 + x_{B25}^2 + x_{C25}^2) + 2\sqrt{3}L_{211}^2x_{C25}\sin 4\varphi_{21}(-x_{A25} + x_{B25}) + \\
& 24\sqrt{3}L_{21}y_{P2}\sin 2\varphi_{21}(x_{A25}^2 - x_{B25}^2) + 48L_{21}L_{211}y_{P2}\cos\varphi_{21}(-x_{A25} + x_{B25}) + \\
& 24\sqrt{3}x_{C25}y_{P2}^2\sin 2\varphi_{21}(x_{A25} - x_{B25}) + 24L_{211}x_{C25}\sin\varphi_{21}(-L_{21}x_{A25} + L_{21}x_{B25} + x_{A25}y_{P2} - x_{B25}y_{P2}) + \\
& 8\sqrt{3}L_{21}L_{211}(x_{A25}x_{B25}\cos\varphi_{21} - 2x_{A25}y_{P2}\sin\varphi_{21} - 2x_{B25}y_{P2}\sin\varphi_{21} + 4x_{C25}y_{P2}\sin\varphi_{21}) + \\
& 8\sqrt{3}L_{211}(2x_{A25}x_{B25}y_{P2}\cos\varphi_{21} - x_{A25}x_{C25}y_{P2}\cos\varphi_{21} - x_{B25}x_{C25}y_{P2}\cos\varphi_{21} - L_{21}x_{A25}x_{B25}\cos 3\varphi_{21} + \\
& L_{21}x_{A25}y_{P2}\sin 3\varphi_{21} + L_{21}x_{B25}y_{P2}\sin 3\varphi_{21} - 2L_{21}x_{C25}y_{P2}\sin 3\varphi_{21} + x_{A25}x_{B25}y_{P2}\cos 3\varphi_{21} + \\
& x_{A25}x_{C25}y_{P2}\cos 3\varphi_{21} + x_{B25}x_{C25}y_{P2}\cos 3\varphi_{21}) + 48\sqrt{3}L_{21}x_{C25}y_{P2}\sin 2\varphi_{21}(-x_{A25} + x_{B25})]^{1/2} + \\
& 6\sin\varphi_{21}(-2L_{21}x_{A25} - 2L_{21}x_{B25} + x_{A25}y_{P2} + x_{B25}y_{P2} - 2x_{C25}y_{P2}) + 3L_{211}\cos 2\varphi_{21}(x_{A25} - x_{B25}) + \\
& 6y_{P2}\cos 2\varphi_{21}(-2L_{21} - \sqrt{3}x_{A25} + \sqrt{3}x_{B25}) + \sqrt{3}L_{211}(2L_{21}\cos 2\varphi_{21} + x_{A25}\sin 2\varphi_{21} + x_{B25}\sin 2\varphi_{21} - \\
& 2x_{C25}\sin 2\varphi_{21})\ \}/(24L_{21}\sin\varphi_{21})
\end{aligned}
\tag{4-41}
$$

The second case is calculated as

$$
\begin{aligned}
x_{p2} = \{\ & [\sqrt{3}(24y_{P2}^2 + 2L_{211}^2)(x_{A25}^2 + x_{B25}^2 + x_{C25}^2) + 18L_{21}^2L_{211}^2 + 24L_{21}^2(x_{A25}^2 + x_{B25}^2) + \\
& 24L_{21}^2(y_{P2}^2 - x_{A25}^2\cos 2\varphi_{21} - x_{B25}^2\cos 2\varphi_{21} + y_{P2}^2\cos 2\varphi_{21}) + \\
& L_{211}^2(x_{A25}^2\cos 4\varphi_{21} + x_{B25}^2\cos 4\varphi_{21} - 2x_{C25}^2\cos 4\varphi_{21}) - 24y_{P2}^2(x_{A25}x_{B25} + x_{A25}x_{C25} + x_{B25}x_{C25}) \\
& + 12y_{P2}^2\cos 2\varphi_{21}(x_{A25}^2 + x_{B25}^2 - 2x_{C25}^2) + L_{21}^2(-16L_{211}^2\cos 2\varphi_{21} + 2L_{211}^2\cos 4\varphi_{21} - 48x_{A25}x_{B25}) \\
& - 2L_{211}^2(x_{A25}x_{B25} + x_{A25}x_{C25} + x_{B25}x_{C25}) - 24L_{21}y_{P2}(x_{A25}^2 + x_{B25}^2) + \\
& 24L_{21}^2L_{211}\cos 3\varphi_{21}(-x_{A25} + x_{B25}) - 8L_{21}L_{211}^2\sin 2\varphi_{21}(x_{A25} + x_{B25}) + \\
& 12L_{21}L_{211}\sin 3\varphi_{21}(-x_{A25}^2 + x_{B25}^2) + L_{21}L_{211}^2(2x_{A25}\sin 4\varphi_{21} + 16x_{C25}\sin 2\varphi_{21} + 2x_{B25}\sin 4\varphi_{21} - \\
& 4x_{C25}\sin 2\varphi_{21}) + 48L_{21}x_{A25}x_{B25}(y_{P2} + L_{21}\cos 2\varphi_{21}) + \\
& L_{211}^2\cos 4\varphi_{21}(-4x_{A25}x_{B25} + 2x_{A25}x_{C25} + 2x_{B25}x_{C25}) + 6\sqrt{3}L_{21}L_{211}^2(-x_{A25} + x_{B25}) + \\
& 24L_{21}y_{P2}(x_{A25}^2\cos 2\varphi_{21} + x_{B25}^2\cos 2\varphi_{21} + x_{A25}y_{P2}\sin 2\varphi_{21} + x_{B25}y_{P2}\sin 2\varphi_{21} - 2x_{C25}y_{P2}\sin 2\varphi_{21}) + \\
& 24y_{P2}^2\cos 2\varphi_{21}(-2x_{A25}x_{B25} + x_{A25}x_{C25} + x_{B25}x_{C25}) + \\
& 24\sqrt{3}L_{21}y_{P2}(3x_{A25}y_{P2} - 2L_{21}x_{A25} - 3x_{B25}y_{P2} + 2L_{21}x_{B25}) + \sqrt{3}L_{211}^2\sin 4\varphi_{21}(x_{A25}^2 - x_{B25}^2) + \\
& 24L_{21}^2L_{211}\cos\varphi_{21}(x_{A25} - x_{B25}) + 12\sqrt{3}y_{P2}^2\sin 2\varphi_{21}(-x_{A25}^2 + x_{B25}^2) + \\
& 12L_{211}\sin\varphi_{21}(L_{21}x_{A25}^2 - L_{21}x_{B25}^2 - x_{A25}^2y_{P2} + x_{B25}^2y_{P2}) - \\
& 4\sqrt{3}L_{21}L_{211}(x_{A25}^2\cos\varphi_{21} + x_{B25}^2\cos\varphi_{21} + 6L_{21}y_{P2}\cos\varphi_{21}) + 24L_{21}L_{211}x_{C25}\sin 3\varphi_{21}(x_{A25} - x_{B25}) + \\
& 4\sqrt{3}L_{211}y_{P2}\cos\varphi_{21}(-x_{A25}^2 - x_{B25}^2 + 2x_{C25}^2) - 48L_{21}x_{A25}x_{B25}y_{P2}\cos 2\varphi_{21} \\
& + 2\sqrt{3}L_{21}L_{211}(4L_{211}x_{A25}\cos 2\varphi_{21} + 2x_{A25}^2\cos 3\varphi_{21} - 4L_{211}x_{B25}\cos 2\varphi_{21} + 2x_{B25}^2\cos 3\varphi_{21} + \\
& L_{211}x_{A25}\cos 4\varphi_{21} - L_{211}x_{B25}\cos 4\varphi_{21} + 4L_{21}y_{P2}\cos 3\varphi_{21}) + \\
& 24\sqrt{3}L_{21}y_{P2}\cos 2\varphi_{21}(-x_{A25}y_{P2} + 2L_{21}x_{A25} + x_{B25}y_{P2} - 2L_{21}x_{B25}) - \\
& 8\sqrt{3}L_{211}y_{P2}\cos 3\varphi_{21}(x_{A25}^2 + x_{B25}^2 + x_{C25}^2) + 2\sqrt{3}L_{211}^2x_{C25}\sin 4\varphi_{21}(-x_{A25} + x_{B25}) + \\
& 24\sqrt{3}L_{21}y_{P2}\sin 2\varphi_{21}(x_{A25}^2 - x_{B25}^2) + 48L_{21}L_{211}y_{P2}\cos\varphi_{21}(-x_{A25} + x_{B25}) + \\
& 24\sqrt{3}x_{C25}y_{P2}^2\sin 2\varphi_{21}(x_{A25} - x_{B25}) + 24L_{211}x_{C25}\sin\varphi_{21}(-L_{21}x_{A25} + L_{21}x_{B25} + x_{A25}y_{P2} - x_{B25}y_{P2}) + \\
& 8\sqrt{3}L_{21}L_{211}(x_{A25}x_{B25}\cos\varphi_{21} - 2x_{A25}y_{P2}\sin\varphi_{21} - 2x_{B25}y_{P2}\sin\varphi_{21} + 4x_{C25}y_{P2}\sin\varphi_{21}) + \\
& 8\sqrt{3}L_{211}(2x_{A25}x_{B25}y_{P2}\cos\varphi_{21} - x_{A25}x_{C25}y_{P2}\cos\varphi_{21} - x_{B25}x_{C25}y_{P2}\cos\varphi_{21} - L_{21}x_{A25}x_{B25}\cos 3\varphi_{21} + \\
& L_{21}x_{A25}y_{P2}\sin 3\varphi_{21} + L_{21}x_{B25}y_{P2}\sin 3\varphi_{21} - 2L_{21}x_{C25}y_{P2}\sin 3\varphi_{21} + x_{A25}x_{B25}y_{P2}\cos 3\varphi_{21} + \\
& x_{A25}x_{C25}y_{P2}\cos 3\varphi_{21} + x_{B25}x_{C25}y_{P2}\cos 3\varphi_{21}) + 48\sqrt{3}L_{21}x_{C25}y_{P2}\sin 2\varphi_{21}(-x_{A25} + x_{B25})]^{1/2} + \\
& 6\sin\varphi_{21}(2L_{21}x_{A25} + 2L_{21}x_{B25} - x_{A25}y_{P2} - x_{B25}y_{P2} + 2x_{C25}y_{P2}) + 3L_{211}\cos 2\varphi_{21}(-x_{A25} + x_{B25}) + \\
& 6y_{P2}\cos 2\varphi_{21}(+2L_{21} + \sqrt{3}x_{A25} - \sqrt{3}x_{B25}) - \sqrt{3}L_{211}(2L_{21}\cos 2\varphi_{21} + x_{A25}\sin 2\varphi_{21} + x_{B25}\sin 2\varphi_{21} - \\
& 2x_{C25}\sin 2\varphi_{21})\ \}/(24L_{21}\sin\varphi_{21})
\end{aligned}
\tag{4-42}
$$

(iii) Workspace analysis

The reachable workspace is one of the most essential indices for a parallel manipulator. The corresponding linkages of three chains have the same dimensions respectively, to realize the symmetric feature. For introductive purpose, the linkages dimensions of this

parallel manipulator are selected as L_{21}= 150mm, L_{22}= L_{24}= L_{26}=120mm, L_{23}= L_{25}= L_{27}=20mm, L_{28}= L_{29}= L_{210}=0, L_{211}=50mm and L_{212}=400mm.

The first factor that affects the workspace volume is the strokes of the driving joints. In this mechanism, the strokes of three actuation joints are provided as $L_{23} \le x_{A25}, x_{B25}, x_{C25} \le L_{212} - L_{23}$. The $\pm$ symbols in Equations (4-23), (4-30) and (4-31) are chosen as $-$, $+$ and $+$, respectively. According to the geometric relations, the passive slopping angels θ_{2i} are computed as

$$\begin{cases} \theta_{21} = \sin^{-1}\left\{[y_{P2} - \sqrt{3}L_{211}/3\sin(\varphi_{21} + \pi/6) - L_{28}]/L_{22}\right\} \\ \theta_{22} = \sin^{-1}\left\{[y_{P2} - \sqrt{3}L_{211}/3\sin(\varphi_{21} + 5\pi/6) - L_{28}]/L_{22}\right\} \\ \theta_{23} = \sin^{-1}\left\{[y_{P2} - \sqrt{3}L_{211}/3\sin(\varphi_{21} + 3\pi/2) - L_{21} + L_{28}]/L_{22}\right\} \end{cases} \tag{4-43}$$

The driven revolute joints are also constrained as

$$\begin{cases} [i\pi/2 - 17\pi/36] \le \theta_{2i} \le [i\pi/2 - \pi/36] \quad i = 1,2,3 \\ -\pi \le \varphi_{21} \le \pi \end{cases} \tag{4-44}$$

To solve the reachable workspace, the position range of the mobile platform $A_{27}B_{27}C_{27}$ is predefined as $2L_{23} \le x_{P2} \le L_{212} - 2L_{23}$ and $2L_{23} \le y_{P2} \le L_{21} - L_{211}$ .The spatial search methodology is employed to obtain the reachable workspace. The flow diagram of this approach is demonstrated in figure 4-8. According to the above conditions, the parameters in this flowchart are listed as $x_{\min} = 2L_{23}$, $x_{\max} = L_{212} - 2L_{23}$, $x_{\text{step}} = 4mm$, $y_{\min} = 2L_{23}$, $y_{\max} = L_{21} - L_{211}$, $y_{\text{step}} = 1mm$, $\varphi_{\min} = -\pi$ rad, $\varphi_{\max} = \pi$ rad and $\varphi_{\text{step}} = \pi/18$ rad. In the provided $\boldsymbol{X}_2$ range, each possible position is employed to compute the corresponding $\boldsymbol{Q}_2$ based on the inverse kinematic model. This position will be feasible once it meets all the aforementioned constraints.

The reachable workspace of this planar parallel mechanism is computed and shown in figure 4-9. The figures 4-9 (a-c) are the standard views while the figure 4-9 (d) presents the 3D view. Three layers those are parallel to the front/side/top views are provided respectively in figure 4-9 (a-c) to better understand the distributions of the workspace. In accordance with figure 4-9, when $\varphi_{21} = 0$, the workspace is the smallest and the workspace

increases when the orientation φ_{21} is larger or smaller. The reachable workspace is irregular and asymmetric, which is difficult to be utilized in applications.

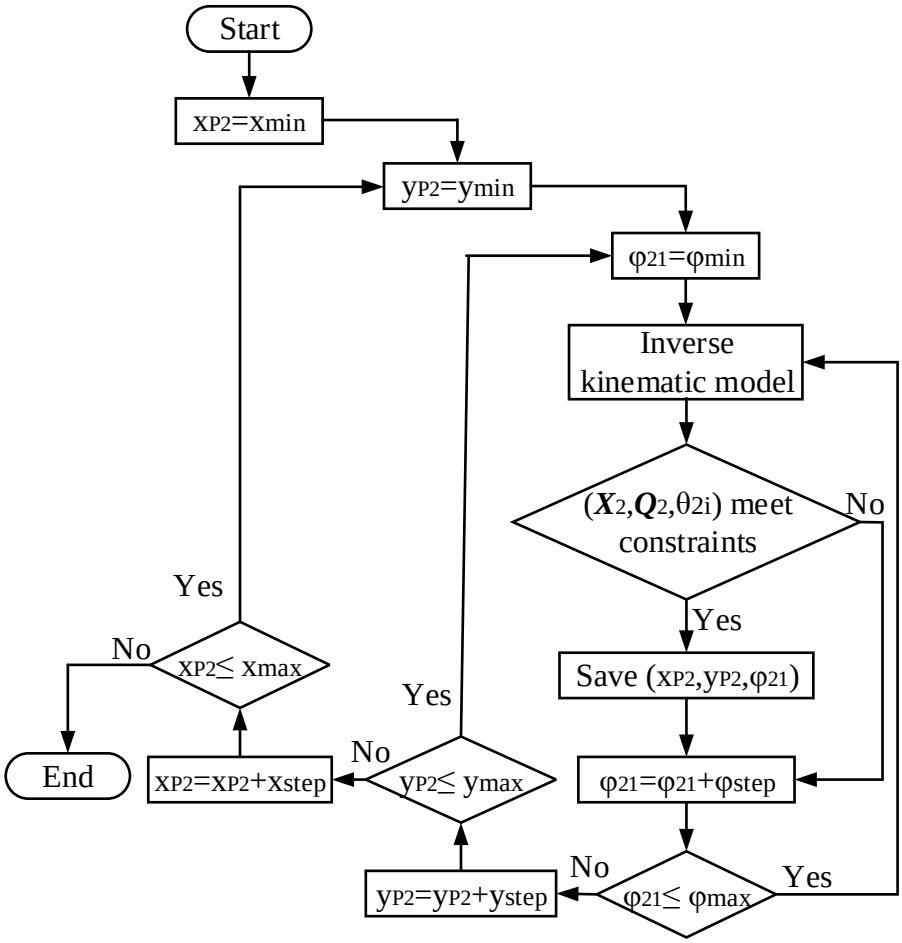

Figure 4-8 Flow diagram for reachable workspace

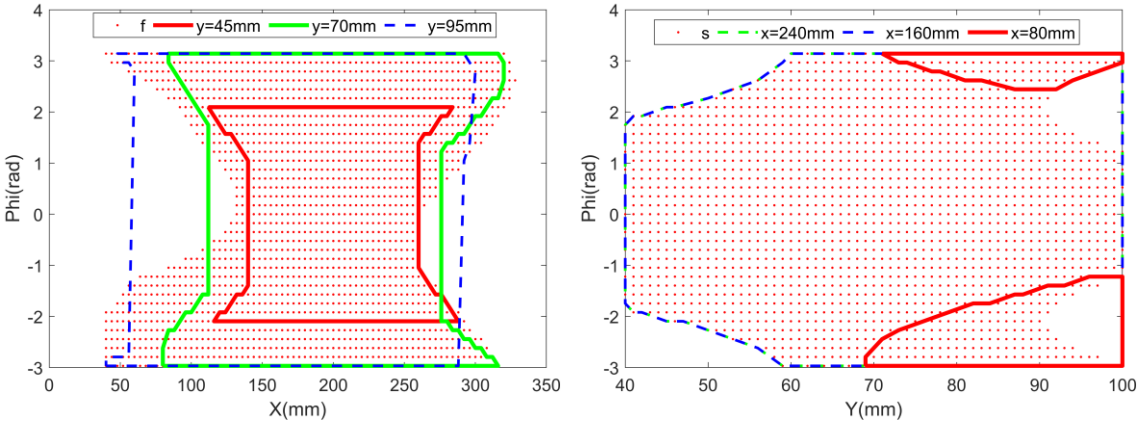

(a) Front view (b) Side view

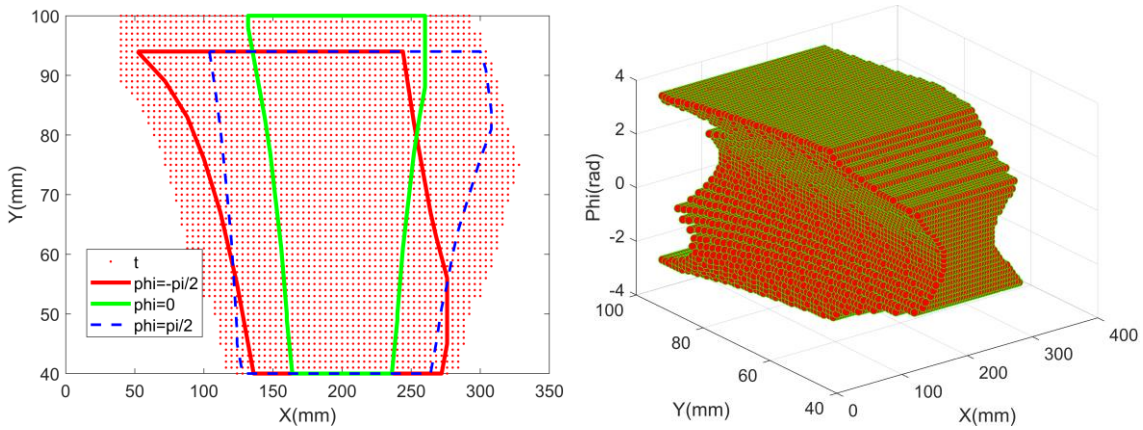

(c) Top view (d) 3D view

Figure 4-9 Reachable workspace and specific layers

A series of linkage dimensions is selected to study their impacts on the volume of the reachable workspace. These influences are depicted in figure 4-10. From figure 4-10(a), the workspace volume continues to grow as L_{21} changes from 130mm to 150mm. The workspace volume decreases when L_{21} changes from 150mm to 152mm. As L_{21} changes from 152mm to 154mm, the workspace volume increases a bit and then reduces as L_{21} extends to 170mm. From figure 4-10(b), the reachable workspace volume improves as L_{22} increases from 110mm to 124mm. Then the workspace volume shows a download trend. From figure 4-10(c-d), the reachable workspace volume and L_{23} or L_{24} are both negative relationships. The workspace volume keeps shrinking as L_{23} or L_{24} gets longer. From figure 4-10(e), the reachable workspace volume and L_{212} are positive relationship. In the predefined range of L_{212}, the workspace volume has a rising trend when L_{212} increases gradually.

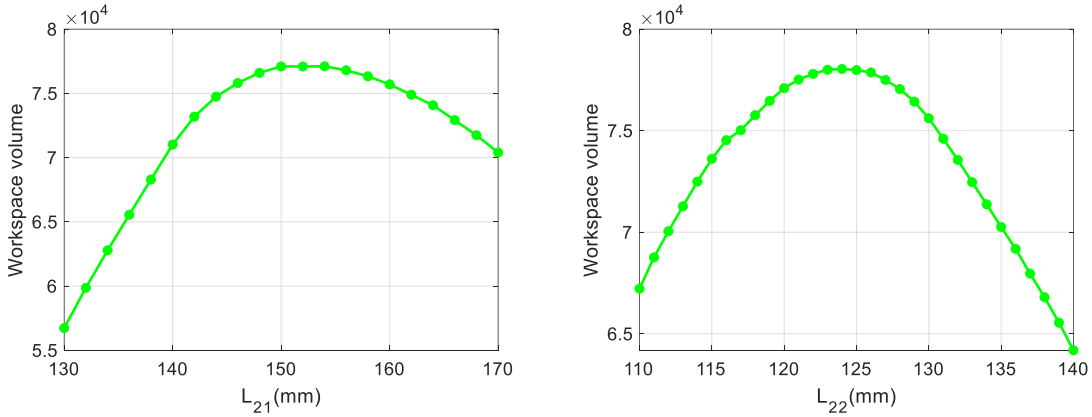

(a) L_{21} (b) L_{22}

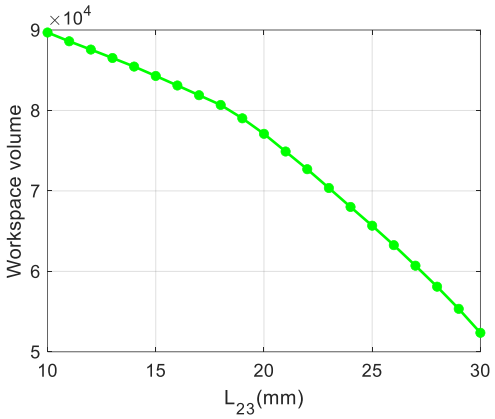

(c) L_{23}

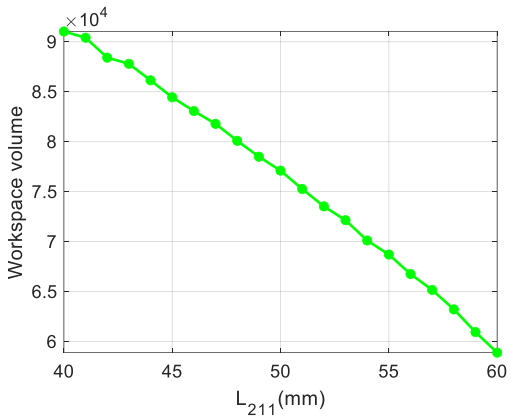

(d) L_{211}

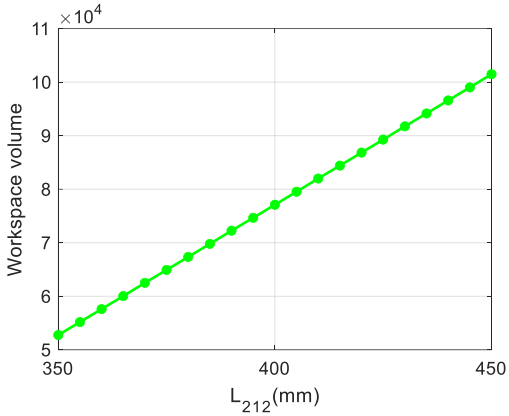

(e) L_{212}

Figure 4-10 Parametric analysis on the reachable workspace

(iv) Dexterity analysis

The Local Condition Index of this planar parallel robot is calculated as

$$LCI = \|\boldsymbol{J}_2\|_f \left\|\boldsymbol{J}_2^{-1}\right\|_f \tag{4-45}$$

Since this planar parallel manipulator has translational and rotational movements, Equation (4-40) is divided into the sum of two terms,

$$\dot{\boldsymbol{Q}}_2 = \boldsymbol{J}_{2V}[\dot{x}_{P2}, \dot{y}_{P2}]^{\mathrm{T}} + \boldsymbol{J}_{2W}[\dot{\varphi}_{21}]^{\mathrm{T}} \tag{4-46}$$

where $\boldsymbol{J}_{2V}$ (3-by-2 matrix) and $\boldsymbol{J}_{2W}$ (3-by-1 matrix) own respectively the first two columns and the last column of the Jacobian matrix $\boldsymbol{J}_2$.

In accordance with the definition in Equation (4-4), the local translational condition index (LTCI) and the local rotational condition index (LRCI) are generated respectively as

$$\begin{cases} \text{LTCI} = LCI(\boldsymbol{J}_V) = \left\|\boldsymbol{J}_{2V}\right\|_f \left\|\boldsymbol{J}_{2V}^{-1}\right\|_f \\ \text{LRCI} = LCI(\boldsymbol{J}_W) = \left\|\boldsymbol{J}_{2W}\right\|_f \left\|\boldsymbol{J}_{2W}^{-1}\right\|_f \end{cases} \tag{4-47}$$

The LTCI can be computed and is not associated with the position along *X* direction. The LTCI- y_{P2} and LTCI- φ_{21} are plotted in figures 4-11 (a-b). The constant parameters are defined as x_{P2} =200mm and φ_{21}=0 to explore the relationships between LTCI (or LRCI) and y_{P2}. The conditions that x_{P2} =200mm and y_{P2}=70mm are pre-set to study the φ_{21} impacts on the LTCI (or LRCI). Both figures show a downward trend at first and then grows as y_{P2} or φ_{21} increases. The lowest points of these plots happen at y_{P2}=60mm and φ_{21} =0, respectively. The LRCI is also not related to x_{P2} and is illustrated in figures 4-11 (c-d). From figure 4-11(c), the LRCI reduces gradually and then grows, while the turning point is y_{P2}=75mm. From figure 4-11(d), the LRCI's distribution seem like cyclic with respect to φ_{21}. From figure 4-11, both LTCI and LRCI are larger than 1. The values of LRCI are much larger than those of LTCI. The LTCI ranges from 1.92 to 10.435 in the whole workspace and the mean value is 2.9783. In the overall workspace, the smallest and largest LRCIs are 9.8333 and 273.21, respectively. The mean LRCI is 54.17.

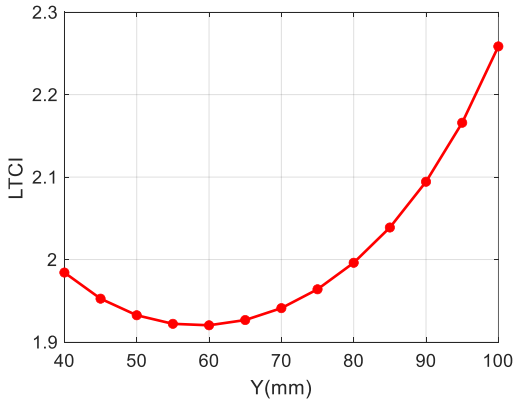

(a) y_{P2}

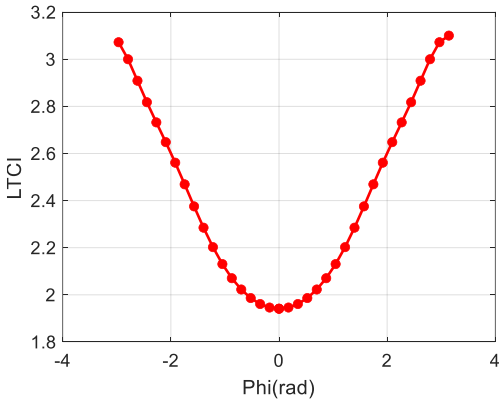

(b) φ_{21}

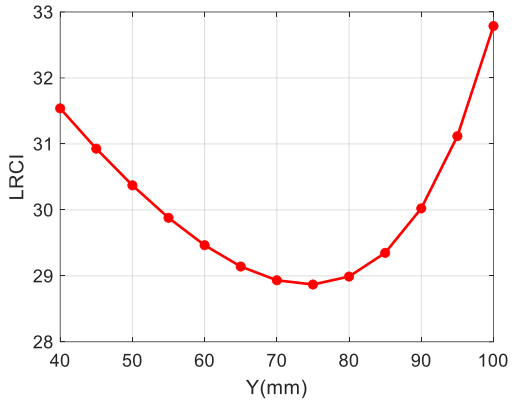

(c) y_{P2}

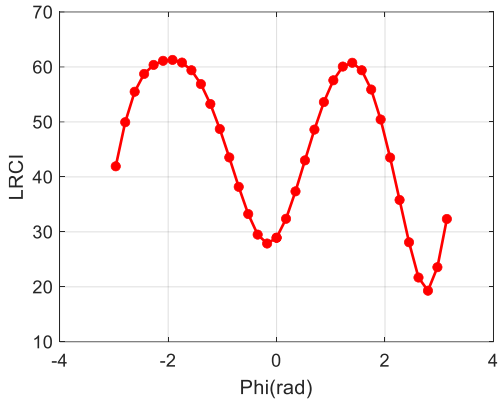

(d) φ_{21}

Figure 4-11 Distributions of LTCI and LRCI

The distributions of the LTLCI and LRLCI are plotted in figure 4-12. The corresponding figures within figure 4-12 have the identical trends as those in figure 4-11, except for the scales are narrowed in figure 4-12. The LTLCI ranges from 0.39201 to 0.43127 in figure 4-12(a). The smallest and largest LTLCIs are 0.39458 and 0.51005 respectively in figure 4-12(b). The LRLCI ranges from 0.34765 to 0.37705 in figure 4-12(c). The smallest and largest LRLCIs are 0.26269 and 0.5308 separately in figure 4-12(d).

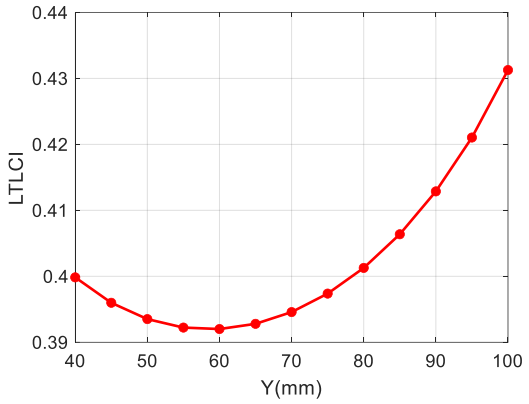

(a) y_{P2}

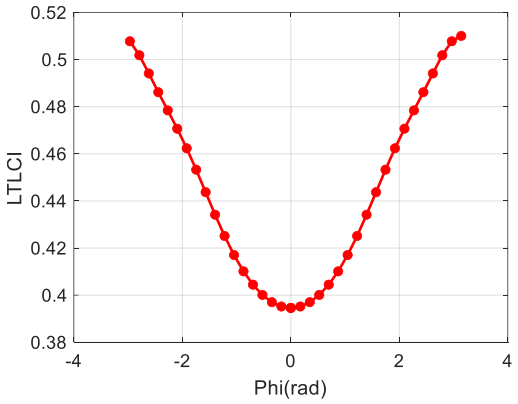

(b) φ_{21}

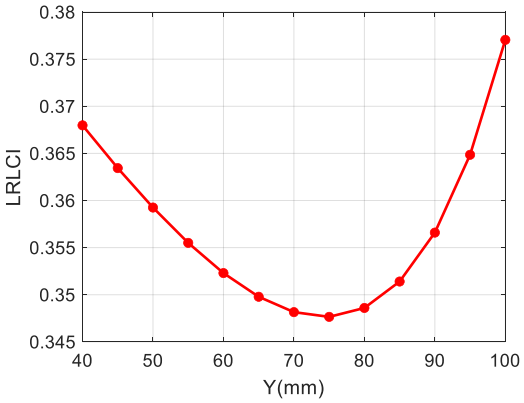

(c) y_{P2}

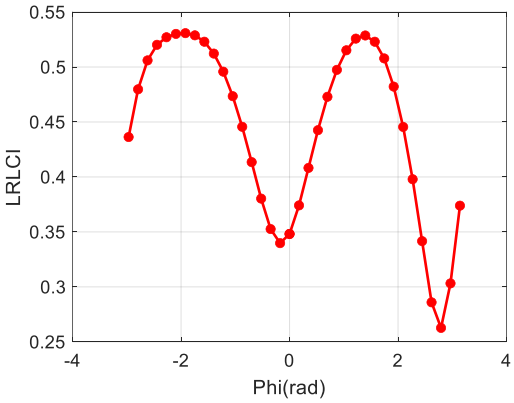

(d) φ_{21}

Figure 4-12 Layouts of LTLCI and LRLCI

4.4 Case three: 3T parallel mechanism

The schematic diagram of this 3T parallel mechanism is demonstrated in figure 4-13. This parallel manipulator with three translational movements is consisted of one fixed platform and moving platform connected by three kinematic chains (A-limb, B-limb, C-limb). In each kinematic branch, there are from the fixed platform to the end-effector, one active prismatic joint, a parallelogram module(four-revolute-joint) and a passive prismatic joint. The global coordinate system is also established as shown in figure 4-13. The driving sliders of first two branches (A-limb and B-limb), and the passive prismatic pair of the branch three (C-limb) move along the same direction(parallel to *X* axis). The parallelogram modules of branch one and branch two are both parallel to *XOZ* plane, while that of branch three is parallel to *YOZ* plane. The passive prismatic joints of branch one and branch two, and the active driving slider of branch three move in the same direction (parallel to *Y* axis). In branch one and branch two, it is noteworthy that both the passive prismatic joints, the connection linkages between the parallelogram modules and the passive prismatic joints, have identical movements respectively in the workspace. For simplification, their connection linkages are merged as linkage $A_{32}A_{34}B_{34}B_{32}$ and two passive sliding joints are combined as one kinematic pair. Overall, the moving platform possesses three translations in space and three actuators are required to be mounted on three prismatic joints connected to the fixed platform to fully drive the whole parallel manipulator.

In figure 4-13, A_{35}, B_{35} and C_{35} denote the virtual center positions of active sliders $A_{31}A_{33}$, $B_{31}B_{33}$ and $C_{31}C_{33}$, respectively. A_{36}, B_{36} and C_{36} stand for the virtual center points of $A_{32}A_{34}$, $B_{32}B_{34}$ and $C_{32}C_{34}$, respectively. The fixed platform is a square with the length of L_{31}. The inclined linkages of parallelogram modules in each branch own the same length and are defined as L_{32}, L_{34} and L_{35}, respectively. L_{33}, L_{35} and L_{37} represent respectively the distances between points A_{31} and A_{35}, B_{31} and B_{35}, C_{31} and C_{35}. Thus $\left|A_iA_{i+2}\right| = 2L_{33}(i=1,2)$, $\left|B_iB_{i+2}\right| = 2L_{35}(i=1,2)$ and $\left|C_iC_{i+2}\right| = 2L_{37}(i=1,2)$. The side length of the square moving platform is denoted as L_{38}. The angles between $A_{31}A_{33}$ and positive *X* axis, $B_{31}B_{33}$ and positive *X* axis, $C_{31}C_{33}$ and positive *Y* axis, are defined as θ_{31}, θ_{32} and θ_{33}, respectively.

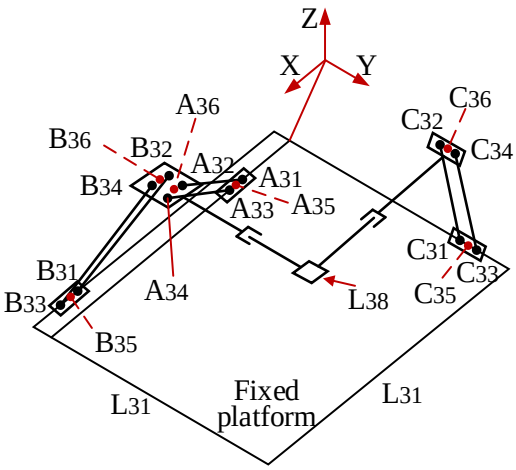

Figure 4-13 Schematic diagram of the 3T parallel robot

(i) Kinematic models

Since the mobile platform can move but not rotate in spatial space, the posture of this moving platform is simplified as $\boldsymbol{X}_3=[x_{P3},y_{P3},z_{P3}]^{\mathrm{T}}$. The displacements of three sliding joints are the inputs of this system, which is represented as $\boldsymbol{Q}_3=[x_{A35},x_{B35},y_{C35}]^{\mathrm{T}}$. Considering the special joint configurations of this parallel architecture, the geometric feature is employed to calculate the mathematical model of the kinematic problem. Ignoring the distance along *Y*-axis between limb one and limb two, the coordinates of three active sliders can be written as (x_{A35},0,0), (x_{B35},0,0), and (0, y_{C35},0), respectively. The positions of the points A_{36} (or B_{36}) and C_{36} are (X_{P2},0,z_{P2}),and (0, y_{P2}, z_{P2}), respectively. The linkages lengths of inclined rods $A_{31}A_{32}$(or $A_{33}A_{34}$), $B_{31}B_{32}$(or $B_{33}B_{34}$) and $C_{31}C_{32}$(or $C_{33}C_{34}$) remain the same in workspace. Therefore

$$\begin{cases}\left\|\boldsymbol{OA}_{36}-\boldsymbol{OA}_{35}\right\|=L_{32}\\ \left\|\boldsymbol{OB}_{36}-\boldsymbol{OB}_{35}\right\|=L_{34}\\ \left\|\boldsymbol{OC}_{36}-\boldsymbol{OC}_{35}\right\|=L_{36}\end{cases} \tag{4-48}$$

where $\|\cdot\|$ represents the Euclidean norm.

Equation (4-48) can be further expressed as

$$\begin{cases} \Gamma_{31}:(x_{P3}-x_{A35})^2+z_{P3}^2-L_{32}^2=0 \\ \Gamma_{32}:(x_{B35}-x_{P3})^2+z_{P3}^2-L_{34}^2=0 \\ \Gamma_{33}:(y_{C35}-y_{P3})^2+z_{P3}^2-L_{36}^2=0 \end{cases} \tag{4-49}$$

If the position of the mobile platform is given, the inverse kinematic solution can be computed as

$$\boldsymbol{Q}_3=\begin{bmatrix} x_{A35} \\ x_{B35} \\ y_{C35} \end{bmatrix}=\begin{bmatrix} x_{P3}\pm\sqrt{L_{32}^2-z_{P3}^2} \\ x_{P3}\pm\sqrt{L_{34}^2-z_{P3}^2} \\ y_{P3}\pm\sqrt{L_{36}^2-z_{P3}^2} \end{bmatrix} \tag{4-50}$$

Equation (4-50) indicates each slider has two kinds of working modes. Thus, there are totally eight sets of theoretical results. For the configuration of the parallel architecture shown in figure 4-13, three $\pm$ signs are respectively –,+ and +. If the linkages relations are predefined, e.g., $x_{P3}<x_{A35}<x_{B35}\ \&\ y_{P3}<y_{C35}$ as depicted in figure 4-13, the corresponding mathematical solution of inverse kinematic problem is unique and simple to be obtained. The corresponding solution of the forward kinematic problem can also be derived from Equation (4-49)

$$\begin{cases} x_{P3}=\dfrac{-(L_{32}^{\ 2}-L_{34}^{\ 2}-x_{A35}^2+x_{B35}^2)}{2\sigma} \\ y_{P3}=\pm\dfrac{\sqrt{-L_{32}^{\ 2}[L_{32}^{\ 2}-2L_{34}^{\ 2}-2\sigma^2]+L_{34}^{\ 2}[L_{34}^{\ 2}-2\sigma^2+4L_{36}^{\ 2}\sigma^2+\sigma^4]}\mp 2\sigma y_{C35}}{2|\sigma|} \\ z_{P3}=\dfrac{\pm\sqrt{-[(L_{32}+L_{34})+\sigma][(L_{32}+L_{34})-\sigma][(L_{32}-L_{34})+\sigma][(L_{32}-L_{34})-\sigma]}}{2|\sigma|} \end{cases} \tag{4-51}$$

where $\sigma=x_{A35}-x_{B35}$.

The forward problem is difficult and multiple solutions in both problems should be avoided. The direct kinematic problem can be simplified once a rule (e.g., $x_{P3}<x_{A35}<x_{B35}$ and $y_{P3}<y_{C35}$) is predefined. In this case, the direct kinematic solution is unique and computation time are reduced. If all inclined linkages lengths are designed with special relations, the forward problem solution can be further simplified, i.e., these lengths are the same, L_{32}=L_{34}=L_{36}. Combined with the working mode ($x_{P3}<x_{A35}<x_{B35}$, $y_{P3}<y_{C35}$)

selected from the inverse kinematics, the corresponding forward kinematic problem is written as

$$\begin{cases} x_{P3} = 0.5(x_{A35} + x_{B35}) \\ y_{P3} = y_{C35} + 0.5\sigma \\ z_{P3} = \sqrt{L_{32}^{\ 2} - 0.25\sigma^2} \end{cases} \tag{4-52}$$

Under this condition, three inclined angles can be obtained as

$$\begin{cases} \theta_{31} = \tan^{-1}[z_{P3} / (x_{P3} - x_{A35})] \\ \theta_{32} = \theta_{33} = \tan^{-1}[z_{P3} / (x_{A35} - x_{P3})] \end{cases} \tag{4-53}$$

(ii) Singularity configurations

Differential both sides of the constraint equations in Equation (4-49) with respect to time, the velocity relation between three actuators and the mobile platform is obtained

$$\boldsymbol{J}_{Q3}\left[\dot{x}_{A35}, \dot{x}_{B35}, \dot{y}_{C35}\right]^{\mathrm{T}} = \boldsymbol{J}_{X3}\left[\dot{x}_{P3}, \dot{y}_{P3}, \dot{z}_{P3}\right]^{\mathrm{T}} \tag{4-54}$$

where

$$\boldsymbol{J}_{Q3} = diag\left[(x_{P3} - x_{A35}), (x_{P3} - x_{B35}), (y_{P3} - y_{C35})\right]$$

$$\boldsymbol{J}_{X3} = \begin{bmatrix} x_{P3} - x_{A35} & 0 & z_{P3} \\ x_{P3} - x_{B35} & 0 & z_{P3} \\ 0 & y_{P3} - y_{C35} & z_{P3} \end{bmatrix}$$

Thereby the Jacobian matrix is computed as

$$\boldsymbol{J}_3 = \boldsymbol{J}_{Q3}^{-1}\boldsymbol{J}_{X3} \tag{4-55}$$

Based on the velocity Equations (4-54) and (4-55), there are two kinds of singularity configurations.

Type-I singularity happens when $Det(\boldsymbol{J}_{Q3}) = 0$. There are three scenarios. (A) $x_{P3} = x_{A35}$ in the condition of $L_{32} \le L_{34}, L_{36}$, as seen in figure 4-14(a). (B) $x_{P3} = x_{B35}$ if $L_{34} \le L_{32}, L_{36}$, as shown in figure 4-14(b). (C) $y_{P3} = y_{C35}$ under the condition of $L_{36} \le L_{32}, L_{34}$, as

illustrated in figure 4-14(c). In any of these cases, the corresponding branch's inclined linkages are vertical (parallel to *Z* axis) and this limb can bear external force that is parallel to *Z* axis without actuation force. For the current assembly configurations shown in figure 4-13, each situation indicates the upper boundary of the reachable workspace. Moreover, L_{32}=0 or L_{34}=0 or L_{36}=0 can also lead to the above situations, respectively. In this scenario, the whole mechanism loses vertical translation and it is reduced to a planar mechanism.

Type-II singularity occurs when $Det(\boldsymbol{J}_{X3})=0$. (A) $x_{A35}=x_{B35}$ when $L_{32}=L_{34}$. Branch one and branch two coincide completely. It can be further divided into two scenarios, $(x_{A35}=x_{B35}=x_{P3}\,\&\,L_{32}=L_{34}\le L_{36})$ and $(x_{A35}=x_{B35}\neq x_{P3}\,\&\,L_{32}=L_{34})$. In the first case shown in figure 4-14(d), all inclined links of branch one and branch two are vertical. They can both stand external force that is parallel to *Z* axis without driving force. For the latter one listed in figure 4-14(e), the end-effector can still move even all active joints are locked. (B) $y_{P3}=y_{C35}$ if $L_{36}\le L_{32},L_{34}$. It is the same with the third type-I singularity. (C) z_{P3}=0. It demonstrates all moving linkages are trapped in *XOY* plane and the mobile platform loses one DOF. It is composed of two cases, $x_{A35}\neq x_{B35}$ ($x_{A35}<x_{P3}<x_{B35}$ or $x_{A35}>x_{P3}>x_{B35}$, these two cases are similar, only the former case is illustrated) and $x_{A35}=x_{B35}\neq x_{P3}$, as depicted in figure 4-14(f) and figure 4-14(g). All links are constrained in the *XOY* plane and the moving platform gains an uncontrollable movement along *Z* axis under both situations.

The combined singularity occurs when both $Det(\boldsymbol{J}_{Q3})=0$ and $Det(\boldsymbol{J}_{X3})=0$ take place. From the above analysis, there are two situations (A) $(x_{A35}=x_{B35}=x_{P3}\,\&\,L_{32}=L_{34}\le L_{36})$,

as depicted in figure 4-14(d). (B) $y_{P3} = y_{C35}$ if $L_{36} \le L_{32}, L_{34}$, as presented in figure 4-14(c).

By the way, it is worthy noticing that there are two kinds of singularities for each parallelogram module. The first kind of singularity configuration happens when the adjacent links are perpendicular to each other, as happened in figures 4-14 (a-d). The second singularity occurs when opposite rods coincide (in the same straight line), as can be seen in figures 4-14 (f-g). Such singularity configurations discussed above should be avoided in the operational workspace for any industrial application by limiting motion ranges of kinematic pairs and selecting proper links dimensions.

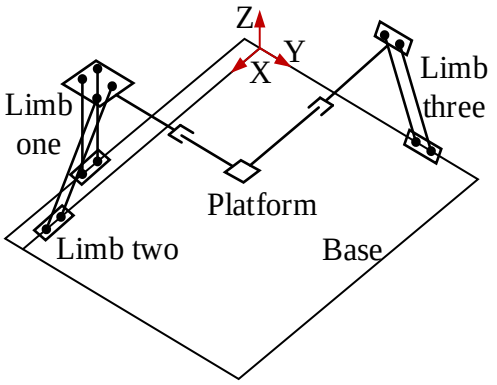

(a)

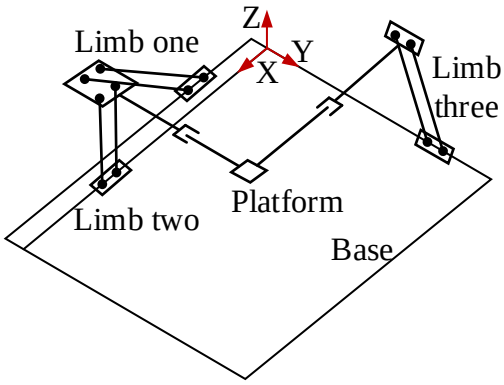

(b)

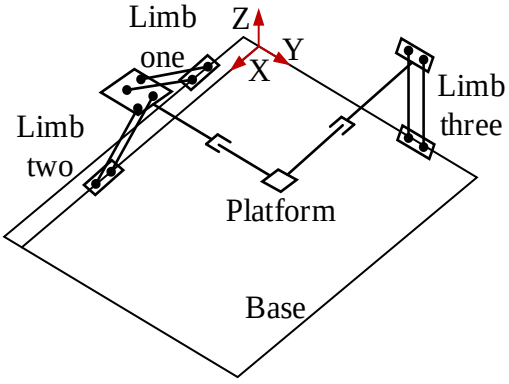

(c)

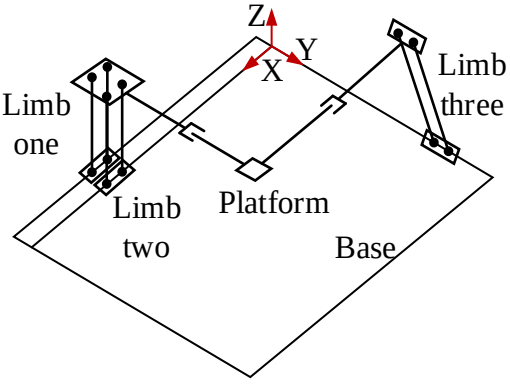

(d)

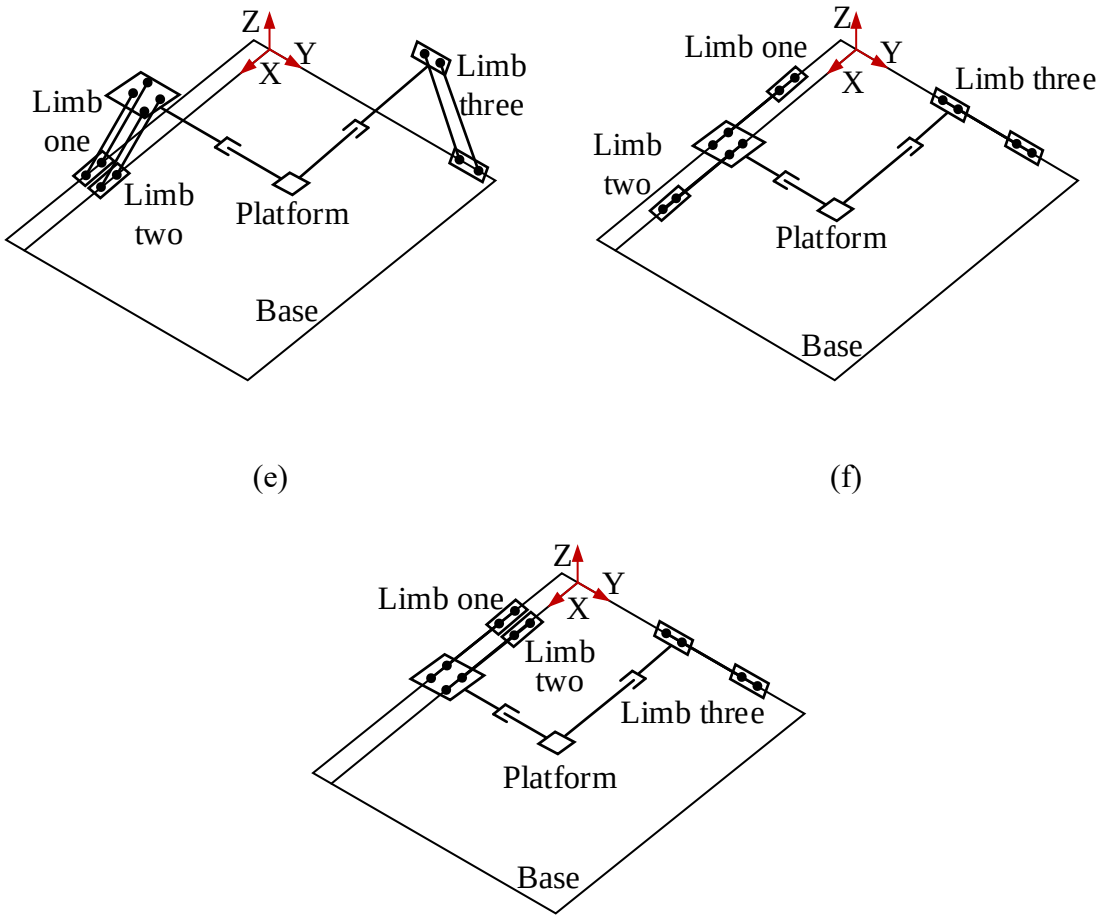

Figure 4-14 Singularity configurations of the 3T parallel robot

(iii) Workspace analysis

To calculate workspace, physically constraints of these joints should be considered. The strokes for three active prismatic joints are constrained as $L_{33} \le x_{A35} \le L_{31} - 4L_{33}$, $4L_{33} \le x_{B35} \le L_{31} - L_{33}$ and $4L_{33} \le y_{C35} \le L_{31} - L_{33}$. Revolute joint generally has a large rotational range. However, they are shrunk when considering singularity avoidance and real assembly condition. $\theta_{31} = [\pi/36, 17\pi/36]$, $\theta_{3i} = [19\pi/36, 35\pi/36]$ (i=2,3). The displacement of any passive prismatic joint is between [L_{38}, L_{31}−L_{38}]. To avoid singularity

configurations, the position of the mobile platform is given as $x_{P3} < x_{A35} < x_{B35}, y_{P3} < y_{C35}$ and $L_{33} \le z_{P3} \le \min(L_{32}, L_{34}, L_{36}) - L_{33}$. The spatial searching algorithm is applied to determine its workspace. Given any possible point, the inverse kinematic solution is employed and it can be regarded feasible if above requirements can be satisfied.

The other active sliders and sloping linkages respectively have the same dimensions to realize a symmetrical architecture and modular design for the parallel manipulator. These parameters are given as: L_{31}=100mm, L_{32}= L_{34}== L_{36}==30mm, L_{33}= L_{35}= L_{37}=5mm and L_{38}=5mm. All the following calculations are based on this set of dimensions. Their reachable workspaces are illustrated in figure 4-15(a). The reachable workspace section along *Z* axis is a rectangle and increases gradually as the height of the mobile platform rises. All sections along *Y* axis are symmetrical. All sections that are parallel to *YOZ* plane are in the shape of right-angled trapezoid due to less constraint along *Y* axis. To further understand the irregular shape of its workspace, five different sections are selected. Figure 4-15(b) presents the plane *X*=50mm and figure 4-15(c) denotes the workspace in plane *Y*=40mm. Three planes along *Z* axis with different heights, *Z*=10mm, *Z*=15mm and *Z*=20 mm are represented in figure 4-15 (d). From figures 4-15(a) and (c), the plane *X*=50mm is the symmetric plane of the workspace. However, the reachable workspace with irregular shape does not fit for real applications. The task workspace is defined as a cuboid within the reachable workspace as denoted in figure 4-15(a).

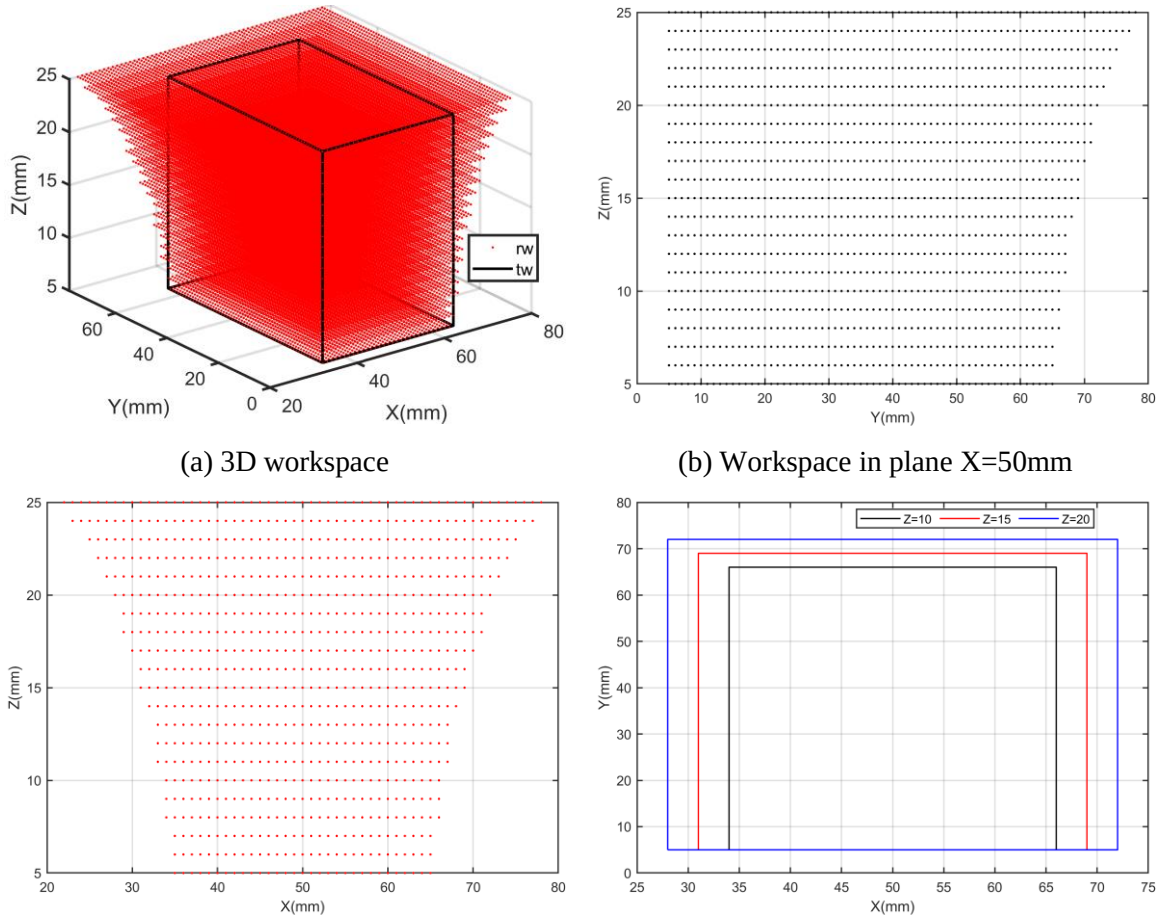

(a) 3D workspace

(b) Workspace in plane X=50mm

(c) Workspace in plane Y=40mm

(d) Workspace in planes Z=10, 15, 20mm

Figure 4-15 Reachable workspaces (rw) and task workspaces (tw)

To understand the parametric effects on workspace, a set of values for each parameter are selected to evaluate and compare the corresponding volumes of task workspace. The reachable workspace utilizes the sum discrete poses as its volume. The operational workspace can be represented by the volume (unit: mm^3) of the cuboid. L_{38} is ignored since end-effector can be fabricated above/below the current platform and it doesn't affect workspace. These ranges of three main parameters are defined as (unit: mm) $75 \le L_{31} \le 125$, $20 \le L_{32} \le 40$ and $3 \le L_{33} \le 10$. The volumes under various dimensions can be seen in figure 4-16. From figure 4-16(a), the both the reachable and task workspace volumes rise as L_{31} increases. From figure 4-16 (b), the volumes for both workspaces

increase at first and then reduces when L_{32} changes from 20mm to 40mm. The turning points for both cases are different, L_{32}=29mm for the reachable workspace and L_{32}=25mm for the task workspace. Figure 4-16(c) illustrates the volumes changes under various L_{33}. Both workspaces are shrunk when a longer L_{33} is employed.

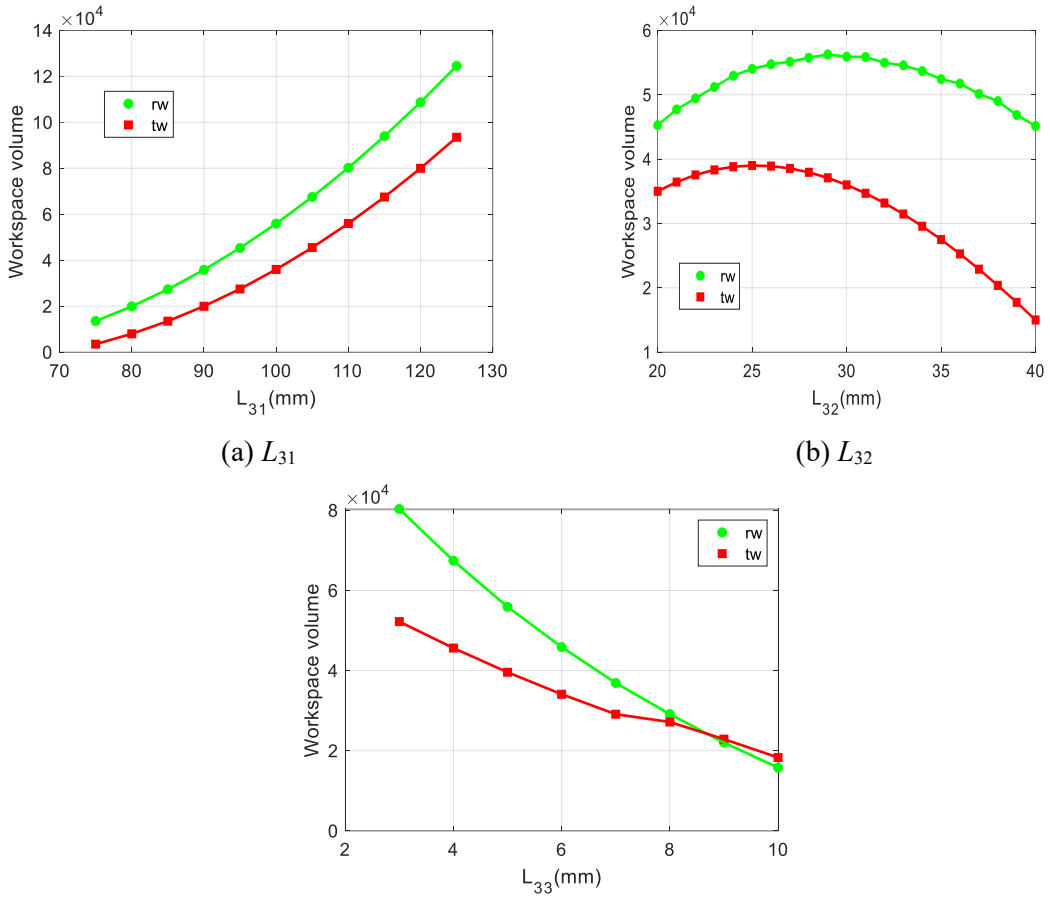

(a) L_{31} (b) L_{32}

(c) L_{33}

Figure 4-16 Parametric effects on reachable and task workspace

(iv) Dexterity analysis

The Local Condition Index of this spatial parallel robot is calculated as the Frobenius norm of its Jacobian matrix, as provided below

$$
\begin{aligned}
LCI &= \sqrt{\left(\frac{z_{P3}}{x_{P3}-x_{A35}}\right)^2+\left(\frac{z_{P3}}{x_{P3}-x_{B35}}\right)^2+\left(\frac{z_{P3}}{y_{P3}-x_{C35}}\right)^2+3} \\
&= \sqrt{\frac{z_{P3}^2}{L_{32}^2-z_{P3}^2}+\frac{z_{P3}^2}{L_{32}^2-z_{P3}^2}+\frac{z_{P3}^2}{L_{32}^2-z_{P3}^2}+3} \\
&= \sqrt{\frac{3L_{32}^2}{L_{32}^2-z_{P3}^2}}
\end{aligned}
\tag{4-56}
$$

In accordance with Equation (4-56), this index is only related to two variables, z_{P3} and L_{32}. The LCI layout with respect to z_{P3} is plotted in figure 4-17(a). The LCI indicator increases as the height of the mobile platform keeps rising. The LCI index has a negative relationship with L_{32}, as displayed in figure 4-17(b). A 3D layout of LCI indicator with respect to both values are shown in figure 4-17(c). The largest LCI index can be found with the highest mobile platform and smallest L_{32} value, while the smallest LCI index is obtained while the mobile platform is lowest and the longest L_{32} value is chosen.

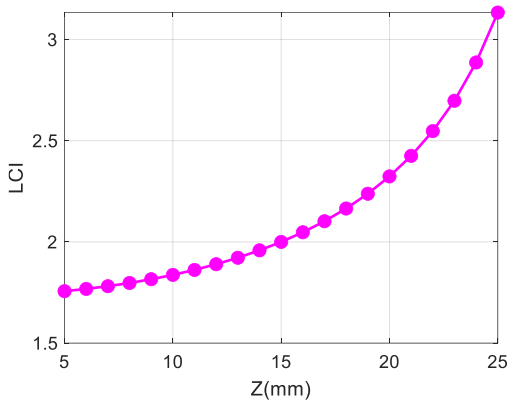

(a) z_{P3}

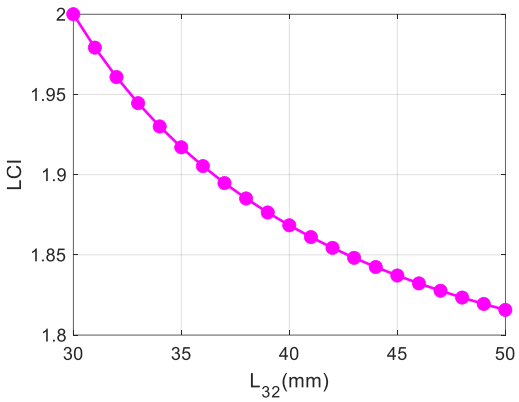

(b) L_{32}

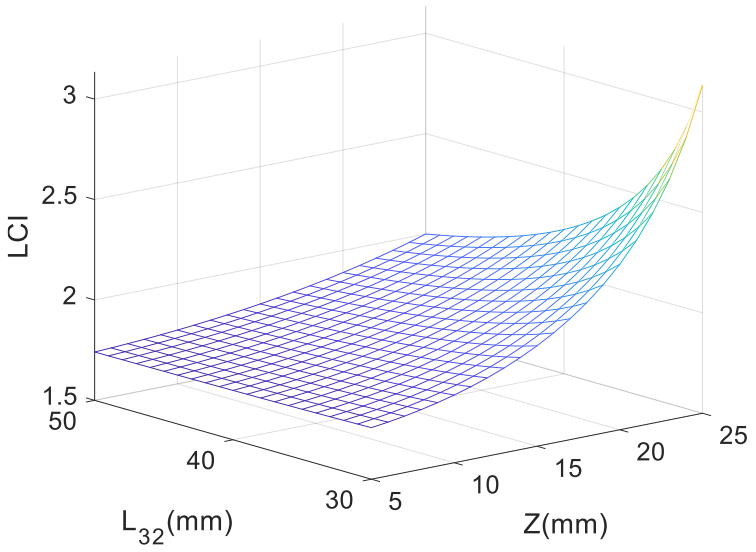

(c) z_{P3} and L_{32}

Figure 4-17 The distribution of the LCI of 3T mechanism

Based on the definition in Equation (4-3), the local level condition index of this spatial parallel robot is computed and its layout is displayed in figure 4-18. The range of this index is from 0.43954 to 0.58314 and it rises as the mobile platform has a higher position along Z direction. The impact from L_{32} is neglected since different L_{32} will lead to the changes of workspace and $\overline{LCI}$.

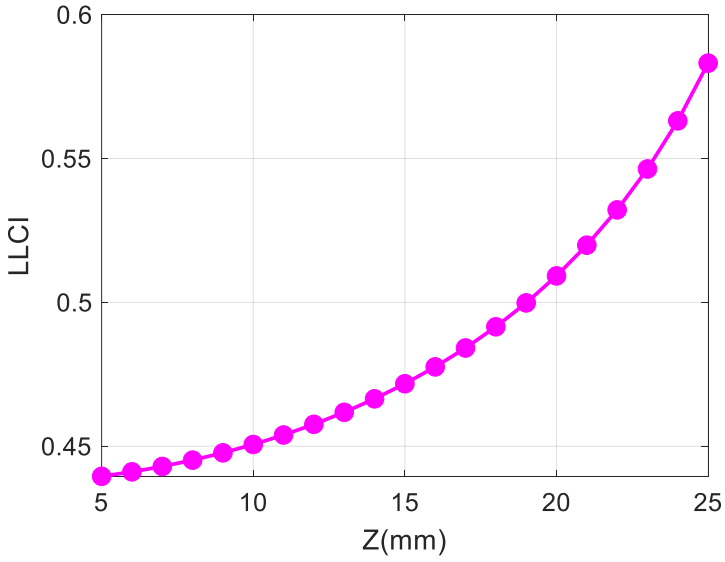

Figure 4-18 The distribution of the LLCI of 3T mechanism

4.5 Case four: 3T1R parallel mechanism

The schematic diagram of this parallel structure is provided in figure 4-19. This parallel robot is composed of four same kinematic limbs with one driving prismatic joint installed on the fixed platform, a parallelogram joint, a passive sliding joint and a rotary joint attached to the mobile platform. The midpoints of links $A_{41}A_{43}$, $A_{42}A_{44}$, $B_{41}B_{43}$, $B_{42}B_{44}$, $C_{41}C_{43}$, $C_{42}C_{44}$, $D_{41}D_{43}$ and $D_{42}D_{44}$ are denoted as A_{45}, A_{46}, B_{45}, B_{46}, C_{45}, C_{46}, D_{45} and D_{46}, respectively.

The length and width of the of fixed platform is L_{41} and L_{411}, respectively. The lengths of the rods $A_{41}A_{42}$ or ($A_{43}A_{44}$) and $A_{41}A_{43}$ or ($A_{42}A_{44}$) are respectively L_{42} and $2L_{43}$. The lengths of the rods $B_{41}B_{42}$ or ($B_{43}B_{44}$) and $B_{41}B_{43}$ or ($B_{42}B_{44}$) are respectively L_{44} and $2L_{45}$. The dimensions of the linkages $C_{41}C_{42}$ or ($C_{43}C_{44}$) and $C_{41}C_{43}$ or ($C_{42}C_{44}$) are respectively L_{46} and $2L_{47}$. The dimensions of the linkages $D_{41}D_{42}$ or ($D_{43}D_{44}$) and $D_{41}D_{43}$ or ($D_{42}D_{44}$) are respectively L_{48} and $2L_{49}$. These four kinematic chains are connected to the mobile platform through A_{47} (or C_{47}), B_{47} and D_{47}. The side length of the mobile platform is denoted as L_{410}. The center point of the mobile platform is P_4. The angles between the positive X axis and linkages $A_{41}A_{42}$, $B_{41}B_{42}$ are θ_{41} and θ_{42}, respectively. The angles between the negative Z axis and linkages $C_{41}C_{42}$, $D_{41}D_{42}$ are θ_{43} and θ_{44}, respectively. The angle between the moving platform and positive Y axis is φ_{41}.

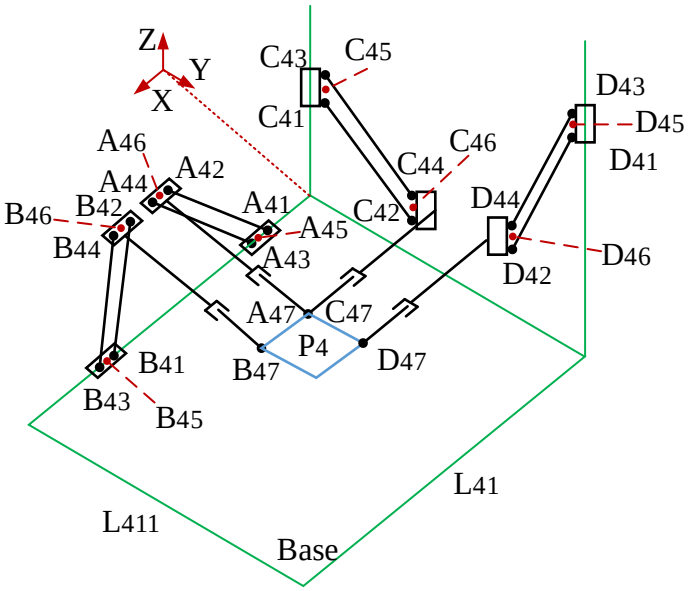

Figure 4-19 Schematic diagram of the 3T1R mechanism

(i) Kinematic models

The coordinate system is also generated as a reference as seen in figure 4-19. The position and orientation of this mobile platform is $\boldsymbol{X}_4=[x_{P4},y_{P4},z_{P4},\varphi_{41}]^{\mathrm{T}}$. The inputs of this parallel robot are four driving prismatic joints, $\boldsymbol{Q}_4=[x_{A45},x_{B45},z_{C45},z_{D45}]^{\mathrm{T}}$. The constant linkage length serves as the main source to calculate the kinematic model. For the first kinematic chain, the following expressions can be obtained

$$\boldsymbol{OA}_{45}+\boldsymbol{A}_{45}\boldsymbol{A}_{46}+\boldsymbol{A}_{46}\boldsymbol{A}_{46}+\boldsymbol{A}_{47}\boldsymbol{P}_4=\boldsymbol{OP}_4 \tag{4-57}$$

$$\boldsymbol{OB}_{45}+\boldsymbol{B}_{45}\boldsymbol{B}_{46}+\boldsymbol{B}_{46}\boldsymbol{B}_{46}+\boldsymbol{B}_{47}\boldsymbol{P}_4=\boldsymbol{OP}_4 \tag{4-58}$$

Equations (4-57) and (4-58) are both projected on the *X* and *Z* axes

$$\begin{cases} x_{A45}+L_{42}\cos\theta_{41}+0.5L_{410}=x_{P4} \\ L_{42}\sin\theta_{41}+0.5L_{410}\sin\varphi_{41}=z_{P4} \end{cases} \tag{4-59}$$

$$\begin{cases} x_{B45}+L_{42}\cos\theta_{42}-0.5L_{410}=x_{P4} \\ L_{44}\sin\theta_{42}+0.5L_{410}\sin\varphi_{41}=z_{P4} \end{cases} \tag{4-60}$$

The sloping angles (θ_{41} and θ_{42}) are moved in one side of the equations.

$$\begin{cases} L_{42}\cos\theta_{41}=x_{P4}-0.5L_{410}-x_{A45} \\ L_{42}\sin\theta_{41}=z_{P4}-0.5L_{410}\sin\varphi_{41} \end{cases} \tag{4-61}$$

$$\begin{cases} L_{44}\cos\theta_{42} = x_{P4} + 0.5L_{410} - x_{B45} \\ L_{44}\sin\theta_{42} = z_{P4} - 0.5L_{410}\sin\varphi_{41} \end{cases} \tag{4-62}$$

Combining two expressions in Equations (4-61) and (4-62) yields constraint condition, as follows

$$\Gamma_{41} : (x_{P4} - 0.5L_{410} - x_{A45})^2 + (z_{P4} - 0.5L_{410}\sin\varphi_{41})^2 - L_{42}^2 = 0 \tag{4-63}$$

$$\Gamma_{42} : (x_{P4} + 0.5L_{410} - x_{B45})^2 + (z_{P4} - 0.5L_{410}\sin\varphi_{41})^2 - L_{42}^2 = 0 \tag{4-64}$$

Then the positions of the actuation linkages can be computed

$$x_{A45} = x_{P4} - 0.5L_{410} \pm \sqrt{L_{42}^2 - (z_{P4} - 0.5L_{410}\sin\varphi_{41})^2} \tag{4-65}$$

$$x_{B45} = x_{P4} + 0.5L_{410} \pm \sqrt{L_{44}^2 - (z_{P4} - 0.5L_{410}\sin\varphi_{41})^2} \tag{4-66}$$

In a similar approach, the vector-loop equations for the remaining kinematic branches are provided as

$$\boldsymbol{OC}_{45} + \boldsymbol{C}_{45}\boldsymbol{C}_{46} + \boldsymbol{C}_{46}\boldsymbol{C}_{46} + \boldsymbol{C}_{47}\boldsymbol{P}_4 = \boldsymbol{OP}_4 \tag{4-67}$$

$$\boldsymbol{OD}_{45} + \boldsymbol{D}_{45}\boldsymbol{D}_{46} + \boldsymbol{D}_{46}\boldsymbol{D}_{46} + \boldsymbol{D}_{47}\boldsymbol{P}_4 = \boldsymbol{OP}_4 \tag{4-68}$$

Both Equations (4-67) and (4-68) can be split into two orthogonal directions, as

$$\begin{cases} L_{46}\sin\theta_{43} + 0.5L_{410}\cos\varphi_{41} = y_{P4} \\ z_{C45} + L_{46}\cos\theta_{43} + 0.5L_{410}\sin\varphi_{41} = z_{P4} \end{cases} \tag{4-69}$$

$$\begin{cases} L_{411} - L_{48}\sin\theta_{44} - 0.5L_{410}\cos\varphi_{41} = y_{P4} \\ z_{D45} + L_{48}\cos\theta_{48} - 0.5L_{410}\sin\varphi_{41} = z_{P4} \end{cases} \tag{4-70}$$

The unknow angles (θ_{43} and θ_{44}) are set in one side of equations. Equations (4-69) and (4-70) can be rearranged as

$$\begin{cases} L_{46}\sin\theta_{43} = y_{P4} - 0.5L_{410}\cos\varphi_{41} \\ L_{46}\cos\theta_{43} = z_{P4} - 0.5L_{410}\sin\varphi_{41} - z_{C45} \end{cases} \tag{4-71}$$

$$\begin{cases} -L_{48}\sin\theta_{44} = y_{P4} + 0.5L_{410}\cos\varphi_{41} - L_{411} \\ L_{48}\cos\theta_{48} = z_{P4} + 0.5L_{410}\sin\varphi_{41} - z_{D45} \end{cases} \tag{4-72}$$

The constraint equations for the remaining two kinematic legs are formulated as

$$\Gamma_{43} : (y_{P4} - 0.5L_{410}\cos\varphi_{41})^2 + (z_{P4} - 0.5L_{410}\sin\varphi_{41} - z_{C45})^2 - L_{46}^2 = 0 \tag{4-73}$$

$$\Gamma_{44} : (y_{P4} + 0.5L_{410}\cos\varphi_{41} - L_{411})^2 + (z_{P4} + 0.5L_{410}\sin\varphi_{41} - z_{D45})^2 - L_{48}^2 = 0 \tag{4-74}$$

Based on Equations (4-73) and (4-74), the positions of the driving linkages $C_{41}C_{43}$ and $D_{41}D_{43}$ are derived as

$$z_{C45} = z_{P4} - 0.5L_{410}\sin\varphi_{41} \pm \sqrt{L_{46}^2 - (y_{P4} - 0.5L_{410}\cos\varphi_{41})^2} \tag{4-75}$$

$$z_{D45} = z_{P4} + 0.5L_{410}\sin\varphi_{41} \pm \sqrt{L_{48}^2 - (y_{P4} + 0.5L_{410}\cos\varphi_{41} - L_{411})^2} \tag{4-76}$$

Equations (4-65), (4-66), (4-75) and (4-76) provide the solutions for the inverse kinematic mathematical model of this parallel structure.

To obtain the forward kinematic solution, combining Equations (4-63) and (4-64) leads to

$$x_{P4} = \frac{L_{44}^2 - (0.5L_{410} - x_{B45})^2 - L_{42}^2 + (0.5L_{410} + x_{A45})^2}{2(L_{410} + x_{A45} - x_{B45})} \tag{4-77}$$

Employing Equation (4-77) in Equation (4-61), the sloping angle of the first kinematic chain can be described as

$$\theta_{41} = \arccos\frac{x_{P4} - 0.5L_{410} - x_{A45}}{L_{42}} \tag{4-78}$$

Hence, z_{P4} can be computed based on the second expression of Equation (4-59). Then solving Equation (4-73) leads to

$$y_{P4} = 0.5L_{410}\cos\varphi_{41} \pm \sqrt{L_{46}^2 - (L_{42}\sin\theta_{41} - z_{C45})^2} \tag{4-79}$$

z_{P4} and y_{P4} are substituted in Equation (4-74). The following expression can be resolved

$$L_{410}^2 + (L_{42}\sin\theta_{41} - z_{D45})^2 + 2L_{410}\sin\varphi_{41}(L_{42}\sin\theta_{41} - z_{D45}) + [\pm\sqrt{L_{46}^2 - (L_{42}\sin\theta_{41} - z_{C45})^2} - L_{411}]^2$$
$$+2L_{410}\cos\varphi_{41}[\pm\sqrt{L_{46}^2 - (L_{42}\sin\theta_{41} - z_{C45})^2} - L_{411}] - L_{48}^2 = 0 \tag{4-80}$$

Equation (4-80) can be rewritten as the following form

$$E_1\sin\varphi_{41} + E_2\cos\varphi_{41} + E_3 = 0 \tag{4-81}$$

where

$$E_1 = 2L_{410}(L_{42}\sin\theta_{41} - z_{D45})$$

$$E_2 = 2L_{410}[\pm\sqrt{L_{46}^2 - (L_{42}\sin\theta_{41} - z_{C45})^2} - L_{411}]$$

$$E_3 = L_{410}^2 + (L_{42}\sin\theta_{41} - z_{D45})^2 + [\pm\sqrt{L_{46}^2 - (L_{42}\sin\theta_{41} - z_{C45})^2} - L_{411}]^2 - L_{48}^2$$

Another angle is defined as $T_1 = \tan(\varphi_{41}/2)$. Equation (4-81) can be established utilizing T_1

$$(E_3 - E_2)T_1^2 + 2E_1T_1 + (E_2 + E_3) = 0 \tag{4-82}$$

The orientation of the mobile platform φ_{41} is then solved from Equation (4-82)

$$\varphi_{41} = 2\arctan\left[(-E_1 \pm \sqrt{E_1^2 + E_2^2 - E_3^2})/(E_3 - E_2)\right] \tag{4-83}$$

Equation (4-83) is substituted in Equations (4-61) to resolve z_{P4} and Equation (4-79) to generate y_{P4}.

(ii) Singularity configurations

Differentiating both sides of the constraint equations (4-63), (4-64), (4-73) and (4-74) with respect to time, the velocity relation between two actuators and the mobile platform can be arranged

$$\boldsymbol{J}_{Q4}[\dot{x}_{A45}, \dot{x}_{B45}, \dot{z}_{C45}, \dot{z}_{D45}]^{\mathrm{T}} = \boldsymbol{J}_{X4}[\dot{x}_{P1}, \dot{y}_{P1}, \dot{z}_{P4}, \dot{\varphi}_{41}]^{\mathrm{T}} \tag{4-84}$$

where

$$\boldsymbol{J}_{Q4} = \begin{bmatrix} M_{41} & 0 & 0 & 0 \\ 0 & M_{43} & 0 & 0 \\ 0 & 0 & M_{46} & 0 \\ 0 & 0 & 0 & M_{48} \end{bmatrix}$$

$$\boldsymbol{J}_{X4} = \begin{bmatrix} M_{41} & 0 & M_{42} & -0.5L_{410}\cos\varphi_{41}M_{42} \\ M_{43} & 0 & M_{44} & -0.5L_{410}\cos\varphi_{41}M_{44} \\ 0 & M_{45} & M_{46} & 0.5L_{410}(\sin\varphi_{41}M_{45} - \cos\varphi_{41}M_{46}) \\ 0 & M_{47} & M_{48} & 0.5L_{410}(\sin\varphi_{41}M_{47} + \cos\varphi_{41}M_{48}) \end{bmatrix}$$

$$M_{41} = x_{P4} - 0.5L_{410} - x_{A45}$$

$$M_{42} = z_{P4} - 0.5L_{410}\sin\varphi_{41}$$

$$M_{43} = x_{P4} + 0.5L_{410} - x_{B45}$$

$$M_{44} = z_{P4} - 0.5L_{410}\sin\varphi_{41}$$

$$M_{45} = y_{P4} - 0.5L_{410}\cos\varphi_{41}$$

$M_{46} = z_{P4} - 0.5L_{410}\sin\varphi_{41} - z_{C45}$

$M_{47} = y_{P4} + 0.5L_{410}\cos\varphi_{41} - L_{411}$

$M_{48} = z_{P4} + 0.5L_{410}\sin\varphi_{41} - z_{D45}$

The Jacobian matrix of this parallel structure is formulated as

$$\boldsymbol{J}_4 = \boldsymbol{J}_{Q4}^{-1}\boldsymbol{J}_{X4} \tag{4-85}$$

There are generally three kinds of singularity configurations based on Equation (4-84).

(A) Type-I singularity happens when $Det(\boldsymbol{J}_{Q4}) = 0$. There are four different cases, $x_{P4} = x_{A45} + 0.5L_{410}$, $x_{P4} = x_{B45} - 0.5L_{410}$, $z_{P4} = 0.5L_{410}\sin\varphi_{41} + z_{C45}$ and $z_{P4} = z_{D45} - 0.5L_{410}\sin\varphi_{41}$. These four cases correspond to $L_{4i}\cos\theta_{4j} = 0$ (j=1, 2, 3, 4. i=2j). This expression can be further derived as $L_{4i} = 0$ or $\theta_{4i} = \pi/2$ (θ_{4i} ranges from 0 to π). When the inclined angle is set as this value, the mobile platform can bear the external force along *Z* direction without any driving force.

(B) Type-II singularity occurs when $Det(\boldsymbol{J}_{X4}) = 0$. The first case is $L_{410} = 0$. The moving platform is degenerated as a point in 3D space under this situation. The second case is $x_{A45} = x_{B45} - L_{410}$, which means $L_{42}\sin\theta_{41} = L_{42}$ & $L_{44}\sin\theta_{42} = L_{44}$. It includes $L_{42} = L_{44} = 0$ or $\theta_{41} = \theta_{42} = \pi/2$. The third case shows $y_{P4} = 0.5L_{410}\cos\varphi_{41}$. It denotes $L_{46}\sin\theta_{43} = 0$ and $L_{411} - L_{48}\sin\theta_{44} = L_{410}$. The fourth case indicates $z_{D45} = z_{P4} + 0.5L_{410}\sin\varphi_{41}$, which means $L_{48}\sin\theta_{44} = L_{48}$. It will happen when $L_{48} = 0$ or $\theta_{44} = \pi/2$. The fifth case is $z_{P4} = 0.5L_{410}\sin\varphi_{41}$. Its means $z_{C45} + L_{46}\cos\theta_{43} = 0$ & $z_{D45} + L_{48}\cos\theta_{48} = L_{410}\sin\varphi_{41}$. The last case is $\cos\varphi_{41} = 0$. It indicates $\varphi_{41} = \pm\pi/2$.

(C) The combined singularity happens when both type-I and type-II scenarios happen. There are in total sixteen cases when $Det(\boldsymbol{J}_{Q4}) = 0 \,\&\, Det(\boldsymbol{J}_{X4}) = 0$. The first case happens when $z_{D45} = z_{P4} + 0.5L_{410}\sin\varphi_{41}$, which is already stated in the above analysis. The second case is $x_{P4} = x_{A45}$ & $L_{410} = 0$, which indicates $L_{42} = 0$ or $\theta_{41} = \pi/2$. The third case is

$x_{P4} = x_{A45} + 0.5L_{410}$ & $x_{B45} = x_{A45} + L_{410}$. This case means $L_{42} = L_{44} = 0$ or $\theta_{41} = \theta_{42} = \pi/2$. The fourth case is $x_{P4} = x_{A45} + 0.5L_{410}$ & $y_{P4} = 0.5L_{410}\cos\varphi_{41}$. It implies $L_{42}\sin\theta_{41} = L_{42}$ and $L_{46}\sin\theta_{43} = 0$. The fifth case occurs when $x_{P4} = x_{A45} + 0.5L_{410}$ & $z_{P4} = 0.5L_{410}\sin\varphi_{41}$. It further means $L_{42}\sin\theta_{41} = L_{42}$ & $z_{C45} + L_{46}\cos\theta_{43} = 0$ & $z_{D45} + L_{48}\cos\theta_{48} = L_{410}\sin\varphi_{41}$. The sixth case takes place while $x_{P4} = x_{A45} + 0.5L_{410}$ & $\cos\varphi_{41} = 0$. It indicates $L_{42}\sin\theta_{41} = L_{42}$ and $\varphi_{41} = \pm\pi/2$. The seventh case happens when $x_{P4} = x_{B45}$ & $L_{410} = 0$. This expression $L_{44}\cos\theta_{42} = 0$ can be further generated based on this case. The eighth case will occur as $x_{P4} = x_{B45} - 0.5L_{410}$ & $x_{A45} = x_{B45} - L_{410}$. This case means $L_{42}\sin\theta_{41} = L_{42}$ & $L_{44}\sin\theta_{42} = L_{44}$. The ninth case displays $x_{P4} = x_{B45} - 0.5L_{410}$ & $y_{P4} = 0.5L_{410}\cos\varphi_{41}$. This case indicates $L_{44}\cos\theta_{42} = 0$ & $L_{46}\sin\theta_{43} = 0$ & $L_{411} - L_{48}\sin\theta_{44} = L_{410}$. The tenth case presents $x_{P4} = x_{B45} - 0.5L_{410}$ & $z_{P4} = 0.5L_{410}\sin\varphi_{41}$. This case can be further explained as $L_{44}\cos\theta_{42} = 0$ & $z_{C45} + L_{46}\cos\theta_{43} = 0$ & $z_{D45} + L_{48}\cos\theta_{48} = L_{410}\sin\varphi_{41}$. The eleventh case displays that $x_{P4} = x_{B45} - 0.5L_{410}$ & $\cos\varphi_{41} = 0$. It can also be understood as $L_{44}\cos\theta_{42} = 0$ and $\varphi_{41} = \pm\pi/2$. The twelfth case happens when $z_{C45} = 0$ & $z_{P4} = 0.5L_{410}\sin\varphi_{41}$. It has another meaning that $z_{C45} = 0$ & $L_{46}\cos\theta_{43} = 0$ & $z_{D45} + L_{48}\cos\theta_{48} = L_{410}\sin\varphi_{41}$. The thirteenth case will occur while $z_{C45} = z_{P4}$ & $L_{410} = 0$. It can be further expressed as $L_{46}\cos\theta_{43} = 0$ and $L_{410} = 0$. The fourteenth case takes place as $z_{C45} = z_{P4} - 0.5L_{410}\sin\varphi_{41}$ & $x_{A45} = x_{B45} - L_{410}$. The other information can also be deduced, $L_{46}\cos\theta_{43} = 0$ and $L_{42}\sin\theta_{41} = L_{42}$ and $L_{44}\sin\theta_{42} = L_{44}$. The fifteenth scenario will arise when $z_{C45} = z_{P4} - 0.5L_{410}\sin\varphi_{41}$ & $y_{P4} = 0.5L_{410}\cos\varphi_{41}$. This case implies that $L_{46}\cos\theta_{43} = 0$ and $L_{46}\sin\theta_{43} = 0$ and $L_{411} - L_{48}\sin\theta_{44} = L_{410}$. The last case shows that $z_{C45} = z_{P4} - 0.5L_{410}\sin\varphi_{41}$ & $\cos\varphi_{41} = 0$. It also demonstrates $L_{46}\cos\theta_{43} = 0$ and $\varphi_{41} = \pm\pi/2$.

(iii) Workspace analysis

The corresponding same rods in all four branches own the identical dimensions. These symmetric linkage parameters are provided in the following analysis. L_{41}=400mm, L_{42}= L_{44}= L_{46}= L_{48}=120mm, L_{43}= L_{45}= L_{47}= L_{49}= 20mm, L_{410}=40mm. L_{411}=200mm. L_{412}=250mm. The positions constraints of all kinematic pairs should be taken into account in order to calculate workspace of the moving platform. Considering the current configuration and the singularities listed above, the strokes for two driving prismatic joints of the first two branches are limited as $L_{43} \le x_{A45} \le L_{41} - L_{43}$, $L_{43} \le x_{B45} \le L_{41} - L_{43}$ and $x_{B45} > x_{P4} > x_{A45}$. The strokes for the remaining active prismatic joints are listed as $L_{43} \le z_{C45}, z_{D45} \le L_{412} - L_{43}$ and $z_{C45}, z_{D45} > z_{P4}$. The rang of motion for θ_{41} and θ_{4i} (i=2,3,4) are defined as $\pi/36 < \theta_{41} < 17\pi/36$ and $19\pi/36 < \theta_{4i} < 35\pi/36$, respectively. The orientation φ_{41} of the mobile platform is also limited as $-\pi/2 < \varphi_{41} < \pi/2$. Given any possible point, the inverse kinematic model is employed. The symbol $\pm$ in Equations (4-65), (4-66), (4-75) and (4-76) are separately selected as −, +, + and +. Any pose in workspace that can meet all the above criteria will be collected within reachable workspace. The reachable workspace of this 4-DOF parallel robot is illustrated as in figure 4-20. Since its three translations and one rotation, there are four subplots in figure 4-20 where each one is composed of three components. These four plots in figure 4-20 are complicated. The symmetrical plane for figures 4-20 (a-c) is plane x_{P4}=200mm.

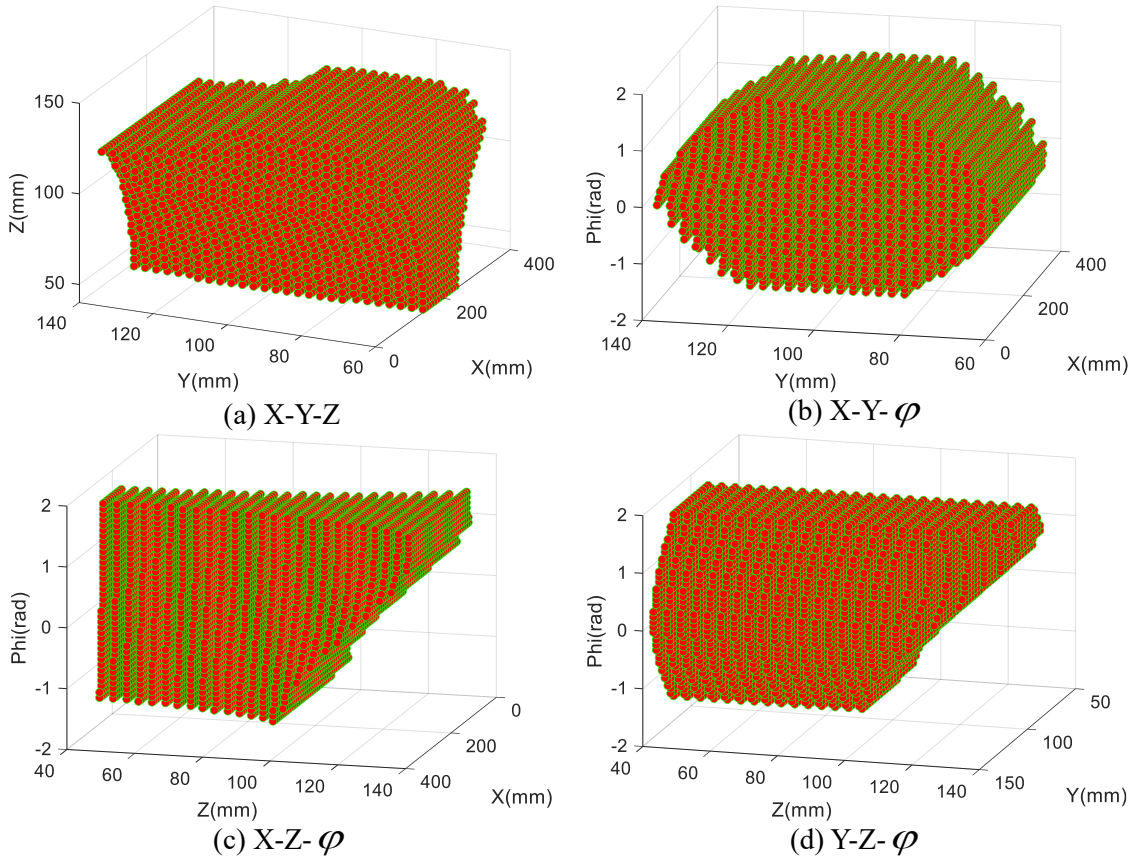

(a) X-Y-Z (b) X-Y-φ

(c) X-Z-φ (d) Y-Z-φ

Figure 4-20 Reachable workspace of the 4-DOF parallel robot

A set of values for each linkage length is chosen to evaluate and compare the corresponding workspace volume. The reachable workspace impacts originated from linkages dimensions are provided in figure 4-21.

The workspace volume and L_{41} are in positive relationship as seen in figure 4-21(a). The workspace volume and L_{41} are in positive relationship. From figure 4-21 (b), the workspace volume shows an upward trend until L_{41} is 124mm, the performance becomes oscillates (improve or reduce) as L_{41} continue to extend. Based on figure 4-21(c), the relation between workspace volume and L_{43} is negative relationship. The performance is reduced as L_{43} increases from 10mm to 30mm. As seen from figure 4-21 (d), the workspace index coming from L_{410} is complicated. The index oscillates as L_{43} changes from 30mm to 50mm. However, the overall workspace trend is downward when a longer L_{4e} is chosen in the pre-set range. The workspace influence from L_{411} is similar to that of L_{43}, the workspace volume is shrunk as L_{411} extends from 180mm to 220mm, as displayed in figure 4-21 (e). The workspace impact from length L_{412} is different, the workspace is improved as the length changes from 230mm to 270mm but the increasement rate is reducing in the overall process.

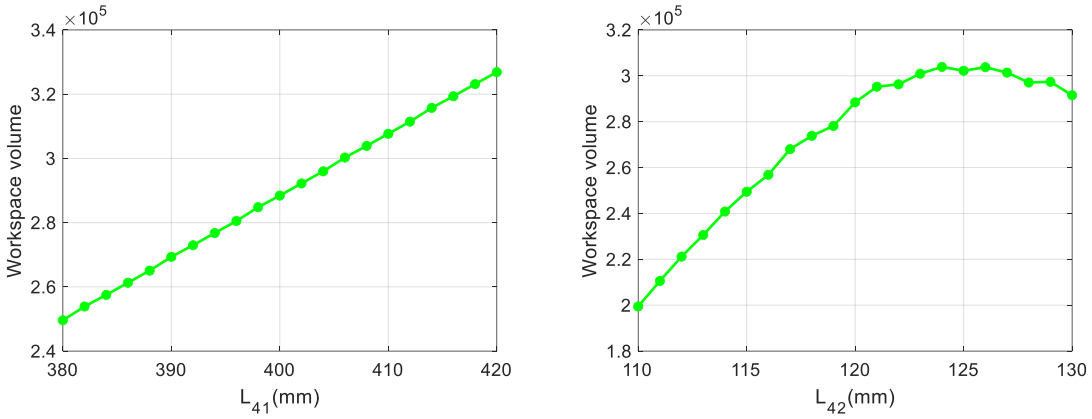

(a) L_{41}

(b) L_{42}

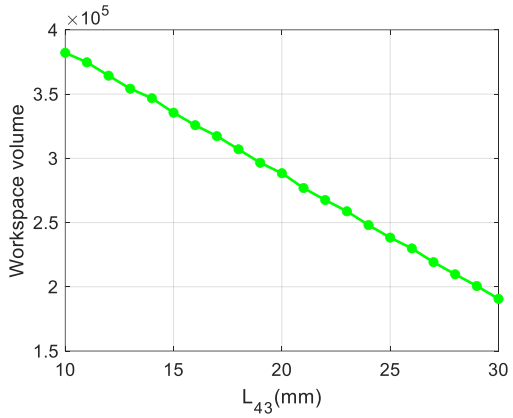

(c) L_{43}

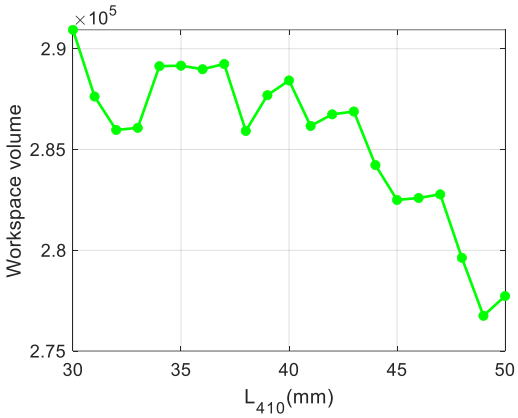

(d) L_{410}

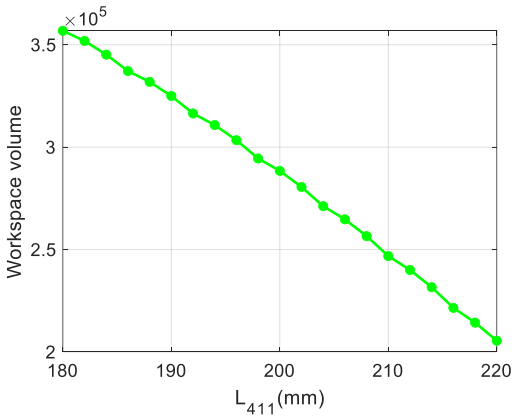

(e) L_{411}

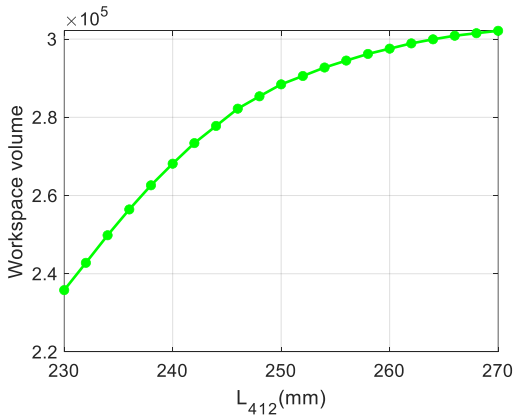

(f) L_{412}

Figure 4-21 Linkages' impacts on the reachable workspace of the 4-DOF robot

(iv) Dexterity analysis

The local condition Index of this spatial parallel robot is calculated as

$$LCI = \left\| \boldsymbol{J}_4 \right\|_f \left\| \boldsymbol{J}_4^{-1} \right\|_f \tag{4-86}$$

Considering the has translational and rotational movements of this parallel structure, Equation (4-85) is divided into the sum of two terms

$$\dot{\boldsymbol{Q}}_4 = \boldsymbol{J}_{4V}[\dot{x}_{P4}, \dot{y}_{P4}, \dot{z}_{P4}]^{\mathrm{T}} + \boldsymbol{J}_{4W}[\dot{\varphi}_{41}]^{\mathrm{T}} \tag{4-87}$$

where $\boldsymbol{J}_{4V}$ and $\boldsymbol{J}_{4W}$ own respectively the first three columns and the last column of the Jacobian matrix $\boldsymbol{J}_4$.

Based on the definitions shown in Equation (4-4), the local translational condition index and the local rotational condition index for this 3T1R parallel robot are generated respectively as

$$\begin{cases} \mathrm{LTCI} = LCI(\boldsymbol{J}_V) = \left\|\boldsymbol{J}_{4V}\right\|_f \left\|\boldsymbol{J}_{4V}^{-1}\right\|_f \\ \mathrm{LRCI} = LCI(\boldsymbol{J}_W) = \left\|\boldsymbol{J}_{4W}\right\|_f \left\|\boldsymbol{J}_{4W}^{-1}\right\|_f \end{cases} \tag{4-88}$$

According to Equation (4-88), the LTCI index is obtained and this indicator is not related to x_{P4} of the mobile platform. The LTCI index with respect to y_{P4}, z_{P4} and φ_{41} is illustrated in figures 4-22 (a-c). The expressions $\varphi_{41} = 0$, $z_{P4} = 80mm$ and $y_{P4} = 100mm$ are employed separately in these three figures. The constant parameter $x_{P4} = 200mm$ is utilized for them since different values of this variable will not affect this performance.

From figure 4-22 (a), the performance has a symmetrical layout about plane $y_{P4} = 100mm$. This performance will gradually grow as y_{P4} is away from this plane. This performance and z_{P4} shows positive trend with a constant predefined y_{P4} value. As seen in figure 4-22 (b), this layout is not asymmetric. The smallest performance happens when $y_{P4} = 100mm$ & $\varphi_{41} = 0$. The performance improves as these two values is far from this pose. The LTCI impact from z_{P4} and φ_{41} is denoted in figure 4-22 (c). The workspace starts to reduce as the mobile platform reaches 100mm. With a constant orientation angle, this performance has an upward trend as the mobile platform is higher. With a predefined moving platform height, the highest LTCI is higher when the orientation angle stays away from 0 and the smallest performance is realized when $\varphi_{41} = 0$.

The same parameters are utilized in figures 4-22 (d-f). From figure 4-22 (d), the LRCI index is not associated with y_{P4}. This index gradually increases as the moving platform is higher. The LRCI index distribution is complicated in figure 4-22 (e), the smallest value takes place but not in the pose $y_{P4}=100mm$ & $\varphi_{41}=0$. The values on four corners are higher than other places. According to figure 4-22 (f), the LRCI layout is complex. The minimal value with a constant z_{P4} does not always happen when $\varphi_{41}=0$. This plot also indicates the workspace is reducing as the mobile platform is higher than 100mm.

The maximal and minimal LTCI values are separately 17.78 and 2.5943. The highest and lowest LRCI indicators are 297.07 and 10.643, respectively. The average values for them are 4.3077 and 56.24, respectively.

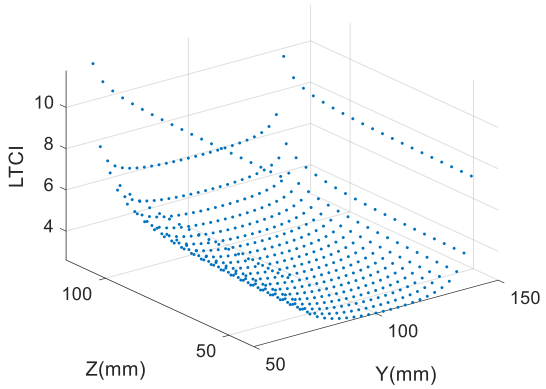

(a) y_{P4} and z_{P4}

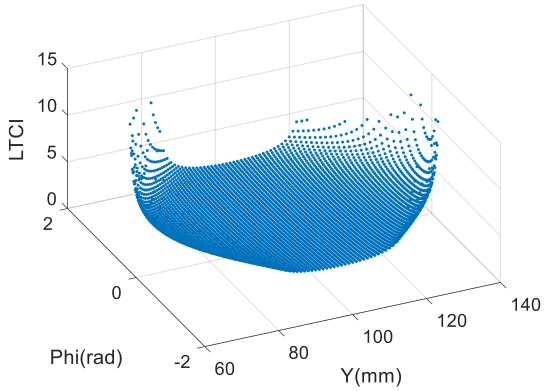

(b) y_{P4} and φ_{41}

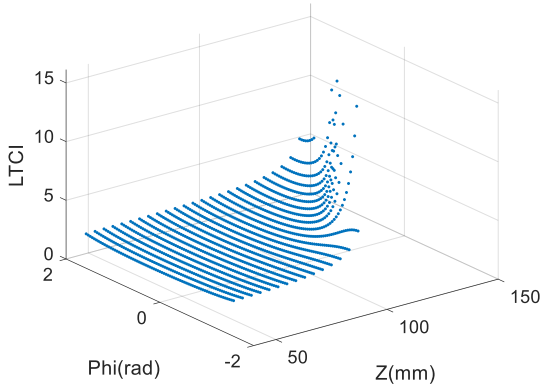

(c) z_{P4} and φ_{41}

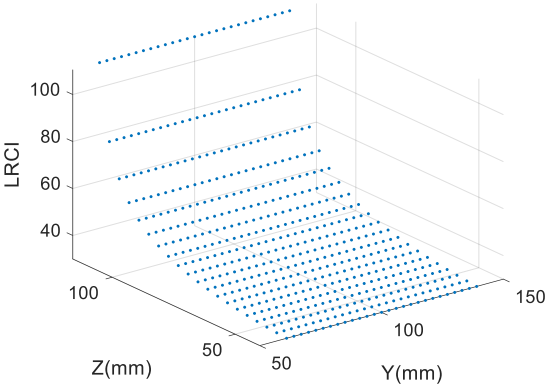

(d) y_{P4} and z_{P4}

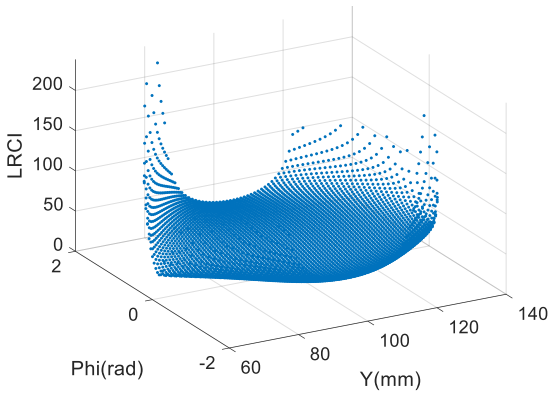

(e) y_{P4} and φ_{41}

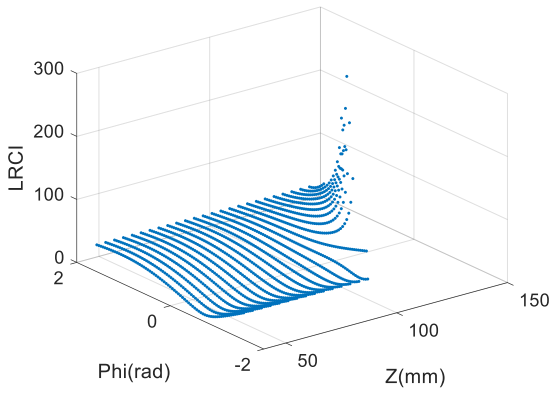

(f) z_{P4} and φ_{41}

Figure 4-22 LTCI and LRCI Distributions of the 4-DOF robot

On the basis of the level index concept, the figures 4-23 (a-f) correspond to figures 4-22 (a-f). The LTLCI or LRLCI layout is identical to that of the related plot in figure 4-22. The only difference is the scales in figure 4-23 are smaller and range from zero to one.

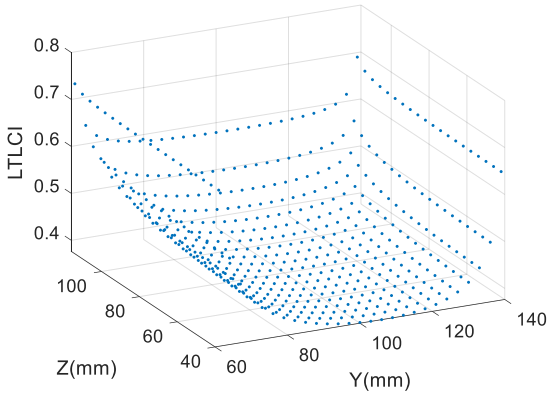

(a) y_{P4} and z_{P4}

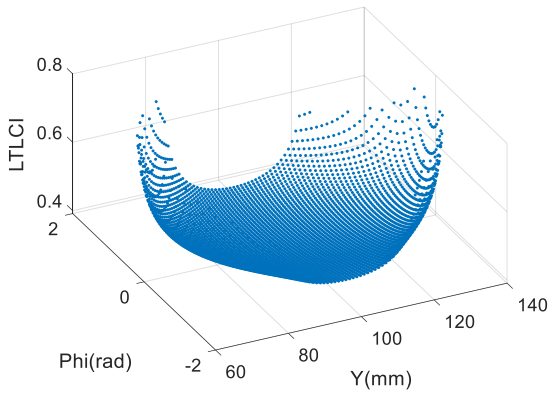

(b) y_{P4} and φ_{41}

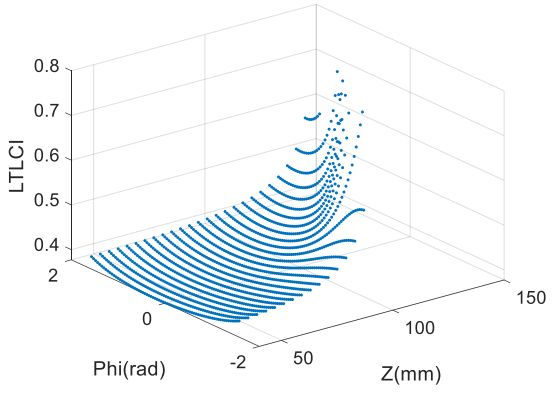

(c) z_{P4} and φ_{41}

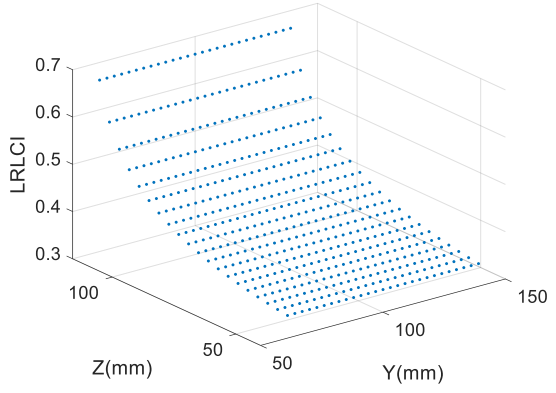

(d) y_{P4} and z_{P4}

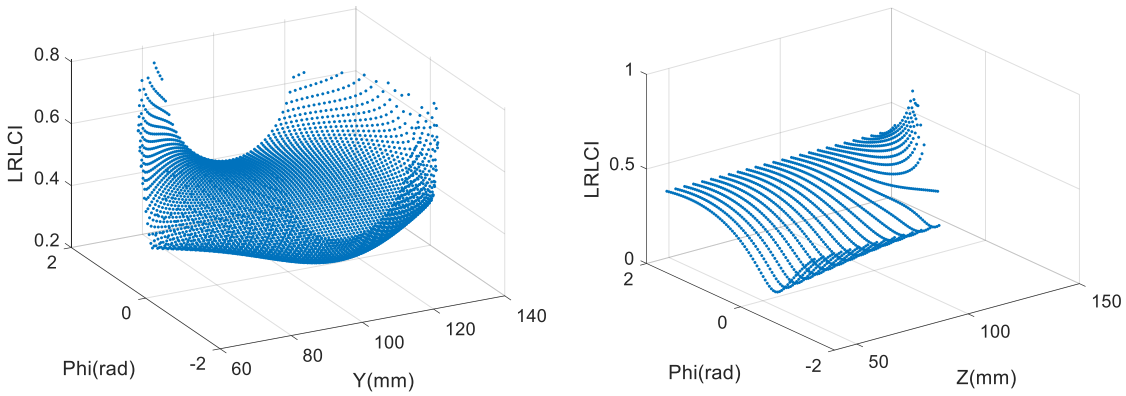

(e) y_{P4} and φ_{41} (f) z_{P4} and φ_{41}

Figure 4-23 LTLCI and LRLCI Distributions of the 4-DOF robot

4.6 Summary

The detailed kinematic models and analysis for 2T, 2T1R, 3T and 3T1R parallel mechanisms are studied in this chapter. Both the inverse and direct kinematic mathematical models are calculated. Three types of singularity configurations are explored for further avoidance. The workspaces of these manipulators are obtained and the parametric analysis is conducted. The novel level index is proposed. The dexterity performance is evaluated and the corresponding level indices are illustrated.

Chapter 5 Dynamic modelling of parallel structures

5.1 Inertia-related indices

The inverse dynamic model for any parallel manipulator can be arranged in the following form

$$\boldsymbol{F} = \boldsymbol{M}(\boldsymbol{Q})\ddot{\boldsymbol{Q}} + \boldsymbol{C}(\boldsymbol{Q},\dot{\boldsymbol{Q}})\dot{\boldsymbol{Q}} + \boldsymbol{G}(\boldsymbol{Q}) + \boldsymbol{E}(\boldsymbol{Q}) \tag{5-1}$$

where $\boldsymbol{F}$ indicates the driving force/torque. $\boldsymbol{Q}$ is the linear/rotary displacements of all active prismatic joints. $\boldsymbol{M}(\boldsymbol{Q})$ means the inertia matrix of the overall mechanism. $\boldsymbol{C}(\boldsymbol{Q},\dot{\boldsymbol{Q}})$ represents the Coriolis force. $\boldsymbol{G}(\boldsymbol{Q})$ denotes the gravity and $\boldsymbol{E}(\boldsymbol{Q})$ indicates the external forces/torques applied on the parallel structure.

It is stated that the $\boldsymbol{M}(\boldsymbol{Q})\ddot{\boldsymbol{Q}}$ in Equation (5-1) plays an important role in the inverse dynamic model without consideration of the external forces/torques [161]. In some applications with low speed and no external loads/forces/torques requirement, Equation (5-1) can be simplified as

$$\boldsymbol{F} \approx \boldsymbol{M}(\boldsymbol{Q})\ddot{\boldsymbol{Q}} \tag{5-2}$$

Hereafter, it is essential to formulate the inertia matrix of this proposed translational parallel structure for further performance evaluation.

(i) The joint-reflected Inertia (JRI) index denotes the mean value of all the items in the *i*-th row and *i*-th column of the inertia matrix, when the moving platform is in any position/orientation in workspace [130]. The JRI index can be computed by

$$JRI = \frac{1}{n}\sum_{i=1}^{n} \boldsymbol{M}_{ii} \tag{5-3}$$

where $\boldsymbol{M}_{ii}$ means the *i*-th row and *i*-th column element of the *n*-by-*n* inertia matrix $\boldsymbol{M}$. $\boldsymbol{M}_{ii}$ depicts the inertia feature of the *i*-th branch. The JRI index indicates the average level of all supporting chains and is a local performance index.

A supplementary assumption should be provided to employ this concept. It is essential to design a single variable to explore its impact on the dynamic performance. The mass property of any linkage will not be increased/decreased with the variations of its length.

(ii) The coefficient of variation of joint-space inertia (CVI) index [131] is also important for performance assessment, which is defined as

$$CVI = \frac{1}{JRI}\sqrt{\frac{1}{n}\sum_{i=1}^{n}(\boldsymbol{M}_{ii} - JRI)^2} \tag{5-4}$$

In accordance with the definition in Equation (5-4), the CVI index is also a local index. A larger CVI value implies the inertia feature of all kinematic chains are more different.

(iii) A novel index named the branch-coupling absolute inertia (BCAI) index is proposed to study the average inertia-coupling characteristic among various kinematic limbs. The BCAI index is formulated as

$$BCAI = \frac{1}{n(n-1)}\sum\left|\boldsymbol{M}_{ij}\right| \quad (i, j = 1, 2, 3, ..., n.\ i \neq j) \tag{5-5}$$

where $\boldsymbol{M}_{ij}$ indicates the i-th row and j-th column element (off-diagonal element) of the n-by-n inertia matrix $\boldsymbol{M}$.

Equation (5-5) shows the BCAI index is a non-negative value for any position and orientation within the reachable workspace. The closer the BACI index approaches to zero, the smaller the influence caused by the inertia-coupling among different kinematic limbs.

(iv) Another new index called the variation of branch-coupling inertia (VBCI) index is designed to evaluate the dispersion property of the inertia-coupling values among all kinematic chains. It can be computed as

$$VBCI = \frac{1}{n(n-1)}\sum\left[\boldsymbol{M}_{ij} - \frac{\sum \boldsymbol{M}_{ij}}{n(n-1)}\right]^2 \quad (i, j = 1, 2, 3, ..., n.\ i \neq j) \tag{5-6}$$

Equation (5-6) indicates the VBCI index is not less than zero for each pose (position and orientation) in workspace. The smaller the VBCI index is, the more similar the inertia-coupling elements are. It is noteworthy that the absolute operator is utilized in Equation (5-5) but not in Equation (5-6). It implies that the BCAI index of Equation (5-5) might not be the smallest even the VBCI index of Equation (5-6) is zero.

5.2 Case one: 2T parallel mechanism

(i) Dynamic models

With the kinematic mathematical models in Section 4.2, the inverse dynamic model can be derived based on the Lagrange method. The masses for the active sliders (linkages $A_{11}A_{13}$ or $B_{11}B_{13}$) and inclined linkages ($A_{11}A_{12}$, $A_{13}A_{14}$, $B_{11}B_{12}$, $B_{13}B_{14}$) are separately represented as m_{11}, m_{12}. The total mass of the moving platform is denoted as m_{13}. It is assumed that the

center of geometry of each linkage coincides with its center of mass. The friction forces are neglected in the dynamic model.

The linear velocities of the linkages $A_{11}A_{13}$, $A_{12}A_{14}$, $B_{11}B_{13}$ and $B_{12}B_{14}$ are denoted as $\dot{\boldsymbol{P}}_{A15}[\dot{x}_{A15},0]^{\mathrm{T}}$, $\dot{\boldsymbol{P}}_{A16}[\dot{x}_{P1},\dot{y}_{P1}]^{\mathrm{T}}$, $\dot{\boldsymbol{P}}_{B15}[\dot{x}_{B15},0]^{\mathrm{T}}$, $\dot{\boldsymbol{P}}_{B16}[\dot{x}_{P1},\dot{y}_{P1}]^{\mathrm{T}}$, respectively. The kinetic energy of the first linear actuator is calculated as

$$K_{A11A13}=\frac{1}{2}m_{11}\dot{x}_{A15}^2 \tag{5-7}$$

The inclined linkages with mixed movements (both translations and rotations) can be regarded as uniform rigid linkages for simplification. A uniform bar NJ with the length of L_{10} is demonstrated in figure 5-1. The overall mass of this bar is denoted as m. The velocities of both endpoints are $\boldsymbol{V}_N=[V_{NX},V_{NY},V_{NZ}]^{\mathrm{T}}$ and $\boldsymbol{V}_J=[V_{JX},V_{JY},V_{JZ}]^{\mathrm{T}}$, respectively. A small section is chosen along this bar. The distance between this section and point N is rL_{10} ($r\in[0,1]$). The corresponding length and mass of this tiny section are dr and dm, respectively. The three orthogonal velocities of this section in space can be computed as

$$\begin{cases}V_{RX}=(1-r)V_{NX}+rV_{JX}\\V_{RY}=(1-r)V_{NY}+rV_{JY}\\V_{RZ}=(1-r)V_{NZ}+rV_{JZ}\end{cases} \tag{5-8}$$

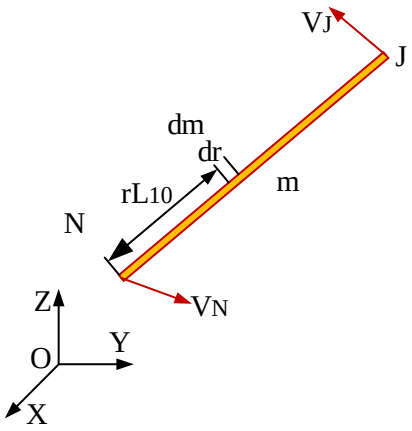

Figure 5-1 Diagram of a rigid linkage in 3-dimensional space

Hereafter, the kinetic energy of this uniform linkage can be calculated as [162]

$$T_{bar}=\frac{1}{2}\int\int_0^1\left(V_{RX}^2+V_{RY}^2+V_{RZ}^2\right)dmdr=\frac{1}{6}m\left(\boldsymbol{V}_N^2+\boldsymbol{V}_J^2+\boldsymbol{V}_N\boldsymbol{V}_J\right) \tag{5-9}$$

According to the proof of Equation (5-9), the kinetic energy of the inclined linkages in the first branch can be solved as

$$K_{A11A12} = K_{A13A14} = \frac{1}{6} m_{12} (\dot{\boldsymbol{P}}_{A15}^2 + \dot{\boldsymbol{P}}_{A16}^2 + \dot{\boldsymbol{P}}_{A15} \dot{\boldsymbol{P}}_{A16}) = \frac{1}{6} m_{12} (\dot{x}_{A15}^2 + \dot{x}_{P1}^2 + \dot{y}_{P1}^2 + \dot{x}_{A15} \dot{x}_{P1}) \quad (5\text{-}10)$$

In the second branch, the kinetic energy of its linear actuator is derived as

$$K_{B11B13} = \frac{1}{2} m_{11} \dot{x}_{B15}^2 \quad (5\text{-}11)$$

The kinetic energy of the inclined linkages in the second chain are computed as

$$K_{B11B12} = K_{B13B14} = \frac{1}{6} m_{12} (\dot{\boldsymbol{P}}_{B15}^2 + \dot{\boldsymbol{P}}_{B16}^2 + \dot{\boldsymbol{P}}_{B15} \dot{\boldsymbol{P}}_{B16}) = \frac{1}{6} m_{12} (\dot{x}_{B15}^2 + \dot{x}_{P1}^2 + \dot{y}_{P1}^2 + \dot{x}_{B15} \dot{x}_{P1}) \quad (5\text{-}12)$$

The kinetic energy of the mobile platform is obtained as

$$K_{P1} = \frac{1}{2} m_{13} (\dot{x}_{P1}^2 + \dot{y}_{P1}^2) \quad (5\text{-}13)$$

The *X* axis is taken as the reference line for potential energy. Therefore, the potential energies of the active sliders are

$$U_{A11A13} = U_{B11B13} = 0 \quad (5\text{-}14)$$

The potential energies of all the inclined linkages can be expressed as

$$U_{A11A12} = U_{A13A14} = U_{B11B12} = U_{B13B14} = m_{12} g_y \frac{y_{P1} + 0}{2} \quad (5\text{-}15)$$

where g_y denotes the Y-axis-component of the gravitational acceleration $\boldsymbol{g}_1 = [0, g_y]^{\mathrm{T}}$.

The potential energy of the mobile platform is generated as

$$U_{P1} = m_{13} g_y y_{P1} \quad (5\text{-}16)$$

The corresponding Lagrangian function [26] is defined as

$$L_1 = K_1 - U_1 = K_{A11A13} + 2K_{A11A12} + K_{B11B13} + 2K_{B11B12} + K_{P1} - 4U_{A11A12} - U_{P1} \quad (5\text{-}17)$$

where K_1 and U_1 stand for the total kinetic energy and total potential energy of all moving linkages.

$q_1 = (x_{P1}, y_{P1}, x_{A15}, y_{B15})$ represents the generalized coordinates to be employed in the Lagrangian equation of the first type. Henceforth, three equations containing Lagrangian multiplier λ_{1i} can be listed as

$$\sum\nolimits_{i=1,2} \lambda_{1i} \frac{\partial \Gamma_{1i}}{\partial q_{1j}} = \frac{d}{dt} \left(\frac{\partial L_1}{\partial \dot{q}_{1j}} \right) - \frac{\partial L_1}{\partial q_{1j}} - f_{1j} \quad j = 1, 2 \quad (5\text{-}18)$$

where f_{11} and f_{12} mean the external force exerted on the moving platform along X and Y axes, respectively.

Expanding Equation (5-18) yields

$$\begin{cases} 2\lambda_{11}(x_{P1}-x_{A15}-L_{13}-L_{16})+2\lambda_{12}(x_{P1}-x_{B15}+L_{15}+L_{16})=\dfrac{1}{3}m_{12}(4\ddot{x}_{P1}+\ddot{x}_{A15}+\ddot{x}_{B15})+m_{12}\ddot{x}_{P1}-f_{11} \\ 2(\lambda_{11}+\lambda_{12})y_{P1}=\dfrac{4}{3}m_{12}\ddot{y}_{P1}+m_{13}\ddot{y}_{P1}+2(m_{12}+m_{13})g_y-f_{12} \end{cases} \tag{5-19}$$

The driving forces on two active prismatic joints can be resolved as

$$F_{1j}=\frac{d}{dt}(\frac{\partial L_1}{\partial \dot{q}_{1j}})-\frac{\partial L_1}{\partial q_{1j}}-\sum\nolimits_{i=1,2}\lambda_i\frac{\partial \Gamma_{1i}}{\partial q_{1j}} \quad \text{j=3,4} \tag{5-20}$$

The inverse dynamic solution is then derived by further expanding Equation (5-20)

$$\begin{cases} F_{11}=m_{11}\ddot{x}_{A15}+\dfrac{1}{3}m_{12}(2\ddot{x}_{A15}+\ddot{x}_{P1})+2\lambda_{11}(x_{P1}-x_{A15}-L_{13}-L_{16}) \\ F_{12}=m_{11}\ddot{x}_{B15}+\dfrac{1}{3}m_{12}(2\ddot{x}_{B15}+\ddot{x}_{P1})+2\lambda_{12}(x_{P1}-x_{B15}+L_{13}+L_{16}) \end{cases} \tag{5-21}$$

(ii) Inertia matrix

Both $\dot{\boldsymbol{Q}}_1$ and $\dot{\boldsymbol{X}}_1$ can be expressed according to Equation (4-16)

$$\begin{cases} \dot{\boldsymbol{Q}}_1=(\boldsymbol{J}_{Q1}^{-1}\boldsymbol{J}_{X1})\dot{\boldsymbol{X}}_1=\boldsymbol{J}_1\dot{\boldsymbol{X}}_1 \\ \dot{\boldsymbol{X}}_1=(\boldsymbol{J}_{X1}^{-1}\boldsymbol{J}_{Q1})\dot{\boldsymbol{Q}}_1=\boldsymbol{J}_1^{-1}\dot{\boldsymbol{Q}}_1 \end{cases} \tag{5-22}$$

The velocity of first active sliding joint can be obtained as

$$\dot{\boldsymbol{P}}_{A15}=\begin{bmatrix}\dot{x}_{A15}\\0\end{bmatrix}=\begin{bmatrix}1&0\\0&0\end{bmatrix}\dot{\boldsymbol{Q}}_1=\boldsymbol{J}_{A15}\dot{\boldsymbol{Q}}_1 \tag{5-23}$$

The velocity of linkage $A_{12}A_{14}$ can be arranged as

$$\dot{\boldsymbol{P}}_{A16}=\begin{bmatrix}\dot{x}_{P1}\\\dot{y}_{P1}\end{bmatrix}=\dot{\boldsymbol{X}}_1=\boldsymbol{J}_1^{-1}\dot{\boldsymbol{Q}}_1 \tag{5-24}$$

Considering Equation (5-23), Equation (5-7) can be expressed as below

$$K_{A11A13}=\frac{1}{2}m_{11}\dot{\boldsymbol{P}}_{A15}^2=\frac{1}{2}m_{11}\dot{\boldsymbol{Q}}_1^{\mathrm{T}}\boldsymbol{J}_{A15}^{\mathrm{T}}\boldsymbol{J}_{A15}\dot{\boldsymbol{Q}}_1 \tag{5-25}$$

Combining Equations (5-23) and (5-24), Equation (5-10) can be computed as

$$K_{A11A12}=K_{A13A14}=\frac{1}{6}m_{12}\dot{\boldsymbol{Q}}_1^{\mathrm{T}}(\boldsymbol{J}_{A15}^{\mathrm{T}}\boldsymbol{J}_{A15}+\boldsymbol{J}_1^{-\mathrm{T}}\boldsymbol{J}_1^{-1}+\boldsymbol{J}_{A15}^{\mathrm{T}}\boldsymbol{J}_1^{-1})\dot{\boldsymbol{Q}}_1 \tag{5-26}$$

The velocity of the second sliding joint can be stated as

$$\dot{\boldsymbol{P}}_{B15}=\begin{bmatrix}\dot{x}_{B15}\\0\end{bmatrix}=\begin{bmatrix}0&1\\0&0\end{bmatrix}\dot{\boldsymbol{Q}}_1=\boldsymbol{J}_{B15}\dot{\boldsymbol{Q}}_1 \tag{5-27}$$

The velocity of the linkage $B_{12}B_{14}$ can be expressed as below

$$\dot{\boldsymbol{P}}_{B16}=\begin{bmatrix}\dot{x}_{P1}\\\dot{y}_{P1}\end{bmatrix}=\dot{\boldsymbol{X}}_1=\boldsymbol{J}_1^{-1}\dot{\boldsymbol{Q}}_1 \tag{5-28}$$

According to Equation (5-27) and (5-28), Equation (5-11) can be rearranged as

$$K_{B11B13}=\frac{1}{2}m_{11}\dot{\boldsymbol{P}}_{B15}^2=\frac{1}{2}m_{11}\dot{\boldsymbol{Q}}_1^{\mathrm{T}}\boldsymbol{J}_{B15}^{\mathrm{T}}\boldsymbol{J}_{B15}\dot{\boldsymbol{Q}}_1 \tag{5-29}$$

Combining Equations (27)-(28), Equation (5-12) can be expressed as below

$$K_{B11B12}=K_{B13B14}=\frac{1}{6}m_{12}\dot{\boldsymbol{Q}}_1^{\mathrm{T}}(\boldsymbol{J}_{B15}^{\mathrm{T}}\boldsymbol{J}_{B15}+\boldsymbol{J}_1^{-\mathrm{T}}\boldsymbol{J}_1^{-1}+\boldsymbol{J}_{B15}^{\mathrm{T}}\boldsymbol{J}_1^{-1})\dot{\boldsymbol{Q}}_1 \tag{5-30}$$

Integrating the second expression of Equation (5-22), Equation (5-13) can be further obtained as

$$K_{P1}=\frac{1}{2}m_{13}\dot{\boldsymbol{Q}}_1^{\mathrm{T}}\boldsymbol{J}_1^{-\mathrm{T}}\boldsymbol{J}_1^{-1}\dot{\boldsymbol{Q}}_1, \tag{5-31}$$

The total kinetic energy of this parallel manipulator will be formulated as

$$K_1=\frac{1}{2}\dot{\boldsymbol{Q}}_1^{\mathrm{T}}\boldsymbol{I}_1\dot{\boldsymbol{Q}}_1 \tag{5-32}$$

where $\boldsymbol{I}_1=\sum_{j=A,B}\left[m_{11}\boldsymbol{J}_{j15}^{\mathrm{T}}\boldsymbol{J}_{j15}+\frac{2}{3}m_{12}(\boldsymbol{J}_{j15}^{\mathrm{T}}\boldsymbol{J}_{j15}+\boldsymbol{J}_1^{-\mathrm{T}}\boldsymbol{J}_1^{-1}+\boldsymbol{J}_{j15}^{\mathrm{T}}\boldsymbol{J}_1^{-1})\right]+m_{13}\boldsymbol{J}_1^{-\mathrm{T}}\boldsymbol{J}_1^{-1}$

Then the inertia matrix [135] of this 2T mechanism can be computed as

$$\boldsymbol{M}_1=\boldsymbol{J}_1^{\mathrm{T}}\boldsymbol{I}_1\boldsymbol{J}_1 \tag{5-33}$$

(iii) Inertia-related performances

According to the definition in Equation (5-3), the JRI index of this parallel mechanism can be fully derived and it is only related to moving platform *Y*-axis position and inclined linkage length L_{12}. In any horizonal line that is parallel to *X* axis, the JRI index remain the same with a constant L_{12}. This is because the JRI index is calculated on the basis of the Jacobian matrix $\boldsymbol{J}_1$ shown in Equation (4-13). m_{11}=0.402g. m_{12}=0.125g. m_{13}=1.356g. The distribution of JRI index is plotted with respect to y_{P1} and L_{12}, as depicted in figure 5-2. The unit of JRI index is $g\cdot mm^2$. From figure 5-2, with a constant L_{12} of 30mm, the JRI index keeps increasing a while the moving platform moves higher. Given a prescribed

moving platform height of 15mm, the JRI index shows a downward trend as L_{12} gets longer. The smallest JRI index can be found when the lowest moving platform height and the longest L_{12} are chosen.

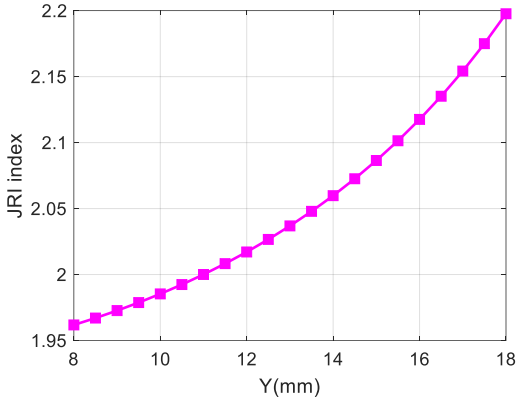

(a) The impact of y_{P1}

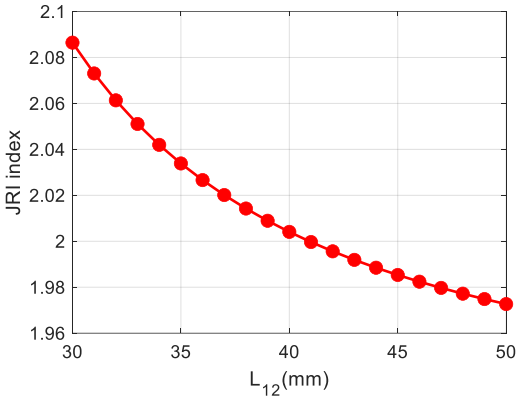

(b) The impact of L_{12}

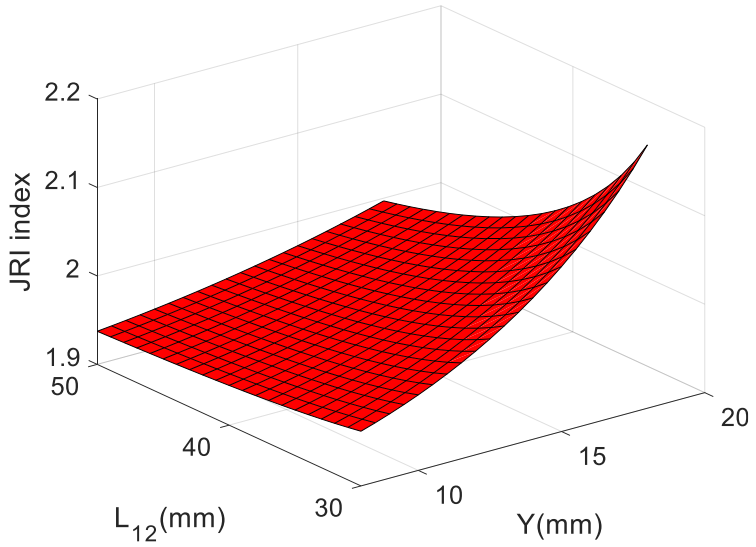

(c) The impact of y_{P1} and L_2

Figure 5-2 JRI index of the parallel mechanism

The CVI index of this parallel mechanism is derived in accordance with the definition in Equation (5-4) and is demonstrated in Figure 5-3. With a pre-set L_{12}, the CVI shows a downward when the moving platform moves up along Y axis. When the mobile platform has a constant Y value, the CVI index keep improving when L_{12} gets longer gradually. A more detailed CVI distribution with respect to y_{P1} and L_{12} is illustrated in figure 5-3(c). The minimal CVI index happens when the shortest L_{12} and highest y_{P1} are selected.

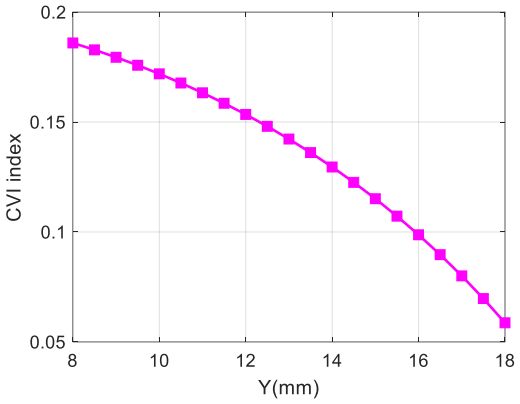

(a) The impact of y_{P1}

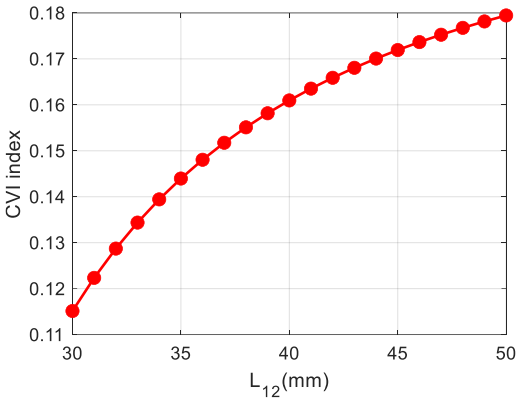

(b) The impact of L_{12}

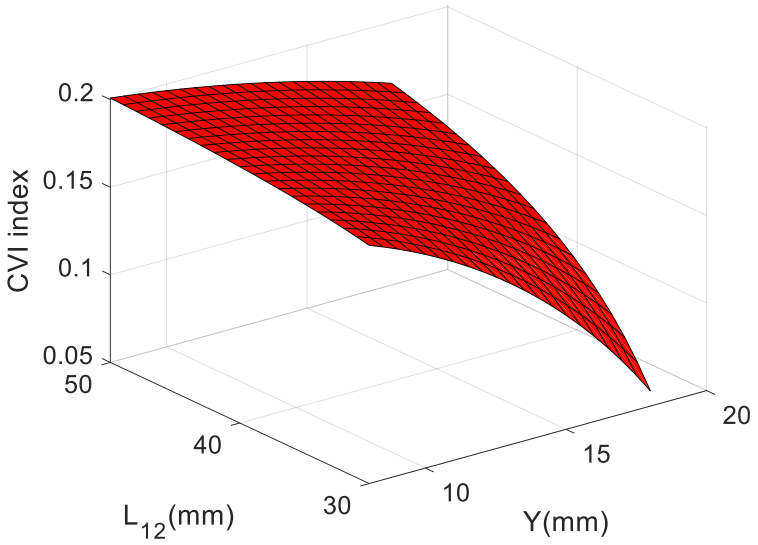

(c) The impact of y_{P1} and L_{12}

Figure 5-3 CVI index of this parallel mechanism

The branch-coupling absolute inertia (BCAI) index is generated by Equation (5-5). The distribution of the BCAI index of the parallel manipulator can be seen in figure 5-4. The unit of BCAI index is $g \cdot mm^2$. Different from the layouts of the JRI and CVI indices, the BCAI index is not only related to parameters y_{P1} and L_{12}, but also influenced by L_{13} and L_{16}. The variable y_{P1} has a complicated influence on the BCAI index. This index is zero with many values, the exceptions are when y_{P1} is selected as 12mm, 13mm, 14mm, 17mm and 17.5mm. The BCAI layout with respect to L_{12} is also irregular. The impact from L_{13} is straightforward. The BCAI index is a constant value when L_{13} is 2mm to 4mm. The BCAI index is zero when L_{13} changes from 4.5mm to 8mm. The influence coming from L_{16} is

similar to that of L_{13}. The BCAI index is a constant that is larger than zero when L_{16} changes from zero to 1mm. When L_{16} is 1.5mm and larger, this index remains zero. The BCAI trend is more complicated than those of JRI and CVI, since it is difficult to find out the maximal or minimal BACI values directly from figure 5-4.

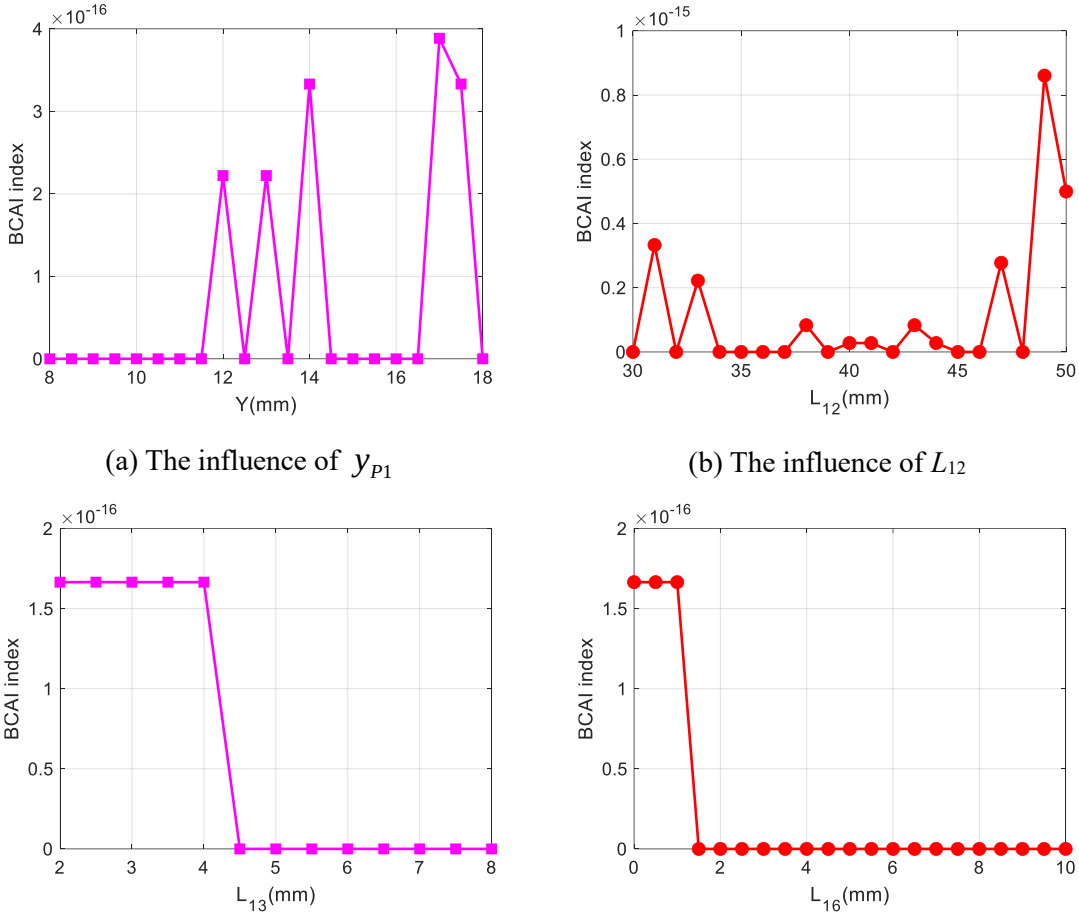

(a) The influence of y_{P1}

(b) The influence of L_{12}

(c) The influence of L_{13}

(d) The influence of L_{16}

Figure 5-4 BCAI index of this 2T parallel mechanism

The variation of branch-coupling inertia (VBCI) index is derived from Equation (5-6). The layout of the VBCI index for this linkage mechanism is demonstrated in figure 5-5. It is noteworthy that the VBCI layouts are similar to the BCAI distributions. Except when y_{P1} equals to 14mm, 17mm and 17.5mm, the VBCI index is zero. The VBCI indices when y_{P1} equals to 14mm and 17.5mm are the same. The relationship between VBCI index and L_{12} is also sophisticated. The VBCI index is larger than zero when L_{12} is set as 31mm, 38mm, 40mm, 41mm, 43mm, 44mm, 47mm, 49mm and 50mm. The VBCI index distribution originated from L_{13} is simple. When L_{13} extends from 2mm to 4mm, the corresponding

VBCI index remains a constant value that is larger than zero. The VBCI indicator is equal to zero when L_{13} changes from 4.5mm to 8mm. There are two regions when the VBCI indicator is constant values, L_{16} ranges from 0 to 1mm, from 1.5mm to 10mm.

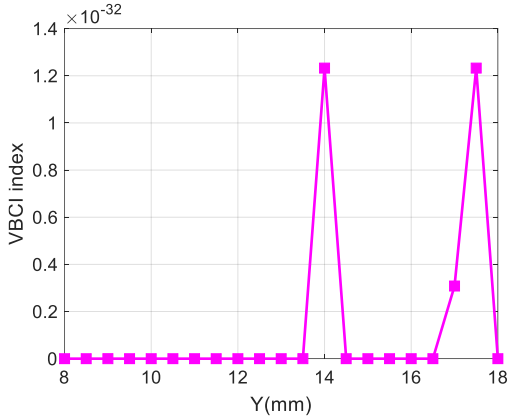

(a) The influence of y_{P1}

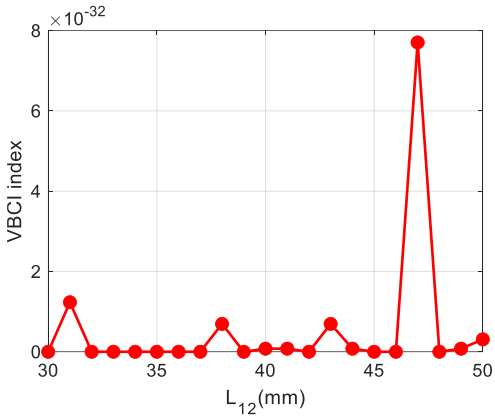

(b) The influence of L_{12}

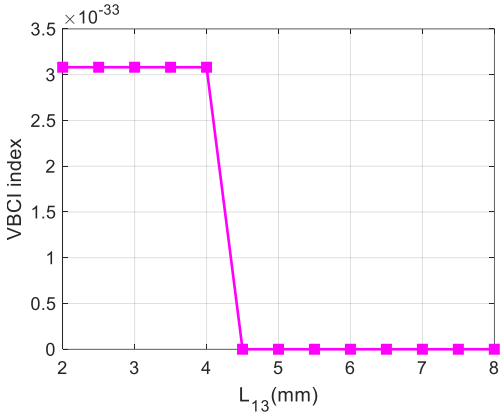

(c) The influence of L_{13}

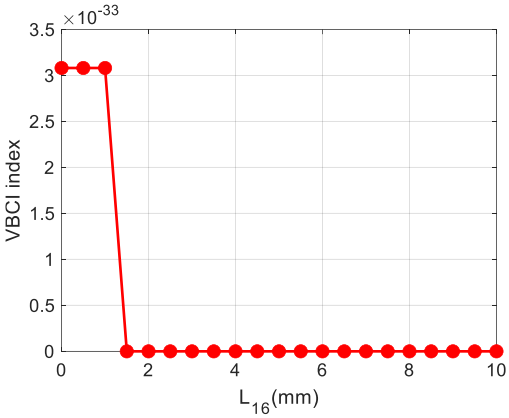

(d) The influence of L_{16}

Figure 5-5 VBCI index of this 2T parallel structure

5.3 Case two: 2T1R parallel mechanism

(i) Dynamic models

In accordance with the kinematic models in Section 4.3, the inverse dynamic model can be derived employing the Lagrange method. The masses for the active sliding linkages $A_{21}A_{23}$ or $B_{21}B_{23}$ or $C_{21}C_{23}$ are all defined as m_{21}. The masses of the inclined linkages $A_{21}A_{22}$, $A_{23}A_{24}$, $B_{21}B_{22}$, $B_{23}B_{24}$, $C_{21}C_{22}$ or $C_{23}C_{24}$ are represented as m_{22}. The masses of the linkages $A_{22}A_{24}$, $B_{22}B_{24}$ or $C_{22}C_{24}$ are denoted as m_{23}. The lumped mass of the mobile platform $A_{27}B_{27}C_{27}$ is set as m_{24}. The assumption is predefined that the center of geometry of every linkage coincides with its center of mass. The frictions are not considered in this dynamic model.

In the first kinematic chain, the positions of linkages $A_{21}A_{23}$ and $A_{22}A_{24}$ are calculated as $P_{A25}(x_{A25},0)$ and $P_{A26}(x_{P2}-\sqrt{3}L_{211}\cos(\varphi_{21}+\pi/6)/3, y_{P2}-L_{211}\sin(\varphi_{21}+\pi/6))$, respectively. Considering this planar parallel robot is consisted of three components (two translations and one rotation), the linear and rotary velocities of any linkage are expressed in one expression. The lumped velocities of rods $A_{21}A_{23}$ and $A_{22}A_{24}$ are respectively calculated as

$$\dot{\boldsymbol{P}}_{A25}=\begin{bmatrix}\dot{x}_{A25}\\0\\0\end{bmatrix} \tag{5-34}$$

$$\dot{\boldsymbol{P}}_{A26}=\begin{bmatrix}\dot{x}_{P2}+\sqrt{3}L_{211}\dot{\varphi}_{21}\sin(\varphi_{21}+\pi/6)/3\\ \dot{y}_{P2}-\sqrt{3}L_{211}\dot{\varphi}_{21}\cos(\varphi_{21}+\pi/6)/3\\0\end{bmatrix} \tag{5-35}$$

The kinetic energy of the first sliding linkage $A_{21}A_{23}$ is expressed as

$$K_{A21A23}=\frac{1}{2}m_{21}\dot{x}_{A25}^2 \tag{5-36}$$

The kinetic energy of the sloping linkages $A_{21}A_{22}$ and $A_{23}A_{24}$ are derived as

$$\begin{aligned}K_{A21A22}=K_{A23A24}&=\frac{1}{6}m_{22}(\dot{\boldsymbol{P}}_{A25}^2+\dot{\boldsymbol{P}}_{A26}^2+\dot{\boldsymbol{P}}_{A25}\dot{\boldsymbol{P}}_{A26})=\frac{1}{6}m_{22}[\dot{x}_{A25}^2+\dot{x}_{P2}^2+\dot{y}_{P2}^2\\&+\frac{1}{3}L_{211}^2\dot{\varphi}_{21}^2+2\sqrt{3}L_{211}\dot{x}_{P2}\dot{\varphi}_{21}\sin(\varphi_{21}+\pi/6)/3-2\sqrt{3}L_{211}\dot{y}_{P2}\dot{\varphi}_{21}\cos(\varphi_{21}+\pi/6)/3\\&+\dot{x}_{A25}\dot{x}_{P2}+\sqrt{3}L_{211}\dot{x}_{A25}\dot{\varphi}_{21}\sin(\varphi_{21}+\pi/6)/3]\end{aligned} \tag{5-37}$$

The kinetic energy of the bar $A_{22}A_{24}$ is formulated as

$$\begin{aligned}K_{A22A24}&=\frac{1}{2}m_{23}\dot{\boldsymbol{P}}_{A26}^2=\frac{1}{2}m_{23}[\dot{x}_{P2}^2+\dot{y}_{P2}^2+\frac{1}{3}L_{211}^2\dot{\varphi}_{21}^2+2\sqrt{3}L_{211}\dot{x}_{P2}\dot{\varphi}_{21}\sin(\varphi_{21}+\pi/6)/3\\&-2\sqrt{3}L_{211}\dot{y}_{P2}\dot{\varphi}_{21}\cos(\varphi_{21}+\pi/6)/3]\end{aligned} \tag{5-38}$$

In the second kinematic limb, the positions of linkages $B_{21}B_{23}$ and $B_{22}B_{24}$ are generated as $P_{B25}(x_{B25},0)$ and $P_{B26}(x_{P2}-\sqrt{3}L_{211}\cos(\varphi_{21}+5\pi/6)/3, y_{P2}-L_{211}\sin(\varphi_{21}+5\pi/6))$, separately.

The velocities of rods $B_{21}B_{23}$ and $B_{22}B_{24}$ are respectively described as

$$\dot{\boldsymbol{P}}_{B25}=\begin{bmatrix}\dot{x}_{B25}\\0\\0\end{bmatrix} \tag{5-39}$$

$$\dot{\boldsymbol{P}}_{B26}=\begin{bmatrix}\dot{x}_{P2}+\sqrt{3}L_{211}\dot{\varphi}_{21}\sin(\varphi_{21}+5\pi/6)/3\\ \dot{y}_{P2}-\sqrt{3}L_{211}\dot{\varphi}_{21}\cos(\varphi_{21}+5\pi/6)/3\\ 0\end{bmatrix} \tag{5-40}$$

The kinetic energy of the second active linkage $B_{21}B_{23}$ is written as

$$K_{B21B23}=\frac{1}{2}m_{21}\dot{x}_{B25}^2 \tag{5-41}$$

The kinetic energy of the sloping linkages $B_{21}B_{22}$ and $B_{23}B_{24}$ are obtained as

$$\begin{aligned}K_{B21B22}=K_{B23B24}&=\frac{1}{6}m_{22}(\dot{\boldsymbol{P}}_{B25}^2+\dot{\boldsymbol{P}}_{B26}^2+\dot{\boldsymbol{P}}_{B25}\dot{\boldsymbol{P}}_{B26})=\frac{1}{6}m_{22}[\dot{x}_{B25}^2+\dot{x}_{P2}^2+\dot{y}_{P2}^2\\ &+\frac{1}{3}L_{211}^2\dot{\varphi}_{21}^2+2\sqrt{3}L_{211}\dot{x}_{P2}\dot{\varphi}_{21}\sin(\varphi_{21}+5\pi/6)/3-2\sqrt{3}L_{211}\dot{y}_{P2}\dot{\varphi}_{21}\cos(\varphi_{21}+5\pi/6)/3\\ &+\dot{x}_{B25}\dot{x}_{P2}+\sqrt{3}L_{211}\dot{x}_{B25}\dot{\varphi}_{21}\sin(\varphi_{21}+5\pi/6)/3\end{aligned} \tag{5-42}$$

The kinetic energy of the link $B_{22}B_{24}$ is computed as

$$\begin{aligned}K_{B22B24}&=\frac{1}{2}m_{23}\dot{\boldsymbol{P}}_{B26}^2=\frac{1}{2}m_{23}[\dot{x}_{P2}^2+\dot{y}_{P2}^2+\frac{1}{3}L_{211}^2\dot{\varphi}_{21}^2+2\sqrt{3}L_{211}\dot{x}_{P2}\dot{\varphi}_{21}\sin(\varphi_{21}+5\pi/6)/3\\ &-2\sqrt{3}L_{211}\dot{y}_{P2}\dot{\varphi}_{21}\cos(\varphi_{21}+5\pi/6)/3]\end{aligned} \tag{5-43}$$

In the last kinematic branch, the positions of links $C_{21}C_{23}$ and $C_{22}C_{24}$ are derived as $P_{C25}(x_{C25},0)$ and $P_{C26}(x_{P2}-\sqrt{3}L_{211}\cos(\varphi_{21}+3\pi/2)/3, y_{P2}-L_{211}\sin(\varphi_{21}+3\pi/2))$, separately. The velocities of links $C_{21}C_{23}$ and $C_{22}C_{24}$ are respectively solved as

$$\dot{\boldsymbol{P}}_{C25}=\begin{bmatrix}\dot{x}_{C25}\\ 0\\ 0\end{bmatrix} \tag{5-44}$$

$$\dot{\boldsymbol{P}}_{C26}=\begin{bmatrix}\dot{x}_{P2}+\sqrt{3}L_{211}\dot{\varphi}_{21}\sin(\varphi_{21}+3\pi/2)/3\\ \dot{y}_{P2}-\sqrt{3}L_{211}\dot{\varphi}_{21}\cos(\varphi_{21}+3\pi/2)/3\\ 0\end{bmatrix} \tag{5-45}$$

The kinetic energy of the last driving linkage $C_{21}C_{23}$ is resolved as

$$K_{C21C23}=\frac{1}{2}m_{21}\dot{x}_{C25}^2 \tag{5-46}$$

The kinetic energy of the sloping linkages $C_{21}C_{22}$ and $C_{23}C_{24}$ are defined as

$$K_{C21C22} = K_{C23C24} = \frac{1}{6} m_{22} (\dot{\boldsymbol{P}}_{C25}^2 + \dot{\boldsymbol{P}}_{C26}^2 + \dot{\boldsymbol{P}}_{C25} \dot{\boldsymbol{P}}_{C26}) = \frac{1}{6} m_{22} [\dot{x}_{C25}^2 + \dot{x}_{P2}^2 + \dot{y}_{P2}^2$$
$$+ \frac{1}{3} L_{211}^2 \dot{\varphi}_{21}^2 + 2\sqrt{3} L_{211} \dot{x}_{P2} \dot{\varphi}_{21} \sin(\varphi_{21} + 3\pi/2)/3 - 2\sqrt{3} L_{211} \dot{y}_{P2} \dot{\varphi}_{21} \cos(\varphi_{21} + 3\pi/2)/3 \quad (5\text{-}47)$$
$$+ \dot{x}_{C25} \dot{x}_{P2} + \sqrt{3} L_{211} \dot{x}_{B25} \dot{\varphi}_{21} \sin(\varphi_{21} + 3\pi/2)/3]$$

The kinetic energy of the link $C_{22}C_{24}$ is arranged as

$$K_{C22C24} = \frac{1}{2} m_{23} \dot{\boldsymbol{P}}_{C26}^2 = \frac{1}{2} m_{23} [\dot{x}_{P2}^2 + \dot{y}_{P2}^2 + \frac{1}{3} L_{211}^2 \dot{\varphi}_{21}^2 + 2\sqrt{3} L_{211} \dot{x}_{P2} \dot{\varphi}_{21} \sin(\varphi_{21} + 3\pi/2)/3 \quad (5\text{-}48)$$
$$-2\sqrt{3} L_{211} \dot{y}_{P2} \dot{\varphi}_{21} \cos(\varphi_{21} + 3\pi/2)/3]$$

The kinetic energy of the moving platform $A_{27}B_{27}C_{27}$ is arranged as

$$K_{P2} = \frac{1}{2} m_{24} (\dot{x}_{P2}^2 + \dot{y}_{P2}^2) + \frac{1}{2} I_{P2} \dot{\varphi}_{21}^2 \quad (5\text{-}49)$$

where I_{P2} means the moment of inertia of the mobile platform about the axis that is parallel to Z direction and passes through point P_2.

The XOY plane is set as the reference for potential energy. The total potential energy of the whole mechanism $U_2 = 0$ since every linkage is trapped in this plane in movement.

The corresponding Lagrangian function is defined as

$$L_2 = K_2 - U_2 = K_{A21A23} + 2K_{A21A22} + K_{A22A24} + K_{B21B23} + 2K_{B21B22} + K_{B22B24} \quad (5\text{-}50)$$
$$+ K_{C21C23} + 2K_{C21C22} + K_{C22C24} + K_{P2}$$

where K_2 stands for the total kinetic energy of all moving linkages.

$q_2 = (x_{P2}, y_{P2}, \varphi_{21}, x_{A25}, x_{B25}, x_{C25})$ represents the generalized coordinates to be utilized in the Lagrangian equation of the first type. Therefore, three equations containing Lagrangian multiplier λ_{2i} can be listed as

$$\sum\nolimits_{i=1,2,3} \lambda_{2i} \frac{\partial \Gamma_{2i}}{\partial q_{2j}} = \frac{d}{dt} (\frac{\partial L_2}{\partial \dot{q}_{2j}}) - \frac{\partial L_2}{\partial q_{2j}} - f_{2j} \quad j = 1,2,3 \quad (5\text{-}51)$$

where f_{21} and f_{22} indicate the external force applied on the moving platform along X and Y axes, respectively. f_{23} is the external torque applied on the moving platform about Z direction.

The actuation forces on three active prismatic joints can be calculated as

$$F_{2j} = \frac{d}{dt} (\frac{\partial L_2}{\partial \dot{q}_{2j}}) - \frac{\partial L_2}{\partial q_{2j}} - \sum\nolimits_{i=1,2,3} \lambda_{2i} \frac{\partial \Gamma_{2i}}{\partial q_{2j}} \quad \text{j=4,5,6} \quad (5\text{-}52)$$

(ii) Inertia matrix

Both $\dot{\boldsymbol{Q}}_2$ and $\dot{\boldsymbol{X}}_2$ can be expressed according to Equation (4-37)

$$\begin{cases} \dot{\boldsymbol{Q}}_2 = (\boldsymbol{J}_{Q2}^{-1}\boldsymbol{J}_{X2})\dot{\boldsymbol{X}}_2 = \boldsymbol{J}_2\dot{\boldsymbol{X}}_2 \\ \dot{\boldsymbol{X}}_2 = (\boldsymbol{J}_{X2}^{-1}\boldsymbol{J}_{Q2})\dot{\boldsymbol{Q}}_2 = \boldsymbol{J}_2^{-1}\dot{\boldsymbol{Q}}_2 \end{cases} \tag{5-53}$$

In the first kinematic chain, the velocity of first active sliding link $A_{21}A_{23}$ can be obtained as

$$\dot{\boldsymbol{P}}_{A25} = \begin{bmatrix} \dot{x}_{A25} \\ 0 \\ 0 \end{bmatrix} = \begin{bmatrix} 1 & 0 & 0 \\ 0 & 0 & 0 \\ 0 & 0 & 0 \end{bmatrix} \dot{\boldsymbol{Q}}_2 = \boldsymbol{J}_{A25}\dot{\boldsymbol{Q}}_2 \tag{5-54}$$

The velocity of the link $A_{22}A_{24}$ can be computed as

$$\dot{\boldsymbol{P}}_{A26} = \begin{bmatrix} 1 & 0 & \sqrt{3}L_{211}\sin(\varphi_{21}+\pi/6)/3 \\ 0 & 1 & -\sqrt{3}L_{211}\cos(\varphi_{21}+\pi/6)/3 \\ 0 & 0 & 0 \end{bmatrix} \dot{\boldsymbol{X}}_2 = (\boldsymbol{J}_{A26}\boldsymbol{J}_2^{-1})\dot{\boldsymbol{Q}}_2 \tag{5-55}$$

Considering Equation (5-54), Equation (5-36) can be derived as

$$K_{A21A23} = \frac{1}{2}m_{21}\dot{\boldsymbol{P}}_{A25}^2 = \frac{1}{2}m_{21}\dot{\boldsymbol{Q}}_2^{\mathrm{T}}\boldsymbol{J}_{A25}^{\mathrm{T}}\boldsymbol{J}_{A25}\dot{\boldsymbol{Q}}_2 \tag{5-56}$$

Combining Equations (5-54) and (5-55), Equation (5-37) can be computed as

$$K_{A21A22} = K_{A23A24} = \frac{1}{6}m_{22}\dot{\boldsymbol{Q}}_2^{\mathrm{T}}[\boldsymbol{J}_{A25}^{\mathrm{T}}\boldsymbol{J}_{A25} + (\boldsymbol{J}_{A26}\boldsymbol{J}_2^{-1})^{\mathrm{T}}(\boldsymbol{J}_{A26}\boldsymbol{J}_2^{-1}) + \boldsymbol{J}_{A25}^{\mathrm{T}}(\boldsymbol{J}_{A26}\boldsymbol{J}_2^{-1})]\dot{\boldsymbol{Q}}_2 \tag{5-57}$$

Considering Equation (5-54), Equation (5-38) can be rearranged as

$$K_{A22A24} = \frac{1}{2}m_{23}\dot{\boldsymbol{Q}}_2^{\mathrm{T}}(\boldsymbol{J}_{A26}\boldsymbol{J}_2^{-1})^{\mathrm{T}}(\boldsymbol{J}_{A26}\boldsymbol{J}_2^{-1})\dot{\boldsymbol{Q}}_2 \tag{5-58}$$

In the second kinematic chain, the velocity of active link $B_{21}B_{23}$ can be generated as

$$\dot{\boldsymbol{P}}_{B25} = \begin{bmatrix} \dot{x}_{B25} \\ 0 \\ 0 \end{bmatrix} = \begin{bmatrix} 0 & 1 & 0 \\ 0 & 0 & 0 \\ 0 & 0 & 0 \end{bmatrix} \dot{\boldsymbol{Q}}_2 = \boldsymbol{J}_{B25}\dot{\boldsymbol{Q}}_2 \tag{5-59}$$

The velocity of the link $B_{22}B_{24}$ can be formulated as

$$\dot{\boldsymbol{P}}_{B26} = \begin{bmatrix} 1 & 0 & \sqrt{3}L_{211}\sin(\varphi_{21}+5\pi/6)/3 \\ 0 & 1 & -\sqrt{3}L_{211}\cos(\varphi_{21}+5\pi/6)/3 \\ 0 & 0 & 0 \end{bmatrix} \dot{\boldsymbol{X}}_2 = (\boldsymbol{J}_{B26}\boldsymbol{J}_2^{-1})\dot{\boldsymbol{Q}}_2 \tag{5-60}$$

In accordance with Equation (5-59), Equation (5-41) can be further expressed as

$$K_{B21B23} = \frac{1}{2}m_{21}\dot{\boldsymbol{P}}_{B25}^2 = \frac{1}{2}m_{21}\dot{\boldsymbol{Q}}_2^{\mathrm{T}}\boldsymbol{J}_{B25}^{\mathrm{T}}\boldsymbol{J}_{B25}\dot{\boldsymbol{Q}}_2 \tag{5-61}$$

On the basis of Equations (5-59) and (5-60), Equation (5-42) can be written as

$$K_{B21B22} = K_{B23B24} = \frac{1}{6} m_{22} \dot{\boldsymbol{Q}}_2^{\mathrm{T}} [\boldsymbol{J}_{B25}^{\mathrm{T}} \boldsymbol{J}_{B25} + (\boldsymbol{J}_{B26} \boldsymbol{J}_2^{-1})^{\mathrm{T}} (\boldsymbol{J}_{B26} \boldsymbol{J}_2^{-1}) + \boldsymbol{J}_{B25}^{\mathrm{T}} (\boldsymbol{J}_{B26} \boldsymbol{J}_2^{-1})] \dot{\boldsymbol{Q}}_2 \quad (5\text{-}62)$$

Considering Equation (5-60), Equation (5-43) is described as

$$K_{B22B24} = \frac{1}{2} m_{23} \dot{\boldsymbol{Q}}_2^{\mathrm{T}} (\boldsymbol{J}_{B26} \boldsymbol{J}_2^{-1})^{\mathrm{T}} (\boldsymbol{J}_{B26} \boldsymbol{J}_2^{-1}) \dot{\boldsymbol{Q}}_2 \quad (5\text{-}63)$$

In the last kinematic limb, the velocity of driving linkage $C_{21}C_{23}$ can be generated as

$$\dot{\boldsymbol{P}}_{C25} = \begin{bmatrix} \dot{x}_{C25} \\ 0 \\ 0 \end{bmatrix} = \begin{bmatrix} 0 & 0 & 1 \\ 0 & 0 & 0 \\ 0 & 0 & 0 \end{bmatrix} \dot{\boldsymbol{Q}}_2 = \boldsymbol{J}_{C25} \dot{\boldsymbol{Q}}_2 \quad (5\text{-}64)$$

The velocity of the rod $C_{22}C_{24}$ can be deduced as

$$\dot{\boldsymbol{P}}_{C26} = \begin{bmatrix} 1 & 0 & \sqrt{3} L_{211} \sin(\varphi_{21} + 3\pi/2)/3 \\ 0 & 1 & -\sqrt{3} L_{211} \cos(\varphi_{21} + 3\pi/2)/3 \\ 0 & 0 & 0 \end{bmatrix} \dot{\boldsymbol{X}}_2 = (\boldsymbol{J}_{C26} \boldsymbol{J}_2^{-1}) \dot{\boldsymbol{Q}}_2 \quad (5\text{-}65)$$

According to Equation (5-64), Equation (5-46) is solved as

$$K_{C21C23} = \frac{1}{2} m_{21} \dot{\boldsymbol{P}}_{C25}^2 = \frac{1}{2} m_{21} \dot{\boldsymbol{Q}}_2^{\mathrm{T}} \boldsymbol{J}_{C25}^{\mathrm{T}} \boldsymbol{J}_{C25} \dot{\boldsymbol{Q}}_2 \quad (5\text{-}66)$$

Take Equations (5-64) and (5-65) into account, Equation (5-47) is resolved as

$$K_{C21C22} = K_{C23C24} = \frac{1}{6} m_{22} \dot{\boldsymbol{Q}}_2^{\mathrm{T}} [\boldsymbol{J}_{C25}^{\mathrm{T}} \boldsymbol{J}_{C25} + (\boldsymbol{J}_{C26} \boldsymbol{J}_2^{-1})^{\mathrm{T}} (\boldsymbol{J}_{C26} \boldsymbol{J}_2^{-1}) + \boldsymbol{J}_{C25}^{\mathrm{T}} (\boldsymbol{J}_{C26} \boldsymbol{J}_2^{-1})] \dot{\boldsymbol{Q}}_2 \quad (5\text{-}67)$$

Based on Equation (5-65), Equation (5-48) is written as

$$K_{C22C24} = \frac{1}{2} m_{23} \dot{\boldsymbol{Q}}_2^{\mathrm{T}} (\boldsymbol{J}_{C26} \boldsymbol{J}_2^{-1})^{\mathrm{T}} (\boldsymbol{J}_{C26} \boldsymbol{J}_2^{-1}) \dot{\boldsymbol{Q}}_2 \quad (5\text{-}68)$$

The variables in Equation (5-49) can be expressed with respect to $\dot{\boldsymbol{Q}}_2$

$$\begin{bmatrix} \dot{x}_{P2} \\ 0 \\ 0 \end{bmatrix} = \begin{bmatrix} 1 & 0 & 0 \\ 0 & 0 & 0 \\ 0 & 0 & 0 \end{bmatrix} \dot{\boldsymbol{X}}_2 = (\boldsymbol{J}_{P21} \boldsymbol{J}_2^{-1}) \dot{\boldsymbol{Q}}_2 \quad (5\text{-}69)$$

$$\begin{bmatrix} 0 \\ \dot{y}_{P2} \\ 0 \end{bmatrix} = \begin{bmatrix} 0 & 0 & 0 \\ 0 & 1 & 0 \\ 0 & 0 & 0 \end{bmatrix} \dot{\boldsymbol{X}}_2 = (\boldsymbol{J}_{P22} \boldsymbol{J}_2^{-1}) \dot{\boldsymbol{Q}}_2 \quad (5\text{-}70)$$

$$\begin{bmatrix} 0 \\ 0 \\ \dot{\varphi}_{21} \end{bmatrix} = \begin{bmatrix} 0 & 0 & 0 \\ 0 & 0 & 0 \\ 0 & 0 & 1 \end{bmatrix} \dot{\boldsymbol{X}}_2 = (\boldsymbol{J}_{P23} \boldsymbol{J}_2^{-1}) \dot{\boldsymbol{Q}}_2 \quad (5\text{-}71)$$

Combining Equations (5-69) to (5-71), Equation (5-49) can be rearranged as

$$K_{P2}=\frac{1}{2}m_{24}\dot{\boldsymbol{Q}}_2^{\mathrm{T}}[(\boldsymbol{J}_{P21}\boldsymbol{J}_2^{-1})^{\mathrm{T}}(\boldsymbol{J}_{P21}\boldsymbol{J}_2^{-1})+(\boldsymbol{J}_{P22}\boldsymbol{J}_2^{-1})^{\mathrm{T}}(\boldsymbol{J}_{P22}\boldsymbol{J}_2^{-1})]\dot{\boldsymbol{Q}}_2+\frac{1}{2}I_{P2}\dot{\boldsymbol{Q}}_2^{\mathrm{T}}(\boldsymbol{J}_{P23}\boldsymbol{J}_2^{-1})^{\mathrm{T}}(\boldsymbol{J}_{P23}\boldsymbol{J}_2^{-1})\dot{\boldsymbol{Q}}_2 \tag{5-72}$$

The total kinetic energy K_2 can be then derived as

$$K_2=\frac{1}{2}\dot{\boldsymbol{Q}}_2^{\mathrm{T}}\boldsymbol{I}_2\dot{\boldsymbol{Q}}_2 \tag{5-73}$$

where

$$\boldsymbol{I}_2=\sum_{j=A,B,C}\{m_{21}\boldsymbol{J}_{j25}^{\mathrm{T}}\boldsymbol{J}_{j25}+\frac{2}{3}m_{22}[\boldsymbol{J}_{j25}^{\mathrm{T}}\boldsymbol{J}_{j25}+(\boldsymbol{J}_{j26}\boldsymbol{J}_2^{-1})^{\mathrm{T}}(\boldsymbol{J}_{j26}\boldsymbol{J}_2^{-1})+\boldsymbol{J}_{j25}^{\mathrm{T}}(\boldsymbol{J}_{j26}\boldsymbol{J}_2^{-1})]$$
$$+m_{23}(\boldsymbol{J}_{j26}\boldsymbol{J}_2^{-1})^{\mathrm{T}}(\boldsymbol{J}_{j26}\boldsymbol{J}_2^{-1})^{\mathrm{T}}\}+m_{24}[(\boldsymbol{J}_{P21}\boldsymbol{J}_2^{-1})^{\mathrm{T}}(\boldsymbol{J}_{P21}\boldsymbol{J}_2^{-1})+(\boldsymbol{J}_{P22}\boldsymbol{J}_2^{-1})^{\mathrm{T}}(\boldsymbol{J}_{P22}\boldsymbol{J}_2^{-1})]$$
$$+I_{P2}(\boldsymbol{J}_{P23}\boldsymbol{J}_2^{-1})^{\mathrm{T}}(\boldsymbol{J}_{P23}\boldsymbol{J}_2^{-1})$$

The inertia matrix of this 2T1R mechanism can be computed as

$$\boldsymbol{M}_2=\boldsymbol{J}_2^{\mathrm{T}}\boldsymbol{I}_2\boldsymbol{J}_2 \tag{5-74}$$

(iii) Inertia-related performances

The workspace that x_{P2}, y_{P2} and φ_{21} respectively range from 180mm to 220mm, 60mm to 80mm and $-\pi/4rad$ to $\pi/4rad$ is selected to evaluate the inertia-related performance indices. The linkage mass information is provided, m_{21}=0.402g. m_{22}=0.108g. m_{23}=0.282g. m_{24}=0.226g. The inertia I_{P2}=14.476 $g\cdot mm^2$.

According to the JRI definition in Equation (5-30), the JRI index of this 2T1R parallel manipulator is calculated and is not pertinent to the variable x_{P2}. The JRI index distribution with respect to y_{P2} and φ_{21} is plotted in figure 5-6(a). The JRI indices have huge differences with various parameter φ_{21} when y_{P2} has a predefined value. If the parameter φ_{21} is fixed, the JRI indices are similar even with different y_{P2}.

A fixed pose (x_{P2}=200mm, y_{P2}=70mm and φ_{21}=0) within the predefined workspace is chosen to further explore the parametric analysis originated from various linkage lengths. The JRI indicator at this specific pose is not related to L_{23} and L_{212}. The impact from the length L_{21} is seen in figure 5-6(b). The JRI indicator keeps growing as a longer L_{21} is

employed, and the increasement rate also improves when L_{21} is chosen from 130mm to 170mm.

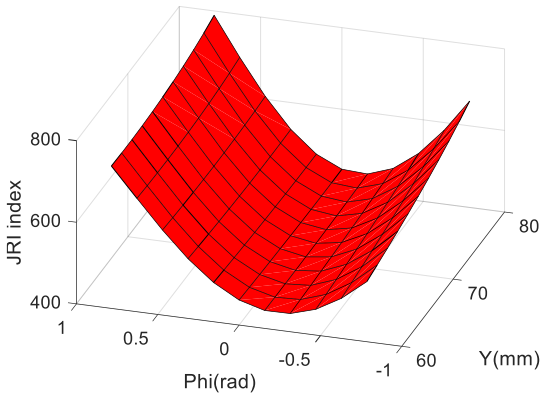

(a) JRI distribution

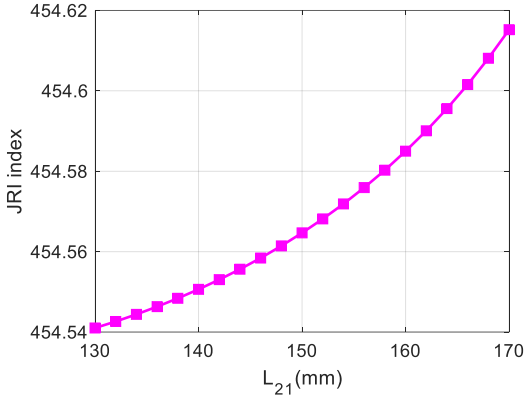

(b) The influence of L_{21}

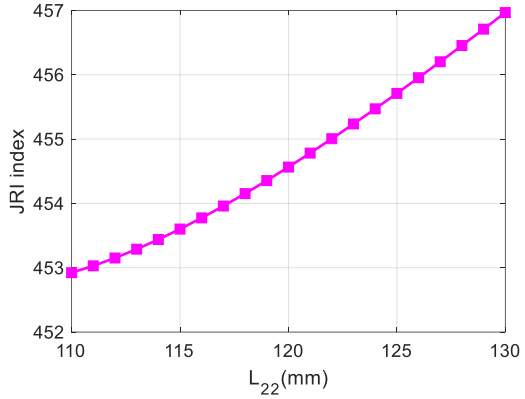

(c) The influence of L_{22}

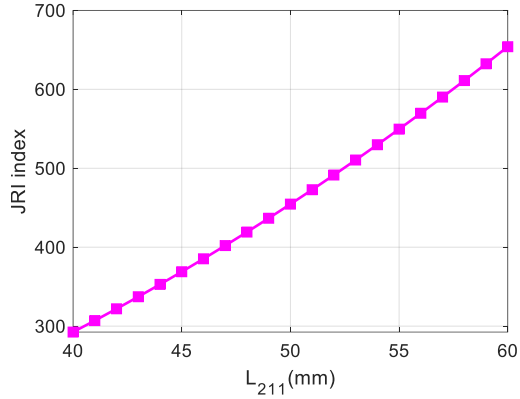

(d) The influence of L_{211}

Figure 5-6 JRI index of this 2T1R parallel mechanism

This index with respect to L_{22} is illustrated in figure 5-6(c). The JRI index rises as L_{22} changes from 110mm to 130mm. The L_{211} influence on this JRI indicator is demonstrated in figure 5-6(d). This index has significantly increasements as a longer L_{211} is chosen. Based on figure 5-6 (a-c), it is noteworthy that the JRI index impact from L_{211} is the largest since the JRI indices have the largest range. The influence coming from L_{211} is the weakest. On the basis of the CVI definition shown in Equation (5-31), the CVI indicator of this parallel mechanism is obtained. This CVI index is not related to the variable x_{P2}. Its layout is shown in figure 5-7(a). Similar to the JRI index distribution, the CVI indices vary significantly with a constant y_{P2} value. The CVI indices are close to each other when φ_{21} is pre-set as a constant. The CVI indices are small when φ_{21} is about 0. The index increases when φ_{21} is far from 0.

The CVI indicator is not related to L_{23} and L_{212}. The CVI impact coming from parameter L_{21} is provided in figure 5-7(b). This index displays a downward trend as L_{21} extends from 130mm to 170mm. The reduction rate is also higher when L_{21} is extended. The impact from the parameter L_{22} is seen in figure 5-7(c). The CVI indicator is rising as L_{22} changes from 110mm to 130mm. The CVI trend illustrated in figure 5-7(d) is similar to that in figure 5-7(c), while the latter curve has a slower increasement rate.

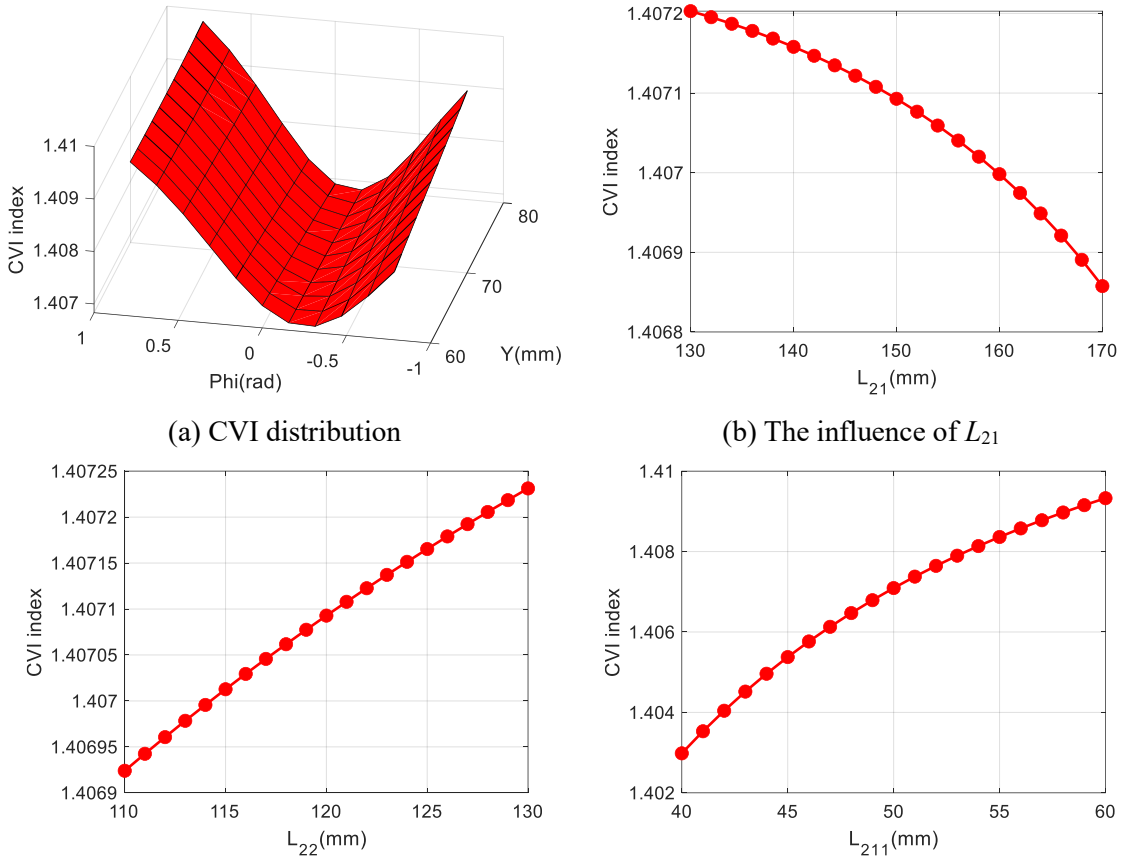

(a) CVI distribution

(b) The influence of L_{21}

(c) The influence of L_{22}

(d) The influence of L_{211}

Figure 5-7 CVI index of this 2T1R parallel mechanism

Its corresponding BCAI index can be generated by directly utilizing Equation (5-32). The BCAI index is a constant when the parameter x_{P2} has various values. The BCAI distribution with respect to y_{P2} and φ_{21} is plotted in figure 5-8(a). The BCAI index has irregular changes when extending y_{P2} and φ_{21}. The largest and smallest BCAI indices are 13.53 $g \cdot mm^2$ and 5.5993 $g \cdot mm^2$, respectively.

In the given position and orientation, the BCAI index is not associated with L_{23} and L_{212}. The BCAI demonstrates an increasing trend as L_{21} changes from 130mm to 170mm, as

seen in figure 5-8(b). Different from that, this index keeps reducing as L_{22} extends from 110mm to 130mm. The BCAI index originated from L_{211} is displayed in figure 5-8(d). This index increases gradually as the parameter L_{211} changes from 40mm to 60mm.

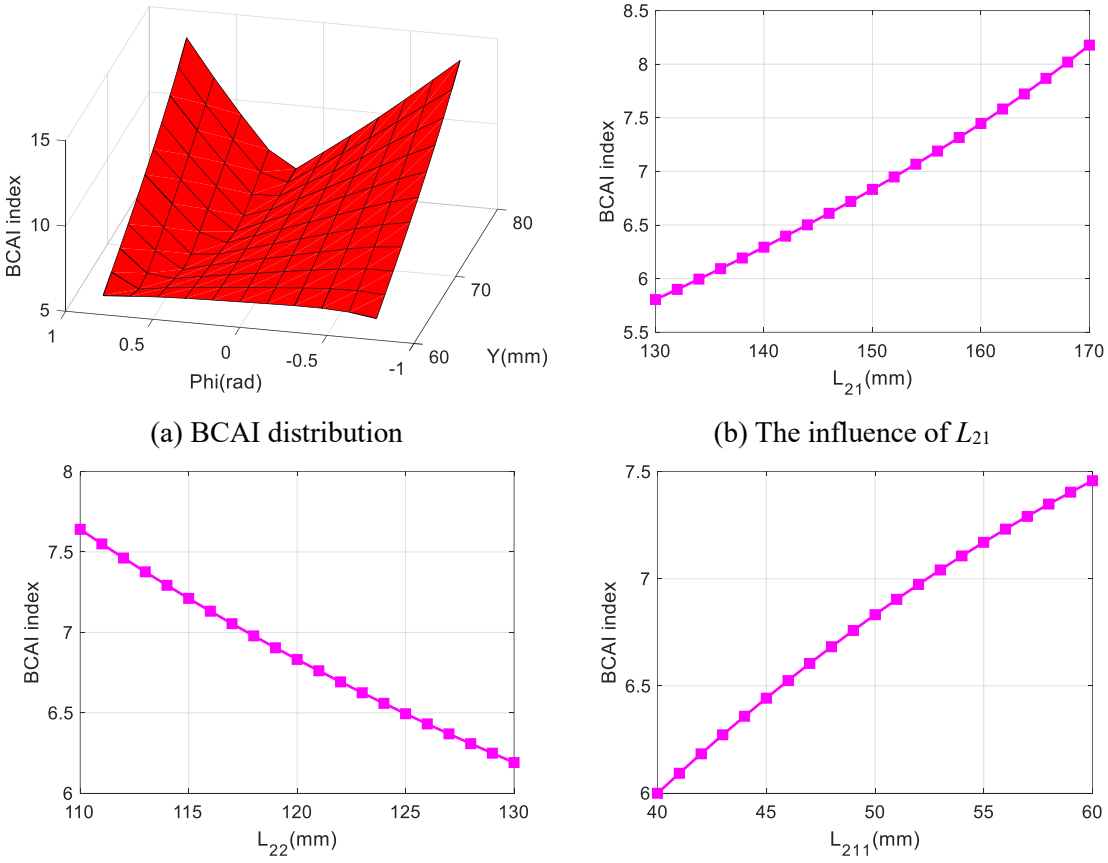

(a) BCAI distribution

(b) The influence of L_{21}

(c) The influence of L_{22}

(d) The influence of L_{211}

Figure 5-8 BCAI index of this 2T1R parallel mechanism

Its corresponding VBCI index can be solved by using Equation (5-33). Based on the calculations, this index is not related to the variable x_{P2}. The distribution of this VBCI index about two parameters y_{P2} and φ_{21} is indicated in figure 5-9(a). Its layout is a smooth surface with the minimal value of 22.57 and the maximal value of 268.91.

When the mobile platform is fixed at the predefined pose, its VBCI index is not related to two parameters L_{23} and L_{212}. From figure 5-9(b), this index presents a downward curve and then an upward curve and the turning point is L_{21}=146mm. The maximal and minimal indices are separately 35.99 $g \cdot mm^2$ and 30.931 $g \cdot mm^2$. In accordance with figure 5-9(c), this index keeps reducing as L_{22} grows from 110mm to 130mm. However, the positive relationship is found between this index and L_{211}, as seen in figure 5-9(d).

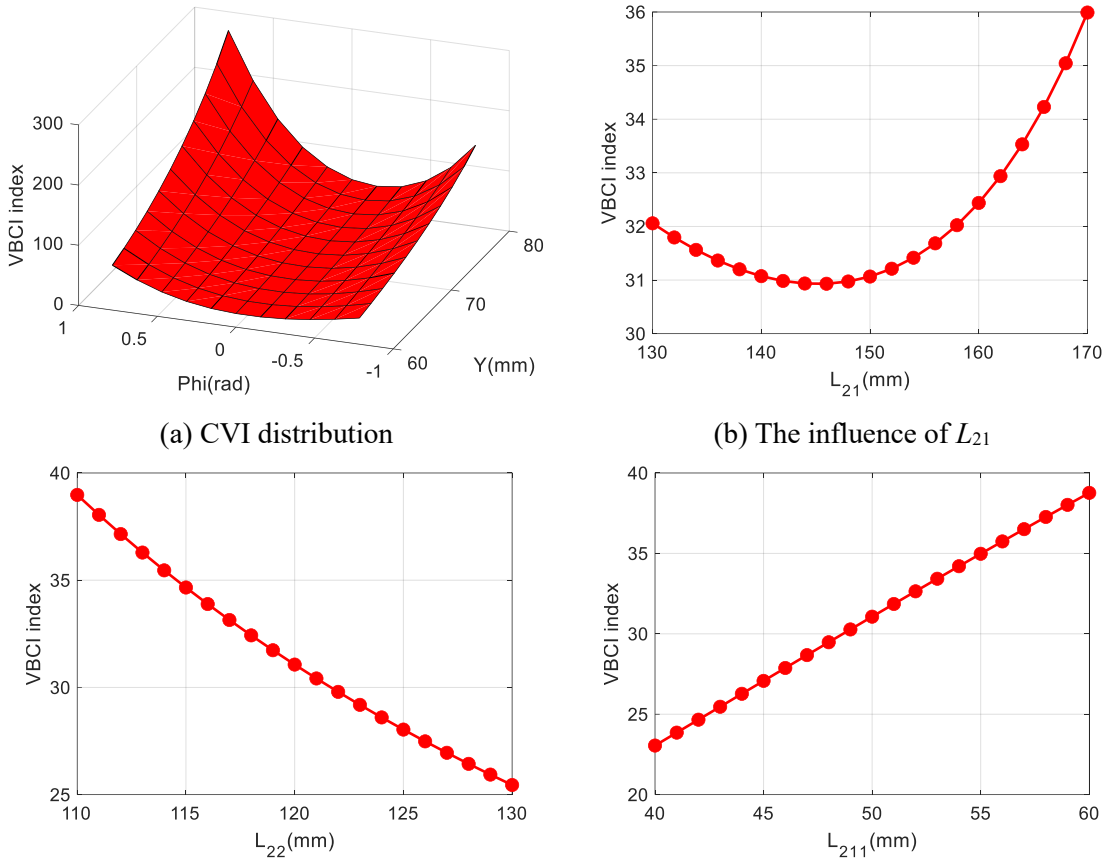

(a) CVI distribution

(b) The influence of L_{21}

(c) The influence of L_{22}

(d) The influence of L_{211}

Figure 5-9 VBCI index of this 2T1R parallel mechanism

5.4 Case three: 3T parallel mechanism

(i) Dynamic models

With the kinematic analysis, the inverse dynamic model can be derived based on the Lagrange method. The masses for active slider ($A_{31}A_{33}$, $B_{31}B_{33}$, $C_{31}C_{33}$), inclined linkage ($A_{31}A_{32}$, $A_{33}A_{34}$, $B_{31}B_{32}$, $B_{33}B_{34}$, $C_{31}C_{32}$, $C_{33}C_{34}$), rod $A_{32}A_{34}B_{34}B_{32}$ and rod $C_{32}C_{34}$ are separately represented as m_{31}, m_{32}, m_{33} and m_{34}. The total mass of the moving platform and two passive linkages installed on it is denoted as m_{35}.

According to the unique configuration of this parallel manipulator, the positions of the slider($A_{31}A_{33}$) and Rod $A_{32}A_{34}B_{34}B_{32}$ can be represented as $P_{A35}(x_{A35},0,0)$ and $P_{A36}(x_{P3},0,z_{P3})$, respectively. The velocities of the slider($B_{31}B_{33}$) and Rod $A_{32}A_{34}B_{34}B_{32}$ are denoted as $P_{B35}(x_{B35},0,0)$ and $P_{B36}(x_{P3},0,z_{P3})$, respectively. The velocities of the slider($C_{31}C_{35}$) and Rod $C_{32}C_{34}$ are defined as $P_{C35}(0,y_{C35},0)$ and $P_{C36}(0,y_{P3},z_{P3})$,

respectively. The corresponding velocity vectors for these aforementioned linkages are denoted as $\dot{\boldsymbol{P}}_{A35}=[\dot{x}_{A35},0,0]^{\mathrm{T}}$, $\dot{\boldsymbol{P}}_{A36}=[\dot{x}_{P3},0,\dot{z}_{P3}]^{\mathrm{T}}$, $\dot{\boldsymbol{P}}_{B35}=[\dot{x}_{B35},0,0]^{\mathrm{T}}$, $\dot{\boldsymbol{P}}_{B6}=[\dot{x}_{P3},0,\dot{z}_{P3}]^{\mathrm{T}}$, $\dot{\boldsymbol{P}}_{C35}=[0,\dot{y}_{C35},0]^{\mathrm{T}}$ and $\dot{\boldsymbol{P}}_{C36}=[0,\dot{y}_{P3},\dot{z}_{P3}]^{\mathrm{T}}$, respectively.

The kinetic energies of three linear actuators are calculated as

$$\begin{cases} K_{A31A33}=\dfrac{1}{2}m_{31}\dot{x}_{A35}^2 \\ K_{B31B33}=\dfrac{1}{2}m_{31}\dot{x}_{B35}^2 \\ K_{C31C33}=\dfrac{1}{2}m_{31}\dot{y}_{C35}^2 \end{cases} \tag{5-75}$$

According to the proof in Equation (5-9), the total kinetic energy of the linkage $A_{31}A_{32}$ and linkage $A_{33}A_{34}$ can be solved as

$$K_{A31A32}=K_{A33A34}=\frac{1}{6}m_{32}(\dot{\boldsymbol{P}}_{A35}^2+\dot{\boldsymbol{P}}_{A36}^2+\dot{\boldsymbol{P}}_{A35}\dot{\boldsymbol{P}}_{A36}) \tag{5-76}$$

In a similar manner, the total kinetic energies of inclined linkages of branch two and branch three are derived as

$$\begin{cases} K_{B31B32}=K_{B33B34}=\dfrac{1}{6}m_{32}(\dot{\boldsymbol{P}}_{B35}^2+\dot{\boldsymbol{P}}_{B36}^2+\dot{\boldsymbol{P}}_{B35}\dot{\boldsymbol{P}}_{B36}) \\ K_{C31C32}=K_{C33C34}=\dfrac{1}{6}m_{32}(\dot{\boldsymbol{P}}_{C35}^2+\dot{\boldsymbol{P}}_{C36}^2+\dot{\boldsymbol{P}}_{C35}\dot{\boldsymbol{P}}_{C36}) \end{cases} \tag{5-77}$$

For the Rod $A_{32}A_{34}B_{34}B_{32}$ and Rod $C_{32}C_{34}$, the kinetic energies of them are determined as

$$\begin{cases} K_{A32A34B34B32}=\dfrac{1}{2}m_{33}(\dot{x}_{P3}^2+\dot{z}_{P3}^2) \\ K_{C32C34}=\dfrac{1}{2}m_{34}(\dot{y}_{P3}^2+\dot{z}_{P3}^2) \end{cases} \tag{5-78}$$

The kinetic energy of the remaining linkages is

$$K_{P3}=\frac{1}{2}m_{35}(\dot{x}_{P3}^2+\dot{y}_{P3}^2+\dot{z}_{P3}^2) \tag{5-79}$$

The total kinetic energy of all the moving links is

$$K_3=K_{A31A33}+2K_{A31A32}+K_{A32A34B34B32}+K_{B31B33}+2K_{B31B32}+K_{C31C33}+2K_{C31C32}+K_{C32C34}+K_{P3} \tag{5-80}$$

According to the coordinate system shown in figure 4-13, the *XOY* plane is taken as a reference. The total potential energy of all moving linkages is

$$U_3 = (3m_{32} + m_{33} + m_{34} + m_{35}) g_z z_{P3} \tag{5-81}$$

where g_z denotes the Z-axis-component of the gravitational acceleration $\boldsymbol{g} = [0, 0, g_z]^{\mathrm{T}}$.

The Lagrangian function is defined as

$$L_3 = K_3 - U_3 \tag{5-82}$$

$q_3 = (x_{P3}, y_{P3}, z_{P3}, x_{A35}, x_{B35}, y_{C35})$ represents the generalized coordinates to be employed in the Lagrangian equation of the first type. Henceforth, three equations containing Lagrangian multiplier λ_{3i} can be listed as

$$\sum\nolimits_{i=1,2,3} \lambda_{3i} \frac{\partial \Gamma_{3i}}{\partial q_{3j}} = \frac{d}{dt}\left(\frac{\partial L_3}{\partial \dot{q}_{3j}}\right) - \frac{\partial L_3}{\partial q_{3j}} - f_{3j} \quad j = 1, 2, 3 \tag{5-83}$$

where $_{3j}$ means the j-th variable of the external force $\boldsymbol{f}_3 = [f_{3x}, f_{3y}, f_{3z}]^{\mathrm{T}}$ exerted on the mobile platform.

Expanding Equation (5-83) yields

$$\begin{cases} 2(x_{P3} - x_{A35})\lambda_{31} + 2(x_{P3} - x_{B35})\lambda_{32} = (\frac{4}{3}m_{32} + m_{33} + m_{35})\ddot{x}_{P3} + \frac{1}{3}m_{32}(\ddot{x}_{A35} + \ddot{x}_{B35}) - f_{3x} \\ 2(y_{P3} - y_{C35})\lambda_{33} = (m_{34} + m_{35})\ddot{y}_{P3} + \frac{1}{3}m_{32}(2\ddot{y}_{P3} + \ddot{y}_{C35}) - f_{3y} \\ 2z_{P3}(\lambda_{31} + \lambda_{32} + \lambda_{33}) = (2m_{32} + m_{33} + m_{34} + m_{35})\ddot{z}_{P3} + (3m_{32} + m_{33} + m_{34} + m_{35})g_z - f_{3z} \end{cases} \tag{5-84}$$

The driving forces on three active prismatic joints can be formulated as

$$F_{3j} = \frac{d}{dt}\left(\frac{\partial L_3}{\partial \dot{q}_{3j}}\right) - \frac{\partial L_3}{\partial q_{3j}} - \sum\nolimits_{i=1,2,3} \lambda_{3i} \frac{\partial \Gamma_{3i}}{\partial q_{3j}} \quad j = 4, 5, 6 \tag{5-85}$$

The inverse dynamic solution is then derived by further expanding Equation (5-85)

$$\begin{cases} F_{31} = m_{31}\ddot{x}_{A35} + \frac{1}{3}m_{32}(2\ddot{x}_{A35} + \ddot{x}_{P3}) - 2(x_{A35} - x_{P3})\lambda_{31} \\ F_{32} = m_{31}\ddot{x}_{B35} + \frac{1}{3}m_{32}(2\ddot{x}_{B35} + \ddot{x}_{P3}) - 2(x_{B35} - x_{P3})\lambda_{32} \\ F_{33} = m_{31}\ddot{y}_{C35} + \frac{1}{3}m_{32}(2\ddot{y}_{C35} + \ddot{y}_{P3}) - 2(y_{C35} - y_{P3})\lambda_{33} \end{cases} \tag{5-86}$$

(ii) Inertia matrix

Both $\dot{\boldsymbol{Q}}_3$ and $\dot{\boldsymbol{X}}_3$ can be expressed according to Equation (4-53)

$$\begin{cases} \dot{\boldsymbol{Q}}_3 = (\boldsymbol{J}_{Q3}^{-1}\boldsymbol{J}_{X3})\dot{\boldsymbol{X}}_3 = \boldsymbol{J}_3\dot{\boldsymbol{X}}_3 \\ \dot{\boldsymbol{X}}_3 = (\boldsymbol{J}_{X3}^{-1}\boldsymbol{J}_{Q3})\dot{\boldsymbol{Q}}_3 = \boldsymbol{J}_3^{-1}\dot{\boldsymbol{Q}}_3 \end{cases} \tag{5-87}$$

The velocity of first active sliding joint can be obtained as

$$\dot{\boldsymbol{P}}_{A35} = \begin{bmatrix} \dot{x}_{A35} \\ 0 \\ 0 \end{bmatrix} = \begin{bmatrix} 1 & 0 & 0 \\ 0 & 0 & 0 \\ 0 & 0 & 0 \end{bmatrix} \dot{\boldsymbol{Q}}_3 = \boldsymbol{J}_{A35}\dot{\boldsymbol{Q}}_3 \tag{5-88}$$

The velocity of rod $A_{32}A_{34}B_{34}B_{32}$ can be arranged as

$$\dot{\boldsymbol{P}}_{A36} = \dot{\boldsymbol{P}}_{B36} = \begin{bmatrix} \dot{x}_{P3} \\ 0 \\ \dot{z}_{P3} \end{bmatrix} = \begin{bmatrix} 1 & 0 & 0 \\ 0 & 0 & 0 \\ 0 & 0 & 1 \end{bmatrix} \dot{\boldsymbol{X}}_3 = \begin{bmatrix} 1 & 0 & 0 \\ 0 & 0 & 0 \\ 0 & 0 & 1 \end{bmatrix} \boldsymbol{J}_3^{-1}\dot{\boldsymbol{Q}}_3 = \boldsymbol{J}_{A36}\dot{\boldsymbol{Q}}_3 = \boldsymbol{J}_{B36}\dot{\boldsymbol{Q}}_3 \tag{5-89}$$

The velocity of the second sliding joint can be stated as

$$\dot{\boldsymbol{P}}_{B35} = \begin{bmatrix} \dot{x}_{B35} \\ 0 \\ 0 \end{bmatrix} = \begin{bmatrix} 0 & 1 & 0 \\ 0 & 0 & 0 \\ 0 & 0 & 0 \end{bmatrix} \dot{\boldsymbol{Q}}_3 = \boldsymbol{J}_{B35}\dot{\boldsymbol{Q}}_3 \tag{5-90}$$

The velocity of the last sliding joint can be expressed as below

$$\dot{\boldsymbol{P}}_{C35} = \begin{bmatrix} 0 \\ \dot{y}_{C35} \\ 0 \end{bmatrix} = \begin{bmatrix} 0 & 0 & 0 \\ 0 & 0 & 1 \\ 0 & 0 & 0 \end{bmatrix} \dot{\boldsymbol{Q}}_3 = \boldsymbol{J}_{C35}\dot{\boldsymbol{Q}}_3 \tag{5-91}$$

The velocity of the rod $C_{32}C_{34}$ can be written as

$$\dot{\boldsymbol{P}}_{C36} = \begin{bmatrix} 0 \\ \dot{y}_{P3} \\ \dot{z}_{P3} \end{bmatrix} = \begin{bmatrix} 0 & 0 & 0 \\ 0 & 1 & 0 \\ 0 & 0 & 1 \end{bmatrix} \dot{\boldsymbol{X}}_3 = \begin{bmatrix} 0 & 0 & 0 \\ 0 & 1 & 0 \\ 0 & 0 & 1 \end{bmatrix} \boldsymbol{J}_3^{-1}\dot{\boldsymbol{Q}}_3 = \boldsymbol{J}_{C36}\dot{\boldsymbol{Q}}_3 \tag{5-92}$$

According to Equations (5-88), (5-90) and (5-91), Equation (5-75) can be rearranged as

$$\begin{cases} K_{A31A33} = \dfrac{1}{2} m_{31} \dot{\boldsymbol{P}}_{A35}^2 = \dfrac{1}{2} m_{31} \dot{\boldsymbol{Q}}_3^{\mathrm{T}} \boldsymbol{J}_{A35}^{\mathrm{T}} \boldsymbol{J}_{A35} \dot{\boldsymbol{Q}}_3 \\ K_{B31B33} = \dfrac{1}{2} m_{31} \dot{\boldsymbol{P}}_{B35}^2 = \dfrac{1}{2} m_{31} \dot{\boldsymbol{Q}}_3^{\mathrm{T}} \boldsymbol{J}_{B35}^{\mathrm{T}} \boldsymbol{J}_{B35} \dot{\boldsymbol{Q}}_3 \\ K_{C31C33} = \dfrac{1}{2} m_{31} \dot{\boldsymbol{P}}_{C35}^2 = \dfrac{1}{2} m_{31} \dot{\boldsymbol{Q}}_3^{\mathrm{T}} \boldsymbol{J}_{C35}^{\mathrm{T}} \boldsymbol{J}_{C35} \dot{\boldsymbol{Q}}_3 \end{cases} \tag{5-93}$$

Combining Equations (5-88) and (5-89), Equation (5-76) can be expressed as below

$$K_{A31A32} = K_{A33A34} = \frac{1}{6} m_{32} \dot{\boldsymbol{Q}}_3^{\mathrm{T}} (\boldsymbol{J}_{A35}^{\mathrm{T}} \boldsymbol{J}_{A35} + \boldsymbol{J}_{A36}^{\mathrm{T}} \boldsymbol{J}_{A36} + \boldsymbol{J}_{A35}^{\mathrm{T}} \boldsymbol{J}_{A36}) \dot{\boldsymbol{Q}}_3 \tag{5-94}$$

On the basis of Equations (5-89)-(5-92), Equation (5-77) can be rewritten as

$$\begin{cases} K_{B31B32} = K_{B33B34} = \frac{1}{6} m_{32} \dot{\boldsymbol{Q}}_3^{\mathrm{T}} (\boldsymbol{J}_{B35}^{\mathrm{T}} \boldsymbol{J}_{B35} + \boldsymbol{J}_{A36}^{\mathrm{T}} \boldsymbol{J}_{A36} + \boldsymbol{J}_{B35}^{\mathrm{T}} \boldsymbol{J}_{A36}) \dot{\boldsymbol{Q}}_3 \\ K_{C31C32} = K_{C33C34} = \frac{1}{6} m_2 \dot{\boldsymbol{Q}}_3^{\mathrm{T}} (\boldsymbol{J}_{C35}^{\mathrm{T}} \boldsymbol{J}_{C35} + \boldsymbol{J}_{C36}^{\mathrm{T}} \boldsymbol{J}_{C36} + \boldsymbol{J}_{C35}^{\mathrm{T}} \boldsymbol{J}_{C36}) \dot{\boldsymbol{Q}}_3 \end{cases} \tag{5-95}$$

Take into consideration the Equations (5-89) and (5-92), Equation (5-78) can be derived as

$$\begin{cases} K_{A32A34B34B32} = \frac{1}{2} m_{33} \dot{\boldsymbol{P}}_{A36}^2 = \frac{1}{2} m_3 \dot{\boldsymbol{Q}}_3^{\mathrm{T}} \boldsymbol{J}_{A36}^{\mathrm{T}} \boldsymbol{J}_{A36} \dot{\boldsymbol{Q}}_3 \\ K_{C32C34} = \frac{1}{2} m_{34} \dot{\boldsymbol{P}}_{C36}^2 = \frac{1}{2} m_{34} \dot{\boldsymbol{Q}}_3^{\mathrm{T}} \boldsymbol{J}_{C36}^{\mathrm{T}} \boldsymbol{J}_{C36} \dot{\boldsymbol{Q}}_3 \end{cases} \tag{5-96}$$

Integrating the second equation of Equation (5-87), Equation (5-79) can be further obtained as

$$K_{P3} = \frac{1}{2} m_{35} \dot{\boldsymbol{X}}_3^2 = \frac{1}{2} m_{35} (\boldsymbol{J}_3^{-1} \dot{\boldsymbol{Q}}_3)^2 = \frac{1}{2} m_{35} \dot{\boldsymbol{Q}}_3^{\mathrm{T}} \boldsymbol{J}_3^{-\mathrm{T}} \boldsymbol{J}_3^{-1} \dot{\boldsymbol{Q}}_3 \tag{5-97}$$

The total kinetic energy of this parallel manipulator will be formulated as

$$K_3 = \frac{1}{2} \dot{\boldsymbol{Q}}_3^{\mathrm{T}} \boldsymbol{I}_3 \dot{\boldsymbol{Q}}_3 \tag{5-98}$$

where

$$\boldsymbol{I}_3 = \sum\nolimits_{j=A,B,C} \left[m_{31} \boldsymbol{J}_{j35}^{\mathrm{T}} \boldsymbol{J}_{j35} + \frac{2}{3} m_{32} (\boldsymbol{J}_{j35}^{\mathrm{T}} \boldsymbol{J}_{j35} + \boldsymbol{J}_{j36}^{\mathrm{T}} \boldsymbol{J}_{j36} + \boldsymbol{J}_{j35}^{\mathrm{T}} \boldsymbol{J}_{j36}) \right] + m_{33} \boldsymbol{J}_{A36}^{\mathrm{T}} \boldsymbol{J}_{A36} + m_{34} \boldsymbol{J}_{C36}^{\mathrm{T}} \boldsymbol{J}_{C36} + m_{35} \boldsymbol{J}_3^{-\mathrm{T}} \boldsymbol{J}_3^{-1}$$

Then the inertia matrix of this this parallel robot can be computed as

$$\boldsymbol{M}_3 = \boldsymbol{J}_3^{\mathrm{T}} \boldsymbol{I}_3 \boldsymbol{J}_3 \tag{5-99}$$

(iii) Inertia-related performances

The parameters of this parallel mechanism are defined at first. The edge length L_{31} of the fixed platform is 320mm. The inclined linkages of three branches are in the same dimension. L_{32}=L_{34}= L_{36}=120mm. L_{33}, L_{35} and L_{37} are 20mm. L_{38}=20mm.The linear slider mass m_{31} is 3.668g. The mass for each inclined linkage m_{32} is 0.696g. The masses for the Rod $A_{32}A_{34}B_{34}B_{32}$ and Rod $C_{32}C_{34}$ are respectively 4.891g and 3.732g. m_{35} is 4.992g. The gravitational acceleration along Z direction g_z is set as -9.8 m/s^2.

According to the definition in Equation (5-30), the JRI index of the spatial parallel robot can be fully derived and it is only related to moving platform height z_{P3} and inclined linkage length L_{32}. In any horizonal plane (parallel to *XOY* plane), the JRI index remain the same. This is because the JRI index is calculated on the basis of the Jacobian matrix $\boldsymbol{J}_3$ shown in Equation (4-54), which only relates to z_{P3} and L_{32} due to its unique configuration and special set of linkage dimensions. Therefore, the distribution of JRI index is plotted with respect to z_{P3} and L_{32}, as depicted in figure 5-10.

From figure 5-10, with a constant L_{32}, the JRI index keeps increasing and the increment gets larger while the moving platform moves higher. Given a pre-described moving platform height z_{P3}, the JRI index shows a downward trend as L_{32} gets longer. The smallest JRI index can be found when the lowest moving platform height and the longest L_{32} are selected.

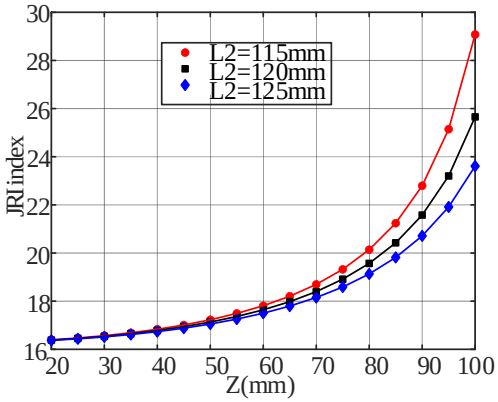

(a) The impact of z

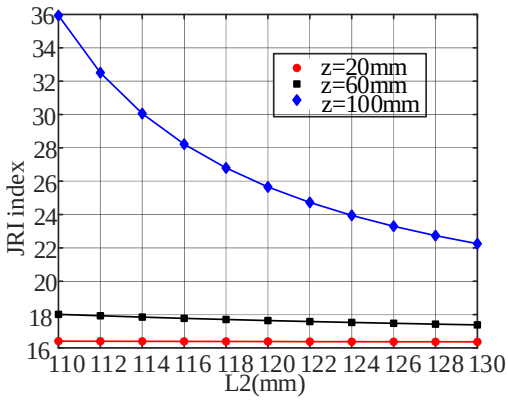

(b) The impact of L_2

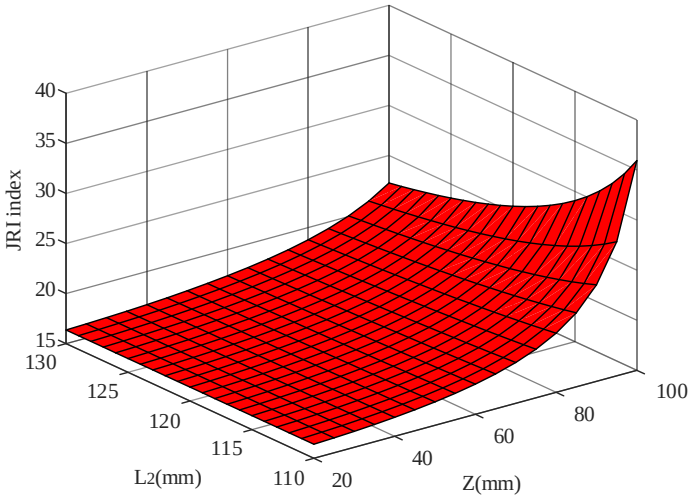

(c) The impact of z and L_2

Figure 5-10 JRI index of the 3T parallel robot

The CVI index of this mechanism is demonstrated in figure 5-11, as calculated from Equation (5-32). With a pre-set L_{32}, the CVI shows a downward trend and then starts to increase when the moving platform moves up. The situation of a constant z_{P3} is complex, as shown in figures 5-11 (b-c). The red line of figure 5-11(b) has an upward trend while enlarging the L_{32} value. However, both the black and blue lines of figure 5-11(b) display downward trends while the L_{32} value grows gradually. It can be seen from figure 5-11(c) that the connection between CVI index and variable L_{32} is not a positive or negative relationship.

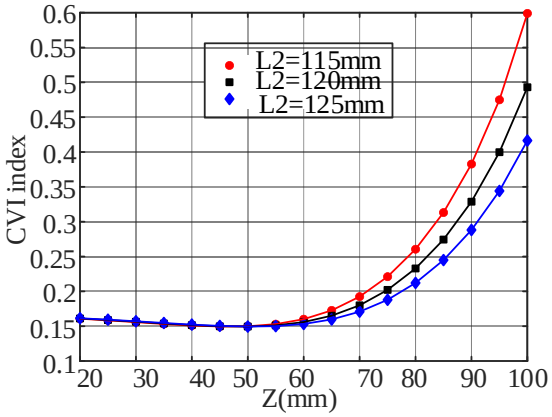

(a) The impact of z

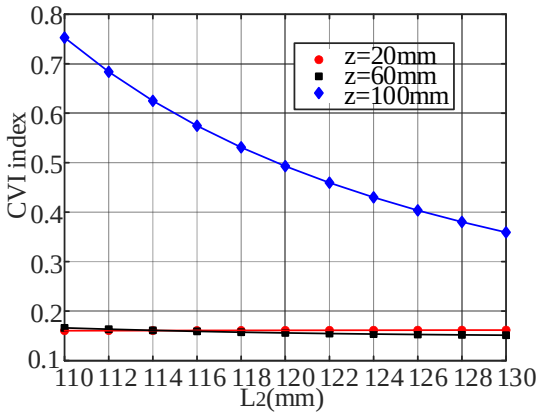

(b) The impact of L_2

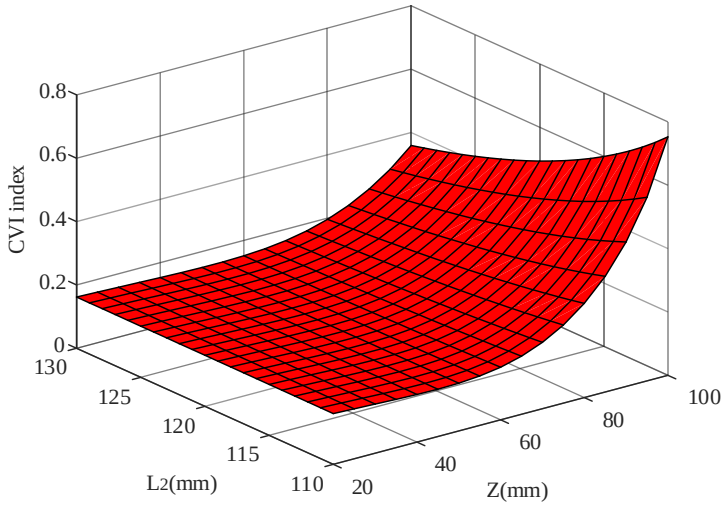

(c) The impact of z and L_2

Figure 5-11 CVI index of the 3T parallel robot

In according to Equation (5-32), the distribution of the BCAI index of this parallel structure is generated and can be seen in figure 5-12. The BCAI rises when the parameter z increases gradually with a constant L_{32}. The BACI index gradually decreases when the variable L_{32} grows gradually with a predefined z_{P3}. Hence, the smallest BCAI value can be achieved with the lowest moving platform height and the largest L_{32} value, as revealed by figure 5-12(c).

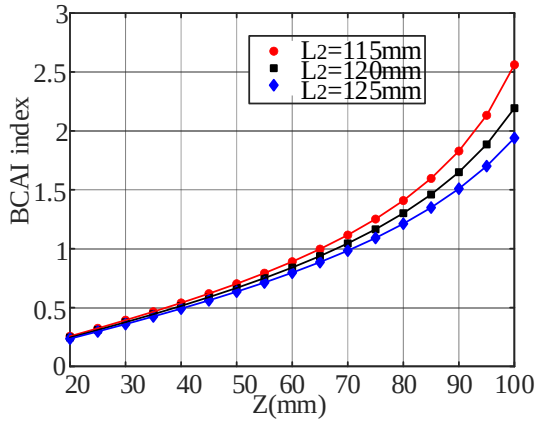

(a) The influence of z

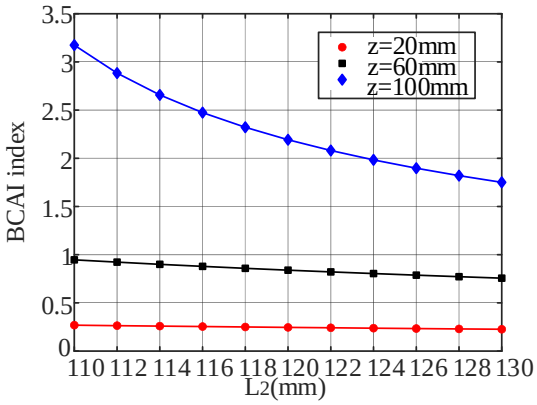

(b) The influence of L_2

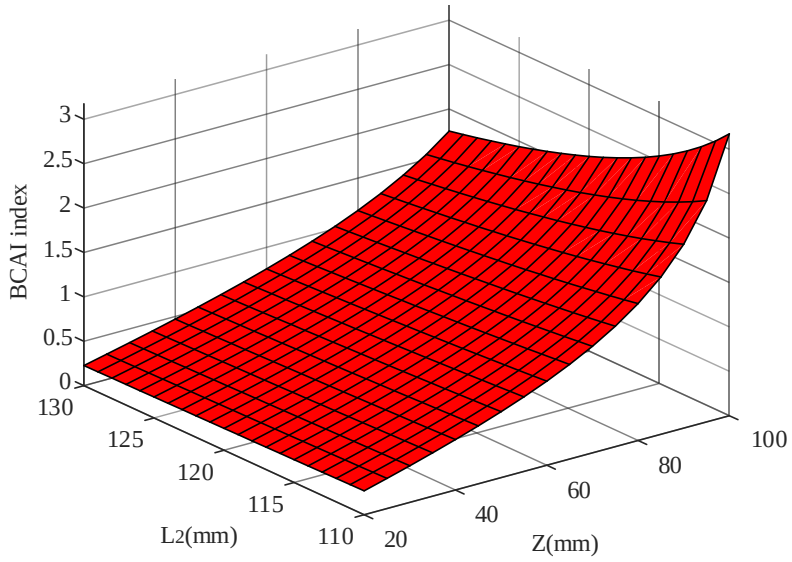

(c) The influence of z and L_2

Figure 5-12 BCAI index of the 3T parallel robot

On the basis of Equation (5-33), The VBCI index of this parallel architecture is calculated and its layout is demonstrated in figure 5-13. The relationship between the VBCI and the variable z_{P3} is positive. The connection between the VBCI index and parameter L_{32} is negative correlation. The largest VBCI value can be fulfilled while employing the highest moving platform height and the shortest L_{32} value, as indicated by figure 5-13 (c).

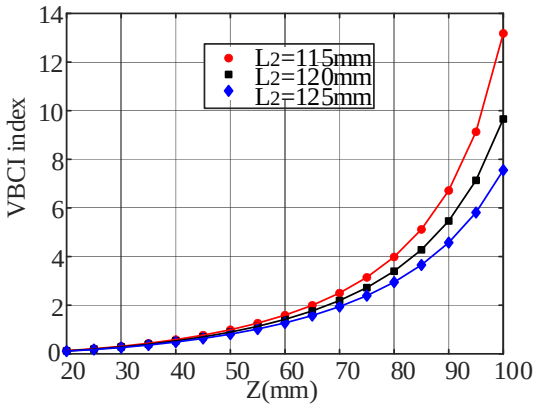

(a) The influence of z

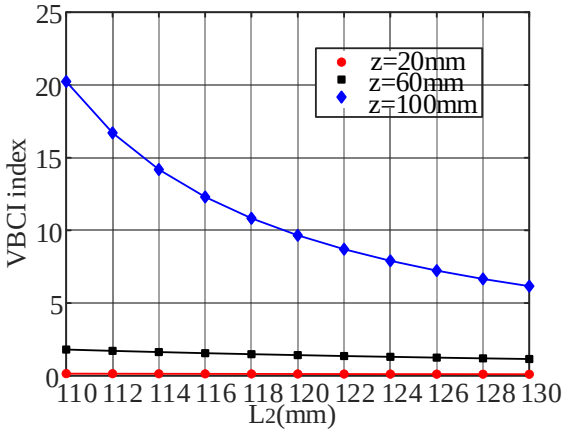

(b) The influence of L_2

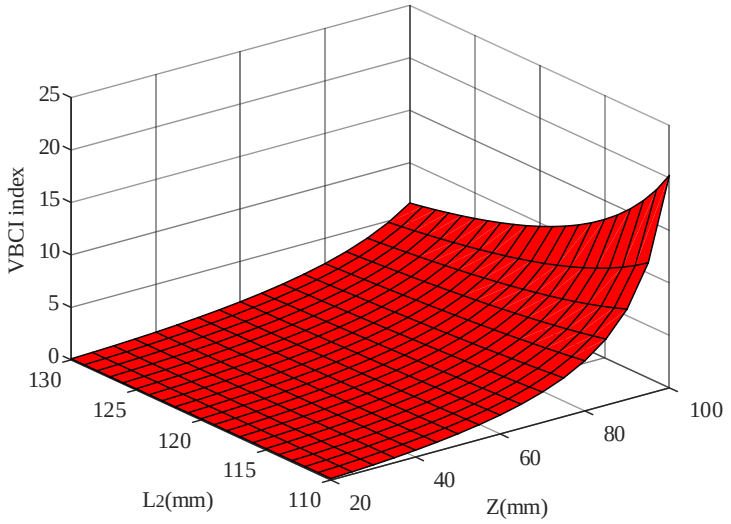

(c) The influence of z and L_2

Figure 5-13 VBCI index of the 3T parallel robot

5.5 Case four: 3T1R parallel mechanism

(i) Dynamic models

The masses of four driving sliders ($A_{41}A_{43}$, $B_{41}B_{43}$, $C_{41}C_{43}$ and $D_{41}D_{43}$) are all indicated as m_{41}. The sloping rods ($A_{41}A_{42}$, $A_{43}A_{44}$, $B_{41}B_{42}$, $B_{43}B_{44}$, $C_{41}C_{42}$, $C_{43}C_{44}$, $D_{41}D_{42}$, $D_{43}D_{44}$) are denoted as m_{42}. The links ($A_{42}A_{44}$, $B_{42}B_{44}$, $C_{42}C_{44}$, $D_{42}D_{44}$) all have the mass of m_{43}. The passive sliding linkage between points A_{46} and A_{47}, B_{46} and B_{47}, C_{46} and C_{47}, D_{46} and D_{47}, have the same sum mass of m_{44}. The total mass of the remaining linkages is m_{45}.

According to the geometric relationship of this 3T1R parallel robot configuration, the positions of several spots can be obtained. $P_{A45}(x_{A45},0,0)$. The position of point P_{A46} is presented as $P_{A46}(x_{P4}-0.5L_{410},0,z_{P4}-0.5L_{410}\sin\varphi_{41})$. The location of the point P_{A47} is denoted as $P_{A47}(x_{P4}-0.5L_{410},y_{P4}-0.5L_{410}\cos\varphi_{41},z_{P4}-0.5L_{410}\sin\varphi_{41})$.

The lumped velocities of rods $A_{41}A_{43}$, $A_{42}A_{44}$ and $A_{46}A_{47}$ are respectively calculated as

$$\dot{\boldsymbol{P}}_{A45}=\begin{bmatrix}\dot{x}_{A45}\\0\\0\\0\end{bmatrix},\dot{\boldsymbol{P}}_{A46}=\begin{bmatrix}\dot{x}_{P4}\\0\\\dot{z}_{P4}-0.5L_{410}\dot{\varphi}_{41}\cos\varphi_{41}\\0\end{bmatrix},\dot{\boldsymbol{P}}_{A47}=\begin{bmatrix}\dot{x}_{P4}\\\dot{y}_{P4}+0.5L_{410}\dot{\varphi}_{41}\sin\varphi_{41}\\\dot{z}_{P4}-0.5L_{410}\dot{\varphi}_{41}\cos\varphi_{41}\\0\end{bmatrix} \quad (5\text{-}100)$$

In the first branch, the kinetic energy of the rod $A_{41}A_{43}$ can be expressed in the following equation

$$K_{A41A43} = \frac{1}{2} m_{41} \dot{\boldsymbol{P}}_{A45}^2 = \frac{1}{2} m_{41} \dot{x}_{A45}^2 \tag{5-101}$$

The kinetic energy for linkage $A_{41}A_{42}$ or $A_{43}A_{44}$ can be deduced as

$$\begin{aligned} K_{A41A42} = K_{A43A44} = \frac{1}{6} m_{42} (\dot{\boldsymbol{P}}_{A45}^2 + \dot{\boldsymbol{P}}_{A46}^2 + \dot{\boldsymbol{P}}_{A45} \dot{\boldsymbol{P}}_{A46}) = \frac{1}{6} m_{42} (\dot{x}_{A45}^2 + \dot{x}_{P4}^2 + \dot{z}_{P4}^2 \\ +0.25 L_{410}^2 \cos^2 \varphi_{41} \dot{\varphi}_{41}^2 - L_{410} \cos \varphi_{41} \dot{z}_{P4} \dot{\varphi}_{41} + \dot{x}_{A45} \dot{x}_{P4}) \end{aligned} \tag{5-102}$$

The kinetic energy of the link $A_{42}A_{44}$ can be computed as

$$K_{A42A44} = \frac{1}{2} m_{43} \dot{\boldsymbol{P}}_{A46}^2 = \frac{1}{2} m_{43} (\dot{x}_{P4}^2 + \dot{z}_{P4}^2 + 0.25 L_{410}^2 \cos^2 \varphi_{41} \dot{\varphi}_{41}^2 - L_{410} \cos \varphi_{41} \dot{z}_{P4} \dot{\varphi}_{41}) \tag{5-103}$$

The kinetic energy of the rod $A_{46}A_{47}$ is expressed as

$$\begin{aligned} K_{A46A47} = \frac{1}{2} m_{44} \dot{\boldsymbol{P}}_{A47}^2 = \frac{1}{2} m_{44} (\dot{x}_{P4}^2 + \dot{y}_{P4}^2 + \dot{z}_{P4}^2 + 0.25 L_{410}^2 \dot{\varphi}_{41}^2 \\ +L_{410} \sin \varphi_{41P4} \dot{y}_{P4} \dot{\varphi}_{41} - L_{410} \cos \varphi_{41} \dot{z}_{P4} \dot{\varphi}_{41}) \end{aligned} \tag{5-104}$$

In the second kinematic chain, $P_{B45}(x_{B45}, 0, 0)$. $P_{B46}(x_{P4} + 0.5L_{410}, 0, z_{P4} - 0.5L_{410} \sin \varphi_{41})$. $P_{B47}(x_{P4} + 0.5L_{410}, y_{P4} - 0.5L_{410} \cos \varphi_{41}, z_{P4} - 0.5L_{410} \sin \varphi_{41})$. Therefore, the overall velocities of linkages $B_{41}B_{43}$, $B_{42}B_{44}$ and $B_{46}B_{47}$ can be solved as

$$\dot{\boldsymbol{P}}_{B45} = \begin{bmatrix} \dot{x}_{B45} \\ 0 \\ 0 \\ 0 \end{bmatrix}, \dot{\boldsymbol{P}}_{B46} = \begin{bmatrix} \dot{x}_{P4} \\ 0 \\ \dot{z}_{P4} - 0.5 L_{410} \dot{\varphi}_{41} \cos \varphi_{41} \\ 0 \end{bmatrix}, \dot{\boldsymbol{P}}_{B47} = \begin{bmatrix} \dot{x}_{P4} \\ \dot{y}_{P4} + 0.5 L_{410} \dot{\varphi}_{41} \sin \varphi_{41} \\ \dot{z}_{P4} - 0.5 L_{410} \dot{\varphi}_{41} \cos \varphi_{41} \\ 0 \end{bmatrix} \tag{5-105}$$

From Equation (5-105), the kinetic energy of link $B_{41}B_{43}$ can be resolved as

$$K_{B41B43} = \frac{1}{2} m_{41} \dot{\boldsymbol{P}}_{B45}^2 = \frac{1}{2} m_{41} \dot{x}_{B45}^2 \tag{5-106}$$

The kinetic energy of linkage $B_{41}B_{42}$ or $B_{43}B_{44}$ can be generated as

$$\begin{aligned} K_{B41B42} = K_{B43B44} = \frac{1}{6} m_{42} (\dot{\boldsymbol{P}}_{B45}^2 + \dot{\boldsymbol{P}}_{B46}^2 + \dot{\boldsymbol{P}}_{B45} \dot{\boldsymbol{P}}_{B46}) = \frac{1}{6} m_{42} (\dot{x}_{B45}^2 + \dot{x}_{P4}^2 + \dot{z}_{P4}^2 \\ +0.25 L_{410}^2 \cos^2 \varphi_{41} \dot{\varphi}_{41}^2 - L_{410} \cos \varphi_{41} \dot{z}_{P4} \dot{\varphi}_{41} + \dot{x}_{B45} \dot{x}_{P4}) \end{aligned} \tag{5-107}$$

The kinetic energy of the rod $B_{42}B_{44}$ is formulated as

$$K_{B42B44} = \frac{1}{2} m_{43} \dot{\boldsymbol{P}}_{B46}^2 = \frac{1}{2} m_{43} (\dot{x}_{P4}^2 + \dot{z}_{P4}^2 + 0.25 L_{410}^2 \cos^2 \varphi_{41} \dot{\varphi}_{41}^2 - L_{410} \cos \varphi_{41} \dot{z}_{P4} \dot{\varphi}_{41}) \tag{5-108}$$

The kinetic energy of the last linkage in the second kinematic limb is written as

$$K_{B46B47} = \frac{1}{2} m_{44} \dot{\boldsymbol{P}}_{B47}^2 = \frac{1}{2} m_{44} (\dot{x}_{P4}^2 + \dot{y}_{P4}^2 + \dot{z}_{P4}^2 + 0.25 L_{410}^2 \dot{\varphi}_{41}^2 + L_{410} \sin \varphi_{41P4} \dot{y}_{P4} \dot{\varphi}_{41} - L_{410} \cos \varphi_{41} \dot{z}_{P4} \dot{\varphi}_{41}) \tag{5-109}$$

In the third kinematic branch, $P_{C45}(0, 0, z_{C45})$. The position of point P_{C46} is $(0, y_{P4} - 0.5 L_{410} \cos \varphi_{41}, z_{P4} - 0.5 L_{410} \sin \varphi_{41})$. The position of point P_{C76} is denoted as $P_{C47}(x_{P4} - 0.5 L_{410}, y_{P4} - 0.5 L_{410} \cos \varphi_{41}, z_{P4} - 0.5 L_{410} \sin \varphi_{41})$.

Hence, the overall velocities of linkages $C_{41}C_{43}$, $C_{42}C_{44}$ and $C_{46}C_{47}$ can be computed as

$$\dot{\boldsymbol{P}}_{C45} = \begin{bmatrix} 0 \\ 0 \\ \dot{z}_{C45} \\ 0 \end{bmatrix}, \dot{\boldsymbol{P}}_{C46} = \begin{bmatrix} 0 \\ \dot{y}_{P4} + 0.5 L_{410} \dot{\varphi}_{41} \sin \varphi_{41} \\ \dot{z}_{P4} - 0.5 L_{410} \dot{\varphi}_{41} \cos \varphi_{41} \\ 0 \end{bmatrix}, \dot{\boldsymbol{P}}_{C47} = \begin{bmatrix} \dot{x}_{P4} \\ \dot{y}_{P4} + 0.5 L_{410} \dot{\varphi}_{41} \sin \varphi_{41} \\ \dot{z}_{P4} - 0.5 L_{410} \dot{\varphi}_{41} \cos \varphi_{41} \\ 0 \end{bmatrix} \tag{5-110}$$

The kinetic energy of the linkage $C_{41}C_{43}$ is described as

$$K_{C41C43} = \frac{1}{2} m_{41} \dot{\boldsymbol{P}}_{C45}^2 = \frac{1}{2} m_{41} \dot{z}_{C45}^2 \tag{5-111}$$

The kinetic energy of the linkage $C_{41}C_{42}$ or $C_{43}C_{44}$ can be formulated as

$$K_{C41C42} = K_{C43C44} = \frac{1}{6} m_{42} (\dot{\boldsymbol{P}}_{C45}^2 + \dot{\boldsymbol{P}}_{C46}^2 + \dot{\boldsymbol{P}}_{C45} \dot{\boldsymbol{P}}_{C46}) = \frac{1}{6} m_{42} (\dot{z}_{C45}^2 + \dot{y}_{P4}^2 + \dot{z}_{P4}^2 + 0.25 L_{410}^2 \dot{\varphi}_{41}^2 + L_{410} \sin \varphi_{41} \dot{y}_{P4} \dot{\varphi}_{41} - L_{410} \cos \varphi_{41} \dot{z}_{P4} \dot{\varphi}_{41} + \dot{z}_{C45} \dot{z}_{P4} - 0.5 L_{410} \cos \varphi_{41} \dot{z}_{C45} \dot{\varphi}_{41}) \tag{5-112}$$

The kinetic energy of the rod $C_{42}C_{44}$ is calculated

$$K_{C42C44} = \frac{1}{2} m_{43} \dot{\boldsymbol{P}}_{C46}^2 = \frac{1}{2} m_{43} (\dot{y}_{P4}^2 + \dot{z}_{P4}^2 + 0.25 L_{410}^2 \dot{\varphi}_{41}^2 + L_{410} \sin \varphi_{41} \dot{y}_{P4} \dot{\varphi}_{41} - L_{410} \cos \varphi_{41} \dot{z}_{P4} \dot{\varphi}_{41}) \tag{5-113}$$

The kinetic energy of the remaining linkage in this branch is derived as

$$K_{C46C47} = \frac{1}{2} m_{44} \dot{\boldsymbol{P}}_{C47}^2 = \frac{1}{2} m_{44} (\dot{x}_{P4}^2 + \dot{y}_{P4}^2 + \dot{z}_{P4}^2 + 0.25 L_{410}^2 \dot{\varphi}_{41}^2 + L_{410} \sin \varphi_{41P4} \dot{y}_{P4} \dot{\varphi}_{41} - L_{410} \cos \varphi_{41} \dot{z}_{P4} \dot{\varphi}_{41}) \tag{5-114}$$

In the last branch, $P_{D45}(0, 0, z_{D45})$. $P_{D46}(0, y_{P4} + 0.5 L_{410} \cos \varphi_{41}, z_{P4} + 0.5 L_{410} \sin \varphi_{41})$. $P_{D47}(x_{P4} - 0.5 L_{410}, y_{P4} + 0.5 L_{410} \cos \varphi_{41}, z_{P4} + 0.5 L_{410} \sin \varphi_{41})$. The overall velocities of linkages $D_{41}D_{43}$, $D_{42}D_{44}$ and $D_{46}D_{47}$ can be defined as

$$\dot{\boldsymbol{P}}_{D45}=\begin{bmatrix}0\\0\\\dot{z}_{D45}\\0\end{bmatrix},\dot{\boldsymbol{P}}_{D46}=\begin{bmatrix}0\\\dot{y}_{P4}-0.5L_{410}\dot{\varphi}_{41}\sin\varphi_{41}\\\dot{z}_{P4}+0.5L_{410}\dot{\varphi}_{41}\cos\varphi_{41}\\0\end{bmatrix},\dot{\boldsymbol{P}}_{D47}=\begin{bmatrix}\dot{x}_{P4}\\\dot{y}_{P4}-0.5L_{410}\dot{\varphi}_{41}\sin\varphi_{41}\\\dot{z}_{P4}+0.5L_{410}\dot{\varphi}_{41}\cos\varphi_{41}\\0\end{bmatrix} \tag{5-115}$$

The kinetic energy of the active sliding linkage is

$$K_{D41D43}=\frac{1}{2}m_{41}\dot{\boldsymbol{P}}_{D45}^2=\frac{1}{2}m_{41}\dot{z}_{D45}^2 \tag{5-116}$$

The kinetic energy of the sloping linkage $D_{41}D_{42}$ or $D_{43}D_{44}$ is computed as

$$\begin{aligned}K_{D41D42}=K_{D43D44}=\frac{1}{6}m_{42}(\dot{\boldsymbol{P}}_{D45}^2+\dot{\boldsymbol{P}}_{D46}^2+\dot{\boldsymbol{P}}_{D45}\dot{\boldsymbol{P}}_{D46})=\frac{1}{6}m_{42}(\dot{z}_{D45}^2+\dot{y}_{P4}^2+\dot{z}_{P4}^2+0.25L_{410}^2\dot{\varphi}_{41}^2\\-L_{410}\sin\varphi_{41}\dot{y}_{P4}\dot{\varphi}_{41}+L_{410}\cos\varphi_{41}\dot{z}_{P4}\dot{\varphi}_{41}+\dot{z}_{D45}\dot{z}_{P4}+0.5L_{410}\cos\varphi_{41}\dot{z}_{D45}\dot{\varphi}_{41})\end{aligned} \tag{5-117}$$

The kinetic energy of the rod $D_{42}D_{44}$ is arranged as

$$K_{D42D44}=\frac{1}{2}m_{43}\dot{\boldsymbol{P}}_{D46}^2=\frac{1}{2}m_{43}(\dot{y}_{P4}^2+\dot{z}_{P4}^2+0.25L_{410}^2\dot{\varphi}_{41}^2-L_{410}\sin\varphi_{41}\dot{y}_{P4}\dot{\varphi}_{41}+L_{410}\cos\varphi_{41}\dot{z}_{P4}\dot{\varphi}_{41}) \tag{5-118}$$

The kinetic energy of linkage $D_{46}D_{47}$ is established as

$$\begin{aligned}K_{D46D47}=\frac{1}{2}m_{44}\dot{\boldsymbol{P}}_{D47}^2=\frac{1}{2}m_{44}(\dot{x}_{P4}^2+\dot{y}_{P4}^2+\dot{z}_{P4}^2+0.25L_{410}^2\dot{\varphi}_{41}^2\\-L_{410}\sin\varphi_{41P4}\dot{y}_{P4}\dot{\varphi}_{41}+L_{410}\cos\varphi_{41}\dot{z}_{P4}\dot{\varphi}_{41})\end{aligned} \tag{5-119}$$

The kinetic energy of the moving platform is generated as

$$K_{P4}=\frac{1}{2}m_{45}(\dot{x}_{P2}^2+\dot{y}_{P2}^2+\dot{z}_{P4}^2)+\frac{1}{2}I_{P4}\dot{\varphi}_{41}^2 \tag{5-120}$$

where I_{P4} indicates the moment of inertia of the mobile platform about the axis that is parallel to X direction and passes through point P_4.

The plane XOY is taken as the reference for gravity. The potential energy of the first kinematic chain is listed as

$$\begin{cases}U_{A41A43}=0\\U_{A41A42}=U_{A43A44}=0.5m_{42}g_z(z_{P4}-0.5L_{410}\sin\varphi_{41})\\U_{A42A44}=m_{43}g_z(z_{P4}-0.5L_{410}\sin\varphi_{41})\\U_{A46A47}=m_{44}g_z(z_{P4}-0.5L_{410}\sin\varphi_{41})\end{cases} \tag{5-121}$$

The potential energy of the second chain is

$$\begin{cases} U_{B41B43} = 0 \\ U_{B41B42} = U_{B43B44} = 0.5m_{42}g_z(z_{P4} - 0.5L_{410}\sin\varphi_{41}) \\ U_{B42B44} = m_{43}g_z(z_{P4} - 0.5L_{410}\sin\varphi_{41}) \\ U_{B46B47} = m_{44}g_z(z_{P4} - 0.5L_{410}\sin\varphi_{41}) \end{cases} \tag{5-122}$$

The potential energy of the third kinematic limb is

$$\begin{cases} U_{C41C43} = m_{41}g_z z_{C45} \\ U_{C41C42} = U_{C43C44} = 0.5m_{42}g_z(z_{C45} + z_{P4} - 0.5L_{410}\sin\varphi_{41}) \\ U_{C42C44} = m_{43}g_z(z_{P4} - 0.5L_{410}\sin\varphi_{41}) \\ U_{C46C47} = m_{44}g_z(z_{P4} - 0.5L_{410}\sin\varphi_{41}) \end{cases} \tag{5-123}$$

The potential energy of the last chain is

$$\begin{cases} U_{D41D43} = m_{41}g_z z_{D45} \\ U_{D41D42} = U_{D43D44} = 0.5m_{42}g_z(z_{D45} + z_{P4} + 0.5L_{410}\sin\varphi_{41}) \\ U_{D42D44} = m_{43}g_z(z_{P4} + 0.5L_{410}\sin\varphi_{41}) \\ U_{D46D47} = m_{44}g_z(z_{P4} + 0.5L_{410}\sin\varphi_{41}) \end{cases} \tag{5-124}$$

The potential energy of the moving platform is

$$U_{P4} = m_{45}g_z z_{P4} \tag{5-125}$$

The corresponding Lagrangian function is introduced as

$$L_4 = K_4 - U_4 \tag{5-126}$$

where the total kinetic energy $K_4 = \sum_{j=A,B,C,D}(K_{j41j43} + 2K_{j41j42} + K_{j42j44} + K_{j46j47}) + K_{P4}$, the total potential energy $U_4 = \sum_{j=A,B,C,D}(U_{j41j43} + 2U_{j41j42} + U_{j42j44} + U_{j46j47}) + U_{P4}$.

$q_4 = (x_{P4}, y_{P4}, z_{P4}, \varphi_{41}, x_{A45}, x_{B45}, z_{C45}, z_{D45})$ indicates the generalized coordinates to be utilized in the Lagrangian equation of the first type. Therefore, four equations containing Lagrangian multiplier λ_{4i} can be listed as

$$\sum_{i=1,2,3,4}\lambda_{4i}\frac{\partial\Gamma_{4i}}{\partial q_{4j}} = \frac{d}{dt}\left(\frac{\partial L_4}{\partial\dot{q}_{4j}}\right) - \frac{\partial L_4}{\partial q_{4j}} - f_{4j} \quad j = 1,2,3,4 \tag{5-127}$$

where f_{41}, f_{42} and f_{42} indicate the external force applied on the moving platform along X, Y and Y directions, respectively. f_{44} denotes the external torque applied on the moving platform about X axis.

The driving forces on these four active prismatic joints can be calculated as

$$F_{4j}=\frac{d}{dt}(\frac{\partial L_4}{\partial \dot{q}_{4j}})-\frac{\partial L_4}{\partial q_{4j}}-\sum\nolimits_{i=1,2,3,4}\lambda_{4i}\frac{\partial \Gamma_{4i}}{\partial q_{4j}}\quad \text{j=5,6,7,8} \tag{5-128}$$

(ii) Inertia matrix

Both $\dot{\boldsymbol{Q}}_4$ and $\dot{\boldsymbol{X}}_4$ can be obtained according to Equation (4-82)

$$\begin{cases}\dot{\boldsymbol{Q}}_4=(\boldsymbol{J}_{Q4}^{-1}\boldsymbol{J}_{X4})\dot{\boldsymbol{X}}_4=\boldsymbol{J}_4\dot{\boldsymbol{X}}_4\\ \dot{\boldsymbol{X}}_4=(\boldsymbol{J}_{X4}^{-1}\boldsymbol{J}_{Q4})\dot{\boldsymbol{Q}}_4=\boldsymbol{J}_4^{-1}\dot{\boldsymbol{Q}}_4\end{cases} \tag{5-129}$$

Based on Equations (5-100) and (5-129), the total velocities of rods $A_{41}A_{43}$, $A_{42}A_{44}$ and $A_{46}A_{47}$ are respectively calculated as

$$\dot{\boldsymbol{P}}_{A45}=\begin{bmatrix}1&0&0&0\\0&0&0&0\\0&0&0&0\\0&0&0&0\end{bmatrix}\dot{\boldsymbol{Q}}_4=\boldsymbol{J}_{A45}\dot{\boldsymbol{Q}}_4$$

$$\dot{\boldsymbol{P}}_{A46}=\begin{bmatrix}1&0&0&0\\0&0&0&0\\0&0&1&-0.5L_{410}\cos\varphi_{41}\\0&0&0&0\end{bmatrix}\dot{\boldsymbol{X}}_4=(\boldsymbol{J}_{A46}\boldsymbol{J}_4^{-1})\dot{\boldsymbol{Q}}_4 \tag{5-130}$$

$$\dot{\boldsymbol{P}}_{A47}=\begin{bmatrix}1&0&0&0\\0&1&0&0.5L_{410}\sin\varphi_{41}\\0&0&1&-0.5L_{410}\cos\varphi_{41}\\0&0&0&0\end{bmatrix}\dot{\boldsymbol{X}}_4=(\boldsymbol{J}_{A47}\boldsymbol{J}_4^{-1})\dot{\boldsymbol{Q}}_4$$

According to Equations (5-101) and (5-130), the kinetic energy of the rod $A_{41}A_{43}$ can be expressed

$$K_{A41A43}=\frac{1}{2}m_{41}\dot{\boldsymbol{P}}_{A45}^2=\frac{1}{2}m_{41}\dot{\boldsymbol{Q}}_4^{\mathrm{T}}\boldsymbol{J}_{A45}^{\mathrm{T}}\boldsymbol{J}_{A45}\dot{\boldsymbol{Q}}_4 \tag{5-131}$$

According to Equations (5-102) and (5-130), the kinetic energy for linkage $A_{41}A_{42}$ or $A_{43}A_{44}$ can be rearranged as

$$K_{A41A42}=K_{A43A44}=\frac{1}{6}m_{42}\dot{\boldsymbol{Q}}_4^{\mathrm{T}}[\boldsymbol{J}_{A45}^{\mathrm{T}}\boldsymbol{J}_{A45}+(\boldsymbol{J}_{A46}\boldsymbol{J}_4^{-1})^{\mathrm{T}}(\boldsymbol{J}_{A46}\boldsymbol{J}_4^{-1})+\boldsymbol{J}_{A45}^{\mathrm{T}}(\boldsymbol{J}_{A46}\boldsymbol{J}_4^{-1})]\dot{\boldsymbol{Q}}_4 \tag{5-132}$$

The kinetic energy of the link $A_{42}A_{44}$ can be rewritten as

$$K_{A42A44}=\frac{1}{2}m_{43}\dot{\boldsymbol{Q}}_4^{\mathrm{T}}(\boldsymbol{J}_{A46}\boldsymbol{J}_4^{-1})^{\mathrm{T}}(\boldsymbol{J}_{A46}\boldsymbol{J}_4^{-1})\dot{\boldsymbol{Q}}_4 \tag{5-133}$$

The kinetic energy of the rod $A_{46}A_{47}$ is resolved as

$$K_{A46A47} = \frac{1}{2} m_{47} \dot{\boldsymbol{Q}}_4^{\mathrm{T}} (\boldsymbol{J}_{A47} \boldsymbol{J}_4^{-1})^{\mathrm{T}} (\boldsymbol{J}_{A47} \boldsymbol{J}_4^{-1}) \dot{\boldsymbol{Q}}_4 \tag{5-134}$$

Equation (5-105) can be rewritten by considering Equation (5-129)

$$\dot{\boldsymbol{P}}_{B45} = \begin{bmatrix} 0 & 1 & 0 & 0 \\ 0 & 0 & 0 & 0 \\ 0 & 0 & 0 & 0 \\ 0 & 0 & 0 & 0 \end{bmatrix} \dot{\boldsymbol{Q}}_4 = \boldsymbol{J}_{B45} \dot{\boldsymbol{Q}}_4$$

$$\dot{\boldsymbol{P}}_{B46} = \begin{bmatrix} 1 & 0 & 0 & 0 \\ 0 & 0 & 0 & 0 \\ 0 & 0 & 1 & -0.5L_{410} \cos\varphi_{41} \\ 0 & 0 & 0 & 0 \end{bmatrix} \dot{\boldsymbol{X}}_4 = (\boldsymbol{J}_{B46} \boldsymbol{J}_4^{-1}) \dot{\boldsymbol{Q}}_4 \tag{5-135}$$

$$\dot{\boldsymbol{P}}_{B47} = \begin{bmatrix} 1 & 0 & 0 & 0 \\ 0 & 1 & 0 & 0.5L_{410} \sin\varphi_{41} \\ 0 & 0 & 1 & -0.5L_{410} \cos\varphi_{41} \\ 0 & 0 & 0 & 0 \end{bmatrix} \dot{\boldsymbol{X}}_4 = (\boldsymbol{J}_{B47} \boldsymbol{J}_4^{-1}) \dot{\boldsymbol{Q}}_4$$

From Equations (5-106) and (5-135), the kinetic energy of link $B_{41}B_{43}$ can be expressed as

$$K_{B41B43} = \frac{1}{2} m_{41} \dot{\boldsymbol{P}}_{B45}^2 = \frac{1}{2} m_{41} \dot{\boldsymbol{Q}}_4^{\mathrm{T}} \boldsymbol{J}_{B45}^{\mathrm{T}} \boldsymbol{J}_{B45} \dot{\boldsymbol{Q}}_4 \tag{5-136}$$

Equation (5-107) can be rearranged as

$$K_{B41B42} = K_{B43B44} = \frac{1}{6} m_{42} \dot{\boldsymbol{Q}}_4^{\mathrm{T}} [\boldsymbol{J}_{B45}^{\mathrm{T}} \boldsymbol{J}_{B45} + (\boldsymbol{J}_{B46} \boldsymbol{J}_4^{-1})^{\mathrm{T}} (\boldsymbol{J}_{B46} \boldsymbol{J}_4^{-1}) + \boldsymbol{J}_{B45}^{\mathrm{T}} (\boldsymbol{J}_{B46} \boldsymbol{J}_4^{-1})] \dot{\boldsymbol{Q}}_4 \tag{5-137}$$

Equation (5-108) is further expressed as

$$K_{B42B44} = \frac{1}{2} m_{43} \dot{\boldsymbol{Q}}_4^{\mathrm{T}} (\boldsymbol{J}_{B46} \boldsymbol{J}_4^{-1})^{\mathrm{T}} (\boldsymbol{J}_{B46} \boldsymbol{J}_4^{-1}) \dot{\boldsymbol{Q}}_4 \tag{5-138}$$

The kinetic energy of the last linkage in the second kinematic limb shown in Equation (5-109) is

$$K_{B46B47} = \frac{1}{2} m_{47} \dot{\boldsymbol{Q}}_4^{\mathrm{T}} (\boldsymbol{J}_{B47} \boldsymbol{J}_4^{-1})^{\mathrm{T}} (\boldsymbol{J}_{B47} \boldsymbol{J}_4^{-1}) \dot{\boldsymbol{Q}}_4 \tag{5-139}$$

The overall velocities of linkages $C_{41}C_{43}$, $C_{42}C_{44}$ and $C_{46}C_{47}$ shown in Equation (5-110) can be rearranged as

$$\dot{\boldsymbol{P}}_{C45} = \begin{bmatrix} 0 & 0 & 0 & 0 \\ 0 & 0 & 0 & 0 \\ 0 & 0 & 1 & 0 \\ 0 & 0 & 0 & 0 \end{bmatrix} \dot{\boldsymbol{Q}}_4 = \boldsymbol{J}_{C45}\dot{\boldsymbol{Q}}_4$$

$$\dot{\boldsymbol{P}}_{C46} = \begin{bmatrix} 0 & 0 & 0 & 0 \\ 0 & 1 & 0 & 0.5L_{410}\sin\varphi_{41} \\ 0 & 0 & 1 & -0.5L_{410}\cos\varphi_{41} \\ 0 & 0 & 0 & 0 \end{bmatrix} \dot{\boldsymbol{X}}_4 = (\boldsymbol{J}_{C46}\boldsymbol{J}_4^{-1})\dot{\boldsymbol{Q}}_4 \tag{5-140}$$

$$\dot{\boldsymbol{P}}_{C47} = \begin{bmatrix} 1 & 0 & 0 & 0 \\ 0 & 1 & 0 & 0.5L_{410}\sin\varphi_{41} \\ 0 & 0 & 1 & -0.5L_{410}\cos\varphi_{41} \\ 0 & 0 & 0 & 0 \end{bmatrix} \dot{\boldsymbol{X}}_4 = (\boldsymbol{J}_{C47}\boldsymbol{J}_4^{-1})\dot{\boldsymbol{Q}}_4$$

The kinetic energy of the linkage $C_{41}C_{43}$ presented in Equation (5-111) is rewritten as

$$K_{C41C43} = \frac{1}{2}m_{41}\dot{\boldsymbol{P}}_{C45}^2 = \frac{1}{2}m_{41}\dot{\boldsymbol{Q}}_4^{\mathrm{T}}\boldsymbol{J}_{C45}^{\mathrm{T}}\boldsymbol{J}_{C45}\dot{\boldsymbol{Q}}_4 \tag{5-141}$$

The kinetic energy of the rod $C_{41}C_{42}$ or $C_{43}C_{44}$ indicated in Equation (5-112) can be generated as

$$K_{C41C42} = K_{C43C44} = \frac{1}{6}m_{42}\dot{\boldsymbol{Q}}_4^{\mathrm{T}}[\boldsymbol{J}_{C45}^{\mathrm{T}}\boldsymbol{J}_{C45} + (\boldsymbol{J}_{C46}\boldsymbol{J}_4^{-1})^{\mathrm{T}}(\boldsymbol{J}_{C46}\boldsymbol{J}_4^{-1}) + \boldsymbol{J}_{C45}^{\mathrm{T}}(\boldsymbol{J}_{C46}\boldsymbol{J}_4^{-1})]\dot{\boldsymbol{Q}}_4 \tag{5-142}$$

The kinetic energy of the rod $C_{42}C_{44}$ displayed in Equation (5-113) is formulated as

$$K_{C42C44} = \frac{1}{2}m_{43}\dot{\boldsymbol{Q}}_4^{\mathrm{T}}(\boldsymbol{J}_{C46}\boldsymbol{J}_4^{-1})^{\mathrm{T}}(\boldsymbol{J}_{C46}\boldsymbol{J}_4^{-1})\dot{\boldsymbol{Q}}_4 \tag{5-143}$$

The kinetic energy of the remaining linkage in this branch is further calculated

$$K_{C46C47} = \frac{1}{2}m_{47}\dot{\boldsymbol{Q}}_4^{\mathrm{T}}(\boldsymbol{J}_{C47}\boldsymbol{J}_4^{-1})^{\mathrm{T}}(\boldsymbol{J}_{C47}\boldsymbol{J}_4^{-1})\dot{\boldsymbol{Q}}_4 \tag{5-144}$$

The lumped velocities of linkages $D_{41}D_{43}$, $D_{42}D_{44}$ and $D_{46}D_{47}$ in Equation (5-115) can be redefined as

$$\dot{\boldsymbol{P}}_{D45} = \begin{bmatrix} 0 & 0 & 0 & 0 \\ 0 & 0 & 0 & 0 \\ 0 & 0 & 0 & 1 \\ 0 & 0 & 0 & 0 \end{bmatrix} \dot{\boldsymbol{Q}}_4 = \boldsymbol{J}_{D45}\dot{\boldsymbol{Q}}_4$$

$$\dot{\boldsymbol{P}}_{D46}=\begin{bmatrix}0&0&0&0\\0&1&0&-0.5L_{410}\sin\varphi_{41}\\0&0&1&0.5L_{410}\cos\varphi_{41}\\0&0&0&0\end{bmatrix}\dot{\boldsymbol{X}}_4=(\boldsymbol{J}_{D46}\boldsymbol{J}_4^{-1})\dot{\boldsymbol{Q}}_4 \tag{5-145}$$

$$\dot{\boldsymbol{P}}_{D47}=\begin{bmatrix}1&0&0&0\\0&1&0&-0.5L_{410}\sin\varphi_{41}\\0&0&1&0.5L_{410}\cos\varphi_{41}\\0&0&0&0\end{bmatrix}\dot{\boldsymbol{X}}_4=(\boldsymbol{J}_{D47}\boldsymbol{J}_4^{-1})\dot{\boldsymbol{Q}}_4$$

The kinetic energy of the active sliding linkage $D_{41}D_{43}$ in Equation (5-116) is then written as

$$K_{D41D43}=\frac{1}{2}m_{41}\dot{\boldsymbol{P}}_{D45}^2=\frac{1}{2}m_{41}\dot{\boldsymbol{Q}}_4^{\mathrm{T}}\boldsymbol{J}_{D45}^{\mathrm{T}}\boldsymbol{J}_{D45}\dot{\boldsymbol{Q}}_4 \tag{5-146}$$

The kinetic energy of the linkage $D_{41}D_{42}$ or $D_{43}D_{44}$ shown in Equation (5-117) is derived as

$$K_{D41D42}=K_{D43D44}=\frac{1}{6}m_{42}\dot{\boldsymbol{Q}}_4^{\mathrm{T}}[\boldsymbol{J}_{D45}^{\mathrm{T}}\boldsymbol{J}_{D45}+(\boldsymbol{J}_{D46}\boldsymbol{J}_4^{-1})^{\mathrm{T}}(\boldsymbol{J}_{D46}\boldsymbol{J}_4^{-1})+\boldsymbol{J}_{D45}^{\mathrm{T}}(\boldsymbol{J}_{D46}\boldsymbol{J}_4^{-1})]\dot{\boldsymbol{Q}}_4 \tag{5-147}$$

The kinetic energy of the link $D_{42}D_{44}$ displayed in Equation (5-118) is rearranged as

$$K_{D42D44}=\frac{1}{2}m_{43}\dot{\boldsymbol{Q}}_4^{\mathrm{T}}(\boldsymbol{J}_{D46}\boldsymbol{J}_4^{-1})^{\mathrm{T}}(\boldsymbol{J}_{D46}\boldsymbol{J}_4^{-1})\dot{\boldsymbol{Q}}_4 \tag{5-148}$$

The kinetic energy of linkage $D_{46}D_{47}$ listed in Equation (5-119) is then solved as

$$K_{D46D47}=\frac{1}{2}m_{47}\dot{\boldsymbol{Q}}_4^{\mathrm{T}}(\boldsymbol{J}_{D47}\boldsymbol{J}_4^{-1})^{\mathrm{T}}(\boldsymbol{J}_{D47}\boldsymbol{J}_4^{-1})\dot{\boldsymbol{Q}}_4 \tag{5-149}$$

The four components in Equation (5-120) can be expressed with respect to $\dot{\boldsymbol{Q}}_4$

$$\begin{bmatrix}\dot{x}_{P4}\\0\\0\\0\end{bmatrix}=\begin{bmatrix}1&0&0&0\\0&0&0&0\\0&0&0&0\\0&0&0&0\end{bmatrix}\dot{\boldsymbol{X}}_4=(\boldsymbol{J}_{P41}\boldsymbol{J}_4^{-1})\dot{\boldsymbol{Q}}\,,\quad \begin{bmatrix}0\\\dot{y}_{P4}\\0\\0\end{bmatrix}=\begin{bmatrix}0&0&0&0\\0&1&0&0\\0&0&0&0\\0&0&0&0\end{bmatrix}\dot{\boldsymbol{X}}_4=(\boldsymbol{J}_{P42}\boldsymbol{J}_4^{-1})\dot{\boldsymbol{Q}}_4$$

$$\begin{bmatrix}0\\0\\\dot{z}_{P4}\\0\end{bmatrix}=\begin{bmatrix}0&0&0&0\\0&0&0&0\\0&0&1&0\\0&0&0&0\end{bmatrix}\dot{\boldsymbol{X}}_4=(\boldsymbol{J}_{P43}\boldsymbol{J}_4^{-1})\dot{\boldsymbol{Q}}_4\,,\quad \begin{bmatrix}0\\0\\0\\\dot{\varphi}_{41}\end{bmatrix}=\begin{bmatrix}0&0&0&0\\0&0&0&0\\0&0&0&0\\0&0&0&1\end{bmatrix}\dot{\boldsymbol{X}}_4=(\boldsymbol{J}_{P44}\boldsymbol{J}_4^{-1})\dot{\boldsymbol{Q}}_4 \tag{5-150}$$

Henceforth, the kinetic energy of the mobile platform shown in Equation (5-120) is computed as

$$K_{P4} = \frac{1}{2} m_{45} \dot{\boldsymbol{Q}}_4^{\mathrm{T}} [(\boldsymbol{J}_{P41} \boldsymbol{J}_4^{-1})^{\mathrm{T}} (\boldsymbol{J}_{P41} \boldsymbol{J}_4^{-1}) + (\boldsymbol{J}_{P42} \boldsymbol{J}_4^{-1})^{\mathrm{T}} (\boldsymbol{J}_{P42} \boldsymbol{J}_4^{-1}) + (\boldsymbol{J}_{P43} \boldsymbol{J}_4^{-1})^{\mathrm{T}} (\boldsymbol{J}_{P43} \boldsymbol{J}_4^{-1})] \dot{\boldsymbol{Q}}_4 + \frac{1}{2} I_{P4} \dot{\boldsymbol{Q}}_4^{\mathrm{T}} (\boldsymbol{J}_{P44} \boldsymbol{J}_4^{-1})^{\mathrm{T}} (\boldsymbol{J}_{P44} \boldsymbol{J}_4^{-1}) \dot{\boldsymbol{Q}}_4 \tag{5-151}$$

The total kinetic energy of this parallel robot is generated as

$$K_4 = \frac{1}{2} \dot{\boldsymbol{Q}}_4^{\mathrm{T}} \boldsymbol{I}_4 \dot{\boldsymbol{Q}}_4 \tag{5-152}$$

where

$$\boldsymbol{I}_4 = \sum_{j=A,B,C,D} \{ m_{41} \boldsymbol{J}_{j45}^{\mathrm{T}} \boldsymbol{J}_{j45} + \frac{2}{3} m_{42} [\boldsymbol{J}_{j45}^{\mathrm{T}} \boldsymbol{J}_{j45} + (\boldsymbol{J}_{j46} \boldsymbol{J}_4^{-1})^{\mathrm{T}} (\boldsymbol{J}_{j46} \boldsymbol{J}_4^{-1}) + \boldsymbol{J}_{j45}^{\mathrm{T}} (\boldsymbol{J}_{j46} \boldsymbol{J}_4^{-1})] + m_{43} (\boldsymbol{J}_{j46} \boldsymbol{J}_4^{-1})^{\mathrm{T}} (\boldsymbol{J}_{j46} \boldsymbol{J}_4^{-1})^{\mathrm{T}} + m_{44} (\boldsymbol{J}_{j47} \boldsymbol{J}_4^{-1})^{\mathrm{T}} (\boldsymbol{J}_{j47} \boldsymbol{J}_4^{-1}) \}$$
$$+ m_{45} [(\boldsymbol{J}_{P41} \boldsymbol{J}_4^{-1})^{\mathrm{T}} (\boldsymbol{J}_{P41} \boldsymbol{J}_4^{-1}) + (\boldsymbol{J}_{P42} \boldsymbol{J}_4^{-1})^{\mathrm{T}} (\boldsymbol{J}_{P42} \boldsymbol{J}_4^{-1}) + (\boldsymbol{J}_{P43} \boldsymbol{J}_4^{-1})^{\mathrm{T}} (\boldsymbol{J}_{P43} \boldsymbol{J}_4^{-1})]$$
$$+ I_{P4} (\boldsymbol{J}_{P44} \boldsymbol{J}_4^{-1})^{\mathrm{T}} (\boldsymbol{J}_{P44} \boldsymbol{J}_4^{-1})$$

At last, the inertia matrix of this this parallel robot can be formulated as

$$\boldsymbol{M}_4 = \boldsymbol{J}_4^{\mathrm{T}} \boldsymbol{I}_4 \boldsymbol{J}_4 \tag{5-153}$$

(iii) Inertia-related performances

The workspace that x_{P4}, y_{P4}, z_{P4} and φ_{41} respectively range from 180mm to 220mm, 80mm to 120mm, 50mm to 90mm, and $-\pi/4 rad$ to $\pi/4 rad$ is selected to evaluate the inertia-related performance indices. The linkage mass information is provided, m_{41}=0.402g. m_{42}=0.108g. m_{43}=0.39g. m_{44}=0.112g. The inertia $I_{P4} = 39636.942\, g \cdot mm^2$.

According to the JRI definition in Equation (5-30), the JRI index of this 3T1R parallel manipulator is computed and this performance is not pertinent to the variable x_{P4}. The JRI index layout with respect to y_{P4} and z_{P4} is plotted in figure 5-14 (a) when x_{P4} is 200mm and φ_{41} is 0. This indicator is not pertinent to y_{P4} from this figure. This performance has a larger value when the mobile platform is higher. The JRI index related to y_{P4} and φ_{41} is displayed in figure 5-14 (b) when x_{P4} is 200mm and z_{P4} is 70mm. This index shows an upward trend as the orientation angle φ_{41} is larger. The impact originated from y_{P4} is

complicated. The JRI index impact from parameters z_{P4} and φ_{41} is displayed in figure 5-14 (c) when x_{P4} is 200mm and y_{P4} is 100mm. The index keeps an upward trend as the moving platform is lifted or the orientation angle φ_{41} is larger.

A fixed position and orientation (x_{P4} =200mm, y_{P4} =100mm, z_{P4} =70mm and φ_{41} =0) within the predefined workspace is selected to conduct the parametric analysis from various linkages. The JRI indicator at this specific pose is not related to L_{41}, L_{43} and L_{412}. The impact from the length L_{42} is shown in figure 5-14 (c). The JRI indicator represents a downward trend as L_{42} changes from 110mm to 130mm. The JRI index keeps grows gradually as L_{410} is extended, as seen in figure 5-14 (e). The JRI index increases and the changing rate grows when L_{411} changes from 180mm to 220mm.

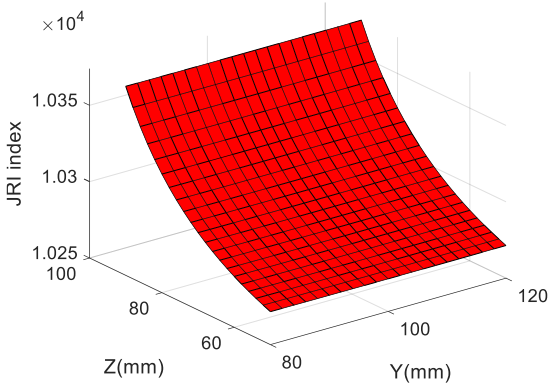

(a) y_{P4} and z_{P4}

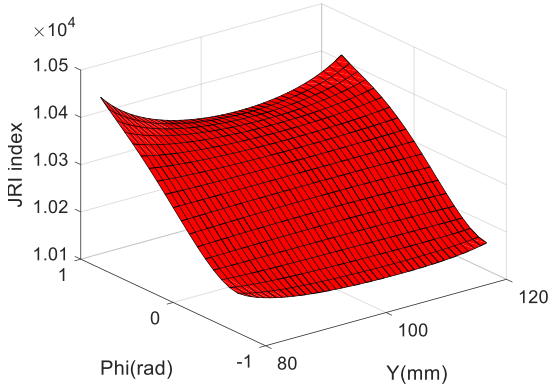

(b) y_{P4} and φ_{41}

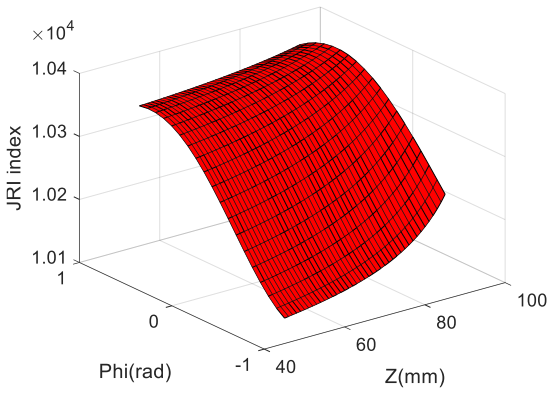

(c) z_{P4} and φ_{41}

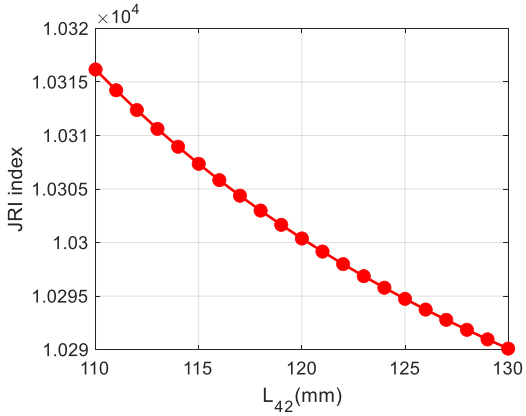

(d) L_{42}

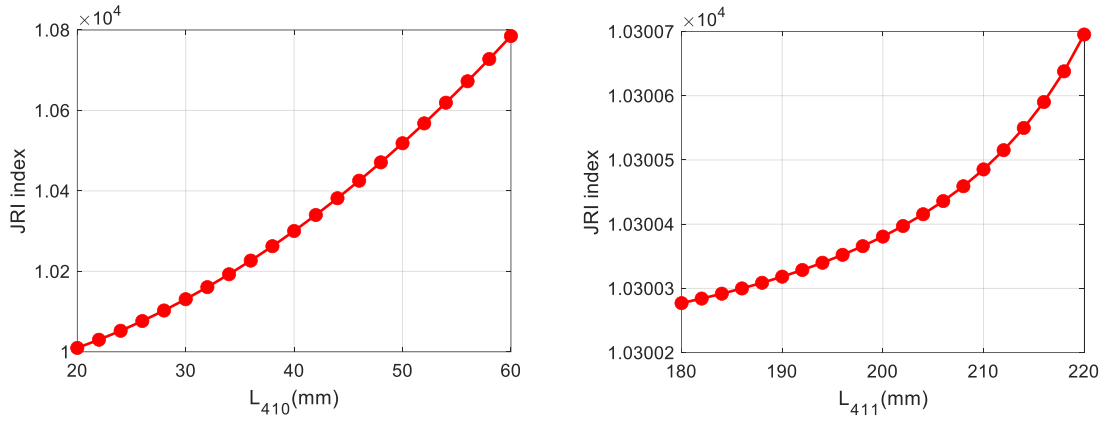

(e) L_{410} (f) L_{411}

Figure 5-14 JRI index of the 3T1R parallel robot

The CVI index is not related to the variable x_{P4}. The distributions of CVI index are illustrated in figures 5-15 (a-c). From the first plot, the CVI index and the mobile platform height have negative relationship with a pre-set y_{P4}. This indicator increases at first and then reduce as the y_{P4} value is larger. The CVI influence from y_{P4} and φ_{41} is displayed in figure 5-15 (b). As the variable y_{P4} changes from 80mm to 120mm, this index improves firstly and then decreases with a constant orientation angle φ_{41}. While the y_{P4} value is fixed, the CVI value also shows an upward trend and then reduces. From figure 5-15 (c), this indicator has a larger value when the mobile platform keeps lower position. This index and the orientation angel φ_{41} have positive relationship.

The CVI index at this special pose is not pertinent to L_{41}, L_{43} and L_{412}. As seen in figures 5-15 (d-f), this index keeps growing and the increasement rate reduces as L_{42} changes from 110mm to 130mm. The CVI value is enhanced as L_{410} extends. The larger L_{411} is, the smaller the index becomes.

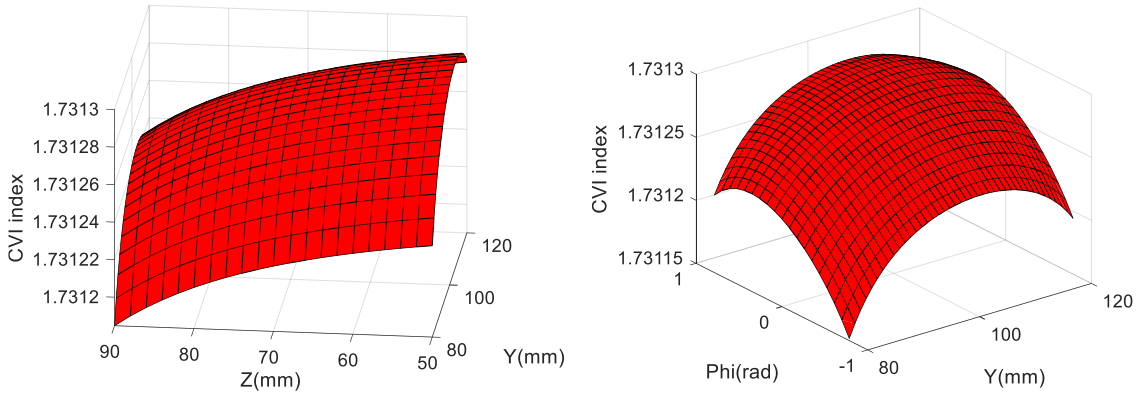

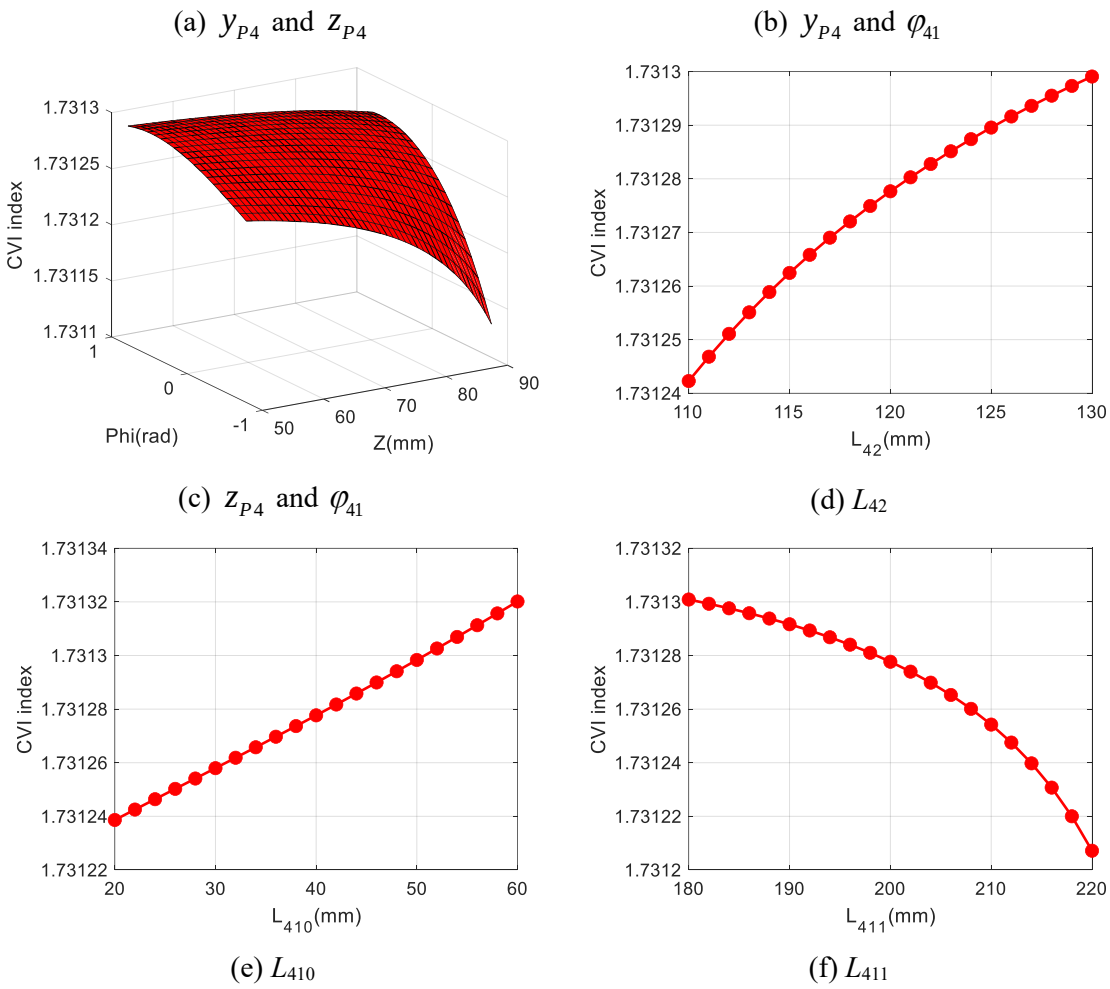

Figure 5-15 CVI index of the 3T1R parallel robot

The BCAI indicator is not associated with the parameter x_{P4}. The layouts of BCAI index are illustrated in figures 5-16 (a-c). As seen from figure 5-16 (a), this indicator and the mobile platform height have negative relationship with a pre-set y_{P4}. This indicator reduces and then improves as a larger y_{P4} value is selected. As demonstrated in figure 5-17 (b), the BCAI index has a complex trend with respect to y_{P4} and φ_{41}. Figure 5-16 (c) provides the impacts from z_{P4} and φ_{41}. The BCAI index shows an upward trend as the height of the mobile platform is higher. The BCAI value originated from φ_{41} is complicated since their relationship is not positive or negative.

In this pose, the BCAI index is not related to L_{41}, L_{43} and L_{412}. As displayed in figures 5-16 (d-f), this index reduces gradually while L_{42} is extended from 110mm to 130mm. The

BCAI value rises when L_{410} changes from 20mm to 60mm. The larger L_{411} is, the higher the index and the increasement rate become.

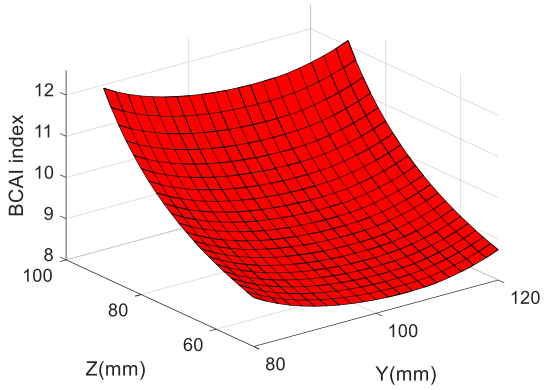

(a) y_{P4} and z_{P4}

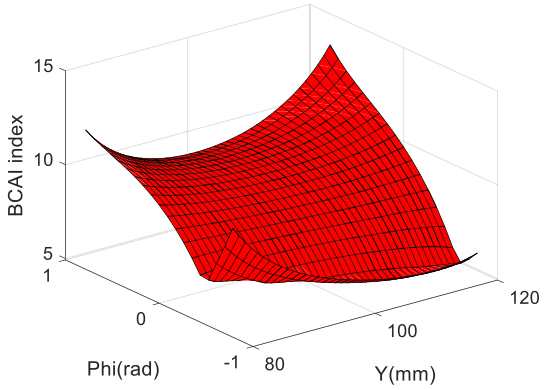

(b) y_{P4} and φ_{41}

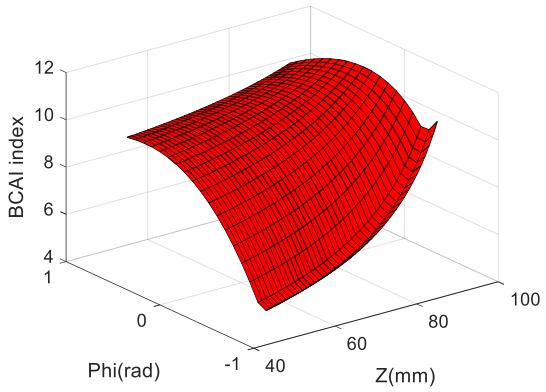

(c) z_{P4} and φ_{41}

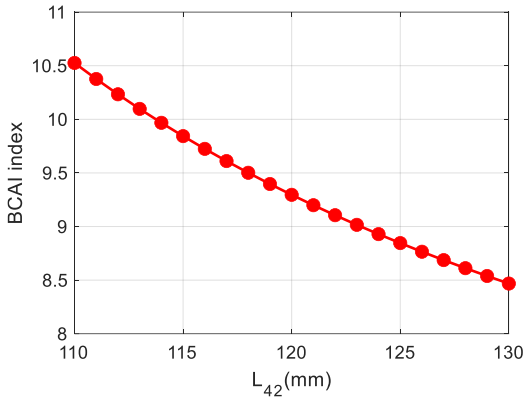

(d) L_{42}

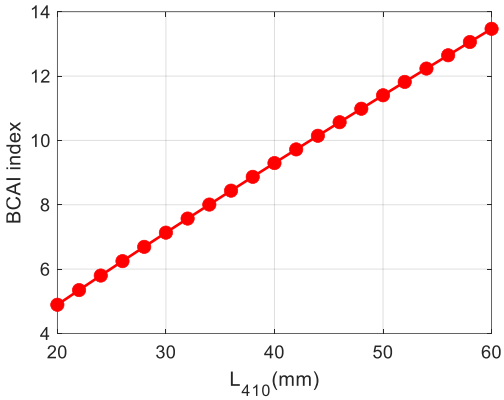

(e) L_{410}

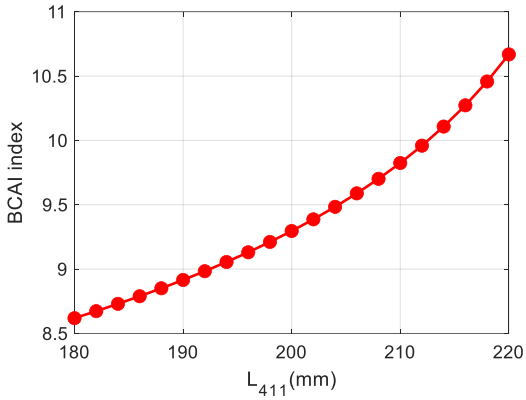

(f) L_{411}

Figure 5-16 BCAI index of the 3T1R parallel robot

The VBCI indicator remains the same value when the parameter x_{P4} is defined by different values. The layouts of VBCI index are demonstrated in figures 5-17 (a-c). From the first figure, with a constant y_{P4} value, this indicator grows gradually as the height of this

moving platform is lifted. This VBCI index reduces and then improves as y_{P4} changes from 80mm to 120mm. The VBCI index relating to y_{P4} and φ_{41} is seen in figure 5-17 (b). The layout of this index is complicated. However, the minimal index can be realized when the largest y_{P4} and the smallest φ_{41} are chosen. The maximal value can be reached when the lowest y_{P4} and the largest φ_{41} are both selected. Figure 5-17 (c) provides the relationship among this index and z_{P4} and φ_{41}. The lowest index value happens when the smallest z_{P4} and φ_{41} are chosen simultaneously.

With the predefined pose, the VBCI indicator can be computed and it is not related to L_{41}, L_{43} and L_{412}. This index decreases as L_{42} changes from 110mm to 130mm, as depicted in figure 5-17 (d). From figures 5-17 (e-f), the VBCI index grows gradually when L_{410} or L_{411} increases within the pre-set ranges.

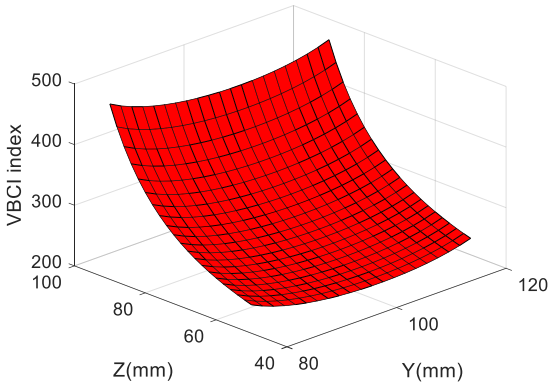

(a) y_{P4} and z_{P4}

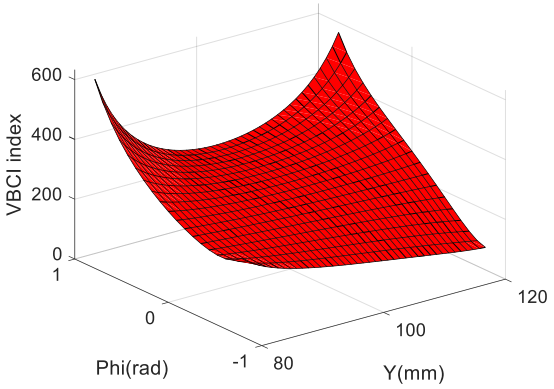

(b) y_{P4} and φ_{41}

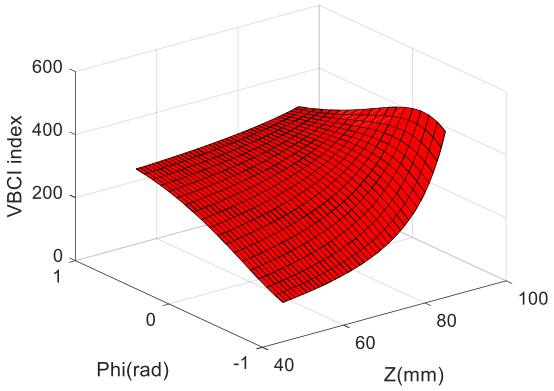

(c) z_{P4} and φ_{41}

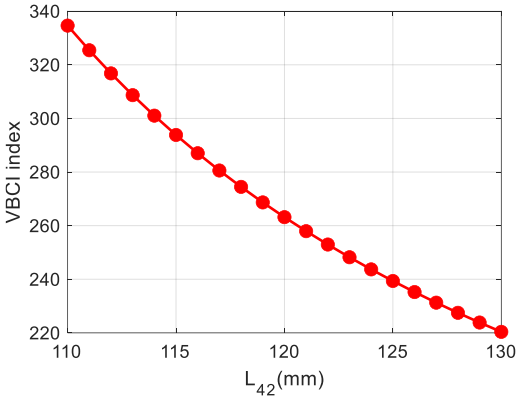

(d) L_{42}

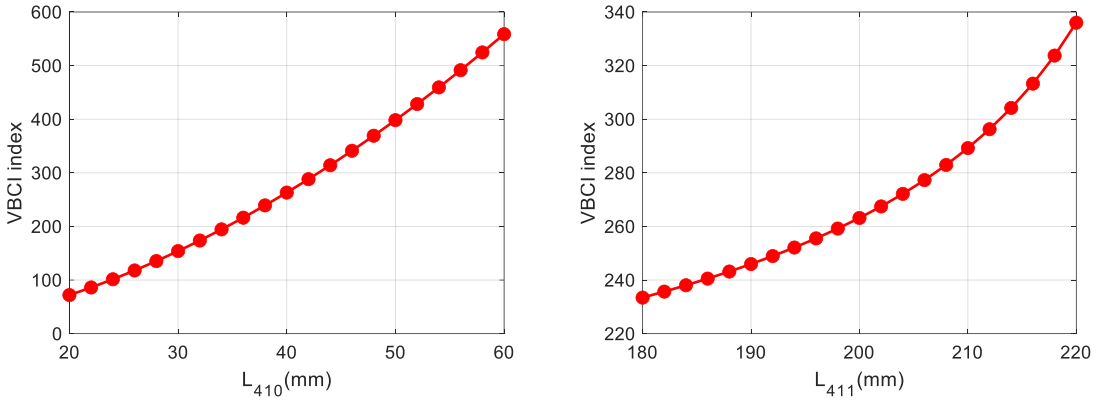

(e) L_{410} (f) L_{411}

Figure 5-17 VBCI index of the 3T1R parallel robot

5.6 Summary

The inverse dynamic models of 2T, 2T1R, 3T and 3T1R parallel manipulators are derived in detail by the Lagrange formulation. The inertia matrix of each parallel structure is generated since the kinetic energy of linkages are rearranged by the relationship with the active linear and rotary velocities. Two novel inertia-related indices, the branch-coupling absolute inertia index and the variation of branch-coupling inertia index, are formulated. The distributions of these two indices and the joint-reflected Inertia index and the coefficient of variation of joint-space inertia index are obtained and compared. The impacts originated from various linkage dimensions on one selected pose are presented.

Chapter 6 Design optimization and experiments

6.1 Dimension optimization

For a parallel structure with various sets of linkages lengths, the overall performance of the is mechanism can be significantly different. As can be seen from Sections 4 and 5, the dimension of any one rod might have impacts on the parallel mechanism. The corresponding linkages (e.g., the sloping linkages in all parallel architectures) may cause distinct influences on the same index. It is essential to determine the best set of linkage dimensions for prototypes. The 2T mechanism in the Section 4.2 is chosen for the optimal design.

This mechanism illustrated in figure 4-1 is a general concept. A modified mechanism is constructed by the coincidence of points A_{12} and B_{12}, points A_{14} and B_{14}, respectively. Under this situation, L_{13}+ L_{16} equals zero. This will retain a more compact structure and increase the reachable workspace under limited strokes of the prismatic joints and small rotary angles of slopping linkages. It is noteworthy that there will be offset in the Z direction between both kinematic chains to avoid limb collision.

The volume of the reachable workspace is one of the most important indicators. The local condition index is necessary to measure the motion transmission of the overall parallel mechanism. The local index only evaluates the performance of one specific pose. The global condition index provides the average performance within the whole reachable workspace. Therefore, the workspace volume and the global condition index are selected to realize the optimal design for this parallel mechanism. In accordance with the special configuration of this mechanism, the lengths L_{11}, L_{12} and L_{13} are the design parameters. The ranges of the linkage lengths are provided below (unit: mm)

$$150 \le L_{11} \le 200, 100 \le L_{12} \le 200, 22.5 \le L_{13} \le 44.5 \tag{6-1}$$

To avoid the singularity configurations, the constraints listed in Section 4.2 are required in this scenario.

The commonly employed non-dominated genetic algorithm II is chosen in this multi-objective optimization process. Compared with the conventional genetic algorithm, this method applies the fast non-dominated sorting algorithm. The crowded comparison and the elitism enable a quick convergence characteristic and the good individuals will retain

in the following generation [163,164]. The steps of this algorithm are briefly introduced below.

In the first step, the population is predefined. The ranges of these variables and constraints are provided. There are 50 individuals in each generation. The maximal generation is set as 100 to guarantee an efficient and global searching process.

In the second step, the fitness functions of the primary population are calculated and these individuals are sorted by their performance. These individuals are arranged into a set of non-dominate fronts.

In each generated front, the crowing distance of each individual is solved, based on which, these individuals are sorted out again. The corresponding selection, mutation and crossover procedures are then implemented and a new generation of individuals are produced.

In the fourth step, all the individuals in these two generations are mixed together. According to the effective elitism approach, only 50 individuals are selected according to the performance rankings.

In the fifth step, the terminal conditions are reviewed. The optimal procedure will be ended if all these requirements are realized. The Pareto optimal or non-dominated solutions are finally found. Otherwise, another generation is introduced and the algorithm will continue to go to the second step for further searching.

The flow diagram of this algorithm is illustrated in figure 6-1. This algorithm searches for the minimal values for both optimization objectives. Therefore, the inverse of the workspace and global condition index are described as

$$\begin{cases} \text{Objective 1}: \dfrac{1}{\text{Workspace Volume}} \\ \text{Objective 2}: \dfrac{1}{\text{GCI}} \end{cases} \tag{6-2}$$

where the volume denotes the amount of discrete feasible configurations.

The dual-objective optimization process is seen in figure 6-2. It can be seen from figure 6-2, the workspace volume continues to increase and keep steady when the generation approaches to the maximal generation. The global condition index increases quickly at the first several generations and then increases slowly. This indicator remains steady since the 20^{th} generation. The variable and performance information of the last generation is listed in table 6-1. It is noteworthy that the 21^{st} to 50^{th} individuals are the same. The Pareto set is

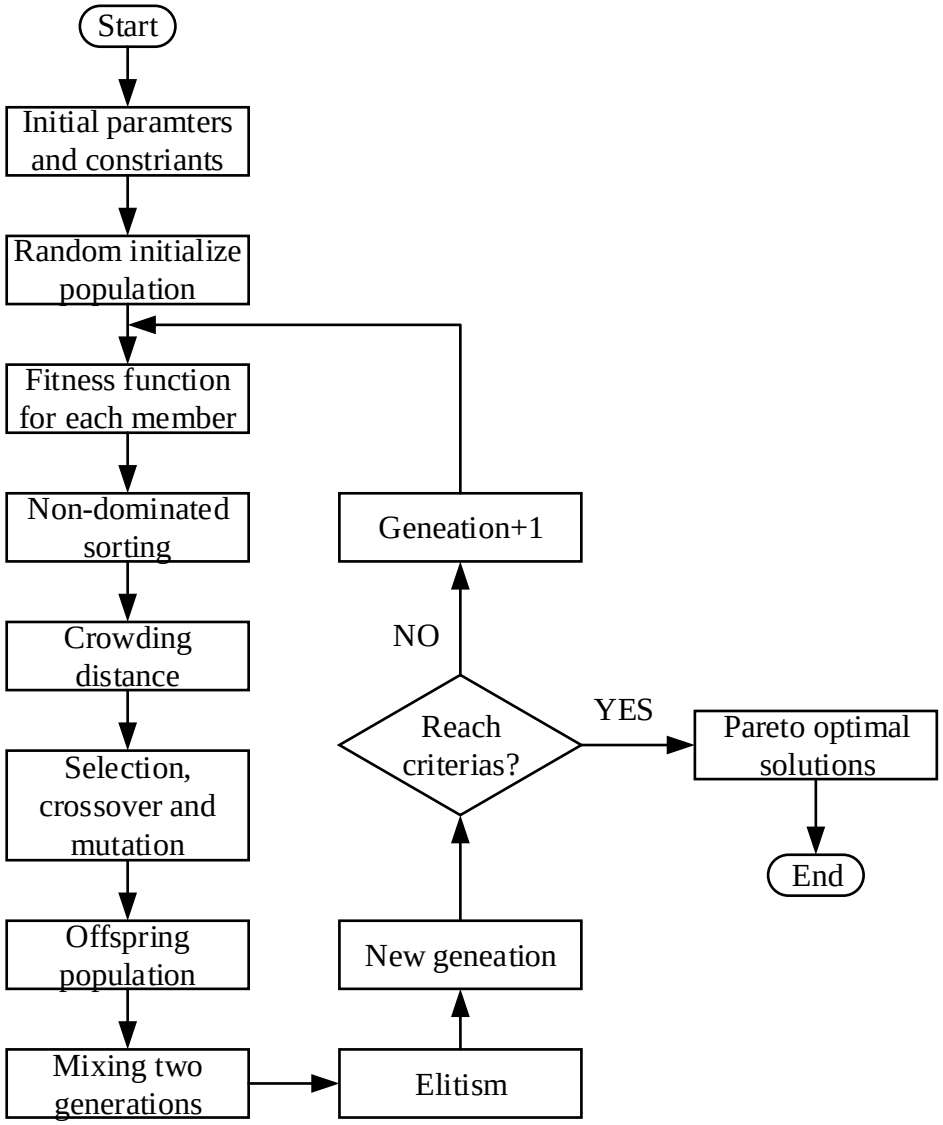

Figure 6-1 Flow diagram of the non-dominated genetic algorithm-II

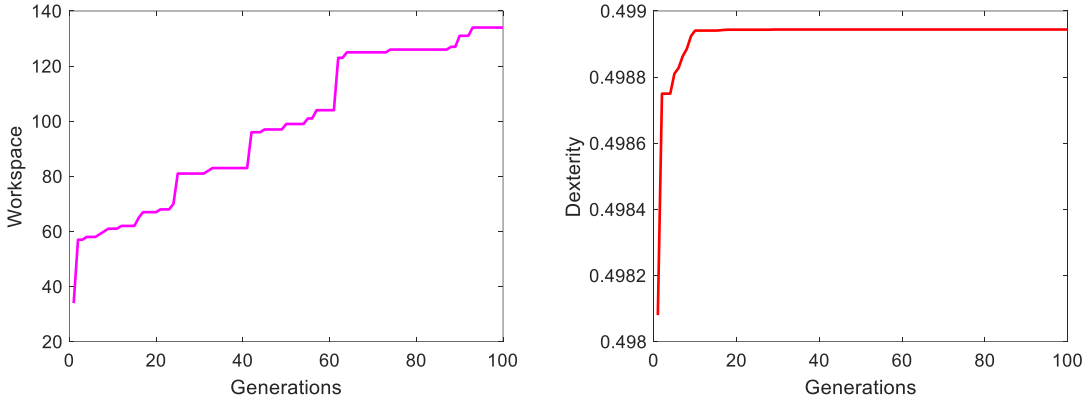

(a) Workspace volume (b) Global condition index

Figure 6-2 Optimization process

Table 6-1 Performances of the last generations

	L_{11}(mm)	L_{12}(mm)	L_{13}(mm)	Workspace	Dexterity
1	195.4	100	25	36	0.49894
2	195.5	101.1	22.5	134	0.49549
3	195.4	100	25	36	0.49894
4	197.5	101.1	25	42	0.49881
5	195.3	100.1	24.5	49	0.49867
6	197.5	101.1	24.1	72	0.49811
7	195.1	100	22.5	121	0.49654
8	197.4	100.8	24.6	64	0.49834
9	195.3	101.5	22.5	122	0.49585
10	195.1	101.3	22.7	100	0.49674
11	197.5	101.1	24.5	56	0.49850
12	197.7	101.1	24	92	0.49720
13	197.4	101	24.4	73	0.49761
14	195.4	100.8	23.5	81	0.49748
15	197.4	100.9	24.5	57	0.49842
16	195.3	101.2	23.1	90	0.49724
17	195.5	101.1	22.5	112	0.49667
18	195.3	100.9	23.5	74	0.49750
19	195.3	101.3	22.5	124	0.49555
20	195.4	101.4	22.5	123	0.49570
21-50	195.4	100	25	36	0.49894

demonstrated in figure 6-3. Since there are 21 data in this figure since there are identical members in this generation. From figure 6-3, some members have supreme global condition index but limited workspace while some individuals own large workspace but unfavourable dexterity. Both performances of the remaining members are not outstanding. The seventh member (denoted by a black pentagram in figure 6-3) of this generation is selected for demonstration. The linkage lengths should be rounded to be easier manufactured. Therefore, L_{11} is 195mm and L_{12} is 100mm. L_{13} remain 22.5mm since 2 L_{13} (e.g., $A_{11}A_{13}$) is often employed in this parallel mechanism.

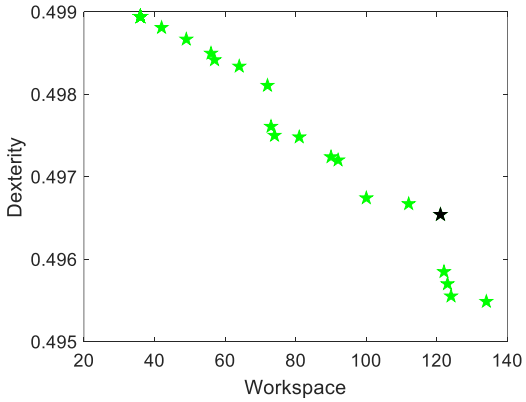

Figure 6-3 The Pareto optimal solutions

6.2 Experiments

On the basis of the optimal design in Section 6.1, the parallel robot in built and the whole system is completed, as demonstrated in figure 6-4. The sliding blocks, sloping linkages and the mobile platform are printed by 3-dimensional (3D) printer. The screw nut units (pitch is 2mm) attached to the sliding blocks are employed for the sliding movement. The DYNAMIXEL MX-64 servo motors are selected to drive the whole robotic system. This power supply could provide direct current with 12-voltage. The motors and the computer are connected by the U2D2 (a communication converter).

In this section, the required movement of the moving platform is designed as (unit: mm)

$$\boldsymbol{X}_1 = [127.5 + \sin t, 152.95 + (\cos t - 1)]^{\mathrm{T}} \tag{6-3}$$

where t denotes time (unit: second).

Considering the real prototype with offsets, the ideal path that can match with Equations (4-7) and (4-8) is $[110 + \sin t, 90 + (\cos t - 1)]^{\mathrm{T}}$ mm. The ideal displacements of two motors both add 17.5mm along X direction and 50.95mm along Y direction, to realize the real positions of these actuators. The following calculations are calculated taking the offsets into account.

The whole running time is 2π seconds. One round of operation for the motor can be divided into 4096 pulses. In accordance with the path of the moving platform, the initial position is (127.5, 152.95) mm. Then the original X-positions for two sliding blocks can be calculated by Equations (4-3) and (4-6), as 83.911 mm and 171.09 mm. The original assembly configuration of the parallel robot is constructed accordingly. The motors can detect its own rotation angles, which will be employed to compute the position of the

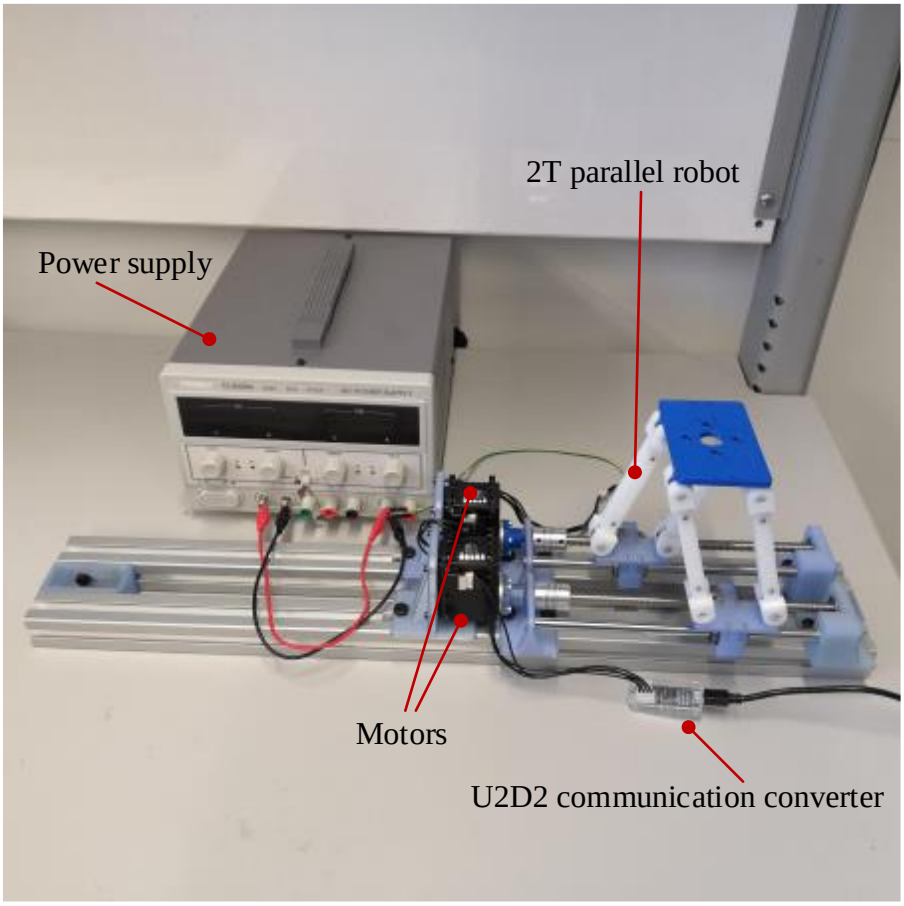

Figure 6-4 The 2T parallel robot prototype

mobile platform by means of the forward kinematic solutions, Equations (4-10) and (4-11). These two motors operate without control strategy and the results are indicated in figure 6-5. From figures 6-5 (a-b), the desired and experimental paths match with each other. The largest errors happen when moving platform moves at the left and right sides of the circular path. The pulse data of these two actuators are seen in figure 6-5 (c). The experimental pulse data of both motors can retain the trends of the desired pulse values, respectively. Since the linear positions of the sliding joints are employed in this design, the displacements of two linear blocks are calculated as indicated in figure 6-5 (d).

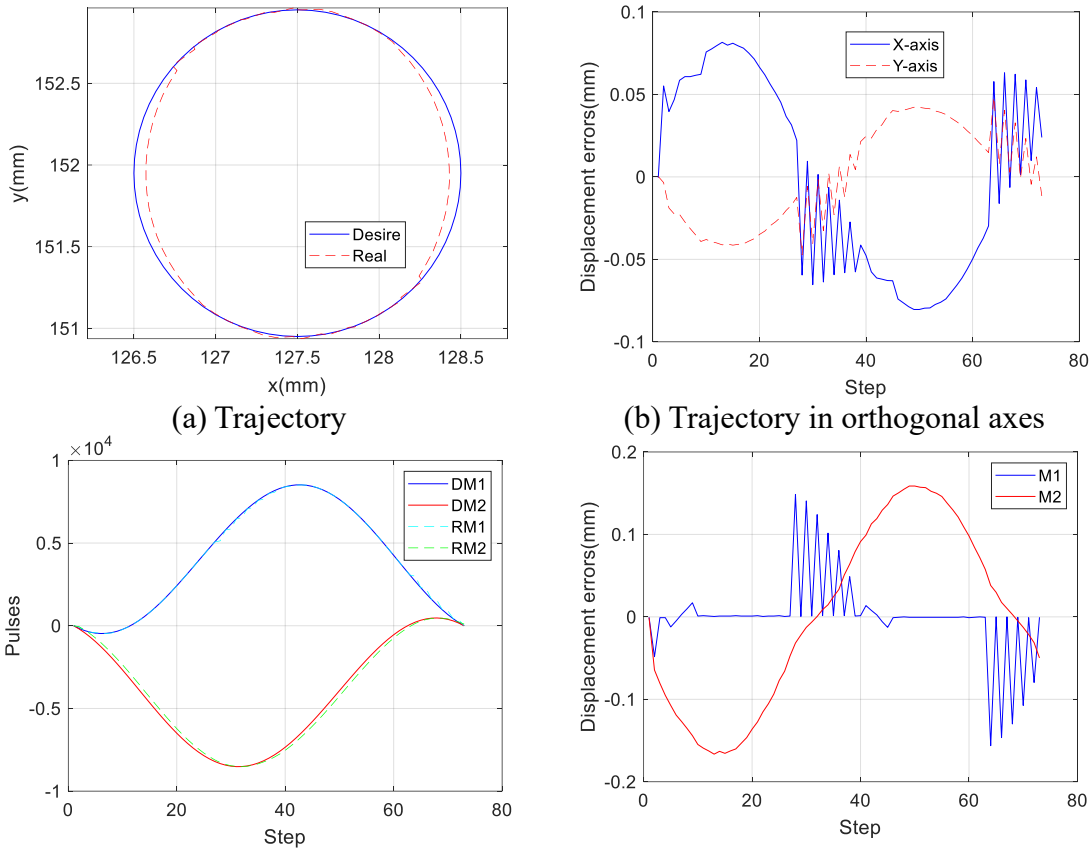

(a) Trajectory (b) Trajectory in orthogonal axes

(c) Pulses of two motors (d) Position errors of two motors

Figure 6-5 The experiment results without controller

(D-Desire solution. R-Real result. M1-Motor 1. M2-Motor 2)

The proportional-integral-derivative (PID) control scheme is utilized to compare with the above results. The PID controller will foster the minimum error between the predefined and experimental results. It has simple algorithm, good robustness and high reliability. It is one of the commonly used controllers both in academic research and industrial products [165,166]. In this section, two independent joint-space PID control strategies are developed for all kinematic branches. Since these controllers are monitoring the displacements of two driving sliding joints, the tracking errors are defined as

$$\begin{cases} e_1(t) = desired\ x_{A15} - actual\ x_{A15} \\ e_2(t) = desired\ x_{B15} - actual\ x_{B15} \end{cases} \tag{6-4}$$

The output of the *i*-th (*i*=1,2) PID control algorithm is expressed as

$$u_i(t) = K_{Pi} e_i(t) + K_{Ii} \int e_i(t)dt + K_{Di} \frac{de_i(t)}{dt} \tag{6-5}$$

where K_{Pi} , K_{Ii} and K_{Di} denote the *i*-th proportional, integral and derivative gains, respectively.

The control scheme is important to instruct the parallel manipulator to run a desired trajectory. The PID control policies illustrated in figure 6-6 are utilized to obtain the required positions of the mobile platform since this parallel manipulator owns a constant orientation in workspace.

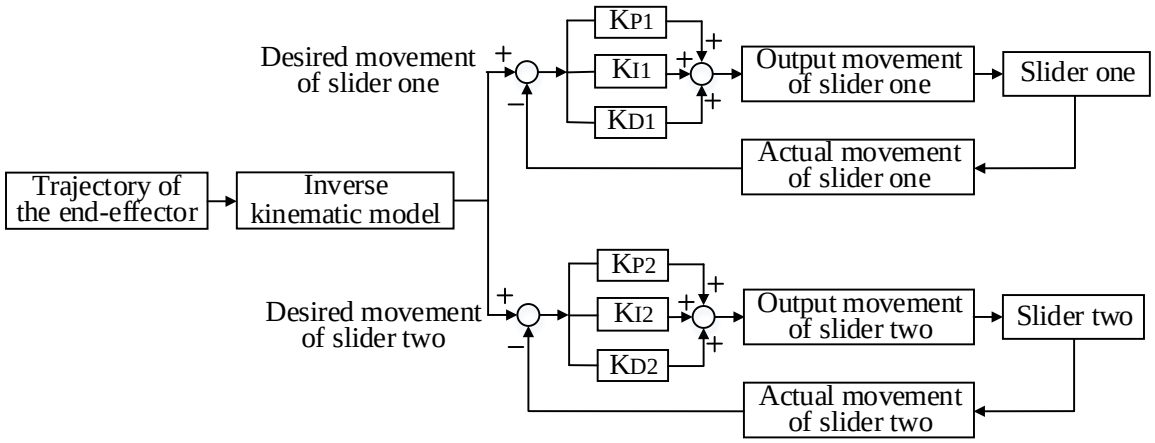

Figure 6-6 Control strategy of the parallel robot

The positions of three active sliders are the control parameters, which are used to promote the proposed parallel mechanism to achieve the desired trajectory smoothly and accurately. These control gains are selected as

$$\begin{cases} K_{P1} = 9 \\ K_{I1} = 0 \\ K_{D1} = 4.5 \end{cases} \quad \begin{cases} K_{P2} = 9.01 \\ K_{I2} = 18.34 \\ K_{D2} = 5.45 \end{cases} \tag{6-6}$$

Both the desired and experimental movements of the moving platform are completed, as illustrated in figure 6-7 (a). The trajectory errors in *X*-direction and *Y*-direction are further computed and presented in figure 6-7 (b). Compare with figures 6-5 (a-b), this moving platform path with controller is closer to the expected trajectory. The differences along both orthogonal directions are shrunk and this result is more stable due to less sawtooth waves. The pulse information of both actuators is illustrated in figure 6-7 (c) and the real results of two motors respectively have better closeness with the desired pulses, compared with the situation without controller as seen in figure 6-5 (c). The displacements for two active sliding joints are also generated as demonstrated in figure 6-7 (d). The errors for both joints are reduced comparing the results in figure 6-5 (d). These errors are small compared with the predefined paths. Overall, the proposed PID control algorithm can achieve the target trajectory smoothly and accurately.

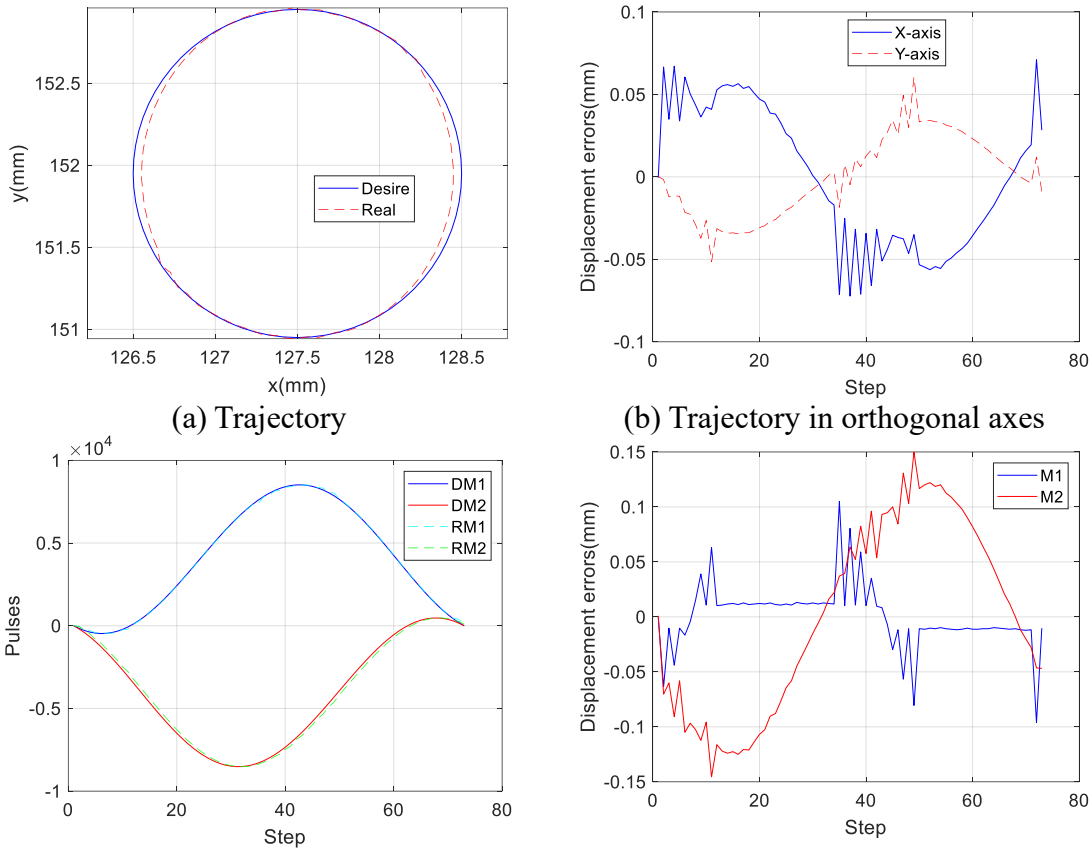

(a) Trajectory (b) Trajectory in orthogonal axes

(c) Pulses of two motors (d) Position errors of two motors

Figure 6-7 The experiment results with controller

(D-Desire solution. R-Real result. M1-Motor 1. M2-Motor 2)

There are several factors that affect the performance of the experimental results.

The first error source comes from the imprecise linkages. These low-cost rods are manufactured by a 3D printer. The lengths of linkages, the distances of rotary shafts are not accurate.

Another factor is the assembly issue. The values in the predefined trajectory and the initial assembly configuration contains decimals, which makes this task more difficult. To achieve the linear motion of the active sliders, the rotary motor, coupler and screw nut system are purchased separately and assembled manually. A higher precision can be realized if the transmission method is simpler. For example, the integrated linear motors can be utilized to avoid accumulated errors.

The target positions with decimal make it harder to send orders to motors. Although there are 4096 pulses for one round of this motor. There are some expected pulses with decimal, which have to be rounded to be sent to motors.

In the experiments, there are some unknown parameters, e.g., friction and joint clearance. The errors for both motors can be reduced if a complete dynamic model including these factors is adopted.

The PID control gains are chosen by trial-and-error approach, which is time consuming. The PID parameter changes of one motor will also cause various performance of another motor. The performance will be improved if better sets of PID variables are applied in this coupled system.

In conclusion, the experiments verify the moving platform can achieve a 2-dimension circular trajectory. The 2-DOF mobility of this parallel robot is confirmed. The mobile platform can realize the expected motions without any control strategy, which denote both the inverse and direct kinematic solutions are correct. The effectiveness of this proposed PID controller is testified with high performance by comparing with the experiment results under no control algorithm.

6.3 Summary

The dimension synthesis of the selected 2T parallel architecture is completed through the non-dominated sorting Genetic Algorithm II. The optimized linkage lengths are generated and chosen after the multi-objective optimization. A position-based control strategy is constructed for the physical prototype. The experiments verify the effectiveness of the movement capability of the robot and the proposed controller.

Chapter 7 Conclusion and future work

7.1 Conclusions

The modified Grübler–Kutzbach equation is further revised to be appropriate to a class of parallel structures containing parallelogram links. A novel kinematic joint matrix is proposed in this research to indicate parallel architectures under predefined conditions. The mapping relationships between the kinematic joint matrix and parallel manipulators can be one-to-one mapping and one-to-many mapping based on the predefined assembly conditions. The special block pattern is essential to distinguish various kinematic joint matrices, especially for matrices with plenty of elements. Therefore, a family of two to six degrees of freedom parallel structures are completely enumerated by the kinematic joint matrices. The unqualified parallel mechanisms are detailed explained with the assistance of the screw theory.

Two planar and spatial parallel manipulators are selected. Their kinematic solutions and singularity configurations are explored. The linkage impacts on the reachable workspaces for four parallel structures and the operational workspaces for 2T and 3T parallel architectures are explored. The novel indicator-level index is proposed to measure the performance rating within reachable workspace. It can be utilized for any performance index larger than zero for every position and orientation. The local condition index is employed to test this concept on these four linkage mechanisms. The inverse dynamic models and inertia matrices for these four parallel robots are calculated in detail, based on which, the distributions of two novel mass-related performance indicators are presented and compared. The optimal sets of linkage dimensions with a large workspace region and good dexterity index for a planar translational parallel structure are obtained through multi-objective optimization algorithm. The experiments demonstrated the correctness of the analytical inverse and forward kinematic solutions, since the experimental results match with the target movements.

7.2 Contributions of the dissertation

(i) Revise the modified Grübler–Kutzbach formula

Although the modified Grübler–Kutzbach equation could solve the mobility problems for most parallel structures, the DOFs of some parallel mechanisms with special configurations can not be revealed correctly. In accordance with one such exception, a family of parallel

architectures with planar joints and parallelogram units is summarized. A special term containing of the order of the parallel mechanism is proposed and supplemented in this equation, in order to disclose the DOFs for this group of parallel manipulators.

(ii) Design kinematic joint matrix to represent mechanisms

The novel kinematic joint matrix is proposed in this research. This square matrix with compact size can indicate parallel manipulators containing of three categories of kinematic pairs. The joints directions can be demonstrated through this kind of matrix. This 3-by-3 square matrix can be treated as a module and additional modules will be provided if the kinematic joints exceed the current unit.

(iii) Create unique block pattern for matrices distinction

Since the kinematic joint matrix is inadequate to represent a concrete parallel mechanism due to various coordinate systems and the one-to-many mapping relations with the parallel structures, a special block pattern is proposed to distinguish different kinds of kinematic joint matrices. Given a kinematic joint matrix, the amounts of various kinematic pairs are collected and located in this block pattern. Different patterns denote distinct matrices. This kind of block pattern is also beneficial to identify the same kind of matrices, eliminate repeated kinematic joint matrices and has the potential to automatically generate all reliable kinematic joint matrices via software under given conditions.

(iv) Establish a systematic approach for structural synthesis

A detailed structural synthesis of a family of parallel robots is proposed. On the basis of the revised mobility equation, the possible parallel manipulators with all kinds of movement types are completed enumerated. In each scenario, the feasible limbs are obtained under predefined conditions and indicated by kinematic joint matrices. The combinations among all matrices are conducted and the same categories of matrices are eliminated. Therefore, two kinds of 2T matrices, ten kinds of 3T matrices, two kinds of 2T1R matrices, twenty-four kinds of 3T1R matrices, forty kinds of 3T2R matrices and seventy-three 3T3R parallel matrices are constructed. The mobility analysis of the structures or kinematic limbs for the remaining 1T1R, 1T2R, 3R, 2T2R, 1T2R, 2T2R, 1T3R, 2T3R parallel structure types are investigated by the theory of screw. Based on the calculations and discussions, they are defined as infeasible structures.

(v) Propose level index for parallel structures

The novel level index is presented to unify the performance indicator and measure the performance rank in the whole reachable workspace. The local condition index is employed to testify its effectiveness. The local level condition indices of the selected 2T and 3T parallel manipulators are computed. The local translational level condition index and the local rotational level condition index of the 2T1R and 3T1R parallel structures are generated. Their distributions with respect to each pose component are established.

(vi) Develop inertia-related performance indices of parallel mechanisms

Two dynamic performance indices about the inertia matrix, the branch-coupling absolute inertia index and the variation of branch-coupling inertia index, are proposed in this research to study the coupling-inertia features among various kinematic limbs within the parallel architecture. These two indicators are mutually complementary and should be employed together to measure the detailed performances of a given parallel structure. The detailed inverse dynamic models and inertia matrices of four different parallel robots are derived, in order to testify the proposed concepts. Furthermore, the parametric impacts on these indicators are investigated.

7.3 Future work

(i) Broaden type synthesis approach

In the future research, this novel structural synthesis will be expanded and completed, to be suitable for some parallel mechanisms with more complicated joint types and configurations. The first aspect is that the current methodology can deal with fully parallel robots. There are still a lot of other kind parallel structures, e.g., parallel manipulators with kinematic redundancy, actuation redundancy, asymmetric kinematic chains, over-constraints. The second concern is that the current approach is applicable for three kinds of kinematic joints (prismatic, rotary and P_a joints). It is expected to be suitable for parallel architectures with more different joints (i.e., helical, cylindrical, universal joints). What's more, it is better to include the other modular generalized kinematic joints (i.e. $(S\text{-}S)_2$, $(S\text{-}S)_2$, five-bar linkage). The kinematic joint matrix already includes the joint direction information. Besides the joint directions are parallel and orthogonal, the joint axes may intersect at one fixed special position (especial for sphere parallel robots). The considerations with all these joints relationships will further widen the functions of this approach.

(ii) Proper limb/joint positions

Their detailed kinematic and dynamic analyses of two planar and spatial parallel mechanisms are conducted in Chapters 4 and 5. However, the kinematic limbs are assembled without consideration of static force/torque balance. Without a proper limb position, the unbalanced static configuration may cause larger joints frictions in the movements. The kinematic pairs will bear larger forces/torques in different directions. This situation is beneficial to lead to link deformation and it is difficult to remain the precise motions. These issues should be avoided before making a physical prototype.

Another target is for the performance of parallel robot. For example, the whole parallel robot configuration remains the same but different positions or offsets for kinematic limbs or joints will lead to various reachable translational or rotary workspace volumes/regions. The consideration should be included to maximum the potential of a given parallel structure.

(iii) Completed mathematical models

The joint clearance that is neglected in the kinematic models will reduce the motion (position and orientation) accuracy of the moving platform. This issue will be worse when there are more passive joints in kinematic chains due to the cumulative impacts. Both the kinematic and dynamic performances based on the kinematic solutions will be influenced. Therefore, a completed kinematic model considering joint clearance is essential to achieve the target accuracy of the parallel robot.

In the dynamic model, each linkage should be modelled in accordance with its real shape and mass distribution instead of a uniform bar. The joint frictions should be taken into account for realizing the real physical scenario.

Bibliography

[1] N. Ma, X. Dong, J.C. Arreguin, C. Bishop, D. Axinte, A class of novel underactuated positioning systems for actuating/configuring the parallel manipulators. Robotica, (2022):1-20.

[2] X.S. Gao, D.L. Lei, Q.Z. Liao, G.F. Zhang, Generalized Stewart-Gough platforms and their direct kinematics, IEEE Transactions on Robotics, 21(2) (2005): 141-151.

[3] T. Sun, B.B. Lian, Y.M. Song, L. Feng, Elastodynamic optimization of a 5-DoF parallel kinematic machine considering parameter uncertainty, IEEE/ASME Transactions on Mechatronics, 24(1) (2019): 315-325.

[4] G. Carabin, L. Scalera, T. Wongratanaphisan, R. Vidoni, An energy-efficient approach for 3D printing with a Linear Delta Robot equipped with optimal springs, Robotics and Computer-Integrated Manufacturing, 67 (2021): 102045.

[5] K.F. Wen, C. Gosselin, Static model based grasping force control of parallel grasping robots with partial cartesian force measurement, IEEE/ASME Transactions on Mechatronics, 27(2) (2021): 999-1010.

[6] P. Miermeister, M. Lächele, R. Boss, C. Masone, C. Schenk, J. Tesch, M. Kerger, H. Teufel, A. Pott, H.H. Bülthoff, The cablerobot simulator large scale motion platform based on cable robot technology, IEEE/RSJ International Conference on Intelligent Robots and Systems (IROS), (2016): 3024-3029.

[7] Y.Q. Wang, J.J. Cao, R.R. Geng, L. Zhou, L. Wang. Study on the design and control method of a wire-driven waist rehabilitation training parallel robot, Robotica, (2022): 1-15.

[8] Z. Huang, J.F. Liu, Y.W. Li, On the degree of freedom-the general formula of the degree of freedom which has been searched for 150 years, Beijing Science Press, (2011).

[9] Q. Zou, D. Zhang, X.L. Luo, G.Y. Huang, L.J. Li, H.Q. Zhang, Enumeration and optimum design of a class of translational parallel mechanisms with prismatic and parallelogram joints, Mechanism and Machine Theory, 150 (2020): 103846.

[10] J.A. Carretero, R.P. Podhorodeski, M.A. Nahon, C.M. Gosselinn, Kinematic analysis and optimization of a new three degree-of-freedom spatial parallel manipulator, Journal of Mechanical Design, 122(1) (2000): 17-24.

[11] Q.C. Li, J.M. Hervé, 1T2R parallel mechanisms without parasitic motion, IEEE Transactions on Robotics, 26(3) (2010): 401-410.

[12] Q.C. Li, Z. Chen, Q.H. Chen, C.Y. Wu, X.D. Hu, Parasitic motion comparison of 3-PRS parallel mechanism with different limb arrangements, Robotics and Computer-Integrated Manufacturing, 27(2) (2011): 389-396.

[13] Z.H. Chong, F.G. Xie, X.J. Liu, J.S. Wang, H.F. Niu, Design of the parallel mechanism for a hybrid mobile robot in wind turbine blades polishing, Robotics and Computer-Integrated Manufacturing, 61 (2020): 101857.

[14] M.L. Husty, An algorithm for solving the direct kinematics of general Stewart-Gough platforms, Mechanism and Machine Theory, 31(4) (1996): 365-379.

[15] T.Y. Lee, J.K. Shim, Forward kinematics of the general 6–6 Stewart platform using algebraic elimination, Mechanism and Machine Theory 36(9) (2001): 1073-1085.

[16] M. Raghavan, Madhusudan, The Stewart platform of general geometry has 40 configurations, (1993): 277-282.

[17] J.P. Merlet, J-P, Solving the forward kinematics of a Gough-type parallel manipulator with interval analysis, The International Journal of robotics research, 23(3) (2004): 221-235.

[18] Y.M. Li, Q.S. Xu, Kinematic analysis and design of a new 3-DOF translational parallel manipulator, (2006): 729-737.

[19] K.F. Wen, C.M. Gosselin, Forward kinematic analysis of kinematically redundant hybrid parallel robots, Journal of Mechanisms and Robotics, 12(6) (2020): 061008.

[20] C. Liu, G.H. Cao, Y.Y. Qu, Safety analysis via forward kinematics of delta parallel robot using machine learning, Safety Science, 117 (2019): 243-249.

[21] A. Morell, M. Tarokh, L. Acosta, Solving the forward kinematics problem in parallel robots using Support Vector Regression, Engineering Applications of Artificial Intelligence, 26(7) (2013): 1698-1706.

[22] P.K. Jamwal, S.Q. Xie, Y.H. Tsoi, K.C. Aw, Forward kinematics modelling of a parallel ankle rehabilitation robot using modified fuzzy inference, Mechanism and Machine Theory, 45(11) (2010): 1537-1554.

[23] J.P. Merlet, Parallel robots, Kluwer Academic Publishers, (2006).

[24] X.W. Kong, C.M. Gosselin, Type synthesis of parallel mechanisms, Springer, (2007).

[25] Y. Jin, I-M. Chen, G.L. Yang, Kinematic design of a family of 6-DOF partially decoupled parallel manipulators, Mechanism and Machine Theory, 44(5) (2009): 912-922.

[26] L.W. Tsai, Robot Analysis: the Mechanics of Serial and Parallel Manipulators, John Wiley & Sons, (1999).

[27] J. Lacombe, C.M. Gosselin, Singularity analysis of a kinematically redundant (6+ 2)-DOF parallel mechanism for zero-torsion configurations, Mechanism and Machine Theory, 170 (2022): 104682.

[28] D. Zlatanov, I.A. Bonev, C.M. Gosselin, Constraint singularities of parallel mechanisms, In Proceedings 2002 IEEE International Conference on Robotics and Automation, 1 (2002): 496-502.

[29] S. Patel, T. Sobh, Manipulator performance measures-a comprehensive literature survey, Journal of Intelligent & Robotic Systems, 77(3) (2015): 547-570.

[30] M.W. Hannan, I.D. Walker, Kinematics and the implementation of an elephant's trunk manipulator and other continuum style robots, Journal of robotic systems, 20(2) (2003): 45-63.

[31] J. Brinker, B. Corves, Y. Takeda, Kinematic performance evaluation of high-speed Delta parallel robots based on motion/force transmission indices, Mechanism and Machine Theory, 125 (2018): 111-125.

[32] X.J. Liu, J.S. Wang, F. Gao, Performance atlases of the workspace for planar 3-DOF parallel manipulators, Robotica, 18(5) (2000): 563-568.

[33] J.P. Merlet, Jacobian, manipulability, condition number, and accuracy of parallel robots, (2006): 199-206.

[34] X.D. Meng, F. Gao, S.F. Wu, Q.D. Ge, Type synthesis of parallel robotic mechanisms: Framework and brief review, Mechanism and machine theory, 78 (2014): 177-186.

[35] Y.D. Xu, Y. Zhao, Y. Yue, F.F. Xi, J.T. Yao, Y.S. Zhao, Type synthesis of overconstrained 2R1T parallel mechanisms with the fewest kinematic joints based on the ultimate constraint wrenches, Mechanism and Machine Theory, 147 (2020): 103766.

[36] S.Y. Long, T. Terakawa, M. Komori, Type synthesis of 6-DOF mobile parallel link mechanisms based on screw theory, Journal of Advanced Mechanical Design, Systems, and Manufacturing, 16(1) (2022): JAMDSM0005-JAMDSM0005.

[37] T. Sun, X.M. Huo, Type synthesis of 1T2R parallel mechanisms with parasitic motions, Mechanism and Machine Theory, 128 (2018): 412-428.

[38] S.F. Yang, T. Sun, T. Huang, Type synthesis of parallel mechanisms having 3T1R motion with variable rotational axis, Mechanism and Machine Theory, 109 (2017): 220-230.

[39] H.F. Ding, W.A. Cao, Z.M. Chen, A. Kecskeméthy, Structural synthesis of two-layer and two-loop spatial mechanisms with coupling chains, Mechanism and Machine Theory, 92 (2015): 289-313.

[40] J. Wei, J.S. Dai, Reconfiguration-aimed and manifold-operation based type synthesis of metamorphic parallel mechanisms with motion between 1R2T and 2R1T, Mechanism and Machine Theory, 139 (2019): 66-80.

[41] Q.C. Li, Z. Huang, J.M. Hervé, Type synthesis of 3R2T 5-DOF parallel mechanisms using the Lie group of displacements, IEEE transactions on robotics and automation, 20(2) (2004): 173-180.

[42] Y. Qi, T. Sun, Y.M. Song, Y. Jin, Topology synthesis of three-legged spherical parallel manipulators employing Lie group theory, Proceedings of the Institution of Mechanical Engineers, Part C: Journal of Mechanical Engineering Science, 229(10) (2015): 1873-1886.

[43] J.Z. Zhang, Z.L. Jin, H.B. Feng, Type synthesis of a 3-mixed-DOF protectable leg mechanism of a firefighting multi-legged robot based on GF set theory, Mechanism and Machine Theory, 130 (2018): 567-584.

[44] J. He, F. Gao, Type synthesis for bionic quadruped walking robots, Journal of Bionic Engineering, 12(4) (2015): 527-538.

[45] J. He, F. Gao, X.D. Meng, W.Z. Guo, Type synthesis for 4-DOF parallel press mechanism using GF set theory, Chinese Journal of Mechanical Engineering, 28(4) (2015): 851-859.

[46] F. Gao, J.L. Yang, Q.D. Ge, Type synthesis of parallel mechanisms having the second class GF sets and two dimensional rotations, Journal of Mechanisms and Robotics, (2011): 011003.

[47] Q. Jin, T.L. Yang, Theory for topology synthesis of parallel manipulators and its application to three-dimension-translation parallel manipulators, Journal of Mechanical Design, 126(4) (2004): 625-639.

[48] H.P. Shen, T.L. Yang, L.Z. Ma, Synthesis and structure analysis of kinematic structures of 6-dof parallel robotic mechanisms, Mechanism and machine theory, 40(10) (2005): 1164-1180.

[49] T.L. Yang, A.X. Liu, H.P. Shen, L.B. Hang, Q.D. Ge, Composition principle based on Single-Open-Chain unit for general spatial mechanisms and its Application—in conjunction with a review of development of mechanism composition principles, Journal of Mechanisms and Robotics, 10(5) (2018): 051005.

[50] H.S. Yan, Creative design of mechanical devices, Springer Science & Business Media, (1998).

[51] H.S. Yan, C.H. Kuo, Structural analysis and configuration synthesis of mechanisms with variable topologies, ASME/IFToMM International Conference on Reconfigurable Mechanisms and Robots, (2009): 23-31.

[52] H.S. Yan, C.H. Kuo, Representations and identifications of structural and motion state characteristics of mechanisms with variable topologies, Transactions of the Canadian Society for Mechanical Engineering, 30(1) (2006): 19-40.

[53] K.T. Zhang, J. S. Dai, Y. F. Fang, Q. Zeng, String matrix based geometrical and topological representation of mechanisms, World Congress in Mechanism and Machine Science, (2011): 19-25.

[54] B.J. Slaboch, P.A. Voglewede, Mechanism state matrices for planar reconfigurable mechanisms, Journal of Mechanisms and Robotics, 3(1) (2011): 011012.

[55] X.L. Ding, Y. Yang, J.S. Dai, Topology and kinematic analysis of color-changing ball, Mechanism and Machine Theory, 46(1) (2011): 67-81.

[56] S. Li, J.S. Dai, Augmented adjacency matrix for topological configuration of the metamorphic mechanisms, Journal of Advanced Mechanical Design, Systems, and Manufacturing, 5(3) (2011): 187-198.

[57] M. Pucheta, A. Cardona, An automated method for type synthesis of planar linkages based on a constrained subgraph isomorphism detection, Multibody System Dynamics, 18(2) (2007): 233-258.

[58] L.H. Wu, A. Mueller, J.S. Dai, A matrix method to determine infinitesimally mobile linkages with only first-order infinitesimal mobility, Mechanism and Machine Theory, 148(2020): 103776.

[59] A. Seibel, S. Schulz, J. Schlattmann, On the direct kinematics problem of parallel mechanisms, Journal of robotics, 2018 (2018).

[60] D. Oetomo, H.C. Liaw, G. Alici, B. Shirinzadeh, Direct kinematics and analytical solution to 3RRR parallel planar mechanisms, In 2006 9th International Conference on Control, Automation, Robotics and Vision, (2006):1-6.

[61] Y. Zhang, X.W. Kong, S.M. Wei, D.L. Li, Q.Z. Liao, CGA-Based approach to direct kinematics of parallel mechanisms with the 3-RS structure, Mechanism and Machine Theory, 124 (2018): 162-178.

[62] H.P. Shen, D. Chablat, B.X. Zeng, J. Li, G.L. Wu, T.L. Yang, A translational three-degrees-of-freedom parallel mechanism with partial motion decoupling and analytic direct kinematics, Journal of Mechanisms and Robotics 12(2) (2020): 021112.

[63] M.S. Tsai, T.N. Shiau, Y.J. Tsai, T.H. Chang, Direct kinematic analysis of a 3-PRS parallel mechanism, Mechanism and Machine Theory, 38(1) (2003): 71-83.

[64] I.A. Bonev, Direct kinematics of zero-torsion parallel mechanisms, In 2008 IEEE international

conference on robotics and automation, (2008): 3851-3856.

[65] X.G. Huang, Q.Z. Liao, S.M. Wei, Closed-form forward kinematics for a symmetrical 6-6 Stewart platform using algebraic elimination, Mechanism and Machine Theory, 45(2) (2010): 327-334.

[66] J. Kim, F.C. Park, Direct kinematic analysis of 3-RS parallel mechanisms, Mechanism and Machine theory, 36(10) (2001): 1121-1134.

[67] J. Gallardo, H. Orozco, J.M. Rico, Kinematics of 3-RPS parallel manipulators by means of screw theory, The International Journal of Advanced Manufacturing Technology, 36(5) (2008): 598-605.

[68] S. Zarkandi, M.R. Esmaili, Direct position kinematics of a three revolute-prismatic-spherical parallel manipulator, International Journal of Recent Research and Applied Studies, 7(1) (2011): 88-95.

[69] H. Ye, D. Wang, J. Wu, Y. Yue, Y.L. Zhou, Forward and inverse kinematics of a 5-DOF hybrid robot for composite material machining, Robotics and Computer-Integrated Manufacturing, 65 (2020): 101961.

[70] D. Gan, Q. Liao, J.S. Dai, S. Wei, L.D. Seneviratne, Forward displacement analysis of a new 1CCC–5SPS parallel mechanism using Gröbner theory, Proceedings of the Institution of Mechanical Engineers, Part C: Journal of Mechanical Engineering Science, 223(5) (2009): 1233-1241.

[71] C.F. Yang, S.T. Zheng, J. Jin, S.B. Zhu, J.W. Han, Forward kinematics analysis of parallel manipulator using modified global Newton-Raphson method, Journal of Central South University of Technology, 17(6) (2010): 1264-1270.

[72] L.J. Puglisi, R. Saltaren, C. Garcia, P. Cardenas, H. Moreno, Implementation of a generic constraint function to solve the direct kinematics of parallel manipulators using Newton-Raphson approach, Journal of Control Engineering and Applied Informatics, 19(2) (2017): 71-79.

[73] C.F. Yang, Q.T. Huang, H.Z. Jiang, O.O. Peter, J.W. Han, PD control with gravity compensation for hydraulic 6-DOF parallel manipulator, Mechanism and Machine theory, 45(4) (2010): 666-677.

[74] M. Góra, J. Knapczyk, M. Maniowski, Estimation of platform spatial pose and displacement of parallel mechanism using wire-based sensors, Archive of Mechanical Engineering, (2007): 365-389.

[75] L.T. Schreiber, C.M. Gosselin, Physical human-robot interaction with a backdrivable (6+ 3)-dof parallel mechanism.

[76] T.S. Nguyen, D. Harton, A. Campeau-Lecours, C.M. Gosselin, Motion control algorithms based on the dynamic modelling of kinematically redundant hybrid parallel robots, Mechatronics, 76 (2021): 102555.

[77] S. Schulz, On using inertial measurement units for solving the direct kinematics problem of parallel mechanisms, Robotics, 8(4) (2019): 99.

[78] S.M. Varedi, H.M. Daniali, D.D. Ganji, Kinematics of an offset 3-UPU translational parallel manipulator by the homotopy continuation method, Nonlinear Analysis: Real World Applications, 10(3) (2009): 1767-1774.

[79] P.J. Parikh, S.S. Lam, A hybrid strategy to solve the forward kinematics problem in parallel manipulators, IEEE Transactions on Robotics, 21(1) (2005): 18-25.

[80] H.Q. Zhang, H.R. Fang, B.S. Jiang, F.Q. Zhao, T. Zhu, A Newton-Raphson and BP neural network hybrid algorithm for forward kinematics of parallel manipulator, In 2019 WRC Symposium on Advanced Robotics and Automation (WRC SARA), (2019): 122-127.

[81] A.H. Elsheikh, E. Showaib, A. Asar, Artificial neural network based forward kinematics solution for planar parallel manipulators passing through singular configuration, Advances in Robotics & Automation, 2(2) (2013): 1000106.

[82] G.Y. Liu, Y. Wang, Y.R. Zhang, Z. Xie, Real-time solution of the forward kinematics for a parallel haptic device using a numerical approach based on neural networks, Journal of Mechanical Science and Technology, 29(6) (2015): 2487-2499.

[83] M. Dehghani, M. Ahmadi, A. Khayatian, M. Eghtesad, M. Farid, Neural network solution for forward kinematics problem of HEXA parallel robot, In 2008 American Control Conference, (2008): 4214-4219.

[84] D. Zhang, J.H. Lei, Kinematic analysis of a novel 3-DOF actuation redundant parallel manipulator using artificial intelligence approach, Robotics and Computer-Integrated Manufacturing, 27(1) (2011): 157-163.

[85] A. Morell, L. Acosta, J. Toledo, An artificial intelligence approach to forward kinematics of Stewart platforms, In 2012 20th Mediterranean Conference on Control & Automation (MED), (2012): 433-438.

[86] W. Ye, X.X. Chai, K.T. Zhang, Kinematic modeling and optimization of a new reconfigurable parallel mechanism, Mechanism and Machine Theory, 149(2020): 103850.

[87] G.L. Wu, S.P. Bai, Design and kinematic analysis of a 3-RRR spherical parallel manipulator reconfigured with four–bar linkages, Robotics and Computer-Integrated Manufacturing, 56(2019): 55-65.

[88] L.P. Wang, Z.K. Zhang, Z.F. Shao, X.Q. Tang, Analysis and optimization of a novel planar 5R parallel mechanism with variable actuation modes, Robotics and Computer-Integrated Manufacturing, 56(2019) : 178-190.

[89] N. Plitea, A. Szilaghyi, D. Pisla, Kinematic analysis of a new 5-DOF modular parallel robot for brachytherapy, Robotics and Computer-Integrated Manufacturing, 31(2015): 70-80.

[90] L.T. Schreiber, C.M. Gosselin, Kinematically redundant planar parallel mechanisms: Kinematics, workspace and trajectory planning, Mechanism and Machine Theory, 119 (2018): 91-105.

[91] C.M. Gosselin, L.T. Schreiber, Kinematically redundant spatial parallel mechanisms for singularity avoidance and large orientational workspace, IEEE Transactions on Robotics, 32(2) (2016): 286-300.

[92] L. Nurahmi, J. Schadlbauer, S. Caro, M. Husty, P. Wenger, Kinematic analysis of the 3-RPS cube parallel manipulator, Journal of Mechanisms and Robotics, 7(1) (2015): 011008.

[93] Z. Huang, Y.F. Fang, “Motion characteristics and rotational axis analysis of three DOF parallel robot mechanisms, IEEE International Conference on Systems, Man and Cybernetics. Intelligent Systems for the 21st Century, Vancouver, BC, Canada, (1995): 67–71.

[94] D.M. Gan, J. Dias, L. Seneviratne, Unified kinematics and optimal design of a 3rRPS metamorphic parallel mechanism with a reconfigurable revolute joint, Mechanism and Machine Theory, 96(2016): 239-254.

[95] C.M. Gosselin, T. Laliberté, A. Veillette, Singularity-free kinematically redundant planar parallel mechanisms with unlimited rotational capability, IEEE Transactions on Robotics, 31(2) (2015): 457-467.

[96] B. Li, Bin, Y.M. Li, X.H. Zhao, Kinematics analysis of a novel over-constrained three degree-of-freedom spatial parallel manipulator, Mechanism and Machine Theory, 104 (2016): 222-233.

[97] G.J. Niu, B. Pan, F.H. Zhang, H.B. Feng, Y.L. Fu, Kinematic analysis of a novel uncoupled and isotropic 2-degree-of-freedom parallel mechanism, Advances in Mechanical Engineering, 8(3) (2016): 1687814016638040.

[98] M.R.C. Qazani, S. Pedrammehr, A. Rahmani, B. Danaei, M.M. Ettefagh, A.K.S. Rajab, H. Abdi, Kinematic analysis and workspace determination of hexarot-a novel 6-DOF parallel manipulator with a rotation-symmetric arm system, Robotica, 33(8) (2015): 1686-1703.

[99] K. Balaji, B.S.H. Khan, Kinematic analysis and performance evaluation of novel PRS parallel mechanism, In IOP Conference Series: Materials Science and Engineering, 310(1) (2018): 012007.

[100] M. Mazare, M. Taghizadeh, M.R. Najafi, Kinematic analysis and design of a 3-DOF translational parallel robot, International journal of Automation and Computing, 14(4) (2017): 432-441.

[101] F.G. Xie, X.J. Liu, X. Luo, M. Wabner, Mobility, singularity, and kinematics analyses of a novel spatial parallel mechanism, Journal of Mechanisms and Robotics, 8(6) (2016): 061022.

[102] Q.Z. Meng, F.G. Xie, X.J. Liu, Conceptual design and kinematic analysis of a novel parallel robot for high-speed pick-and-place operations, Frontiers of Mechanical Engineering, 13(2) (2018): 211-224.

[103] X.L. Shan, G. Cheng, Nonlinear dynamic behaviour of joint effects on a 2(3PUS+S) parallel manipulator, Proceedings of the Institution of Mechanical Engineers, Part K: Journal of Multi-body Dynamics, 233(2019): 470-484.

[104] Z.S. Chen, L.M. Xu, W.Z. Zhang, Q.C. Li, Closed-form dynamic modeling and performance analysis of an over-constrained 2PUR-PSR parallel manipulator with parasitic motions, Nonlinear Dynamics, 96(2019): 517-534.

[105] J. He, H.C. Zheng, F. Gao, H.B. Zhang, Dynamics and control of a 7-DOF hybrid manipulator for capturing a non-cooperative target in space, Mechanism and Machine Theory, 140(2019): 83-103.

[106] X.W. Kong, C.M. Gosselin, Kinematics and singularity analysis of a novel type of 3-CRR 3-DOF translational parallel manipulator, The International Journal of Robotics Research, 21(9) (2002): 791-798.

[107] M. Sharifzadeh, M.T. Masouleh, A. Kalhor, P. Shahverdi, An experimental dynamic identification & control of an overconstrained 3-DOF parallel mechanism in presence of variable friction and feedback delay, Robotics and Autonomous Systems, 102(2018): 27-43.

[108] G.X. Wang, L. Wang, Dynamics investigation of spatial parallel mechanism considering rod flexibility

and spherical joint clearance, Mechanism and Machine Theory, 137(2019): 83-107.

[109] X.R. Li, S.P. Bai, O. Madsen, Dynamic modeling and trajectory tracking control of an electromagnetic direct driven spherical motion generator, Robotics and Computer-Integrated Manufacturing, 59(2019): 201-212.

[110] L. Milica, A. Năstase, G. Andrei, A novel algorithm for the absorbed power estimation of HEXA parallel mechanism using an extended inverse dynamic model, Proceedings of the Institution of Mechanical Engineers, Part K: Journal of Multi-body Dynamics, 234(2019): 185-197.

[111] R.F. Abo-Shanab, Dynamic modeling of parallel manipulators based on Lagrange–D'Alembert formulation and Jacobian/Hessian matrices, Multibody System Dynamics, 48(2020): 403-426.

[112] D.S. Zhang, Y.D. Xu, J.T. Yao, B. Hu, Y.S Zhao, Kinematics, dynamics and stiffness analysis of a novel 3-DOF kinematically/actuation redundant planar parallel mechanism, Mechanism and Machine Theory, 116(2017): 203-219.

[113] J. Enferadi, K. Jafari, A Kane's based algorithm for closed-form dynamic analysis of a new design of a 3RSS-S spherical parallel manipulator, Multibody System Dynamics, 49(2020): 377–394.

[114] G.Y. Xin, G.L. Zhong, Closed-form dynamics of a 3-DOF spatial parallel manipulator by combining the Lagrangian formulation with the virtual work principle, Nonlinear Dynamics, 86(2016): 1329-1347.

[115] J. Brinker, P. Ingenlath, B. Corves, A study on simplified dynamic modeling approaches of Delta parallel robots, In Advances in Robot Kinematics 2016, (2018): 119-128.

[116] S.N. Nabavi, A. Akbarzadeh, J. Enferadi, Closed-form dynamic formulation of a general 6-PUS robot, Journal of Intelligent & Robotic Systems, 96(2019): 317-330.

[117] J. Du, Y. Lou, Simplified dynamic model for real-time control of the delta parallel robot, 2016 IEEE International Conference on Information and Automation (ICIA), Ningbo, (2016): 1647-1652.

[118] Z.H. Chong, F.G. Xie, X.J. Liu, J.S. Wang, Evaluation of dynamic isotropy and coupling acceleration capacity for a parallel manipulator with mixed DoFs, Mechanism and Machine Theory, 163 (2021): 104382.

[119] V. Muralidharan, A.Bose, K. Chatra, S. Bandyopadhyay, Methods for dimensional design of parallel manipulators for optimal dynamic performance over a given safe working zone. Mechanism and Machine Theory, 147(2020): 103721.

[120] X.J. Wang, J. Wu, Y.T. Wang, Dynamics evaluation of 2UPU/SP parallel mechanism for a 5-DOF hybrid robot considering gravity, Robotics and Autonomous Systems, 135 (2021): 103675.

[121] J.V. Fontes, M.M.D. Silva, On the dynamic performance of parallel kinematic manipulators with actuation and kinematic redundancies, Mechanism and Machine Theory, 103(2016): 148-166.

[122] H. Asada, A geometrical representation of manipulator dynamics and its application to arm design, Journal of Dynamic Systems, Measurement, and Control, 105(1983): 131–135.

[123] J.,Wu, J.S. Wang, T.M. Li, L.P. Wang, L.W. Guan, Dynamic dexterity of a planar 2-DOF parallel manipulator in a hybrid machine tool, Robotica, 26(1) (2008): 93-98.

[124] T. Yoshikawa, Dynamic manipulability of robot manipulators, International Conference on Robotics and Automation, (1985): 1033–1038 .

[125] G.L. Chen, W.D Yu, Q.C. Li, H. Wang, Dynamic modeling and performance analysis of the 3-PRRU 1T2R parallel manipulator without parasitic motion, Nonlinear Dynamics, 90(1) (2017): 339-353.

[126] Z.S. Chen, L.M. Xu, W.Z. Zhang, Q.C. Li, Closed-form dynamic modeling and performance analysis of an over-constrained 2PUR-PSR parallel manipulator with parasitic motions, Nonlinear Dynamics, 96(1) (2019): 517-534.

[127] M. Chen, Q. Zhang, X.R. Qin, Y.T. Sun, Kinematic, dynamic, and performance analysis of a new 3-DOF over-constrained parallel mechanism without parasitic motion, Mechanism and Machine Theory, 162(2021): 104365.

[128] X.X. Chai, M. Wang, L.M. Xu, W. Ye, Dynamic modeling and analysis of a 2PRU-UPR parallel robot based on screw theory, IEEE Access, 8 (2020): 78868-78878.

[129] J.F. Li, S.P. Zuo, L.Y. Zhang, M.J. Dong, Z.K. Zhang, C.J. Tao, R. Ji, Mechanical design and performance analysis of a novel parallel robot for ankle rehabilitation, Journal of Mechanisms and Robotics, 12(5) (2020): 051007.

[130] Z.F. Shao, X.Q. Tang, X. Chen, L.P. Wang, Research on the inertia matching of the Stewart parallel manipulator, Robotics and Computer-Integrated Manufacturing, 28(6) (2012): 649-659.

[131] J. Mo, Z.F. Shao, L.W. Guan, F.G. Xie, X.Q. Tang, Dynamic performance analysis of the X4 high-speed pick-and-place parallel robot, Robotics and Computer-Integrated Manufacturing, 46 (2017): 48-57.

[132] V. Muralidharan, A. Bose, K. Chatra, S. Bandyopadhyay, Methods for dimensional design of parallel manipulators for optimal dynamic performance over a given safe working zone, Mechanism and Machine Theory, 147(2020): 103721.

[133] D. Liang, Y.M. Song, T. Sun, G. Dong, Optimum design of a novel redundantly actuated parallel manipulator with multiple actuation modes for high kinematic and dynamic performance, Nonlinear Dynamics, 83(1) (2016): 631-658.

[134] L.P. Wang, H.Y. Xu, L.W.Guan, Optimal design of a 3-PUU parallel mechanism with 2R1T DOFs, Mechanism and Machine Theory, 114 (2017): 190-203.

[135] R. Kelaiaia, O. Company, A. Zaatri, Multiobjective optimization of a linear Delta parallel robot, Mechanism and Machine Theory, 50 (2012): 159-178.

[136] G.L. Wu, S. Caro, S.P. Bai, J. Kepler, Dynamic modeling and design optimization of a 3-DOF spherical parallel manipulator, Robotics and Autonomous Systems, 62 (2014): 1377-1386.

[137] L. Garcia, A. Campos, Maximal singularity-free orientation subregions associated with initial parallel manipulator configuration, Robotics, 7 (2018): 57.

[138] Y.M. Song, B.B Lian, T. Sun, G. Dong, Y. Qi, H. Gao, A novel Five-Degree-of-Freedom parallel manipulator and its kinematic optimization, Journal of Mechanisms and Robotics, 6 (2014): 041008.

[139] H. Wang, W. Li, H.T. Liu, J.X. Zhang, S.T. Liu, Conceptual design and dimensional synthesis of a

novel parallel mechanism for lower-limb rehabilitation, Robotica, 37(3) (2019): 469-480.

[140] X.J. Liu, J.S. Wang, H.J. Zheng, Optimum design of the 5R symmetrical parallel manipulator with a surrounded and good-condition workspace, Robot. Auton. Syst. 54 (2006): 221-233.

[141] X.J. Liu, L.P. Wang, F.G. Xie, I.A. Bonev, Design of a 3-axis articulated tool head with parallel kinematics achieving desired motion/force transmission, Journal of Manufacturing Science & Engineering, 132 (2010): 021009.

[142] X.J. Liu, J. Li, Y.H. Zhou, Kinematic optimal design of a 2-degree-of-freedom 3-parallelogram planar parallel manipulator, Mechanism and Machine Theory, 87(2015): 1-17.

[143] K.K. Oh, X.J. Liu, D.S. Kang, J.W. Kim, Optimal design of a micro parallel positioning platform, Part II: Real machine design, Robotica, 23(1) (2005): 109-122.

[144] M.L. Li, Y.Q. Gu, H.L. Zhang, L.Q. Liu, W.E.N.D. Juan, G.S. Lan, Parallel mechanism structure optimization design based on multi-objective differential evolution algorithm, China Mechanical Engineering, 21(16) (2010): 1915.

[145] C.Z. Wang, Y.F. Fang, S. Guo, Multi-objective optimization of a parallel ankle rehabilitation robot using modified differential evolution algorithm, Chinese Journal of Mechanical Engineering, 28(4) (2015): 702-715.

[146] W.X. Zhang, W. Zhang, X.L. Ding, L. Sun, Optimization of the rotational asymmetric parallel mechanism for hip rehabilitation with force transmission factors, Journal of Mechanisms and Robotics, 12(4) (2020).

[147] L. Weihmann, D. Martins, L.D.S. Coelho, Modified differential evolution approach for optimization of planar parallel manipulators force capabilities, Expert Systems with Applications, 39(6) (2012): 6150-6156.

[148] A.R. Shirazi, M.M.S. Fakhrabadi, A. Ghanbari, Optimal design of a 6-DOF parallel manipulator using particle swarm optimization, Advanced Robotics, 26(13) (2012): 1419-1441.

[149] Z. Gao, D. Zhang, Workspace representation and optimization of a novel parallel mechanism with three-degrees-of-freedom, Sustainability, 3(11) (2011): 2217-2228.

[150] G. Abbasnejad, H.M. Daniali, A. Fathi, Architecture optimization of 4PUS+ 1PS parallel manipulator, Robotica, 29(5) (2011): 683-690.

[151] S. Farooq, A. Baqai, M. Shah, Optimal design of tricept parallel manipulator with particle swarm optimization using performance parameters, Journal of Engineering Research, 9(2) (2021): 378-395.

[152] J. Enferadi, R. Nikrooz, The performance indices optimization of a symmetrical fully spherical parallel mechanism for dimensional synthesis, Journal of Intelligent & Robotic Systems, 90(3) (2018): 305-321.

[153] L.X Che, G.W. Chen, H.Y. Jiang, L. Du, S.K. Wen, Dimensional synthesis for a Rec4 parallel mechanism with maximum transmission workspace, Mechanism and Machine Theory, 153 (2020): 104008.

[154] M. Russo, S. Herrero, O. Altuzarra, M. Ceccarelli, Kinematic analysis and multi-objective

optimization of a 3-UPR parallel mechanism for a robotic leg, Mechanism and Machine Theory, 120(2018): 192-202.

[155] T. Sun, Y.M. Song, Y.G. Li, J. Zhang, Workspace decomposition based dimensional synthesis of a novel hybrid reconfigurable robot, Journal of Mechanisms and Robotics, 2 (2010): 031009.

[156] D. Liang, Y.M. Song, T. Sun, G. Dong, Optimum design of a novel redundantly actuated parallel manipulator with multiple actuation modes for high kinematic and dynamic performance, Nonlinear Dynamics, 83 (2016): 631-658.

[157] D.M. Gan, J.S. Dai, J. Dias, R. Umer, L. Seneviratne, Singularity-free workspace aimed optimal design of a 2T2R parallel mechanism for automated fiber placement, Journal of Mechanisms and Robotics, 7(4) (2015): 041022.

[158] A. Karimi, M.T. Masouleh, P. Cardou, Avoiding the singularities of 3-RPR parallel mechanisms via dimensional synthesis and self-reconfigurability, Mechanism and Machine Theory, 99 (2016): 189-206.

[159] Y. Jin, Z. M. Bi, H. T. Liu, C. Higgins, M. Price, W. H. Chen, T. Huang, Kinematic analysis and dimensional synthesis of exechon parallel kinematic machine for large volume machining, Journal of Mechanisms and Robotics, 7(4) (2015): 041004.

[160] S. Khan, K. Andersson, J. Wikander, Jacobian matrix normalization-A comparison of different approaches in the context of multi-objective optimization of 6-DOF haptic devices, Journal of Intelligent & Robotic Systems, 79(1) (2015): 87-100.

[161] J. Wu, Y. Gao, B.B. Zhang, L.P. Wang, Workspace and dynamic performance evaluation of the parallel manipulators in a spray-painting equipment, Robotics and Computer-Integrated Manufacturing, 44(2017): 199-207.

[162] A. Codourey, Dynamic modeling of parallel robots for computed-torque control implementation, The International Journal of Robotics Research, 17(12) (1998): 1325-1336.

[163] K. Deb, A. Pratap, S. Agarwal, T.A.M.T. Meyarivan, A fast and elitist multiobjective genetic algorithm: NSGA-II, IEEE transactions on evolutionary computation 6(2) (2002): 182-197.

[164] K. Deb, H. Jain, An evolutionary many-objective optimization algorithm using reference-point-based nondominated sorting approach, part I: solving problems with box constraints. IEEE Transactions on Evolutionary Computation, 18(4) (2014):577–601.

[165] H.R. Nohooji, Constrained neural adaptive PID control for robot manipulators, Journal of The Franklin Institute, 357(7) (2020): 3907-3923.

[166] J. Zhong, C. Zhao, A phenomenological model-based controller for position tracking of a pneumatic muscle actuator driven setup, IEEE Access, 7 (2019): 45662-45669.